LITHOFACIES, PETROGRAPHY AND GEOCHEMISTRY OF THE NEOGENE MOLASSE SEQUENCE OF HIMALAYAN FORELAND BASIN, SOUTHWESTERN KOHAT, PAKISTAN

By
Kafayat Ullah

Doctorate of Philosophy in Geology

National Centre of Excellence in Geology, University of Peshawar

2009

LITHOFACIES, PETROGRAPHY AND GEOCHEMISTRY OF THE NEOGENE MOLASSE SEQUENCE OF HIMALAYAN FORELAND BASIN, SOUTHWESTERN KOHAT, PAKISTAN

By
Kafayat Ullah

A Dissertation submitted to the University of Peshawar in partial fulfillment for the Degree of
Doctoral of Philosophy in Geology

National Centre of Excellence in Geology, University of Peshawar

2009

Dissertation Acceptance Certificate

I hereby declare that the work presented in this dissertation is original (excluding where referred) and has not been used for the award of any degree by any university or institution.

Kafayat Ullah (Author)
National Center of Excellence in Geology (NCEG)
University of Peshawar
2008

Dedication

My degree of Doctor of Philosophy, including this thesis is dedicated to my beloved parents, family members and respected teachers.

Abstract

The Himalayan Foreland Basin (HFB) is one of the largest and dynamic terrestrial basins, stretching between the northwestern and northeastern Himalayas before arching southward to the Arabian Sea in the west and the Indian Ocean in the east. Molasse sediments eroded from the Himalayan orogen, representing the post-Eocene sedimentary record of the collision of the Indian and Eurasian plates occur in this basin from Pakistan through India to Nepal. In Pakistan, this sedimentary sequence is well preserved and exposed in the Kohat and Potwar plateaus other than Sulaiman and Kirthar ranges. The source area, sedimentation pattern, drainage organization, tectonic and climatic conditions generally differ at sub-basin level. For present study, the Neogene molasse sequence of the southwestern Kohat plateau is selected, which constitutes the westernmost deformed part of the HFB. Here, the Neogene molasse sequence consists of the Kamlial, Chinji and Nagri formations. All these formations are composed of sandstones, mudstones and conglomerates.

On the basis of field observations and presence of various sedimentary structures, different lithofacies of the Kamlial Formations are identified, namely; Channel Conglomerates Facies (K1), Cross-bedded Sandstone Facies (K2), Interbedded Mudstone, Sandstone and Siltstone Facies (K3) and Mudstone Facies (K4). In Chinji Formation, based on various sedimentary structures, lithofacies identified include; Cross-bedded Channel Sandstone Facies (C1), Cross-bedded and Cross-laminated Sandstone Facies (C2), Interbedded Mudstone, Siltstone and Sandstone Facies (C3) and Mudstone Facies (C4). Alike, lithofacies identified in the Nagri Formation include Channel Conglomerate Facies (N1), Cross-bedded Channel Sandstone Facies (N2), Interbedded Sandstone, Siltstone and Mudstone Facies (N3) and Mudstone Facies (N4).

The above mentioned facies propose that the Kamlial Formation was possibly deposited by sandy bedload or major mixed load river, the Chinji Formation by mixed-load rivers with significant fine suspended sediment and the Nagri Formation by sandy bedload rivers. The floodplain deposits of the Chinji Formation seem to be deposited by suspended-load rivers during major flood events. Low lateral and vertical connectivity of the sandstone bodies suggests high subsidence rates. The change from thick channel sandstones of Kamlial Formation to dominantly overbank accumulation with minor, thin, channel-sandstone lenses of the Chinji Formation could either be due to a change in climate or palaeodrainage of the area. Again a major change from mudstone-siltstone facies-dominant Chinji Formation to channel sandstone facies-dominant Nagri Formation occurs, which might reflect one or more factors including (1) low subsidence rates, or (2) arid climatic regime and limited vegetation, or (3) strongly seasonal discharge resulting in flash flooding.

Detailed petrographic studies of representative sandstone samples from three different sections reveal that the Kamlial, Chinji and Nagri formations contain abundant quartz with subordinate feldspars and variable proportions of lithic grains. Monocrystalline quartz dominates over polycrystalline quartz in all the three studied formations. The feldspar content mostly ranges from 18 to 30%, 24 to 28% and 16 to 36% in the Kamlial, Chinji and Nagri sandstones, respectively. The abundance of lithic grains shows a wide range of variation (4 to 35%). Although the lithics are mainly sedimentary, but fragments of volcanic and low-grade metamorphic rocks also occur in appreciable amounts. Micas, including both muscovite and biotite, are generally less than 10 % of the total detrital grains. The observed heavy minerals include epidote, monazite, apatite, garnet, zircon, rutile and brown hornblende. The crystals of zircon, monazite, rutile, epidote and mica also occur as tiny inclusions in quartz grains.

On the basis of modal composition, sandstones of the Kamlial, Chinji and Nagri formations fall into the groups of feldspathic and lithic arenites indicating to be the products of feldspar-rich crystalline rocks and rugged high-relief source areas, respectively. The presence of appreciable amount of feldspars in the sandstone samples favors either high relief or arctic climate at the source area. The overall variation in the relative abundance of different types of quartz grains (monocrystalline including both non-undulatory and undulatory types and polycrystalline containing 2-3 and >3 subgrains) shows contribution from both medium-high grade and low-grade metamorphic rocks provenance for sandstones of the Kamlial, Chinji and Nagri formations, supported by the consistent presence of minerals like mica, epidote and garnet as well as relative dominance of polycrystalline quartz grains composed of 2-3 crystals (Qp_{2-3}). Alike, the presence of illite in mudstone also suggests a source area composed of metamorphic and sedimentary rocks. On the other hand, the average contents of different types of quartz grains from the Kamlial, Chinji and Nagri formations show granitic and/or gneissic source. The greater abundance of alkali feldspar than plagioclase further supports this conclusion. The relatively greater abundance of monocrystalline quartz also suggests that the presence of granitic and volcanic rocks in the source areas cannot be ruled out, or else the quartz grains have traveled a longer distance of transportation. Furthermore, the inter-sectional variation in modal composition and types of quartz grains in both the Kamlial and Chinji sandstones suggest a strong spatial control on their deposition.

Petrographic results of the studied sandstones were also processed using different provenance discriminatory diagrams suggesting Magmatic arc, Recycled Orogens and a mixed provenance for the Kamlial, Chinji and Nagri formations.

Similarly, geochemical data of the major element oxides of the sandstone was used for classification and provenance determination applying different tectonic discriminatory plots. Sandstone of the Kamlial, Chinji and Nagri formations predominantly classify as litharenite and Fe-sand. The shift of sandstone to various fields in classification is due to a wide range in the variation of relative proportion of matrix, feldspar and lithic components. Different provenance discriminatory plots suggest continental island arc and Active Continental Margin (ACM) provenance for the sandstone of the three studied formations of southwestern Kohat. Similarly, discriminatory plot of SiO_2 vs log (K_2O/Na_2O) indicate a dominant influx from ACM for the studied sandstone. Other geochemical parameters like Fe_2O_3+MgO, TiO_2 and Al_2O_3/SiO_2 and the contents of the major element oxides except MnO of the Neogene molasse sandstone show major provenance from continental island arc and partial influx from ACM settings. Furthermore, the Th/U ratio of the Neogene molasse sequence is lower than the UCC and PAAS, which also show that these sediments are first cycled in origin; however, Zr/Sc ratio proposes minor contribution from recycled sedimentary sources.

In regional tectonic scenario of the study area, it is assumed that the recycled orogen sediments are sourced from the Himalayan tectonic units, the active continental margin orogen sediments from the Asian active continental margin (the Trans-Himalaya and Karakoram) and the magmatic arc orogen sediments from the Kohistan-Ladakh arc.

Values of the Chemical Index of Alteration (CIA) of the Neogene sandstone (mostly 64 to 76) and mudstone (mostly 70 to 80) suggest moderate to slightly intense weathering of these sediments, respectively. However, Index of Compositional Variability (ICV) values and lower contents of Rb and Cs than UCC and PAAS of the mudstone indicate relatively moderate weathering. The more abundance of feldspar (plagioclase) than clay minerals in the mudstone suggests high denudation rates or high relief or limited chemical weathering in the source area(s). The presence of illite in the mudstone suggests cold and dry glacier conditions whereas kaolinite indicates warm and humid conditions. This conclusion either favors a source region of vast area that had different climates in different parts, or major shifts in extreme climatic conditions. Red coloration of the Neogene mudstone of the Kohat Plateau most probably indicates deposition under hot, semi-arid and oxidizing diagenetic conditions. Furthermore, the values of the authigenic U, and ratios of U/Th, V/Cr, Cu/Zn and Ni/Co of the Neogene molasse sediments show that these sediments were deposited in oxidizing conditions.

Greater abundance of alkali feldspar than plagioclase in the Neogene sandstone of the Kohat Plateau, and dominance of plagioclase in the associated mudstone suggest granitic and mafic/ultramafic sources for these sediments, respectively. However, the lower values of Zr, Nb and Y, and ratios of the Ba/Sc, Ba/Co, Cr/Zr, Sc/Th and Y/Ni in sandstone and mudstone indicate the consistent presence of basic/mafic phases in the source area, still values of La/Th, La/Sc, Th/Zr and binary plot of Th/Co vs La/Sc propose provenance similar to Upper Continental Crust (UCC)/Post Archaen Australian Shale (PAAS)/felsic rocks. Generally, there exist a significant positive correlation of TiO_2, Zr, Rb and V with Al_2O_3 indicating their association with clay minerals and associated phases.

Acknowledgements

First and above all, I wish to thank almighty “ALLAH” for HIS blessings to accomplish this task.

This work is the result of a long journey in which I received support from many peoples. I extend my sincere gratitude to all of them. The first person I would like to thank is my co-supervisor, Prof. Dr. M. Arif. In fact, I don’t have words to express his generosity. All through this work, he has provided his support and guidance, and he was always ready to help whenever required.

I am also grateful to my supervisor, Prof. Dr. M. Tahir Shah for his endless support and encouragement during this study. His suggestion, help and supplies were integral to the timely completion of this study.

I am also indebted to my co-supervisor, Prof. I. A. Abbasi for his expert advice and attention at various stages of this project.

Appreciation and invaluable suggestions given by the dissertation examiners, namely Prof. Dr. Eduardo Garzanti, Dipartimento di Scienze Geologiche e Geotecnologie, UNIVERSITA' DI MILANO-BICOCCA, Milano, Italy, Prof. Dr. Christian Koeberl, Head, Department of Lithospheric Research, Center for Earth Sciences, University of Vienna, Austria and Prof. Dr. Abdul Salam Khan, Director, Center of Excellence in Mineralogy, Balochistan University, Quetta are highly acknowledged.

This project was fully funded by the Higher Education Commission (HEC), Government of Pakistan. I am obliged for their monetary support as well as the free access to a large number of international journals. I would like to express my profound gratitude to Mr. Sajid Hussain, Mr. Shahid Saleem and Mr. Asif of HEC, who have always been very positive in dealing with official matters.

I would also like to extend my true gratitude to my parent organization, Pakistan Atomic Energy Commission (PAEC) for allowing me to conduct this project. I offer special thanks to my seniors Mr. Aziz A. Qureshi, Dr. Imthinan Elahi Qureshi, Dr. J. I. Akhtar, Dr. Ikram Shehzad and Mr. M Akram there in. Indispensable support was provided by all of them regarding PAEC official matters.

Dr. Ray Ingersoll, Department of Earth and Space Sciences, University of California is highly acknowledged for providing relevant literature, and Drs. Rohtas Kumar of Wadia Institute of Himalayan Geology, Mary J. Kraus, Department of Geological Sciences, University of Colorado and Adrian Hartley, Department of Geology & Petroleum Geology, University of Aberdeen for their useful discussion and answering my queries regarding field photographs and suggestions about field work.

I would like to thank Mr. Sher Muhammad, PAEC and Mr. Muhammad Shahid, OGDCL for their help and company in the field work. Thanks to Mr. Muhammad Khan, driver National Center of Excellence in Geology (NCEG) for being a helping hand during samples collection in the field.

I again offer my undying gratitude to Prof. M. Arif for allowing me to use petrographic microscope and point counting instruments of the Department of Geology, University of Peshawar.

I give my thanks to Profs. M. Asif Khan and Irshad Ahmad for granting permission to use the XRF and XRD facilities of the NCEG. I am very grateful to Mr. Iqbal Hussain for his help in carrying out analysis with XRD and XRF. Special thanks go to Mr. Liaqat Ali, Mr. Bilal and Mr. Tariq for their contribution regarding the geochemical analysis with atomic absorption spectrometer.

Special thanks are due to the faculty and staff members of the NCEG for creating a friendly working environment. Account and administrative personals were always supportive and encouraging, and I extend my sincere gratitude to all of them. I express deep sense of gratitude to NCEG for the use of field camera, office space and internet facility.

Heartfelt thanks are extended to Prof. Nimat Ullah, Zahid Shah, Jawad Zeb, Rahman Ullah, M. Hassan Agheem, Ahmad Nabi, Shamsul Hadi, Dr. Rashid Ahmad, Maj. Tamiz, Abdul Raziq, Anwarul Haq, Shahid Saleem, Nawab Ali and Safeer Hussain for their help and support. Discussion with them and their brotherly advices helped me a lot in studying at the high track.

I sincerely thank to all my friends who helped one way or another to complete this study. Due to space constraint, it is not possible to name all of them.

I am greatly indebted to my parents, uncle and aunt for their endless and consistent efforts to bring me to this level. I would also like to highly acknowledge the support of my brothers, sisters and other family members. All of them stayed by my side and showered me with their love, kindness and care, which make me feel extremely lucky to have been blessed with such a family.

Kafayat Ullah

Table of Contents

List of Figures

List of Photographs

List of Plates

List of Tables

CHAPTER 1

Introduction

1.1 General

The Himalayan Foreland Basin (HFB) is one of the largest and dynamic terrestrial basins flanking Himalayan mountain ranges. The basin stretches between the northwestern and northeastern Himalayas before arching southward to the Arabian Sea in the west and the Indian Ocean in the east (Burbank et al., 1996). The Himalayan Basin is divided into a number of sub-basins separated by several pre-Tertiary basement highs (Raiverman, 2002) and lineaments (Virdi, 1979). In Pakistan, two main sedimentary basins are identified, namely, the Indus and the Balochistan basins. The Neogene molasse sequence in the Indus Basin is exposed in the Kohat and Potwar plateaus (Upper Indus Basin), and Sulaiman and Kirthar ranges (Southern/Central Indus Basin) (Kadri, 1995) (Fig. 1.1). This sequence of the foreland basin represents the post-Eocene sedimentary record of the collision of the Indian and Eurasian plates (Tahirkheli, 1979; Zeitler, 1985) preserved in northern Pakistan, India and Nepal (Fig. 1.2). The source area, sedimentation pattern, drainage organization, tectonic and climatic conditions generally differ at sub-basin level (Kumar et al., 2003). For present study, the Neogene molasse sequence of the southwestern Kohat i.e., the westernmost part of the Himalayan Foreland Basin is selected (Fig. 1.2).

1.2 Study Area

The Kohat Plateau constitutes the westernmost deformed part of the HFB covering an approximately 10,000 km^2 area of anticlinal hills resulted from the ongoing collision of the Indian and Eurasian plates (Pivnik and Wells, 1996). It is bounded by the Main Boundary Thrust (MBT) in the north, Surghar Range Thrust (Salt Range Thrust) in the south, Kalabagh Fault (and Indus River) in the east and Kurram Fault in the west (Gee, 1983; Khan, M. A. et al., 1986; Lillie et al., 1987; Jaume and Lillie, 1988) (Fig. 1.3). It is located between latitude 32°-34° N and longitude 70°-72° E. The geological map of Kohat Plateau has been published by the United States Geological Survey (Meissner et al., 1974, 1975).

The southwestern part of Kohat Plateau is dominated by regional scale folds and thrust faults, trending mostly east-west. Important folds in this region include Karak

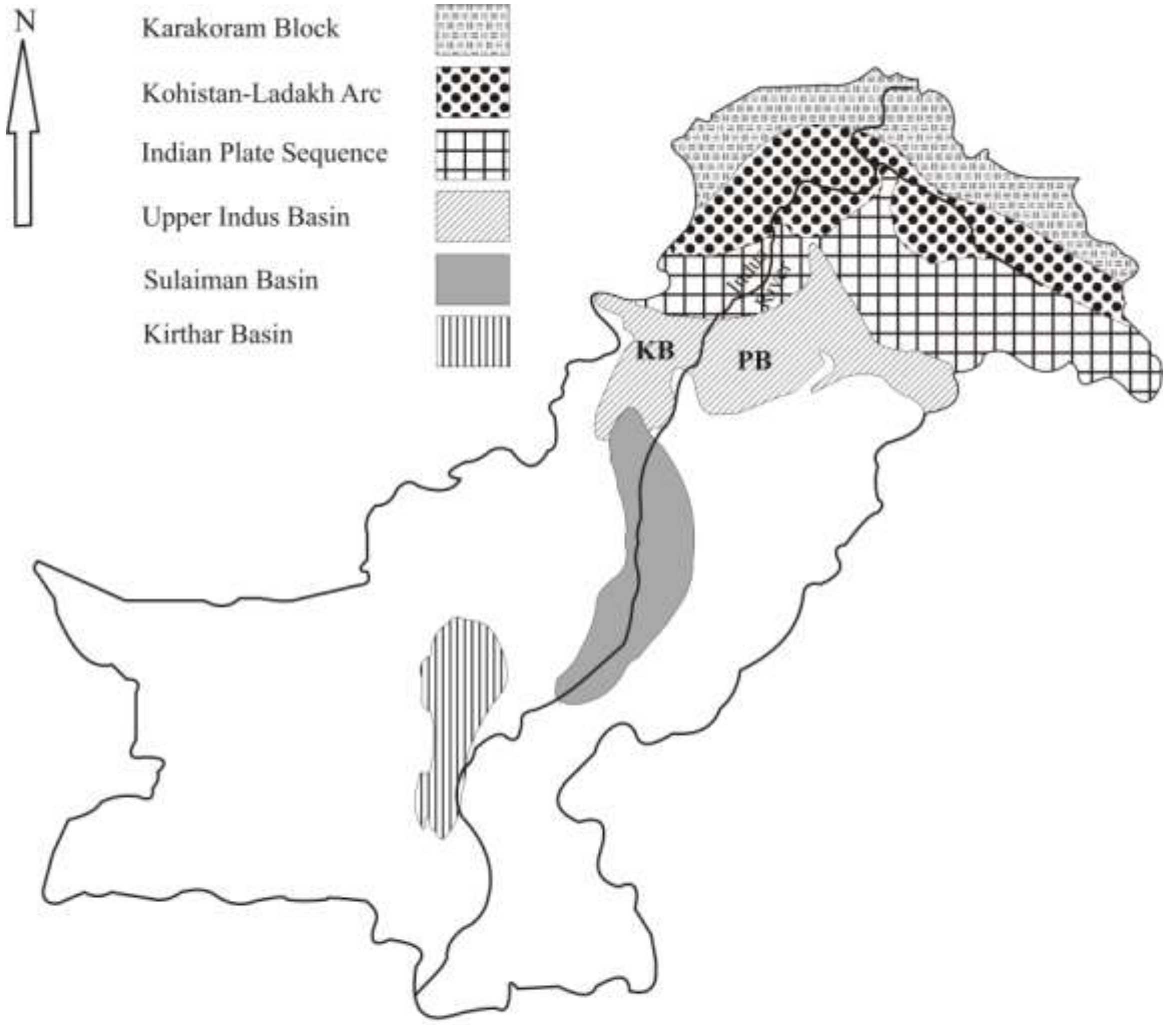

Fig 1.1. Map of Pakistan showing post-Eocene molasse basins architecture as well as main tectonic units of northern part. KB = Kohat Basin and PB = Potwar Basin.

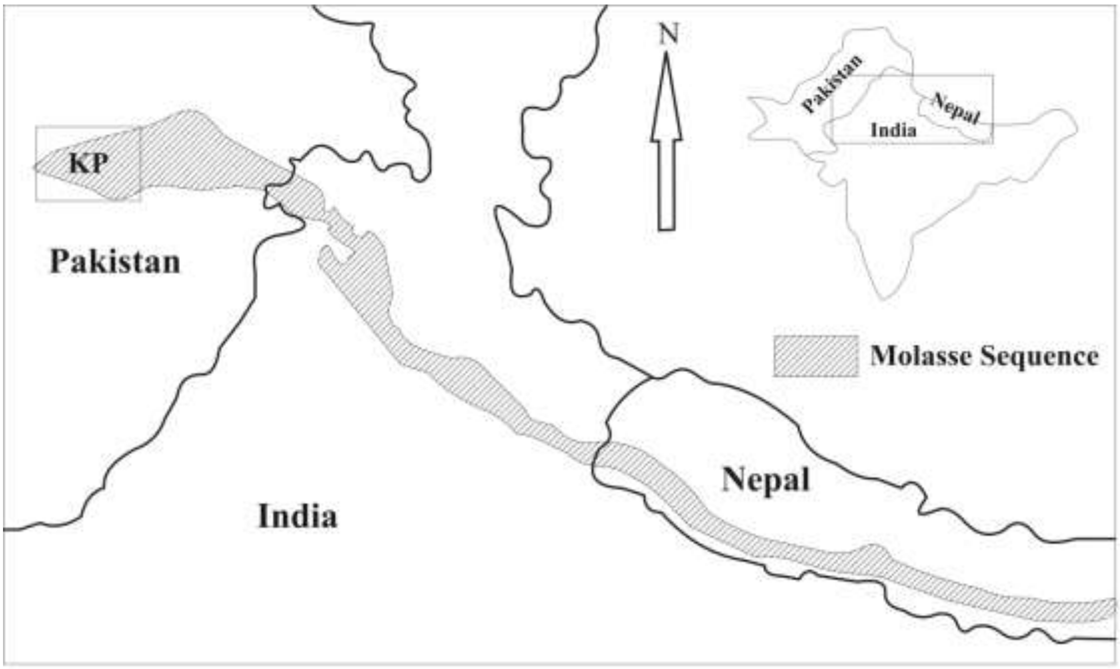

Fig. 1.2. Geographical extension of the molasse sequence of the Himalayan Foreland Basin. KP = Kohat Plateau

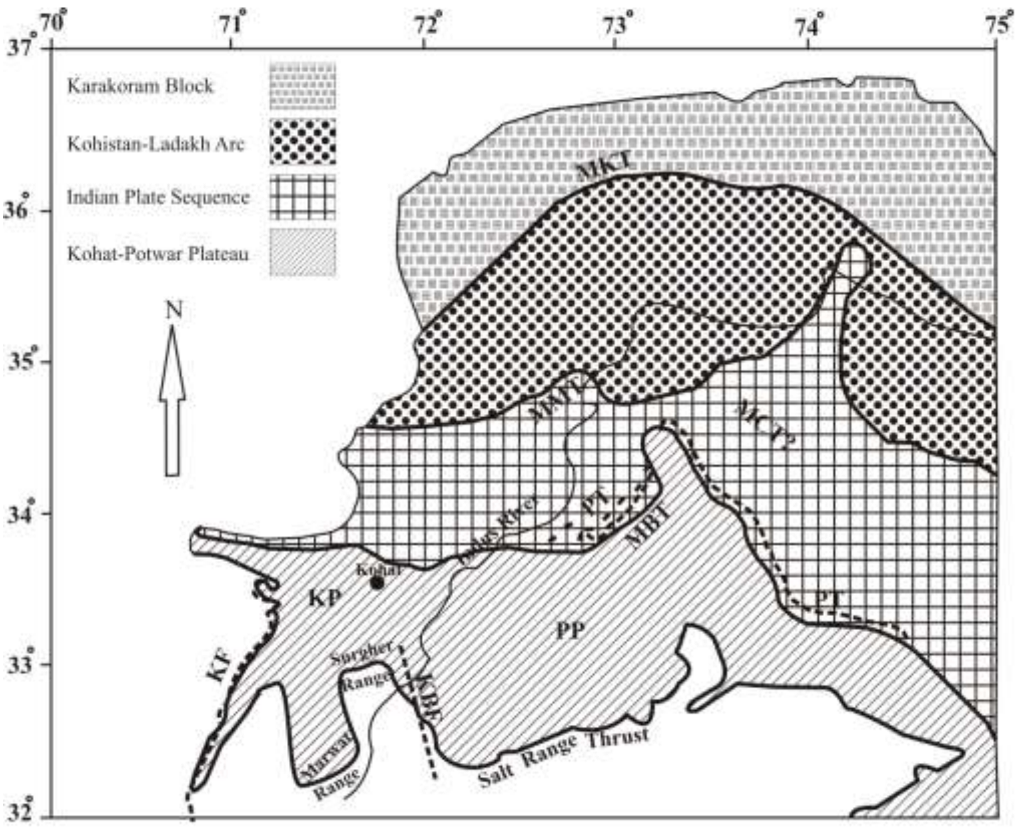

Fig. 1.3. Regional tectonic map of Northern Pakistan (modified after Kazmi and Rana, 1982). MKT = Main Karakoram Thrust, MMT = Main Mantle Thrust, PT = Panjal Thrust, MBT = Main Boundary Thrust, KP = Kohat Plateau, PP = Potwar Plateau, KF = Kurram Fault, KBF = Kalabagh Fault.

anticline, Nari Panoos syncline, Chashmai anticline, Banda Assar syncline and Bahadar Khel anticline. In these, the last three structures (i.e., Chashmai anticline latitude 33° 06' 34 N and longitude 70° 47' 77 E, Banda Assar syncline latitude 33° 07' 52 N and longitude 70° 55' 88 E, and Bahadar Khel anticline latitude 33° 09' 79 N and longitude 70° 57' 64 E), where the present study is conducted, have good exposures of the Neogene molasse sequence (Fig. 1.4). The lower contact of the Neogene molasse sequence in these structures is unconformable with underlying Eocene limestone. These structures are approachable through Indus Highway and old Bannu-Kohat road.

1.3 The Neogene Molasse Sequence

The high uplift rates of the Himalayan orogenic belt during Miocene time (Zeitler, 1985) exposed deep-seated metamorphic and igneous rocks for denudation and then the Himalayan drainage system analogous to the present day river systems of Indus, Ganges and Brahmaputra started flowing axially into their respective basins that deposited thick detrital sediments commonly known as the “molasse deposits” (Abid et al., 1983; Abbasi and Friend, 2000). These molasse sediments provide information about the lithologies uplifted in the source area, the type of drainage system, the position of the depositional site relative to the orogenic belt and basin subsidence (Dickinson, 1985). The sediments become progressively younger southward as the deformational front and resultant depocentre migrated away from the collision belt (Raynolds and Johnson, 1985).

The Neogene molasse sequence of the Kohat Plateau comprises of the Rawalpindi and Siwalik groups underlain by marine sequence of Eocene age. These rocks have been tightly folded and form narrow ridges of lower altitude separated by broad flat valleys, while the Paleocene rocks in the study area form rugged mountainous terrain of the same altitude ranges from 300-550m (Kazmi and Jan, 1997).

The Rawalpindi Group exposed in the Kohat Plateau consists of the Murree and Kamlial formations, and the Siwalik Group includes Chinji, Nagri, Dhok Pathan and Soan formations (Meissner et al., 1974). However, the study area consisting of the Chashmai anticline, Banda Assar syncline and Bahadar Khel anticline dominantly contains well-exposed sequences of Kamlial, Chinji and Nagri formations. These formations are composed of sandstones, overbank fines and conglomerates. In general, the foreland sequence of the Rawalpindi and Siwalik groups represents less than 18 million years of fluvial deposition, most likely by the ancestral Indus River (Cerveny et al., 1988).

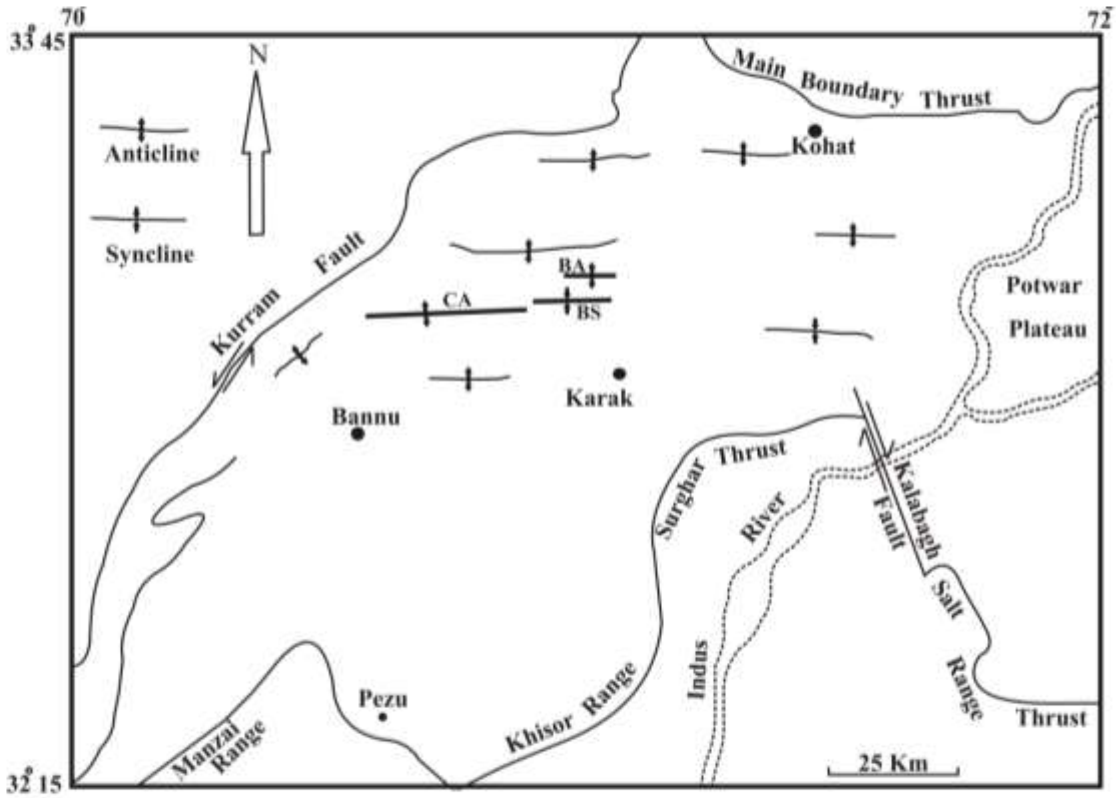

Fig. 1.4. Tectonic map of the Kohat Plateau (after Meissner et al., 1974). CA = Chashmai anticline latitude 33° 06' 34 N and longitude 70° 47' 77 E, BA = Bahadar Khel anticline latitude 33° 09' 79 N and longitude 70° 57' 64 E, BS = Banda Assar syncline latitude 33° 07' 52 N and longitude 70° 55' 88 E.

1.4 Aims and Objectives

Studies of molasse sequences in foreland basins are carried out in different perspective. Sedimentary structures in sandstone, and association of sandstone with mudstone and conglomerate are useful for investigation of depositional environment. Petrographic modal composition and geochemical studies of sandstone are reliable indicators for tracing source area sediments. Phase analysis and geochemistry of the mudstone reveal the paleoclimatic conditions of the source area and/or basin. Sediments of the Neogene molasse sequence of the Himalayan Foreland Basin are studied in different perspective. These sediments are extensively studied in different sub-basins of India (e.g., Raiverman et al., 1983; Kumar and Tandon, 1985; Kumar and Nanda, 1989; Kumar and Ghosh, 1994; Najman et al., 1997, 2000, 2003b, 2004; Kumar et al., 1999, 2003, 2004; Raiverman, 2002) and Potwar Plateau of Pakistan (e.g., Raynolds, 1981; Behrensmeyer and Tauxe, 1982; Johnson, N. M. et al., 1985; Raynolds and Johnson, 1985; Behrensmeyer, 1987; Quade et al., 1989, 1992; Willis, 1993a, 1993b; Willis and Behrensmeyer, 1994, 1995; Zaleha, 1997a, 1997b). In Kohat, such studies are conducted by Abbasi (Abbasi et al., 1983; Abbasi and Friend, 1989, 2000; Abbasi, 1991, 1994, 1998), which are mostly limited to the eastern part of the plateau. No detailed investigations of the lithofacies, petrography and geochemistry of the molasse sequence of southwestern Kohat Plateau are available, and the project was designed for collecting these data.

The aims and objective of the proposed study are as follows:

1) To describe and interpret the regional lithofacies distribution and overall depositional environment of the sediments comprising the Neogene molasse sequence (i.e., the Kamlial, Chinji, and Nagri formations) of the Kohat Plateau from the measured sections i.e., the Chashmai anticline, Banda Assar syncline and Bahadar Khel anticline.

2) To carry out petrographic, mineralogical and geochemical characterization of the molasse sequence and determine the origin of the poorly understood rock units from the Kohat Plateau.

3) To investigate provenance of the molasse sequence in a specific tectonic setting.

4) To utilize the data of sedimentology, petrography and geochemistry of the molasse sequence in interpretation of the tectonic evolution of the Himalayan Ranges.

1.5 Methodology

A) Fieldwork: Field/outcrops features such as bed geometry, texture, sedimentary structures, erosional surfaces etc. serve as evidence for depositional environments. Such features were carefully observed in the field. Field techniques also included documentation of the geometry of features (description, photos, measurement). Field descriptions were aided with the use of a 10x hand lens, dilute HCl (to test for carbonate cement) and grain size chart (to standardize grain size descriptions). Samples were collected for petrographic studies and geochemical analysis from beds of representative and variable lithologies.

B) Laboratory work: Thin sections were prepared for petrographic studies from sandstone samples collected in the field. The mudstone samples were analyzed for the structural and mineralogical composition using x-ray diffractometer. Chemical analysis of the whole rock samples were carried out using x-ray fluorescence/atomic absorption spectrophotometer under established standard conditions.

1.6 Interpretation of Data and Significance

Sedimentary structures and field photographs were briefly described in terms of lithofacies associations. These lithofacies associations are then interpreted for depositional environment of the studied sections.

Petrographic results were processed using different provenance discriminatory diagrams (e.g., Basu et al., 1975; Dickinson and Suczek, 1979; Dickinson, 1985) for tectonic setting. These discriminatory diagrams are based not only on the study of the thin sections but also upon knowledge of the regional geology and stratigraphy. The kind and proportion of the detrital minerals portray the character and location of the source rocks and tell something about the relief and climate of the source region.

Similarly, the geochemical analyses of the Neogene molasse sequence of the Kohat Plateau are utilized for provenance determination of these sediments. Sandstone geochemical data was plotted following the classification schemes of Herron (1988) and Pettijohn et al. (1987). Composition of the major element oxides of the sandstone was used for provenance determination applying tectonic discriminatory plots of Bhatia, M. R. (1983) and Roser and Korsch (1986). Furthermore, major elements oxides were plotted against Al_2O_3 for comparison with Upper Continental Crust (UCC) and Post Archian Australian Shale (PAAS). Alike, ratios of the La/Sc vs Th/Co of the sandstone and mudstone on binary plots were used for the characterization of the source rock composition.

It is known to us that the only uranium deposits of Pakistan are being mined from the Siwalik sequence for its nuclear power plants. The present studies will, of course help us in designing a detailed future plan for locating the source of these uranium deposits. The study of depositional environment will also be helpful in locating the uranium deposits as uranium dissolves easily in oxidizing environment and precipitates under reducing conditions.

CHAPTER 2

Regional Tectonics

2.1 Introduction

This chapter of the thesis consists of broadly two parts. First part of the chapter discusses a brief tectonic history of Himalaya and its lithotectonic units. Mentioning regional tectonics of the hinterland is important as it directly controls the type and rate of sediment supply and the drainage system in the foreland basin. In addition, the orogenic tectonic activities also play vital role in controlling paleoclimate. Second part of this chapter briefly describes the Eocene stratigraphy of the Kohat Plateau.

2.2 The Himalayan Tectonic System

The Himalayan mountain belt consists of a series of southward-propagating thrust sheets, which began soon after the collision between the Indian and Eurasian plates in the Eocene (Ratschbacher et al., 1994; Searle et al., 1997) (Fig. 2.1). The Indus Tsangpo Suture Zone (ITSZ) separates the Indian and Asian crusts, and is composed of sedimentary rocks, melange and ophiolitic material (Fig. 2.1). Obduction period of ophiolite onto the northern Indian margin is uncertain. Searle et al. (1997) suggested a Late Cretaceous ophiolite obduction with Eocene reactivation (associated with Himalayan collision), whereas Garzanti et al. (1987) and Gaetani and Garzanti (1991) favor Paleocene-Early Eocene obduction. In the south of the suture zone is the Paleozoic-Eocene Tethyan/Tibetan Himalaya Zone (THZ), deposited on the northern passive margin of India (Gaetani and Garzanti, 1991) (Fig. 2.1). Further to the south are the metamorphosed Indian plate rocks of the Greater Himalayan Crystalline Complex (GHC) that are separated from the THZ by the South Tibetan Detachment Zone (STDZ) above, and by the Main Central Thrust (MCT) from the Lesser Himalaya below (Hodges et al., 1996; Searle et al., 1997; Vance and Harris, 1999; Godin et al., 1999; Prince et al., 1999; Foster et al., 2000; Simpson et al., 2000) (Fig. 2.1). South of the Greater Himalaya lies the Lesser Himalaya, consisting of low-grade or unmetamorphosed Indian crust material of mostly Precambrian to Paleozoic age (Tewari, 1993; Frank et al., 1995; Hodges, 2000), further categorized into inner and outer Lesser Himalaya based on the geochemical differences (Ahmad, T. et al., 2000). South of the Lesser Himalaya, lies the

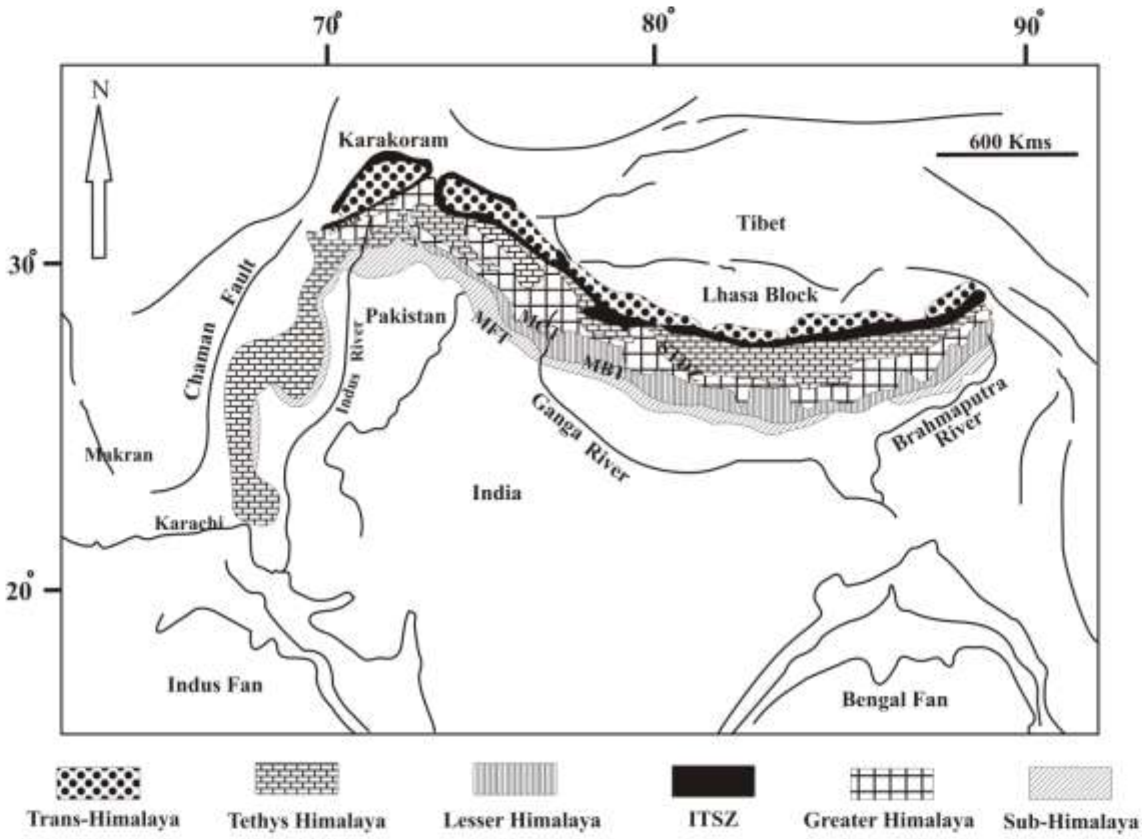

Fig. 2.1. Location map of the Himalayan Range (after Critelli and Garzanti, 1994; Najman, 2006). ITSZ = Indus Tsangpo Suture Zone, STDZ = South Tibetan Detachment Zone, MKT = Main Karakoram Thrust, MCT = Main Central Thrust, MBT = Main Boundary Thrust, MFT = Main Frontal Thrust.

Sub-Himalaya foreland basin sedimentary rocks, separated from the Lesser Himalaya by the MBT (Meigs et al., 1995).

According to Najman (2006), the total convergence between 1400 and 3215 km is estimated across the entire Himalayan orogen (including the Tibet) since the start of collision (Molnar and Tapponnier, 1975; Dewey et al., 1989; Lepichon et al., 1992; Hodges, 2000; Guillot et al., 2003). Different mechanisms, which also differ in the timing and rates of major events, are proposed for accommodation of this convergence. These include: distributed shortening followed by lithospheric delamination (Dewey et al., 1988); underthrusting of the Indian crust beneath Eurasian (Zhao et al., 1993); and lateral extrusion along major transform faults, which pushed out material to the east (Tapponnier et al., 1982).

2.2.1 Tectonic Regime-features of the Himalaya

Himalayan Range: According to Yin (2006), the Himalayan Range occurs between the eastern and western syntaxes of Himalaya i.e., the Namche Barwa (NB) and Nanga Parbat (NP) peaks, respectively (Fig. 2.2). Northern boundary of the Himalayan Range is marked by the east-flowing Yalu Tsangpo and west-flowing Indus rivers and the southern boundary is delineated by the Main Frontal Thrust (MFT) from the Indo-Gangetic depression. To the west and north of the Himalayan Range are the Hindu Kush and Karakoram Mountains, respectively.

Himalayan orogen: The Himalayan orogen is defined by the Indus-Tsangpo Suture Zone (ITSZ) in the north, the right-slip Sagaing Fault in the east, the left-slip Chaman Fault in the west, and the MFT in the south (LeFort, 1975) (Fig. 2.1). It extends all the way from the Himalayan Range to the Arabian Sea and the Bay of Bengal (Yin, 2006).

Himalayan tectonic system: The Himalayan tectonic system is a broader concept that consists of the Himalayan orogen, the active Himalayan foreland basin (the Indo-Gangetic depression), and the Indus and Bengal fans. All of these features were shaped by the Cenozoic Indo-Eurasian collision (Yin, 2006) (Fig. 2.1).

2.2.2 Himalayan Divisions

Yin (2006) categorized the Himalayan orogen into the North Himalaya and South Himalaya separated by its high crest line. In this categorization, the former is approximately equivalent to the geographically defined Tethyan Himalaya of Heim and

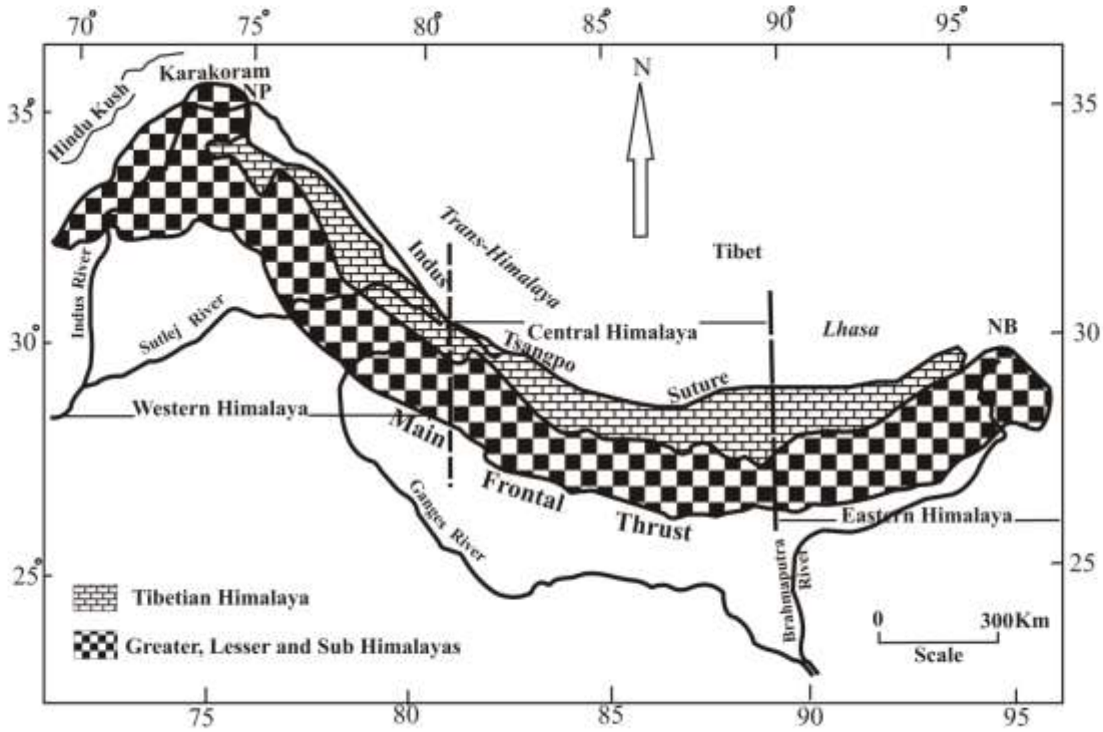

Fig. 2.2. Map of the Himalayan Range showing Western (66-81E), Central (81-89E) and Eastern Himalaya (89-98E). The map also shows major river system of the Himalaya. The Tibetian Himalaya is separated from the Greater, Lesser and Sub Himalayas by the South Tibetian Dtachment Zone (STDZ). The southern contact of the Himalayan Range is marked by the Main Frontal Thrust (MFT). NP= Nanga Parbat, NB= Namche Barwa.

Gansser (1939) or the Tibetan Himalaya of LeFort (1975), whereas the latter is divided into Higher, Lower, and Sub-Himalaya (Heim and Gansser, 1939; Gansser, 1964) from north to south (Fig. 2.1).

The Himalayan orogen is also subdivided along strike into the Western, Central and Eastern segments (Fig. 2.2). The Western Himalayan orogen includes Zanskar, Spiti, Chamba, Himachal Pradesh, Lahul, Kashmir and the Salt Range (Pakistan). The Central Himalayan orogen consists of Nepal, Sikkim and south-central Tibet, while the Eastern Himalayan orogen occupies Bhutan, Arunachal Pradesh (India) and southeastern Tibet (Yin, 2006).

This along-strike change in the Himalayan topography is also expressed by the geometrical variation of the modern intermontane basins in the south Himalaya, which range from ~80-100 km north-south widths (e.g., Jalalabad and Peshawar basins) in northern Pakistan and Kashmir (Kashmir Basin) to ~30-40 km north-south width in the central Himalayan orogen and are completely absent in the eastern Himalaya. This variation in basin width can be related to an eastward increase in the total crustal shortening along the Himalayan orogen (Yin, 2006).

Tectonic evolution of the Himalaya can be divided into two stages: the Eohimalayan event (Middle Eocene to Oligocene i.e., 45-25 Ma) and the Neohimalayan event (since the Early Miocene) (LeFort, 1996; Hodges, 2000).

2.2.3 Major Himalayan Tectonic Units

The Himalaya consists of nine lithotectonic zones (Gansser, 1964). From north to south, these belts and their representative rock types are as follows (Fig. 2.1).

The Trans-Himalayan Zone: This zone predominantly consists of Upper Cretaceous to Eocene calc-alkaline plutons, interpreted as the Andean-type northern margin of Tethys (LeFort, 1996), partly covered by forearc rocks and continental molasse derived from the uplift of magmatic rocks (Fig. 2.1). The igneous complex was formed as a result of partial melting of a subducting NeoTethyan slab beneath the Asian Plate (Sorkhabi and Macfarlane, 1999). To the west, in the Kohistan-Ladakh region, this zone is represented by an island arc environment (Windley, 1995).

The Hindu Kush terrain in Trans-Himalayan zone consists mainly of amphibolite and greenschist facies metapelites, marbles, cherts and sandstones, intruded by granodiorite and granite (Karim, 1998).

The Karakoram Range in Trans-Himalaya is subdivided into a granitic batholith in the center (~ 500 km long and upto 20 km wide), flanked in the south by a high-grade metamorphic belt consisting of interbedded pelites, marbles and amphibolites, and in the north by a sedimentary/metasedimentary zone (Searle et al., 1996; Karim, 1998).

Rocks similar in chemistry and age to the Karakoram batholith can also be found along a nearly continuous belt, further southeast, known as the Trans-Himalaya batholith that is about 50 km wide and 2500 km long. The same chemistry and ages of the Karakoram and Trans-Himalaya batholiths (LeFort et al., 1983; Debon et al., 1987) are interpreted for similar origin (LeFort, 1988).

The Main Karakoram Thrust (MKT): The Karakoram terrain is joined to the Kohistan-Ladakh arc along a suture zone known in Pakistan as the Northern Suture (Pudsey, 1986) or the Main Karakoram Thrust, and in India as the Shyok Suture (Tahirkheli, 1982). The suture zone is 150 m to 4 km wide and contains blocks of volcanic greenstones, limestones, shales, conglomerates, quartzites and serpentinites in northern Pakistan (Karim, 1998).

The Kohistan-Ladakh Island Arcs: The Kohistan includes most of the area along the Indus valley, between Nanga Parbat in the east and upper Swat valley in the west. It is bounded in the north and northwest by the MKT and in the south and southeast by the Main Mantle Thrust (MMT), and consists predominantly of mafic, ultramafic and calc-alkaline layered plutonic and volcanic rocks (Fig. 2.3). The Kohistan terrain has been divided into six major units, from bottom to top (Karim, 1998).

Jijal-Pattan Complex*:* To the north of the MMT along the Indus River is an isolated outcrop of granulites (mainly garnet granulites) and ultramafic rocks known as the Jijal-Pattan Complex ~150 km^2 (Jan and Howie, 1980). The granulites consist of garnet, clinopyroxene, and quartz ± plagioclase ± orthopyroxene. The protolith of the complex is interpreted to represent either the Tethyan lower crust or magmatic cumulates at the base of the Kohistan arc (Jan, 1985).

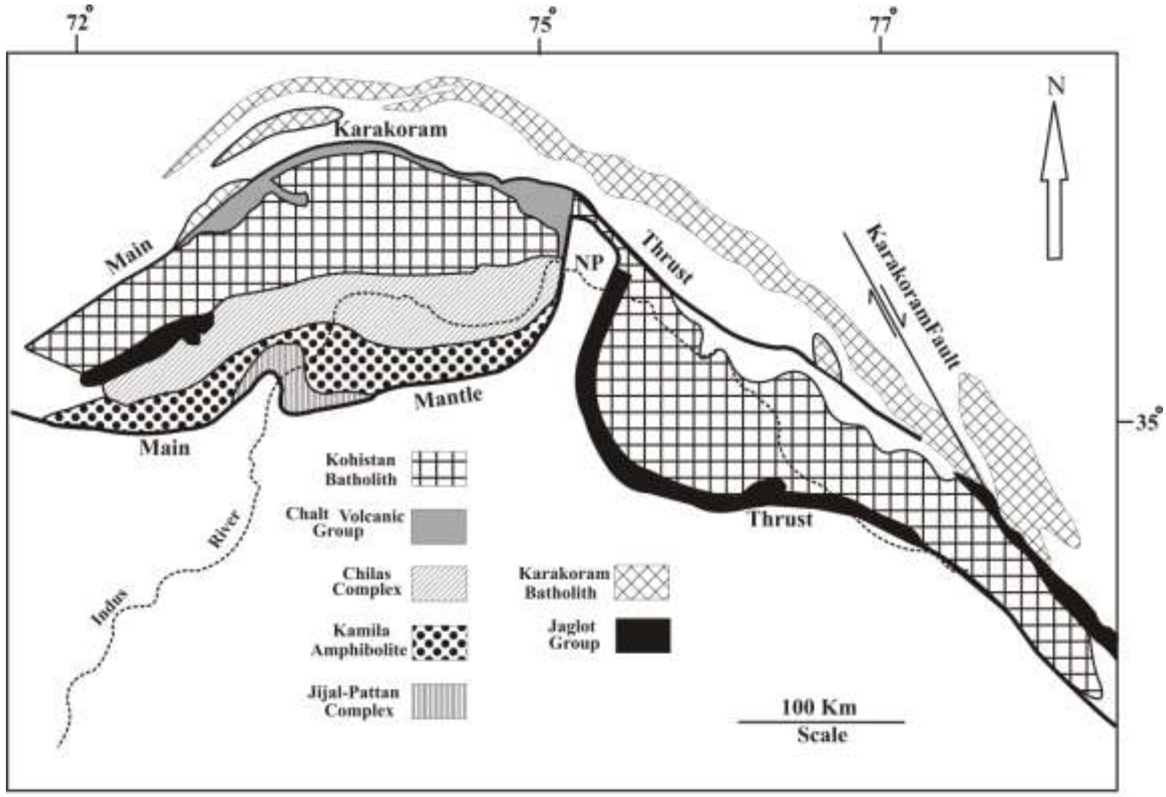

Fig. 2.3. Geological map of the Kohistan-Ladakh region (after Sharma, 1991; Searle and Khan, 1996). NP = Nanga Parbat.

The Jijal-Pattan complex has yielded a Sm-Nd modal age of 104 Ma (Coward et al., 1986), and Sm-Nd isochron cooling ages of 91±3 Ma (Yamamoto and Nakamura, 1996) and 96±3 Ma (Anczkiewicz and Vance, 2000). Its magmatic age is 118±12 Ma (Anczkiewicz and Vance, 2000; Yamamoto and Nakamura, 2000).

Kamila Amphibolite: The Kamila Amphibolite is ~40 km wide, and extends from the Nanga Parbat Massif in the east to the eastern Afghanistan in the west. Amphibolite is the predominant rock type but ultramafic rocks also occur. The amphibolites consist essentially of hornblende, plagioclase ± epidote ± garnet ± clinopyroxene (Jan, 1988). Bard et al. (1980) suggested an oceanic crust origin for the amphibolites due to scarcity of siliceous rocks, however, Coward et al. (1986) and Jan (1988) preferred an island arc origin.

Chilas Complex: The Chilas Complex is up to 40 km wide and stretches for 300 km, which is composed of layered mafic, ultramafic rocks and quartz diorites (Jan et al., 1984; Khan, M. A. et al., 1989; Khan, T. et al., 1994; Treloar et al., 1996). This intrusion is dated around 111±24 Ma on the basis of Rb-Sr whole rock isochron of the gabbronorite of the main facies (Mikoshiba et al., 1999). However, Zeitler et al. (1980) and Jagoutz et al. (2004) reported 84 Ma (U-Pb) and 102±5 Ma (the Sm-Nd whole-rock clinopyroxene-plagioclase isochron method) crystallization ages for the Chilas Complex, respectively. The cooling age of the gabbronorite through 500 °C, estimated by K-Ar and ^{40}Ar-^{39}Ar ages of hornblende, is ~ 80 Ma (Treloar et al., 1990).

Jaglot Group: The northern part of Kohistan arc consists of large-scale granitic plutons (the Kohistan Batholith), a sequence of arc-type volcanic rocks (the Chalt Volcanics) (Petterson and Windley, 1985, 1991), and a sequence of slates, turbidites and shallow marine Tethyan limestones (the Mid-Cretaceous Yasin and Jaglot groups) (Pudsey, 1986). The Jaglot Group is considered to represent rock assemblages of a back-arc basin, including greenschist facies metabasalts, interbedded with volcanoclastic and schistose metasediments (Khan, T. et al., 1994; Treloar et al., 1996). The Kalam volcanics and metasediments, Thelichi volcanics and metasediments, Majne volcanics and Gilgit paragneiss are also considered part of this group (Sullivan et al., 1994; Khan, T. et al., 1994).

Chalt Volcanic Group: The Chalt Volcanic Group consists of two formations, i.e., the Ghizar and Hunza formations (Petterson and Treloar, 2004), of which the latter is interpreted as a back-arc basin (Treloar et al., 1996; Rolland et al., 2000; Robertson and Collins, 2002; Bignold and Treloar, 2003).

Kohistan Batholith: The Kohistan Batholith forms part of the Trans-Himalaya Batholith and is intrusive into both the Chalt Volcanic Group and the Jaglot Group (Bignold and Treloar, 2006). The Kohistan Batholith, 300 km long and 60 km broad, consists of numerous large and small plutons, sills, dikes and sheets, composed of gabbro, hornblendite, diorite, quartz diorite, adamellite, granodiorite, granite, tonalite, trondhjemite, aplite and pegmatite (Petterson and Windley, 1991; Treloar et al., 1996).

On the basis of Rb-Sr whole-rock isochron ages, Petterson and Windley (1985, 1991) identified three distinct stages of emplacement of the Kohistan Batholith. Stage 1 plutons, which include the deformed Matum Das tonalite, were emplaced between 110 and 90 Ma, prior to suturing of the arc to Eurasia. Stage 2 plutons, with undeformed low- to high-K calc-alkaline gabbros and diorites, and granodiorites were emplaced between 85 and 40 Ma. Stage 3 plutons were emplaced as granite sheets at about 30 Ma (George et al., 1993). Both Stages 2 and 3 were emplaced after suturing with Eurasia.

The Indus-Tsangpo Suture Zone (ITSZ): It is the zone of collision between Indian and Eurasian plates. This zone is composed of deep-water Indian continental rise sediments, Trans-Himalayan accretionary complexes, ophiolites and ophiolitic melange, island arc volcanic rocks, and forearc basin sedimentary rocks (Fig. 2.1) (Searle, 1983; Robertson and Degnan, 1993).

In Pakistan, the Kohistan terrain is separated from the Indian plate sequence by a north dipping thrust known as the "Main Mantle Thrust" (MMT) or Indus Suture Zone (ISZ) (Tahirkheli et al., 1979), which is the western extension (Jan et al., 1981b) of the roughly 2000 km long ITSZ, and named after the Indus River, which follows it for several hundred kilometers in the Ladakh region (Gansser, 1964; Allègre et al., 1984).

The ISZ consists of three thrust bounded blocks in the Shangla-Mingora area of northern Pakistan (Kazmi et al., 1984). From north to south, these are: (1) The Shangla blueschist melange, mainly composed of metavolcanics and phyllite schist with smaller lensoidal masses of serpentinite, metadolerite, metagraywacke, metachert and marble; (2) The Charbagh greenschist melange, consisting of greenstone, greenschist and minor tectonized metasediments; and (3) The Mingora ophiolite melange, typified by abundant ophiolite suit rocks and emerald mineralization. Other rock types include serpentinite, talc-carbonate schist, greenschist, metagabbro, metasediments and metachert.

The Tibetan or Tethys Himalayan Zone (THZ): This zone preserves Proterozoic to Eocene sedimentary rocks (both siliciclastic and carbonate) interbedded with Paleozoic and Mesozoic volcanic rocks (Yin, 2006; and references therein) (Fig. 2.1).

The Greater Himalayan Crystalline Complex (GHC): The Greater Himalayan Crystalline Complex consists of Indian continental crust and sedimentary rocks of mainly Late Proterozoic-Cambrian age (Parrish and Hodges, 1996), now regionally metamorphosed (consisting of gneisses, granite gneisses, schists and marble) and intruded by leucogranite crustal melts in the uppermost part (Treloar and Searle, 1993) (Fig. 2.1).

The ITSZ near the confluence of the Indus and Gilgit-Hunza rivers, is folded into a crustal scale antiform forming the Nanga-Parbat Haramosh Massif (NPHM) (Coward, 1985). The NPHM is mainly composed of a series of biotite augen gneisses derived from an igneous (Butler and Prior, 1988) or metasedimentary (Chaudhry and Ghazanfar, 1990) precursor. Radiometric ages ranging from 2500 Ma to 2.3 Ma have been obtained on these rocks (Zeitler, 1985; Zeitler et al., 1989).

Though the GHC is generally considered to be composed of high grade rocks, but in northern Pakistan these rocks are low-grade to unmetamorphosed and thus it becomes difficult to differentiate them from the THZ (Pogue et al., 1999). Though a high-grade equivalent of the GHC lacks in northern Pakistan (Yeats and Lawrence, 1984), high-grade Lesser Himalayan rocks within and adjacent to the Nanga Parbat syntaxis have been noted (DiPietro and Isachsen, 2001). The GHC thrust over the unmetamorphosed or low grade late Palaeoproterozoic rocks (Valdiya and Bhatia, 1980) of the Lesser Himalayan Zone (LHZ) along Main Central Thrust (MCT).

In Pakistan, the southern boundary of the Greater Himalayas is based on its position relative to the MCT (Gansser, 1964), as it is not clear in northern Pakistan and Kashmir. Coward et al. (1988) considers the Panjal and the Mansehra thrusts to be equivalent to, but not necessarily coeval with the MCT.

South of the MMT in the Swat valley, Alpurai Group, Swat Granite Gneisses and Manglaur Schist are the dominant lithologic units. The Alpurai Group is composed of Early Paleozoic calcareous schist, marbles and amphibolites (Humayun, 1986; Lawerence et al., 1989). The Manglaur Schists consist of tectonized, non-calcareous quartz-feldspar, quartz-mica-kyanite and quartz-mica-garnet schists. The Swat Granite Gneisses are sheet-like intrusive within the Manglaur Schist (Kazmi et al., 1984).

Lithologically, the Indus valley exposes Precambrian gneisses of the Besham Group including metasedimentary schists, marbles and amphibolites (Treloar, 1989), not very different from the adjacent Swat valley, except for different proportions of rock types. The pelitic rocks predominate in the former, whereas the calcareous rocks of Alpurai Schist predominate in the latter (Karim, 1998).

The Hazara region is composed of metapelites and metapsammite of the Precambrian Tanawal Formation and Mansehra Granite. Other important lithologies of this area include Salkhala Formation (composed largely of slates, phyllites and granitic schists) (Wadia, 1953), Hazara Formation (predominantly composed of slates and phyllites) and Kingriali Formation (mainly composed of dolomite, quartzite and phyllite) (Calkins et al., 1975). In the south/southwest, the Peshawar Basin contains alluvial sediments with scattered outcrops of alkaline igneous rocks (Kempe and Jan, 1970), of which the Ambela Granitic Complex (~ 900 km^2) is the largest (Rafiq, 1987).

The Kaghan valley contains extensive Salkhala Formation rocks, subdivided into the Mid-Proterozoic to Archean Sharda Group and Late Proterozoic Kaghan Group (Chaudhry and Ghazanfar, 1990). The former consists of gneisses, marbles with sheet granites, migmatites and amphibolites, whereas the latter is mainly composed of quartz schists, quartzites, graphitic schists, marbles, gypsum and metaconglomerates (Chaudhry and Ghazanfar, 1990).

The southern margin of the Peshawar Basin is marked by the Attock-Cherat Range that consists of three east-west trending fault-bound blocks from north to south, and mainly composed of (i) Precambrian metapelites and minor limestone and quartzite, (ii) siltstone, argillite, quartzite and subordinate limestone of Precambrian Dakhner Formation, and (iii) unfossiliferous limestone and dolomite, and argillite and quartzite (Hussain et al., 1989). Among these lithologic units, the Dakhner Formation is the most extensive in the Attock-Cherat Range (Karim, 1998).

The Lesser Himalayan Zone (LHZ): The Lesser Himalayan Zone includes the nonfossiliferous low-grade metasedimentary rocks (Heim and Gansser, 1939; LeFort, 1975), overlain by Permian to Cretaceous strata (the Gondwana Sequence) (Gansser,

1964) (Fig. 2.1). This zone completely lacks Ordovician to Carboniferous strata that have been noted in the THZ (Yin, 2006).

The Sub-Himalaya: The Outer or Sub-Himalaya of the Western Himalaya contains the molasse sediments in Pakistan, best preserved in the fold-thrust belts of Potwar, Kohat, Trans Indus ranges, Sulaiman and Kirthar belts, and have mostly unconformable contacts with underlying Eocene carbonate rocks (Thakur, 1992) (Figs. 1.1, 2.1). The Main Boundary Thrust (MBT) is defined as the thrust placing the LHZ over the sub-Himalayan sedimentary strata (Heim and Gansser, 1939) (Fig. 2.1).

South of the Sub-Himalayas is the Salt Range, an arcuate mountain range that constitutes the drainage divide between the Jhelum and Soan rivers. The Salt Range consists of Eocambrian Salt Range Formation, marine sediments of Cambrian age, followed by a complete succession from Permian to Eocene. The Eocene strata are separated from the overlying Miocene fluviatile and lacustrine clastic sediments by a major unconformity (Gee and Gee, 1989).

The Active Himalayan Foreland Basin: According to Yin (2006), the Indo-Gangetic depression represents an active foreland basin that receives sediments both from the Himalayan orogen as well as the Indian Peninsula Highlands. The basin has been divided into four sub-basins: the Indus Basin, the Ganga Basin, the Brahmaputra Basin and the Bengal Basin covering the drainage areas of the Indus River, the Ganges River, the Brahmaputra River, and the joined Brahmaputra-Ganges River south of the Rajmahal-Garo gap, respectively.

2.2.4 Major Himalayan Structures

South Tibet Detachment Zone (STDZ): The South Tibet Detachment Zone juxtaposes unmetamorphosed or low-grade THZ over high-grade GHC (Burg et al., 1984; Burchfiel et al., 1992) (Fig. 2.1).

Main Central Thrust (MCT): The Main Central Thrust is identified as a lithologic contact separating the LHZ below from the GHC above (Heim and Gansser, 1939), or is the fault with an abrupt change in metamorphic grade (LeFort, 1975; Peˆcher, 1989), or it is the surface of a broad shear zone several kilometers thick across the uppermost part of the LHZ and the lowermost part of the GHC (Arita, 1983; Peˆcher, 1989; Searle et al., 2003) (Fig. 2.1).

Main Boundary Thrust (MBT): Heim and Gansser (1939) identify MBT as the thrust placing the LHZ over Tertiary sedimentary strata (Fig. 2.1).

Main Frontal Thrust (MFT): The fault that places the Neogene Siwalik strata above the Quaternary deposits of the Indo-Gangetic depression is named as the MFT (Gansser, 1964, 1983; Yeats and Lillie, 1991; Lave´ and Avouac, 2000) (Fig. 2.1).

Main Himalayan Thrust (MHT): The idea of Main Himalayan Thrust suggests that major Himalayan thrusts (MFT, MBT and MCT) in eastern Nepal of the South Himalaya may sole into a low angle fault termed as the Main Detachment Fault (Schelling and Arita, 1991). This idea was later supported by the INDEPTH (International Deep Profiling of Tibet and the Himalaya) seismic reflection profiles from the North Himalaya (Zhao et al., 1993).

2.2.5 Tectonic History of the Pakistan Himalaya

The mountain belt in Pakistan consists of three tectonostratigraphic units that formed during a series of orogenic events, both prior to and during collision of Indian and Eurasian plates (Fig. 2.1). Farthest north lies the southern margin of the Asian crust, including the Hindu Kush and the Karakoram, consisting of Paleozoic-Mesozoic succession intruded by a Jurassic to Cretaceous batholith and affected by metamorphic events pre- and post- India-Eurasia collision (Debon et al., 1987; Gaetani et al., 1990; Searle, 1996; Hildebrand et al., 2001; Fraser et al., 2001). Sandwiched between the Asian crust along the Northern or Shyok Suture or Mian Karakoram Thrust (MKT) (to the north) and the Indian crust along the Main Mantle Thrust (MMT) (to the south) is the Cretaceous-Eocene Kohistan Island Arc (KIA), which is intruded by the Kohistan batholith of pre- and post-collisional stages of formation (Treloar et al., 1989b; Khan, M. A. et al., 1993) (Fig. 2.1).

The north-dipping Kohistan Fault (= MMT) juxtaposes the Kohistan arc over the northern Indian margin and has been interpreted as a normal fault by Treloar et al. (2000), however, DiPietro et al. (2000) and DiPietro and Pogue (2004) showed that the fault was mainly a thrust, active between the Early Eocene and Early Miocene and noted that the juxtaposition relationship across the Kohistan Fault was similar to the Gangdese thrust of Yin et al. (1994) in south Tibet.

The Indian plate to the south of MMT is subdivided into three tectonic units. From north to south these are (1) an internal metamorphosed unit, (2) an external unmetamorphosed or low-grade metamorphic unit, and (3) the foreland basin sediments (Treloar et al., 1991b). The internal unit consists of cover and basement rocks. The basement rocks are predominantly high-grade gneisses that in some areas are unaffected by the Himalayan metamorphism, but the cover rocks are predominantly greenschist to amphibolite grade metapelites and metapsammites, metamorphosed during the Himalayan orogeny (Butler and Prior, 1988; Treloar et al., 1989a; Argles, 2000). The internal zone is separated from the unmetamorphosed to low-grade metamorphic Precambrian sediments and dominantly Mesozoic to Eocene Tethyan shelf sediments of external zone by the Panjal Thrust (PT) (Fig. 1.3). The Panjal Thrust equivalent to MCT, can be traced continuously south of the Nanga Parbat syntaxis and around the Hazara syntaxis (Greco et al., 1989; Thakur and Rawat, 1992; DiPietro and Pogue, 2004). However, further west, the MCT splits into three fault branches: the Oghi shear zone, the Mansehra Thrust and the Khairabad Thrust from north to south (Calkin et al., 1975; Coward et al., 1988; Searle et al., 1989; Pogue et al., 1999). Among them, the Khairabad Thrust is considered to be the main strand of the MCT west of the Hazara syntaxis, supported by the similar stratigraphic juxtaposition across the Panjal Thrust east of the Hazara syntaxis (see Yin, 2006).

Farther to the south, the MBT separates these rocks from the Tertiary foreland basin deposits (Fig. 2.1). The MFT (= Salt Range Thrust) delineates the southernmost extent of the foreland basin fold and thrust belt (Fig. 2.1).

The formation of KIA started in the Early Cretaceous times (144 to 99 Ma), and collided with the Eurasian Plate sometimes between 70 and 100 Ma (Coward et al., 1986). Since then, it acted as an Andean-type margin until India-Eurasia/Kohistan collision between 65 and 50 Ma (Powell and Conaghan, 1973; Maluski and Matte, 1984; Tonarini et al., 1993; Smith, H. A. et al., 1994; Chamberlain and Zeitler, 1996). Prior to final closure of the Neotethys, oceanic lithosphere was being subducted beneath the Eurasian active margin, exposed today in the Trans-Himalayan belt. Collision between the India and Eurasia along the ITSZ, and the subsequent formation of the Himalaya began circa 55 Ma (latest Paleocene) (LeFort, 1996; Rowley, 1996). In the west, at circa 55 Ma (Klootwijk et al., 1991), the KIA collided with the Indian crust along the MMT. Subsequent to collision, metamorphism of the subducting Indian crust took place, diachronous from west to east and an eclogite facies metamorphism occurred by 49 Ma (Pognante and Spencer, 1991; Tonarini et al., 1993). Two main phases of later metamorphism have also been recognized: phase 1 metamorphism (M_1) circa 40 Ma (but younging eastward) is barrovian metamorphism of the Greater Himalaya, the result of crustal thickening due to thrust stacking. The climax of phase 2 metamorphism (M_2) and production of leucogranite melts circa 20 Ma (also younging eastward) is associated with movement along the MCT and normal faulting at the base of the THZ along the STDZ (Staubli, 1989; Searle and Rex, 1989; Metcalfe, 1993). The MCT, active at 24-21 Ma, was responsible for bringing the GHC over the LHZ (Hubbard and Harrison, 1989; Harrison et al., 1995). A period of rapid cooling between 25 and 20 Ma is tentatively associated with tectonic denudation, as the overlying KIA slid northward on normal faults. From circa 20 Ma, faulting ceased and the KIA and Indian crust have only undergone simple uplift and erosion (Treloar et al., 1989b, 1991a; Pognante and Spencer, 1991; Chamberlain and Zeitler, 1996; Burg et al., 1996). The Nanga Parbat Haramosh Massif (NPHM) is an anomalous region of the Indian crust that has been undergoing to metamorphism of granulite grade and extremely rapid exhumation since at least 10 Ma (Treloar et al., 1989b; Zeitler, 1985; Zeitler et al., 1989, 1993).

Continued convergence of India with Eurasia resulted in southward propagation of the thrust belt. As a result, the MBT, which was active in Middle-Late Miocene ~ 10 Ma (Hodges et al., 1988; Meigs et al., 1995) or Pliocene time (DeCelles et al., 1998b), placed the LHZ over the Sub-Himalaya. Similarly, the active MFT lies to the south of the Sub-Himalaya, separates it from the Indian foreland basin (Indo-Gangetic plain) in the south (Powers et al., 1998). In the present day Himalaya, convergence is largely accommodated along the MFT (Molnar, 1984). On the other hand, the steady-state model suggests a gradual shift of the deformational front towards the foreland, and the MBT and MCT are considered to be contemporaneous features that are still active (Seeber et al., 1981). This view is supported by several geological and geomorphological evidences which indicate ongoing tectonic activity along the MCT (Seeber and Gornitz, 1983) as well as along the MBT (Valdiya, 1992; Nakata, 1989; Malik and Nakata, 2003).

2.3 The Eocene Sequence of the Kohat Plateau

The stratigraphic sequence of the Kohat Plateau can easily be categorized into the Pre-Paleocene stratigraphy (deposited on the passive, northern Indian continental margin), the Eocene stratigraphy (deposited in the remnant Tethys sea, isolated among

India, Asia and microplates located to the northwest of India), and the Miocene-Pleistocene stratigraphy (deposited in a terrestrial foreland basin) (Pivnik and Wells, 1996). In the Early Eocene, marine continental shelf and shallow sea conditions prevailed with extensive evaporates and restricted marine fauna, depositing muddy facies of Panoba Shales in the northwestern portion and the Shekhan Formation consisting of limestone, shale and dolomitized limestone in the northeast of the Kohat Basin. The Panoba Shale was most likely deposited in a small, restricted massive basin that had limited outlet to the closing Tethys Sea (Wells, 1984). The Panoba Shale is followed by the deposition of Shekhan Formation (on carbonate platform) in the northeast and Jatta Gypsum (on evaporitic plateau or sabkha) in the south and southeast. The overlying Kuldana/Mami Khel Formation records the southward propagation of the fluvial/deltaic system, followed by the deposition of the Kohat Formation (shallow water carbonate) (Pivnik and Sercombe, 1993). Then there is an unconformity between the carbonate shelf sediments and the overlying Oligocene (?)-Miocene synorogenic Rawalpindi and Siwalik groups (Pivnik and Sercombe, 1993). A brief account of the Eocene sequence of the Kohat Plateau is given below.

Panoba Shale: The "Panoba Shale" of Eames (1952) has type section in the south of Panoba village (Late. 33° 37´ N, Long. 71° 35´ E), and is comprised of calcareous, olive green, greenish-grey and yellowish-grey shale interbedded with finely laminated dark grey siltstone beds. The formation is 97 m thick at type locality, 160 m thick at Uch Bazar and 40 m thick at Tarkhobi (Kazmi and Abbasi, 2008). Lithofacies association of the formation is interpreted as an offshore environment of deposition (Tanoli et al., 1993). The formation conformably overlies the Patala Shale and is conformably overlain by the Shekhan Formation/ Bahadar Khel Salt/ Jatta Gypsum. Different foraminifera from the formation indicate an age of Early Eocene (Meissner et al., 1969).

Shekhan Formation: The Shekhan Formation (Fatmi, 1973) has a type section of 50 m thickness, exposed in the Shekhan Nala (Late. 33° 35´ N, Long. 71° 30´ E), where it is composed of yellowish-grey, medium- to thin-bedded, nodular, highly bioturbated limestone with interbedded shale partings. The formation is developed only in the northern and northeastern part of the Kohat Basin and passes laterally into evaporite sequence of the central part. The formation is 77 m thick in Panoba section (Tanoli et al., 1993) and 30 m at Mami Khel (Meissner et al., 1974), and has conformable lower and upper contacts with Panoba Shale and Kuldana Formation, respectively. Sedimentary facies and fauna record show an upward shallowing deposition on a relatively open carbonate shelf to mud flats and brine rich lagoon (Wells, 1984). Different fossils including large foraminifera, corals and echinoids indicate Early Eocene age for the formation.

Chashmai Formation/Gurguri Sandstone: The Gurguri Formation of Wells (1984) was named Chashmai Formation by Tanoli et al. (1993), is well exposed in northeast of Chashmai village (Late. 33° 60´ N, Long. 70° 47´ E). The formation coarsens upward and consists dominantly of clay in the basal part, sandstone interbedded with clay in the middle part, and sandstone and conglomerate in the upper part. Thickness of the sandstone beds increases up-section, but several of them pinch out laterally over short distances. The formation is 40 m thick at Lodikhel and 14 m thick near Gurguri village, and has conformable contacts with Panoba Shale at the base and with Kohat Formation at the top except Gurguri, where the upper contact with Kohat Formation is unconformable (Kazmi and Abbasi, 2008). The formation was deposited in nearshore environments including sand and cobble beaches, stream led deltas, mud flats, offshore bars and channels (Pivinik and Wells, 1996). Different fossils and stratigraphic position of the formation suggest an Early Eocene age.

Bahadar Khel Salt: The Bahadar Khel Salt (Meissner et al., 1974) exposure in the Bahadar Khel (Late. 33° 09´ N, 70° 59´ E), generally crops out in the south-central part of the Kohat Plateau at the Manzalai anticline and along the Karak-Hunki fault system as diapers overlain by the Jatta Gypsum (Pivnik and Wells, 1996). Thickness of the salt is not known in the type section as the base is not exposed.

The salt was most likely deposited in restricted small basin(s) that resulted from Early Eocene regression (Tanoli et al., 1993). Absence of the subaerial features in the salt and its current position in the south-central part of the Kohat Plateau indicate that the formation was deposited in the center of the basin, bordered by the sabkha flat (Jatta Gypsum) and carbonate shelf (Shekhan Limestone) in the northeast. The brine probably generated on sabkhas and lagoon to the northeast or in shallow water environments to the south, flowed to the center of the basin because of its density and precipitated when warm brine was cooled (Pivnik and Wells, 1996). An Early Eocene age has been assigned to the formation on the basis of its stratigraphic position.

Jatta Gypsum: The Jatta Gypsum (Late. 33° 18´ N, Long. 71° 17´ E) of Meissner et al. (1974) is mostly present in southern Kohat. The gypsum is light grey to greenish grey and white, massive to well bedded, and mostly pure and homogeneous (Pivnik and Wells, 1996). The gypsum is 70 m thick in Bahadar Khel, and 40 m thick at Mami Khel (Meissner et al., 1974, 1975). Shallow marine and fluvial facies are suggestive of intertidal to supratidal environments, but organic rich layers were deposited in oxygen-depleted conditions (Kazmi and Abbasi, 2008). The gypsum has conformable lower contact with Bahadar Khel Salt in the south, and conformable sharp upper contact with Kuldana Formation. An Early Eocene age has been assigned to the formation on the basis of its stratigraphic position.

Kuldana/Mami Khel Formation: The Kuldana Formation of Latif (1970) is also known as Mami Khel Formation (Meissner et al., 1974) having a type section near the village of Kuldana (Late. 33° 56´ N, Long. 73° 27´ E), north of Murree, but crops out in the eastern two-thirds of the Kohat Plateau, thickest in the center and thins in the east, west and south. The “lower Kuldana beds” comprised of about 95% uniform brick-red shale and 5 % channel sandstone, are fluviatile in origin, while the “upper Kuldana beds” consisting of purple clasts and marls are transitional marine in origin in Kohat Basin (Wells, 1983). The red clays of the terrestrial beds represent overbank floodplains while the sandstone beds resulted from single, small, shallowly incised streams switching due to avulsions (Kazmi and Abbasi, 2008).

The Kuldana formation is 100-150 m thick in Kohat and 110 m thick in Bahadar Khel. The formation has conformable lower contact with the Jatta Gypsum/Shekhan Formation and Chashmai Formation and upper contact with Kohat Formation in Kohat Basin. Late-Early Eocene to early Middle Eocene age is assigned to the formation on the basis of its stratigraphic position (Latif, 1970; Gingerich, 2003)

Kohat Formation: The Kohat Formation has a type section along Kohat-Khushalgarh Highway (Late. 33° 27´ N, Long. 71° 35´ E), and is 115 m thick at Shekhan Nala section, 37 m at Bahadar Khel, 111 m at Jozara, 81 m at Dalan-Thal and 70 m at Mardan Khel (Kazmi and Abbasi, 2008) The formation is thickest in the north-central part of the Kohat Plateau near Hangu (> 200 m thick) and pinches out in the south and west near Karak and Thal, respectively (Pivnik and Wells, 1996). Meissner et al. (1974, 1975) have divided the formation into three members. The lowermost member consists of interbedded thin foraminiferal limestone and yellow green shale. The middle member is foraminiferal grainstone while the upper member is a diagenetic, condensed, homogenized, porcelain-like limestone.

CHAPTER 3

The Neogene Molasse Sequence of the Himalayan Foreland Basin

3.1 Introduction

The terms flysch and molasse are old Swiss stratigraphic terms but they acquired a general meaning in early geosynclinal theory. Flysch refers to deep-water clastic sediments deposited under what were described as preorogenic or early-orogenic conditions. It commonly passes up, stratigraphically into molasse, a shallow-marine to nonmarine deposits formed under late-orogenic to postorogenic conditions (Hsu, 1970; Reading, 1972; Van Houten, 1973, 1981). Most flysch and molasse, including those in Switzerland, occur in what are now known to be remnant ocean basins and proforeland (peripheral) basins (Graham et al., 1975; Homewood and Caron, 1982; Homewood et al., 1986; Ingersoll et al., 1995). However, the sedimentary facies comprising flysch and molasse can occur in many tectonic settings, including some that are not orogenic in the original sense (Reading, 1972). Earlier part of this chapter briefly describes foreland basin in general, followed by a thorough discussion on the Neogene molasse sequence of the Himalayan Foreland Basin in rest of the chapter.

3.2 Foreland Basin

Foreland basins are large sedimentary basins that form upon continental crust alongside compressional plate mountain belts. Due to compression, the earth's crust shortens and thickens at the plate margin producing an elongate mountain belt. At the same time, an increase in crustal load upon the relatively thin and weaker crust of the adjacent continental interior forces the thinner crust to subside, forming a wide sedimentary basin which extends along the length of the mountain belt (Schwartz and DeCelles, 1988; DeCelles and Giles, 1996). The foreland basin receives lithic-rich sediment (i.e., sedimentary, metamorphic and igneous debris) that is eroded from the adjacent mountain belt. Because of this dynamic relationship, sedimentary layers within the basin reflect mountain-belt growth by means of their particle composition and physical features that indicate transport by ancient rivers into the basin.

There are two major types of foreland basin, differentiated on the basis of position relative to the orogenic belt:

A) ***Peripheral foreland basins*** form in collisional belts in response to flexural loading of the lithosphere by the adjacent thrust belt (Beaumont, 1981; Jordan, 1981). The term proforeland basin was suggested for foreland basins situated on the downgoing plate by Johnson, D. D. and Beaumont (1995). These basins generally result from arc-arc, arc-continent, or continent-continent collision (Dickinson, 1976). The traditional description of basin geometry is that of a 'wedge-shaped' basin that deepens towards the hinterland.

The evolution of the basin fill in terms of sedimentary environment, succession thickness and vertical trends, is strongly dependent on the degree of compressional tectonic activity (Munoz-Limenez and Casas-Sainz, 1997). Proforeland basins are typically occupied by longitudinal drainage systems. Drainage directions in tectonically partitioned foreland basins, however, may show local divergence from the over-all paleoslope direction (DeCelles, 1986). These basins are typified by the active Indo-Gangetic foreland basins south of the HFT and the inactive molasse basins of the Alps and Pyrenees (Leeder, 1999).

One of the unique characteristics of foreland basins is the style of syndepositional tectonism in most of them. Thrusts gradually step outward, resulting in widening of the fold-thrust belt (Dahlstrom, 1970). The structural style varies in detail, depending on pre-existing basement fabric, including the presence or absence of suitable surfaces of decollement, such as salt beds (for example, the Swiss Molasse Basin; Allen, P. A. et al., 1986). The faults propagate from below the basin, gradually cutting through and uplifting the sediments of the basin itself (Ori and Friend, 1984; Ori et al., 1986). Local intraformational and interformational unconformities are produced in areas proximal to the fold-thrust belt and within the foreland basin proper (Miall, 1977).

DeCelles and Giles (1996) noted that a foreland basin system is an elongate region of potential sediment accommodation. Within a foreland basin system four discrete depozones, comprising wedge top, fore-deep, fore-bulge and back bulge areas, may be recognized. As a result of the continuing evolution of the belt and the basin itself, these zones are not fixed in either space or time and the interaction between them can result in an extremely complex sediment distribution pattern within any foreland basin system. Both subsidence and uplift can cause significant local variations in sediment erosion and deposition, while the relative sense of thrust movement can have significant influence on sediment transport pathways. Most suture zones form by the consumption of an ocean between irregular continental margins that do not match in shape when they collide. The suturing process, therefore, is a diachronous one such that collision is progressive as the uplift and closure of the remnant ocean basin proceed. Sediment transport is both axial and normal to the fold thrust belt (Jordan, 1995).

B) ***Retro-arc foreland basins*** form on the continental side of the magmatic arc during the subduction of oceanic plates (Dickinson, 1976). The sedimentary record of retro-arc basins includes fluvial, deltaic, and marine strata as much as 5 km thick deposited in terrestrial lowlands and epicontinental seas along elongate pericratonic belts between continental margin arcs and cratons (Dickinson, 1974).

This type of sedimentary basin is retroforeland basin in Johnson, D. D. and Beaumont (1995) terminology. Retro-arc foreland basins should not be confused with proforeland or peripheral foreland basins, which are located on the downgoing plate adjacent to continental sutures but display similar structural and stratigraphic histories to retro-arc basins (Miall, 2000).

3.3 The Neogene Molasse Sequence of Western Himalayan Foreland Basin (Pakistan)

The Miocene-Pleistocene molasse sequence of the Kohat Plateau is a part of the Himalayan Foreland Basin (Fig. 3.1), and is composed of Rawalpindi and Siwalik groups. The Rawalpindi Group consists of the Murree and Kamlial formations, and the Siwalik Group consists of the Chinji, Nagri, Dhok Pathan and Soan formations (Table 3.1) (Meissner et al., 1974). All these formations are composed of sandstones, shales and conglomerates, deposited in a terrestrial foreland basin in response to Himalayan orogenic movements during the collision (Meissner et al., 1974; Powell, 1979; Tahirkheli et al., 1979; Johnson, N. M. et al., 1985).

3.3.1 Rawalpindi Group: The Rawalpindi Group is composed of the Murree and Kamlial formations of Miocene age in the Kohat Plateau, and is also widely distributed in the Potwar, Hazara and Kashmir areas. It generally thins out to the south and only Kamlial Formation of the group is present in the Salt and Surghar ranges. The group laterally correlates with the Gaj Formation of the Kirthar Range and Chitarwata Formation of the Sulaiman Basins (Table 3.1).

Sedimentary sequence of the group is composed of freshwater clastics of rhythmically alternating deep and shallow water environments, and consists of sandstones of dark red, purple and gray color alternating with purple and red shales (Fatmi, 1973).

This group represents the early detritus shed by the Himalayan orogenic belt and deposited in the Kohat-Potwar Foreland Basin as a coarsening upward sequence. These sediments are characterized by a succession of transient depocenter which migrated outward from the orogenic belt as the deformation rippled southward (Raynolds and Johnson, G. D., 1985).

Table. 3.1. The Neogene molasse stratigraphy from selected sections of the Himalayan Foreland Basin (Kazmi and Jan, 1997; Yin, 2006; Najman, 2006). Also see Table 9.1 for Eocene stratigraphy.

<table>
<tr><th>Geol Time</th><th>Kohat (in study area)</th><th>Potwar</th><th>Sulaiman</th><th>Kirthar</th><th>Kangra</th><th>Subathu</th></tr>
<tr><td>Late Pliocene</td><td></td><td>Soan Fm</td><td>Chaudhwan Fm</td><td>Soan Fm</td><td rowspan="4">Siwalik Group</td><td rowspan="4">Siwalik Group</td></tr>
<tr><td>Middle Pliocene</td><td>Dhok Pathan Fm</td><td>Dhok Pathan Fm</td><td rowspan="2">Litra Fm</td><td rowspan="2">Dhok Pathan Fm</td></tr>
<tr><td>Early Pliocene</td><td>Nagri Fm</td><td>Nagri Fm</td></tr>
<tr><td>Late Miocene</td><td>Chinji Fm</td><td>Chinji Fm</td><td>Vihowa Fm</td><td>Nagri Fm</td></tr>
<tr><td>Middle Miocene</td><td>Kamlial Fm</td><td>Kamlial Fm</td><td rowspan="2">Chitarwata/ Gaj Fm</td><td rowspan="2">Gaj Fm</td><td rowspan="2">Dharamsala Fm</td><td>Kasauli Fm</td></tr>
<tr><td>Early Miocene</td><td>Unconformity</td><td>Murree Fm</td><td>Dagshai Fm</td></tr>
</table>

According to Abbasi (1991, 1998), the paleoriver system of the Rawalpindi Group was a medium to high sinuosity as reflected by the abundance of trough cross-bedding and low angle plane bedding facies with a stream depth ranging from 6 to 8 meters. High proportions of intraformational conglomerates are due to reworking of overbank fines by major channels, while absence of extrabasinal conglomerate is probably because the site of deposition was toward the distal part of the foreland basin, where streams could not transport large clasts in sufficient amount.

The Neogene terrestrial sediments (Chitarwata Formation in case of Sulaiman Range) (Table 3.1, Fig. 1.1) disconformably overlie the marine Eocene strata in the

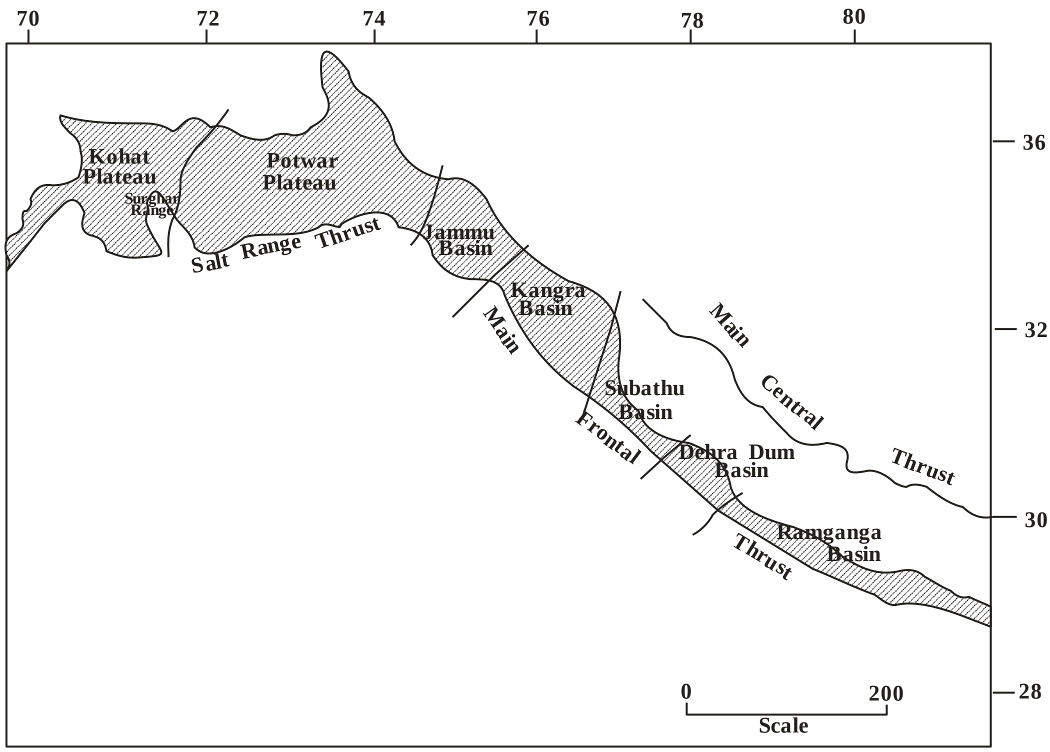

Fig. 3.1 General and simplified map showing sub-basins of the Himalayan Foreland Basin.

Middle Indus Basin, as they do elsewhere in the western Himalayan foredeep. But the duration of the hiatus in the Sulaiman Range, however, is much less, spanning only about 14 Ma, as opposed to around 20-25 Ma in the Potwar Plateau. Apparently the Eocene marine sedimentation continued in the Middle Indus Basin as the Tethys seaway was being squeezed out from the east (the area now forming the Western Himalaya) due to continued underthrusting of the Indo-Pakistan Plate beneath the Eurasian Plate. The Chitarwata Formation of the Sulaiman Basin ranges in age from 22.3-18.6 Ma (Early Miocene) (Friedman et al., 1992), from 22-17.4 Ma (Lindsay, E. H. and Downs, 2000) and Oligocene at its base and earliest Miocene at the contact with the Vihowa Formation (Lindsay, E. H. et al., 2005) in the Zinda Pir Dome. According to this age assessment, the Chitarwata Formation temporally overlaps with the Murree Formation in the northwest regions of the Potwar Plateau (Abbasi and Friend, 1989; Najman et al., 2003a), the uppermost Shaigalu member of the Khojak Formation in the Katawaz Basin (Qayyum et al., 2001) and the Kasauli Formation in the Indian Himalayan Foreland Basin (Najman and Garzanti, 2000).

The variations in lithofacies associations through time reflect the changing depositional regime in the region. The Chitarwata Formation is interpreted as a terrestrial near-shore deposit giving way upwards to low energy meandering river deposits of the Vihowa Formation (Waheed and Wells, 1990; Downing et al., 1993). The river system changed to more sandy braided rivers during deposition of Litra Formation and eventually shallower pebbly to cobbly braided rivers during deposition of the upper Chaudhwan Formation (Waheed and Wells, 1990).

In the Sulaiman Range, the facies association of Chitarwata Formation has been interpreted as fluvial (Waheed and Wells, 1990), deltaic (Welcomme et al., 2001) and tidal flat/tidal channel (Downing et al., 1993). The overlying fluvial Vihowa Formation is correlated with the Kamlial Formation, possibly slightly older on the basis of mammalian fauna, followed by Siwalik-like fluvial facies that persist to present day (Friedman et al., 1992).

Paleocurrent measurements of the Chitarwata Formation at Dalana indicate a predominant southeastward mean resultant direction for the planar cross-bedding (Downing et al., 1993) (Table 3.2). Southeastward drainage is also supported by trough cross-bedding and planar cross-bedding data from the lowermost major sandstone units of the Vihowa Formation (Downing et al., 1993).

Table 3.2. Eocene-Miocene post-collisional paleocurrent trends in the Himalayan Foreland Basin (Lindsay, E. H. et al., 2005).

Formation	Location	Age	Dominant Paleocurrent Trends	Drainage Interpretation	Source
Kamlial Formation	Potwar Plateau	Middle Miocene	SE, E	Fluvial system indicating regional flow Flow from alluvial fans equivocal to regional flow	Johnson N. M. et al., 1985 Willis, 1993a, b
Upper units of the Choksti Formation (Indian Molasse)	Indian Himalaya	Oligocene-Early Miocene	SW	May represent the initiated Indus River with source from the Karakoram or Lhasa blocks (=Indian Plate)	Clift et al. 2001b
Chitarwata and Vihowa Formations	Zinda Pir Dome (Dalana)	Early Miocene (Oligocene?-Early Miocene)	SE	Coastal shelf system draining the Katawaz block highlands supplanted by the Indus river drainage	Lindsay et al., 2005
Chitarwata, Vihowa, Litra and Chaudhwan Formations	Zinda Pir Dome (Raki Nala and Chaudwan Zam)	Oligocene-Pliocene	SE, SW	Sequence of meandering river deposits to larger braided rivers to conglomerates, with drainage from W foothills and NW highland	Waheed and Wells, 1990
Khojak Formation	Katawaz Basin	Eocene-Early Miocene	SW	Delta-Fan complex which drained the Indus River system longitudinally into the Katawaz remnant ocean	Qayyum et al., 1996, 2001
Gurguri Sandstone	Kohat Basin	Early Eocene	SE	Nearshore environments with a NW source	Wells,1984; Pivnik and Wells, 1996
Ghazij Formation	Balochistan	Early Eocene	SE	From areas to the NW where uplift near initial zone of continent-continent contact and compression	Clyde et al., 2003
Ghazij Formation	Zinda Pir Dome (Raki Nala and Chaudwan Zam)	Early Eocene	SE	Post-collisional shelf slope reversal	Waheed and Wells, 1990

In the Potwar Plateau, the fluvial system of the Middle Miocene Kamlial Formation was dominated by southeastward and eastward-directed paleodrainage associated with a large river system (Johnson, N. M. et al., 1985) or alluvial fans (Willis, 1993b) and is considered to represent the first stratigraphic evidence of the Indus River diversion to its current position at about 18 Ma (Najman et al., 2003a).

Murree Formation: The “Mari Group” of Wynne (1874), “Murree Beds” of Feistmantel (1880) and “Murree Series” of Pilgrim (1910) have been formalized as the Murree Formation after the hill station of Murree (Late. 33° 54′ N, Long. 73° 27′ E). This formation is dominantly composed of sandstone and siltstone while shale beds occur at places. The sandstone is dark brownish-gray, greenish-gray and in places purple, medium- to coarse-grained or conglomeratic, while the shale is purple or reddish brown (Fatmi, 1973; Meissner et al., 1974). The formation is nicely exposed in most parts of the Himalayan fold belt (Bossart and Ottigar, 1989) and Shakardara (Abbasi, 1994) but missing from the Salt and Surghar range front (e.g., Gee, 1981a, 1982b, 1982c). The formation is time transgressive, dated to be Early Eocene in the Hazara-Kashmir syntaxis (Bossart and Ottigar, 1989), but is believed to be Late Oligocene-Early Miocene in the Kohat-Potwar area (Pinfold, 1918; Pascoe, 1963; Latif, 1970; Fatmi, 1973).

Pilgrim (1910) and Pinfold (1918) concluded that the Murrees were entirely continental deposits. Wadia (1926, 1931) and the subsequent workers (Rashid, M. A., 1965: Latif, 1970: Fatmi, 1973: Meissner et al., 1974) also accepted the continental origin for these Oligocene to Middle Miocene rocks in the Kohat-Potwar Plateau. On the other hand, the Murree Formation equivalent Balakot Formation in the Hazara-Kashmir Syntaxis is of shallow marine origin (tidal flat deposits), though the base shows channel-fill deposits. Subaerial exposures of the interchannel and supratidal areas are indicated by the presence of pedogenic carbonates and gypsiferous horizons (Bossart and Ottiger, 1989).

Pilgrim (1919) and Wadia (1931) believed that the predominant red and purple colors are because of high iron content and concluded that Murrees were sourced from the iron bearing Precambrian Purana Formation occurring south of the Murree deposits on the Indian shield. But Bossart and Ottiger (1989) found chrome-spinel grains in Balakot Formation in the Hazara-Kashmir syntaxis suggesting an ophiolitic rocks provenance and detrital zircon crystals of euhedral shape suggesting a relatively short distance of transport. Furthermore, they suggested two possible sources for the Murree Formation, a southern one of the Kirana Hills, also supported by Gansser (1964) and a northern one of the nearby Trans-Himalayas, supported by Karunkaran and Rao (1979), and Raiverman et al. (1983).

Bossart and Ottiger (1989) noted the presence of sandstone channel facies, thinly interbedded sandstones and mudstones, with fining up cycles, ripple marks, caliche, flaser bedding and marine marl bands, and interpreted a tidal facies depositional environment for the Balakot Formation red bed sediments. But keeping the fossiliferous marl bands as a separate formation to that of the red bed succession, the remaining evidences are ample that favor fluvial depositional environment for Balakot Formation (Najman et al., 2002). For example, the Balakot Formation red bed succession shows fining up sequences, often beginning with thick-bedded, medium-grained sandstones which are quite commonly erosively based and/or channel lagged, with rare groove and flute marks and cross-beds. Overlying these sandstones, thinner-bedded and finer-grained sandstones are often found. Thick mudstones at the top of the cycle can be interbedded with thin or medium-bedded siltstones and sandstones. Caliche is also present. Sedimentary structures present in the sandstones include grading, asymmetrical ripple marks, flasers, climbing ripples, convolute bedding and parallel laminations. Interlaminations of mudstone and sandstone on a fine scale are also present (Najman et al., 2002). Furthermore, Murree Formation in the southernmost outcrops of the Kohat-Potwar region is of fluviatile origin (Bossart and Ottigar, 1989).

The Murree Formation in the Potwar area (Fig. 3.1) is a monotoneous sequence of dark red to maroon and purple siltstone and clay, gray to greenish gray, fine- to medium-grained sandstone and subordinate intraformational conglomerate. The sandstone-siltstone ratio is almost equal in the type section but siltstone is dominant to the south and west. The intraformational conglomerate is best developed in the basal part of the formation near Fatehjang and has been designated as "Fatehjang member" by Shah (1977).

In the Kohat area (Fig. 3.1), the Murree Formation is comprised of gray and purple sandstone interbedded with bright red and maroon clays and siltstone with subordinate intraformational conglomerates. Lower contact of the formation with Eocene marine sequence represents a major unconformity while its upper contact with Kamlial Formation is conformable and transitional (Kazmi and Abbasi, 2008).

The formation in the Kohat-Potwar area (Fig. 3.1) was deposited by meandering streams with large flood plains, flowing along the orogenic front from west to east and laterally migrating from north to south (Stix, 1982; Abbasi, 1994). The dark red and maroon color of the siltstone represents a long period of aerial exposure of flood plain. The provenance of the formation is interpreted as the rising Himalayas, as the sediments include low-grade metamorphic lithics high quartz and epidote (Abbasi and Friend, 1989: Critelli and Garzanti, 1994).

Since the Kamlial Formation of Middle to Late Miocene age overlies the Murree Formation, its age is essentially Early to (early) Middle Miocene (Fatmi, 1973; Meissner et al., 1974) (Table 3.1). The presence of nummulites and assilines in Balakot Formation indicates a Late Paleocene to Middle Eocene age for these strata (Bossart and Ottiger, 1989). However, on the basis of ^{40}Ar/^{39}Ar dating of white detrital mica, Najman et al. (2000, 2001) suggested an age not older than 35 Ma. They further stated that the fossiliferous limestone beds are tectonically emplaced and that the lower contact of the formation with Patala Formation is not depositional. The deposition in the northeast started in Late Paleocene and in the southwest most probably in the Early Miocene (Bossart and Ottigar, 1989).

Kamlial Formation: The name “Kamlial Formation” proposed by Lewis (1937) and later accepted by Stratigraphic Committee of Pakistan (1964a), was used for the rocks exposed near Kamlial village (Late. 33° 15′ N, Long. 72° 50′ E) in the Attock district, previously named “Kamlial Stage” by Pinfold (1918). The formation is 580 meter thick around Shakardara area, 50 meter in Surghar Range, 90 meter at Kamlial, 650 meter at Soan gorge and 120-300 meter in western Kohat.

The Kamlial Formation is comprised of dark gray to greenish-gray sandstone (about 75%) exhibiting spheroidal weathering, interbedded with dark red to maroon color siltstone (about 20%) and subordinate intraformational conglomerates (about 5%). The sandstone is fine- to medium-grained, cross-bedded, channelized and intercalated with lenses of intraformational conglomerates or thin layers of clay flakes. The sandstone is multistoreyed defined either by fining or coarsening upward sequence or by the presence of channel lag deposits, whereas thickness of the individual storey rarely exceeds 4 meter (Abbasi, 1991). Overbank fines were either not deposited or had low preservation potential. The cross-sets data show a paleoflow direction to ESE (Stix, 1982; Abbasi, 1991).

Abbasi (1991) divided the Kamlial Formation into two major types in southeastern Kohat (Fig. 3.1) on the basis of sandstone body geometry, namely; (i) the major channel type sand bodies, the dominant ones, and (ii) the floodplain type tabular sand bodies interbedded with siltstone. The major sandstone bodies are composed of greenish-gray, medium-grained, fining or coarsening upward multistoreyed sandstone as marked by the presence of a number of erosional surfaces commonly indicated by thin lag deposits with dominant paleocurrent directions to the east. The individual storeys are either trough cross-bedded or plane-bedded or the both; usually trough cross-bedding is overlain by the plane bedding. Individual cross-sets bounded by the erosional surfaces at top and bottom, reach upto 3 m in size, were deposited by the migration of large dunes or megaripples. Plane beds probably indicate deposition by plane bedded simple bars (Allen, 1982), whereas thick sandstone deposits and vertical stacking of the sandstone bodies is probably due to low subsidence rates in the basin coupled with a dominant sand supply from source area into the foreland basin (Allen, 1978; Kraus and Middleton, 1987). Interbedded siltstone beds in the sandstone sequences pinch out laterally within short distances, possibly because of low preservation potential or were eroded by the major channels. On the other hand the siltstone sequences in the lower part are commonly brownish-gray to brown in color and contains subordinate sandstone beds of brownish gray color, medium-grained, and brown intraformational conglomerates. The sandstone bodies have sharp contacts with siltstone. The sandstone bodies were deposited by a local high sinuosity or large-scale crevasse splays or by a mixed load local stream activity flowing at right angle to the main river flow direction.

In summary, the sediments of the Kamlial Formation were deposited by well-channelized high sinuosity to low sinuosity streams active on a major floodplain. Multistoreyed sandstone sequences with individual storeys in the order of 4-6 meter thick, were deposited probably by 6-10 meter deep streams (Abbasi, 1991, 1998). High proportions of intraformational conglomerates are due to reworking of overbank fines and calcrete by major channels. The major river system was flowing to the ESE in Kohat (Kazmi and Abbasi, 2008), whereas trough cross-bedding of the formation in the Potwar area shows a dominant flow direction to the east (Stix, 1982).

Chinji Formation conformably overlies the Kamlial Formation while lower contact with the Murree Formation is transitional but in Kohat Plateau it unconformably overlies the Kohat Formation. Age of the Kamlial Formation is Middle to Late Miocene (Fatmi, 1973; Meissner et al., 1974). The Kamlial Formation is assigned an age from 18.3 to 14.3 Ma on the basis of magnetic stratigraphic studies (Johnson, N. M. et al., 1982).

3.3.2 Siwalik Group: The Siwalik Group represents the Neogene basin sediments that extend from northern Pakistan across northern India, Nepal and into Burma with a length of more than 2000 km. Medlicott (1864) was the first who introduced the term Siwaliks for the fresh water deposits of Late Tertiary age from Siwalik Hills in Indian held Kashmir, later on extended by Wynne (1879) to similar rocks of the Potwar Plateau, North-West Frontier Province, Kashmir, Baluchistan and Sindh areas of Pakistan.

In Nepal, the Siwaliks are commonly known as the Churia Range, and are 5-6 km thick. The Himalayan Frontal Thrust (HFT) bound this to the south and the Main Boundary Thrust (MBT) to the north. The Siwaliks have been classified into three units as "Lower Siwalik", "Middle Siwalik", and “Upper Siwalik" in Nepal.

In Pakistan, the “Siwalik Series” of Oldham (1893) has been formalized as “Siwalik Group” by the Stratigraphic Committee of Pakistan (1964b). The group includes the Chinji, Nagri, Dhok Pathan and Soan formations (Table 3.1), dominantly comprising sediments of clastic origin of the molasse type (Fatmi, 1973). The various formations of the Siwalik Group are distinguished by gross sandstone percentages, with Chinji Formation less than 50 % sand, the Nagri Formation more than 50% and the Dhok Pathan Formation again less than 50% sand (Fatmi, 1973; Pilbeam et al., 1979).

Abid et al. (1983) described several sedimentary features and lithological characteristics from the Siwalik Group from Surghar Range. These include frequent occurrence of cross-bedding, ripple marks, logs of vertebrate fossils and wood, and association of pebble and cobble size fragments with sand size detritus. The presence of thin beds of conglomerate in sandstone and occurrence of thinly laminated black shale in the middle part of the sequence favor channel lag or braided stream deposition under swampy conditions. But, the huge thickness of Siwalik can only be explained if considered that quick deposition took place in a shallow, fast sinking basin with rapid erosion and short transportation from the source area.

The Siwalik Group sediments are time transgressive (Raynolds and Johnson, 1985) and exhibit remarkable lithological variations. Several million years mismatch in lithostratigraphy between the Potwar Plateau and other areas (Burbank, 1992) resulted in different nomenclature used for the Siwalik Group sediments in different areas. For example, it is divided into (in younging order) Vihowa Formation, Litra Formation and Chaudhwan Formation in Waziristan area and Sulaiman fold belt (Hemphill and Kidwai, 1973) (Table 3.1). Detailed stratigraphy of the Pakistani Siwaliks has been established through collaborative studies among University of Peshawar, Geological Survey of Pakistan, Darth Mouth College, Yale University, Lonont-Dohery Geological Observation and the University of Arizona (published in Paleo. Paleo. Plaeo., 1982, Special Issue, V. 37).

Chinji Formation: The terms “Chinji Zone” of Pilgrim (1913) and “Chinji Stage” of Pascoe (1963) for stratigraphic units consisting of interbedded sandstone, silty clay and siltstone were later on reformed as “Chinji Formation”. The type section is exposed near Chinji village (Late. 32° 41′ N, Long. 72° 22′ E).

The Chinji Formation is dominantly composed of interbedded bright red and brown orange siltstone and ash-gray sandstone, with siltstone: sandstone ratio of 4:1 in the type section that decreases northward. The interbedded in-channel and overbank siltstone sequences are 10-50 meter thick while major sand bodies are multistoreyed with individual storeys generally 5-10 meter thick that are complexly stacked both vertically and laterally (Behrensmeyer, 1987; Willis, 1993a, 1993b; Willis and Behrensmeyer, 1994).

In Potwar Plateau (Khaur area), the Chinji Formation is divided into three facies, namely, a) thick sandstone (5 meters to tens of meters thick), b) thin sandstone (decimeters to few meters thick) and c) laminated mudstone (decimeters to several meters thick) (Zaleha, 1997b).

a) Thick sandstone: The thick-bedded sandstones extend along strike for hundreds of meters to several kilometers, are gray to light brown and very fine- to fine-grained. These sandstones are composed of one to ten storeys (complete storey generally 5-33 m thick), the bases of which are delineated by an erosion surface with/out overlying intraformational conglomerate (cut bank material). Other sedimentary structures include trough cross-stratification, finer-grained planar stratification (whose thickness decreases with decreasing grain size), current ripple cross-lamination, wave ripple cross-lamination (tops of thick sandstone), gutter casts, load casts and tool marks (Zaleha, 1997a).

These thick sandstones seem to be river-channel deposits, with individual large-scale inclined strata representing channel-bar deposits of a single flood. Connected storeys are formed either by lateral migration and superposition of different bars within the same channel belt or superposition of different channel belts. The trough cross-stratification and planar stratification are formed by deposition associated with migrating sinuous-crested and straight-crested dunes, respectively. Current and wave ripple cross-lamination record deposition by migrating current ripples in relatively slow moving water and wind action on ponded water on some bar tops and/or within some abandoned channel belts, respectively. Fining upward sequences represent decreasing flow velocities associated with waning flood stages. Bankfull channel depths were generally $\leq$ 15 m and widths of channel segments (single channel) were 320-710 m (Zaleha, 1997a).

b) Thin sandstones: Thin sandstones extend laterally upto hundreds of meters, and are generally gray to light brown, typically very fine- to fine-grained (medium-grained locally). These sandstones are trough and planar cross-stratified, and wave ripple and current ripple cross-laminated, which represent deposition from channelized (crevasse channels) and non-channelized (levee and splay) floodplain deposits. Current ripple cross-lamination, trough cross-stratification and planar stratification were formed by deposition associated with migrating current ripples, dunes and upper stage plane beds, respectively. Each large-scale stratum of these sandstones is interpreted as the deposit of a single flood. Intraformational clasts locally occur associated with basal erosion surfaces in these sandstones (Zaleha, 1997a). Intraformational conglomerate lenses are composed of clasts, mainly calcareous nodules, manganese/iron nodules, and silt and clay fragments (Badgley, 1986). Burrows and root traces are common with varying degree of bioturbation in these sandstones. Desiccation cracks indicate subaerial exposure (Zaleha, 1997a).

c) Laminated mudstone: The laminated mudstones are composed typically of clay and fine silt which are red, brown, green and gray in color. Desiccation cracks are common in the upper part that indicate periods of subaerial exposures. Sedimentary structures include planar lamination (indicating settling of suspended sediments from slow moving or stagnant water) and wave ripple lamination (suggesting deposition under oscillatory flow of ponded water) (Zaleha, 1997a). At places, secondary structures such as disrupted bedding, slikensides, nodules, root and burrow casts etc. have largely destroyed primary sedimentary structures. Nodules are of variable composition, dominantly calcareous, spheroidal in shape and 2-10 mm (but upto 0.1 m across) in size (Behrensmeyer and Tauxe, 1982; Badgley, 1986). This sequence is interpreted as floodplain (mostly flood basin) and lacustrine deposits (Zaleha, 1997a).

Thick overbank fines of the Chinji Formation contain well-developed paleosol horizons and thin sheet type sandstone bodies of crevasse splay origin. Paleosols are generally 1-3 meter thick, laterally continuous for tens of kilometers, characteristically underlain by leached carbonate concretions, which reflect substantially long periods of aerial exposures of overbank fines during sedimentation hiatuses. These paleosols are good marker horizons for lateral correlation in such sedimentary sequences (Willis and Behrensmeyer, 1994, 1995).

The multistoreyed channel type sandstone-bodies of the Chinji Formation in southeastern Kohat area (Fig. 3.1) are about 10 m thick and extend laterally for many kilometers. They are gray in color, medium-grained and contain lenses of intraformational conglomerates. There is a simple lithofacies association of plane bedding, low angle plane bedding and trough cross-bedding sandstone, but relationship among these lithofacies is complex and does not follow any trend. Trough cross-beds across the formation suggest a consistent flow direction to the SSE (Abbasi, 1998).

Azizullah and Khan (1998) have observed two types of sandstone bodies in Chinji Formation at Takhti Nasrati-Shanawah section, Shinghar-Surghar Range (Fig. 3.1). These are, A) the multistoreyed major sandstone bodies; at least 3 meter thick and the individual storey is 3-5 meter thick, and B) the overbank fines; consist of intercalated sandstone and mudstone, mainly present in the lower part of the formation. The various types of sedimentary structures suggest that the sandstone bodies were deposited by paleochannels dominated by sand with subordinate gravels while the overbank fines are flood sediments that were deposited by a meandering river system.

The ages of Kamlial-Chinji and Chinji-Nagri boundaries (Table 3.1) are interpreted as 14.3 Ma and 10.8 Ma, respectively (Johnson, N. M. et al., 1985) while to the west in the Surghar Range, the base and top of the Chinji Formation are believed to be 11.8 Ma and 8 Ma old, respectively (Khan, M. J. and Opdyke, 1993). On the basis of different fauna, the age of the formation is considered to be Late Miocene (Sarmatian) (Fatmi, 1973).

Nagri Formation: The “Nagri Zone” of Pilgrim (1913) formalized as “Nagri Formation” by Lewis (1937), and the Stratigraphic Committee of Pakistan accepted the same for the middle part of the Siwalik Group. The type section of the formation is the village of Dhok Sethi Nagri (Late. 32° 45′ N, Long. 72° 14′ E).

In the central and eastern Potwar Plateau (Fig. 3.1), the formation consists of tens of meters thick multistoreyed sandstone bodies which are normal to paleoflow and extend laterally for kilometers. The individual storeys represent deposits of single flood. The sandstone bodies are medium-grained, trough and planer cross-bedded, low angle cross bedded and are interpreted as deposits of sinuous, braided channels that migrated laterally across the alluvial plain. The interbedded overbank fines comprising red-brown-yellow claystone to coarse siltstone constitute about one-fifth of the formation and are interpreted as flood plain deposits. The disruption of strata by desiccation cracks, roots and burrows indicates some degree of pedogenesis (Khan, I. A. et al., 1997). The formation was deposited by channels 15-30 m deep and typically 200-400 m wide (Burbank and Beck, 1991).

The Nagri Formation in Potwar Plateau (Khaur area) is composed of three lithofacies. a) thick sandstone (> 5 m thick), b) thin sandstone (< 5 m thick) and c) laminated mudstone (decimeters to several meters thick) (Zaleha, 1997b).

a) Thick sandstone: The multistory (single storey generally 5-33 m thick) thick-bedded sandstones of the Nagri Formation extend along strike for hundreds of meters to several kilometers. The sandstone is gray to light brown and medium-grained, in which bases of individual storeys are delineated by erosion surfaces with/out overlying intraformational conglomerate (cut bank material) (Zaleha, 1997a). Sets of the large-scale inclined strata (storeys) are meters to tens of meters thick (Khan, I. A. et al., 1997). Sedimentary structures in this sandstone include trough cross-stratification, finer-grained planar stratification (whose thickness decreases with decreasing grain size), current ripple cross-lamination, wave ripple cross-lamination (tops of thick sandstone), gutter casts, load casts and tool marks (Zaleha, 1997a).

This sandstone is interpreted as deposits of sinuous, braided channel and the stacking pattern represents the movement of channels within single or multiple channel belts (Khan, I. A. et al., 1997). The individual storey represents channel-bar deposits of a single flood. The trough cross-stratification and planar stratification are formed by deposition associated with migrating sinuous-crested and straight-crested dunes, respectively. Planar stratification formed under conditions of relatively higher flow velocities associated with upper stage plane beds. Current and wave ripple cross-lamination record deposition by migrating current ripples in relatively slow moving water and wind action on ponded water on some bar tops and/or within some abandoned channel belts, respectively. Fining upward sequences represent decreasing flow velocities associated with waning flood stages. Single channel bankfull depths and widths were generally 33 m and 320-1050 m, respectively (Zaleha, 1997a).

b) Thin sandstones: The gray to light brown, typically very fine- to fine-grained (medium-grained locally) thin sandstones facies of the Nagri Formation extend laterally for hundreds of meters. These sandstones represent deposition from channelized (crevasse channels) and non-channelized (levee and splay) floodplain deposits, and each large-scale stratum is interpreted as the deposit of a single flood. Current ripple cross-lamination, trough cross-stratification and planar stratification were formed by deposition associated with migrating current ripples, dunes and upper stage plane beds, respectively. Intraformational clasts locally occur associated with basal erosion surfaces in these sandstones. Burrows and root traces are common with varying degree of bioturbation in these sandstones. Desiccation cracks indicate subaerial exposure (Zaleha, 1997a).

c) Laminated mudstone: The laminated mudstones are composed typically of clay and fine silt which are red, brown, green and gray in color. Sedimentary structures like planar lamination and wave ripple lamination indicate deposition of sediments from slow moving/ stagnant water and oscillatory flow of ponded water, respectively (Zaleha, 1997a). At places, secondary structures such as disrupted bedding, slikensides, nodules, root and burrow casts etc. have largely destroyed primary sedimentary structures (Zaleha, 1997a). Desiccation cracks, common in the upper part, indicate periods of subaerial exposures. Nodules are of variable composition, dominantly calcareous, spheroidal in shape and 2-10 mm (but upto 0.1 m across) in size (Behrensmeyer and Tauxe, 1982; Badgley, 1986). This sequence is interpreted mostly as floodplain (Zaleha, 1997a).

In the eastern Potwar, Khan, I. A. et al. (1997) interpreted the mudstone-sandstone strata of Nagri Formation as overbank deposits, mainly composed of mudstone with relatively thin sandstone bodies and distinct paleosol horizons. The mudstones represent mainly floodbasin and lacustrine deposits while thin sandstone bodies represent crevasse splays, levees and floodplain channels (individual channel rivers typically 5 m deep and 100 m wide). The floodplain channels had limited lateral migration possibly because of low power/short life span/limited erodibility of muddy banks protected by vegetation and/or soil concretion. Current ripples represent relatively low flow velocities on shallow areas of the bars and channel fills. Non-calcareous upper horizons of paleosols were resulted from non-precipitation or leaching of carbonates (Khan, I. A. et al., 1997).

The tens of meters thick alternation of thick sandstones and mud dominated strata of the Nagri Formation suggest small-scale variations, whereas one hundred to a few hundreds meters, and formation-scale changes over one km thickness indicate medium-scale and large-scale variations, respectively. These variations were associated with autucyclic and/or mountain-front tectonism (e.g., faulting and earthquakes). The Chinji-Nagri transition records the diversion or establishment of a larger river system attributed to an increase and spatially variable mountain belt uplift rates in the hinterland areas or drastic change in climate (Zaleha, 1997b). However, the nature of the paleosols (Quade et al., 1989; 1992; Cerling et al., 1993; Willis, 1993b), plant material (Sahni and Mitra, 1980) and climate modeling (Ruddiman and Kutzbach, 1989; Ruddiman et al., 1989; Raymo and Ruddiman, 1992; Kutzbach et al., 1993) suggest warm, humid, sub-tropical to tropical and monsoonal climate for the Siwalik Group.

The Nagri Formation in Takhti Nasrati-Shanawah section and Shinghar-Surghar Range (Fig. 3.1) is composed of immature, poorly to moderately sorted, mainly medium-grained, thick massive sandstone constituting different storeys that are stacked both vertically and laterally. Pebbles (upto 1 cm in diameter) of different lithologies like quartzite, limestone, gneiss, granite, andesite, dacite, tonalite, amphibolite, cherts and graywakes are also occasionally present. The formation was deposited by paleochannels of a braided river system dominated by sand and subordinate gravels (Azizullah and Khan, 1998).

In Shakardara area of Kohat Plateau, the 1800 m thick Shakardara Formation (Miocene), equivalent to the Nagri Formation in the other parts of the Kohat-Potwar Plateau is composed of sandstone and siltstone with a ratio 1:1 in the lower part (600 m thick), dominantly sandstone in the middle part (800 m thick), and sandstone and conglomerate in the upper part (400 m thick). The sand bodies are mainly medium-grained and their contacts with the intraformational conglomerate or fine-grained overbank sediments are sharp (Abbasi, 1994, 1998).

The major sand bodies of the Shakardara Formation are 10-15 m thick with a lateral extent of a few hundreds meters indicating their extensive multistoreyed and multilateral nature. The internal geometry of the sandstone bodies is fairly complex, which includes macroform, bar complexes, channel-fill, minor channel scours on bar surfaces, local shale lenses and thin lag deposits. They internally consist of plane-bedding, low angle plane-bedding, and trough cross-bedding with several meters of thick cosets. The well preserved bar macroforms defined on the basis of their internal lithofacies bounding surfaces, are dominantly of mid-channel origin indicating upper flow regime plane-bed conditions, which are common in rivers that undergo high seasonal discharge (Abbasi, 1994, 1998). The internal setting of the bars probably suggests deposition by intermediate to high flow in 10-15 meters deep braided channels with a dominant paleoflow direction to the SSW, which is fairly similar to the present day Indus River system (Abbasi, 1994, 1998). The clasts composition of pebble and gravel beds is also similar to that of the Indus River system (Abbasi and Friend, 2000). High proportion of coarse-grained facies and increased sediment accumulation rates (Johnson, N. M. et al., 1985) correspond to accelerated basin subsidence in response to high uplift rates along MMT at that time (Zeitler, 1985). High subsidence rate and abundant sediment supply resulted in large-scale vertical and lateral sand body amalgamation (Abbasi, 1994, 1998).

The Nagri Formation is time transgressive between various section within the Potwar Plateau and ranges from about 11.4 Ma to 10.8 Ma age (Johnson, N. M. et al., 1985). Zircons from the locally present bentonized air fall tuff have yielded a fission track date of 9.5±0.5 Ma (Johnson, G. D. et al., 1982). The formation is interpreted to have been deposited during 8-2.7 Ma in the Surghar Range (Khan and Opdyke, 1993). The Nagri Formation is assigned an age from 10.8 to 8.5 Ma on the basis of magnetic stratigraphic studies (Johnson, N. M. et al., 1982). An Early Pliocene (Pohtian) age has been suggested on the basis of fossils reported from the Nagri Formation (Fatmi, 1973).

Dhok Pathan Formation: The “Dhok Pathan Stage” of Pilgrim (1913) was referred to as the “Dhok Pathan Formation” by Lewis (1937), and finally the Stratigraphic Committee of Pakistan accepted the same name. Dhok Pathan village (Late. 33° 07′ N, Long. 72° 14′ E) in the Attock district is the type section of the formation.

The formation is comprised of deep orange to red color siltstone and gray sandstone with occasional bands of conglomerate. It is differentiated from the underlying Nagri Formation on the basis of higher content of overbank fines. Behrensmeyer and Tauxe (1982) have identified two types of sandstone units within the formation from Khaur area (Potwar) (Fig. 3.1), a blue gray sandstone system laterally persistent on regional scale, and a buff sandstone system that typically contains many ribbon-type sandstone bodies whose average thickness is 10 meter but of limited lateral extent. The difference in color is due to texture and mineralogy. The blue gray sandstones are clean, spar cemented and contain fragments of schists, biotite and hornblende. The buff sandstone system has silty matrix and abundant weathered rock fragments. The blue gray sandstone system has a maximum channel belt width at least 25 km and was deposited by a very large river system, probably the ancestral Indus while the buff system has a channel belt width of 1-3 km and was deposited by smaller tributary rivers. The overbank fines constitute about 75% of the buff system and consist of silt and clay with intercalations of sandstone. Bedding units identified on the basis of colors, are mostly 1-2 meter thick but some are 8 meters thick. Paleosol horizons are common in the fine-grained facies and mostly formed under drier conditions (Barry et al., 2002).

Zaleha (1997b) categorized Dhok Pathan Formation in the Potwar Plateau (Khaur area) into a) thick sandstone (generally > 5 m thick), b) thin sandstone (generally decimeters to few meters thick) and c) laminated mudstone (generally decimeters to several meters thick).

a) Thick sandstone: The thick sandstone, gray to light brown, very fine- to fine-grained, commonly contains fining upward large-scale inclined strata (deposits of single floods), that extend along strike for hundreds of meters to several kilometers. Sets of the large-scale inclined strata (storeys) are meters to tens of meters thick. This sandstone is interpreted as deposits of sinuous, braided channel and the stacking pattern represents the movement of channels within single or multiple channel belts. The medium scale trough cross-strata, planar strata, small-scale cross-strata, fining upward sequence and bioturbation are associated with dunes, upper-stage plane beds, ripples, decrease in flow velocity and post flood organic activity, respectively (Zaleha, 1997a; Khan, I. A. et al., 1997).

b) Thin sandstones: Thin sandstone units of the Dhok Pathan Formation, generally gray to light brown, typically very fine- to fine-grained (medium-grained locally) extend laterally upto hundreds of meters. Intraformational clasts locally occur associated with basal erosion surfaces in these sandstones. These sandstones represent deposition from channelized (crevasse channels) and non-channelized (levee and splay) floodplain deposits, and each large-scale stratum is interpreted as the deposit of a single flood. Current ripple cross-lamination, trough cross-stratification and planar stratification were formed by deposition associated with migrating current ripples, dunes and upper stage plane beds, respectively. Burrows and root traces are common with varying degree of bioturbation in these sandstones. Desiccation cracks indicate subaerial exposure (Zaleha, 1997a).

c) Laminated mudstone: The laminated mudstones are composed typically of clay and fine silt which are red, brown, green and gray in color. Sedimentary structures include planar lamination (indicating settling of suspended sediments from slow moving or stagnant water) and wave ripple lamination (suggesting deposition under oscillatory flow of ponded water) (Zaleha, 1997a). At places, secondary structures such as disrupted bedding, slikensides, nodules, root and burrow casts etc. have largely destroyed primary sedimentary structures. Nodules are of variable composition, dominantly calcareous, spheroidal in shape and 2-10 mm (but upto 0.1 m across) in size (Behrensmeyer and Tauxe, 1982; Badgley, 1986). Desiccation cracks are common in the upper part that indicate periods of subaerial exposures. This sequence is interpreted as floodplain (mostly flood basin) and lacustrine deposits (Zaleha, 1997a).

The interbedded mudstone-sandstone strata of the Dhok Pathan Formation from eastern Potwar indicate overbank deposition. Thick mudstone bodies represent floodbasin and lacustrine deposition while thin sandstone bodies represent crevasse splays, levees and floodplain channels. The thin sandstone bodies suggest single channel rivers typically five meters deep and 100 m wide with limited lateral migration possibly because of low power/short life span/limited erodibility of muddy banks protected by vegetation and/or soil concretion. Current ripples represent relatively low flow velocities on shallow areas of the bars and channel fills (Khan, I. A. et al., 1997).

Generally tens of meters thick alternation of thick sandstones and mud dominated strata were resulted from small-scale variations, whereas one hundred to a few hundreds meters, and formation-scale changes over one km thickness resulted from medium-scale and large-scale variations, respectively. These variations were associated with autucyclic and/or mountain-front tectonism (e.g., faulting and earthquakes). The Nagri-Dhok Pathan transition records the establishment of a smaller river system directly related to changes in hinterland mountain belt (Zaleha, 1997b), as the nature of the paleosols (Quade et al., 1989; 1992; Cerling et al., 1993;

Willis, 1993b), plant material (Sahni and Mitra, 1980) and climate modeling (Ruddiman and Kutzbach, 1989; Ruddiman et al., 1989; Raymo and Raddiman, 1992; Kutzbach et al., 1993) indicate warm, humid, sub-tropical to tropical and monsoonal climate for the Siwalik Group.

The formation becomes coarse-grained in the Kohat Plateau (Fig. 3.1) and is composed of an alternation of sandstone and clay with lenses and layers of extrabasinal conglomerates. In some areas, the base of Dhok Pathan Formation is entirely composed of igneous and metamorphic cobbles bedded conformably over the underlying Nagri Formation. Sandstone of the formation is light gray or white, coarse-grained and soft, while the clay is light reddish brown or gray in color (Fatmi, 1973; Meissner et al., 1974).

The Dhok Pathan Formation in the Puki Gudikhel area of district Karak is dominantly composed of alternating sandstone and shale with many pebbly beds, indicating fluvial system of laterally migrating streams. Sandstone units resulted from lateral accretion as point bar deposits while mudstones resulted from the overbank flooding. A few clasts thick gravel beds show channel lag deposits. The sandstone is fine- to medium-grained, moderately sorted and the presence of gravelly layers marks cyclic deposition, where the depth of the basin did not exceed than the thickness of the two consecutive gravelly layers (Abbasi et al., 1983).

In Takhti Nasrati-Shanawah section and Shinghar-Surghar Range (Fig. 3.1), the Dhok Pathan Formation shows an excellent cyclic deposition of shales and fine- to medium-grained multistoreyed sandstone. The formation was deposited by paleochannels of a braided river system dominated by sand and subordinate gravels. The presence of boulders in the upper part of Dhok Pathan Formation is the result of some extreme flash flooding or Pleistocene glaciation (Azizullah and Khan, 1998).

Different fossils suggest a Middle Pliocene age for the formation (Fatmi, 1973). However, magnetic stratigraphic studies indicate the age of 8.5-5.5 Ma for the Dhok Pathan Formation (Johnson, N. M. et al., 1982).

Soan Formation: The term “Soan Formation” after the Soan River was introduced by Kravtochenko (1964) for the formation composed of alternations of compact, massive, coarse-grained conglomerate and vari-colored, soft, dirty claystone, siltstone and sandstone. Kravtochenko (1964) carried out the detailed lithological studies in the type locality and the adjoining areas (Late. 32° 22′ N, Long. 72° 47′ E).

The formation is comprised of friable, brown sandstone that is interbedded with pale brown clays and conglomerates. Composition of the sandstone and conglomerate changes over short distances as material was contributed from locally uplifted areas through tributary systems which were displacing the trunk river system in most part of the foreland basin. This is due to the fact that the deposition of the formation coincides with southward migrating deformation, uplifting not only the range fronts but had also migrated within the foreland basin itself (Burbank and Raynolds, 1984, 1988; Burbank et al., 1996).

Cotter (1933) proposed the provenance of a peculiar graphic pink color granitic gravel bed found near Bahun and Dhok Talian, to be derived from the Talchir Boulder Beds (Tobra Formation) in the Salt Range. Burbank and Beck (1989) dated the conglomerate interval to be about 5 Ma suggesting initial uplift of the Salt Range, and that it was deposited by the streams flowing northeastward from the range front.

The Soan Formation in the Takhti Nasrati-Shanawah section and Shinghar-Surghar Range consists of massive conglomerates, sandstone and siltstone/mudstone. The conglomerates contain clasts of limestone, quartzite, andesite, rhyolite, granite, chert, glauconitic sandstone, greywacke and amphibolite. A few boulders of granite, andesite and sandstone upto 1.5 meters across have also been recorded. The formation was deposited by pebbly braided river system and the presence of boulders in the formation shows some extreme flash flooding or Pleistocene glaciation (Azizullah and Khan, 1998). An Early Pleistocene age has been assigned to the formation on the basis of different fossils reported (Fatmi, 1973).

3.4 Siwaliks in Sulaiman Range and Waziristan Area (Pakistan)

The Vihowa Formation of the Sulaiman Range (Table 3.1, Fig. 1.1), equivalent to the Lower Siwalik is composed of about 700 m of gray sandstone and reddish brown mudstone with a few thin conglomerate interbeds. Sandstone and mudstone often form fining-upward couplets where the lower contact is erosional and lined with clasts of the underlying mottled and reddish brown claystone (Raza et al., 2002). On the basis of abundant proximal deposits and distal floodplain deposits, and the fining-upward sequences with common lateral accretion surfaces, Waheed and

Wells (1990) interpreted a clayey to sandy meandering river system for the Vihowa Formation. Downing et al. (1993) had placed the lower contact of the Vihowa Formation at the base of a thick, poorly sorted, light olive gray sandstone overlying the red siltstone of the Chitarwata Formation. The upper contact of the Vihova Formation with the Litra Formation is marked by a thick pebbly sandstone unit with large subangular to rounded pebbles of brown mottled claystone (Raza et al., 2002).

The transition from the Vihowa to Litra formations (Table 3.1) marks a change in topographic expression accompanied by a sudden increase in thickness and lateral continuity of the sandstone units and an influx of common conglomerate interbeds at circa 11 Ma (Raza et al., 2002), about the same time when the similar sandstone-rich Nagri lithofacies develops in the Potwar Plateau (Johnson, N. M. et al., 1985). The Litra Formation is substantially coarser-grained than the underlying Vihowa Formations and perhaps indicates a change in the depositional regime. The Litra Formation is about 1700 m thick multistoreyed gray sandstone unit with subordinate reddish brown siltstone and conglomerate interbeds. Substantially thicker, vertically stacked and laterally extensive individual gray sandstone unit forms a fining-upward sequence with thinner dull red to brown siltstone on top. Varicolored, mottled, highly bioturbated paleosol horizons form distinct and laterally extensive units within the siltstone or at the transition of sandstone to siltstone facies. The upper contact of the Litra Formation with the Chaudhwan Formation (Table 3.1) is gradational, usually placed when the conglomerates frequently occur as massive to crudely bedded units, 1-3 m thick (Raza et al., 2002).

The Chaudhwan Formation, about 1500 m thick, consists of thick massive to stratified conglomerate and pebbly gray sandstone with subordinate medium- to fine-grained friable gray sandstone and grayish-brown siltstone. The facies associations of both the Litra and Chaudhwan formations suggest a braided river system with an increasingly coarse bedload during the deposition of the Chaudhwan Formation (Waheed and Wells, 1990). The more easterly paleoflows in the Zinda Pir region (particularly in the upper Chaudhwan Formation) is attributed to local tectonics, such as movement of the Domanda Fault (Hemphill and Kidwai, 1973; Waheed and Wells, 1990).

The Late Cenozoic molasse in Sulaiman Range (Fig. 1.1) has been divided into lower, middle and upper parts in the Rakhi Nala, and lower and upper parts in Chaudhwan Zam gorge (Waheed and Wells, 1990). The basal beds sandstone in both the sections have mostly been homogenized and overprinted by root/burrow mottles, nodules, casts and breakage of the beds into vertical columns. The lower units of both sections show classical meandering features such as channels with epsilon cross-bedding. The channel sands typically show strong upward fining and classic point bar cross-bedding with abundant overbank clay and many intraformational clay clasts presumably formed by bank collapse. The middle part in Rakhi Nala comprises multistorey, both fining and coarsening upward minisequences with few floodplain clays. This part indicates in-channel braiding with overbank deposition which is more typical of meandering rivers. The upper parts in both the sections are principally conglomeratic with distinctive clasts of Cretaceous to Eocene strata suggesting that the Sulaiman Range was uplifted very recently. The upper part was deposited in stony plains and even stonier braided channels (Waheed and Wells, 1990).

Fluvial system in the entire region of the Sulaiman Basin was well established by deposition of the Vihowa Formation (circa 17 Ma). The anomalously high sedimentation rate in the Kohat ‘Siwaliks’ suggests that being proximal to the mountain front, the Paleo-Indus deposited more sediments in that region and also that the Kohat area was subsiding at a faster rate than the Sulaiman Basin (Khan, M. J. et al., 1988; Khan, M. J. and Opdyke, 1993) (Fig. 1.1). There was also an increasing input of sediments from the nearby westerly hill ranges brought by relatively smaller tributaries in the Middle Indus Basin, as evidenced by dispersion of paleocurrents in the upper Litra and Chaudhwan formations (Waheed and Wells, 1990) (Table 3.2). The enormous thickness of the ‘Siwalik’ deposits in this region and the lack of any obvious lithological discontinuities suggest that any depositional hiatuses were minor (Raza et al., 2002).

Siwalik in the Waziristan are also represented by the Vihowa, Litra and Chaudhwan formations. The Vihowa Formation is predominantly composed of red to maroon sandy and silty claystone, with subordinate greenish-gray, subangular, medium- to coarse-grained, thick-bedded and commonly cross-bedded sandstone. The Litra Formation mainly consists of light gray, friable sandstone with some red to reddish-brown clay beds. Moderate angularity and sorting along with high content of feldspar evince the textural immaturity of these sandstones. The upper Chaudhwan Formation comprises calcite-cemented petromict orthoconglomerate that contains granule-, pebble-, cobble-, and boulder-sized phenoclasts. Upto 90% of the phenoclasts are of limestone (mostly Paleocene-Eocene), sandstone (some of the Pab Sandstone), quartzite, chert, along with some intrabasinal pebble-sized rip-up clasts of mudstone (Khan, M. J. and Ahmad, 1991). The sediments of the upper Litra Formation were predominantly derived from the northern provenance. The sporadic occurrence of Paleocene-Eocene Limestone, and Pab Sandstone bearing conglomerates at various stratigraphic levels in the upper Litra Formation and Chaudhwan Formation indicates uplift along Fort Monro anticline. The fluvial system that deposited these sediments flowed towards SSE (Khan, M. J. and Ahmad, 1991).

Southern paleoflow directions in the Neogene Siwalik rocks of the Surghar-Shinghar and Trans-Indus Salt ranges (Abbasi and Friend, 1989; Khan, M. J. and Opdyke, 1993; Friend et al., 1999) to the Sulaiman Range (Raza et al., 2002) and different paleoflow directions in the Potwar Plateau indicate that different river systems were draining the basin at that time (Figs. 1.1, 3.1). The southwards flow in case of former is like the modern Indus River and southeast to east is more like the flow of the present-day Ganga and its tributaries (Khan, M. J. and Opdyke, 1993; Friend et al., 1999). The precursor of the Paleo-Indus River was also an east-west flowing axial fluvial system, which drained the newly risen Himalayas during the late Paleogene and deposited siliciclastic sediments in the Katawaz basin (Qayyum et al., 1996).

3.5 Indian Siwaliks

The Siwalik succession in India has been divided into three sub-groups: Lower, Middle and Upper Siwalik. In general, the Lower Siwalik subgroup is characterized by an alternation of sandstone and mudstone (mudstone >50%). The transition from the Lower to Middle Siwalik succession is reflected by a change in sandstone geometry (ribbon type to sheet type) and decrease of mudstone abundance. The switch from mudstone to sandstone-dominated succession occurred at about 11 Ma in the Potwar Plateau (Johnson, N. M. et al., 1985), 10 Ma in the Kangra subbasin (Kumar et al., 2003) and 9 Ma in Nepal (DeCelles et al., 1998a, 1998b).

3.5.1 The Kangra Sub-basin (Table 3.1, Fig. 3.1): Kumar et al. (2004) have identified five major lithofacies for the Middle and Upper Siwalik in the Kangra Sub-basin, namely, i) the disorganized conglomerate characterized by boulder to cobble-size clasts, poorly stratified and ungraded to poorly graded (resulted from rapid deposition of hyperconcentrated flood flow), ii) the crudely stratified matrix supported conglomerates characterized by pebble to boulder-size imbricated clasts, fine to coarse sand matrix which fines upward (resulted from traction bed load with persistent stream flow), iii) the stratified matrix supported conglomerate characterized by pebble to boulder-size clasts and low angle cross-stratification (resulted from lateral accretion and slip face deposition on longitudinal bars), iv) the stratified sandstone which is pebbly in places and characterized by fine- to coarse-grained cross-stratified sandstone (resulted from 3-dimentional dune migration in active channel) and v) the massive mudstone characterized by parallel lamination and pedogenic features (overbank deposits). The conglomerate facies indicate a complex provenance from the hanging wall of the Main Boundary Thrust and Chail Thrust. These conglomerates were deposited between 10 to 7 Ma by confined braided streams with well-developed floodplains flowing in the axial part of the basin followed by an alluvial fan deposition from unconfined braided streams flowing toward SW direction.

3.5.2 The Dehra Dun Sub-basin: The Middle Siwalik succession (9-5.23 Ma) of the Dehra Dun subbasin (DSB) shows vertical facies variation from sandstone-mudstone (300-450 m thick) to sandstone (900-1200 m thick) and finally to sandstone-mudstone-conglomerate (100-250 m thick) facies (Kumar and Nanda, 1989; Kumar, 1993; Kumar and Ghosh, 1994). The grey sandstones are medium- to fine-grained multistoreyed units that exhibit sheet geometry. Individual storeys vary in thickness from 0.5 to more than 3 m and each is underlain by a major erosional surface, which extends laterally for hundreds of meters. Individual stories within the multistorey sandstone are recognized by the presence of intra- and extra-formational clasts along the base of each storey, differences in paleocurrent azimuths (in order of ±90°) and the orientation of erosional surface. Prominent internal structures are trough and planar cross-stratification (Kumar et al., 2003). Paleoflow data obtained from trough cross-stratification show high variability in space and time with mean paleoflow toward the south (Kumar and Nanda, 1989; Kumar, 1993; Kumar and Ghosh, 1994). The presence of sheet geometry, low mudstone content and frequent erosional surfaces in the Middle Siwalik succession of the DSB (9-5.23 Ma) suggest deposition by sheet floods in a braided channel environment (Kumar et al., 2003).

3.5.3 The Subathu Sub-basin (Table 3.1, Fig. 3.1): The Middle Siwalik succession (6-5.23 Ma) of Subathu Sub-basin (SSB) is composed of gray, thick-bedded (>40 m), multistorey sheet sandstone (>80%) with subordinate mudstone (<20%). The characteristic features of the sandstone are similar to the Middle Siwalik sandstone of DSB (Kumar et al., 2003), suggesting deposition by a braided river system (Rust and Jones, 1987; Bridge and Mackey, 1993) that flowed southeast like the present day Ganga River (Kumar et al., 1999).

The Upper Siwalik succession of the Subathu Sub-basin shows three facies assemblages and represents an upward coarsening succession. The two important facies associations in ascending order are (A) sandstone-mudstone, and (B) conglomerate-sandstone-mudstone (Kumar et al., 2003).

Facies association A is dominantly composed of grey sandstone, mudstone with subordinate buff sandstone. The mudstone facies are variegated, show extensive pedogenic modification and contain evidence of biogenic activity such as trace fossils and root casts (Kumar et al., 2003). This facies suggests deposition in floodplain environment by a low-sinuosity stream system (Kumar et al., 1999). The presence of local lateral-accretion surfaces within the major sheet bodies indicates rare high-sinuosity channels. The multistorey nature of the sheet bodies represents an episodic pattern of channel avulsion and reoccupation (Kumar and Tandon, 1985; Gordon and Bridge, 1987; Kumar, 1993). Extensive pedogenic modification of the mudstone facies and their lateral variability in maturation indicates that vertical accretion took place on a broad floodplain. The grey sheet sandstone with frequent erosional surfaces indicates a major transverse channel deposit flowing toward southwest (Kumar et al., 2003).

3.6 Fossils of the Molasse Sequence

During the Neogene, changes in climate, oceanic circulation and position of the continent have profoundly affected Earth's biota (Raup and Sepkoshi, 1984;

Stanley, 1984). The Murree Formation of Rawalpindi Group is poorly fossileferous except the Fatehjang member, well developed in the basal part of the formation near Fatehjang area. It has yielded plant remains, frogs and identifiable mammal remains. Different nummulites and assilines have been reported from the fossiliferous marly limestone and shales near Balakot area (Bossart and Ottigar, 1989). The overlying Kamlial Formation of this group contains the important mammal fossils including pelidae (Fatmi, 1973; Thakur, 1992), as well as gastropod, reptilia, chelonia, carnivora, proboscidea, perissodactyla and artiodactyla, which indicates Middle Miocene age for this formation (Pascoe, 1963).

Fluvial sedimentation of the Neogene Siwalik formations of Pakistan in the Chinji area of Potwar started at about 18.3 Ma and continued with only minor interruption until after 8 Ma (Johnson, N. M. et al., 1985). On the other hand, the early discoveries of numerous vertebrate fossils, including humanoid primates, particularly for the period between 13 Ma to about 1 Ma provided base for extensive biostratigraphic studies (Johnson, G. D. et al., 1983; Barry et al., 1985; Flynn et al., 1990; Badgley and Behrensmeyer, 1995; Barry et al., 2002). The fauna include the oldest bovids, thryonomyid, rhizomyid, advanced muroid rodents, small gibbinlike hominoid, tragulids and large giraffoid (Barry et al., 1985).

The prominent groups of Chinji fauna include crocodiles, turtles, lizards, aquatic birds, dinotheres, primitive trilophodonts, forest dwelling suidae, water deer, few hominoids and chelonian remains. Other important fossils of Chinji Formation are pongidae, hystricidae, hyaenodontidae, tayssuidae, cervidae and bovidae.

The Nagri Formation largely contains crocodilians, perrosodactyles, artiodactyls, carnivores, proboscideans, primates, lorisidae, pongidae and orycteropodidae (Pascoe, 1963; Thakur, 1992). Similarly, the Dhok Pathan Formation is highly fossiliferoue and mainly contains primates, carnivora, rodentia, perrosodactyles, artiodactyls and proboscideans (Pascoe, 1963), as well as cercopithecidae, canidae, ursidae, mustelidae, hyaenidae, felidae, trilophodontidae, suidae, tragulidae, giraffidae and bovidae (Thakur, 1992).

The Soan Formation is more fossiliferous in the buff system containing fossil remains of artiodactyla, aves, bovidae, canidae, cervidae, equidae, felidae, ranidae, suidae and uesidae (Jenkinson et al., 1989). A summary of the Middle Siwalik fauna is given by Barry et al. (2002) and is listed in Table 3.3.

Table 3.3. Stratigraphic range of the small mammal in the Siwalik Group (From Barry et al., 2002).

S. No	Mammal fauna	1st occurrence (Inferred 1st appearance) Ma	Last occurrence (Inferred last appearance) Ma
1	Hominoidea	12.5 (14.0)	8.5 (8.4)
2	Deinotheriidae	12.9 (14.0)	8.0 (7.9)
3	Listriodontinae	13.7 (14.0)	10.3 (10.3)
4	Tetraconodontinae	13.1 (14.0)	10.3 (10.3)
5	Suinae	11.3 (11.4)	3.3 (2.2)
6	Anthracotheriidae	13.6 (14.0)	3.3 (2.2)
7	Tragulidae	12.8 (14.0)	3.3 (2.2)
8	Sivatheriinae	13.6 (14.0)	7.1 (7.1)
9	Bovidae	11.3 (14.0)	7.0 (6.3)
10	Boselaphini	11.5 (14.0)	6.2 (2.2)
11	Antilopini	11.3 (14.0)	6.2 (2.2)
12	Hipparionini	10.7 (10.9)	5.5 (3.7)
13	Chalicotherini	12.9 (14.0)	8.0 (8.0)
14	Tupaiidae	13.0 (13.6)	8.1 (6.5)
15	Crocidurinae	12.7 (13.6)	6.4 (5.7)
16	Copemyinae	13.6 (13.6)	8.6 (8.2)
17	Tachyoryctinae	11.5 (13.6)	6.4 (5.7)
18	Rhizomyinae	9.6 (10.3)	8.0 (5.7)
19	Murinae	11.5 (13.6)	6.4 (5.7)
20	Gliridae	13.6 (13.6)	7.9 (7.3)
21	Ctenodactylidae	12.3 (13.6)	10 (9.4)

CHAPTER 4

The Indus River System

4.1 Introduction

It has been documented that big rivers are affected by major, continental-scale tectonic movements (Potter, 1978), and alluvial channel patterns are sensitive to active movements of individual geologic structure (Adams, J. 1980; Burnett and Schumm, 1983; Ouchi, 1985; Schumm, 1986). In case of the Indus River and other Himalayan drainage system, which are believed to have deposited the molasse sequence in the Himalayan Foreland Basin, their behavior is linked to the collisional tectonics of the Himalayan orogen; where the uplift terrains serve as headwaters (Tamburi, 1974) and the Indo-Gangetic as foredeep (Seeber and Armbruster, 1979). This chapter briefly reviews the origin of the Indus River, its behavior downstream to orogenic belt, followed by discussion covering its bedload modal composition.

4.2 Origin of the Indus River

The Himalaya is drained by 19 major rivers, of which the Indus and Brahmaputra are the largest (Fig. 2.1). The Indus system in the Western Himalaya includes the Jhelum, the Chenab, the Ravi, the Beas and the Sutlej (Fig. 4.1). The Jhelum rises in the vale of Kashmir; the Chenab is fed by the Chandra and Bhaga in the Lahaul valley (Himachal Pradesh, India), while the Ravi starts from the snowy peaks of Bara Bhangal in Chamba (Himachal Pradesh, India). The Beas and the Sutlej originate from a glacial lake near Rohtang in the Kulu valley (Himachal Pradesh, India) and Mansarowar in the Trans-Himalaya region, respectively (Thakur, 1992).

The Indus River appears to have formed shortly after India-Asia collision and its drainage is dominated by western Tibet, the Indus Suture Zone and Karakoram as well as significant influx from the Indian Plate (Clift, 2002). It has drainage of circa. 1 x 10^6 km^2 (Clift, 2002), an annual water discharge of 238 km^3 and an annual sediment discharge of 110 x 10^9 kg (Milliman and Meade, 1983) that result in one of the largest deep sea fans totaling circa. 5 x10^6 km^3 in the Arabian Sea (Naini and Kolla, 1982). The Indus River has 44% sand and 56% silt and clay at Attock while the suspended load in Jhelum and Chenab rivers constitute 28% sand and 72% silt and clay each near Mithan Kot area (Attaullah, 1970).

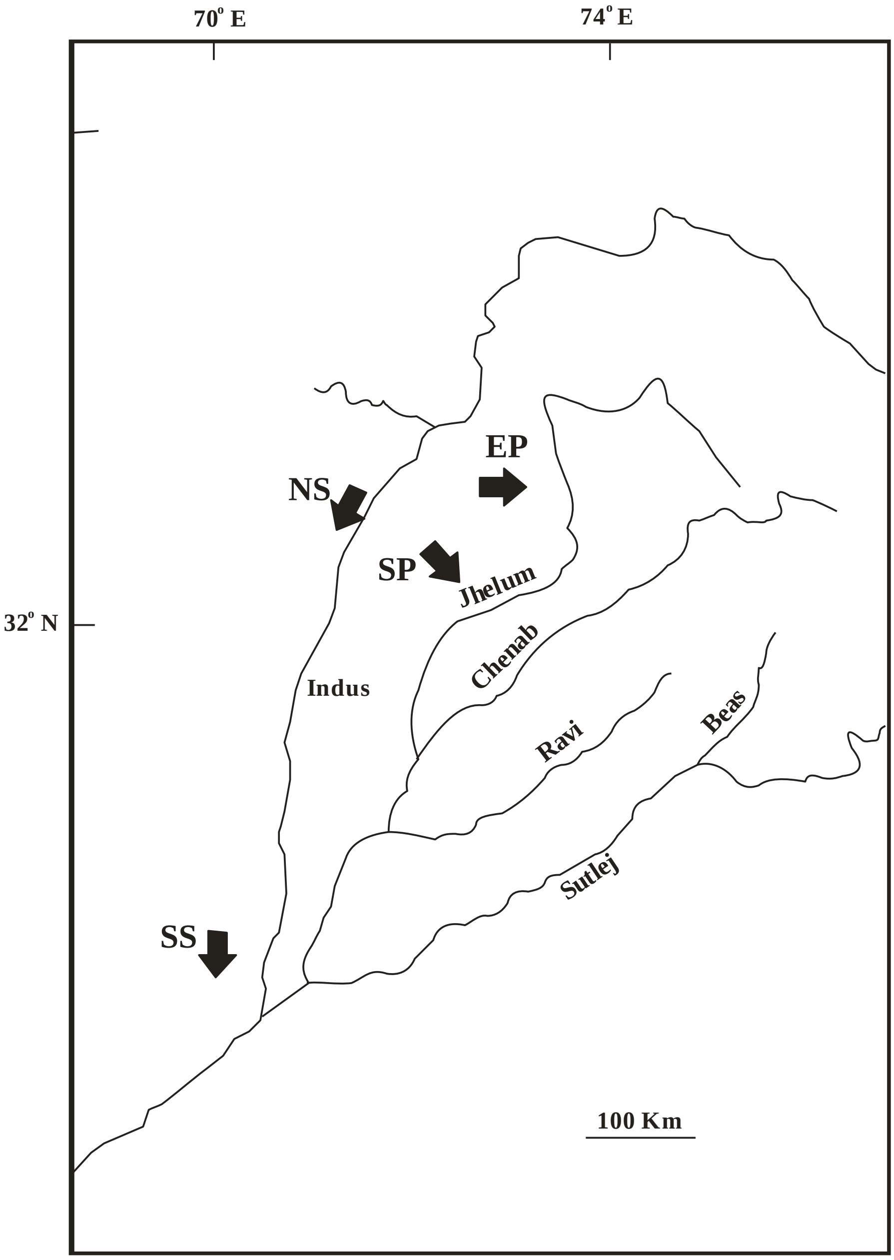

Fig. 4.1. Paleoflow directions of the Neogene fluvial system in different parts of northwestern Pakistan (Friend et al., 1999). NS = Northern Surgher, SS = Southern Sulaiman, EP = Eastern Potwar and SP = Southern Potwar. The figure also shows the present day Indus River system.

The Indus River enters the Indus-Tsangpo Suture Zone about 210 km north-west of its birth place i.e., Mount Kailas, western Tibet (Searle and Owen, 1999). The river follows the NW-SE trend of the Karakoram Fault before cutting westwards into the Indus Suture Zone (Shroder and Bishop, 1999; Searle and Owen, 1999) (Fig. 2.1). The northwest linear flow of the river through the Ladakh, parallel to the general structural trend of the region probably reflects the original Eurasian and Indian plate boundary (Shroder and Bishop, 1999). In Early Miocene time (~ 20 Ma), the marine delta of the ancestral Indus-like river was apparently some 500 km north of its present location, near Bugti (Kazmi, 1984). The same river deposited a thick sedimentary sequence (~ 1500 m) in Shakardara area at about ~ 15 Ma (Abbasi and Friend, 1989). Similarly, a large sandy river similar to the modern Indus existed from at least 13.5-11.5 Ma in this region (Beck and Burbank, 1990). However, major changes in the drainage directions are suggested due to enhanced subsidence of the Indo-Gangetic foredeep in the Late Miocene (~ 11 Ma). The molasse sediments of the Upper Siwalik Group (prior to ~ 5 Ma) suggest a major river, flowing east to north-east (Raynolds, 1981), which was probably diverted back to the south again at ~ 4.5 Ma, because of rising structures in the eastern Salt Range (Beck and Burbank, 1990). The river responded to the migration of the Himalayan foredeep to south at ~ 2 cm yr^{-1} and the coarsening upwards conglomerates advanced south ~ 3 cm yr^{-1} in response to outward displacement of the Pir Panjal orogenic front (Raynolds and Johnson, 1985). The other tributaries of the Indus i.e., the Chenab, Jhelum and Sutlej drain the reduced topography of the crystalline Greater Himalaya.

The Siwalik sedimentary rocks of the Miocene to Recent have different paleocurrent directions in exposures to the east (flow to the SE) and to the west (north to south) of the modern Indus River (Friend et al., 1999). Fig 4.1 shows model paleocurrent directions for four selected areas; Eastern Potwar (EP) (Khan, I. A. et al., 1997), Southern Potwar (SP) (Willis, 1993b), Northern Surghar (NS) (Bonis, 1985) and Southern Sulaiman (SS) (Baig, 1984), in which three sets of data (SS, NS, and EP) are synchronous (from about 8.5-5.5 Ma) while SP is for the period from about 15 Ma to about 8 Ma. Fig 4.1 clearly shows that the flow was generally to the south (parallel to present day Indus) and to the east (parallel to the tributaries of present day

Ganga) in areas west and east of the present day Indus, respectively (Friend et al., 1999).

4.3 Behavior of Indus River

The slope and sediment load control the nature of the river system braiding in the north and meandering in the south. Channel of the Indus River is multi-thread above Sukkur and single thread below Sukkur (Jorgensen et al., 1993). The multi-thread channel is clearly braided and characterized by large bars or islands (3-8 km long) and frequently shifting channels between Mithankot and Machka. The less frequent large bars or islands and more permanent channel between Unhar Head and Sukkur are described as anastomosing, consisting of a large main channel and smaller anastomosing flood channels. The single thread channel best described as meandering from Sukkur to the Arabian Sea. The channel is highly sinuous with large and mobile meanders between Sukkur and Kamal Dero, and is generally straighter between Kamal Dero and Sehwan. From Sehwan to Hala, the channel is comprised of strongly asymmetrical meanders (Jorgensen et al., 1993). The downstream change from braided to meandering pattern results partially from loss of water used for irrigation of the modern floodplains. Channel braiding in the upstream shows high sediment load, high valley slope, and high discharge. Flood depth increases downstream despite of continual water loss (Jorgensen et al., 1993).

Abbasi (1989) classified the channel pattern of the Indus River system in the Punjab Plain into multichannel low sinuosity in the northern reaches, intermediate in the middle reaches and single chain high sinuosity in the southern reaches. The multichannel low sinuosity channel pattern is dominated by first order channels commonly 5 km wide and second order channels 1-2 km wide and separated by macroforms or large complexes. These macroforms are up to 10 km long and 2 km wide, dissected at places by small third order channels. Major deposition in these reaches takes place by accretion along medial and bank attached bars, which finally results in macroforms.

The channel pattern in the middle reaches is transitional between braided and meandering, and composed of fairly sinuous multichannels separated by macrobars. The individual channels are upto 1 km wide while the maximum width of the river course is over 12 km at some places. The macroforms are up to 40 km long and 6 km wide, and dissected by smaller channels. Deposition in the middle reaches takes place by lateral accretion along the medial or tributary bars (Abbasi, 1989).

4.4 Composition of Indus Sands

4.4.1 Karakoram and Hindu Kush Tributaries: The Indus River receives abundant detritus from the Karakoram and Hindu Kush via three major right-bank tributaries. (i) Hushe sand, derived from granodioritic batholiths and Baltoro Granite is mainly plutoniclastic, (ii) Braldu and Hispar sands, largely derived from the South Karakoram are dominantly metamorphiclastic, (iii) Hunza and Kabul sands, derived from North Karakoram and Hindu Kush, respectively, consist of sedimentary to low grade metasedimentary grains. Heavy minerals of the Karakoram and Hindu Kush tributaries include abundant to dominant blue-green to subordinately green and brown hornblende, epidote, garnet, sphene and diopside (Garzanti et al., 2005).

4.4.2 Ladakh and Kohistan Tributaries: The Ladakh Batholith supplies arkosic detritus to the Indus River. Heavy mineral assemblages of the Ladakh Batholith include dominant blue-green and subordinately brown hornblende, epidote, hypersthene, clinopyroxene and trace glaucophane (Swat and Panjkora River sands) (Anczkiewicz et al., 2000). Metabasite detritus with abundant brown hornblende in Kandia River sand derive from the granulite-facies of Chilas Complex (Garzanti et al., 2005).

The Shyok and Gilgit rivers, which drain the Shyok Suture, and carry quartz, feldspars, sedimentary and metamorphic lithic grains (heavy minerals dominated by hornblende) from the Karakoram and Trans-Himalayan arcs (Garzanti et al., 2005).

4.4.3 Himalayan Tributaries: High-rank metamorphiclastic grains including blue-green to subordinately green and brown hornblende, garnet, staurolite, kyanite, sillimanite and epidote from the Greater Himalaya are carried by the Zanskar and Nandihar rivers. The Astor River carries high-rank quartzofeldspathic sands with dominant blue-green hornblende from the Nanga-Parbat Massif and Ladakh Arc (Garzanti et al., 2005).

According to Garzanti et al. (2005), the Soan River has its course through the Tertiary foreland-basin units across the Potwar Plateau, and thus dominantly carries polycyclic sands of recycled orogen. Heavy minerals in sand of Soan River are dominantly epidote, with subordinate amount of garnet and hornblende. The Himalayan tributaries of Punjab mainly transmit quartzolithic, sedimentary (carbonate, shale/sandstone) and metasedimentary grains. The Chenab and Sutlej sands are richer in feldspars and high-rank metamorphic grains; whereas the Jhelum and Ravi sands are richer in shale/slate sediments.

4.4.4 West Central Pakistan Tributaries: Rivers of west central Pakistan are characterized by abundant sedimentary and low-rank metasedimentary grains. The lithic grains mostly consist of limestone, shale/slate, sandstone/ metasandstone and chert. The Kurram River transmits K-feldspar and blue-green hornblende from the Spinghar, whereas the Tochi River sands mostly contain ultramafic, volcanic, metabasite and plagioclase grains, carried from the Waziristan Ophiolite. Rivers of southern Pakistan carry purely sedimentaclastic detritus (limestone grains in Bolan River sand and recycled quartz and feldspars in Sibi River sand) (Garzanti et al., 2005). Lithic signatures of these sands become homogenized across the plains, where quartz sharply increases, indicating recycled provenance from foreland-basin or alluvial sediments (Kurram, Gomal and Sangarh rivers) (Garzanti et al., 2005).

4.4.5 Trunk River: According to Garzanti et al. (2005), the Indus River sand in the Ladakh consists of carbonate and shale/slate grains sourced by the sedimentary to low-rank metasedimentary cover rocks, and quartz and feldspars from the Ladakh Arc, with heavy minerals mostly blue-green hornblende and epidote. The sands become enriched in quartz, K-feldspar, carbonate and high-rank metamorphic grains (from Greater Himalayas) downstream of the Zanskar confluence.

Indus sands in Baltistan (Hushe/Shyok River sands) are enriched in feldspars and blue-green hornblende from the Asian active margin. Here too, the metamorphiclastic detritus, including marble, hornblende and epidote is shed to it from the South Karakoram Belt (Braldu/Shigar River sands) (Garzanti et al., 2005). Further downstream, increases in dolostone and metabasite grains indicate supply from Karakoram and Kohistan sources. Blue-green hornblende prevails over epidote, and other heavy minerals of arc and amphibolite rocks (Karakoram and Himalayan units) (Garzanti et al., 2005).

The increase in the Q/F ratio, sedimentary (limestone, shale/sandstone, chert) and very low rank metasedimentary lithic grains across the Potwar Plateau suggest a dominant recycled orogen (Garzanti et al., 2005).

4.5 Indus Bedload and Sediment Erosion Rates

4.5.1. Indus sands upstream of Tarbela Dam: The active-margin units provide 81±2% of the Indus bed load (60±6% from Karakoram; 6±4% from the Ladakh Arc and South Tibet; 14±4% from the Kohistan Arc) entering Tarbela Lake, with the remaining 19±2% accounted by the Himalayan units (Nanga Parbat 13±3%, Tethys and Greater Himalaya 6±3%). Half of total pre-Tarbela flux is contributed by two Karakoram tributaries, the Braldu/Shigar (34±6%) and Hunza Rivers (17±5%) (Garzanti et al., 2005).

Heavy minerals concentration varies strongly in detritus derived from different geological units i.e., the Ladakh and Kohistan Arcs (supply 29±9%), the Karakoram-Hindu Kush (5±2%), Nanga Parbat (7±6%) and Himalayan units (5±3%). Heavy minerals in sands of the West Pakistan ranges are scarce (2±2%), except the Tochi River sand (21±3%), whereas Indus sands are rich in heavy minerals (11±7%) (Garzanti et al., 2005).

4.5.2. Sediment yields and erosion rates: Sediment flux entering Tarbela Lake (250±50x10^6 t/year) (Milliman et al., 1984; Rehman et al., 1997; Einsele and Hinderer, 1997; Tate and Farquharson, 2000) imply sediment yields of 6000±1800 t km^{-2} yr^{-1} for Karakoram (25,000 km^2), 130±100 t km^{-2} yr^{-1} for the Ladakh Arc and South Tibet (120,000 km^2), 1400±700 t km^{-2} yr^{-1} for the Kohistan Arc (25,000 km^2), 8100±3500 t km^{-2} yr^{-1} for the Nanga Parbat Massif (4000 km^2), and 600±400 t km^{-2} yr^{-1} for the Tethys and Greater Himalaya (25,000 km^2), and average erosion rates (assuming a mean rock density of 2.75 g cm^{-3} (Einsele and Hinderer, 1997)) are 2.2±0.7 mm yr^{-1} for Karakoram, 0.05±0.05 mm yr^{-1} for the Ladakh Arc and South Tibet, 0.5±0.2 mm yr^{-1} for the Kohistan Arc, 3.0±1.3 mm/year for the Nanga Parbat Massif, and 0.2±0.1 mm yr^{-1} for the Tethys and Greater Himalaya. The highest sediment yields and erosion rates are for the Braldu/Shigar (12,500±4700 t km^{-2} yr^{-1}; 4.5±1.7 mm yr^{-1}) and Hispar catchments (11,000±5000 t km^{-2} yr^{-1}; 4.0±1.8 mm yr^{-1}), both draining the South Karakoram Belt northeast and north of Nanga Parbat, and much lower values for the upper Hunza basin in the North Karakoram (2500±1600 t km^{-2} yr^{-1}; 0.9±0.6 mm yr^{-1}) (Garzanti et al., 2005).

This data is compatible with the lower end of denudation rates of the Nanga Parbat (3-4 mm yr^{-1}) (Whittington, 1996; Moore and England, 2000) and South Karakoram domes (5 mm yr^{-1}) (Rolland et al., 2001), and with the sediment yields for the Hunza (5000-8000 t km^{-2} yr^{-1}) (Ferguson, 1984) and Chitral/Konar rivers draining the Hindu Kush (1842 t km^{-2} yr^{-1}) (Rehman et al., 1997). The sediment yields indicate that erosion rates decrease exponentially eastward, northward and westward away from the sharp peak recorded in the syntaxis region (Garzanti et al., 2005).

Indus sands at the Salt Range front suggests extensive recycling of older Indus sediments (54±3%), with subordinate contributions from Kabul (33±2%), Soan (11±2%) and other tributaries draining the West Pakistan ranges (3±2%; Kurram, Tochi, Gomal, Sangarh Rivers) (Garzanti et al., 2005).

Table 4.1 shows sand composition of selected modern rivers and old fluvial deposits (from Critelli and Garzanti, 1994).

Table 4.1. Available data for modern river sands (Potter, 1978). Note that the Chulung La Formation and coeval Indus Group feldspathlithic sandstones (Garzanti and Van Haver, 1988) are much less quartzose and richer volcanic detritus than all other quartzolithic "recycled orogen" clastic wedges (Critelli and Garzanti, 1994). N = Number of samples, Q = Quartz, F = Feldspar, L = Lithics, Qm = Monocrystalline Quartz, P = Plagioclase, K = Alkali Feldspar, Qp = Polycrystalline Quartz, Lvm = meta-volcanic Lithics, Lsm = meta-sedimentary Lithics, Lm = metamorphic Lithic, Lv = volcanic Lithics and Ls = sedimentary Lithics.
The data is recalculated to 100% for use in triangles Q-F-L, Qm-P-K, Qp-Lvm-Lsm, Lm-Lv-Ls.

	N	Q	F	L	Qm	P	K	Qp	Lvm	Lsm	Lm	Lv	Ls
Indus	1	61	7	32	-	-	-	-	-	-	35	11	54
Ganges	1	74	10	16	-	-	-	-	-	-	64	0	36
Brahmaputra	2	51	26	24	-	-	-	-	-	-	40	27	33
Indus Fan	15	44	30	26	59	27	14	4	10	86	52	11	37
Bengal Fan	22	58	28	13	67	22	11	6	5	89	87	4	9
Siwaliks	29	57	7	36	88	12		11	0	89	29	0	71
Nias	24	73	11	16	86	9	5	17	23	60	35	29	36
Makran	62	56	10	34	83	12	5	9	36	55	31	37	32
Chulung La	18	24	26	50	44	55	1	5	93	2	2	96	2
Indus Group	26	24	34	41	41	45	14	8	68	25	13	70	17
Murree Group	28	68	5	26	92	8	1	21	27	52	39	28	33

CHAPTER 5

Lithofacies of the Neogene Molasse Sequence of Southwestern Kohat

5.1 Introduction

The lithological, structural and biological features of modern and ancient sedimentary deposits can be grouped into classes that collectively characterize particular sedimentary environments. These classes are known as facies. The vertical and lateral relationships of facies can further be summarized into facies associations that occur together and are considered to be environmentally or genetically related. The concept of facies associations is based on Walther's law, which states that facies occurring in a conformable vertical sequence represent laterally adjacent depositional environments.

The sedimentary sequences described in this chapter are strongly believed to be of fluvial origin (Kumar and Tandon, 1985; Behrensmeyer, 1987; Kumar and Nanda, 1989; Willis, 1993a, 1993b; Kumar and Ghosh, 1994; Abbasi, 1994, 1998; Willis and Behrensmeyer, 1995; Zaleha, 1997a; Kumar et al., 1999; Kumar et al., 2003; Kumar et al., 2004). Thus, the early sections of this chapter present an overview of the braided river system and its different facies. This overview is followed by detailed sedimentological work carried out for the present research in southwestern Kohat.

5.2 River Systems

In a sedimentary basin, rivers are generally transverse to major structures, and produce depositional plains that extend over lengths hardly exceeding a few hundred kilometers. On the other hand, longitudinal streams are much better developed and extend over thousands of kilometers (Cojan and Renard, 1999). The major controlling parameters of fluvial systems include the stream slope, the scale of the drainage network, the climate, tectonics, sedimentary load and vegetation (Biju-Duval, 2002). These parameters are divided into autocyclic and allocyclic (Beerbower, 1964). Autocyclic controls include variations in flow strength and flow direction in the alluvial environment, whereas allocyclic include major changes in base level, gradient, discharge and sediment load type directly related to external factors such as climate, tectonism and eustacy (Sutter, M. W. and Steidtmann, 1987). A river adjust its cross-sectional size (w-d i.e., width-depth), cross-sectional ratio (w/d), bed configuration, sediment grain size, planform shape (sinuosity) and size (meander wavelength), and channel bed slope in response to these independently imposed allocyclic factors (Leeder, 1999).

For example, the influx of coarse sediment through uplift in the source area changes a river character from meandering to braided, and in any siliciclastic sequence, it could be marked by a change in sediment composition and/or texture (Tucker, 2001). Previous works suggest that coarsening upwards alluvial mega sequences result from the reworking of proximal gravels during periods of decreased subsidence following tectonic activity (Allen, 1978; Blair and Bilodeau, 1988; Heller et al., 1988; Paola, 1988; Heller and Paola, 1989). Progradation of the gravel front is accompanied by increased incision in more proximal areas of the basin. Conversely, fining upwards mega sequences occur during periods of increased subsidence related to renewed tectonic activity, resulting in the restriction of coarse-grained detritus to the more proximal areas of the basin (Blair and Bilodeau, 1988; Heller et al., 1988).

The change in base level affects whether a river aggrades or erodes. If the fall is small, a channel can adjust by changing its pattern or shape; whereas, if the fall is large, incision is likely. Likewise, when a base level fall occurs slowly, the channel can adjust its slope by lateral migration, however, when the change is rapid, flow will be concentrated in a narrow deep valley and incision can migrate upstream (Yoxall, 1969). Table 5.1. presents characteristics of fluvial depositional systems according to grain size.

5.2.1 Braided Rivers: The fundamental processes that control whether a river has a braided or meandering pattern are not completely understood. But it is known that braiding is favored by rapid discharge fluctuations of a greater absolute magnitude than in meandering rivers. The average annual discharge of braided rivers is low, but a few times annually, enormous amounts of water pass along the course of the river during very short periods of time. Braided rivers also tend to have higher slopes, a heavy load of coarse sediment, and more easily erodible banks. In combination these features would suggest that braiding is more characteristic of the upstream reaches of a river, with meandering becoming more common downstreams the slope when the coarseness of load decreases. Braiding would also be more common in semi-arid or arid areas (Walker and Cant, 1984). Other factors that favor braiding include impermeable subsoil in the catchment area and along the course of the river and little vegetation (Doeglas, 1962). Of our interest are the sandy braided systems, which are discussed below in details.

Table 5.1. Summary of characteristics of fluvial depositional systems according to grain size (Orton and Reading, 1993; Emery and Myers, 1996).

	Gravel and sand	**Fine sand**	**Mud/silt**
Hinterland			
Catchment area	Intermediate (<10^5 km^2)	Intermediate (<10^6 km^2)	Large
Relief	Intermediate	Intermediate	Low
Climate	Temperate	Temperate	Humid, tropical
Alluvial form			
Size of stream	Intermediate	Intermediate	Large
Stream gradient	Intermediate (>0.5 km^{-1})	Intermediate (>0.5 km^{-1})	Low
Flow velocity	Intermediate	Intermediate	Low
Discharge	Intermediate (<10^3m^{3}s^{-1})	Intermediate (<10^3m^{3}s^{-1})	High
Discharge variability	Irregular to regular	Regular to irregular	Regular
Sediment load	Intermediate (< 10^7ton yr^{-1})	Intermediate (<10^8 ton yr^{-1})	High (< 10^{10} ton yr^{-1})
Load:discharge ratio	Intermediate	Intermediate	Low
Channel type	Bed-load	Mixed load	Suspended load
Channel pattern	Braided	Meandering/braided	Straight/meandering
Bank strength	Low to moderate	Low	High
Width : depth ratio	High to intermediate	High	Low
Channel mobility	High to intermediate	High	Low (fixed)

Sandy braided systems: Sedimentary sequences of braided fluvial systems generally show multistorey nature and weak to poor cyclicity both for grain size and structures. Sandy braided stream sequences start with channel lag deposits at the bottom, and change to cross-bedded sandy facies, overlain by finer-grained cross-bedded and cross-laminated bar-top deposits, mostly consisting of siltstones and mudstones (Sengupta, 1994).

According to Ashmore (1991), in sandy braided systems, braiding occur by four different processes: deposition and accumulation of central bars, chute cutoff of point bars, conversion of single transverse unit bars to mid-channel braid bars, and dissection of multiple bars. Experiments show that the chute cutoff mechanism was most common. However, the direct physical sedimentary cause of primary braiding is essentially the same in all the processes (i.e., local aggradation and loss of competence in a lateral flow expansion).

Channel characteristics and dynamics of braided rivers: Bristow (1987) identified three scales of channels within the braided river. The first order channel encompasses the whole river and has a variable number of second order channels within it. Each second order channel is itself a large alluvial stream termed an anabranch, and within the second order channels the flow divides and rejoins again to form third order sub-channels. Changes in third order channels occur rapidly and within a season, while changes occur annually in the second order channels.

Deposits of braided systems range from gravel to coarse and fine sand, at times with several grain size stacks and often with internal erosion figures (reactivation surfaces) (Table 5.2) (Biju-Duval, 2002). Horizontally bedded sands and fine gravels with a few intercalated scour-and-fill structures probably deposit from shallow upper flow regimes and are similar to sandy proximal braided stream deposits (Rust, 1978a). Thicknesses of horizontally bedded sand range from 1 to 4 m (McKee et al., 1967). Long axis of pebbles and grains will be perpendicular to the current direction (Doeglas, 1962). Table 5.3 presents characteristic features of channel belt and crevasse sandstone.

Table 5.2. Principal facies assemblages in sand-dominated braided river deposits (modified from Miall, 1977).

Facies assemblage	**Environmental setting**	**Main facies**
S. Saskatchewan type	Sandy braided rivers (cyclic deposits)	St
Platte type	Sandy braided rivers (virtually non cyclic)	St, Sp
Bijou type	Ephemeral or perennial rivers subject to flash floods	Sh, Sl

5.3 Facies of the Braided River System

The most common lithofacies of fluvial system are described below, whereas Table 5.4 lists lithofacies and sedimentary structures of braided river deposits.

5.3.1 Sandstone Facies: The sandstone facies of fluvial origin are classified into four types.

Table 5.3. Characteristic features of channel belt and crevasse sandstones (Ghosh, 1987).

Feature	Channel-belt	Crevasse
Frequency of occurrence	Less common	Abundant
External form	Tabular	Mostly symmetrical, concave-up base; top planar or convex
Thickness	Multistoreyed, as much as 15 m	Channel facies 5 m or less; splay lobe facies 3 to 4 m thick
Width-depth ratio	> 40	Between 5 and 20
Basal contact	Erosional scoured	Erosional scoured or planar
Channel lag deposit	Well developed; polymictic	Only scattered mud clasts
Grain size	Pebbly coarse to fine sand	Fine to very fine silty sand
Grain size trend	Sandstone fines upward	Sandstone do not fine upward; lateral fining observed in some beds
Texture	Better sorted	Poorly sorted and micaceous
Sedimentary structures	Large trough cross-strata at base and ripple lamination at top	Mostly medium-scale trough cross-strata and ripple lamination. Some flutes, load-and-grove casts at base
Bioturbation	Not common	Vertical traces very common
Nodules	Siderite and pyrite nodules in some beds	Calcareous nodules very common

i). Cross-bedded sandstones: These are the most abundant facies in fluvial channel sandstones that are the product of migrating three-dimensional dune. In some cases, they account for virtually all the channel sediments. Grain sizes range from coarse pebbly sandstones to fine sandstone (Collinson, 1996).

ii). Cross-laminated sandstones: These sandstones make up significant volumes of channel sandstones and usually occur towards the tops of the channel units, and are finer-grained, micaceous and carbonaceous than underlying sandstones. They reflect relatively low energy conditions (Collinson, 1996).

iii). Parallel-laminated sandstones: These sandstones are usually fine-grained with well defined horizontal lamination and parting lineation on bedding surfaces. They tend to be more common towards the top of the channel sandstone (Collinson, 1996).

iv). Massive structureless sandstones: These sandstones occur both as tabular beds and as more lenticular bodies within stratified sandstones (Collinson, 1996). Where tabular, they commonly occur towards the base of the channel sandbodies (McCabe, 1977) and are attributed to rapid deposition from suspension during floods (Collinson, 1996).

5.3.2 Conglomerates / Channel Conglomerates: Conglomerates are commonly only a few clasts thick that record winnowing by strong currents, either at erosion surfaces or, in some cases, on the tops of bars. Clasts may be of intraformational or extrabasinal origin. The intraformational clasts are more commonly associated with erosion surfaces related to channel migration, when overbank floodplain sediments have been eroded and reworked (Collinson, 1996).

Channel conglomerate deposits consist of interbedded sandstones and conglomerates. Such deposits commonly occur as stacked multistorey sheets with little or no preserved overbank fines, and reflect the lateral mobility of high-energy bedload streams (Collinson, 1996). Some channel conglomerate bodies fine upward into sandstones, suggesting either gradual diminution of flow through diversion or systematic lateral migration of a curved channel reach (Campbell and Hengry, 1987). Where channel conglomerates contain very thick sets of cross-bedding and are interbedded with thick units of overbank fines, flows were probably confined within cohesive banks (Massari, 1983).

5.3.3 Fine-grained Facies: These facies most commonly comprise mudstones, siltstones and fine-grained sandstones although coarser intraclasts occur in some sandstones (Collinson, 1996). The following subfacies are common in fine-grained sediments.

i). Mudstones and siltstones facies may be thin bedded and laminated or homogeneous. Such facies deposit from suspension either in extensive lakes on the floodplain or abandoned channels such as ox-bow lakes. Well-laminated examples are commonly rich in mica and/or organic matter if the sediment is unoxidized (Collinson, 1996).

Color of this facies ranges from black through gray, green, brown and red. Red color suggests good drainage and oxidizing conditions in early diagenetic regime, while grey beds and the preservation of organic matter record water-logged conditions and reducing porewater (Collinson, 1996). Gray massive siltstone are the result either of rapid deposition by flood or of homogenization by bioturbation. Such facies were mainly laid down on floodplains submerged only during floods (Collinson, 1996).

ii). Sharp-based sandstone beds are commonly interbedded with mudstone or siltstones. They are usually thin, less than 20 cm thick and seldom over 2 m.

Examples over 2 m are more likely to be products of ephemeral streams (Collinson, 1996).

Table 5.4. Lithofacies and sedimentary structures of modern and ancient braided stream deposits (modified from Miall, 1977, 1996).

Facies Code	Facies	Sedimentary structures	Interpretation
Gmm	Matrix-supported gravel	Weak grading	Plastic debris flow (high-strength, viscous)
Gmg	Matrix-supported gravel	Inverse to normal grading	Pseudoplastic debris flow (low strength, viscous)
Gh	Clast-supported, crudely bedded gravel	Horizontal bedding, imbrication	Longitudinal bedforms, lag deposits, sieve deposits
Gt	Gravel, stratified	Trough crossbeds	Minor channel fills
Gp	Gravel, stratified	Planar crossbeds	Transverse bedforms
St	Sand, fine to very coarse, may be pebbly	Solitary or grouped trough crossbeds	Sinuously crested and linguoid (3-D) dunes (lower flow regime)
Sp	Sand, fine to very coarse, may be pebbly	Solitary or grouped planar crossbeds	Transverse and linguoid bedforms (2-D dunes), sand waves (high flow regime)
Sr	Sand, very fine to coarse	Ripple marks (all types)	Ripples (lower flow regime)
Sh	Sand, very fine to coarse, may be pebbly	Horizontal lamination, parting	Plane-bed flow (critical flow), lower and upper flow regime
Sl	Sand, very fine to coarse, may be pebbly	Low-angle ($<15^o$) crossbeds	Scour fills, washed-out dunes (crevasse splays), antidunes
Ss	Sand, fine to very coarse, may be pebbly	Broad, shallow scours	Scour fill
Sm	Sand, fine to coarse	Massive, or faint lamination	Sediment-gravity flow deposits
Sb	Sand, fine to medium	Massive or mottled	Bioturbation
Se	Erosional scour with intraclasts	Crude cross-bedding	Scour fills
Fl	Sand, silt, mud	Fine lamination, very small ripples	Overbank, abandoned channel, or waning flood deposits
Fsm	Silt, mud	Laminated to massive	Back swamp or abandoned channel deposits
Fm	Mud, silt	Massive, desiccation cracks	Overbank, abandoned channel or drape deposits
Fr	Mud, silt	Massive, bioturbation	Root bed, incipient soil
C	Coal, carbonaceous mud	Plants, mud films	Vegetated swamp deposits
P	Paleosol carbonate	Pedogenic features	Soil with chemical precipitation

D, dimensional.

5.4 Lithofacies of the Kamlial Formation

The Kamlial Formation is composed of sandstone interbedded with clay/claystone (Figs. 5.1A-D). At Bahadar Khel anticline, the Kamlial Formation has a total thickness of 70 m from its lower contact with Eocene Kohat Limestone (Fig. 5.1A, Photo 5.1). The lower and upper units of sandstone of this formation are more than 16 m and 10 m thick, respectively (Fig. 5.1A). Sequence in between these sandstone units is composed of interbedded mudstone/clay beds, sandstone, siltstone and intraformational conglomerate (Fig. 5.1A). Some mudstone/clay beds are dominantly maroon in colour and seem to be pedogenic surfaces that are bioturbated.

The Kamlial Formation in the Chashmai anticline has a thickness of 60 m from its lower contact marked by gravel and pebbles embedded in the sandstone unit (Fig. 5.1B). The formation is dominantly composed of sandstone with occasional beds of intraformational clasts (Fig. 5.1B). The upper 30 m unit of the formation is solely composed of sandstone and occasional conglomerate beds and lack overbank deposits. Some sandstone beds in the upper middle unit are well cemented and are termed “hard bands”. The upper unit of the formation is composed of alternate beds of these hard bands and loosely cemented sandstone. Burrow structures are prominent in the top three meters zone of the formation. Clasts embedded in sandstone are intraformational, dominantly balls of clay, siltstone and sandstone with occasional limestone. Some clasts measured at site were: 4x2.5x2 cm, 3.5x2x1 cm, 2x1.5x1 cm, 1.5x1x0.5 cm, 2x1x0.5 cm and 2x1x1 cm. Calcareous nodules of maroon color were observed at places. The Kamlial Formation in the Banda Assar syncline has a total thickness of 147 m from its lower unconformable contact with Eocene limestone to its upper conformable contact with Chinji Formation (Fig. 5.1C).

On the basis of field observations and presence of various sedimentary structures, the following lithofacies have been identified in the Kamlial Formation.

5.4.1 K1: Channel Conglomerates Facies

Description: Channel conglomerate facies is characterized by lenticular beds of massive or crudely stratified conglomerate (Figs. 5.1A, D; Photo 5.2). Clasts are typically less than 5 cm in diameter. Conglomerates are mostly confined to thin beds, only a few clasts thick. The lower contact of the conglomerate beds is

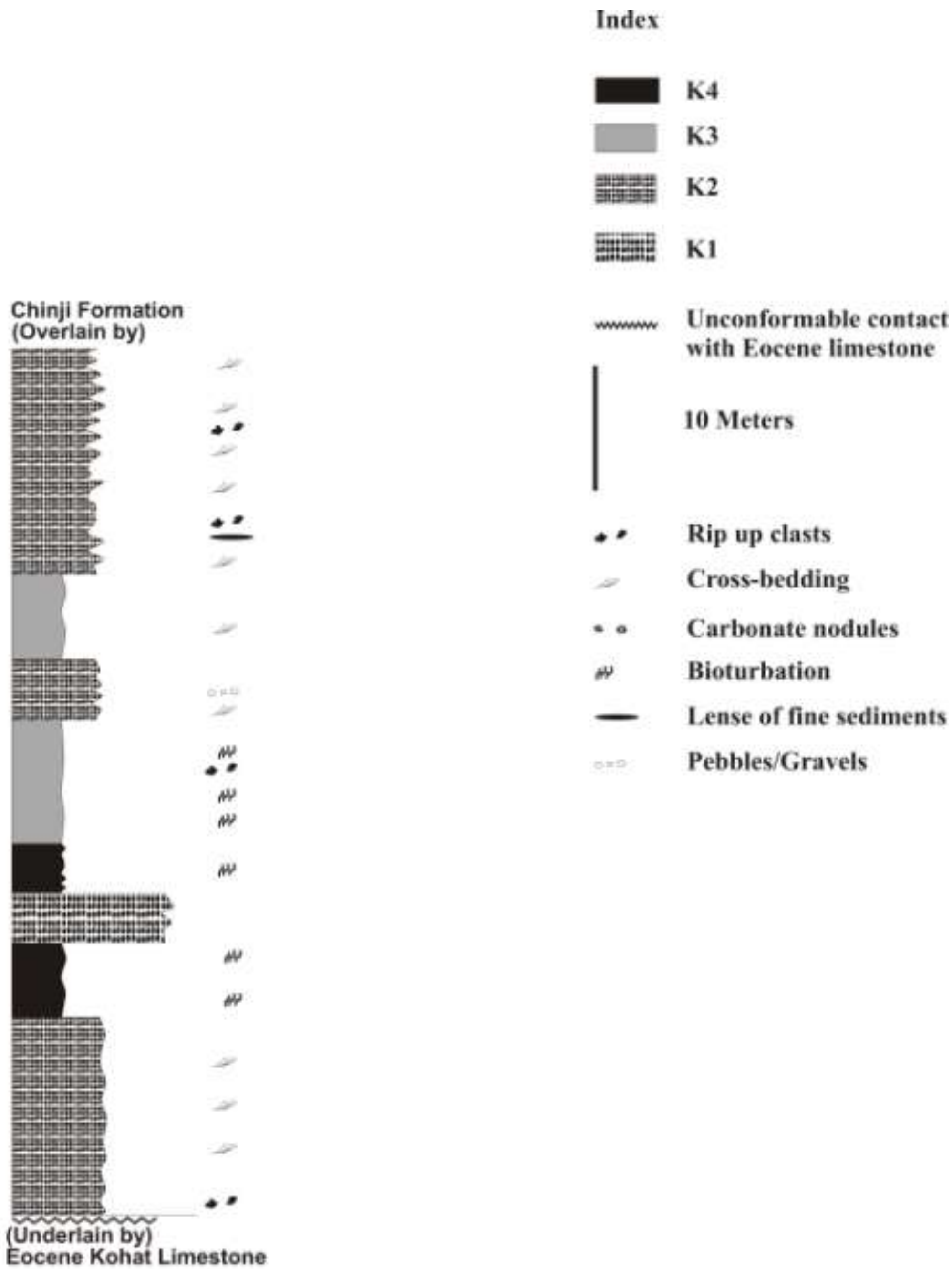

Fig. 5.1A. Measured lithocolumns of the Bahadar Khel anticline, latitude 33° 09' 79 N and longitude 70° 57' 64 E (southwestern Kohat Plateau), showing lithofacies of the Kamlial Formation. (For location, see Fig. 1.4)

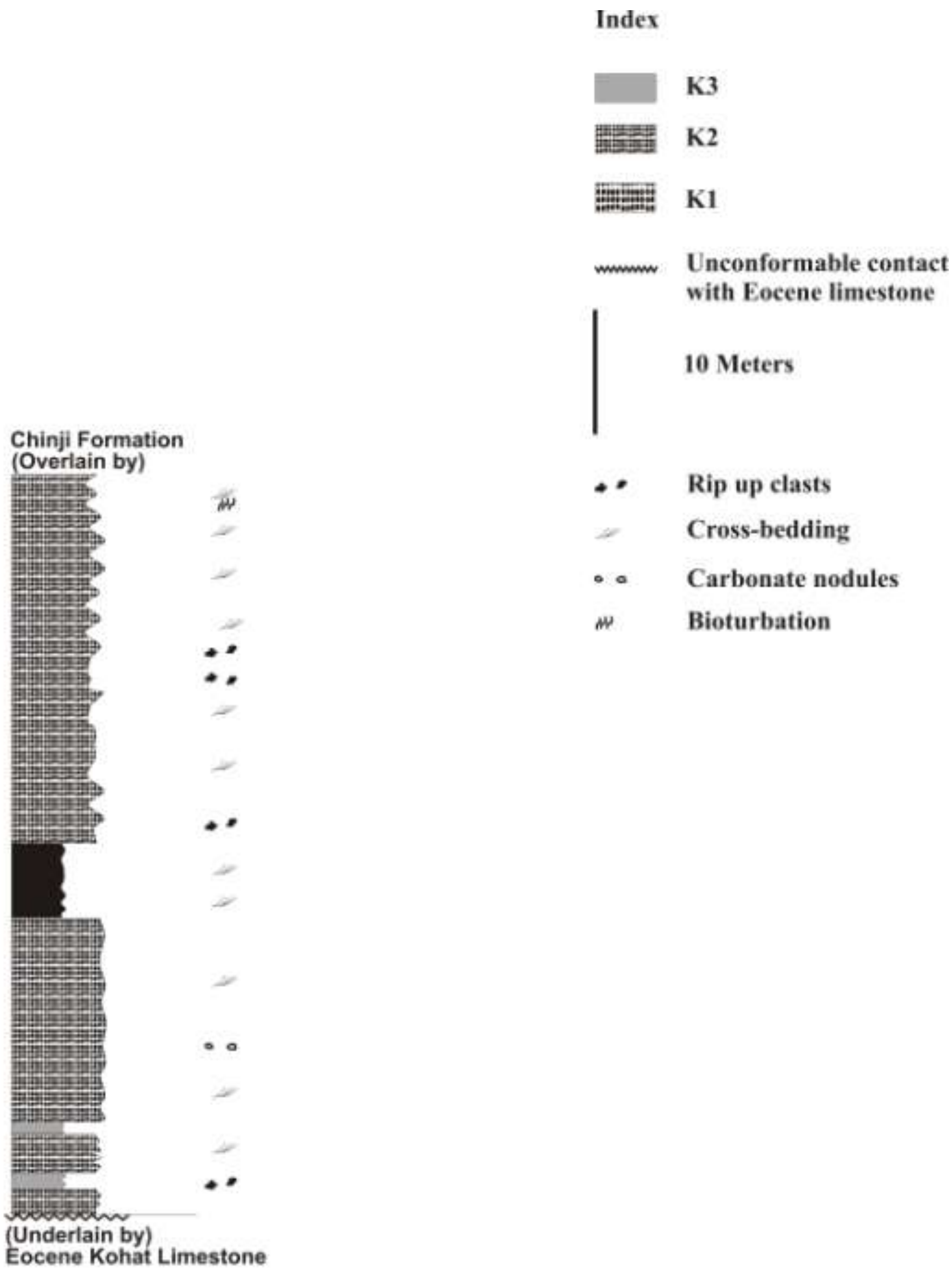

Fig. 5.1B. Measured lithocolumns of the Chashmai anticline, latitude 33° 06' 34 N and longitude 70° 47' 77 E (southwestern Kohat Plateau), showing lithofacies of the Kamlial Formation. (For location, see Fig. 1.4)

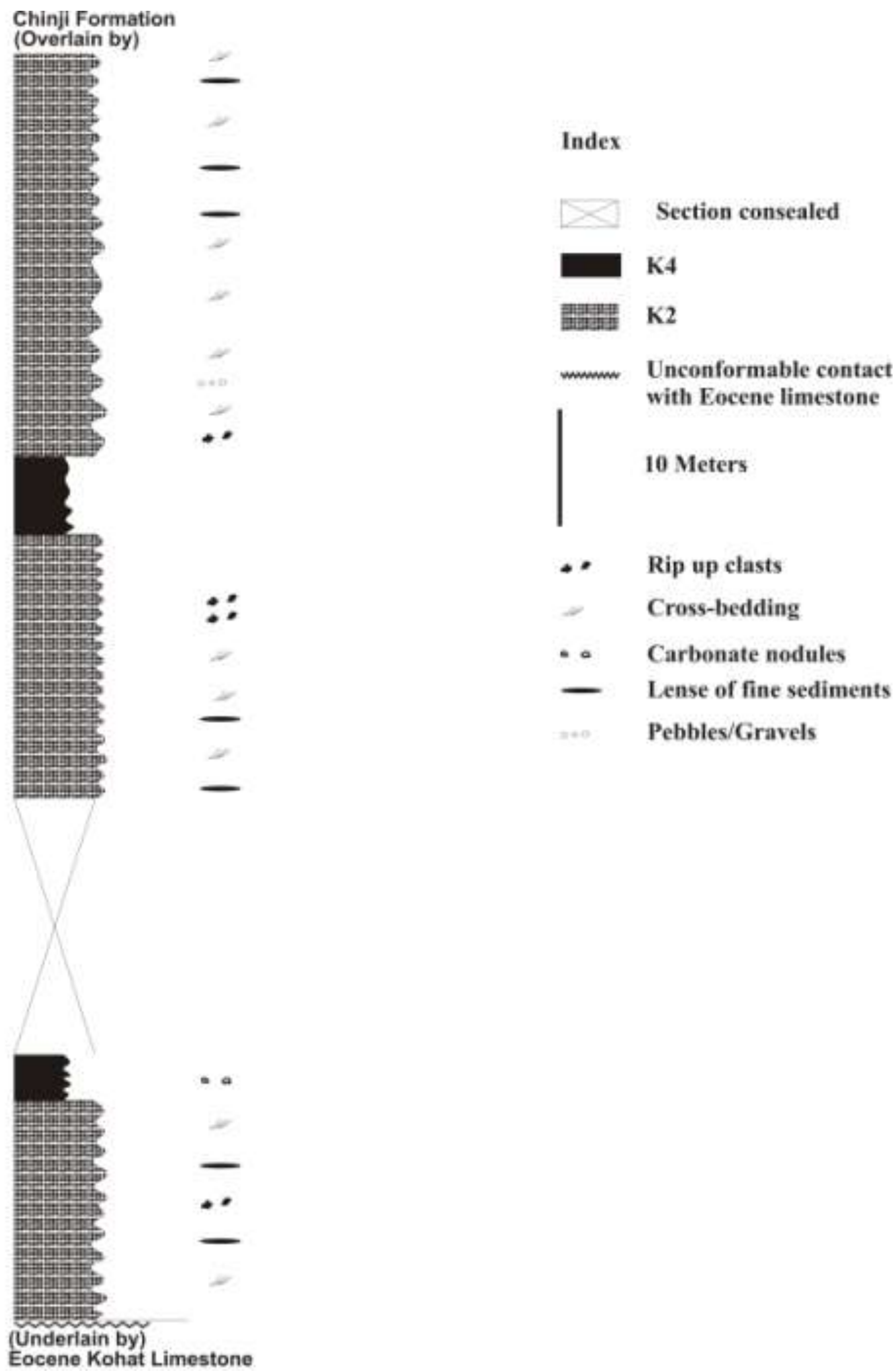

Fig. 5.1C. Measured lithocolumns of the Banda Assar syncline, latitude 33° 07' 52 N and longitude 70° 55' 88 E (southwestern Kohat Plateau,) showing lithofacies of the Kamlial Formation. (For location, see Fig. 1.4)

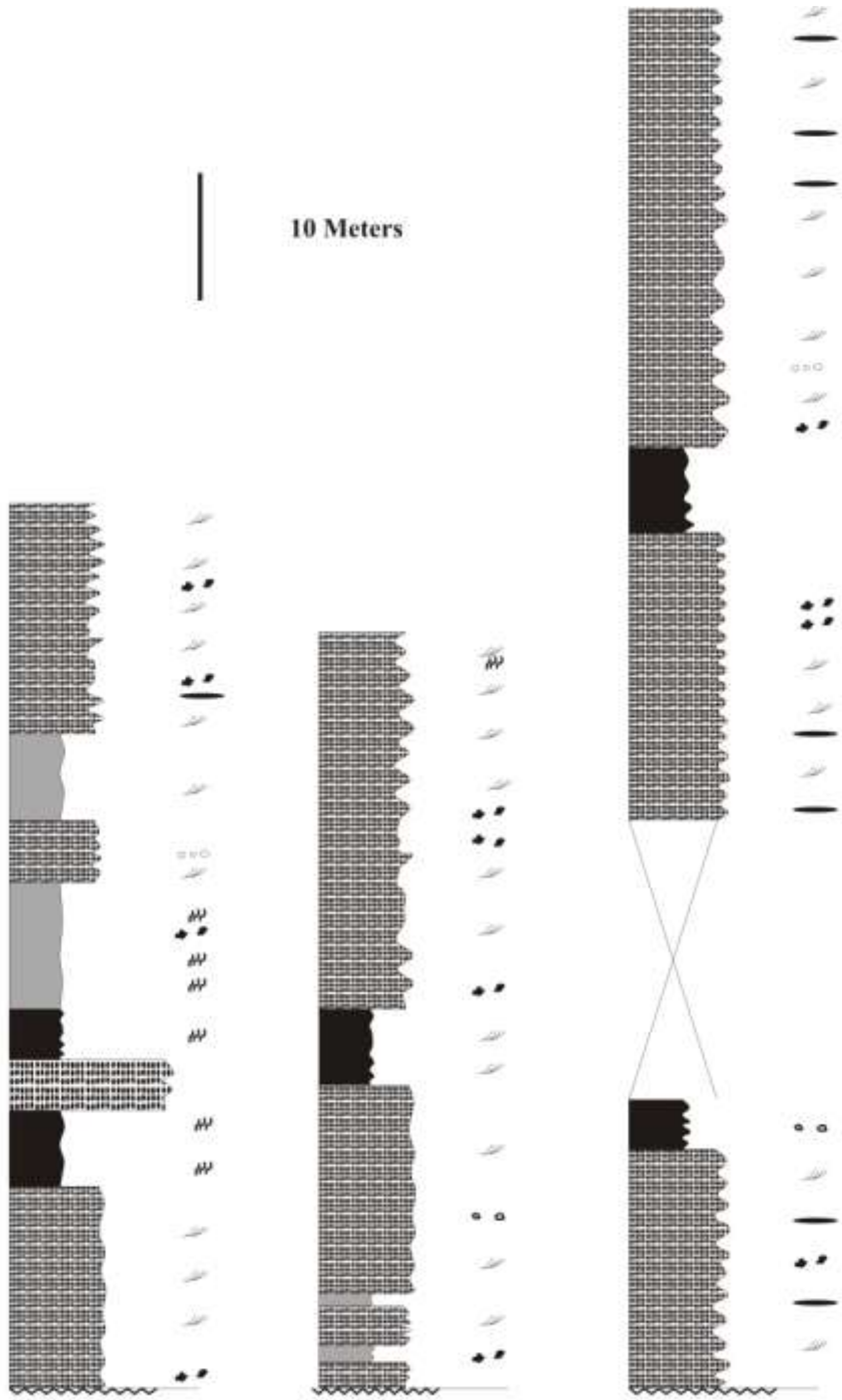

Fig. 5.1D. Measured lithocolumns of the Kamlial Formation from (left to right) Bahadar Khel anticline, Chashmai anticline and Banda Assar syncline (southwestern Kohat Plateau) showing facies association. (For locations, see Fig. 1.4)

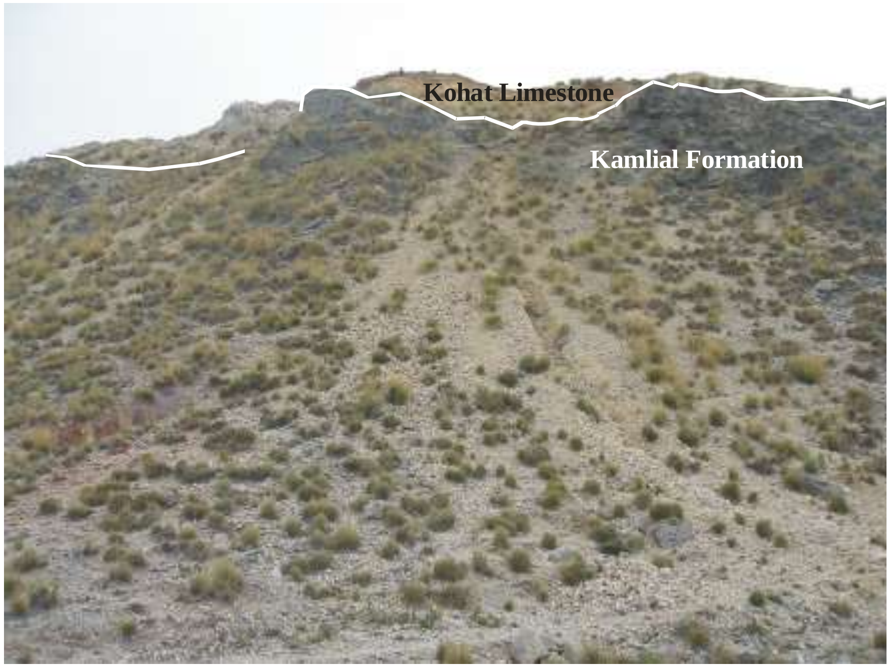

Photo 5.1. Contact (white line) of the Miocene clastic sediments with Eocene Kohat Limestone. The clastic input in the Kamlial Formation could be related to the rising of Himalayas.

Photo 5.2. Channel conglomerate bed, shows deposition in a braided fluvial channel. Hammer head pointing upward.

typically erosional and most commonly fine upward into sandstone. This facies is observed in Bahadar Khel anticline.

Interpretation: Classifying as channel floor deposits, they are composed of a coarse fraction, made up of poorly sorted extra- and intra-formational pebbles (Williams and Rust, 1969; Selley, 1970; Smith, N. D., 1970; Laury, 1971). Coarse channel-floor deposits are essentially lag gravels deposited in the deeper parts of a channel, from which much of the finer material has been winnowed (Beerbower, 1964; Allen, 1965). The subangular fragments and poor sorting show little or no reworking by water. They are probably the result of the collapse of cohesive bank sediments into nearby channels. This explains the preservation of such angular material in, or adjacent to a high energy environment (Laury, 1971).

Conglomeratic channel deposits commonly occur as stacked multistorey sheets with little or no preserved overbank fines, a reflection of the lateral mobility of high-energy bedload streams (Collinson, 1996). Fining upward of channel conglomerate bodies into sandstones suggests either gradual diminution of flow through diversion or systematic lateral migration of a curved channel reach (Cambell and Hengry, 1987).

5.4.2 K2: Cross-bedded Sandstone Facies

Description: Cross-bedded sandstone facies is the most dominant facies of the Kamlial Formation that consists of laterally persistent sheets of sandstone, dominated by large trough cross-stratification (Photo 5.3) with subordinate small-scale planar and trough cross-stratification (Figs. 5.1A-D). Sandstone of this facies is grey to brownish grey, fine- to medium-grained and mostly thick bedded, characteristically upper 60 m sequence of the formation in Banda Assar syncline (Fig. 5.1C). Similarly, the upper unit of K2 sandstone is grey, fine- to medium-grained, thick-bedded with occasional presence of embedded gravel in lower contact and some boulders above it in Bahadar Khel anticline (Photo 5.4). The sandstone beds are broadly lenticular or wedge shaped (up to several tens of meters in lateral extent) with sharp lower and upper contacts.

Interpretation: The laterally persistent sheets of sandstone, dominated by large trough cross-stratification with subordinate small scale planar and trough cross-stratification are

Photo 5.3. Large scale cross-stratified beds, top of pencil shows top of bed-broadly planar tabular low angle cross bedding which suggests dune migration (megaripple) in fluvial environment. Upper surface is truncated.

Photo 5.4. Large limestone boulders in sandstone beds of Kamlial Formation near Bahadar Khel old bridge.

interpreted as the deposit of a distal, sand-dominant braided fluvial system. The planer tabular low angle cross-bedding suggests dune migration (megaripples) in fluvial environment (Photo 5.3). The large scale trough cross-stratified sandstone also shows asymptotic downlap of trough cross-bed foresets which suggests fairly rapid depositional energy conditions (Photo 5.5). Photo 5.6 shows cross-cutting trough cross-bedding that usually result from variations in flow strength i.e., flood and slack periods in fluvial environments. Individual channel fill sequences are stacked directly upon each other, with no intervening vertical accretion deposits. The lack of vertical accretion deposits probably resulted from the erosive capability of numerous concurrently active, shifting channels (Allen, 1982; DeCelles, 1986).

Broad, wedge and lens shaped beds suggest sand deposition in very wide, shallow channels. The lack of land plants must have had a profound effect on sand body geometry (Fedo and Cooper, 1989). Fuller (1985) discussed the empirical analysis of channel form for several active braided systems and derived a 100:1 width/depth ratio for the lower reaches of the Yellow River. High lateral and vertical connectivity of the sandstone bodies was probably due to low subsidence rates, resulting in low preservation of overbank fines (Allen, 1978; Kraus and Middleton, 1987).

The intraformational mudclasts and scours suggest erosion of significant amounts of cohesive mud of the overbank facies during bankfull flow. The ripple cross-laminations, occasionally found at the bed tops indicate gradual waning in flow and channel abandonment (Smith, N. D. et al., 1989; Miall, 1996). The presence of root traces and carbonate nodules in some channel sandstones indicates that some channel areas were emergent during low flows and stable enough for colonization by vegetation.

5.4.3 K3: Interbedded Mudstone, Sandstone and Siltstone Facies

Description: The interbedded mudstone, sandstone and siltstone facies consists of interbedded mudstone, siltstone and sandstone unit (max. of 6 m thickness) that is persistent, although thicknesses of subunits vary laterally. Cross-lamination and asymmetric ripples are characteristics of the sandy and silty layers, whereas parallel lamination, burrows, root marks and calcareous concretions are typical of the finer mudrock subunits. Lithic clasts, dominantly of gravel size of both extrabasinal and

Photo 5.5. Large scale trough cross-stratified sandstone shows asymptotic downlap of trough cross bed foresets indicating fairly rapid depositional energy conditions.

Photo 5.6. Cross cutting trough cross beddings that usually result from variations in flow strength. In fluvial environments, such conditions are caused by flood stage and slack stage periods.

intraformational origin also occur at places in this lithofacies. This lithofacies occurs in Bahadar Khel and Chashmai anticlines (Figs. 5.1A, B, D).

Interpretation: This unit probably represents levee and minor distal splay deposits, as indicated by the abundant burrows and root structures, alternating laminae of mainly sandy silt and mud-clay rocks, and abundant calcareous concretions (Coleman, 1969; Ethridge et al., 1981; Sutter, L. J. et al., 1985). Levee sediments should be particularly suitable for concretion development because leaching and precipitation would be most intense in well drained areas above mean annual water table (Ghosh, 1987). Extensive burrows and rootlets have acted as pathways for movement of calcareous solutions in these levee sediments (Ethridge et al., 1981).

5.4.4 K4: Mudstone Facies

Description: These fine-grained mud bodies consist of massive and laminated mud/clay (Figs. 5.1A-D). The interbedded clay/claystone is brownish-grey to maroon red in color. Clay/claystone occurs both as continuous beds and lenses pinching out at short distances (about or more than 20 m). Some mudstone/clay beds are bioturbated, dominantly maroon in color and seem to be pedogenic surfaces. Bioturbation, subordinate small calcareous nodules and minor desiccation cracks are occasionally present. In some places the mud-clay rocks are multistoreyed in which vertical burrows and caliche horizon are abundant toward the top of an individual story.

Interpretation: This facies assemblage represents a mud-dominated floodplain or repeated mud drapes from a low-energy fluvial system. Furthermore, lateral and vertical association, geometry, red color and pedogenic horizons also imply a flood basin origin for this facies in a well drained oxygenated environment (Ghosh, 1987). Thick mud-clay rock units imply copious sedimentation, whereas the formation of soil horizons suggests rather low subsidence (Ghosh, 1987). The development of calcareous nodules and bioturbation indicates pedogenic modification after deposition (Wright and Tucker, 1991; Retallack, 1997).

5.4.5 Depositional System of the Kamlial Formation

The Kamlial Formation was possibly deposited by sandy bedload or major mixed load river. Sandy bedload rivers dominantly contain sand, though gravel may be present dispersed in sand. These rivers, especially during floods, may have heavy load of suspended sediment some of which may be deposited temporarily in overbank and channel settings. Accumulation of fine sediments is seldom thick enough to significantly resist channel migration and erosion. Highly erodible banks give rise to high width/depth ratios and to lateral movement both of the whole channel tract and of bars and island within the tract. Thus sinuosity is rather low and braiding is well developed (Collinson, 1996). The availability of sand is a major control on braided patterns (Smith, N. D. and Smith, 1984).

Abbasi (1991) divided the Kamlial Formation into two major types in southeastern Kohat on the basis of sandstone body geometry. (a) Major channel type sand bodies, the dominant ones and (b) floodplain type tabular sand bodies interbedded with siltstone. The major sandstone bodies are marked by the presence of a number of erosional surfaces commonly indicated by thin lag deposits with dominant paleocurrent directions to the east. These sediments of the Kamlial Formation were deposited by well-channelized high sinuosity to low sinuosity streams active on a major flood plain. Individual storeys of the major channel type sand bodies are in the order of 4-6 meters thick, deposited probably by streams 6-10 meter deep.

The floodplain type tabular sand bodies interbedded with siltstone were deposited by a local high sinuosity or large-scale crevasse splays or by a mixed load local stream activity flowing at right angle to the flow direction of the main river (Abbasi, 1991).

The low proportion of mudstone–siltstone facies in Kamlial Formation might reflect one or more factors including: (1) low subsidence rates promoting rapid lateral migration of channels and regular erosive removal of flood-basin deposits, (2) an arid climatic regime and limited vegetation allowing greater potential for lateral migration of channels and lesser potential for trapping of fine clastic particles and (3) strongly seasonal discharge resulting in flash flooding and reworking of unconsolidated or semi-consolidated flood-basin deposits as intraclasts.

5.5 Lithofacies of the Chinji Formation

The Chinji Formation in Bahadar Khel anticline has a thickness of 140 m between its conformable lower and upper contacts with Kamlial and Nagri formations, respectively (Figs. 5.2A, D, Photos 5.7, 5.8). The formation is dominantly composed of overbank fines (Figs. 5.2A, D, Photo 5.7).

The Chinji Formation has sharp lower contact with Kamlial Formation in the Chashmai anticline, and has a thickness of 100 m. The formation is composed of overbank fines and sandstone; the overbank fines being the dominant, and has a sharp upper contact with overlying Nagri Formation (Figs. 5.2B, D, Photo 5.9). Pedogenic surfaces/calcareous nodules were observed at seven horizons in the formation, generally associated with overbank fines. Some of these pedogenic surfaces/calcareous nodules are lense shaped. Overbank fines are reddish brown to reddish maroon and include clay beds, shale and siltstone. Sandstone is grayish brown to yellowish gray, soft/hard, dominantly fine-grained/fine- to medium-grained and medium-to thick-bedded. Some units of the sandstone are bioturbated.

The Chinji Formation in the Banda Assar syncline has a thickness of 133 m from its lower conformable contact with Kamlial Formation upto its upper conformable contact with Nagri Formation (Figs. 5.2C, D). The formation is dominantly composed of overbank fines (silty clay/clay/shale/mudstone) with subordinate sandstone and siltstone beds (Figs. 5.2C, D, Photo 5.10). The thick sequences of overbank fines clearly show a major change in the source area conditions from Kamlial Formation to Chinji Formation. The following lithofacies have been identified in Chinji Formation from southwestern Kohat.

5.5.1 C1: Cross-bedded Channel Sandstone Facies

Description: The cross-bedded channel sandstone facies is grey to brownish grey, fine-grained/fine- to medium-grained, medium- to thick-bedded, and contains some sparsely embedded gravel/pebbles at places in a couple of units (Figs. 5.2A-D, Photo 5.11). Individual beds show very little fining-upward tendencies, possibly due to the lack of available grain size variability.

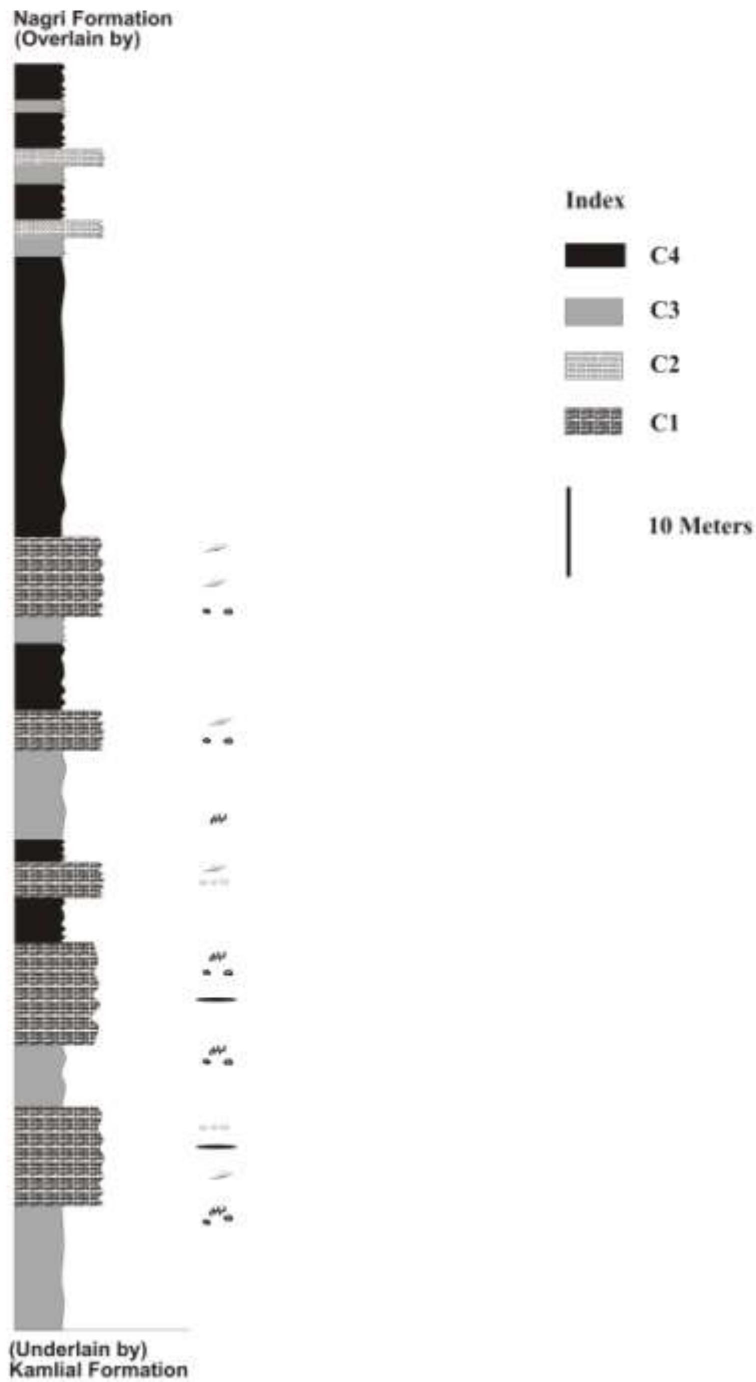

Fig. 5.2A. Measured lithocolumns of the Bahadar Khel anticline, latitude 33° 09' 79 N and longitude 70° 57' 64 E (southwestern Kohat Plateau) showing facies of the Chinji Formation, characterized by subordinate amount of sandstone facies. (For location, see Fig. 1.4)

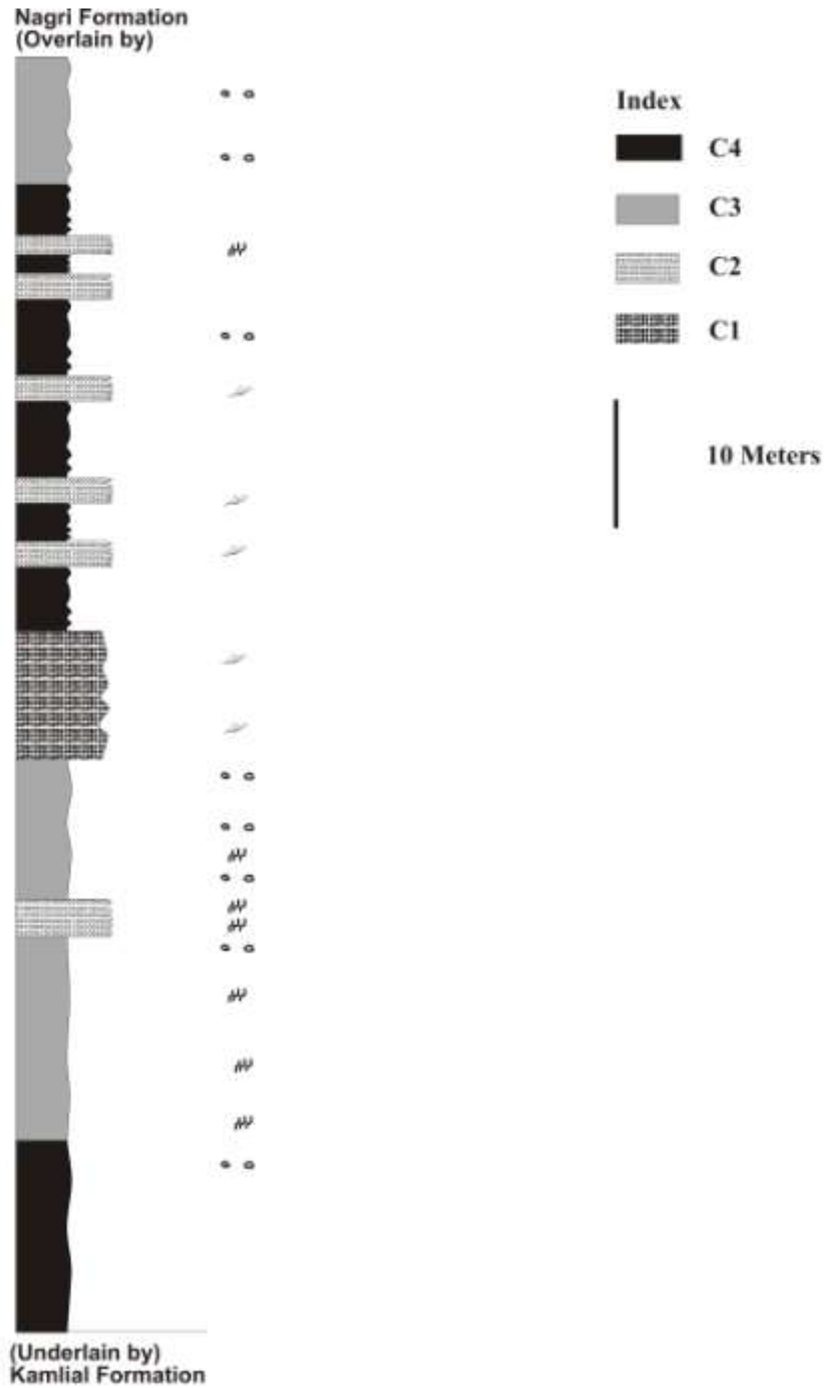

Fig. 5.2B. Measured lithocolumns of the Chashmai anticline, latitude 33° 06' 34 N and longitude 70° 47' 77 E (southwestern Kohat Plateau) showing facies of the Chinji Formation, characterized by subordinate amount of sandstone facies. (For location, see Fig. 1.4)

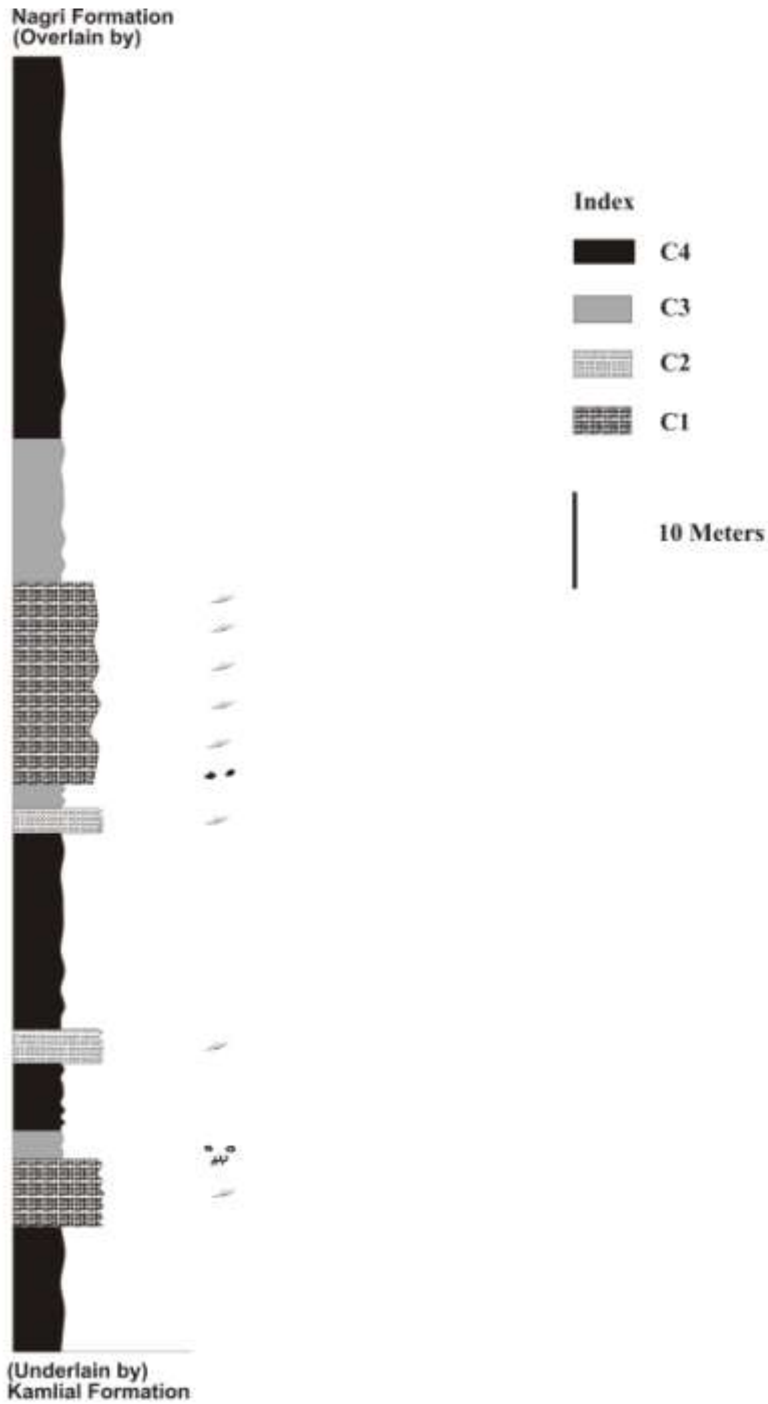

Fig. 5.2C. Measured lithocolumns of the Banda Assar syncline, latitude 33° 07' 52 N and longitude 70° 55' 88 E (southwestern Kohat Plateau) showing facies of the Chinji Formation, characterized by subordinate amount of sandstone facies. (For location, see Fig. 1.4)

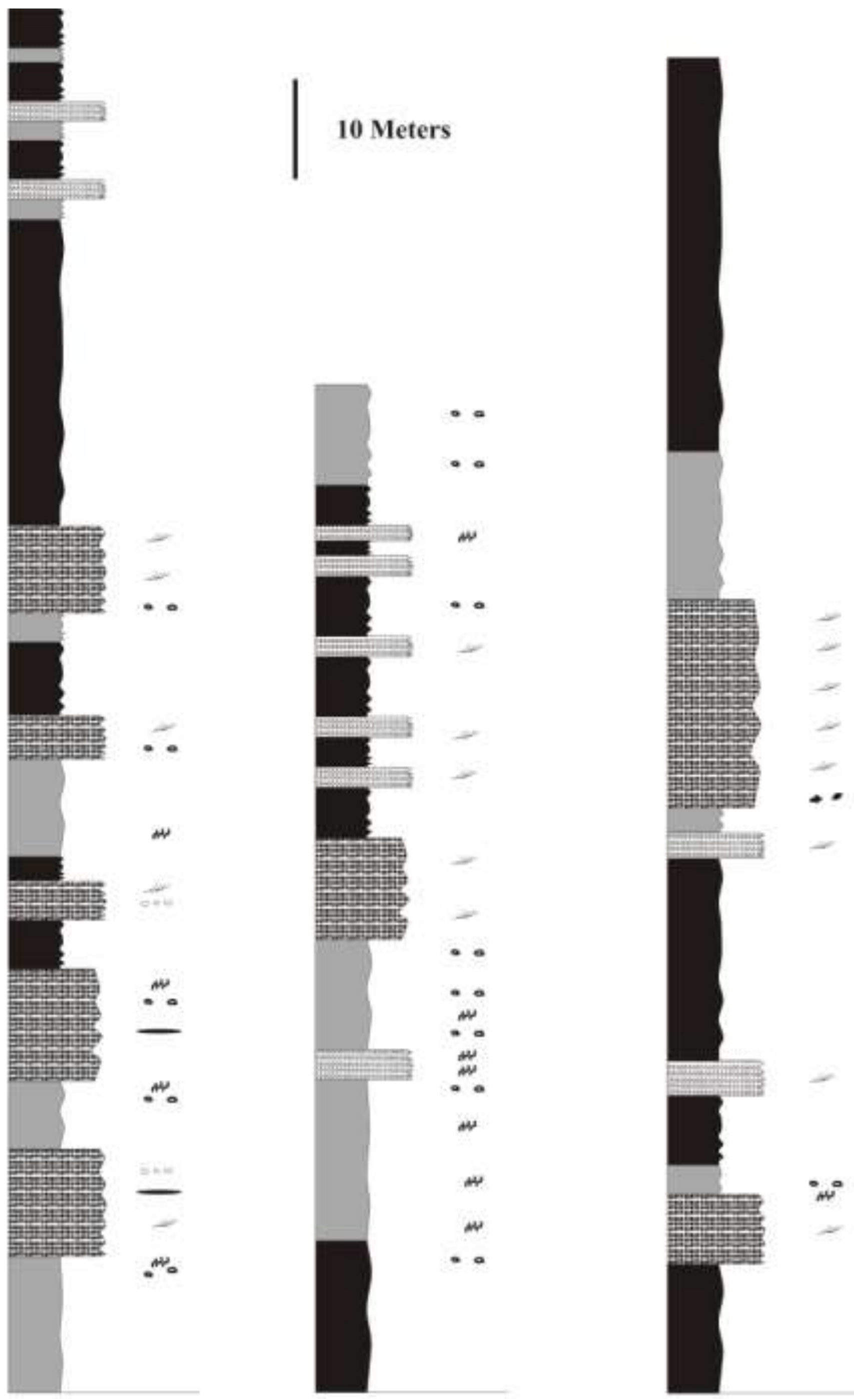

Fig. 5.2D. Measured lithocolumns of the Chinji Formation from (left to right) Bahadar Khel anticline, Chashmai anticline and Banda Assar syncline (southwestern Kohat Plateau) showing facies association. (For locations, see Fig. 1.4)

Photo 5.7. Panoramic view of Bahadar Khel Section (looking north). Contacts of the formations are marked by white lines. The Chinji Formation in the middle is dominantly composed of maroon red mudstone.

Photo 5.8. Thickly bedded purple-red mudstone sequence of Chinji Formation capped by thick sandstone dominated succession of Nagri Formation in Gore Nala, near Bahadar Khel old bridge. A thick unit of sandstone (base marked by a white line) shows lower contact of the Nagri Formation.

Photo 5.9. Maroon red mudstone (overbank) dominated Chinji Formation followed by sandstone (Channel) dominated Nagri Formations with sharp contact marked by a white color line.

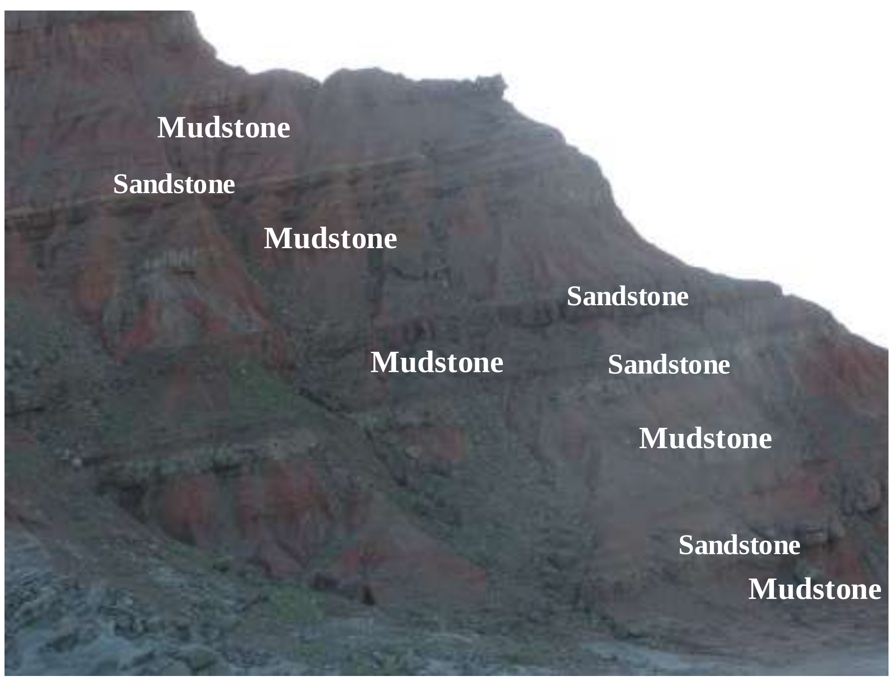

Photo 5.10. Alternation of thin sheets of sandstone and maroon red mudstone succession of the Chinji Formation. Overbank ratio is more than 50% having characteristic of Chinji Formation. Thick overbank deposits also consist of thin lenticular sandstone of crevasse splay deposits. Thin, grey/ brownish-grey beds of sandstone show more resistant to weathering than the associated mudstone.

Photo 5.11. Sparsely pedogenic concretions in trough cross-stratified sandstone beds of Chinji Formation, near Bahadar Khel old bridge.

Photo 5.12. Large scale cross-bedding in sandstone of the Chinji Formation.

C1 facies consists of laterally persistent sheets of sandstone, dominated by large trough cross-stratification with subordinate small-scale, planar and trough cross-stratification (Photos. 5.12, 5.13).

Interpretation: The laterally extensive and erosive-based sandstone of the Chinji Formation probably represent deposits of mixed-load channels with varying stream competence. The aggrading floodplain architecture and the dominance of vertically stacked channels suggest a very limited channel migration tendency (Smith, D.G. and Smith, 1980; Smith, D. G., 1983; Kirschbaum and McCabe, 1992; McCarthy et al., 1997; Makaske et al., 2002). The channel base experienced alternating scouring, bed-load transport and deposition. In addition, this facies is dominated by frequent crevassing and avulsion, which led to the formation of new channels on the floodplain, while active channels were abandoned (Smith, D. G., 1986; Smith, N. D. et al., 1989; Makaske et al., 2002). The ripple cross-laminations (Sr) occasionally found at the bed tops indicate gradual waning in flow and channel abandonment (Smith, N.D. et al., 1989; Miall, 1996).

5.5.2 C2: Cross-bedded and Cross-laminated Sandstone Facies

Description: The cross-bedded and cross-laminated sandstone facies is grey, fine- to medium-grained and thin to medium bedded/medium-to thick-bedded (Figs. 5.2A-D, Photo 5.14). Some units of the sandstone are bioturbated (Photo 5.15). Individual beds show fining-upward tendencies at places and grade vertically from cross-bedded sandstone into cross-laminated sandstone.

This facies grades vertically into overbank deposits (Figs. 5.2A-D, Photo 5.16). The sandstone beds are broadly lenticular or wedge shaped (up to several tens of meters in lateral extent) with sharp lower contact (Photos. 5.17, 5.18). The sandstone sequences contain pebbles embedded in it at a couple of places, whereas a couple of 20 to 30 cm intraformational and extrabasinal conglomerate units were also noted (Photo 5.19). At places multistoreyed sandstone bodies are also separated by channel lag deposits.

Interpretation: The sandstone is interpreted as the deposit of crevasse splay channels of a distal, sand-dominant braided fluvial system in associated floodplains (Photo 5.16)

Photo 5.13. Cross bedding in Chinji Formation.

Photo 5.14. Red/purple mudstone overlain by cross-bedded multistoried channel sandstone suggesting amalgamated braided streams.

Photo 5.15. Animal/root trails and some of these are rip up clasts in fine-grained sandstone unit of Chinji Formation.

Photo 5.16. Thick- to thinly-bedded sandstone with sharp contact of underlying mudstone. The topmost unit of mudstone comprises alternation of thin sheets of fine-grained sandstone and mudstone. Mudstone suggests river overbank episodes in an arid setting whereas sandstone units indicate crevasse splays in river floodplain.

Photo 5.17. Thick multistoried sandstone having sharp erosional contact with underlying red pedogenic mudstone. The erosional surface comprises intra-conglomerate at the base of channel sandstone. Classic channel lag (thalweg of channel center).

Photo 5.18. Sharp, irregular erosional contact of mudstone with overlying channel sandstone shows deep incision of fluvial channel into arid oxidized floodplain.

Photo 5.19. Thick channel lag deposit consisting of intrabasinal, disorganized pedogenic mud clasts in Chinji Formation, near Bahadar Khel old bridge.

Photo 5.20. Load marks in sandstone of Chinji Formation suggesting rapid deposition of sand onto semi-liquefied floodplain.

(DeCelles, 1986). Broad, wedge and lens shaped beds suggest sand deposition in very wide shallow channels (Fedo and Cooper, 1989).

The channel base experienced alternating scouring, bed-load transport, and deposition (Photos 5.18, 5.20). The frequent crevassing and avulsion led to the formation of new channels on the floodplain, while active channels were abandoned (Photo 5.21) (Smith, D. G., 1986; Smith, N. D. et al., 1989; Makaske et al., 2002). Mud clasts at the base are of intraformational origin and are derived locally from the levee and floodplain sediments through which the channel was cut. Textural immaturity implies rapid sedimentation from mixed-load streams and minimum winnowing. Upward increase of shaly lenses, burrows and root traces may be due to progressive crevasse channel abandonment and waning of current energy (Photos 5.22, 5.23) (Ghosh, 1987). The ripple cross-laminations occasionally found at the bed tops also indicate gradual waning in flow and channel abandonment (Smith, N. D. et al., 1989; Miall, 1996).

5.5.3 C3: Interbedded Mudstone, Siltstone and Sandstone Facies

Description: The interbedded mudstone, siltstone and sandstone facies is dominantly composed of shale, interbedded with thin- to medium-bedded, reddish brown sandstone and thin-bedded, thinly laminated siltstone (Figs. 5.2A-D). In the upper part, this facies is solely composed of clay beds interbedded with subordinate siltstone (Photo 5.24). Red, laterally very extensive, horizontally laminated or massive mudstone separates the sand sheets (Photo 5.24). Rare, poorly developed nodular horizons in them indicate weakly developed paleosols. Rootlets and burrows are common, though most of the original stratification is preserved. However, no sedimentary structures were observed where invertebrate burrows and pedogenic carbonate nodules are common.

Interpretation: Strata of the C3 facies are interpreted as overbank deposits produced by the waning flow strength of sandy to muddy sheetfloods through crevasse splays. In particular, sand bodies of lenticular shape represent crevasse splay and levee deposits by virtue of their proximity to major channels and occasionally observable coarsening-upward trends (Smith, N. et al., 1989; Ferrell, 2001) whereas horizontal bedding surfaces probably represent products of distal splays and waning flow energy (Miall, 1996). Laminated mudstones mark suspended-load deposition from low-velocity floods, where

Photo 5.21. Close-up view of contact relationship of channel and overbank facies. The sandstone unit also shows channels within primary channel. At least three channels in the photograph are marked by white lines.

Photo 5.22. Mud ball in sandstone suggests collapsed banks of river, probably related to undercutting of bank during river flood.

Photo 5.23. Mud balls in channel sandstone representing river bank failure.

Photo 5.24. Thin lenticular fine-grained sandstone encased by thick mudstone representing crevasse splay/levee deposits.

reworked by bioturbation and pedogenic processes prevail, they result in massive mudstone. Mudstone color, burrows and calcareous nodules suggest well-drained or even partially emergent floodplains (Retallack, 1997; Mack et al., 2003) and substantial aerial exposure (McCarthy et al., 1997).

Levee sediments are suitable for concretion development as leaching and precipitation would be most intense in well drained areas above mean annual water table (Ghosh, 1987). Extensive burrows and rootlets act as pathways for movement of calcareous solutions in such environment (Ethridge et al., 1981).

Preservation of structure in a rapidly vegetated setting is largely dependent on rapid burial. This facies, therefore, probably represent either deposition in environments flanking the channel, where overbank sedimentation rates would be highest, or deposition in topographically low parts of the floodplain, such as lakes or abandoned channels (Johnson, S. Y., 1984). The sandstone units indicate episodic injections of coarse material into a muddy environment (Reading, 1996).

5.5.4 C4: Mudstone Facies

Description: These fine-grained mud bodies consist of massive and laminated mud, and are characterized by the overbank fines (OF) architectural elements (Figs. 5.2A-D). Individual mudstone units are laterally persistent, red to purple and range from 0.5 cm to 2 m in thickness. Bioturbation, subordinate small calcareous nodules and minor desiccation cracks are occasionally present.

Interpretation: Lateral and vertical association, geometry, predominant red color and extensive pedogenic horizons imply a flood basin origin for the mud/clay rocks in a well drained oxygenated environment (Photo 5.16), while the development of calcareous nodules and bioturbation indicates pedogenic modification after deposition (Wright and Tucker, 1991; Retallack, 1997). The pedogenic caliche horizons develop during periods of little sedimentation and subsidence. Extensive burrowing near the top of individual sedimentary units makes the mudrocks sufficiently porous and facilitates formation of concretions (Ghosh, 1987). Thick mud/clay rock units imply copious sedimentation (Ghosh, 1987). Mottling is commonly associated with seasonally oscillating water tables, and may develop during pedogenesis as a result of either fluctuating Eh-pH conditions or through redistribution of iron oxide/hydroxide particles (Buurman, 1980).

5.5.5 Depositional System of the Chinji Formation

Sandstone of the Chinji Formation was most probably deposited by mixed-load rivers. These rivers transport fine suspended sediment as well as significant bedload (Collinson, 1996). Their bedload is dominantly sandy though there may be some gravel and sufficient fine-grained sediment accumulates to enhance bank stability (Bluck, 1971). But, during a flood, channel banks are breached and a new channel course is established on the lowest part of the floodplain, commonly taking place after several years (Collinson, 1996). The floodplain deposits of the Chinji Formation seem to be deposited by suspended-load rivers. These rivers carry a very high proportion of their load in suspension, and that flow on low gradients, deposit fine-grained sediment both on the floodplain and, to some degree within the channels (Collinson, 1996).

Low lateral and vertical connectivity of the sandstone bodies in Chinji Formation is probably due to high subsidence rates, resulting in high preservation of overbank fines (Allen, 1978: Kraus and Middleton, 1987). The change from thick channel sandstones to dominantly overbank accumulation with minor, thin, channel-sandstone lenses could be due to a change in climate or a change in the palaeodrainage of the area.

Considering the fluvial lithofacies assemblages, the sequences are typical of a braided river system (Miall, 1977, 1978) and may be related to S. Saskatchewan type. Variability in grain size reflects differences in provenance and/or water stage fluctuations. The deposition can thus be described as a distal braided system in which siltstones represent over 80 % of the sediment thickness (Cojan, 1993).

Detailed sedimentologic reconstruction of the Chinji Formation in Chinji village (Willis, 1993b) shows multistoried sandstones representing braided rivers with typical maximum depth of 4-13 m and channel widths of 80-200 m. Foreland strata of the similar age at Surai Khola accumulated at 0.17 km/m.y (Appel et al., 1991), and are dominated by mudstone with common calcareous paleosols, organic rich horizons and sandstone beds (usually less than one meter thick) (West, 1984).

In Potwar, the Chinji Formation contains well-developed paleosol horizons and thin sheet type sandstone bodies of crevasse splay origin. Paleosols are generally 1-3 meter thick and laterally continuous for tens of kilometers and characteristically underlain by leached carbonate concretions that reflect substantially long periods of aerial exposures of overbank fines during sedimentation hiatuses (Willis and Behrensmeyer, 1994, 1995).

The multistoreyed channel-type sandstone bodies of the Chinji Formation in eastern Kohat are about 10 m thickness and extend laterally for many kilometers. These sandstone bodies are gray in color, medium-grained and contain lenses of intraformational conglomerates. A simple lithofacies association of plane bedding, low angle plane bedding and trough cross-bedding sandstone exists, but interrelationship among these lithofacies is complex and do not follow any trend. Trough cross-beds across the formation suggest a consistent flow direction to the SSE (Abbasi, 1998).

Similarly, two types of sandstone bodies in Chinji Formation at Thakhti Nasrati-Shanawah section, Shinghar-Surghar Range have been identified as i) the multistoried major sandstone bodies where the individual storey is at least 3 meter thick, ii) the intercalated sandstone and mudstone, mainly present in the lower part of the formation (Azizullah and Khan, 1998). The former sequences were deposited by paleochannels dominated by sand and subordinate gravels, and the latter by meandering river system.

5.6 Lithofacies of the Nagri Formation

The exposed Nagri Formation in the Chashmai anticline is 256 m thick from its lower contact with Chinji Formation (Figs. 5.3A, D). Upper contact of the formation is not exposed and is covered by recent alluvium deposits. The exposed section of the formation is more than 80 % of sandstone. Overbank fines are also directly associated with sandstone. Sandstone of the formation is gray to brownish gray, dominantly fine to medium-grained and thin- to thick-bedded. Clasts that occur at places are dominantly of intraformational origin, mostly clay and sand balls. Moreover, pedogenic surfaces/calcareous nodules were observed at two horizons in the overbank fines, indicating subaerial exposure.

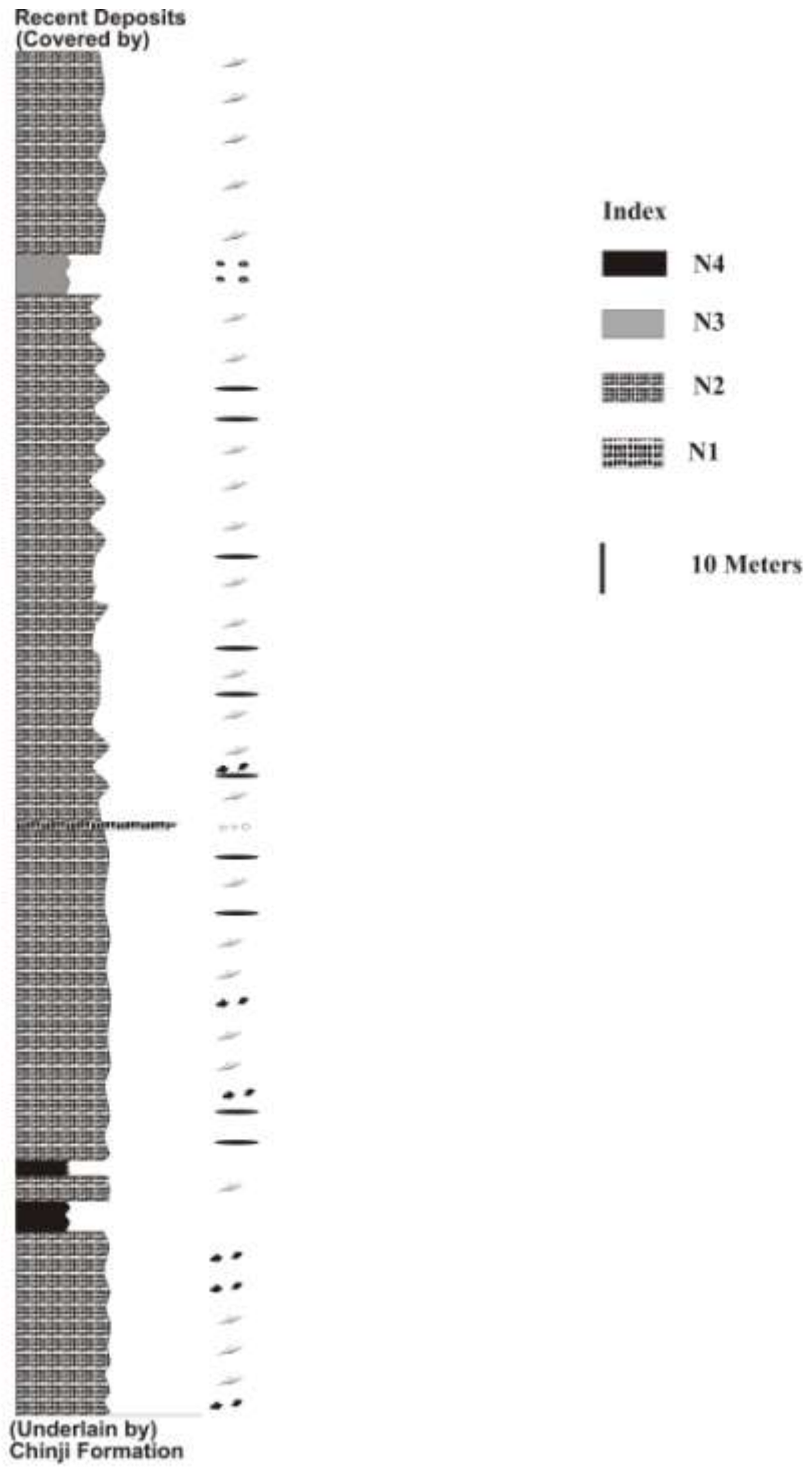

Fig. 5.3A. Measured lithocolumns of the Chashmai anticline, latitude 33° 06' 34 N and longitude 70° 47' 77 E (southwestern Kohat Plateau), showing facies association of the Nagri Formation. (For location, see Fig. 1.4)

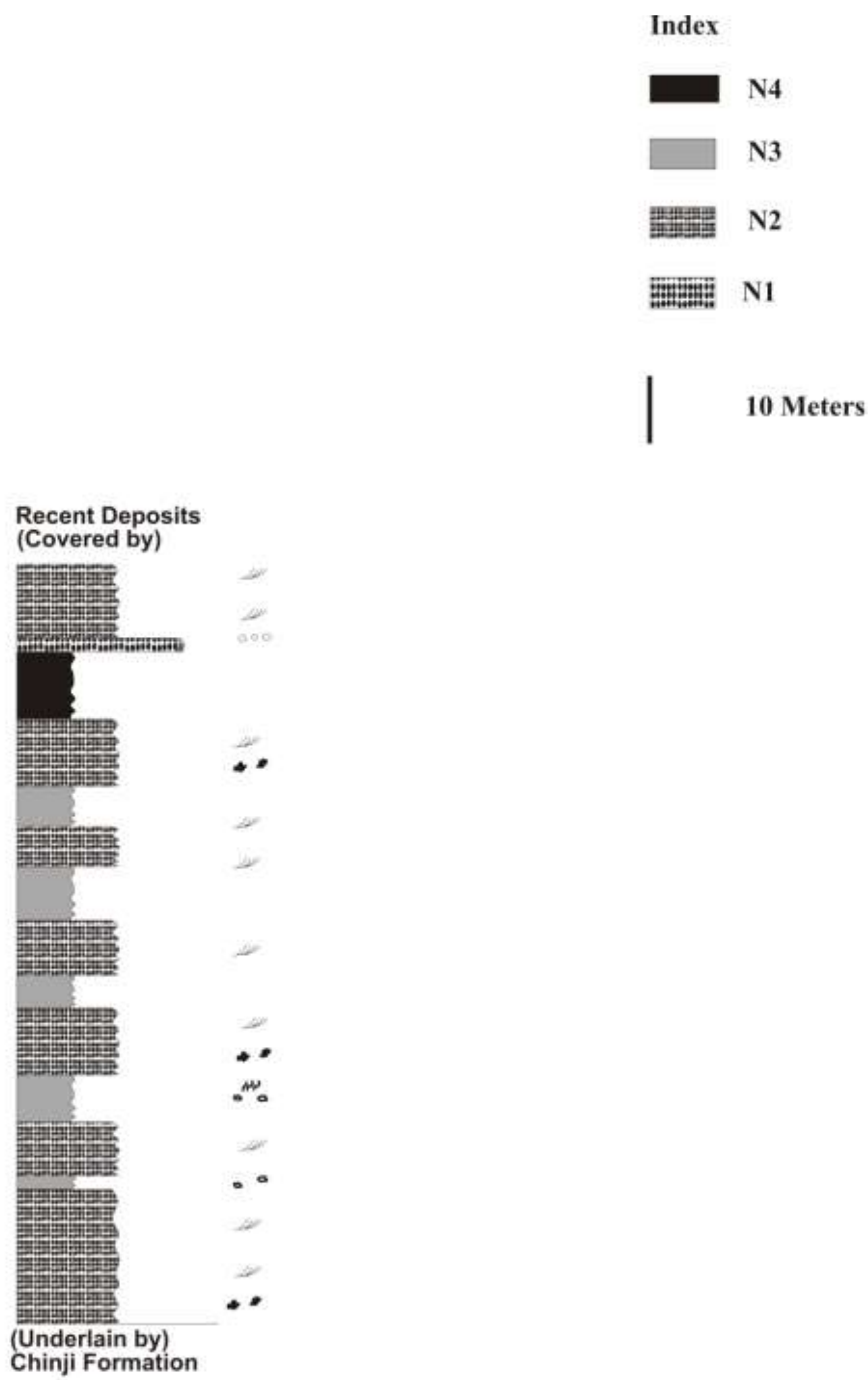

Fig. 5.3B. Measured lithocolumns of the Banda Assar syncline latitude, 33° 07' 52 N and longitude 70° 55' 88 E (southwestern Kohat Plateau), showing facies association of the Nagri Formation. (For location, see Fig. 1.4)

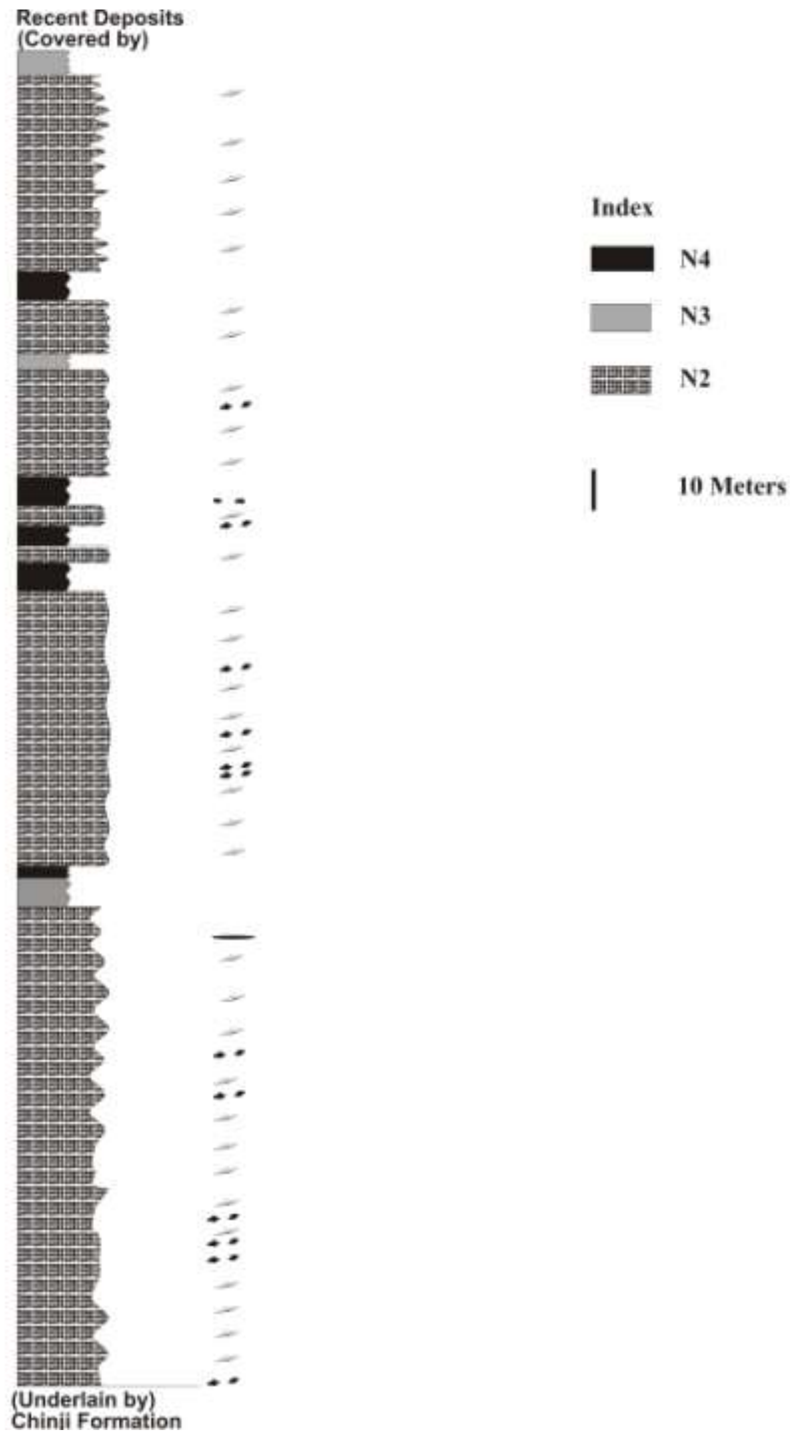

Fig. 5.3C. Measured lithocolumns of the Bahadar Khel anticline, latitude 33° 09' 79 N and longitude 70° 57' 64 E (southwestern Kohat Plateau), showing facies association of the Nagri Formation. (For location, see Fig. 1.4)

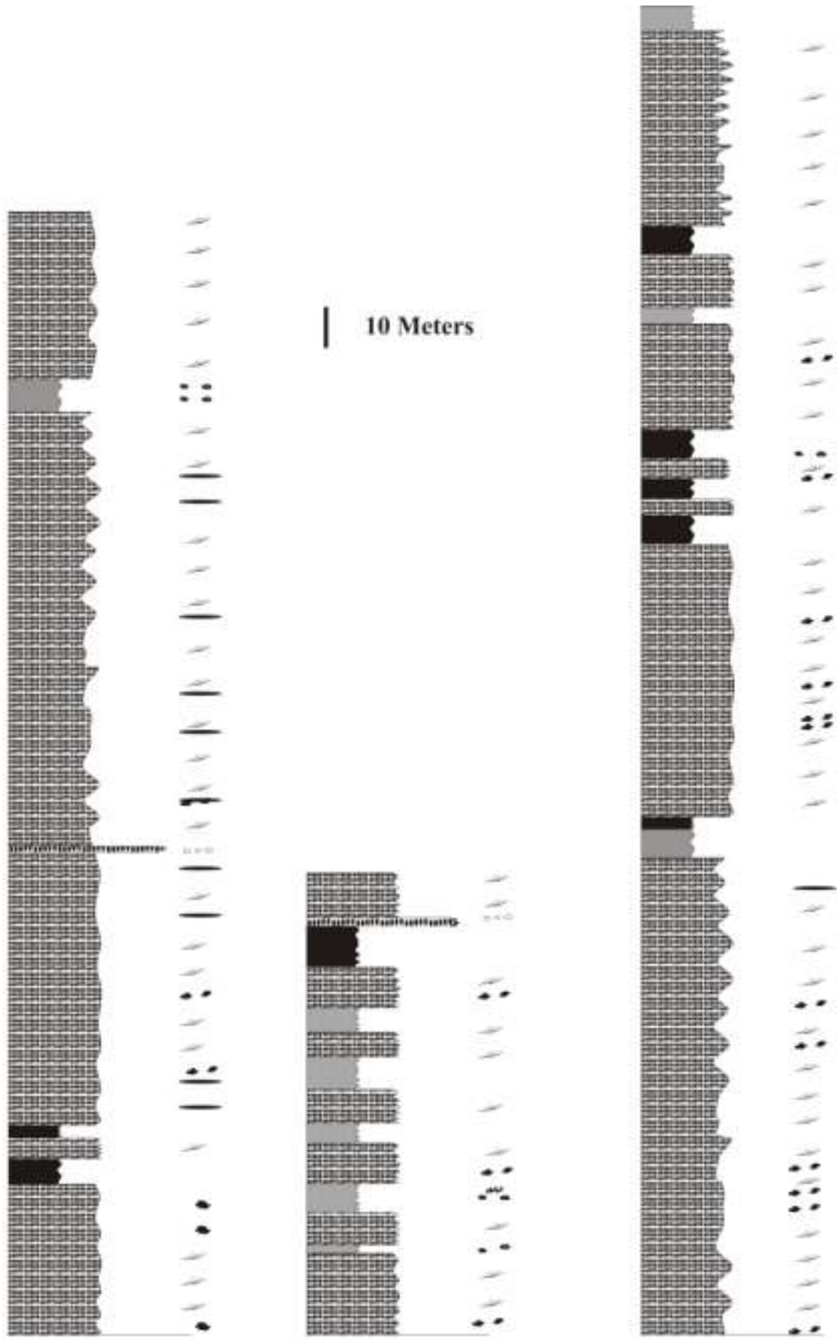

Fig. 5.3D. Measured lithocolumns of the Nagri Formation from (left to right) Chashmai anticline, Banda Assar syncline and Bahadar Khel anticline (southwestern Kohat Plateau) showing facies association. (For locations, see Fig. 1.4)

Thick sequence of sandstone marks the base of the Nagri Formation at Banda Assar syncline (Figs. 5.3B, D). The formation has an exposed thickness of 107 m in this section (Figs. 5.3B, D). The formation is composed dominantly of sandstone interbedded with shale and subordinate clay beds and siltstone (Figs. 5.3A, D). Sandstone grain size ranges from very fine/fine-grained to medium-grained and medium- to thick-bedded. Floodplain deposits are light red/red in color, and some beds are bioturbated.

The Nagri Formation in Bahadar Khel anticline has an exposure of 326 m thick, and is dominantly composed of sandstone with subordinate siltstone, shale and clay beds (Figs. 5.3C, D, Photo 5.25). Sandstone is dominantly grey, fine- to medium-grained and thin- to thick-bedded, and contains lenses of intraformational conglomerate and sparsely embedded gravel/pebbles (Figs. 5.3C, D). Siltstone of the N4 facies exhibits fine lamination. The dominance of sandstone sequences indicates static climatic conditions in the source area.

5.6.1 N1: Channel Conglomerate Facies

Description: This facies represents channel floor deposit, characterized by lenticular beds of crudely stratified conglomerate (Figs. 5.3A, B, D, Photos 5.26, 5.27). The lower contact of the conglomerate beds is typically erosional and most commonly fine upward into sandstone. Conglomerates are mostly confined to thin beds, commonly only a few clasts thick. Clasts sizes of the conglomerate in the base of the formation measured in the field are; 14x10x7 cm, 11x9x7 cm, 5x4x3x cm, 6x4x2 cm, 4x3x2 cm 3x2x1.5 cm, 4x3x3 cm and 5x3x2 cm. Clasts of N1 facies are dominantly intraformational, exceptionally in the middle of the exposed section, where the conglomerate unit is dominantly composed of extrabasinal clasts including quartzite, chert and gneisses. Intraformational clasts are dominantly clay and sand balls.

Interpretation: This facies indicates stream flow deposits, but it may also be a product of rapidly decelerating, high-magnitude, gravel-dominated stream flow under flashy discharge (Rust and Koster, 1984). Coarse channel-floor deposits result from lag gravels deposition in the deeper parts of a channel after winnowing of the finer material (Beerbower, 1964; Allen, 1965). The subangular fragments and poor sorting indicate little reworking by the stream, most probably from the collapse of cohesive bank

Photo 5.25. Thick multistoried sandstone of Nagri Formation overlain by red mudstone with sharp contact. The sandstone represents multistoreyed channel deposits and the maroon red mudstone represents floodplain deposits.

Photo 5.26. Sporadic distribution of gravel in the Nagri Formation. These gravels are disorganize, massive without any orientation indicating rapid deposition.

sediments into the nearby channels. Laury (1971) described a mechanism for cohesive bank collapse involving shearing by rotational slumping, which results in the brecciation of material below thalweg depth.

Conglomeratic channel floor deposits commonly occur as stacked multistory sheets with little or no preserved overbank fines (Collinson, 1996). Some channel conglomerate bodies fines upward into sandstones, suggesting either gradual diminution of flow through diversion or systematic lateral migration of a curved channel reach (Cambell and Hengry, 1987).

5.6.2 N2: Cross-bedded Channel Sandstone Facies

Description: Cross-bedded channel sandstone facies is generally grey in color, fine- to medium-grained and medium to thick bedded. It contains lenses of intraformational conglomerate and sparsely embedded gravel/pebbles at places (Figs. 5.3A-D, Photo 5.28). Individual beds show very little fining-upward tendencies, possibly due to the lack of available grain size variability.

N2 facies is characterized by dominantly trough cross-bedded sandstone (Photos 5.29, 5.30, 5.31, 5.32). Cross-bedded strata most commonly pass upward into ripple laminated sandstone, although in many outcrops they are either erosionally overlain by coarser-grained strata or abruptly overlain by siltstone and mudstone.

N2 facies typically displays sheet geometry and multistorey nature. The base of individual body is delineated by an erosion surface, generally planar or concave-upward (Photos 5.33, 5.34, 5.35, 5.36, 5.37, 5.38). Some thick sandstones consist of single storeys, whereas others consist of several laterally and/or vertically connected storeys. The thickness of individual bodies in the multistorey complex varies from less than one meter to several meters.

Interpretation: The laterally persistent sheets of sandstone, dominated by large trough cross-stratification with subordinate small scale, planar and trough cross-stratification are interpreted as the deposit of a distal, sand-dominant braided fluvial system. Individual channel fill sequences are stacked directly upon each other, with no intervening vertical accretion deposits (Photo 5.39). Storeys exhibiting large-scale inclined strata are channel

Photo 5.27. Intra-formational conglomerate at base of thick sheet sandstone of the Nagri Formation in Gore Nala, near Bahadar Khel old bridge. Limestone clast of intraformational origin can also be seen in the photograph.

Photo 5.28. Grey, thick sheet sandstone of Nagri Formation. Infrequent gravel (both extra- and intra-formation) embedded in sandstone, near Kasho Bridge (Ziarat). Scale in the photo is 15 cm (6”).

Photo 5.29. Thick bed of sandstone with large scale very gentle cross-bedding.

Photo 5.30. Lenticular erosional surface with igneous pebbles in Nagri Formation.

Photo 5.31. Co-set of trough cross-stratification in sandstone of Nagri Formation.

Photo 5.32. Co-set of trough cross-stratification. Close up of Fig. 5.31.

Photo 5.33. Intra-formational conglomerate along the basal part of sandstone bed of Nagri Formation. The conglomerate comprises rip up clast of pedogenic concretions and large mudstone representing channel avulsion on the floodplains.

Photo 5.34. Channel lag deposits at the erosional contact of a multistory sandstone sequence in Nagri Formation near Bahadar Khel old bridge.

Photo 5.35. Multistoried sandstone body separated by erosional surface having intraformational conglomerate. Sandstone beds have trough and planar cross-stratification in Nagri Formation, near Bahadar Khel old bridge.

Photo 5.36. Planar cross-stratified multistoried sandstone body separated by erosional surface in the Nagri Formation, near Bahadar Khel old bridge.

Photo 5.37. Channel lag deposits composed of intraformational pedogenic mudstone in the Nagri Formation, near Bahadar Khel old bridge.

Photo 5.38. Channel lag deposit having sharp, irregular contact with underlying grey sandstone. The sandstone is a small bar on the back of a larger coarser grained conglomerate. The conglomerate bar represents major flooding and bar progradation. During slack and low stage periods, sand is deposited on the lee side. This sand is cross-bedded, while a weak low angle planar fabric is evident in the bigger bars.

5.39. Thick grey sandstone of Nagri Formation having sharp contact with underlying mudstone, near Kasho Bridge (Ziarat). This sandstone bed is calcareous (protruded). The contact of the sandstone with mudstone (white color) shows outline of the channel.

bar deposits, formed by the lateral migration and superposition of different bars within the same channel belt, or by the superposition of different channel belts. Associated intraformational conglomerates along erosion surfaces of storeys are cut bank material eroded during lateral channel migration. The multistorey sandstone bodies result from the superposition of channel bars and fill within the large aggrading channel-belt in fluvial environments before the channel-belt is abandoned (Friend, 1978; Gordon and Bridge, 1987; Bridge and Mackey, 1993). Most of the storeys do not show any upward variation in grain-size, however a few bodies show incomplete cycles.

The presence of trough and planar cross-stratification shows the presence of migrating sinuous-crested and migrating straight-crested dunes, respectively. The latter was formed under conditions of relatively higher flow velocities. The lack of mudcracks and root traces in lowermost portions of channel deposits suggest perennial river flow (Vishnu-Mittre, 1984; Quade and Cerling, 1995). The lack of vertical accretion deposits probably resulted from the erosive capability of numerous concurrently active shifting channels (DeCelles, 1986).

The lack of land plants must have had a profound effect on sand body geometry (Fedo and Cooper, 1989). Smith, D. G. (1976) concluded that loose, non-vegetated sediment could be 20,000 times less stable than the same sediment with 16-18% by volume plant root. The lack of land plants could indicate channel widening rather than channel incising. High lateral and vertical connectivity of the sandstone bodies was probably due to low subsidence rates, resulting in low preservation of overbank fines (Allen, 1978: Kraus and Middleton, 1987).

5.6.3 N3: Interbedded Sandstone, Siltstone and Mudstone Facies

Description: The interbedded sandstone, siltstone and mudstone facies consists of fine- to very fine-grained, thin- to medium-bedded sandstone which shows yellowish/brownish tint in color. Sedimentary structures include small- and large-scale cross-strata, ripple-lamination, parallel-lamination and occasional root marks. No orderly variation of sedimentary structures has been noted, though burrows and root marks tend to occur near the top.

Lateral extents of thin sandstones are meters to tens of meters. Individual large-scale strata in this facies have erosional bases with scour and load structures. Burrow and root traces exhibit various degrees of bioturbation, from a few burrow and/or root traces, to complete obliteration of primary sedimentary structures. Incipient pedogenic features are evident locally, and are typically best developed in the upper few centimeters or decimeters of large-scale strata.

Interpretation: This sandstone is interpreted to be a crevasse channel-fill deposit. Lack of fining upward trend implies low sinuosity of the paleostreams (Ghosh, 1987). Mud clasts at the base are of intraformational origin and are derived locally from the levee and floodplain sediments through which the channel was cut. Textural immaturity implies rapid sedimentation from mixed-load streams. Upward increase of shaly lenses, burrows and root traces may be due to progressive crevasse channel abandonment and waning of current energy (Ghosh, 1987).

In theory, each splay sandstone is likely to have been associated with a single crevasse channel. Furthermore, current ripple cross-lamination, trough cross-stratification and planar stratification were formed by deposition associated with migrating current ripples, dunes, and upper stage plane beds, respectively (Bridge and Diemer, 1983; Bridge, 1993). Trace fossils and incipient pedogenic features indicate that many overbank sand deposits were sites of insect burrowing, plant growth, and weak soil development.

5.6.4 N4: Mudstone Facies

Description: Overbank fines of N4 facies are light red/red in color. There is an internal bedding relationship between the mudstone and thin/medium-bedded siltstone. Siltstone units exhibit fine lamination. Some beds of the overbank fines are bioturbated. Pedogenic surfaces/ calcareous nodules where occur indicates subaerial exposure. No sedimentary structures were observed where invertebrate burrows and pedogenic carbonate nodules are common.

Interpretation: The sandy silt and mud-clay units probably represent levee and minor distal splay deposits, as indicated by the abundant burrows and calcareous concretions (Coleman, 1969; Ethridge et al., 1981; Sutter et al., 1985). Extensive burrows and rootlets acted as pathways for movement of calcareous solutions (Ethridge et al., 1981).

Considering the fluvial lithofacies assemblages, the sequence of N4 facies are typical of a braided river system (Miall, 1977, 1978) and may be related to S. Saskatchewan type. Variability in grain size reflects differences in provenance and/or water stage fluctuations (Cojan, 1993).

The pedogenic characteristics of the fine-grained members indicate that a major proportion of the material was deposited in overbank areas (DeCelles, 1986). The coexistence of red mud intraclasts with reworked accrete nodules in channel sandstones indicates that the red coloration of the fine-grained members developed on a time scale commensurate with that of calcrete development. Therefore, the red colors probably resulted from subaerial exposure and oxidation of iron-rich compounds in overbank areas (DeCelles, 1986).

5.6.5 Depositional System of the Nagri Formation

The Nagri Formation was most probably deposited by sandy bedload rivers. These rivers are dominated by sand, but gravel may be present dispersed in sand. Highly erodible banks of such give rise to high width/depth ratios and to lateral movement both of the whole channel tract and of bars, and island within the tract. Thus sinuosity is rather low and braiding is well developed (Collinson, 1996). The availability of sand is a major control on braided patterns (Smith and Smith, 1984).

The low proportion of mudstone-siltstone facies in Nagri Formation might reflect one or more factors including: (1) low subsidence rates promoting rapid lateral migration of channels and regular erosive removal of flood-basin deposits, (2) an arid climatic regime and limited vegetation allowing greater potential for lateral migration of channels and lesser potential for trapping of fine clastic particles and (3) strongly seasonal discharge resulting in flash flooding and reworking of unconsolidated or semi-consolidated flood-basin deposits as intraclasts.

The consistent presence of purple and brown colored paleosols with calcareous nodules throughout the Himalayan Foreland Basin between 9.7 and 5.23 Ma suggests warm humid climate for deposition of these sediments (Kumar et al., 2004). The change in fluvial architecture from Chinji Formation to Nagri Formation at around 10 Ma suggests a gradual increase in the drainage network (Willis, 1993a, 1993b; Khan, I. A. et al., 1997; Zaleha, 1997a, 1997b; Kumar et al., 2003).

CHAPTER 6

Petrography of the Neogene Sandstone of Southwestern Kohat

6.1 Introduction

Relationship between the detrital components of clastic sedimentary rocks and the tectonic setting of their source area has been discussed by Dickinson (1970), Schwab (1971, 1975), Dickinson and Rich (1972), and Crook (1974), followed by recent syntheses and reviews of Potter (1978, 1984, 1986), Dickinson and Suczek (1979), Ingersoll and Suczek (1979), Valloni and Maynard (1981), Valloni and Mezzadri (1984) and Dickinson (1985, 1988). However, it should be pointed out that detrital composition is controlled by several other important variables including transport history (Suttner 1974; Franzinelli and Potter, 1983), depositional environment (Davies and Ethridge, 1975) and paleoclimate in addition to tectonic provenance (Basu, 1976; Suttner et al., 1981), and nor can diagenetic modifications of sand content be ignored (McBride, 1985). Potter (1978) discussed the inter-relationship of climate and tectonics. Ingersoll (1983) carried out statistical tests of the relationship between composition and depositional facies and showed that the relationship was weak and was far overshadowed by the control imposed by changes in source-area geology.

The provenance of sediment includes all aspects of the source area, e.g., source rocks, climate and relief (Pettijohn et al., 1987). Intensity of weathering is controlled primarily by climate and vegetation. The duration of weathering is controlled by many factors, including relief, slope and sediment storage prior to ultimate deposition, and sedimentation rate. The contribution of various source rocks in a given source area to sand populations derived from that source is largely dependent on intensity of weathering that may be different for different rock types, and relief (Critelli et al., 1997). For example, in areas of intense tectonic/ magmatic activity, source-rock type determines sediment composition more than do climate and relief (Dickinson, 1970). Where tectonism/magmatism is absent, climate and relief are more important in determining composition (Basu, 1976).

This chapter presents petrographic study of medium to fine-grained sandstone of Kamlial, Chinji and Nagri formations collected from three sections i.e. Banda Assar syncline, Bahadar Khel anticline and Chashmai anticline of the southwestern Kohat Plateau. Due to tectonized nature of the region and hence the lack of continuous sedimentary sections and impossibility of along-strike correlation, it is often not possible to identify the stratigraphic placement of a sample more accurately than an assignment to its formation. The quantitative petrographic data is used to establish the composition and also classify the rocks using the scheme designed by Okada (1971) and Basu et al. (1975) after adopting modifications of Tortosa et al. (1991).

6.2. Grain Size Variations and Scale of Sampling

In modern depositional environments, composition of sediments varies with grain size due to four factors: (1) multiple sources providing mineralogically and texturally different sediments, (2) mechanical breakdown of rock fragments into finer sediments, (3) chemical weathering of labile sediments into alteration products, and (4) sorting of compositionally different grains by hydraulic processes (Johnsson, 1993). There are two opposing schools of thought concerning the dependence of sediment composition on grain size; one believes that there is a fundamental dependence of sediment composition on grain size and the other believes that sediment composition is independent of grain size (Ingersoll et al., 1984). The dilemma is unclear as variations in sediment composition downstream are ambiguous. Some researchers have found no clear downstream variation (Pollack, 1961; Naidu, 1966; Breyer and Bart, 1978; Franzinelli and Potter, 1983; Morton and Johnsson, 1993), others have indicated downstream trends of increasing quartz/feldspar ratios, decreasing abundance of unstable lithic fragments and increasing abundance of stable heavy minerals (Mackie, 1986; McBride and Picard, 1987; Johnsson, 1990; Savage and Potter, 1991; Ingersoll et al., 1993; Le Pera and Critelli, 1997).

Similarly, compositional variations for coarse- to fine-grained samples from the New Guinea collisional zone are generally greater than 50% which exceed the analytical error. Medium sand samples generally display average values for most variables (Whitmore et al., 2004). The most consistent variation with decreasing grain size is decreasing rock fragment abundance which indicates that variation in overall composition is dominated by weathering of rock fragments into their constituent minerals. The presence of ubiquitous unaltered volcanic glass and other pristine labile grains suggests the chemical weathering has been relatively minor compared to mechanical weathering (Whitmore et al., 2004).

So, the scale of sampling becomes important for sandstone provenance studies. Some provenance types (e.g., magmatic arc and fold-thrust belts) consist of homogeneous source rocks, and hence order of sampling scale becomes less important. In such settings, Dickinson's provenance types can be used successfully at any scale. In contrast, continental rifts, continental transforms and other complex continental settings contain diverse source rocks, which result in diverse composition at first and second order scale (Ingersoll et al., 1993). Thus the most reliable is the third order sampling of major river systems, deltas and submarine fans that are to be used for developing continental scale petrofacies model (Dickinson and Suczek, 1979; Dickinson, 1985; 1988). However, care should be taken to differentiate between the tectonic setting of the provenance area and that of the basin. In some cases, a sedimentary basin may not receive the greater part of its detritus from a genetically related terrain (Valloni and Maynard, 1981). Similarly, Ingersoll (1990) pointed out that interpretations of the plate-tectonic setting of sandstones should only be carried out at the largest (basin) scale. Ambiguous or misleading results can be obtained if the data are collected locally and reflect only part of a potential source terrain (Ingersoll et al. 1993).

6.3 Petrographic Method

Chips of rock were cut from forty three sandstone samples and were impregnated with casting resin, thinner and a catalyst, and then heated to enable setting of the friable material. Further impregnation with petropoxy was used to make the thin sections (Garzanti et al., 2005).

Grains in thin sections were counted randomly, and grid spacing was adjusted such that to allow more than 300 framework counts per thin section without counting any single grain more than once (Rumelhart and Ingersoll, 1997). The Gazzi-Dickinson method (Gazzi, 1966; Dickinson, 1970) of point counting was used; and crystals greater than 0.0625 mm within lithic fragments were counted as monocrystalline grains (Ingersoll et al., 1984). There are two basic schools of thought concerning the subject: 1) there is a fundamental dependence of modal composition on grain size (the traditional method of the Indiana school i.e., Suttner, 1974; Basu, 1976; Mack and Suttner, 1977); and 2) that modal composition can be determined independently of grain size (the Gazzi-Dickinson method i.e., Gazzi, 1966; Dickinson, 1970).

The primary way in which the Gazzi-Dickinson method differs from the traditional method is that monomineralic crystals and other grains of sand size (> 0.0625 mm) that occur within larger lithics are classified in the category of the crystal or other grain, rather than in the category of the larger lithic (L). The Gazzi-Dickinson method reduces the effects of grain size and alteration on composition and thereby allows accurate determination of original detrital mode and provenance (Ingersoll et al., 1984). Points that did not fall on grains were not counted, so that the totals represent the number of total grains counted (Rumelhart and Ingersoll, 1997).

6.4 Grain Counting

Two point counts were made on each sample, one for quartz-feldspar-lithic (QFL) mode and a second for lithic types. The main categories of grains identified include nonundulatory monocrystalline quartz (Qm_{nu}), undulatory monocrystalline quartz (Qm_{u}), polycrystalline quartz with 2-3 subgrains (Qp_{2-3}), polycrystalline quartz with >3 subgrains ($Qp_{>3}$), plagioclase (P), potash feldspar (K), sedimentary lithic (Ls), carbonate lithic (Lc), volcanic lithic (Lv), metamorphic lithic (Lm) and chert. Undulatory quartz was counted as quartz that becomes extinct with greater than five degrees of stage rotation (Basu et al., 1975). Heavy minerals, carbonate grains, mica and miscellaneous grains were also included in this count (Ingersoll and Suczek, 1979). In the second row 150 lithic points were counted at a spacing of 0.5 mm, and were categorized into volcanic-hypabyssal, quartz-mica tectonites, quartz-mica aggregate, quartz-mica feldspar aggregate, polycrystalline quartz, argillite-shale and miscellaneous (Ingersoll and Suczek, 1979).

For quartz grains types, more than 100 median grains (i.e. grains between 0.25-0.5 mm in size) per thin section of the sandstone of the Neogene molasse sequence were identified and counted as Qm_{nu}, Qm_{u}, Qp_{2-3}, and $Qp_{>3}$ following the procedures recommended by Basu et al. (1975). The relative percentages of the four types of quartz have been plotted on the provenance-discrimination diagram of Basu et al. (1975) with modification of Tortosa et al. (1991). The Qnu-Qu-Qp diagram of Basu et al. (1975) is recommended by Girty et al. (1988) for the discrimination of quartz grains derived from plutonic rocks as well as from metasedimentary rocks. However, Tortosa et al. (1991) suggest that the diagram must be used with caution if plutonic and middle-upper grade metamorphic rocks are present in the source area.

Identifying certain mineral grains and lithics under microscope may present some uncertainties. All microquartz chert grains were classified as cherts, except those with relic mineralogical or structural features, i.e. twinnings for feldspars, laminations and texture for sedimentary rocks; and siliceous shards for volcanic rocks (A´lava and Jaillard, 2005). Only virtually pure silica is classified as polycrystalline quartz (Q_p) using the Gazzi-Dickinson method. The slightest amount of impurities within a chert grain makes it to be classified as sedimentary lithic (Ls); and a single flake of primary mica within a polycrystalline-quartz grain makes it metamorphic lithic (Lm) (Ingersoll et al., 1984).

Lithic were identified using the criteria of Ingersoll and Suczek (1979), given below:

1) volcanic-hypabyssal: lithic grains recognized by the presence of felsitic, microlitic or lathwork texture;
2) quartz-mica tectonite: lithic grains composed of quartz and mica, and having a preferred planar fabric;
3) quartz-mica aggregate: lithic grains composed of quartz and mica, but without a preferred planar fabric;
4) quartz-mica-feldspar aggregate: lithic grains composed of quartz, mica and feldspar, and generally without planar fabric;
5) polycrystalline quartz (including chert);
6) argillite-shale: dark, semi-opaque, fine-grained detrital aggregates;
7) indeterminate-miscellaneous: lithic grains not clearly fitting into any of the above categories.

Metamorphic lithics were divided into schists and tectonites, and grains with well-developed schistosity were classified as schist. Sedimentary lithics were divided into sandstone, mudstone and limestone (extrabasinal carbonate) classes (Zuffa, 1980).

6.5. Sandstone Modal Composition and Tectonic Settings

Dickinson and Suczek (1979), Valloni and Maynard (1981), and Ingersoll et al. (1984) found that the following modal quantities are useful in diagnosing the tectonic environment of clastic sedimentary rocks.

Qm: Monocrystalline quartz

Qp: Polycrystalline quartz

Q: Monocrystalline and polycrystalline quartz grains, Q = Qm +Qp

P: Plagioclase

K: Potassium feldspar

F: Monocrystalline feldspar; F = P + K

Lv: Volcanic (hypabyssal) fragments

Ls: Sedimentary fragments, including chert

Lm: Metamorphic fragments

L: Polycrystalline lithic fragments; L = Lv + Ls + Lm

Lt: L + Qp

D: Dense minerals

On the basis of these modal parameters, Dickinson and Suczek (1979) distinguished nine provenance types with different tectonic setting (Table 6.1):

Different discriminatory plots have been proposed for determining sandstone provenance including Q-F-L, Qm-F-Lt, Lm-Lv-Ls, Qp-Lv-Ls (Qp-Lmv-Lms) and Qm-P-K, which identify specific tectonic setting for arrenaceous sediments. On the Q-F-L diagram, points for continental block, magmatic arc, and recycled orogen provenances occupy discrete fields. Owing to their high chert content, subduction complex suites plot far away from nearly all points of other recycled orogen suites on the Qm-F-Lt diagram (toward the Lt pole). The Qp-Lv-Ls diagram is particularly useful for distinguishing magmatic arc suites (with sources in arc orogens) from recycled orogen suites (with sources mainly in collision orogens). Most continental block suites do not appear on the diagram, for the Qp-Lv-Ls values are not calculated when the total content of lithic fragments is less than 10% (Dickenson and Suczek, 1979). Lithic populations of magmatic arc sand and sandstone are dominated by volcanic grains, whereas lithic populations of rifted continental margin sand and sandstone are dominated by polycrystalline quartz and sedimentary grains (Ingersoll, and Suczek, 1979).

The fundamental differences expressed by the Qp-Lvm-Lsm and Lm-Lv-Ls triangular plots are that: 1) magmatic arcs consist of fine-grained volcanics with subordinate amounts of fine-grained metasedimentary material; 2) suture belts lack

Table 6.1. Framework composition, depositional basins and weathering effects on sandstones of different tectonic provenance (Dickenson and Suczek, 1979).

Tectonic provenance	Source rocks	Derived sediment		Type of depositional basin	Influence of climate and transport
		Sand	Gravel		
Continental Block					
A. Craton interior	Granitic and gneissic basements; subordinate sedimentary and metasedimentary rock from marginal belts.	Quartz arenites and minor arkoses; high ratio of K-feldspar to plagioclase; minor lithic arenites	Minor quartzite(?); most clasts probably do not survive transport(?)	Platform settings, interior basins, foreland basins, passive continental margins and bordering oceans	Severe under humid conditions and long transport
B. Uplifted basement blocks	Granitic and gneissic basement plus sedimentary or metasedimentary cover; possible volcanic rocks	Feldspathic arenites and arkoses; minor sedimentary/ metasedimentary or volcanic lithic arenites	Granite and gneiss clasts; minor sedimentary/ metasedimentary clasts	Fault-bounded interior basins formed by incipient rifting or wrench faulting	Probably minimal owing to rapid erosion and short transport distance
Magmatic Arc					
A. Undissected	Mainly andesitic to basaltic volcanic rocks	Lithic arenites composed of volcanic rock fragments and plagioclase grains; minor volcanic quartz	Andesite or basalt clasts	Forearc, backarc, and intra-arc basins; trenches; possibly abyssal-plain basins	Probably minimal owing to rapid erosion and short transport distance
B. Dissected	Andesitic to basaltic volcanic rocks; plutonic igneous, metaigneous(?)	Mixtures of volcanic-derived rock fragments and plagioclase plus K-feldspar and quartz from plutonic sources	Andesite, basalt, plutonic igneous, or metaigneous clasts	Same as undissected arcs	Moderate effect of climate(?); minimal effect of transport
Recycled Orogen					
A. Subduction complexes	Ophiolite sequences (ultramafic rocks, volcanic rocks, chert); greenstones; argillites, graywackes; limestones; blueschists	Chert a key component (may exceed combined quartz and feldspar); may include sedimentary, ultramafic, volcanic rock fragments	Chert, greenstone, argillite, sandstone, limestone, serpentinite	Forearc basins, trenches; possibly abyssal-plain basins	probably minimal owing to rapid erosion and short transport distance
B. Collision orogens	Mainly sedimentary and metasedimentary rocks; subordinate ophiolite sequences, plutonic basement rocks, volcanic rocks	Intermediate quartz content; high quartz/feldspar ratio; abundant sedimentary and metasedimentary clasts, which may include chert from mélange terrains or nodular limestones	Sedimentary and metasedimentary clasts, minor plutonic igneous, volcanic clasts, chert.	Remnant ocean basins, foreland basins, basins developed along suture belts	Probably moderate to minimal
C. Foreland uplifts	Mainly sedimentary successions within fold-thrust belts; minor plutonic igneous, and metamorphic(?) rocks	Most diagnostic is high quartz with low feldspar content, but variable association of quartz, feldspar, chert	Sedimentary clasts, chert, minor plutonic igneous or metamorphic clasts	Mainly in foreland basins	Probably moderate to minimal.

significant volcanics, but primarily consist of uplifted sedimentary and metasedimentary terrains as well as high-grade gneisses terrains (the latter produce mainly quartz and feldspar, as do plutonic terrains) (Ingersoll and Suczek, 1979).

According to Gergen and Ingersoll (1986):

1) The continental margin forearc sands have approximately equal proportions of quartz, feldspar and lithic grains. On the Lm-Lv-Ls diagram, the forearc samples show moderate proportions of metamorphic, volcanic and sedimentary lithics.
2) The backarc samples are characterized by low amounts of quartz and feldspar and high lithic content. P/F is 0.96. The backarc samples on Lm-Lv-Ls plot show low proportions of metamorphic and sedimentary, and high proportions of volcanic lithics.
3) Sands from continental margin transform-fault setting are predominantly lithic. The lithic fragments are mainly composed of sedimentary and metasedimentary types, with low to moderate proportions of volcanic types. Qp/Q is 0.03, and P/F is 0.86.
4) Sands from continental margin trench settings consist of moderate proportions of quartz and feldspar, and low to moderate proportions of lithic grains; lithic grains are dominantly volcanic, with moderate proportions of metamorphic and low proportions of sedimentary types. Qp/Q is 0.01, and P/F is 0.74.
5) Sands from the continental margin ridge-trench-fault triple-junction setting are characterized by high feldspar, moderate quartz and low lithic proportions. Lithic fragments are dominantly sedimentary, with moderate proportions of metamorphic and volcanic types. Qp/Q is 0.01, and P/F is 0.87.
6) Both the Qp-Lvm-Lsm and Lm-Lv-Ls triangular plots are useful in differentiating among sands derived from suture belts, magmatic arc and rifted continental margins (Ingersoll and Suczek, 1979).

Similarly, Dickinson and Rich (1972) have reported that 1) sandstones derived from andesitic volcanics are characterized by L > F, Q low, and V/L high; 2) sandstones derived from highlands in which volcanic, sedimentary, and low grade metamorphic rocks are exposed are characterized by L exceeds F, Q is moderate, and V/L is low; and 3) sandstones derived from deeply eroded areas exposing plutonic igneous rocks and high grade gneisses are characterized by F exceeds L, Q is moderate, and V/L is low.

6.6 Sandstone Framework Particles

Quartz: The high overall abundance of quartz in sandstone is unsurprising. Quartz is a common constituent in rocks such as granite, gneiss and schist, which make up much of the Earth's crust. Quartz is also resistant to both physical and chemical attacks (Prothero and Schwab, 2003). Monocrystalline quartz grains having fluid-filled vacuoles indicate hydrothermal veins provenance. The quartz grains exhibiting uneven or undulose/undulatory/wavy extinction indicate distortion of their crystal lattice during tectonic deformation, prior to deposition in sedimentary basin. Stresses in sedimentary sequences are usually insufficient to produce this degree of deformation. Undulatory extinction characterizes quartz derived from metamorphic source rocks; nonundulatory extinction indicates volcanic rocks sources or grains recycled from older sandstones (Basu, 1985).

Quartz grains of metamorphic origin are generally polycrystalline in nature. Extinction may be straight or undulose. Inclusions of metamorphic minerals (e.g. micas, garnets) may also be present (Basu, 1985). Young (1976) has shown that polycrystalline quartz can develop from monocrystalline quartz during metamorphism. Under the influence of increasing pressure and temperature, nonundulatory monocrystalline quartz changes progressively to undulatory quartz, polygonized quartz (quartz that shows distinct zones of extinction with sharp boundaries), and finally to polycrystalline quartz.

The content of the four quartz types varies with grain size and source lithology. Qp content decreases with decreasing grain size. This trend is produced by grains breaking along crystalline boundaries. Thus $Qp_{>3}$ break down to $Qp_{2\text{-}3}$ and, finally to monocrystalline quartz types in the fine fractions. The Q_u content tends to decrease in the fine sand fractions in samples of granitic and gneissic origin. Basu (1976) related this to their low mechanical and chemical stability compared with Q_{nu}. However, Tortosa et al. (1991) pointed out the difficulty of observation of this character in fine sand.

The influence of source lithology on quartz types is considered for the medium sand fraction. Granite derived sands have Q_{nu} = 42 %, Q_u = 40 %, $Qp_{2\text{-}3}$ = 14 % and $Qp_{>3}$ = 4 %. Sands of gneissic origin have Q_{nu} = 51 %, Q_u = 15 %, $Qp_{2\text{-}3}$ = 23 % and $Qp_{>3}$ = 11 %. Sands derived from slates and schists have Q_{nu} = 20 %, Q_u = 12 %, $Qp_{2\text{-}3}$ = 5 % and $Qp_{>3}$ = 63 %. Monocrystalline quartz types are predominant in sands from granitic and gneissic sources, whereas polycrystalline quartz types constitute the main population of quartz grains in sands derived from slates and schist (Tortosa et al., 1991).

The difference in the Q_u contents of Basu et al. (1975) i.e. 4% and Tortosa et al. (1991) i.e. 40% for the same type of source (i.e., granitic source) made the latter of the view that the content of Q_u may not be used to distinguish between plutonic and high rank metamorphic provenances. Tortosa et al. (1991) related the difference in Q_u contents in sands of granitic origin to a number of factors, including strain history, magma crystallization conditions, particularly high viscosity, emplacement of the pluton, uplift and decomposition.

All fractions of sands derived from slates and schists plot near the quartz-lithic (QL) edge. Quartz-grain proportions increase at the expense of lithics with decreasing grain size. In very fine-grained source rocks, the lithic percentage is high even in the fine-grained fractions. Variation of feldspar content is very low (Tortosa et al., 1991).

Sands from gneissic sources plot variably on diamond-shaped diagram according to metamorphic rank rather than lithology. Sands of granitic origin have remarkable variations due to different Q_u contents of different massifs. These sands plot in all three fields of the diagram, although they always plot in the central area with low amounts of polycrystalline quartz. In short, the diamond-shaped diagram of Basu et al. (1975) acceptably discriminates sands derived from slates and schists, but sands of plutonic origin show wide dispersion (Tortosa et al., 1991).

Feldspar: High feldspar content in sandstone carries specific implications about source area climate and topography. It means that chemical weathering is not extensive, probably because of climate and/or high source relief. Low precipitation in an arid setting, or an arctic climate in which precipitation occurs as snow and ice rather than as rain, limits hydrolysis and produces feldspar-rich debris. Even in climates that usually promote decomposition to clays (for example, a warm and humid climate), feldspars can survive if relief is high because fast-moving streams will erode feldspar before it decompose (Prothero and Schwab, 2003).

The two principal feldspar families, potash feldspar (orthoclase, sanidine, and microcline) and plagioclase (Na-Ca), differ in abundance in sedimentary rocks. The potash feldspar is much more common in sandstones than the plagioclase because i) K-feldspar has a greater chemical stability than plagioclase, and ii) the fact that K-feldspar is much more common in continental basement rocks (granites and acid gneisses). Plagioclase is relatively common in sandstones sourced from uplifted oceanic island-arc terrains, which have been rare source areas in sedimentary history (Tucker, 2001). Detrital feldspars from metamorphic sources are mostly microcline, while those from volcanic sources are generally sanidine (Basu, 1976). Sanidine is a high-temperature alkali feldspar that has retained its high-temperature structure because it cooled quickly. Microcline's pericline-albite ("tartan") twinning records its inversion from high-temperature monoclinic form to lower-temperature triclinic form during slow cooling, such as occurs in large plutons or after regional metamorphism but never in volcanics. Thus, microcline in detrital rocks indicates that old shields or the cores of orogens have been unroofed (Mclane, 1995).

The anorthite component of plagioclase is far less frequently encountered in continental source rocks than is the albite component. It is because of the commonness of intermediate and silicic rocks at the surface of the continents. However, it is also the result of the low stability of anorthite (Pettijohn et al., 1987). In plagioclase, compositional zoning occurs primarily in igneous rocks of intermediate composition and their gneissic equivalents but rarely in granites or gabbros or their extrusive equivalents (Mclane, 1995).

Chemical alteration of feldspar typically involves replacement by clay minerals such as sericite (a variety of muscovite), kaolinite and illite. Incipient alteration gives the feldspars a dusty appearance, where complete replacement produces clay-mineral pseudomorphs. Feldspar alteration takes place at the site of weathering, if it is dominantly chemical rather than physical weathering, and during diagenesis, either on burial or subsequent uplift. Diagenetic replacement of feldspar by calcite is also common (Tucker, 2001).

Lithics: A variety of lithic clasts may occur in sedimentary rocks those have a wealth of knowledge about their provenance. Identification criteria of lithics are given earlier in detail in section 2 of this chapter.

Heavy Minerals: Heavy minerals generally form <1% of a sand or sandstone, but they are important indicator of provenance. These mineral suites with their attested provenances are listed in Table 6.2. Certain heavy minerals, for example, garnet, epidote and staurolite indicate a metamorphic source terrain, whereas rutile, apatite and tourmaline suggest igneous source rocks (Tucker, 2001).

Coarse micas: Muscovite and chlorite are derived primarily from metamorphic rocks, but biotite also occurs in basic intrusive and volcanic rocks, and in granites. Muscovite also occurs in granites, pegmatites, aplites and rhyolite porphyries, but is less common than biotite (Boggs, 1992). Muscovite's greater abundance in sandstones, compared to biotite, probably reflects both its superior chemical stability and its abundance in metamorphic rocks. Abundant micas in sandstone suggest, but do not prove, a metamorphic source (Boggs, 1992).

Table 6.2. Heavy mineral assemblages of the major source rocks (condensed from Blatt et al., 1980; Pettijohn et al., 1987; Boggs, 1992)

Heavy mineral assemblages	Source rock
Apatite, biotite, hornblende, rutile, tourmaline (pink variety), zircon, monazite, sphene, magnetite, muscovite.	Acidic igneous rocks
Fluorite, topaz, tourmaline (blue variety), beryl, monazite, cassiterite, muscovite.	Granite pegmatites
Augite, chromite, diopside, ilmenite, olivine, magnetite, anatase, brookite, rutile	Basic igneous rocks
Phlogopite, staurolite, zoisite etc.	Contact metamorphic rocks
Andalusite, epidote, garnet, glaucophane, kyanite, silliminite etc.	Dynamothermal metamorphic rocks
Rutile, tourmaline (rounded grains), zircon (rounded grains), sphene	Reworked sediments
Andalusite, staurolite, chondrodite, corundum, topaz, tourmaline, vesuvianite, zoicite, wollastonite, chlorite, muscovite.	Low-grade metamorphic, contact metamorphic
Garnet, epidote, zoicite, staurolite, kyanite, sillimanite, andalusite, magnetite, ilmenite, sphene, zircon, biotite.	Higher-grade metamorphic, dynamothermal metamorphic

Diagenesis: Quartz overgrowth is one of the most common types of silica cement that indicate diagenesis. In quartz overgrowth, silica cement is precipitated around the quartz grain in optical continuity, so that the grain and cement extinguish together under crossed polarizers. In many cases the shape of the original grain is defined by a thin iron oxide/ clay coating between the overgrowth and the grain, termed as dust-line. However, a thicker clay rim around the quartz grain does not allow precipitation of a syntaxial overgrowth (Tucker, 2001).

Silica cement has frequently been attributed to pressure dissolution. Pore solutions become enriched in silica which is then reprecipitated as overgrowths when supersaturation is achieved. Quartz overgrowths in sandstones without pressure dissolution effects may reflect significant upward migration of silica-rich solutions from more distant sites of pressure dissolution, or indicate another source of silica. Possible sources are dissolution of silica dust, biogenic silica and ground water. Silica dust could be derived from grain abrasion, especially if it is an aeolian sandstone. Dissolution of feldspars, amphiboles and pyroxenes as well as minerals transformations from montmorillonite to illite and feldspar to kaolinite would provide silica (Tucker, 2001).

Carbonates, commonly the early precipitated cement in sandstone are another important type of cement. Calcite, a common carbonate cement usually occurs in grain-supported sandstones, for example in quartz arenites and litharenites. The presence of early precipitation of calcite generally stops later quartz overgrowth formation and feldspar alteration to clays but may result in total loss of porosity and permeability. In other sandstones, calcite is a later precipitate, postdating quartz overgrowths and authigenic kaolinite (Tucker, 2001).

6.7 Petrography of the Neogene Molasse Sequence

The petrologic composition of the “molasse” and “flysch” sediments deposited in an area > 10^7 km^2 south/southwest of Himalayan Range records the continental collision history of the India and Asia. The sandstone petrology unveils the geological evolution of a suture belt, from initial subsidence of collisional basins to later stages of uplift, exhumation and unroofing (Garzanti et al., 1996). The stratigraphic succession in study area has been conventionally divided into (1) the basal section, i.e. the Kamlial

Formation; (2) the middle section, i.e. the Chinji Formation; and (3) the upper section, i.e. the Nagri Formation, and is discussed below.

6.7.1 Kamlial Formation (n = 10): Sandstone of the Kamlial Formation is mostly matrix (dominantly carbonate) supported. The sandstone is mainly well to moderately sorted, with sand particles generally subangular to subrounded. Quartz (Q), chiefly monocrystalline, is the dominant detrital constituent of the Kamlial sandstone. The abundance of quartz generally increases upsection from < 60% in the lower and middle parts to ≥ 60% in the upper part of the formation. The average quartz and feldspar (F) contents are, respectively, 50.9 and 25.3% (Q/F=2.0) in the Banda Assar syncline, 60 and 23.6% (Q/F=2.5) in the Chashmai anticline, and 54 and 22.9% (Q/F=2.4) in the Bahadar Khel anticline. The average abundance of feldspar is approximately similar in all the three sections. Though the overall range of feldspar is 9 to 33%, but generally falls between 18 to 30%. Lithic grains show a much wider range of variation from 11 to 35%.

The nonundulatory type of monocrystalline quartz (Q_{nu}) is more dominant than the undulatory one (Q_u) in the Chashmai anticline and Banda Assar syncline, but Q_u is more at the Bahadar Khel anticline. The detrital feldspar component of the Kamlial Formation is dominated by alkali feldspar. The average P/F ratios are 0.39, 0.32 and 0.26 in the Banda Assar syncline, Chashmai anticline and Bahadar Khel anticline, respectively. Some of the feldspar grains are kaolinized or sericitized (Plate 6.1). Grains of microcline and perthitic alkali feldspar as well as fresh plagioclase have also been noted (Plate 6.2).

Lithic fragments are mainly sedimentary (Ls) (argillite, shale and chert) (Plate 6.3). However, volcanic (Lv) and low-grade metamorphic (Lm) (slate and schist) lithics also occur in appreciable amounts (Plates 6.4, 6.5, 6.6). The average contents of lithic fragments are: Lm = 23%, Lv = 37%, Ls = 40% in the Banda Assar syncline, Lm = 24%, Lv = 13%, Ls = 63% in the Chashmai anticline and Lm = 23%, Lv = 22%, Ls = 55% in the Bahadar Khel anticline.

Metamorphic lithics are dominantly of quartz-mica schist and slate in all the three sections (Plates 6.4, 6.5, 6.6). Other metamorphic lithics include mica-schist, phyllite and quartzite (Plates 6.5, 6.6). Mica-schist is consistently present throughout the Banda Assar syncline and Bahadar Khel anticline. Sedimentary lithics include mudstone, lime mudstone and siltstone.

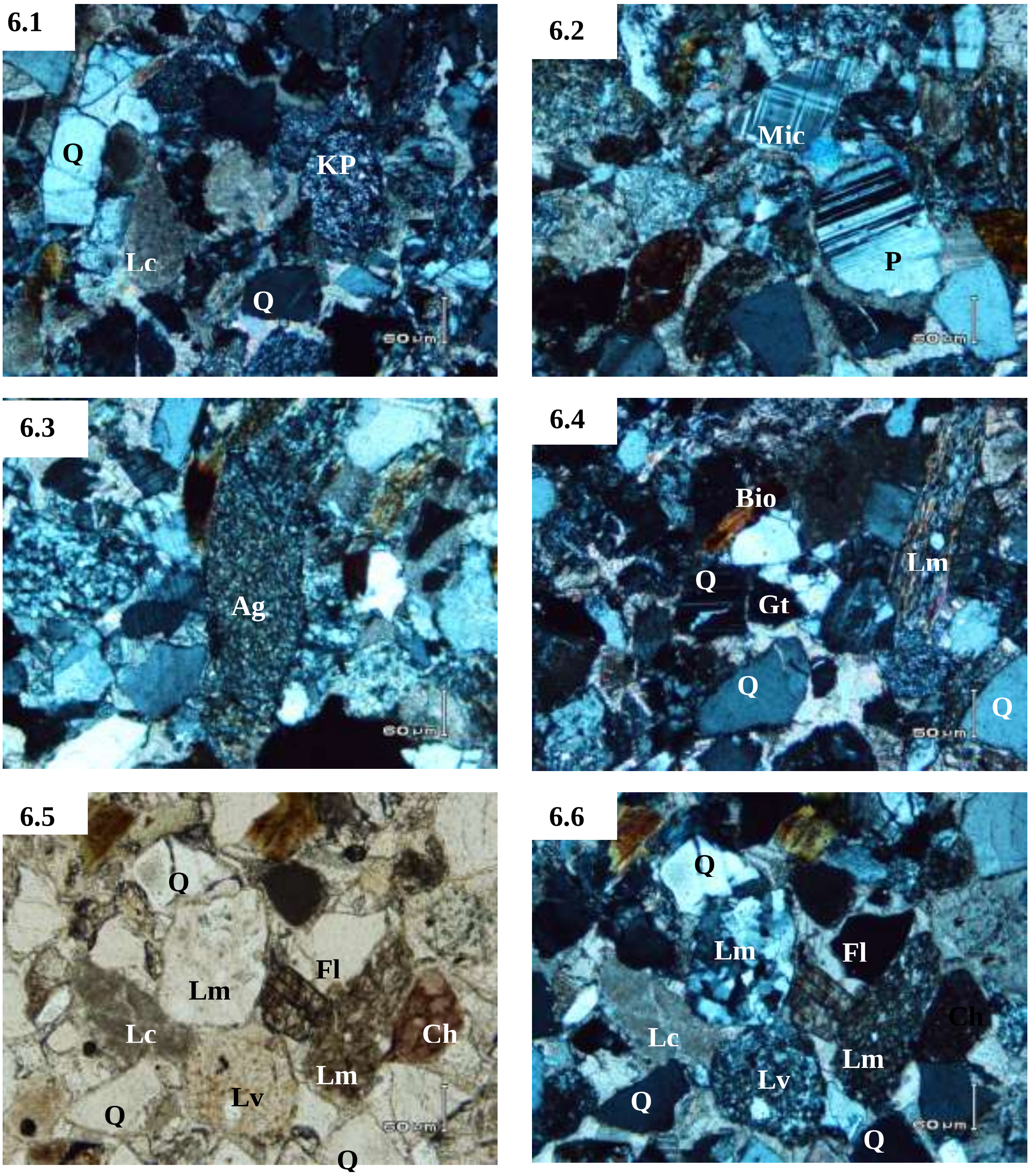

Plates 6.1-6.6: Photomicrographs of the Kamlial and Chinji sandstones: **6.1** Kaolinized plagioclase (KP), carbonate lithic (Lc) (micritic) and quartz (Q) (XPL). Fractures in quartz grain (left) are filled with carbonate. **6.2** Fresh plagioclase (P) and microcline (Mic) displaying the characteristic albite polysynthetic and cross-hatched twinning, respectively (XPL). **6.3** Argillite (Ag). A lithic clast composed of fine grained material (XPL). **6.4.** Quartz (Q), garnet (Gt), metamorphic lithic (Lm) and biotite (Bio) (XPL). Quartz grains are subangular to subrounded, garnet is isotropic, biotite is oxidized, and the metamorphic lithic is of quartz-mica schist. **6.5, 6.6.** Quartz (Q), volcanic lithic (Lv), metamorphic lithic (Lm), carbonate lithic (Lc), chert (Ch) and fluorite (Fl) (PPL, XPL). Subangular quartz grain having a fracture filled with carbonate. A number of lithic grains can be identified. Metamorphic lithic grains shown in the photomicrograph are of quartzite and quartz-mica schist. Chert (Ch) derived from sedimentary sources can be mistaken for very finely crystalline volcanic rock fragments or clay clasts if not carefully examined.

Of the total frameworks in the Kamlial Formation, mica (Plates 6.7, 6.8) ranges from 3 to 6% at the Chashmai anticline, 2.6 to 7% at the Banda Assar syncline, and 1.3 to 15% at the Bahadar Khel anticline. The maximum amounts of mica (i.e., 7% and 15%) occur in the upper part of the formation at the Banda Assar syncline and Bahadar Khel anticline, respectively. Biotite prevails in all the three sections and is dominantly oxidized. Some of the mica flakes are highly deformed.

Trace amounts of a number of heavy minerals also occur in the Kamlial Formation. These include epidote, garnet, monazite, ilmenite, rutile, apatite, chromite and fluorite (Plates 6.4, 6.5, 6.6, 6.9, 6.10, 6.11, 6.12). In addition to discrete grains, zircon, monazite and muscovite also occur as inclusions in different grains of quartz. As pointed out earlier, carbonate is the dominant constituent of the matrix. Besides, carbonate also occurs as fracture-fills and/or replacing relatively unstable framework grains along cracks and cleavages in several of the studied thin sections. Fractures in grains of quartz are divisible into two: (1) filled with calcite and (2) those without any calcite filling. The former probably developed by compaction during burial and the latter during tectonic uplift (Abbasi and Friend, 1989). A few quartz grains have incipient silica overgrowths. The quartz overgrowths may be the result of pressure dissolution, when the grains are buried under the pressure of the overlying rocks (Pettijohn et al., 1987).

6.7.2 Chinji Formation (n = 12): The dominantly matrix supported sandstone of the Chinji Formation is moderately to well sorted and its framework grains are angular to rounded. The matrix is dominantly carbonate. The average framework composition of the sandstone is Q= 44%, F= 24%, L = 32% (Q/F = 1.9) at the Banda Assar syncline, Q = 59, F= 27, L= 12% (Q/F = 2.2) at the Chashmai anticline, and Q= 54, F=28, L = 18 %(Q/F = 2.0) at the Bahadar Khel anticline, respectively. Monocrystalline quartz (Qm) dominates in all the three sections of the Chinji Formation with average Qm/Qp ratio of 25.8 at the Banda Assar syncline, 18.5 at the Chashmai anticline and 15.3 at the Bahadar Khel anticline. Q_{nu} is dominant at the Chashmai anticline, but is suppressed by Q_u at the Banda Assar syncline and Bahadar Khel anticline. Alkali feldspar is the dominant feldspar in the Chinji Formation, increasing upsection relative to plagioclase in the Chashmai anticline, but decreasing upsection at the Banda Assar syncline. The average P/F ratios of the Chinji Formation are 0.40, 0.42 and 0.28 in the Banda Assar syncline, Chashmai anticline and

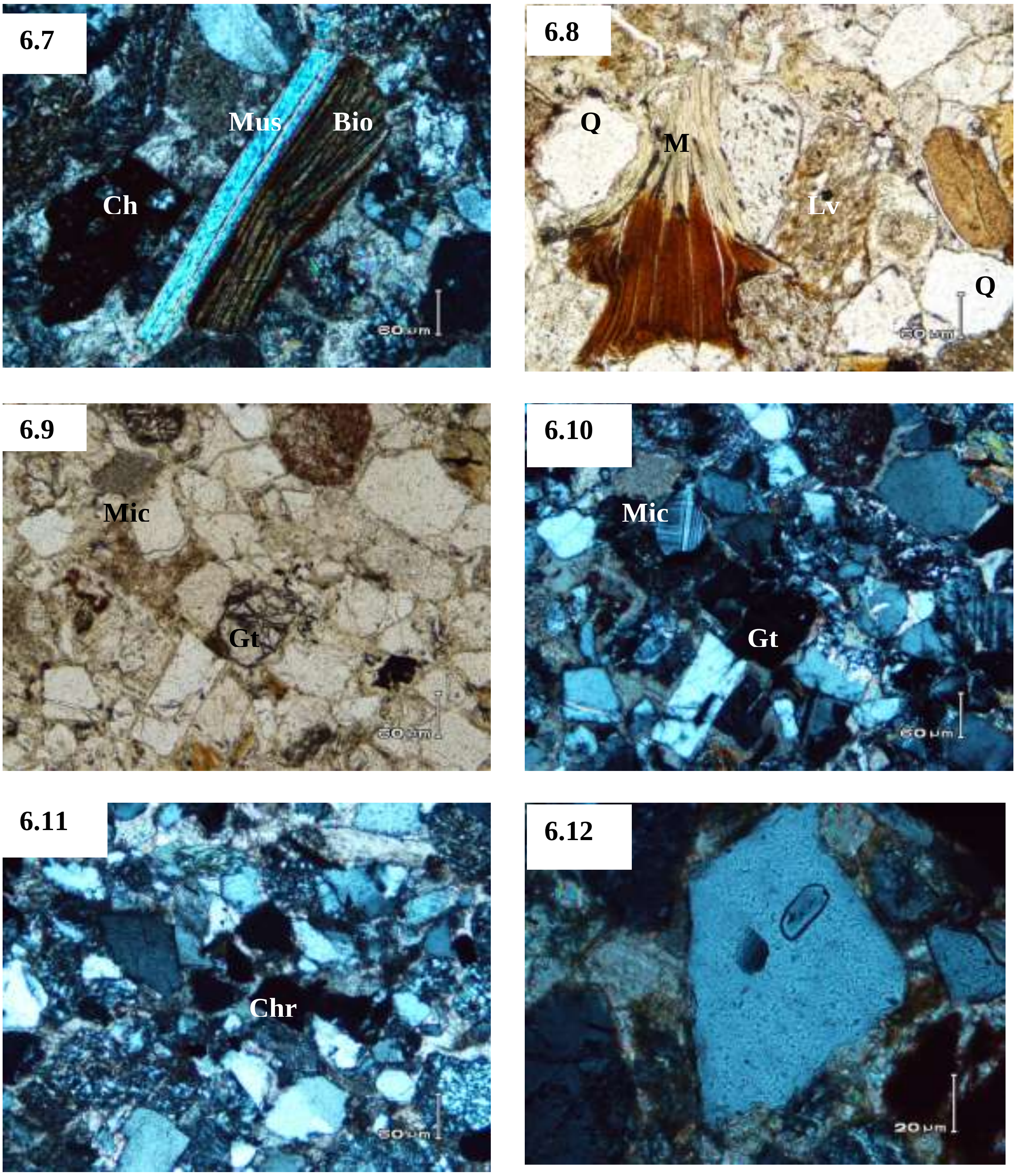

Plates 6.7-6.12: Photomicrographs of the Kamlial and Chinji sandstones: **6.7.** This photomicrograph contains biotite (Bio), muscovite (Mus) and chert (Ch) (XPL). **6.8.** Mica (M), quartz (Q) and volcanic lithic (Lv) can easily be identified (PPL). **6.9 & 6.10.** Garnet (Gt) and microcline (Mic) (PPL & XPL). Garnet has high relief and is isotropic. Microcline with typical grid twinning. **6.11.** Chromite (Chr) is in the center of the photomicrograph (XPL). **6.12.** Quartz containing tiny inclusions of zircon/monazite (XPL).

Bahadar Khel anticline, respectively. The occurrence of microcline is also relatively more common in the Chinji sandstone than in the Kamlial sandstone (Plates 6.2, 6.9, 6.10).

Lithic fragments range from 12 to 32% in the Chinji sandstone and are dominated by sedimentary lithics including chert (Plate 6.3). The lithic fragment composition of the formation at the Chashmai anticline is dominated by Ls (averaging 81%) followed by Lm (averaging 16%) (Plates 6.4, 6.5, 6.6). The occurrence of Lv (Plates 6.5, 6.6) is confined to the upper part of the formation only and constitutes 10% of the lithic grains. Lm decreases upsection at the Chashmai anticline. At the Banda Assar syncline, the formation is dominated by Lv (averaging 48%), followed by Ls (averaging 36%), and Lm (averaging 16%). Lv shows an upsection increase from 43 to 53% whereas Lm shows upsection decrease from 19 to 13%. The average content of lithic fragments at the Bahadar Khel anticline is: Ls = 52%, Lv = 27% and Lm = 29%. Metamorphic clasts are dominantly low-grade mica-schist, quartz-mica schist (Plates 6.4, 6.5, 6.6) and slate while the sedimentary clasts include mudstone and lime mudstone.

Of the total frameworks in the Chinji Formation, mica (Plates 6.7, 6.8) ranges from 3 to 9% at the Chashmai anticline, 0 to 3% at the Banda Assar syncline and 1 to 9% at the Bahadar Khel anticline. The dominantly oxidized and/or highly deformed flakes of biotite occur in almost all the three sections.

Heavy minerals of the Chinji Formation include epidote, monazite, apatite, garnet, rutile and brown hornblende (high-grade metamorphic hornblende) (Plates 6.4, 6.5, 6.6, 6.9, 6.10, 6.11). The quartz grains contain inclusions of zircon, monazite, rutile, epidote and mica. Authigenic carbonate is abundant in all the samples and appears to have selectively replaced unstable framework components. Besides, carbonate also occurs as fracture-fills in some framework grains along cracks and cleavages. These carbonate-filled fractures in quartz grains are probably developed by compaction during burial, and unfilled fractures are developed during tectonic uplift (Abbasi and Friend, 1989). The incipient silica overgrowths in some quartz grains also suggest pressure dissolution under the pressure of the overlying rocks (Pettijohn et al., 1987).

6.7.3 Nagri Formation (n = 16): Sandstone of the Nagri Formation is dominantly matrix supported, however, grain supported sandstone also occur locally. The matrix is mainly carbonate, but rarely clay also occurs. Texturally, the sandstone is moderately sorted to well sorted. Constituent grains of the sandstone are chiefly subangular to subrounded. Composition of the Nagri sandstone is Q = 62.9-73.4 % (Ave. 67.5 %), F = 18.2-31.5 % (Ave. 22.1 %) and L = 4.5-16.7 % (Ave. 9.7 %) at Chashmai anticline, Q = 43.9-63.4 % (Ave. 52.5 %), F = 24.3-36.3 % (Ave. 29.3 %) and L = 11.7-25.6 % (Ave. 18.1 %) at Bahadar Khel anticline and Q = 44.5-55.9 % (Ave. 49 %), F = 16-21.9 % (Ave. 19.5 %) and L = 28.7-34.5 % (Ave. 31.2 %) at Banda Assar syncline. The ratio of Q/F is 3 at Chashmai anticline, 2.5 at Banda Assar syncline, and 1.8 at Bahadar Khel anticline. Monocrystalline quartz dominates over polycrystalline quartz in all the three sections. In monocrystalline quartz, Q_u dominate over Q_{nu} at all the three studied sections, except in upper part of the formation at Chashmai anticline.

Alkali feldspar dominates over plagioclase in all sections of the Nagri Formation. The average ratios of P/F of the Nagri Formation are 0.36 at the Chashmai anticline, 0.3 at the Banda Assar syncline and 0.22 at the Bahadar Khel anticline. Perthitic feldspar, microcline, fresh plagioclase and altered feldspar have also been observed (Plates 6.13-6.19).

Lithic fragments of the Nagri Formation show cumulative dominance of the Ls and Lv over Lm. Lithic fragments range from 8-26% of the total framework grains in Chashmai anticline, 29-38% in Banda Assar syncline, and 12-26% in Bahadar Khel anticline. Metamorphic clasts include mica schist (also biotite schist), quartz-mica schist (also quartz-muscovite schist), slate/phyllite and quartzite (Plates 6.18, 6.20-6.24). Some volcanic clasts have laths of plagioclase (Plates 6.25-6.28). Sedimentary clasts include mudstone, lime mudstone and siltstone (Plates 6.29-6.33). The percent content of lithic fragments are Ls =24.2-40.9 % (33.7 %), Lv =40.2-59.7 % (48.1 %), Lm =11.1-23.5 % (18.2 %) at the Chashmai anticline, Ls =23.9-52.1 % (35.8 %), Lv =22.7-52.0 % (35.4 %), Lm =23.9-35.0 % (18.2 %) at the Banda Assar syncline, Ls =26.9-50.0 % (40.5 %), Lv =25.0-57.7 % (35.8 %), Lm =15.4-31.9 % (23.7 %) at the Bahadar Khel anticline.

Mica content in Nagri Formation ranges from 2-6% at Chashmai anticline and Assar Banda syncline, and 1-8% at Bahadar Khel anticline of the total frameworks. The grains of biotite are usually oxidized, and some of them are highly deformed (Plates 6.34, 6.35).

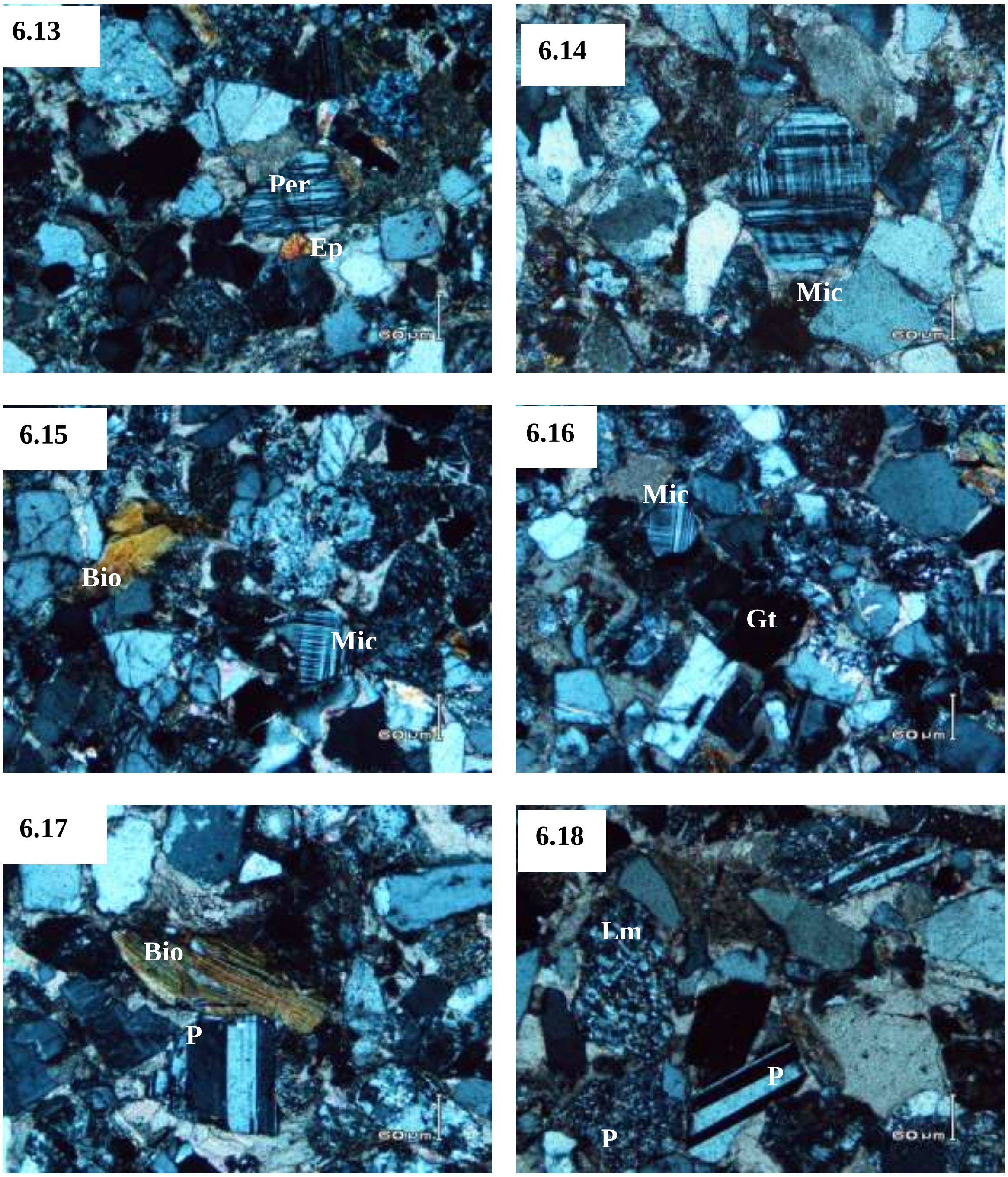

Plates 6.13-6.18: Photomicrographs of the Chinji and Nagri sandstones: **6.13.** Perthite (Per) and epidote (Ep) (XPL). **6.14.** Microcline (Mic) (XPL). **6.15.** Microcline (Mic) and biotite (Bio) (XPL). **6.16.** Garnet (Gt) and microcline (Mic) (XPL). **6.17.** Fresh plagioclase (P) and biotite (Bio) (XPL). **6.18.** Fresh plagioclase (P), alteration of plagioclase (P) and quartz-mica schist (Lm) (XPL).

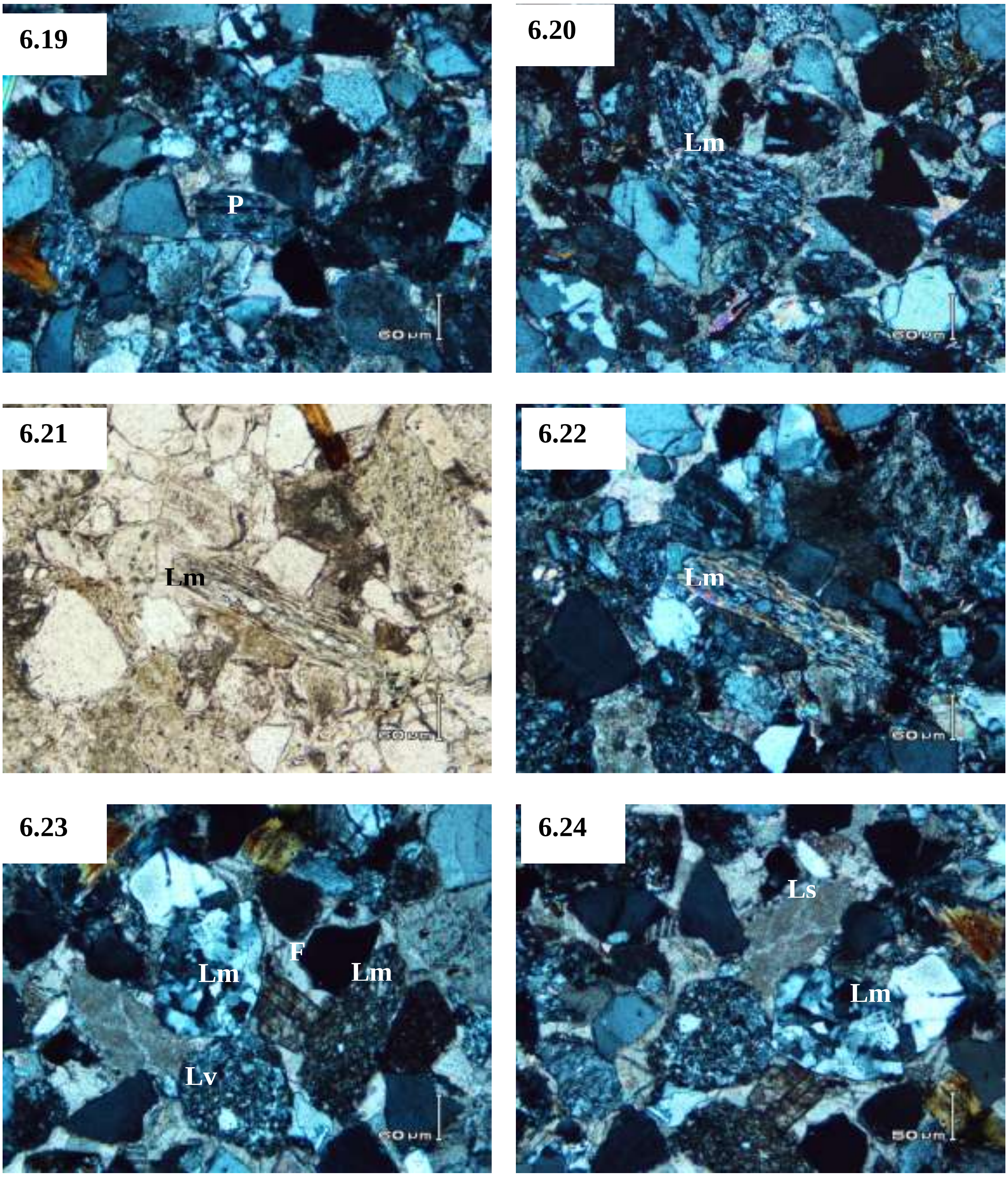

Plates 6.19-6.24: Photomicrographs of the Chinji and Nagri sandstones: **6.19.** Altered plagioclase (P) (XPL). **6.20.** Quartz-mica schist (Lm) (XPL). **6.21. & 6.22.** Quartz-mica schist (Lm) (PPL & XPL). **6.23.** Quartzite (Lm), volcanic lithic (Lv), quartz-mica schist (Lm) and fluorite (F) (XPL). **6.24.** Quartzite (Lm) and micritic fragment (Ls) (XPL).

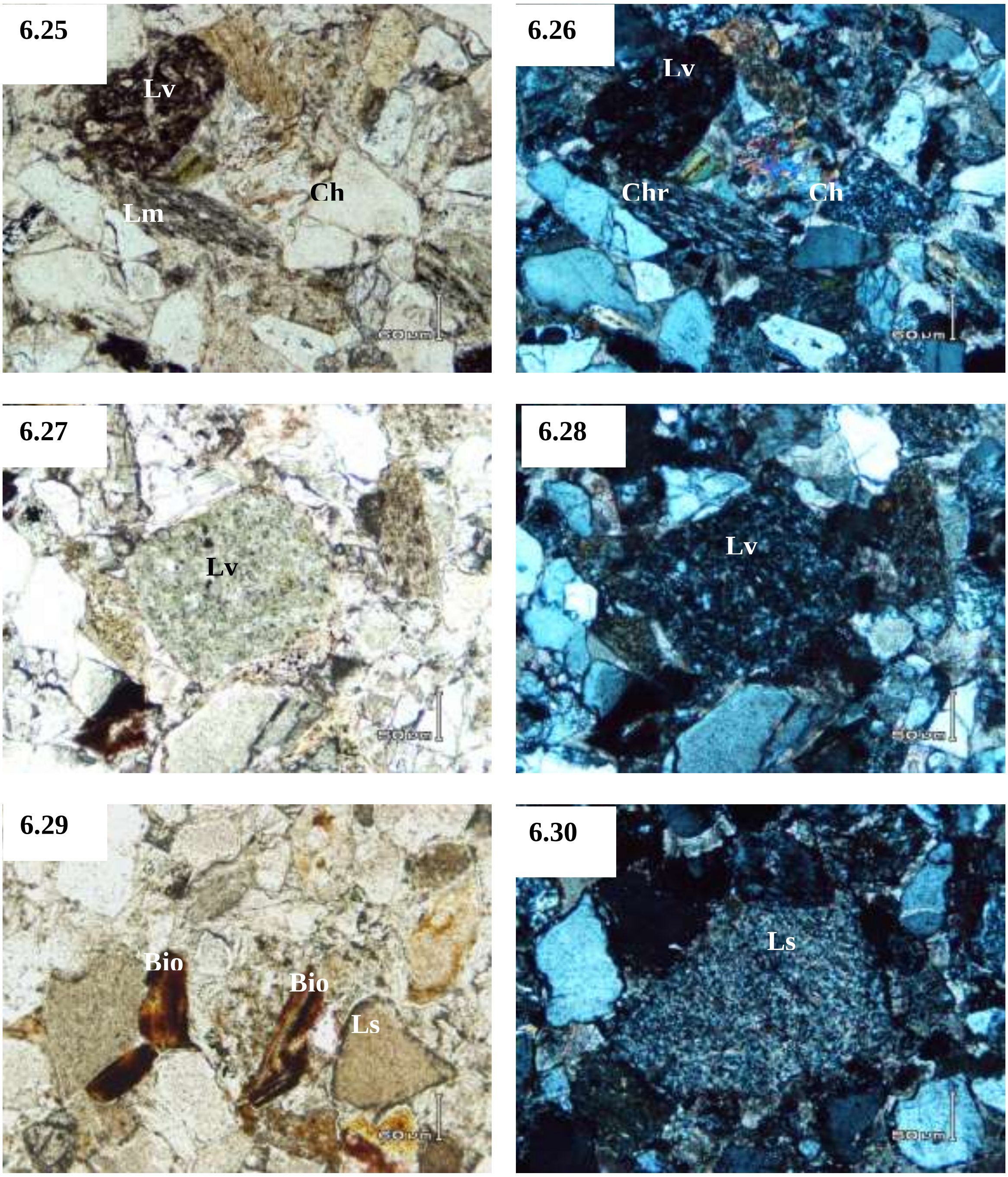

Plates 6.25-6.30: Photomicrographs of the Chinji and Nagri sandstones: **6.25. & 6.26.** Chert, volcanic lithic (Lv), metamorphic lithic (Lm) (PPL & XPL). **6.27 & 6.28.** Volcanic lithic (Lv) (PPL & XPL). **6.29.** Mud clast (Ls) and biotite (Bio) (PPL). **6.30.** Mud fragment (Ls) (XPL).

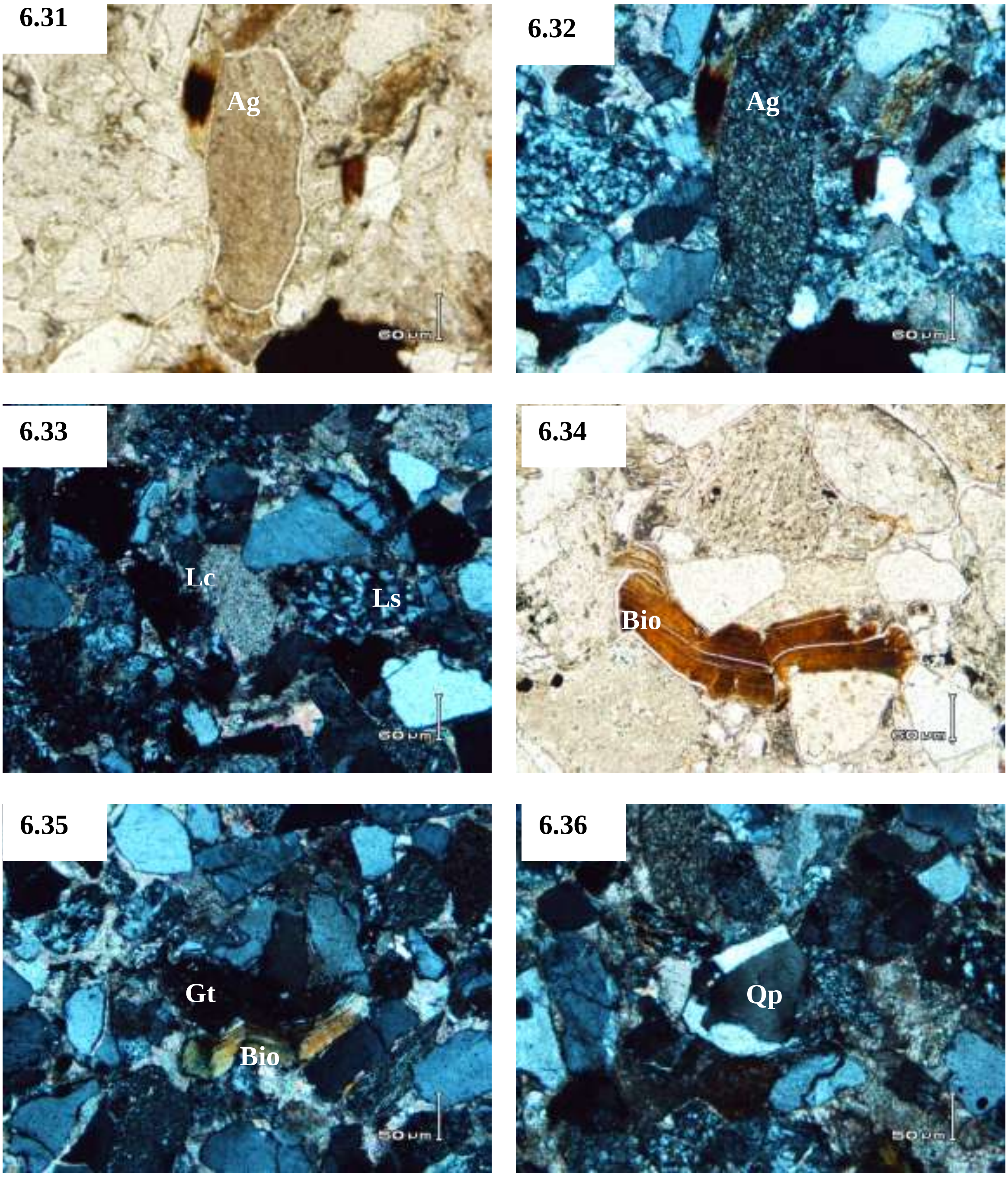

Plates 6.31-6.36: Photomicrographs of the Chinji and Nagri sandstones: **6.31 & 6.32.** Argillite (Ag) (PPL & XPL). **6.33.** Lc (micritic) and Ls (siltstone) (XPL). **6.34.** Biotite (Bio) (PPL). **6.35.** Biotite (Bio) and garnet (Gt) (XPL). **6.36.** Polycrystalline quartz (Qp) (XPL).

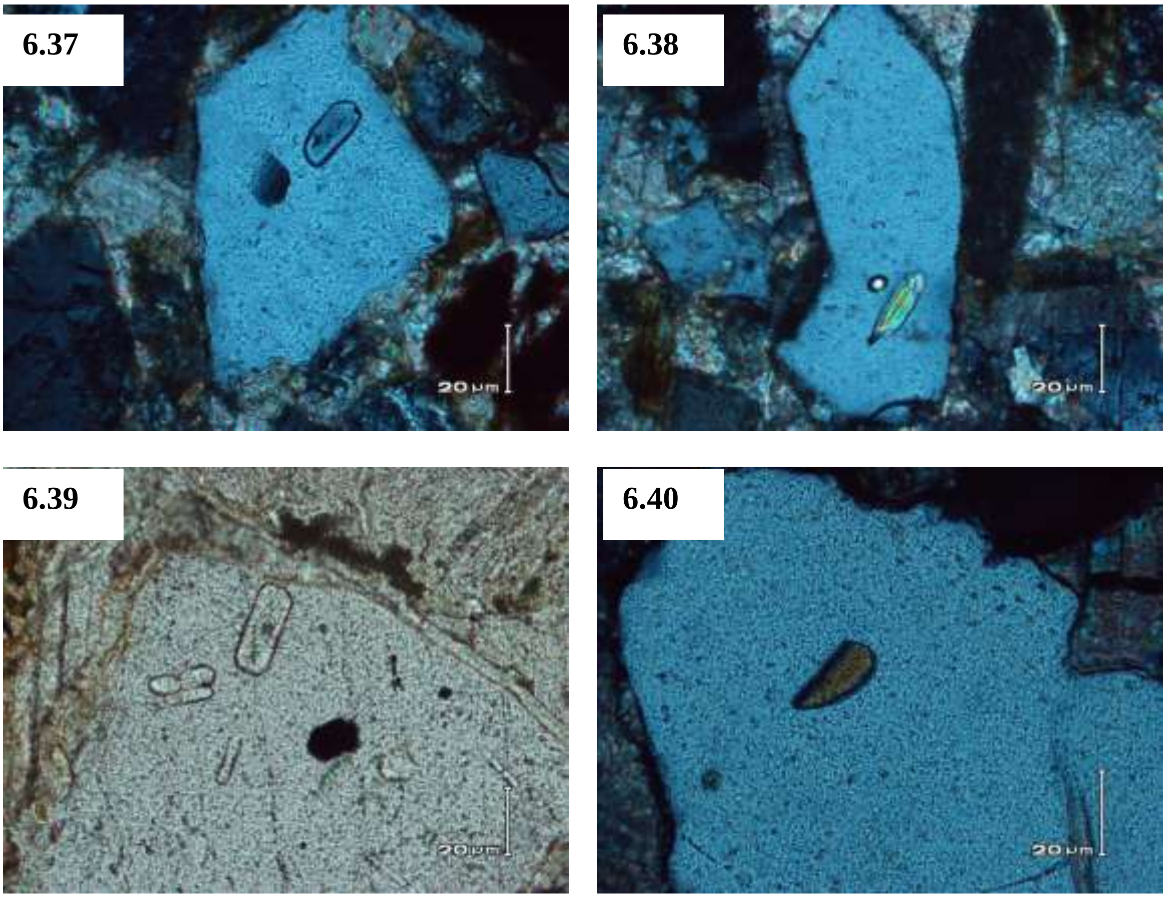

Plates 6.37-6.40: Photomicrographs of the Chinji and Nagri sandstones: **6.37. 6.38. 6.39. 6.40.** Inclusion in quartz (XPL).

Common heavy minerals of the Nagri Formation include epidote, garnet, sphene, amphibole, fluorite, zircon, monazite, apatite, rutile and chromite. Inclusions of zircon, monazite, epidote, tourmaline, sphene and mica in quartz grains have been observed (Plates 6.36-6.40). Authigenic carbonates are abundant in all samples.

Mechanical deformation of some grains shows compaction during burial as revealed by fractures filled with calcite in some quartz grains. On the other hand, fractures not affected by the calcite replacement, were developed during tectonic uplift (Abbasi and Friend, 1989). A few quartz grains have incipient silica overgrowths. These overgrowths may be the result of pressure dissolution at the grain contacts, when the grains were buried under the pressure of the overlying rocks (Pettijohn et al., 1987).

The varying amount of calcite represents the primary cementing material of the Siwalik sandstone, precipitated as pore-filling in the sub-aerial vadoze zone due to capillary action under wet and dry climatic conditions (Tandon and Varshney, 1991). The amount of cement in sandstones depends on the timing of cementation relative to that of compaction. During early diagenesis, sediments have high pore space, which permits precipitation of a large amount of calcium carbonate by capillary evaporation of water. However, pore space of sediments reduces continuously with enhanced burial leaving less pore space for calcite precipitation (Sanyal et al., 2005). The average calcium carbonate in Surai Khola is low (25.1%) in late diagenetic sandstone compared to the early diagenetic carbonate nodules (37.6%) of Potwar Plateau (Quade and Roe, 1999).

6.8 Sandstone Classification and Types of Quartz Grains of the Kamlial, Chinji and Nagri Formations

Mineralogically, the sandstones of the Kamlial, Chinji and Nagri formations of the studied sections belong to both feldspathic and lithic arenites (Fig. 6.1) (Okada, 1971; Folk, 1974). However, sandstone of the Kamlial, Chinji and Nagri formations from the Banda Assar syncline is totally lithic arenite while that of the Chinji Formation from the Chashmai anticline is exclusively feldspathic arenite (Fig. 6.2).

Feldspathic arenites are assumed to be first-cycled deposits that mainly originate by the weathering of feldspar-rich igneous and metamorphic rocks. The formation of feldspathic arenites implies preservation of large quantities of feldspars during the process of weathering. This may happen due either to (1) very cold or very arid climatic conditions that inhibit the chemical weathering processes, or (2) warmer, more humid climates where rapid uplifts allow faster erosion of feldspars before they can be decomposed (Boggs, 1992). The findings by Dickinson and Suczek (1979) also support the latter possibility for the origin of feldspathic arenites.

The higher proportion of unstable lithics and the moderately higher feldspar content of lithic arenites suggest their derivation from rugged high-relief source areas. This is because the detritus is stripped off rapidly from such elevated areas before the weathering processes could destroy the unstable clasts. Furthermore, lithic arenites mostly contain fine-grained lithic clasts presumably derived from source regions dominated by volcanic rocks, schists, phyllites, slates, fine-grained sandstones, shales and limestone.

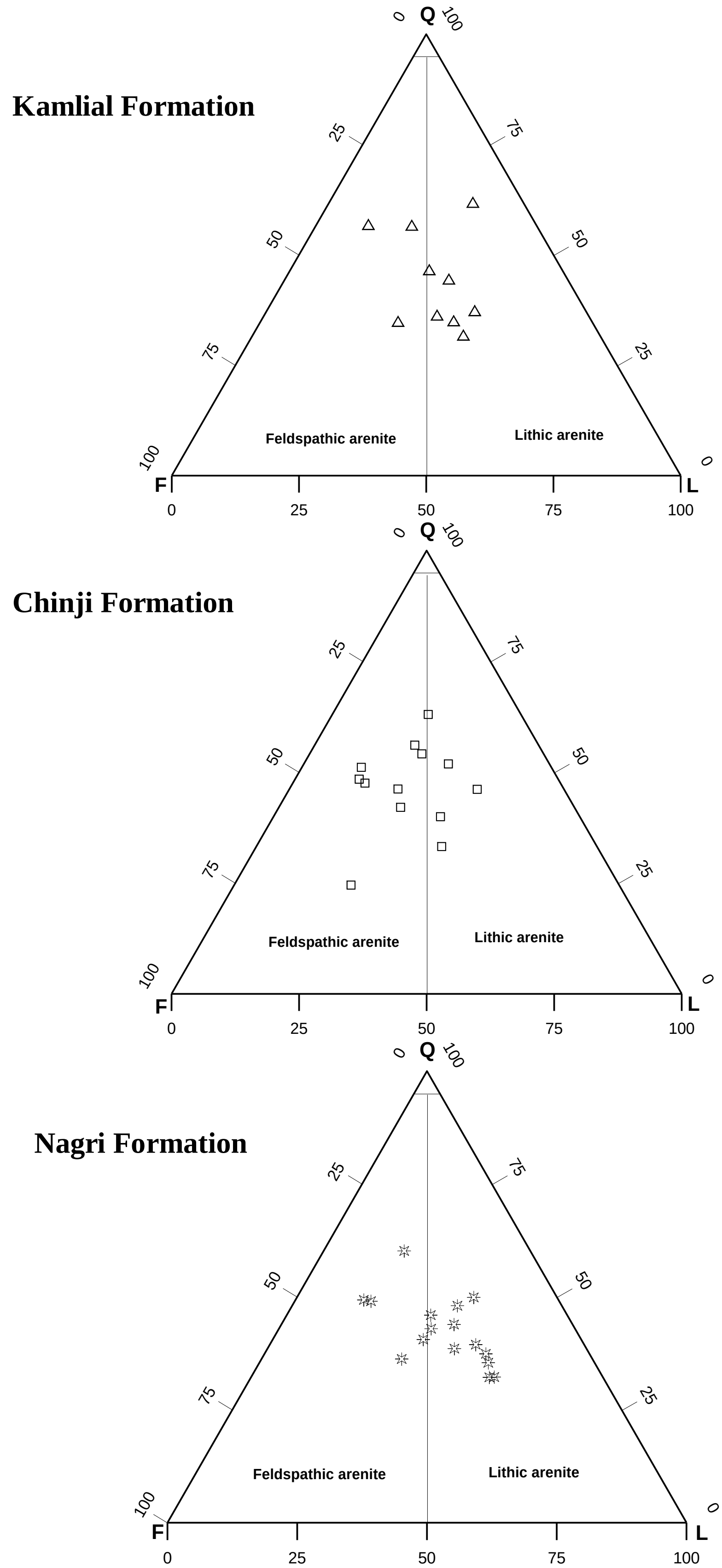

Figs. 6.1. Mineralogical characterization of the Kamlial, Chinji and Nagri sandstone (fields after Okada, 1971), respectively. Q = Quartz; F = Feldspar; L = Lithics.

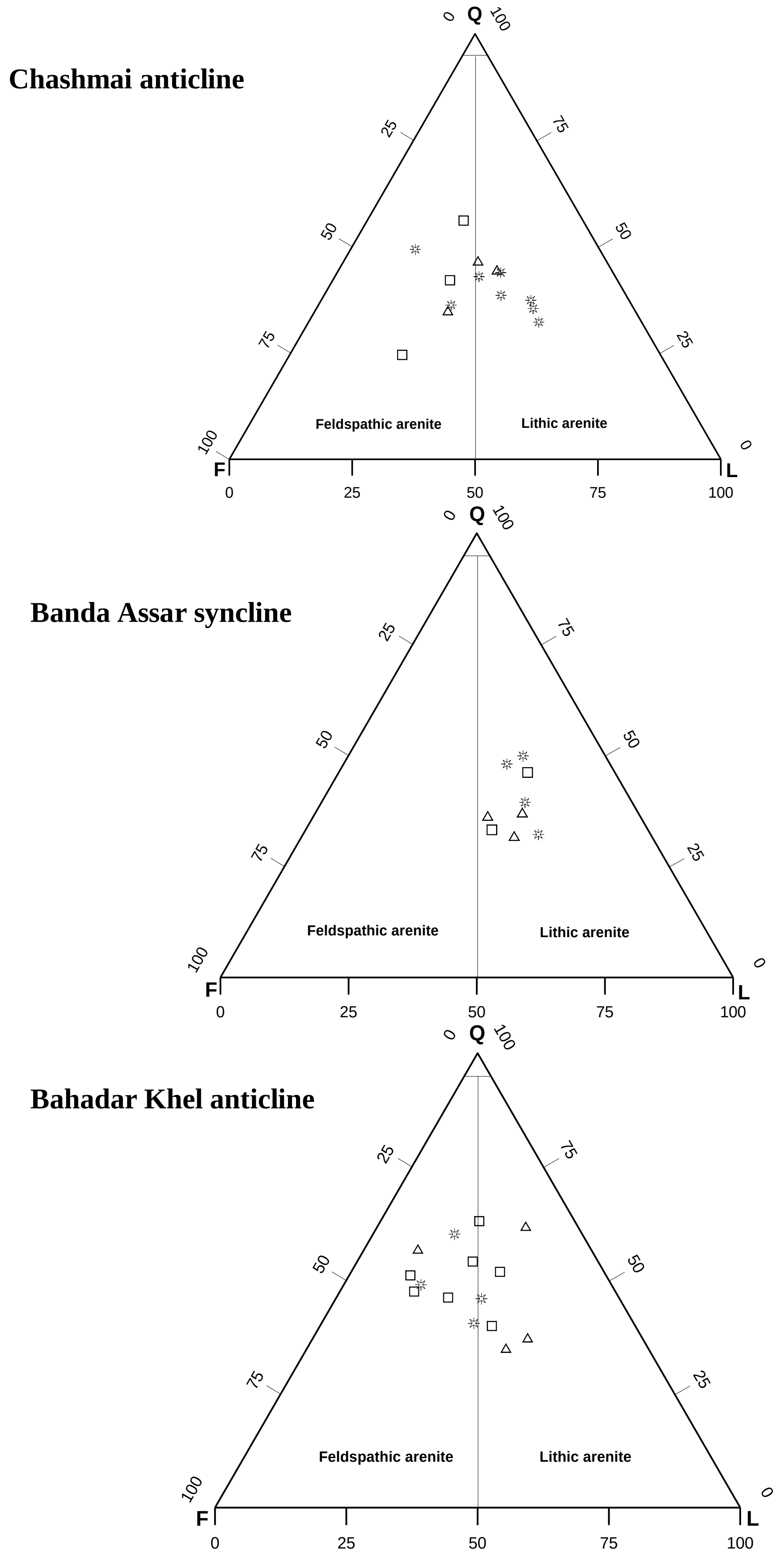

Figs. 6.2. Mineralogical characterization of the Kamlial, Chinji and Nagri sandstone (fields after Okada, 1971) for Chashmai anticline, Banda Assar syncline and Bahadar Khel anticline.

Source areas with such lithological characteristics occur primarily in orogenic belts located along suture zones and magmatic arcs (Dickinson and Suczek, 1979; Dickinson, 1985).

The relative proportions of different types of quartz grains in the Kamlial sandstone suggest that they are mostly derived from medium- and high-grade metamorphic rocks, with only subsidiary contribution from low-grade metamorphics (Fig. 6.3) whereas those from the overlying Chinji Formation indicate both medium-high grade and low-grade metamorphic rock provenance (Fig. 6.3). Only one sample of the Kamlial Formation from the Chashmai anticline falls along the boundary line between metamorphic and plutonic provenances thereby indicating the possibility of an igneous origin for some of the quartz grains (Fig. 6.3). Similarly, comparative study of different types of quartz grains from sandstone of the Nagri Formation indicates medium- and high-grade metamorphic rocks as well as low-grade metamorphic provenance (Fig. 6.3). The detrital modes of the Middle Siwalik sandstones of the Dehra Dun sub-basin also show its derivation from the northerly exposed sedimentary, low- to medium-grade metamorphics and subordinate igneous rocks (Kumar et al., 2004).

It is noteworthy that the types of quartz grains from the Chashmai anticline indicate their derivation exclusively form medium- and high-grade metamorphic rocks for all the three formations whereas the quartz grains of all the three formations from the Banda Assar syncline and Bahadar Khel anticline suggest a dominant contribution from low grade metamorphic rocks (Fig. 6.4). The low content of polycrystalline quartz in the Kamlial and Chinji formations possibly indicates a long distance of transportation (Dabbagh and Rogers, 1983). The dominance of Qp_{2-3} over $Qp_{>3}$ in the Kamlial and Chinji formations indicates an origin from metamorphic source rocks (Blatt et al., 1980; Asiedu et al., 2000).

The abundance of monocrystalline quartz in all the studied sections of the Kamlial, Chinji and Nagri formations indicates that the presence of granitic and volcanic rocks in the source areas cannot be ruled out (Young, 1976). The abundance of Q_{nu} over the Q_u in the Kamlial Formation at the Chashmai anticline and the Banda Assar syncline suggests plutonic and volcanic source rocks (Basu, 1985); while the abundance of Q_u over the Q_{nu} in the Bahadar Khel anticline shows a metamorphic and/or tectonically deformed

Kamlial Formation

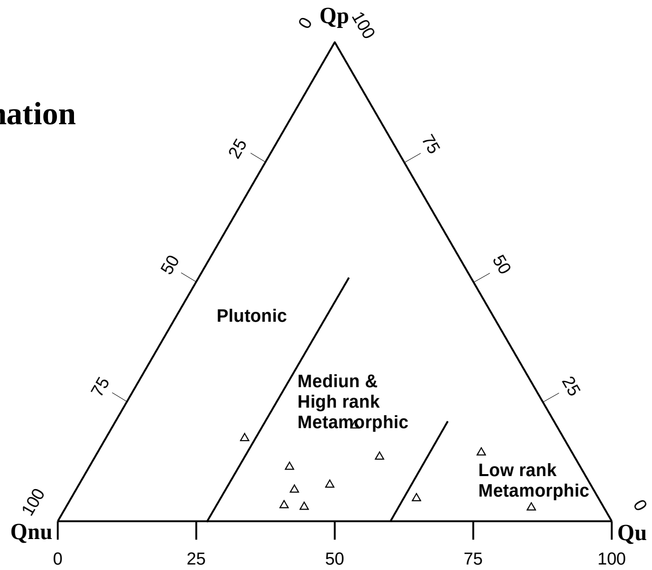

Chinji Formation

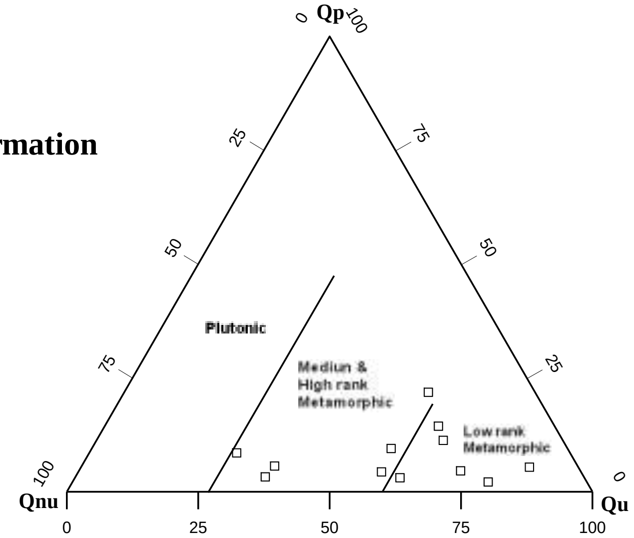

Nagri Formation

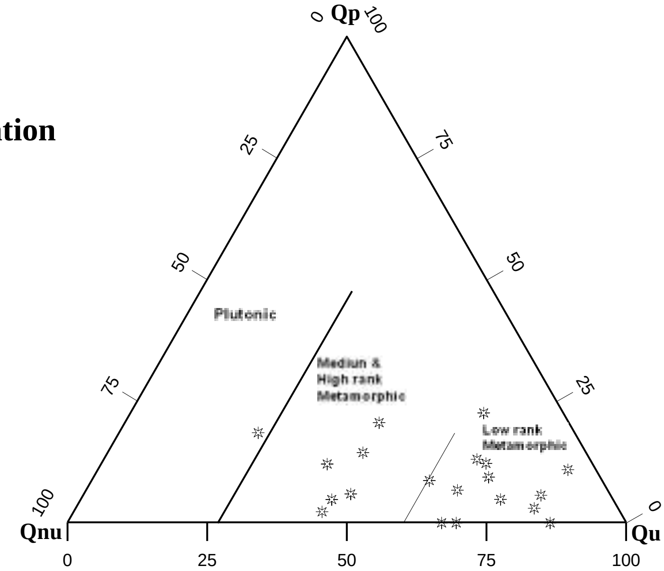

Figs. 6.3. Ternary plots of detrital quartz types of the Kamlial, Chinji and Nagri sandstones, respectively (after Basu et al., 1975). Qp = Quartz polycrystalline; Qnu = Quartz nonundulatory (monocrystalline); Qu= Quartz undulatory (monocrystalline).

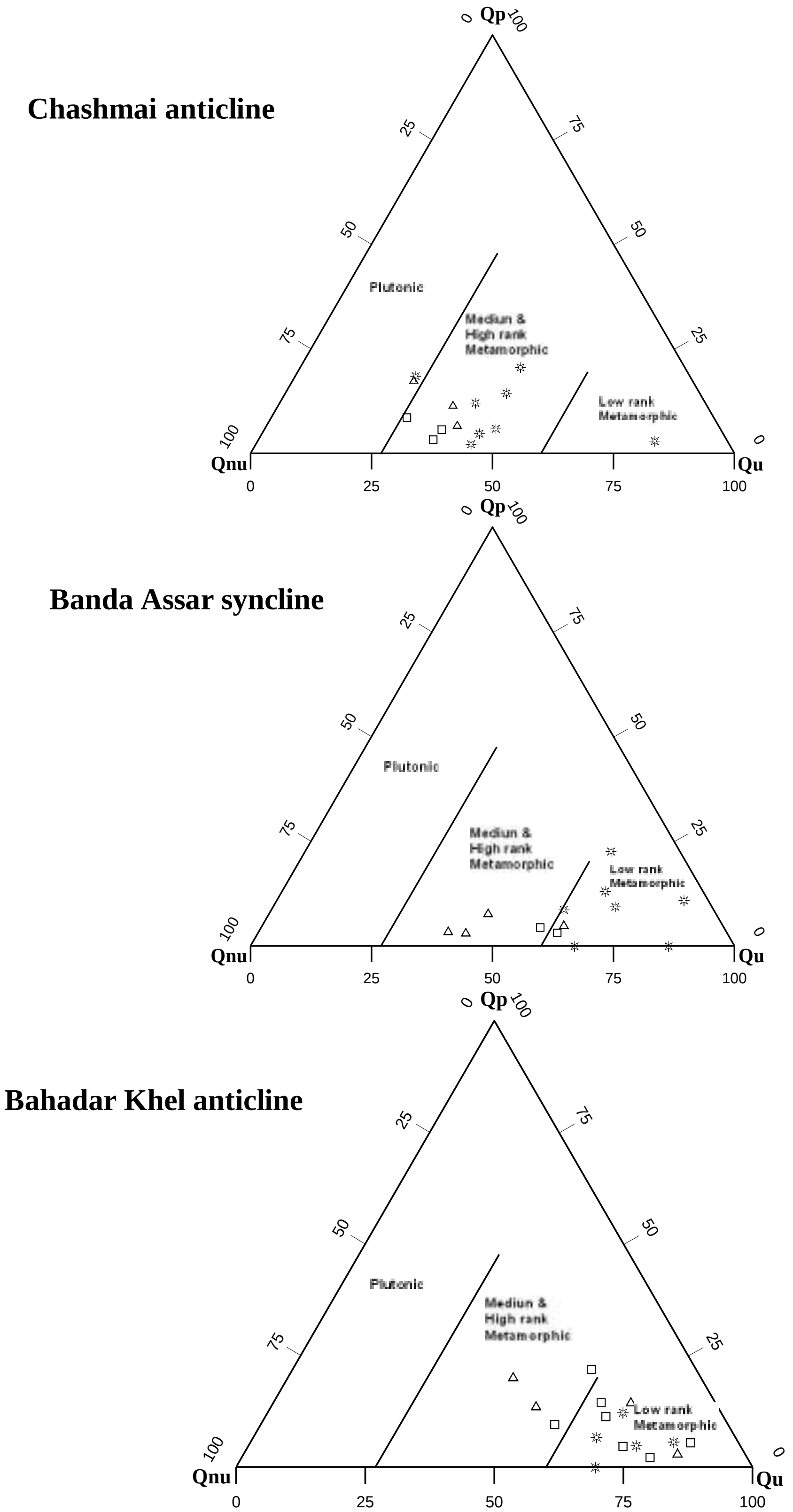

Figs. 6.4. Ternary plots of detrital quartz types of the Kamlial, Chinji and Nagri sandstones for Chashmai anticline, Banda Assar syncline and Bahadar Khel anticline, respectively (after Basu et al., 1975). Qp = Quartz polycrystalline; Qnu = Quartz nonundulatory (monocrystalline); Qu =Quartz undulatory (monocrystalline). Symbols as in Fig. 6.1.

source area. Q_{nu} dominates over the Q_u in the Chinji Formation at the Chashmai anticline. The reverse is true in case of the other two studied sections of the Chinji Formation.

The contrasting ratios of Q_m/Q_p in all the sections of the Nagri Formation (i.e. increasing Q_m/Q_p ratio at Chashmai anticline, and decreasing Q_m/Q_p ratio at the Bahadar Khel anticline upsection) are suggestive of either a large catchment area or active tectonics in the source area. Similarly, the ratio of nonundulatory monocrystalline quartz to undulatory monocrystalline quartz is variable in all the sections that also favor a source area of active tectonics. Nonundulatory monocrystalline quartz indicates plutonic and volcanic origin, while undulatory quartz indicate high-grade metamorphic source (Basu, 1985).

The average contents of different quartz types from the Kamlial Formation are: Q_{nu} = 53, Q_u = 42, $Qp_{2\text{-}3}$ = 4 and $Qp_{>3}$ = 1% at the Banda Assar syncline, Q_{nu} = 25, Q_u = 62, $Qp_{2\text{-}3}$ = 9 and $Qp_{>3}$ = 4% at the Bahadar Khel anticline, and Q_{nu} = 55, Q_u = 33, $Qp_{2\text{-}3}$ = 7 and $Qp_{>3}$ = 5% at the Chashmai anticline. The average contents of different quartz types in the Chinji Formation are: Q_{nu} = 36, Q_u = 60, $Qp_{2\text{-}3}$ = 3 and $Qp_{>3}$ = 1% at the Banda Assar syncline, Q_{nu} = 21, Q_u = 68, $Qp_{2\text{-}3}$ = 9 and $Qp_{>3}$ = 2% at the Bahadar Khel anticline, and Q_{nu} = 61, Q_u=33, $Qp_{2\text{-}3}$=5 and $Qp_{>3}$=1% at the Chashmai anticline. Similarly, the average contents of quartz types in Nagri Formation are Q_{nu} = 18, Q_u = 68, $Qp_{2\text{-}3}$ = 8 and $Qp_{>3}$ = 6% at Banda Assar syncline and Q_{nu} = 22, Q_u = 72, $Qp_{2\text{-}3}$ = 5 and $Qp_{>3}$ = 1% at Bahadar Khel anticline, and Q_{nu} = 47, Q_u = 42, $Qp_{2\text{-}3}$ = 8 and $Qp_{>3}$ = 3% at Chashmai anticline. All these data suggest a granitic source (Tortosa et al., 1991).

6.9. Provenance of the Kamlial Formation

Modal point count data of the Kamlial Formation is presented in Table 6.3, and has been plotted on different discriminatory diagrams. Plotted on the Q-F-L diagram (Fig. 6.5) of Dickinson (1985), which emphasizes the maturity of the sediments (Tucker, 2001), the Kamlial Formation shows a mixed provenance from Dissected magmatic Arc (DA) and Recycled Orogens (RO). Magmatic arc provenance has been divided into three suits, those eroded from undissected arcs, in which nearly continuous volcanic cover is present, those eroded from dissected arcs, in which cogenetic plutons are widely exposed from erosional unroofing, and transitional arcs, which have undergone less erosion than dissected arcs (Dickinson and Suczek, 1979; Boggs and Seyedolali, 1992). Qm-F-Lt plot

Table 6.3. Recalculated key indices for framework composition of the sandstones of the Neogene molasse sequence of the Kohat Plateau.

Sample No.	Q %	Ft%	L %	Qm %	F %	Lt %
Kamlial Fm						
KCK-1	44.66	23.32	32.02	36.76	23.32	39.92
KCK-4	46.77	26.13	27.10	38.55	24.40	37.05
KCK-10	35.06	38.11	26.83	30.57	35.71	33.71
KAK-40	31.95	26.84	41.21	29.39	26.84	43.77
KAK-42*	56.86	24.51	18.63	51.64	23.47	24.88
KAK-44	36.49	29.73	33.78	33.88	28.66	37.46
KAK-52	37.24	22.59	40.17	34.54	21.69	43.78
KBK-88	35.20	27.10	37.69	28.04	27.10	44.86
KBK-95	37.50	21.80	40.70	31.79	21.68	46.53
KBK-97	62.05	9.90	28.05	54.36	10.07	35.57
KBK-102	57.04	32.96	10.00	56.02	33.46	10.53
Chinji Fm						
KCC-17	42.18	34.12	23.70	38.57	32.29	29.15
KCC-18	56.22	24.32	19.46	52.49	24.86	22.65
KCC-20	24.64	52.61	22.75	21.97	49.78	28.25
KAC-56	33.33	30.50	36.17	31.06	29.35	39.59
KAC-63	46.25	17.05	36.69	43.29	16.71	40.00
KBC-104	51.23	37.30	11.48	47.88	38.56	13.56
KBC-106	40.07	27.36	32.57	32.88	28.77	38.36
KBC-111	46.33	32.55	21.11	41.42	32.84	25.74
KBC-114	54.25	23.91	21.84	51.86	24.19	23.95
KBC-121	63.14	18.22	18.64	60.68	18.38	20.94
KBC-125	51.98	19.84	28.17	45.53	20.33	34.15
KBC-127	47.67	38.35	13.98	46.26	38.08	15.66
Nagri Fm						
KCN-24	37.50	20.00	42.50	32.08	20.00	47.92
KCN-26	35.53	20.51	43.96	28.62	20.29	51.09
KCN-31	49.44	37.55	13.01	48.13	37.69	14.18
KCN-33	38.65	25.50	35.86	31.43	26.12	42.45
KCN-36	36.36	36.80	26.84	33.91	36.48	29.61
KCN-37	43.06	27.78	29.17	38.25	28.07	33.68
KCN-38	44.01	22.89	33.10	40.89	22.34	36.77
KCN-39	32.35	20.96	46.69	28.86	19.13	52.01
KAN-67	48.17	20.16	31.68	44.56	20.42	35.01
KAN-78	39.53	20.93	39.53	34.98	20.79	44.22
KAN-80	50.00	16.07	33.93	40.88	16.98	42.14
KAN-84*	57.48	31.50	11.02	57.48	31.50	11.02
KAN-87	32.31	21.92	45.77	25.98	20.28	53.74
KBN-135	40.66	30.49	28.85	38.19	30.10	31.72
KBN-137	49.16	36.31	14.53	46.37	36.31	17.32
KBN-147	60.29	24.35	15.36	56.73	24.56	18.71
KBN-152	46.08	26.33	27.59	40.82	26.58	32.59

Table 6.3 (Continued)

Sample No.	Qp %	Lv %	Ls %	Lm %	Lv %	Ls %
Kamlial Fm						
KCK-1	24.69	2.47	72.84	24.69	2.47	72.84
KCK-4	21.79	6.41	71.79	27.38	5.95	66.67
KCK-10	10.13	32.91	56.96	19.32	29.55	51.14
KAK-40	8.25	34.02	57.73	31.01	25.58	43.41
KAK-42*	15.38	28.21	56.41	13.16	28.95	57.89
KAK-44	4.40	57.14	38.46	13.00	52.00	35.00
KAK-52	3.95	48.68	47.37	23.96	38.54	37.50
KBK-88	23.71	24.74	51.55	38.84	19.83	41.32
KBK-95	14.84	35.94	49.22	22.14	32.86	45.00
KBK-97	28.89	24.44	46.67	24.71	25.88	49.41
KBK-102	16.67	6.67	76.67	7.41	7.41	85.19
Chinji Fm						
KCC-17	6.98	0.00	93.02	20.00	0.00	80.00
KCC-18	23.08	0.00	76.92	16.67	0.00	83.33
KCC-20	6.67	11.11	82.22	12.50	10.42	77.08
KAC-56	3.49	51.16	45.35	18.63	43.14	38.24
KAC-63	6.11	58.02	35.88	13.38	53.52	33.10
KBC-104	36.36	21.21	42.42	25.00	25.00	50.00
KBC-106	24.55	20.91	54.55	17.00	23.00	60.00
KBC-111	21.95	28.05	50.00	11.11	31.94	56.94
KBC-114	14.44	34.44	51.11	18.95	32.63	48.42
KBC-121	16.67	33.33	50.00	20.45	31.82	47.73
KBC-125	26.39	33.33	40.28	25.35	33.80	40.85
KBC-127	9.68	12.90	77.42	28.21	10.26	61.54
Nagri Fm						
KCN-24	14.29	47.25	38.46	23.53	42.16	34.31
KCN-26	15.38	43.59	41.03	17.50	42.50	40.00
KCN-31	14.81	14.81	70.37	34.29	11.43	54.29
KCN-33	20.00	46.00	34.00	11.11	51.11	37.78
KCN-36	8.77	64.91	26.32	16.13	59.68	24.19
KCN-37	18.07	53.01	28.92	19.05	52.38	28.57
KCN-38	7.50	57.50	35.00	21.28	48.94	29.79
KCN-39	1.90	48.57	49.52	18.90	40.16	40.94
KAN-67	14.81	58.33	26.85	23.97	52.07	23.97
KAN-78	13.68	45.26	41.05	31.09	36.13	32.77
KAN-80	33.93	31.25	34.82	35.09	30.70	34.21
KAN-84*	0.00	0.00	100.00	35.71	0.00	64.29
KAN-87	11.00	27.00	62.00	25.21	22.69	52.10
KBN-135	8.33	30.56	61.11	25.00	25.00	50.00
KBN-137	18.52	55.56	25.93	15.38	57.69	26.92
KBN-147	25.45	30.91	43.64	22.64	32.08	45.28
KBN-152	23.08	32.05	44.87	31.82	28.41	39.77

Table 6.3 (Continued)

Sample No.	Qm %	K %	P %
Kamlial Fm			
KCK-1	61.18	28.29	10.53
KCK-4	61.24	30.62	8.13
KCK-10	46.12	28.45	25.43
KAK-40	52.27	28.98	18.75
KAK-42*	68.75	26.88	4.38
KAK-44	54.17	26.04	19.79
KAK-52	61.43	25.00	13.57
KBK-88	50.85	40.11	9.04
KBK-95	59.46	28.65	11.89
KBK-97	84.38	11.46	4.17
KBK-102	62.61	26.47	10.92
Chinji Fm			
KCC-17	54.43	24.05	21.52
KCC-18	67.86	18.57	13.57
KCC-20	30.63	45.00	24.38
KAC-56	51.41	33.33	15.25
KAC-63	72.15	14.35	13.50
KBC-104	55.39	34.31	10.29
KBC-106	53.33	28.89	17.78
KBC-111	55.78	31.87	12.35
KBC-114	68.20	17.74	14.07
KBC-121	76.76	17.84	5.41
KBC-125	69.14	22.22	8.64
KBC-127	54.85	38.82	6.33
Nagri Fm			
KCN-24	61.60	24.00	14.40
KCN-26	58.52	25.19	16.30
KCN-31	56.09	36.96	6.96
KCN-33	54.61	27.66	17.73
KCN-36	48.17	32.93	18.90
KCN-37	57.67	27.51	14.81
KCN-38	64.67	21.20	14.13
KCN-39	60.14	29.37	10.49
KAN-67	68.57	20.00	11.43
KAN-78	62.72	24.26	13.02
KAN-80	70.65	20.65	8.70
KAN-84*	64.60	29.20	6.19
KAN-87	56.15	35.38	8.46
KBN-135	55.92	35.07	9.00
KBN-137	56.08	33.78	10.14
KBN-147	69.78	21.22	8.99
KBN-152	60.56	33.80	5.63

of the Kamlial sandstones indicates dissected arc provenance (DA), although one sample from Bahadar Khel shows Quartzose Recycled (QR) provenance and one other from the same section suggests Transitional Continental provenance (TC) (Fig. 6.6). Qp-Lvm-Lsm plot also indicates a magmatic provenance (MA), and a magmatic and subduction complex provenance (SC + MA) for Kamlial Formation (Fig. 6.7).

Dissected arcs expose the plutonic core that compositionally approaches to sediments derived from uplifted continental basement, although the former is characterized by a greater abundance of feldspar (Ingersoll et al., 1984). More mature and eroded magmatic arcs, especially those along continental margins, shed detritus of mixed plutonic and volcanic origin into both forearc and backarc basins. Sand compositions are complex but both types of feldspars are commonly present in significant proportions, and nonvolcanic lithic fragments are prominent in varying degrees. The volcanic cover and the batholithic core of the volcano-plutonic arc orogen thus serve jointly and simultaneously as sediment sources (Dickinson and Suczek, 1979). These sediments are affected little to moderately by climate.

Recycled orogens on the other hand are the source regions created by upfolding or upfaulting of sedimentary or metasedimentary terrains, allowing detritus from these rocks to be recycled into the associated basin. Many recycled orogens result from the collision of continental blocks. This process creates uplift and welds the terrains together along a suture zone (collision orogen provenances) (Boggs, 1992). Recycled orogens are characterized by an abundance of quartz and sedimentary-metasedimentary lithic fragments (Fig. 6.5).

Collision orogens are composed dominantly of nappes and thrust sheets of sedimentary and metasedimentary rocks but may include subordinate amounts of plutonic or volcanic rocks, or even ophiolitic mélanges. It thus sheds a complex suites of sediments. Dickenson and Suczek (1979) suggested that sandstones typical of collision orogens are composed of recycled sedimentary materials, have intermediate quartz contents, and contain an abundance of sedimentary-metasedimentary lithic fragments. Less typical sandstones derived from collision orogens are also feldspathic arenites. Such sandstones indicate probably significant contributions from igneous terrains uplifted adjacent to the crustal sutures. Sandstone with high chert contents may include significant

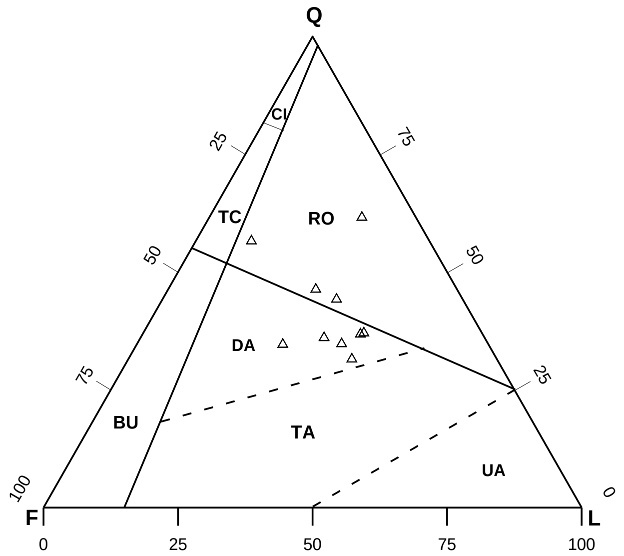

Fig. 6.5.

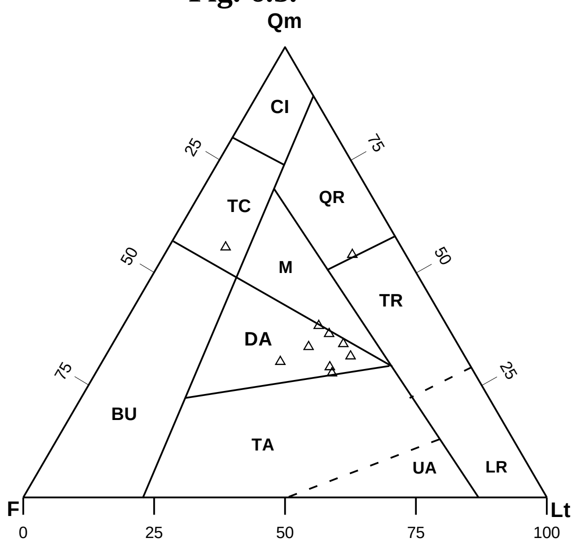

Fig. 6.6.

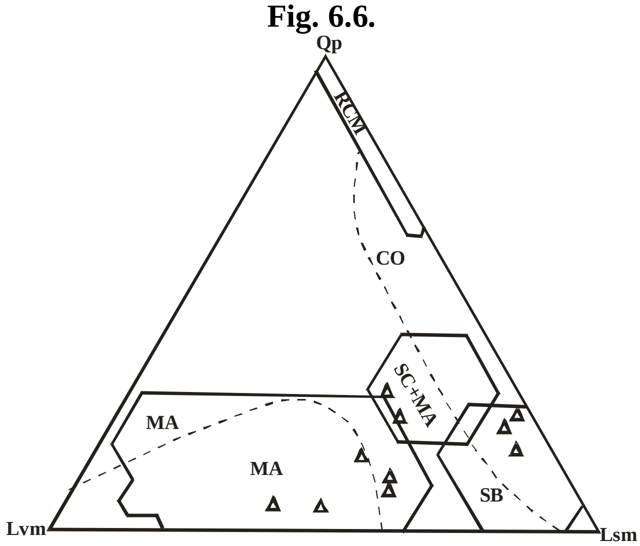

Fig. 6.7

Figs. 6.5-6.7. Ternary diagrams for provenance following Dickinson and Suczek (1979) and Dickinson (1985) for the Kamlial Formation sandstones. 6.5. Framework-grain assemblage Q-F-L. Q =Qm + Qp; F, feldspars; L, rock fragments (chert+quartzite+shale); RO, recycled orogen; BU, basement uplift; TA, transitional arc; DA, dissected arc; UA, undissected arc; TC, transitional arc; CI, continental interior. 6.6. Framework-grain assemblage Qm-F-Lt showing sandstone composition of samples from the Kamlial Formation sandstone. Lt = L + Qp. QR, quartzose recycled; TR, transitional recycled; LR, lithic recycled. 6.7. Qp-Lvm-Lsm triangle of the sandstone of the Kamlial Formation. MA, magmatic arcs (forearc areas); SC+MA, mixed magmatic arcs and subduction complexes; SB, suture belts (remnant ocean basins); RCM, rifted continental margin; CO, collision orogeny. Dashed-line fields from Dickinson and Suczek (1979).

contributions from mélange terrains caught along the suture belts, though chert nodules from carbonate succession may also be important sources. Sediments from collision orogens may be shed into foreland basins or may be transported longitudinally into adjacent ocean basins. Some recycled orogens are foreland uplifts associated with foreland fold-thrust belts. These foreland uplift provenances may contain a complex variety of source rocks, including siliciclastic sediments, carbonate rocks, metasediments, plutonic rocks in exposed basement blocks and volcanic rocks (Boggs, 1992).

Detritus derived from the recycling of orogenic belts is highly varied in composition, reflecting the different types of orogen (broadly either continent-continent or continent-ocean collision). Lithic grains dominate in many recycled-orogen, and quartz plus sedimentary rock fragments along with the metamorphosed equivalents of the latter commonly occur in sandstones derived from continental collision belts. Feldspars will also be more abundant (Tucker, 2001). High Qm contents may reflect derivation from deformed mature platform sediments, whereas high Qp contents would indicate that the suture zone and/ or fold-thrust belt are the sources (Ingersoll et al., 1984).

Qp-Lvm-Lsm plot attests a subduction complex and magmatic provenance as well as a suture belt and collisional orogen provenance for Kamlial Formation (Fig. 6.7). Tectonically uplifted subduction complexes consist of deformed ophiolitic and other oceanic materials from a structural high along the trench-slope break between the trench axis and the volcanic chain within arc-trench systems. In some places, this structural high is emergent as an isolated sediment source along the so-called outer sedimentary arc where varying proportions of greenstone, chert, argillite, greywacke, and some limestone are exposed as constituents of mélanges, thrust sheets and isoclines, formed by deformation within the subduction zone. Sediment derived from such uplifted terrains can be shed either toward the arc into forearc basins or into the trench, where it again becomes incorporated into the subduction complex. Effects of climate are little (Dickinson and Suczek, 1979).

Crook (1974) and Schwab (1975) have shown that that quartz poor rocks are mostly of volcanogenic derivation from magmatic island arcs and that rocks of intermediate quartz content are associated mainly with active continental margins or other orogenic belts.

6.10. Provenance of the Chinji Formation

Petrographic point count data of the sandstone of the Chinji Formation and the Q-F-L discriminatory plot show provenance from dissected arc and recycled orogen for the Chinji Formation (Table 6.3; Fig. 6.8). The Qm-F-Lt plot also shows dominantly mixed and dissected arc provenances, except two samples from Bahadar Khel and one sample from Chashmai those fall into the basement uplift and transitional arc fields, respectively (Fig. 6.9). Qp-Lvm-Lsm plot indicates a magmatic provenance for samples from Banda Assar, and a dominantly magmatic and subduction complex provenance for samples from Bahadar Khel (Fig. 6.10). Dissected magmatic arcs expose the plutonic core that produce sediments matching to uplifted continental basement, but the former is characterized by the greater abundance of both types of feldspar (Ingersoll et al., 1984). Plutonic quartz having inclusions of heavy minerals dominates over clear volcanic quartz. The volcanic cover and the batholithic core of the volcano-plutonic arc orogen thus serve jointly and simultaneously as sediment sources (Dickinson and Suczek, 1979). Mature and eroded magmatic arcs along continental margins shed detritus of mixed plutonic and volcanic origin into forearc and backarc basins.

Sandstones of recycled orogen are characterized by abundance of quartz and sedimentary-metasedimentary lithic fragments. Source regions of recycled orogens are created by upfolding or upfaulting of sedimentary or metasedimentary terrains, mainly result from the collision of continental blocks (Boggs, 1992). Minor lithologies include plutonic rocks, volcanic rocks, or even ophiolitic mélanges. Typical sandstones of recycled sedimentary materials have intermediate quartz contents and abundant sedimentary-metasedimentary lithic fragments, but may also produce feldspathic arenites

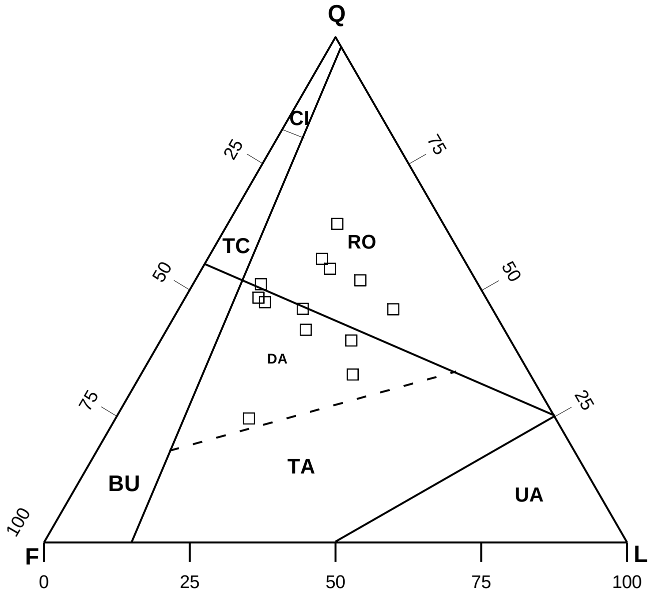

Fig. 6.8

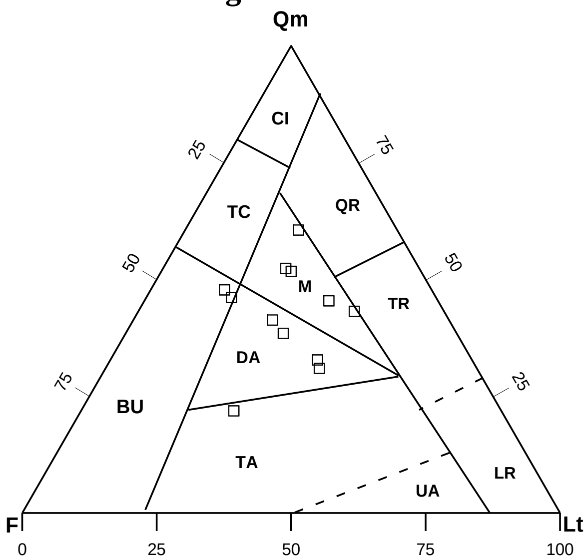

Fig. 6.9

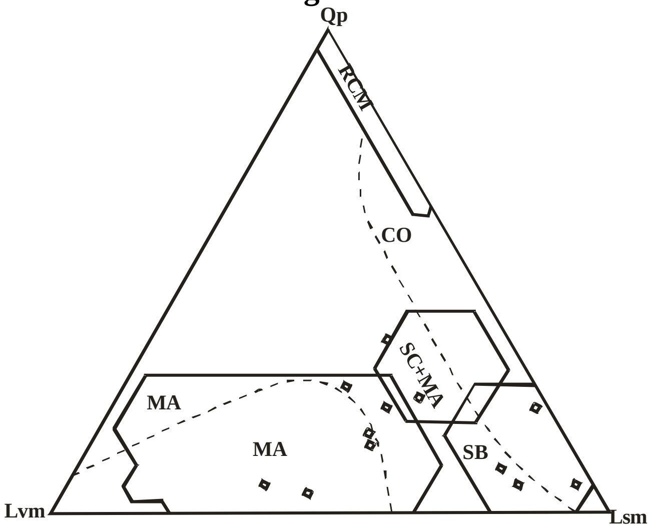

Fig. 6.10

Figs. 6.8-6.10. Ternary diagrams for provenance following Dickinson and Suczek (1979) and Dickinson (1985) for the Chinji Formation sandstones. 6.8 Framework-grain assemblage Q-F-L. 6.9 Framework-grain assemblage Qm-F-Lt showing sand composition of samples from the Chinji Formation sandstone. 6.10 Qp-Lvm-Lsm triangle of the Chinji formation sandstone. For explanation see Figs. 6.5-6.7.

(Dickenson and Suczek, 1979). Sediments of these orogens are transported into foreland basins or adjacent ocean basins. Some recycled orogens are foreland uplifts, which contain a complex variety of source rocks, including siliciclastic sediments, carbonate rocks, metasediments, plutonic rocks in exposed basement blocks, and volcanic rocks (Boggs, 1992).

Sediments of the recycling of orogenic belts broadly range in composition from continent-continent to continent-ocean collision. Dominance of quartz plus lithic grains, especially sedimentary lithics, and then the metasediments indicate continental collision mountain belts (Tucker, 2001). High Qm contents may reflect derivation from deformed, mature platform sediments, whereas high Qp contents would indicate that the suture zone and/or fold-thrust belt are the sources (Ingersoll et al., 1984).

Qp-Lvm-Lsm plot shows a suture belt and collisional orogen provenance for samples from Chashmai anticline (Fig. 6.10). Sediments derived from such orogens are composed largely of recycled sedimentary materials, with intermediate quartz contents, high ratio of quartz to feldspar and abundant sedimentary-metsedimentary lithic fragments. High feldspar contents and high chert contents in such sandstones indicate significant contributions from igneous terrains uplifted adjacent to the crustal sutures, and mélange terrains caught along the suture belts, respectively, though chert nodules from carbonate succession may also be important sources for high chert contents. Collision derived detritus from suture belts are little affected by climate (Dickinson and Suczek, 1979).

6.11. Provenance of the Nagri Formation

Modal point count data of the sandstone of the Nagri Formation suggest dissected arc and recycled orogen provenance for the Nagri Formation (Table 6.3, Fig. 6.11). The Qm-F-Lt plot indicate a mixed and dissected arc origin for Nagri Formation excluding two samples, one from Chashmai anticline and other from Banda Assar syncline, which mark basement uplift and transitional arc provenance, respectively (Fig. 6.12). Qp-Lvm-Lsm plot also reveals magmatic arc as dominant source for Nagri Formation (Fig. 6.13). Arc-derived sandstones are immature and rich in volcanic lithic fragments. These sediments have a wide variety of sand types ranging from lithic-rich volcaniclastic debris to more quartzo-feldspathic (largely of plutonic origin).

Dissected arcs uncover plutonic core, and sediments of such sources are characterized by the greater abundance of feldspar, particularly plagioclase and volcanic fragments (Ingersoll et al., 1984). Mature and eroded magmatic arcs along continental margins shed detritus of mixed plutonic and volcanic origin into both forearc and backarc basins. Both feldspars are commonly present in significant proportions. Plutonic quartz having vacuoles and inclusions occurs commonly. These sediments are little to moderately affected by climate (Dickinson and Suczek, 1979).

Recycled orogen sandstones are produced from regions created by upfolding or upfaulting of sedimentary or metasedimentary terrains, and are deposited in the associated basins. These orogens result from collision of continental block terrains that get welded together along a suture zone (Boggs, 1992). Collision orogens consist dominantly of nappes and thrust sheets of sedimentary and metasedimentary rock with subordinate amounts of plutonic or volcanic rocks, or even ophiolitic mélanges, and thus produces a complex suite of sediments. Typical sandstones contain intermediate quartz content and abundant sedimentary-metasedimentary lithic fragments (Dickenson and Suczek, 1979). Less-typical sandstones are quartz arenites, feldspathic arenites and chert-rich sandstones. Sediments are shed into foreland basins or are transported longitudinally into adjacent ocean basins. Recycled orogens of foreland uplifts, associated with foreland fold-thrust belts may contain a complex variety of source rocks including siliciclastic sediments, carbonate rocks, metasediments, plutonic and volcanic rocks (Boggs, 1992). Varied composition of detritus derived from recycled orogenic belts also suggest different source rocks of orogen (i.e. either continent-continent or continent-ocean collision). Lithic grains dominate in many continental collision recycled-orogen sandstones, followed by abundance of quartz plus sedimentary-rock fragments, and then the metamorphosed equivalents of the latter as deeper levels of the orogen are uplifted (Tucker, 2001). High Qm and high Qp (chert) contents may indicate a mature platform provenance, and suture zone and/or fold-thrust belt sources, respectively (Ingersoll et al., 1984).

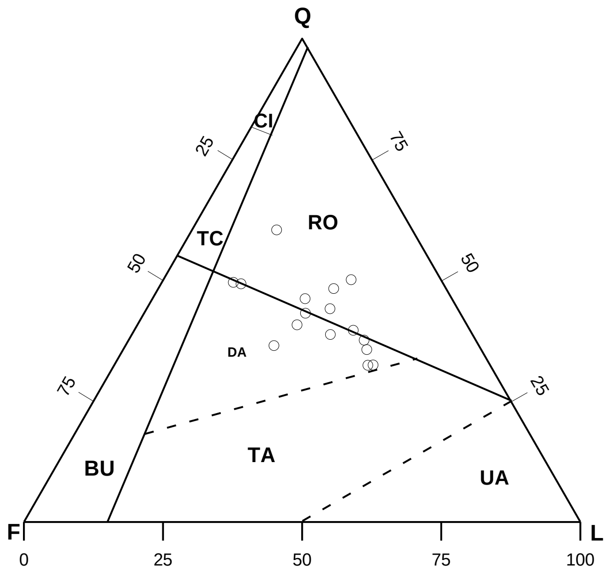

Fig. 6.11

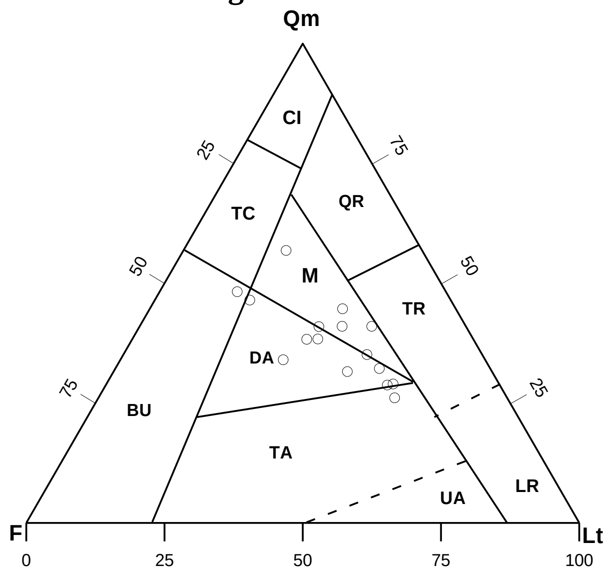

Fig. 6.12

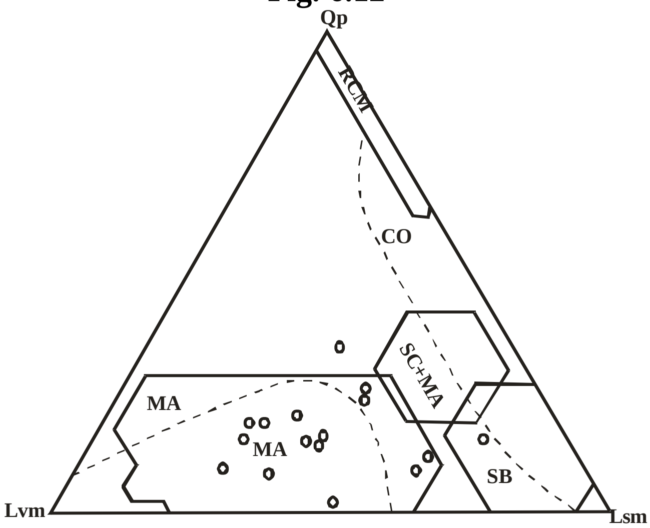

Fig. 6.13

Figs. 6.11-6.13. Ternary diagrams for provenance following Dickinson and Suczek (1979) and Dickinson (1985) for the Nagri Formation sandstones. 6.11 Framework-grain assemblage Q-F-L. 6.12 Framework-grain assemblage Qm-F-Lt showing sand composition of samples from the Nagri Formation sandstone. 6.13 Qp-Lvm-Lsm triangle of the Nagri formation sandstone. For explanation see Figs. 6.5-6.7.

Continental block setting includes major shields and platforms, as well as locally upfaulted basement blocks. Major shields or craton interior provenances are composed dominantly of basement rocks consisting largely of felsic plutonic igneous and metamorphic rocks. Associated platform succession may include abundant sedimentary rocks. Sands derived from craton interiors are typically quartzose containing minor amount of feldspars, reflecting multiple recycling and perhaps intense weathering and long distances of transport (Boggs, 1992). According to Ingersoll et al. (1984), the presence of K-feldspar reflects the ultimate derivation from silicic (granitic or rhyolitic) igneous sources, though it may be recycled. Ingersoll et al. (1984) also reported most feldspathic sandstones from basement uplifts than those reported by Dickinson and Suczek (1979). It confirms a long-held impression that arkoses are typically local deposits related to block faulting or residual deposits above a granitic basement (Potter, 1978; Pettijohn et al., 1987). K-feldspar-to-plagioclase ratios also tend to be high (Boggs, 1992).

The Siwalik Group sandstone in Surghar Range is quartzolithic with metamorphic lithic fragments prevailing over the sedimentary and volcanic types, and enriched in feldspar, especially the K-feldspar (Critelli and Ingersoll, 1994). The molasse sediments in this area also contain a fair amount of red and green chert, which is not common in the suture zone and volcanic arc of Pakistan but more common in southeastern Afghanistan (Azizullah and Khan, 1998). The cement supported detrital grains in sandstone of the lower Siwalik are fine-grained, rounded to subrounded, and characterized by moderate to good sorting. The quartz grains in the Middle Siwaliks sandstone contain inclusions of zircon, epidote, sillimanite, apatite and ore. In some cases, calcite replaces the plagioclase grains completely, indicating post-depositional processes of cementation (Abid et al., 1983).

6.12 Conclusions

- Mineralogically, the sandstones of the Kamlial, Chinji and Nagri formations of the southwestern Kohat Plateau are feldspathic and lithic arenites. But there is a systematic spatial shift in sandstone composition; all the three formations from the Banda Assar syncline are totally lithic arenite while that of the Chinji Formation from the Chashmai anticline is exclusively feldspathic arenite.

- The quartz grains of the Kamlial sandstone are mainly derived from medium- and high-grade metamorphic rocks, with subsidiary contribution from low grade metamorphics, whereas the types of quartz grains from sandstone of the overlying Chinji and Nagri formation indicates subequal contribution from medium-high grade and low-grade metamorphic rock provenances. Spatial control in types of quartz grains is again noteworthy as the quartz grains from the Chashmai anticline indicate their derivation exclusively form medium- and high-grade metamorphic rocks for all the three formations whereas the quartz grains of all the three formations from the Banda Assar syncline and Bahadar Khel anticline suggest a dominant contribution from low grade metamorphic rocks. The relative dominance of polycrystalline quartz grains composed of 2-3 crystals (Qp_{2-3}) also proposes an origin from metamorphic source rocks. Similarly, the presence of mica and other heavy minerals indicate that the source area was composed of metamorphic rocks. However, the relatively greater abundance of monocrystalline quartz suggests that the presence of granitic and volcanic rocks in the source areas cannot be ruled out, or else the quartz grains have traveled a longer distance of transportation.

- Section to section spatial and temporal increase in the relative abundance of non-undulatory and undulatory monocrystalline quartz within formation suggests plutonic/volcanic and metamorphic/tectonically deformed source lithologies, respectively.

- Although the alkali feldspar is chemically more stable than plagioclase, its high proportion indicates dominance of granite and acidic gneisses in the source area. Similarly, the average contents of different quartz types from the Kamlial, Chinji and Nagri formations are suggestive of a granitic and/or gneissic source. Furthermore, appreciable amount of feldspar in the studied formations indicates either high relief of the source area or arctic climate.

- Lithic particles of the studied formations suggest a recycled orogen, except the Banda Assar section for Chinji Formation that indicates a provenance from magmatic arc settings.

CHAPTER 7

Mudstone of the Neogene Sequence of Southwestern Kohat

7.1 Introduction

Clay-mineral distribution in sediments gives information about the geology and climatically controlled weathering conditions of the source area, and has been widely used to reconstruct paleoclimate (Biscaye, 1965; Griffin et al., 1986; Chamley, 1989; Thiry, 2000). Clay mineral assemblages in ancient sediments are affected by both pre- and post-burial conditions. Pre-burial controls include source area lithology, depositional environment, paleoclimate and topography (Chamley, 1989). Post-burial processes, on the other hand, modify the original detrital composition of clays and completely obliterate primary depositional features (Hower et al., 1976). Therefore, sediments that have not undergone intense diagenesis, the vertical and lateral variations of detrital clay minerals can significantly be used as a tool to untie the depositional history of fine-grained sedimentary rocks (Net et al., 2002).

Mudstones of the Neogene sedimentary sequence of southwestern Kohat is mainly red-brown-gray in colors. These mudstones consist of decimeters to meters thick mudstone strata mainly composed of claystone to coarse siltstone, and generally contain 10-25% micron-scale matrix calcite (See Chapter 8). It generally attains a sheet form extending laterally up to hundreds of meters, though lenticular units are also present. Different strata of mudstone in the field were identified on the basis of variation in color, texture and degree of bioturbation. Bioturbation associated with burrows, root casts and desiccation cracks occurs near the tops of strata indicating degree of pedogenesis. The pedogenic features and distinctive red color of some laterally extensive mudstone layers suggest a mature nature of paleosols (Behrensmeyer & Tauxe, 1982; Johnson, N. M. et al., 1985; Behrensmeyer, 1987; Retallack, 1986, 1997; Willis, 1993a; Willis & Behrensmeyer, 1994). These paleosols can be divided into two horizons. The upper horizons are decimeters to several meters thick with abundant desiccation cracks, burrow tubes/root casts and different colors (mottling). Whereas the lower horizons with similar thickness are dominated by calcium carbonate nodules of varying sizes (few cm in diameter), shapes and composition, which form loosely interconnected networks. However, there are also paleosols which do not display well developed horizons. Carbonate nodules indicate precipitation of calcium carbonate due to evaporation of groundwater. The co-existence of iron oxide and calcite concretions in these paleosols suggests marked dry and wet seasons, more likely the modern monsoonal climate at that time. This chapter presents discussion regarding identification and distribution of minerals present in mudstones of the Neogene sedimentary sequence of southwestern Kohat Plateau.

7.2 Methods of Sampling and Analyses

A total of 76 unweathered mudrock samples from three sections of the Neogene sedimentary sequence of southwestern Kohat Plateau were collected and downsized to 250 g each by coning and quartering. On the basis of variation in color and texture, thirty seven samples were selected for X-ray diffractometer (XRD) analysis. All the samples were dried at 60°C for 10-12 h before running through XRD. Selected samples were also analyzed sequentially on air-dried and then glycolated. The dried powdered (< 200 mesh) samples were taken in a sample holder and pressed with a glass slide (press mount method). All the samples were analyzed by a fully automated computerized Rigaku Geiger Flex XRD, using Cu-Kα radiation at the Geoscience Advance Research Labs., Islamabad. The XRD was operated at 40 kV/30 mA and the samples were scanned from 2° to 70° 2θ, at a running speed of 1° 2θ per minute. The diffraction patterns thus obtained were first interpreted by computer software and then checked manually. For cross check, the samples were also analyzed using Rigaku XRD based in the National Center of Excellence in Geology, University of Peshawar, by continuous scanning from 2° to 70° 2θ angle at 40kV/20mA with Cu-Kα radiation.

Semi-quantitative estimations of the relative concentrations of the constituent minerals were carried out on computer program and manually based on the peak area method (Biscaye, 1965). The peak areas of glycolated samples were first computed 10 A° for illite and 7 A° for kaolinite. These values were multiplied by the weighting factors 4 and 2, for illite and kaolinite, respectively (Biscaye, 1965). Intensities of selected peaks were corrected using the intensity factors suggested by Cook et al. (1975) with slight modifications, and used to describe the XRD results which are semiquantitative.

Illite is characterized by 10 Aº (001) and 5 Aº (002) reflections which remained unchanged on treating with glycol and on heating at 450º C (Bagati and Kumar, 1994).

The XRD patterns of whole-rock samples obtained following Brown and Brindley (1984) show that, in general, the mudstone of the Neogene sedimentary sequence is rich in quartz followed by the calcite cement, plagioclase, muscovite and clays.

7.3 Weathering and Formation of Clay Minerals

Clay minerals in sediments or sedimentary rocks have three origins: (a) inheritance (detrital clay), (b) neoformation (in situ clay) and (c) transformation (rearrangement of cation in pre-existing clay) (Tucker, 2001).

In the study of mudrocks, it is essential to know about the type and origin of the clays. Inherited clays give information about the provenance of the deposit and probably the climate there, whereas neoformed clays indicate the chemistry of the pore-fluid, degree of leaching and temperature of the existing mudstone. Transformed clays, on the other hand, carry a memory of inherited characteristics from the source area, together with information on the chemical environment to which the sample was later subjected (Tucker, 2001).

The limited amount of clay fraction in mudstones indicates that weathering-limited conditions prevailed in large parts of the drainage area, and the soil-formed neo-minerals were not dominating the suspended river load. Fluvial erosion processes removed mainly parent rock material and little soils. The neo-mineral group includes minerals of the (1) montmorillonite/smectite type indicating temperate to subtropical climates, (2) illite/muscovite type indicating humid temperate climate, and (3) kaolinite and gibbsite indicating semi-arid to tropical climates (Einsele, 1992).

The most important transformation in clay minerals is that of the smectite not illite and chlorites. Where smectite is dioctahedral, its transformation produces illite through an intermediary called illite/smectite, I/S, and when trioctahedral, the transformation produces chlorite through an intermediary called illite/chlorite, I/C (Boggs, 1992). Genesis of clay minerals is primarily controlled by climate and rock type.

7.3.1 Rock-type Control: Non-indurated and weakly indurated sediments are easily eroded, in contrast to granitic or metamorphic rocks. The large rivers draining the Himalayas, have considerably different average sediment yields from one another because of different rock sources. The Indus exhibits a comparatively low specific transport rate (100 t/km^{2}a), and the Ganges and Brahmaputra Rivers deliver 600 and 900 t/km^{2}a, respectively (Einsele, 1992).

Similarly, the relative abundance of clay minerals in shales is a function of source lithology. For example, chlorite and micas are common in low- and medium-rank metamorphic rocks, and kaolinite, smectite, illite, chlorite, mixed-layer clays and micas may be present in sedimentary rocks (Boggs, 1992). Principle constituents of the mudstone are listed in Table 7.1.

Table 7.1. Principal constituents in shale (Potter et al., 2005).

Constituents	Remarks
Silicate minerals	
Quartz	Make up 20-30 % of the average shale; probably mostly detrital
Feldspar	Plagioclase generally more abundant than alkali feldspar
Zeolites	Commonly present as alteration product of volcanic glass
Clay minerals	
Kaolinite (7 °A)	Forms under strong leaching conditions; abundant rainfall, good drainage, acid waters
Smectite-illite-muscovite (10 °A and greater)	Smectite is hydrated, expandable clay; common in soil and an alteration product of volcanic glass; alters to illite during burial; illite is the most abundant clay mineral in shales; derived mainly from pre-existing shales; alters to muscovite during diagenesis; muscovite may also be detrital
Chlorite,	Chlorite forms particularly during burial diagenesis
Sepiolite	Mg-rich clays that form under special conditions where pore waters are rich in Mg
Oxides and hydroxides	
Iron oxide	Hematite is most common in shales, commonly present as coating on clay minerals
Gibbsite	Consists of $Al(OH)_3$; derived from the weathering of tropical landmasses
Sulfur minerals	
Sulfates: gypsum, anhydrite	Occur as concretions in shales and may indicate the presence of hypersaline conditions during or after deposition
Sulfides	Mainly the iron sulfides pyrite and marcasite

7.3.2 Climate Control: Humid climates and well drained topographies lead to extensive weathering of feldspars to kaolinite (Pettijohn et al., 1987). Kaolinite, in fact, is often the first mineral to form as a product of chemical weathering (Sengupta, 1994). The newly formed clay minerals (neo-minerals), for example kaolinite, reflect the climate of their drainage area rather than the mineralogical composition of the source rocks (Einsele, 1992).

Chlorite is a major constituent of slates and greenschists and its presence in considerable quantities results from the mechanical erosion of pre-existing minerals. However, chlorite is destroyed in warm, humid climates, because it is very sensitive to chemical weathering. Hence, the presence of detrital chlorite indicates a cold or possibly arid climate (Einsele, 1992).

In semi-arid regions (10 to 50 cm rainfall) Na^{+} and K^{+} are mainly, and Ca^{++} and Mg^{++} are partially in solutions (Potter et al., 2005). Consequently, calcium carbonate can be reprecipitated in the soil zone. If often forms nodules close to the surface (calcrete or caliche), such soils are called pedocals. In more temperate humid zones, illite is a characteristic weathering product (Einsele, 1992). In arid regions (less than 10 cm) or regions with excess irrigation, many soils do not follow the common depletion equation because evaporation exceeds precipitation, and calcite and evaporitic minerals are precipitated to form crusts such as calcretes and gypcretes (Potter et al., 2005). Lower rainfall and poorer drainage may result in the formation of smectite. Mafic silicates in many climates will go to smectite (Pettijohn et al., 1987).

The presence of either kind of kaolinite may be evidence of an invasion of relatively fresh groundwater entering the sandstone from a recharge outcrop belt in which there was a supply of distilled silica from chemical weathering (Pettijohn et al., 1987). The formation of a stable clay mineral assemblage of illite and chlorite in sandstones as in shales is a result of long time and/or deep burial (Pettijohn et al., 1987).

In regions of high-latitude and arid zones, the soil generating processes and hence the formation of new minerals are slow that can provide even relatively unstable minerals as sediment components for basin fill e. g., pyroxene, hornblende groups and different types of feldspar etc. Consequently, the terrigenous material derived from such source areas is controlled primarily by source rocks in the drainage area (Einsele, 1992).

7.3.3 Formation of Clay Minerals: Clay minerals chiefly form via the weathering of primary minerals in soils in the following way (Potter et al., 2005).

H^{+} + Primary mineral $\rightarrow$ Intermediate clay mineral + Solution $\rightarrow$ Gibbsite + Solutions.

Two examples of the above general equation are:

H^{+} + Feldspar $\rightarrow$ Illite $\rightarrow$ Smectite $\rightarrow$ Kaolinite $\rightarrow$ Gibbsite,

H^{+} + Muscovite $\rightarrow$ Illite $\rightarrow$ Smectite $\rightarrow$ Kaolinite $\rightarrow$ Gibbsite, The needed H^+ comes via release form water, which is facilitated by excess of CO_2. Thus the more CO_2 dissolved in the water (supplied by bacterial respiration), faster the weathering process. The total flux of water through the soil system also play a very important role in this reaction; the larger the flux, the greater the tendency for these reactions to move to the right. Another important factor is the time interval. With enough time even slow reactions go to completion. The above reactions may tend to be reversed during burial e.g., illite and quartz may form at the expense of smectite (Potter et al., 2005). Table 7.2 shows average feldspar content of igneous rocks and some ancient mudstone.

Illites are the most common weathering products of feldspars and micas. Illites are also often produced by the weathering of pre-existing shales, and they are common in deeply buried muds and shales, where they are formed by the transformation of smectite (Prothero and Schwab, 2003).

Table 7.2. Comparison of the average feldspar content of various plutonic igneous rock with that of ancient red beds. Data are from: Selley (1966) and Krynine (1950)

Rock Types	Potash feldspars (%)	Plagioclase (%)
Granite	40	26
Syenite	72	12
Granodiorite	15	46
Quartz diorite	06	56
Diorite	03	64
Gabbro	0	65
Precambrian sandstone	24	02
Paleozoic sandstone	8.3	01
Mesozoic sandstone	24	06
Cenozoic sandstone	18.5	0.4

7.4 Diagenesis of Clay Minerals and Mudrocks

Changes in the clay mineralogy during diagenesis take place principally due to a rise in temperature associated with increased depth of burial. Studies of long cores through thick mudrock sequences show that the main changes involve an alternation of smectites to illite via mixed-layer clays of smectite-illite. This alternation involves the incorporation of K^+ ions into the smectite structure and loss of interlayer water. The process is largely temperature dependent and the temperature at which smectite begins to disappear is in the order of 70-95º C. This temperature range indicates depths of 2-3 km in areas of average geothermal gradient (30º C km^{-1}). At slightly higher temperatures and greater depths, kaolinite is replaced by illite and chlorite (Turner, 1980). Least altered mudstones identification can be made by:

1) Presence of kaolinite. Detrital kaolinite is stable to temperature between 200 to 550 ºC (Carroll, 1970), so its presence indicates relatively low levels of thermal alteration.
2) Low illite crystallinity indicates that the less ordered (i.e., low temperature) illites are relatively abundant (Weaver, 1989).

7.5 Mudstone of the Sedimentary Sequence of Himalayan Foreland Basin

The Himalayan foredeep created in the last phase of Himalayan orogeny provided the basin in which the well-known Siwalik sediments were deposited (Johnson, N. M., et al., 1985). These sediments are dominantly fluvial in nature, and are characterized by the presence of intercalated overbank facies formed during episodes of non-deposition on the river floodplain (Johnson, G. D., 1977; Tandon and Narayan, 1981). An abrupt change in carbon and oxygen isotope ratios of soil carbonates of the Siwalik from Nepal suggest a major shift in vegetation at circa 7 Ma. It is assumed that this shift was associated with hydrological changes induced by the onset of the Asian monsoon (Quade et al., 1989, 1995). This shift in vegetation at Pakistan Siwalik was circa 10 Ma (Morgan et al., 1994).

The mudstone of the Indian Siwalik is usually associated with overbank facies having thicknesses varying from a few tens of centimeters to several meters. It is generally light red, reddish-brown and dark red in colors, and is invariably mottled at different levels. Rhizoliths and rhizoconcretions are also common. The majority of the mudstone contains carbonate nodules ranging in size from 1 to 5 cm in diameter (Sanyal et al., 2004).

The mudstone in the Kohat Plateau is studied from three sections for present work namely, the Banda Assar syncline, the Bahadar Khel and the Chashmai anticlines (Figs. 5.1-5.3). All the three sections contain exposures of the Kamlial, Chinji and Nagri formations (Detailed discussion in Chapter 3). Mudstone of the Kamlial Formation is light brown to dark brown and reddish-brown in color. Some of the mudstone units are characterized by gray, brown and yellow paleosols mostly arranged in variegated multiple horizons. Paleosols with red mottling are most common and contain calcareous nodules, root traces and bio-tubes. In the lower part of the section, brown, purple and red paleosols are common.

The overlying Chinji Formation in all the three sections is dominantly composed of overbank facies (Fig. 5.2). These facies are light brown to dark brown and reddish-brown in color and are generally represented by interbedded clay beds, siltstone and very fine grained sandstone. The overbank facies are characterized by red, reddish-brown and dark gray paleosols mostly arranged in variegated multiple horizons. These paleosols typify red mottling and contain calcareous nodules, root traces and bio-tubes. Calcareous nodules are common and occur in the formation at different places at Chashmai anticline. In contrast to the Chashmai anticline, the calcareous nodules are relatively uncommon in the Banda Assar and the Bahadar Khel anticline. By definition, the Himalayan Foreland Basin was a muddy basin at the time of deposition of the Chinji Formation. A muddy basin is a sedimentary basin of any size having at least 50% mudstone. The mudstones sequences were accumulated by many small rivers closely coupled to actively subsiding foreland basin (Potter et al., 2005).

The Nagri Formation from all the studied sections in the Kohat Plateau contains several units of mudstone which are mainly composed of clay beds or silty clay or interbedded clay, silt and fine grained sand (Fig. 5.3).

Paleosols in the Neogene sedimentary sequence of Kohat Plateau are identified by mottles, soil peds, rootlets (now filled), concentrations of calcareous nodules (caliche), enhanced clay content, absence of primary stratification and color changes (Retallack, 1988). The calcareous nodules occur either discretely or in isolated/coalesced form, vary in shape from spherical to irregular. These nodules grow within the sediment during diagenesis and this may take place just below the sediment-water interface or much deeper in the sediment column. The growth of nodules arises from the localized precipitation of cement from pore waters within the sediments. The composition, Eh and pH of these pore waters are important in controlling nodule mineralogy and growth rates. More commonly nodules are without nucleus, and form along definite horizons or within particular beds, reflecting a level at which supersaturation of pore waters was achieved. In some cases, nodules form around a nucleus, for example a fossil (Tucker, 2001).

The color of mudrocks: Red and purple colors in mudstone of the Neogene sedimentary sequence of the southwestern Kohat are due to the presence of ferric oxide (hematite), occurring chiefly as grain coatings and intergrowths with clay particles. It also develops within biotite cleavage planes and in some cases replaces the biotite. The hematite is chiefly amorphous or consists of micron-size crystals. It is generally accepted that the red color develops after deposition, through an ageing process of a hydrated iron oxide precursor. In most cases the precursor is, however, detrital, mostly unstable ferromagnesian minerals (commonly hornblende and biotite) that may have already been at least partially altered prior to deposition. This idea is also supported by the impermeable nature of many red mudrocks (Tucker, 2001).

In the floodplain environment of the alluvial setting, periodic drying and lowering of the water table produce oxidizing conditions which change iron hydroxides eventually into hematite (Friend, 1966). In contrast, the channel sediments remain mostly below the water table after deposition alongwith the presence of substantial organic matter and bacteria which consume oxygen and cause reducing conditions. In reducing environment, ferric hydroxides become unstable and are removed in solution resulting the channel sediments to drab (Friend, 1966).

Generally, downward movement of water dissolves material from the upper layer and reprecipitates within the soil as siderite, calcite or sulphates, depending on the pore water chemistry. In humid settings the net water movement is downwards, which results in progressive leaching of soluble ions from the upper levels. Iron mobilized in soil waters is precipitated in both ferrous and ferric form, but ferrous oxide or hydroxide may transform to ferric oxide, depending on Eh of the ground water (Collinson, 1996) (Table 7.3). Red coloration in alluvial sediments occurs most commonly because of deposition under hot, semi-arid conditions and diagenetic hematite coatings on detrital grains, commonly quartz (Walker, T. R., 1967). If the diagenetic environment is oxidizing, then the iron is reprecipitated as hematite or rather a hydrated iron oxide precursor, which converts to hematite on ageing. The length of time involved in the ageing process is the order of millions years. Only a small quantity of iron, 0.1%, is sufficient to impart a bright red color to the sediments. The hematite develops above the water table, and below if the ground water is alkaline and oxidizing (Tucker, 2001).

Other colors in mudrocks result from a mixing of the color-producing components. Olive and yellow mudrocks for, example, may owe their color to a mixing of green minerals and organic matter. Different shades of gray may simply be due to bioturbation, and yellows/reds/browns can be the result of pedogenic processes. Water moving through a soil may cause an irregular distribution of iron oxides/hydroxides and/or carbonate. The term marmorization has been applied to this process (Tucker, 2001).

Table 7.3. Naturally occurring forms of ferric oxyhydroxide (Potter et al., 2005).

Ferric oxyhydroxide	Ideal formula
Goethite	FeOOH
Acaganeite	FeOOH
Lepidocricite	FeOOH
Haematite	Fe_2O_3
Maghemite	Fe_2O_3

7.6 Data and Discussion

The XRD data indicate that the mudstone of the Neogene sedimentary sequence of the Kohat plateau is mainly composed of quartz, calcite and feldspars with clay minerals as accessory phases (Appendix A & B). Table 7.4 displays the mineral composition of these mudrocks. Notable are the very low proportions of clay minerals and the high amounts of quartz and calcite, with clay minerals <15%, and quartz and calcite jointly range from 75 to 85% in many of the mudstone samples (Table 7.4). Different types of feldspars are also present in the range of 10 to 25% in nearly all the mudstone samples (Table 7.4). In all the studied rocks, the clay mineral associations in the fine fractions consist mainly of micaceous phases (i.e. muscovite/illite) and kaolinite, with minor amounts of montmorillonite in a few samples (Table 7.4).

Feldspar in the mudstone samples of the Neogene sedimentary sequence is chiefly plagioclase, whereas alkali-feldspar is rare and occur only in a couple of samples. These analyses indicate the dominance of albite from plagioclase series (Appendix A). In a few samples where albite is absent, the XRD peaks indicate the presence of orthoclase (Appendix A). Feldspar occurs in more than half of the samples analyzed through XRD.

The presence of plagioclase may indicate high denudation rate or high relief or limited chemical weathering in the source areas. The limited amount of clay fraction and high contents of quartz and feldspar in mudstones of Neogene sedimentary sequence indicate that chemical weathering was limited and the soil-formed neo-minerals were not dominating in the source area. River system load was, therefore, dominated by parent rock material and little soils.

Table 7.4. Quantitative analysis of mudstone of the Neogene sedimentary sequence of southwestern Kohat.

Sample No.	Quartz	Calcite	Feldspar	Muscovite (Illite)	Kaolinite	Montmo rillonite
KAK-41	55.6± 2.2	30.5 ±2.1	3.3 ±2 microcline	4 ±1.3	6.6 ±1.7	
KAK-49	73.4 ±1.5	5.4 ±1.6	13.6 ±1.5 albite	5 ±0.9	2.6 ±1.2	
KAN-72	53.1 ±2.2	34.5 ±2.1		6.5 ±1.5	5.8 ±1.4	
KBC-106	40.6 ±7	45.0 ±6.9	14.4 ±5.6 anorthite			
KBC-106 2nd search	23.0 ±4.2	61.6 ±4.2		2.5 ±2.8	6.4 ±3.1	6.5 ±2.9
KBC-106 3rd search	28.5 ±4.8	55.0 ±4.8		3.7 ±3.4	7.4 ±3.2	5.4 ±2.2
KBC-107	70.7 ±2.4		22.4 ±4.4 albite	3.1 ±1.4	3.7 ±1.8	
KBC-111	59.9 ±2.9	33.0 ±2.8	4.7 ±2.2 anorthite	2.3 ±2		
KAN-77	49.7 ±1.7	16 ±1.7	23.6 ±4.2 albite	5.4 ±0.9	5.31 ±1.2	
KAN-90	46.8 ±2.9	22.1 ±2.9	20.4 ±6.1 albite	5.8 ±1.9	4.9 ±1.4	
KAN-98	40.9 ±1.4	42.7 ±1.4	9.7 ±3.6 albite	1.9 ±1	4.8 1.1	
KBN-153	55.7 ±1.4	28.0 ±1.4	5.4 ±1.1 anorthite	7.5 ±0.9	3.3 1	

Chlorite content is higher in the Rawalpindi Group than the Siwalik Group and is usually Fe-rich in the eastern Kohat (Abbasi, 1989). However, this conclusion is not supported by the present study from southwestern Kohat Plateau. Chlorite in sedimentary rocks usually comes from low-grade metamorphic rocks. It is a major constituent of slates and schists. Chlorite is particularly abundant in soils formed at higher latitudes where chemical weathering is less intense than physical weathering (Biscaye, 1965; Abbasi, 1989). This concludes that either the source area for the studied sequence was lacking slates and schists, or chlorite from the studied sediments was destroyed during transportation and deposition. As the petrography of associated sandstone indicates that source area was composed of metamorphic rocks. Thus absence of chlorite indicates warm and humid climates, because it is very sensitive to chemical weathering (Einsele, 1992). Furthermore, the absence of chlorite may also be the result of low-grade diagenesis. But at slightly higher temperatures and greater depths, kaolinite is replaced by illite and chlorite (Turner, 1980). The formation of a stable clay mineral assemblage of illite and chlorite in sandstones as in shales is a result of long time and/or deep burial (Pettijohn et al., 1987).

The mica/illite occurs commonly in the molasse sequence of eastern Kohat Plateau, however, its crystallinity increases up-section (Abbasi, 1989). The abundance of mica in this sequence is probably due to high concentrations of mica in most rocks and soils (Biscaye, 1965; Abbasi, 1989). Illite is consistently present in all the studied mudstone samples of the present study, from southwestern Kohat Plateau (Appendix A). Illites are the most common weathering products of feldspars and micas and are also often produced by the weathering of pre-existing shales (Prothero and Schwab, 2003). Thus, illite/muscovite indicates humid temperate climate (Einsele, 1992), and a source area composed of metamorphic and sedimentary rocks (Boggs, 1992). They are also common in deeply buried muds and shales, where they are formed by the transformation of smectite (Prothero and Schwab, 2003).

Illite, kaolinite and mixed layer clays are important constituents of the clay mineral assemblage of sandstone and associated facies of the Middle Siwalik in the Mohand area, Dehra Dun, India. The clay mineral suites show temporal variation and are not related to lithofacies, rather they show good relationship with provenance and climate (Bagati and Kumar, 1994).

The sediments in the Haripur Khol, India indicate their provenance from crystalline, low- to medium grade metamorphic and sedimentary rocks occurring in the Higher, Lesser and Sub-Himalayas (Kumar et al., 1999; Ghosh et al., 2003). Rocks in a high relief region of the Higher Himalaya under physical weathering tend to produce illite- and chlorite-rich clay mineral suites (Suresh et al., 2004).

The dominant presence of illite and chlorite in mudstone indicates less hydrolyzing, and cold and dry glacial periods, whereas dominance of smectite and kaolinite indicates more hydrolyzing warm and humid conditions during interglacial stages. This suggests these clay minerals were sourced from the narrow belt of basic rocks exposed in the Lesser Himalayan hinterland but high rainfall may have also played an important role in controlling smectite distribution in the Middle and Upper Siwalik sequence of the Haripur Khol, India (Suresh et al., 2004).

Kaolinite, another clay fraction, occurs in majority of the mudstone samples studied from the southwestern Kohat Plateau (Appendix A). Kaolinites develop mostly by intense chemical weathering of aluminosilicates, e.g. feldspars and micas, in warm and humid climates (Chamley, 1989). Kaolinite, in fact, is often the first mineral to form as a product of chemical weathering (Sengupta, 1994) and reflects the climate of the drainage area rather than the mineralogical composition of the source rocks (Einsele, 1992). The presence of either kind of kaolinite may also be an evidence of invasion of relatively fresh groundwater entering the sandstone from a recharge outcrop belt in which there was a supply of distilled silica from chemical weathering (Pettijohn et al., 1987).

The occurrence of kaolinite can be explained by erosion from kaoline sand deposits formed under formerly warmer climatic conditions (Streif, 1996). Alternatively, the kaolinite is the erosion product of granitic feldspar-rich rocks from the source area. The overall difference in contents of illite and kaolinite in the molasse sequence is interpreted either to represent the general intensification and reduction of the glaciation of the surrounding areas or source areas of different climatic conditions (Kuhlmann et al., 2004).

Kaolinite formation is favored under tropical to subtropical humid climatic conditions (Chamley, 1989), however, it may also develop by diagenetic processes due to the circulation of acid solutions (Ghandour et al., 2003). In the present study, the sedimentary successions do not have sufficient thickness to cause any significant burial diagenetic changes. Moreover, petrographic studies of sandstone show that the feldspar is least altered and that there is no development of authigenic mica. These features also suggest that diagenetic modification is insignificant (Suresh et al., 2004).

The weathering of high-latitude noncrystalline rocks (such as altered volcanic rocks) produces smectite (Chamley, 1989). Though, smectite may form during chemical weathering in warm temperatures, it principally develops under wet and dry seasons with less water percolation than that needed for kaolinite formation (Chamley, 1989; Gibson et al., 2000). Smectite of the Haripur Khol, India is interpreted to be derived from the weathering narrow belts of volcanic rocks in the Lesser Himalayan hinterland (Raiverman and Suresh, 1997; Suresh et al., 2004). However, this interpretation is not supported by the petrographic data of the associated sandstone that has rare volcanic and mafic rock fragments (Ghosh et al., 2003). The absence of smectite in mudstone of the Neogene sedimentary sequence of the southwestern Kohat Plateau suggests negligible exposures of volcanic rocks in the source area.

It is generally accepted that the Tibetan-Himalayan uplift between 12 and 9 Ma (Amano and Taira, 1992) has led to the intensification of the monsoon system in South

Asia (Ruddiman and Kutzbach, 1989; Raymo and Ruddiman, 1992). Based on their "abrupt uplift model", Prell and Kutzbach, (1992) suggested that rapid uplift began at around 10 Ma. After approximately the present elevation (5 km) was attained at about 5 Ma, further uplift ceased. Prell and Kutzbach (1992) also suggested that monsoons as strong as today might have started around 7-8 Ma, when the elevation was half (2.5 km) of the present one. Evidence in support of this hypothesis comes from both continental and oceanic records.

Burbank et al. (1996) showed that almost all the Siwalik sections recorded acceleration in sedimentation and increase in basin subsidence rate at around 11 Ma. This shift in sediment flux was probably due to the combined action of intensified monsoonal precipitation and tectonic activity (Sanyal et al., 2004). Table 7.5 points out to tectonic control on mudstone.

Table 7.5. Suggested components of muds and sands from different tectonic settings and weathering intensities (Potter et al., 2005).

Tectonic Setting	**Moderate Weathering**	**Strong Weathering**
Igneous Rocks		
Plateau basalts	Fe oxides, smectite, little sand	Fe oxides, some smectite with kaolinite and gibbsite
Island arcs	Smectite with volcaniclastic sands	Smectite and kaolinite with volcaniclastic sands
Continental margin arcs	Smectite and illite with quartzo feldspathic and volcaniclastic sands	Smectite, illite and kaolinite with qartzofeldspathic and volcaniclastic sands kaolinite with quartzose sands
Basement uplifts	Illite with quartzo feldspathic sands	Kaolinite with quartzose sands
Sedimentary Rocks		
Fold-thrust belts and strike-slip terrains	Recycled illite, chlorite, kaolinite plus some new smectite; quartzo feldspathic sands	Recycled illite, chlorite and kaolinite plus abundant new kaolinite; quartzose sands
Craton Interiors	Recycled illite, chlorite and kaolinite: quartzo feldspathic sands	Recycled illite, chlorite and kaolinite plus abundant new kaolinite; quartzose sands
Metamorphic Rocks		
Mountain belts	Recycled chlorite, muscovite, illite; quartzo feldspathic sands	Recycled chlorite, muscovite, illite with kaolinite; quartzose sands
Precambrian shields	Recycled muscovite, illite; qartzofeldspathic sands	Recycled muscovite, illite; quartzose sands

Large amount of granitic rocks in the Higher Himalayan are considered to produce illite and chlorite rich clays, whereas volcanic rocks of Lesser Himalayan produce smectite (Sanyal et al., 2005). Kaolinite can develop from Lesser Himalayan rocks during chemical weathering in warm temperature, but it generally forms in climate that has wet and dry seasons. It needs more percolation water than that required for smectite formation (Chamley, 1989).

Due to loss of water from the crystal lattice, smectite changes into illite during burial diagenesis (Keller, 1970). The transformation of smectite to illite depends on time, potassium availability, water/ rock ratio, fluid and rock composition and starting composition of mixed layer illite-smectite (Sanyal et al., 2005).

7.7 Conclusions

- The Himalayan Foreland Basin acted as a sandy basin during deposition of the Kamlial and Nagri formations, and as a muddy basin during deposition period of the Chinji Formation.
- Red coloration of the Neogene mudstone of the Kohat Plateau most probably indicates deposition under hot, semi-arid and oxidizing diagenetic conditions.
- The more abundance of feldspar (plagioclase) than the clay minerals in the mudstone suggests high denudation rates or high relief or limited chemical weathering in the source area(s).
- The presence of illite in the mudstone suggests cold and dry glacier conditions whereas kaolinite indicates warm and humid conditions. This conclusion favors a source region of vast area that had different climates in different parts. Alternatively this conclusion can also be interpreted by shifts in extreme climatic conditions.
- The presence of illite in mudstone also suggests a source area composed of metamorphic and sedimentary rocks.
- Abundance of alkali feldspar than plagioclase in the associated sandstone, and dominance of plagioclase in mudstone suggest a major change in source area lithologies at time of erosion of these sediments. Dominance of plagioclase suggests source rocks of basic composition, which more readily alter to clay minerals than acidic rocks.

CHAPTER 8
Geochemistry of the Neogene Molasse Sequence of Southwestern Kohat

8.1 Introduction

The geochemistry of clastic sediments has effectively been used for the evaluation of tectonic setting and provenance determination (Bhatia, M. R., 1983, 1985a, b; McLennan et al., 1983; Taylor and McLennan, 1985; Roser and Korsch, 1986, 1988; Condie et al., 1992; Condie, 1993). Though, the chemical record of clastic sedimentary rocks is affected by many other factors such as chemical weathering, transport distance, sorting processes during transport, sedimentation and post-depositional diagenetic reactions (McLennan, 1989; Nesbitt and Young, 1996; Nesbitt et al., 1996), still if the influence of these processes is minor (e.g., the first-cycle sandstones), the composition of siliciclastic rocks predominantly reflect the nature and proportion of their detrital components and hence their provenance (Bhatia, M. R., 1983; Roser and Korsch, 1988). Bhatia, M. R. (1983) classified the tectonic settings of sedimentary basins, containing significant wackes, into four main types: Oceanic Island Arc (OIA), Continental Island Arc (mainly sourced from felsic volcanic rocks), Active Continental Margin (ACM) and Passive Margin (PM) on the basis of relative enrichment and depletion of the immobile and mobile elements. Other authors (Bhatia and Crook, 1986; Roser and Korsch, 1986, 1988) have also presented different discrimination diagrams by which one can infer the provenance and tectonic settings of sandstone.

The most important clues for the tectonic setting of the basin comes from the relative depletion in oxides like CaO and Na_2O (the most mobile phases) and enrichment of SiO_2 and TiO_2 (the most immobile phases). These oxides are assumed to show enrichment or depletion in quartz, K-feldspar, micas, and plagioclase. The ratio of the most immobile elements to the most mobile ones increases from OIA through continental island arc and ACM to the PM tectonic setting due to relative chemical stability (Bhatia, M. R., 1983; Roser and Korsch, 1988).

Similarly, certain trace elements such as Y, Sc, Th, Zr, Hf, Cr, Co and rare-earth elements (REEs) are assumed to be useful indicators of geological processes, provenance and tectonic setting, for their immobility during erosion and sedimentation (Cullers et al., 1979, 1987, 1988; Bhatia and Taylor, 1981; Taylor and McLennan, 1985; Bhatia and Crook, 1986; Cullers and Stone, 1991; McLennan et al., 1993; Bauluz et al., 2000). Th and Sc are generally accepted as among the most reliable indicators of sediment provenance because their distribution is less affected by heavy-mineral fractionation than that of elements such as Zr, Hf, and Sn (Taylor and McLennan, 1985). These recognitions have led to several studies using trace elements in sedimentary rocks to determine their provenance and tectonic setting (McLennan et al., 1993; Eriksson et al., 1994; Bahlburg, 1998; Burnett and Quirk, 2001; Zimmermann and Bahlburg, 2003). Also, it is agreed upon that the fine-grained clastics are more liable to preserve trace element signatures than coarse-grained sediments (McLennan, 2001).

The abundance of La and Th is high in felsic igneous rocks and their weathering products, whereas Co, Sc, Ni, and Cr are more concentrated in mafic than in felsic igneous rocks (Osae et al., 2006). Similarly, higher concentrations of La and Th in silicic than in basic igneous rocks result in high La/Sc, La/Co, Th/Sc and Th/Co ratios in fine-grained sedimentary rocks derived from silicic sources. The extent to which the above elemental ratios are preserved in sandstones and mudstones in a given tectonic environment, however, is somewhat uncertain (Cullers, 1995). Recent studies of size fractions of Holocene soils and stream sediment at the source of uplifted continental blocks in Colorado have given some insight into the problem (Cullers et al., 1987, 1988; Cullers, 1988, 1993). The analyses of clay and silt fractions had shown similar mineralogy and trace element concentrations to the source. In contrast, the sands and gravels are enriched in quartz and feldspar and depleted in heavy minerals relative to the source and thus have lower trace element concentrations than the source (Cullers, 1995). The variability of the chemical composition of sandstones is a reflection of the variable mineralogy produced by sedimentary processes (Cullers, 1994).

Most of the pioneering work that deals with provenance analysis of multidimensional major and trace element geochemical data sets was carried out using multiple discriminant analysis (MDA; Bhatia, 1983; Roser and Korsch, 1988) or principal component analysis (PCA; Bhatia and Crook, 1986). Both are multivariable statistical techniques, and use to visualize first-order differences between groups of samples. MDA is a ‘‘supervised’’ technique as it distinguishes ‘‘natural’’ groups within sets of data, and relies upon prior knowledge of the groupings (Le Maitre, 1982). However, PCA may differentiate between natural groups without prior assumptions (Lacassie et al., 2004).

But on the other hand, several studies suggest that the tectonic settings determination based on geochemical discrimination diagrams are not in agreement with those inferred from plate tectonic reconstructions of ancient terrains (Valloni and Maynard, 1981; Maynard et al., 1982; Van de Kamp and Leake, 1985; Haughton, 1988;

Winchester and Max, 1989; Holail and Moghazi, 1998; Toulkeridis et al., 1999; Shao et al., 2001). Winchester and Max (1989) suggested further tests of these discrimination diagrams using sediments from known tectonic settings. Van de Kamp and Leake (1985) recommended use of individual analyses instead of the average values as suggested by Bhatia, M. R. (1983). In case of ancient collisional settings, the timing, duration, and spatial variation in tectonic activity can be assessed by analysis of the preserved sedimentary record in adjacent foreland basins (Garver et al., 1996).

8.2 Analytical Methods

A total of 41 unweathered sandstone and 44 mudstone samples representing a large variety in color and texture, were selected from three different sections of the Neogene molasse sequence of the Kohat Plateau. The analytical work included major element analyses by Atomic Absorption Spectrometer (AAS) /UV-visible spectrophotometer as well as X-ray Fluorescence (XRF), and trace element analyses by XRF. Each of these samples was crushed to an average particle size of between 1 and 2 mm between the hardened steel face of a ‘fly press'. The crushed samples were pulverized in an agate swing mill for 2-3 min to 200 mesh.

For major element oxides using XRF, approximately 5 g of each sample was dried overnight at 110°C to remove absorbed water. The samples were kept in a muffle furnace at 950°C for two hours to determine the loss on ignition (LOI). Each sample was cooled in a desiccator and then 0.7 g of sample was mixed with 3.5 g of lithium tetraborate flux. An amount equal to the weight loss was added to the 3.5 g to make a bead. The sample-flux mixture was fused in a platinum-gold crucible at 1100°C for 25 min. During this period the crucible was removed periodically and swirled over a Bunsen burner to remove gas bubbles and ensure a thorough mixing and homogeneity of the melt. The melt was cast between aluminum discs and left there for some time to ensure annealing. The bead was cooled by leaving between sindanyo bricks on a hot plate. Major elements were measured from the fusion discs alongwith corresponding GSJ (Geological Survey of Japan) standard samples with every batch of ten samples using the RIGAKU XRF-3370E spectrometer at the Geoscience Advance Research Laboratories, Geological Survey of Pakistan, Islamabad. The results of analyses were then compared with the recommended values of USGS standard reference samples (Govindaraju, 1989). The detection limits of XRF for major elements are as follow: SiO_2 (0.27%), TiO_2 (0.014%), Al_2O_3 (0.13%), Fe_2O_3 (0.08%), MnO (0.005%), MgO (0.03%), CaO (0.09%), Na_2O (0.02%), K_2O (0.03%) and P_2O_5 (0.03%).

Chemical determinations of trace elements were also obtained by X-ray fluorescence spectrometry (Philips PW 1480) on pressed powder pellets at the XRF Laboratory, National Center of Excellence in Geology, University of Peshawar, Peshawar. To avoid particle size effects, the very fine powdered samples were homogenized with a fusion material (wax). Furthermore, major elements were also analyzed by AAS/UV spectrophotometer at the Geochemistry Laboratory, National Center of Excellence in Geology, University of Peshawar. All of the analyses are quite well in agreement in duplicate and replicate.

The precision of the major elements is normally better than 6%; the precision of most of the trace elements is better than 5%. The exception is Yb whose precision is normally better than 7%. Total iron is reported as Fe_2O_3 (Cullers, 2000**)**. Methods of chemical analysis, descriptions of sample sets, and estimates of analytical error are given by Connor (1990).

8.3 Chemical Composition as a Function of Mineral Constituents and Grain Size

In modern sediments, chemical composition of sediments varies with grain size due to four factors: (1) different sources contributing mineralogically and texturally distinct grain sizes, (2) mechanical weathering of lithic grains into finer components, (3) chemical weathering of labile grains into alteration products and (4) sorting of compositionally distinct grains during transport. A number of authors have pointed out that sediment grain size have effects on both modal composition (e.g., Blatt, 1967; Boggs, 1968; Young et al., 1975; Basu, 1976; Mack and Suttner, 1977; Ingersoll et al., 1984; Mack, 1984; Decker and Helmold, 1985; Johnsson, 1990; Marsaglia and Ingersoll, 1992; Heins, 1993; Nesbitt et al., 1996) and geochemistry (e.g. Bhatia and Crook, 1986; Roser and Korsch, 1986; Ergin, 1995; Cox and Lowe, 1996). Whitmore et al. (2004) observed downstream increase in silica content and downstream decrease of Fe_2O_3, Cr and Ni. However, sediment suites derived from magmatic arc show the least compositional variation with decreasing grain size, and medium sand samples generally display average values for most variables (Whitmore et al., 2004). The samples of the Neogene sandstone of the Himalayan Foreland Basin collected from three different section are dominantly medium-grained and medium- to fine-grained, as already discussed in the previous chapter.

8.4 Chemical Classification of the Neogene Molasses Sandstone

The Neogene sandstone of the Himalayan Foreland Basin from Kohat Plateau has been classified into feldspathic arenites and lithic arenites on the basis of petrography. Accordingly, chemical composition of the Neogene sandstone of the Kohat Plateau (Table 8.1) is well within the range of the mean chemical composition of the lithic arenites and feldspathic arenites (Table 8.3). The very high content of CaO in the Neogene sandstone of the Kohat, which ranges from 6 to 24% (with an average value of 13.8%) is because of the secondary $CaCO_3$ and has reduced the contents of the rest of the oxides accordingly. The mean contents of CaO in lithic and feldspathic arenites are 6.2% and 2.0%, respectively.

Medium to fine-grained sandstone samples of the Kamlial, Chinji and Nagri formations from the three sections i.e. the Banda Assar syncline, Bahadar Khel and Chashmai anticlines appear to be well classified by the scattergrams log (SiO_2/Al_2O_3) versus log (Na_2O/K_2O) and log (SiO_2/Al_2O_3) versus log (Fe_TO_3/K_2O) (Figs. 8.1-8.3). The log (SiO_2/Al_2O_3) versus log (Na_2O/K_2O) scattergram shows that sandstones of the studied sections predominantly are the litharenite. A few samples fall in the greywacke field and one sample in the arkose (Figs. 8.1A, 8.2A, 8.3A). The log (SiO_2/Al_2O_3) versus log (Fe_TO_3/K_2O) scattergram shows that the same sandstone samples dominantly fall in the Fe-sand field (Figs. 8.1B, 8.2B, 8.3B), though a few samples mark an Fe-shale field, and a couple of samples of the Kamlial Formation from the Banda Assar section shift to the wacke field of the diagram. The shift of sandstone to various fields is due to a wide range in the variation of relative proportion of matrix, feldspar and lithic components (Lindsey, D. A. et al., 2003).

Variation in Na_2O/K_2O on log (Na_2O/K_2O) scattergrams (Figs. 8.1A, 8.2A, 8.3A) may have been resulted from (a) mixing of two source rocks, one K_2O-rich (i.e. potassium feldspar) and one Na_2O-rich (plagioclase), or (b) varying degrees of weathering of initially Na_2O-rich (plagioclase) rock either in the source area or during transit to the depositional basin, or both. If log (Na_2O/K_2O) values represent mixing of two rock types, then the ratios at the ends of the line should approximate those of the source rocks. If log (Na_2O/K_2O) represents weathering of an originally Na_2O (plagioclase)-rich source rock, then the ratio at the Na_2O-rich end of the trend should approximate the value of the source. Commonly, in unmetamorphosed arkosic rocks, weathering of the source area and sediment during transit is the probable cause of variation in log (Na_2O/K_2O). Furthermore, all the sandstone samples contain varying proportions of ore minerals (Van de Kamp and Leake, 1994; Lindsey, D. A. et al., 2003).

Table 8.1. Major and trace element data of the sandstone of the Neogene molasse sequence for whole-rock samples. Major elements concentration is in weight percent, whereas trace element concentrations in ppm. Last alphabet in each sample number is for "Formation" whereas the middle alphabet is for locality. Last alphabets; K for Kamlial Formation, C for Chinji Formation and N for Nagri Formation. Middle alphabets; C for Chashmai anticline, A for Banda Assar syncline and B for Bahadar Khel anticline. CIA = Chemical Index of Alteration, CIW = Chemical Index of Weathering, ICV = Index of Compositional Variability.

Sample No.	KCK-1	KCK-4	KCK-10	KCC-17	KCC-20	KCN-24	KCN-26	KCN-31
SiO_2	48.94	57.21	56.23	55.04	58.82	53.25	47.66	47.86
Al_2O_3	8.35	9.14	10.30	9.95	8.98	11.40	8.24	10.20
Fe_2O_3	3.75	4.21	4.47	3.37	4.64	3.50	3.89	4.33
MgO	3.48	2.07	3.18	1.69	2.30	1.76	2.18	2.67
CaO	16.15	12.16	11.01	11.75	9.50	11.67	16.47	14.10
Na_2O	1.01	0.51	0.73	1.46	1.76	1.41	1.38	1.45
K_2O	1.50	1.49	1.66	1.58	1.54	1.54	1.45	1.50
TiO_2	0.32	0.82	0.70	0.66	0.46	0.54	0.46	0.68
P_2O_5	0.11	0.09	0.13	0.09	0.10	0.07	0.08	0.12
MnO	0.18	0.11	0.15	0.21	0.12	0.15	0.17	0.14
LOI	16.22	12.18	11.40	14.33	11.80	14.68	18.09	16.89
Total	100.02	99.99	99.96	100.13	100.01	99.97	100.07	99.95
CIA	71.72	78.80	77.44	70.79	66.30	74.06	68.22	71.80
CIW	0.89	0.95	0.93	0.87	0.84	0.89	0.86	0.88
ICV	1.23	1.01	1.06	0.90	1.20	0.78	1.16	1.06
Trace elements								
Sc	14	12	13	15	18	15	19	18
V	51	52	58	73	68	46	46	62
Cr	162	285	86	55	79	203	57	177
Co	43	51	48	35	32	50	42	31
Ni	112	114	40	22	40	77	30	33
Cu	6	17	12	15	10	15	9	10
Zn	29	32	40	30	40	31	28	34
Ga	6	7	8	7	8	7	6	7
Rb	45	52	56	58	52	54	46	50
Sr	168	134	239	201	285	238	218	230
Y	13	13	17	18	17	14	15	15
Zr	81	104	102	149	80	84	74	120
Nb	6	7	6	6	5	6	5	6
Ag	4	5	6	5	8	4	3	5
Cd	2	3	3	5	5	1	4	2
Sn	1	6	4	7	4	5	1	1
Sb	6	-	1	6	2	5	2	7
Cs	-	-	-	4	-	-	-	1
Ba	132	165	188	357	166	168	149	153
La	30	28	17	31	24	33	20	24
Ce	37	56	20	19	8	22	8	15
Nd	19	25	17	23	8	22	12	17
Sm	-	11	-	-	-	-	-	-
Yb	4	-	-	-	1	-	-	5
Hf	5	4	6	8	5	7	4	9
Ta	1	-	4	-	-	-	2	-
W	548	480	499	302	230	375	318	217
Pb	7	9	10	11	9	11	8	9
Th	5	7	6	8	5	6	4	6
U	1	3	4	3	4	4	2	4

Table 8.1 (Continued)

Sample No.	KCN-33	KCN-36	KCN-37	KCN-38	KCN-39	KAK-40	KAK-42	KAK-44
SiO_2	49.01	61.55	60.30	50.66	64.15	51.25	52.24	46.87
Al_2O_3	8.51	10.03	11.12	17.50	6.05	14.51	7.45	23.33
Fe_2O_3	3.73	4.86	3.47	3.69	3.56	3.07	2.52	4.48
MgO	1.83	3.32	1.49	2.04	1.78	1.49	0.94	2.64
CaO	15.49	6.14	8.11	10.38	9.54	15.46	20.41	9.10
Na_2O	1.75	1.98	1.79	1.59	1.71	1.18	1.12	1.41
K_2O	1.33	1.40	1.74	1.51	1.44	1.34	1.16	1.38
TiO_2	0.58	0.80	0.65	0.74	0.70	0.64	0.60	0.93
P_2O_5	0.08	0.10	0.07	0.07	0.05	0.06	0.07	0.15
MnO	0.09	0.21	0.13	0.11	0.10	0.13	0.19	-
LOI	17.54	9.61	10.92	11.71	11.04	10.94	13.26	9.78
Total	99.95	100.00	99.78	100.01	100.12	100.08	99.95	100.06
CIA	66.32	67.71	69.77	80.44	58.05	81.06	70.60	85.93
CIW	0.83	0.83	0.86	0.92	0.78	0.92	0.87	0.94
ICV	1.09	1.25	0.83	0.55	1.54	0.54	0.88	0.46
Sc	17	13	11	11	41	10	12	12
V	41	69	42	44	43	33	33	64
Cr	130	164	113	157	207	230	161	224
Co	30	52	41	54	56	45	22	44
Ni	24	42	23	68	86	34	27	31
Cu	5	7	7	6	5	10	5	11
Zn	28	37	33	34	30	26	23	39
Ga	5	9	8	7	6	7	6	10
Rb	49	68	68	59	57	59	46	64
Sr	202	280	291	240	221	219	207	221
Y	14	16	14	16	12	14	18	18
Zr	66	185	85	124	95	95	97	121
Nb	4	8	6	7	6	5	6	8
Ag	4	6	3	4	3	5	4	7
Cd	2	2	5	2	1	4	3	4
Sn	1	5	5	4	4	7	4	6
Sb	10	4	1	1	4	5	9	-
Cs	3	1	-	1	11	3	-	-
Ba	141	254	235	226	186	232	156	222
La	20	29	20	28	19	23	20	23
Ce	44	41	24	37	5	38	27	42
Nd	25	28	21	2	3	30	21	33
Sm	-	-	-	-	-	-	-	-
Yb	-	-	-	-	-	1	-	-
Hf	3	6	4	-	4	1	1	5
Ta	-	-	-	3	2	-	-	-
W	206	327	261	388	383	362	29	331
Pb	10	11	10	11	9	11	10	11
Th	4	9	6	7	5	5	6	8
U	2	3	4	3	3	3	3	3

Table 8.1 (Continued)

Sample No.	KAK-52	KAC-56	KAC-63	KAN-67	KAN-71	KAN-78	KAN-80	KAN-84
SiO_2	49.81	51.13	53.07	59.85	54.08	56.30	60.27	56.30
Al_2O_3	6.70	11.58	10.83	11.28	11.33	9.30	7.78	8.97
Fe_2O_3	2.74	4.84	4.33	4.58	3.67	4.04	3.36	3.38
MgO	0.98	2.66	3.71	2.72	2.79	2.32	1.65	2.09
CaO	18.50	12.24	12.26	7.23	11.15	12.01	11.11	12.50
Na_2O	1.06	1.77	1.65	1.86	2.07	1.39	1.09	1.16
K_2O	1.07	1.36	1.12	1.94	1.85	1.51	1.36	1.44
TiO_2	0.54	0.58	0.72	0.63	0.62	0.94	0.75	0.77
P_2O_5	0.06	0.09	0.10	0.07	0.09	0.08	0.06	0.11
MnO	0.09	0.12	0.11	0.08	0.10	0.12	0.11	0.11
LOI	16.79	13.38	12.53	9.93	12.03	11.88	12.26	13.16
Total	98.33	99.76	100.43	100.18	99.77	99.90	99.81	99.97
CIA	69.75	72.52	73.36	68.56	67.71	70.34	70.45	72.11
CIW	0.86	0.87	0.87	0.86	0.85	0.87	0.88	0.89
ICV	0.97	0.98	1.08	1.05	0.98	1.11	1.07	1.00
Sc	15	12	16	8	12	15	11	11
V	29	92	56	58	59	53	42	38
Cr	59	150	316	154	61	366	535	305
Co	39	39	37	47	51	32	44	25
Ni	35	35	60	46	49	29	82	63
Cu	14	13	9	9	11	8	8	7
Zn	26	40	37	36	41	38	29	29
Ga	5	8	9	9	9	8	7	7
Rb	53	55	52	73	83	65	54	57
Sr	176	191	223	200	147	211	180	180
Y	10	16	16	12	12	15	14	15
Zr	74	102	112	112	79	90	136	135
Nb	5	7	7	8	7	6	6	7
Ag	5	5	3	7	6	-	7	3
Cd	4	3	5	4	3	2	3	1
Sn	5	3	3	6	5	4	5	2
Sb	1	-	3	-	3	7	2	5
Cs	14	13	-	4	10	-	-	8
Ba	154	165	157	254	293	205	179	167
La	22	21	29	24	26	24	28	26
Ce	8	10	39	38	52	30	62	28
Nd	16	16	38	21	18	27	41	27
Sm	-	-	-	-	-	-	1	-
Yb	1	-	1	-	-	-	-	-
Hf	1	5	14	4	10	11	1	5
Ta	-	3	1	-	-	2	-	1
W	310	285	247	350	354	184	356	161
Pb	11	12	10	11	12	10	9	11
Th	6	7	6	7	5	6	7	7
U	2	4	4	3	2	3	3	3

Table 8.1 (Continued)

Sample No.	KAN-87	KBK-88	KBK-95	KBK-97	KBK-100	KBC-104	KBC-106	KBC-111
SiO_2	54.72	63.43	47.41	56.10	49.68	53.86	49.76	49.58
Al_2O_3	6.64	6.88	6.51	8.88	6.06	8.39	8.87	10.54
Fe_2O_3	3.56	4.76	4.42	3.73	2.83	4.26	4.42	4.29
MgO	3.08	3.52	1.97	1.96	1.59	2.92	2.22	2.29
CaO	15.31	7.48	19.26	10.00	19.81	11.55	16.36	13.59
Na_2O	0.87	0.87	0.76	0.94	0.81	1.02	0.98	1.76
K_2O	1.05	1.34	1.15	1.18	1.09	1.46	1.33	1.43
TiO_2	0.53	0.70	0.84	0.86	0.57	0.86	0.50	0.68
P_2O_5	0.05	0.11	0.11	0.09	0.07	0.09	0.13	0.09
MnO	0.14	0.09	0.23	0.12	0.19	0.11	0.17	0.19
LOI	13.98	10.72	17.47	16.14	17.57	15.47	15.28	15.44
Total	99.93	99.91	100.12	100.00	100.26	100.00	100.01	99.88
CIA	72.08	70.44	72.34	75.86	70.74	71.99	74.40	70.32
CIW	0.88	0.89	0.90	0.90	0.88	0.89	0.90	0.86
ICV	1.39	1.64	1.44	0.99	1.17	1.27	1.08	1.01
Sc	11	12	19	13	16	14	11	15
V	43	54	58	65	36	124	57	72
Cr	288	191	175	409	183	80	142	201
Co	50	44	30	41	43	24	33	38
Ni	129	222	41	92	78	78	43	37
Cu	10	5	13	7	3	50	10	13
Zn	32	41	34	33	25	98	39	37
Ga	5	8	8	7	5	16	8	8
Rb	39	58	49	48	41	126	54	62
Sr	191	135	190	127	147	143	233	213
Y	15	12	21	15	10	20	16	14
Zr	84	91	96	120	105	134	85	94
Nb	6	7	6	7	6	11	6	6
Ag	-	3	7	7	4	5	6	4
Cd	2	-	2	5	4	1	1	3
Sn	4	2	4	4	3	6	2	3
Sb	8	-	6	-	13	1	1	6
Cs	-	-	-	-	6	4	-	-
Ba	137	176	186	173	138	206	192	212
La	18	28	28	26	25	29	20	27
Ce	28	23	54	13	39	48	30	51
Nd	30	27	31	26	21	31	14	30
Sm	2	-	-	-	-	1	-	-
Yb	-	2	-	13	1	4	-	1
Hf	-	6	2	3	2	6	4	2
Ta	2	-	3	1	3	-	-	2
W	381	264	183	297	311	29	192	264
Pb	7	6	11	8	6	22	10	13
Th	6	5	6	6	6	13	5	7
U	4	3	5	4	14	4	3	3

Table 8.1 (Continued)

Sample No.	**KBC-114**	**KBC-125**	**KBC-127**	**KBN-130**	**KBN-135**	**KBN-137**	**KBN-142**	**KBN-144**
SiO_2	44.50	42.56	53.07	36.65	51.19	42.29	46.75	47.27
Al_2O_3	9.49	7.42	10.85	9.62	10.82	9.70	11.59	8.36
Fe_2O_3	4.19	3.25	3.75	3.88	2.58	3.76	4.62	3.95
MgO	2.70	1.72	2.35	3.16	2.86	1.94	2.76	2.25
CaO	19.43	23.65	9.74	24.24	14.11	22.68	9.39	18.05
Na_2O	1.89	1.57	1.70	1.98	1.34	0.94	1.43	0.79
K_2O	1.25	1.19	1.49	1.48	1.36	1.34	1.71	1.15
TiO_2	0.88	0.45	0.77	0.70	0.71	0.54	0.60	0.71
P_2O_5	0.09	0.08	0.10	0.10	0.09	0.10	0.10	0.09
MnO	0.19	0.14	0.11	0.28	0.14	0.25	0.10	0.24
LOI	15.28	17.89	15.92	18.16	14.84	16.29	20.74	17.03
Total	99.89	99.91	99.86	100.24	100.04	99.84	99.79	99.90
CIA	68.07	65.73	71.08	66.41	74.63	76.40	73.36	76.70
CIW	0.83	0.83	0.86	0.83	0.89	0.91	0.89	0.91
ICV	1.17	1.12	0.94	1.19	0.83	0.91	0.97	1.09
Sc	16	21	19	9	14	18	13	15
V	67	39	47	56	65	46	61	66
Cr	158	121	258	90	97	44	139	342
Co	34	42	29	42	42	26	31	45
Ni	24	87	29	23	32	21	25	74
Cu	11	6	8	21	10	5	14	9
Zn	34	26	31	36	39	32	40	36
Ga	8	6	6	8	8	7	10	7
Rb	52	44	52	66	62	56	76	52
Sr	262	201	257	218	204	214	227	205
Y	19	11	16	12	17	14	16	20
Zr	125	75	111	91	102	78	138	169
Nb	6	6	5	6	6	5	7	8
Ag	5	3	5	2	6	4	5	3
Cd	4	1	3	3	4	1	3	2
Sn	3	1	1	5	5	-	6	4
Sb	6	7	8	-	2	6	5	7
Cs	3	3	5	1	4	10	-	10
Ba	157	122	160	224	215	164	231	177
La	27	26	26	27	28	23	26	36
Ce	22	6	42	36	34	28	28	53
Nd	27	22	32	21	27	18	27	39
Sm	-	-	-	-	-	-	-	-
Yb	-	-	1	2	-	-	2	4
Hf	10	2	9	10	-	7	5	13
Ta	-	-	-	1	-	-	-	3
W	210	273	162	271	287	188	182	270
Pb	11	10	10	11	10	9	13	12
Th	6	5	6	6	7	5	8	8
U	3	3	4	3	3	4	2	4

Table 8.1 (Continued)

Sample No.	KBN-152
SiO_2	50.99
Al_2O_3	6.29
Fe_2O_3	3.27
MgO	1.65
CaO	18.37
Na_2O	0.91
K_2O	1.28
TiO_2	0.46
P_2O_5	0.05
MnO	0.18
LOI	16.73
Total	100.17
CIA	68.53
CIW	0.87
ICV	1.23
Sc	12
V	44
Cr	143
Co	60
Ni	54
Cu	10
Zn	29
Ga	6
Rb	53
Sr	165
Y	14
Zr	96
Nb	6
Ag	4
Cd	4
Sn	5
Sb	9
Cs	9
Ba	183
La	27
Ce	23
Nd	19
Sm	-
Yb	-
Hf	6
Ta	2
W	403
Pb	10
Th	6
U	3

Table 8.2. Ratios of major element oxides and trace elements of the sandstone of the Neogene molasse sequence for whole-rock samples. Last alphabet in each sample number is for "Formation" whereas the middle alphabet is for locality. Last alphabets; K for Kamlial Formation, C for Chinji Formation and N for Nagri Formation. Middle alphabets; C for Chashmai anticline, A for Banda Assar syncline and B for Bahadar Khel anticline.

Sample No.	KCK-1	KCK-4	KCK-10	KCC-17	KCC-20	KCN-24	KCN-26	KCN-31
SiO_2/Al_2O_3	5.86	6.26	5.46	5.53	6.55	4.67	5.78	4.69
Al_2O_3/SiO_2	0.17	0.16	0.18	0.18	0.15	0.21	0.17	0.21
Al_2O_3/Na_2O	8.25	17.82	14.02	6.83	5.10	8.07	5.98	7.05
Na_2O/K_2O	0.67	0.34	0.44	0.92	1.14	0.92	0.95	0.96
K_2O/Na_2O	1.48	2.91	2.25	1.08	0.88	1.09	1.06	1.04
K_2O/Al_2O_3	0.18	0.16	0.16	0.16	0.17	0.14	0.18	0.15
Fe_2O_3+MgO	7.23	6.27	7.65	5.06	6.94	5.26	6.07	7.01
La/Th	5.82	4.09	2.88	4.00	4.70	5.96	5.13	4.19
La/Y	2.28	2.11	1.04	1.74	1.39	2.39	1.29	1.61
La/Sc	2.11	2.38	1.35	2.08	1.28	2.23	1.04	1.34
Th/Sc	0.36	0.58	0.47	0.52	0.27	0.37	0.20	0.32
Th/Co	0.12	0.13	0.13	0.22	0.16	0.11	0.09	0.19
Th/Cr	0.03	0.02	0.07	0.14	0.06	0.03	0.07	0.03
Ba/Co	3.06	3.24	3.91	10.20	5.15	3.38	3.57	4.99
Ba/Sc	9.38	14.06	14.65	24.12	9.05	11.18	7.95	8.53
Rb/Cs	-	-	-	14.02	-	-	-	50.20
Y/Ni	0.12	0.12	0.42	0.81	0.42	0.18	0.51	0.44
Ti/Zr	39.75	78.39	68.47	44.41	57.59	64.68	62.20	56.76
Cr/Ti	0.05	0.03	0.01	0.01	0.02	0.04	0.01	0.03
Cr/V	3.17	5.48	1.47	0.76	1.17	4.38	1.25	2.86
V/Cr	0.32	0.18	0.68	1.32	0.85	0.23	0.80	0.35
K/Rb	332.36	288.71	295.25	274.66	294.61	288.00	319.59	299.26
Cr/Ni	1.45	2.50	2.16	2.52	1.97	2.63	1.91	5.32
Cr/Th	31.85	41.91	14.27	7.16	15.86	36.24	15.03	31.08
Cr/Sc	11.52	24.36	6.69	3.72	4.33	13.53	3.04	9.90
Ni/Co	2.60	2.25	0.83	0.63	1.25	1.55	0.71	1.09
Cu/Zn	0.20	0.53	0.30	0.48	0.25	0.50	0.33	0.29
Zr/Th	15.78	15.31	16.97	19.39	15.94	15.02	19.42	21.02
Zr/Sc	5.71	8.90	7.95	10.09	4.36	5.61	3.93	6.69

Table 8.2 (Continued)

Sample No.	KCN-33	KCN-36	KCN-37	KCN-38	KCN-39	KAK-40	KAK-42	KAK-44
SiO_2/Al_2O_3	5.76	6.14	5.43	2.89	10.61	3.53	7.01	2.01
Al_2O_3/SiO_2	0.17	0.16	0.18	0.35	0.09	0.28	0.14	0.50
Al_2O_3/Na_2O	4.86	5.05	6.23	11.00	3.54	12.29	6.63	16.50
Na_2O/K_2O	1.31	1.42	1.03	1.05	1.18	0.88	0.97	1.03
K_2O/Na_2O	0.76	0.71	0.97	0.95	0.85	1.13	1.03	0.98
K_2O/Al_2O_3	0.16	0.14	0.16	0.09	0.24	0.09	0.16	0.06
Fe_2O_3+MgO	5.55	8.18	4.96	5.73	5.34	4.57	3.46	7.12
La/Th	5.15	3.38	3.56	4.06	3.71	4.98	3.19	2.74
La/Y	1.42	1.79	1.47	1.76	1.59	1.70	1.11	1.28
La/Sc	1.20	2.17	1.78	2.58	0.46	2.27	1.65	2.00
Th/Sc	0.23	0.64	0.50	0.64	0.12	0.46	0.52	0.73
Th/Co	0.13	0.16	0.14	0.13	0.09	0.10	0.28	0.19
Th/Cr	0.03	0.05	0.05	0.04	0.02	0.02	0.04	0.04
Ba/Co	4.62	4.85	5.68	4.16	3.33	5.20	7.04	5.05
Ba/Sc	8.36	18.95	20.61	20.50	4.53	23.00	12.81	19.30
Rb/Cs	15.41	48.79	-	45.23	5.13	23.60	-	-
Y/Ni	0.59	0.39	0.60	0.24	0.14	0.39	0.67	0.58
Ti/Zr	87.44	43.31	75.91	60.00	74.15	67.71	61.44	76.53
Cr/Ti	0.02	0.02	0.02	0.02	0.03	0.04	0.03	0.02
Cr/V	3.16	2.37	2.70	3.54	4.82	6.91	4.87	3.52
V/Cr	0.32	0.42	0.37	0.28	0.21	0.14	0.21	0.28
K/Rb	270.55	205.30	254.87	257.37	251.73	226.69	252.69	216.83
Cr/Ni	5.42	3.94	4.93	2.32	2.42	6.69	5.98	7.25
Cr/Th	33.36	19.10	19.82	22.42	40.63	49.91	25.52	26.66
Cr/Sc	7.75	12.26	9.91	14.26	5.04	22.73	13.18	19.47
Ni/Co	0.79	0.80	0.55	1.25	1.53	0.77	1.21	0.70
Cu/Zn	0.16	0.19	0.21	0.18	0.15	0.40	0.21	0.27
Zr/Th	16.95	21.45	14.93	17.64	18.57	20.65	15.46	14.43
Zr/Sc	3.93	13.77	7.46	11.23	2.30	9.41	7.98	10.54

Table 8.2 (Continued)

Sample No.	KAK-52	KAC-56	KAC-63	KAN-67	KAN-71	KAN-78	KAN-80	KAN-84
SiO_2/Al_2O_3	7.43	4.41	4.90	5.31	4.77	6.05	7.75	6.28
Al_2O_3/SiO_2	0.13	0.23	0.20	0.19	0.21	0.17	0.13	0.16
Al_2O_3/Na_2O	6.32	6.54	6.56	6.05	5.47	6.68	7.15	7.74
Na_2O/K_2O	0.99	1.30	1.47	0.96	1.12	0.92	0.80	0.80
K_2O/Na_2O	1.01	0.77	0.68	1.04	0.89	1.08	1.25	1.24
K_2O/Al_2O_3	0.16	0.12	0.10	0.17	0.16	0.16	0.17	0.16
Fe_2O_3+MgO	3.71	7.50	8.05	7.30	6.46	6.36	5.02	5.46
La/Th	3.91	2.96	4.91	3.53	5.49	4.42	3.89	3.75
La/Y	2.17	1.32	1.79	1.95	2.08	1.68	2.03	1.75
La/Sc	1.54	1.84	1.77	3.04	2.22	1.59	2.58	2.34
Th/Sc	0.39	0.62	0.36	0.86	0.41	0.36	0.66	0.62
Th/Co	0.15	0.18	0.16	0.14	0.09	0.17	0.16	0.28
Th/Cr	0.10	0.05	0.02	0.04	0.08	0.02	0.01	0.02
Ba/Co	3.93	4.20	4.24	5.40	5.79	6.42	4.05	6.77
Ba/Sc	10.63	14.22	9.72	32.13	25.25	13.42	16.76	15.34
Rb/Cs	3.74	4.14	-	19.76	8.73	-	-	7.35
Y/Ni	0.29	0.47	0.27	0.27	0.25	0.51	0.17	0.23
Ti/Zr	72.88	56.83	63.89	56.77	78.23	104.72	55.32	56.80
Cr/Ti	0.01	0.03	0.04	0.02	0.01	0.04	0.07	0.04
Cr/V	2.02	1.63	5.64	2.65	1.04	6.87	12.84	8.00
V/Cr	0.50	0.62	0.18	0.38	0.96	0.15	0.08	0.13
K/Rb	202.29	247.80	216.31	265.99	222.62	232.68	250.36	251.63
Cr/Ni	1.69	4.35	5.32	3.34	1.26	12.81	6.56	4.88
Cr/Th	10.40	20.84	54.54	22.70	13.06	66.59	75.40	44.92
Cr/Sc	4.09	12.93	19.65	19.54	5.29	23.94	50.03	28.02
Ni/Co	0.90	0.88	1.61	0.98	0.97	0.89	1.84	2.53
Cu/Zn	0.53	0.32	0.25	0.24	0.27	0.22	0.29	0.24
Zr/Th	12.96	14.19	19.38	16.41	16.87	16.27	19.15	19.82
Zr/Sc	5.10	8.81	6.98	14.13	6.84	5.85	12.71	12.37

Table 8.2 (Continued)

Sample No.	KAN-87	KBK-88	KBK-95	KBK-97	KBK-100	KBC-104	KBC-106	KBC-111
SiO_2/Al_2O_3	8.24	9.22	7.28	6.31	8.20	6.42	5.61	4.71
Al_2O_3/SiO_2	0.12	0.11	0.14	0.16	0.12	0.16	0.18	0.21
Al_2O_3/Na_2O	7.64	7.87	8.59	9.42	7.49	8.20	9.06	5.98
Na_2O/K_2O	0.82	0.65	0.66	0.80	0.74	0.70	0.74	1.23
K_2O/Na_2O	1.21	1.53	1.51	1.25	1.34	1.43	1.36	0.81
K_2O/Al_2O_3	0.16	0.19	0.18	0.13	0.18	0.17	0.15	0.14
Fe_2O_3+MgO	6.64	8.28	6.39	5.68	4.42	7.17	6.64	6.58
La/Th	3.10	5.29	4.70	4.08	4.43	2.27	3.92	3.91
La/Y	1.21	2.37	1.32	1.77	2.41	1.44	1.27	1.91
La/Sc	1.71	2.24	1.47	2.04	1.56	2.06	1.82	1.82
Th/Sc	0.55	0.42	0.31	0.50	0.35	0.91	0.46	0.47
Th/Co	0.12	0.12	0.20	0.15	0.13	0.54	0.15	0.18
Th/Cr	0.02	0.03	0.03	0.02	0.03	0.16	0.04	0.03
Ba/Co	2.75	4.01	6.15	4.20	3.19	8.62	5.79	5.57
Ba/Sc	13.05	14.29	9.70	13.74	8.67	14.60	17.41	14.55
Rb/Cs	-	-	246.50	-	7.23	28.52	269.00	-
Y/Ni	0.12	0.05	0.51	0.16	0.13	0.26	0.37	0.38
Ti/Zr	63.72	77.35	87.87	71.94	54.26	64.51	58.70	72.54
Cr/Ti	0.05	0.03	0.02	0.05	0.03	0.01	0.03	0.03
Cr/V	6.66	3.54	3.02	6.26	5.14	0.64	2.52	2.78
V/Cr	0.15	0.28	0.33	0.16	0.19	1.55	0.40	0.36
K/Rb	269.72	232.83	232.76	245.44	263.67	116.43	247.42	231.48
Cr/Ni	2.24	0.86	4.23	4.46	2.35	1.02	3.31	5.44
Cr/Th	49.60	36.72	29.19	64.95	32.69	6.24	27.93	29.52
Cr/Sc	27.40	15.52	9.12	32.47	11.51	5.67	12.95	13.75
Ni/Co	2.58	5.06	1.37	2.23	1.80	3.28	1.30	0.97
Cu/Zn	0.32	0.13	0.37	0.21	0.13	0.51	0.26	0.36
Zr/Th	14.47	17.48	15.92	19.02	18.66	10.44	16.67	13.79
Zr/Sc	7.99	7.39	4.97	9.51	6.57	9.48	7.73	6.42

Table 8.2 (Continued)

Sample No.	KBC-114	KBC-125	KBC-127	KBN-130	KBN-135	KBN-137	KBN-142	KBN-144
SiO_2/Al_2O_3	4.69	5.74	4.89	3.81	4.73	4.36	4.03	5.66
Al_2O_3/SiO_2	0.21	0.17	0.20	0.26	0.21	0.23	0.25	0.18
Al_2O_3/Na_2O	5.03	4.72	6.37	4.85	8.08	10.32	8.09	10.61
Na_2O/K_2O	1.51	1.32	1.14	1.34	0.98	0.70	0.84	0.69
K_2O/Na_2O	0.66	0.76	0.88	0.74	1.02	1.42	1.20	1.46
K_2O/Al_2O_3	0.13	0.16	0.14	0.15	0.13	0.14	0.15	0.14
Fe_2O_3+MgO	6.89	4.96	6.10	7.03	5.43	5.71	7.38	6.20
La/Th	4.68	5.74	4.56	4.43	3.84	4.31	3.39	4.38
La/Y	1.38	2.47	1.66	2.22	1.64	1.69	1.64	1.80
La/Sc	1.63	1.27	1.40	2.86	2.10	1.29	2.03	2.43
Th/Sc	0.35	0.22	0.31	0.65	0.55	0.30	0.60	0.55
Th/Co	0.17	0.11	0.20	0.14	0.18	0.20	0.25	0.18
Th/Cr	0.04	0.04	0.02	0.07	0.08	0.12	0.05	0.02
Ba/Co	4.60	2.91	5.60	5.31	5.18	6.21	7.50	3.96
Ba/Sc	9.57	5.84	8.58	24.11	15.93	9.11	18.19	11.98
Rb/Cs	17.47	16.85	10.25	50.69	14.49	5.66	-	5.10
Y/Ni	0.82	0.12	0.55	0.52	0.54	0.66	0.63	0.27
Ti/Zr	70.65	60.40	69.78	77.35	70.01	69.56	43.74	42.31
Cr/Ti	0.02	0.03	0.03	0.01	0.01	0.01	0.02	0.05
Cr/V	2.37	3.08	5.49	1.61	1.50	0.96	2.27	5.23
V/Cr	0.42	0.32	0.18	0.62	0.67	1.04	0.44	0.19
K/Rb	237.97	270.72	285.23	224.04	218.98	241.22	224.42	220.92
Cr/Ni	6.65	1.40	9.01	3.92	3.04	2.13	5.57	4.61
Cr/Th	27.78	26.31	45.23	14.97	13.14	8.23	18.34	41.75
Cr/Sc	9.65	5.82	13.86	9.66	7.21	2.47	10.97	23.13
Ni/Co	0.70	2.08	1.00	0.54	0.77	0.79	0.81	1.66
Cu/Zn	0.33	0.21	0.25	0.60	0.27	0.16	0.34	0.26
Zr/Th	21.96	16.33	19.39	15.15	13.77	14.41	18.13	20.56
Zr/Sc	7.63	3.61	5.94	9.77	7.55	4.32	10.85	11.39

Table 8.2 (Continued)

Sample No.	**KBN-152**
SiO_2/Al_2O_3	8.11
Al_2O_3/SiO_2	0.12
Al_2O_3/Na_2O	6.88
Na_2O/K_2O	0.71
K_2O/Na_2O	1.40
K_2O/Al_2O_3	0.20
Fe_2O_3+MgO	4.92
La/Th	4.96
La/Y	1.98
La/Sc	2.22
Th/Sc	0.45
Th/Co	0.09
Th/Cr	0.04
Ba/Co	3.03
Ba/Sc	14.86
Rb/Cs	-
Y/Ni	-
Ti/Zr	47.21
Cr/Ti	0.03
Cr/V	3.24
V/Cr	0.31
K/Rb	243.59
Cr/Ni	2.66
Cr/Th	26.01
Cr/Sc	11.63
Ni/Co	0.89
Cu/Zn	0.36
Zr/Th	17.53
Zr/Sc	7.84

Table 8.3. Mean composition of principal sandstone classes (after Pettijohn et al., 1987). Composition of the present study is also given in ranges and averages (in parenthesis).

Oxides	Lithic arenite (Pettijohn et al., 1987)	K-feldspar-rich arenites (Pettijohn et al., 1987)	Kamlial Formation (This study)	Chinji Formation (This study)	Nagri Formation (This study)
SiO_2	66.1	66.2	46.9-63.4 (52.6)	42.6-58.8 (51.1)	36.6-64.2 (52.6)
Al_2O_3	8.1	10.2	6.1-23.3 (9.83)	7.4-11.6 (9.7)	6.1-17.5 (9.74)
Fe_2O_3	3.8	7.0 (T)	2.5-4.8 (3.7) (T)	3.2-4.9 (4.1) (T)	2.6-4.9 (3.78) (T)
FeO	1.4				
MgO	2.4	4.5	0.9-3.5 (2.2)	1.7-3.7 (2.4)	1.5-3.3 (2.3)
CaO	6.2	2.0	7.5-20.4 (14.5)	9.5-23.6 (14.0)	6.1-24.2 (13.4)
Na_2O	0.9	1.8	0.5-1.4 (1.0)	1.0-1.9 (1.6)	0.8-2.1 (1.4)
K_2O	1.3	1.6	1.1-1.7 (1.3)	1.1-1.6 (1.4)	1.1-1.9 (1.5)
H_2O^+	3.6	-	-	-	-
H_2O^-	0.7	0.5	-	-	-
TiO_2	0.3	-	0.3-0.9 (0.7)	0.4-0.9 (0.7)	0.5-0.9 (0.7)
P_2O_5	0.1	-	(0.1)	(0.1)	(0.1)
MnO	0.1	0.2	0-0.2 (0.13)	0.1-0.2 (0.15)	0.1-0.3 (0.15)
CO_2	5.0	6.2?	-	-	-
LOI	-	-	-	-	-

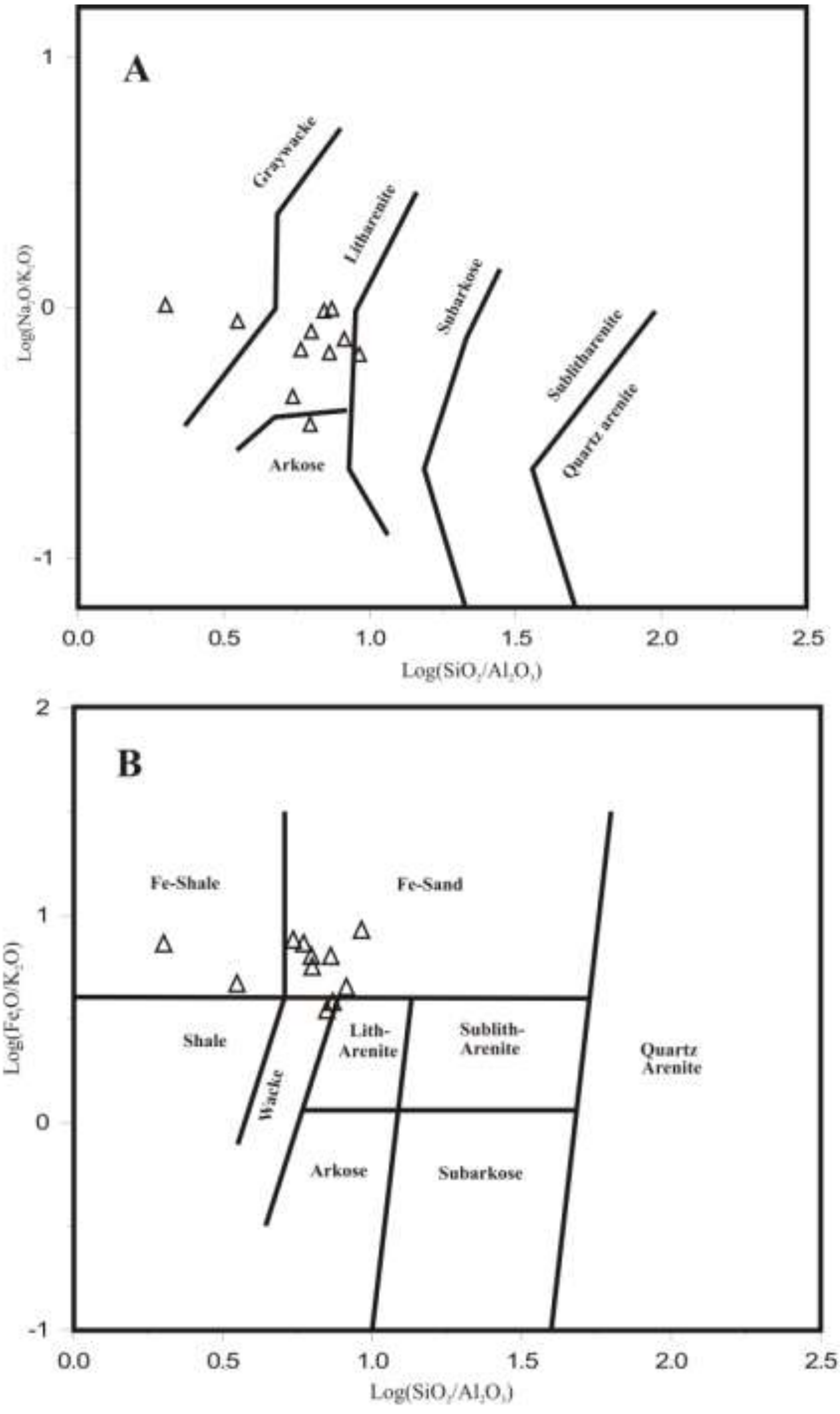

Fig. 8.1 (A) Log(Na_2O/K_2O) vs log(SiO_2/Al_2O_3) plot of the Kamlial Formation sandstone from Kohat Plateau on a geochemical classification diagram after Herron (1988), and (B) log(Fe_2O_3/K_2O) vs (SiO_2/Al_2O_3) plot after Pettijohn et al. (1987).

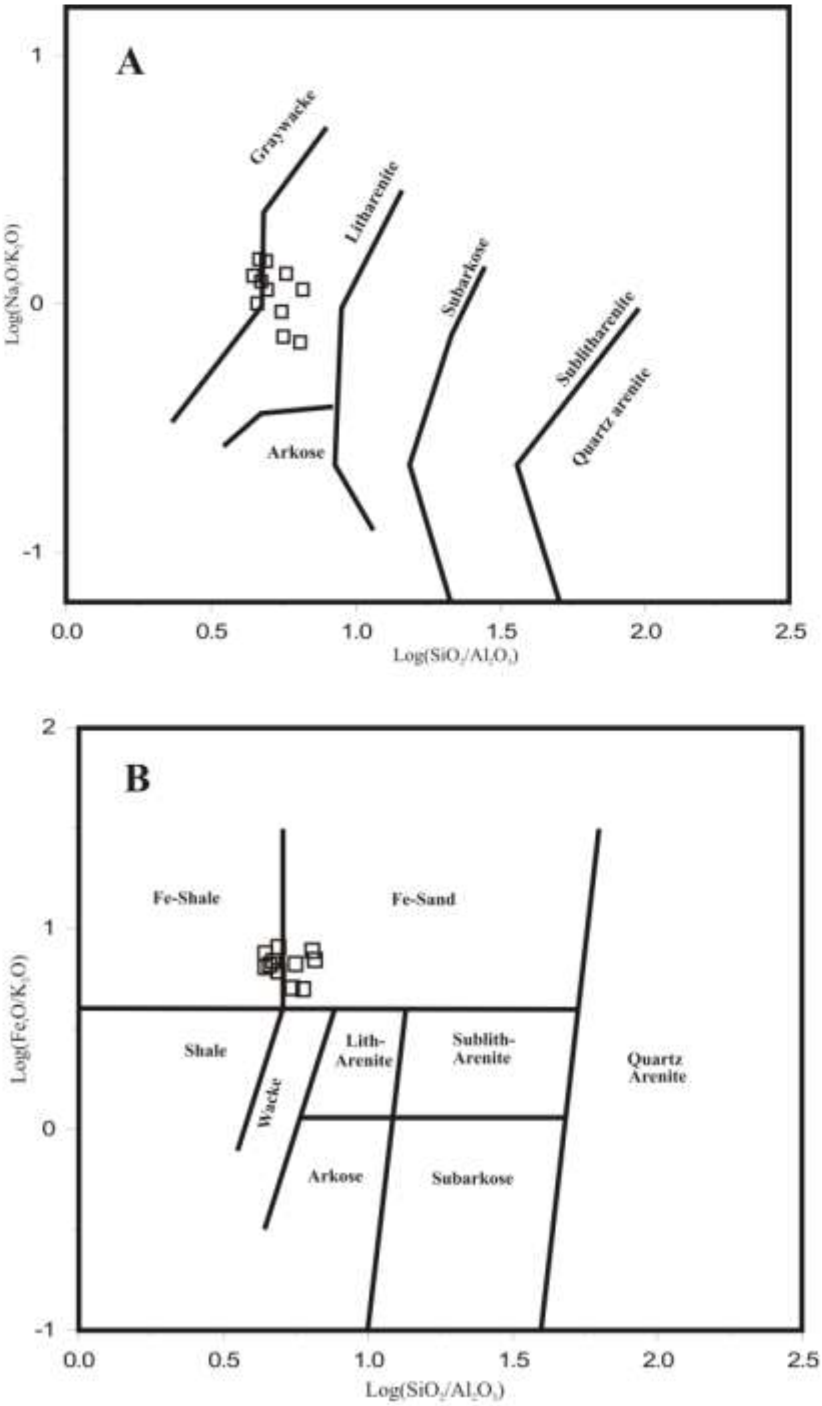

Fig. 8.2 (A) Log(Na_2O/K_2O) vs log(SiO_2/Al_2O_3) plot of the Chinji Formation sandstone from Kohat Plateau on a geochemical classification diagram after Herron (1988), and (B) log(Fe_2O_3/K_2O) vs (SiO_2/Al_2O_3) plot after Pettijohn et al. (1987).

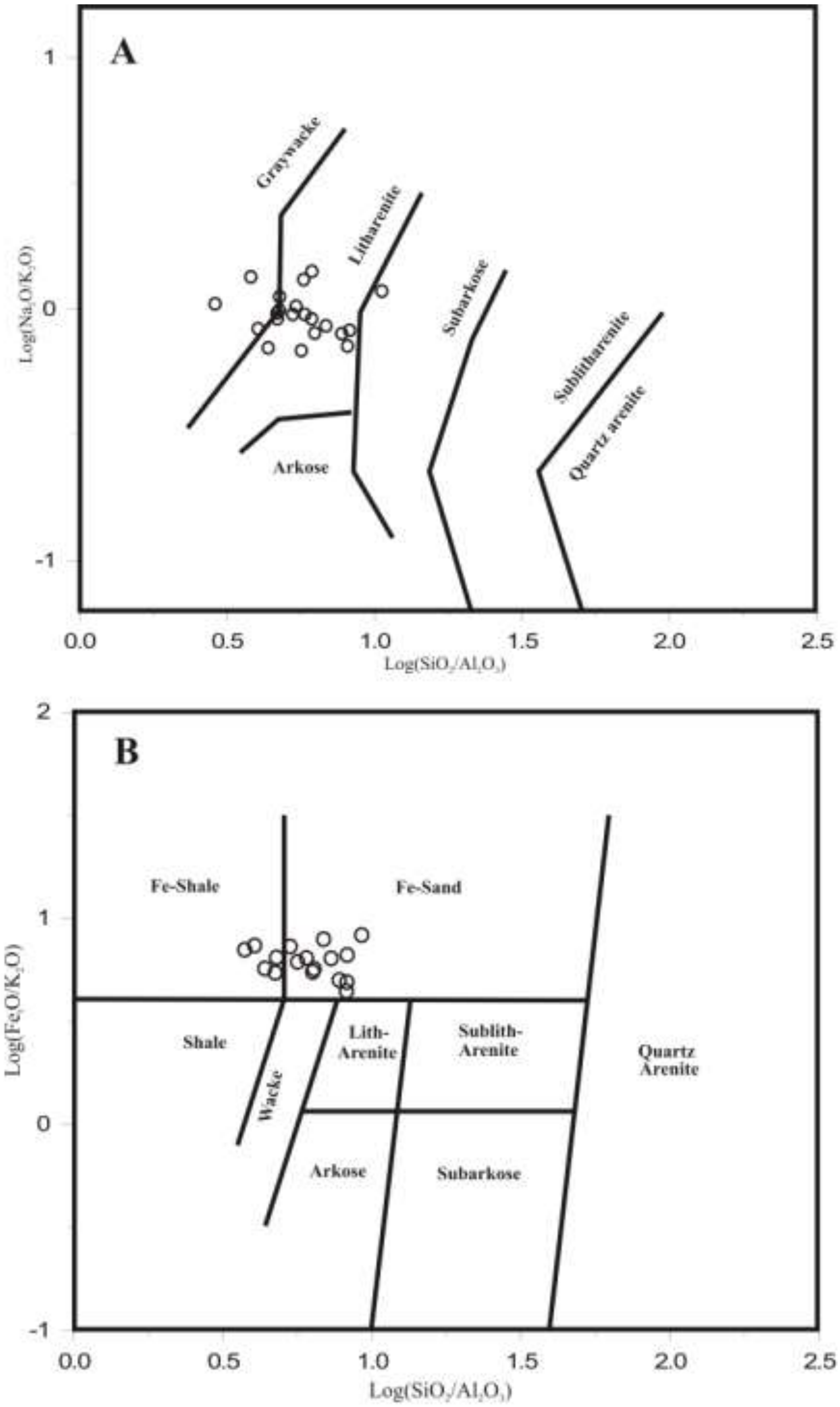

Fig. 8.3 (A) Log(Na_2O/K_2O) vs log(SiO_2/Al_2O_3) plot of the Nagri Formation sandstone from Kohat Plateau on a geochemical classification diagram after Herron (1988), and (B) log(Fe_2O_3/K_2O) vs (SiO_2/Al_2O_3) plot after Pettijohn et al. (1987).

The K_2O/Na_2O ratio has also been used as an indicator of sandstone-type and tectonic setting (Crook, 1974; Roser and Korsch, 1986). This ratio is inferred to increase with sedimentary maturation as feldspars and other labile minerals are converted to K-rich clays, however, both K and Na are commonly mobile during diagenesis. Similarly, the SiO_2/Al_2O_3 ratio has been used as an indicator of maturity in sandstones, because it increases as quartz is progressively concentrated at the expense of less resistant minerals during weathering, transport and recycling (Maynard et al., 1982; Roser and Korsch, 1986).

8.5 Chemical Composition and Plate Tectonic Setting

Roser and Korsch (1986) defined three main tectonic provenances on the basis of chemical composition of sandstones: (a) Passive Continental Margin (PM)- mineralogically mature (quartz-rich) sediments deposited in plate interiors at stable continental margins or intracratonic basins (mainly sourced from recycled sedimentary and metamorphic source rocks); (b) Active Continental Margin (ACM)- sediments with intermediate quartz content derived from tectonically active continental margins and deposited on or adjacent to active plate boundaries (e.g. trench, forearc and backarc settings) (mainly sourced from granites, gneisses, siliceous volcanics); and (c) Oceanic Island Arc (OIC)-quartz poor volcanogenic sediments derived from oceanic island arcs and deposited in a variety of settings including forearc, intra-arc and backarc basins etc. (mainly sourced from calc-alkaline or tholeiitic rocks).

8.5.1 Interpreting Tectonic Setting from Sandstone Geochemistry: The SiO_2 content and K_2O/Na_2O ratios of sandstone appear to be particularly sensitive indicators of geotectonic setting. Crook (1974) demonstrated that the quartz-poor graywackes (quartz <15%, average SiO_2 = 58%, K_2O/Na_2O <<1) are indicative of magmatic island arcs. The average composition of these rocks approximates the average composition of the tholeiitic andesites. Quartz intermediate graywackes (quartz = 15-65%, average SiO_2 = 68-74%, K_2O/Na_2O <1) are indicative of Andean-type continental margins and have approximately the same composition as the upper level of the continental crust. Quartz-rich graywackes (quartz >65%, average SiO_2 = 89%, K_2O/Na_2O >1) are characteristic of Atlantic-type continental margins and are similar in composition to the sand fraction of the continental platform cover. This idea was also supported by Schwab (1975).

Maynard et al. (1982) also used K_2O/Na_2O ratios and SiO_2 content to discriminate between passive-margin and active-margin sandstones. They suggest that passive-margin sandstones have K_2O/Na_2O ratios greater than 1 and active-margin sandstones have ratios less than 1. Also passive-margin sandstones are enriched in SiO_2 compared to active-margin sandstones.

Bhatia, M. R. (1983) concluded that sandstones of sedimentary basins adjacent to oceanic island arcs (e.g., Marianas- and Aleutians-type arcs) are characterized by high abundances of Fe_2O_3+MgO (8-14%) and TiO_2 (0.8-1.4%) and high Al_2O_3/SiO_2 (0.24-0.33) and lower K_2O/Na_2O (0.2-0.4) ratios. He further distinguished sandstones of basins adjacent to continental island arcs (e.g., Cascades-type arc, western USA) from oceanic island-arc types by lower Fe_2O_3+MgO (5-8%), TiO_2 (0.5-0.75) and Al_2O_3/SiO_2 (0.15-0.22) and higher K_2O/Na_2O (0.4-0.8) ratios. According to him sandstones from basins on active continental margins (Andean-type) have very low Fe_2O_3+MgO (2-5%) and TiO_2 (0.25-0.45%) and K_2O/Na_2O ratio of approximately 1. The passive margin (Atlantic-type) sandstones are generally enriched in SiO_2 and depleted in Al_2O_3, TiO_2, Na_2O, CaO with K_2O/Na_2O ratio more than 1. These sandstones may show large variations in composition, sometimes even overlapping the compositions of active continental margin sandstones. Different parameters of Bhatia, M. R. (1983) listed here (Tables 8.1, 8.2 8.4) indicate that the sandstone of the Neogene molasse sequence of the Kohat Plateau is within the range of the continental island arc provenance and partially shifting to the active continental margin provenance. The values of the fourth parameter i.e. K_2O/Na_2O is highly variable and shifts among the continental island arc, active continental margin and passive continental margin setting provenances. The present study also ruled out the use of parameters suggested by Crook (1974) and Maynard et al. (1982) for discrimination of the Neogene molasse sandstone, keeping in view the conclusions of petrography discussed in chapter 6.

Except for MnO, the contents of other individual major element oxides of the sandstone of Neogene sequence of the Kohat Plateau (Tables 8.1, 8.2) support a dominant continental island arc source (Table 8.4). A little difference in the composition of the studied Neogene sandstone (Tables 8.1, 8.2) and the average composition of the continental island arc sandstone is possibly because of the high content of secondary CaO, which averages ~14% for the former. The relatively low content of Al_2O_3 may be due to the immature nature of the Neogene sandstone as evidenced by the presence of substantial amount of feldspar. The average 0.14% MnO is very much in agreement with that of the oceanic island arc provenance i.e. 0.15% (Table 8.4).

Table 8.4. Average chemical composition and some chemical parameter of sandstones of various tectonic settings (after Bhatia, M. R., 1983), and of present study. OIA = Oceanic island arc, CIA = Continental island arc and ACM = Active continental margin

Oxides	OIA	CIA	ACM	Kamlial Formation	Chinji Formation	Nagri Formation
SiO_2	58.83	70.69	73.86	46.9-63.4 (52.6)	42.6-58.8 (51.1)	36.6-64.2 (52.6)
TiO_2	1.06	0.64	0.46	0.3-0.9 (0.7)	0.4-0.9 (0.7)	0.5-0.9 (0.7)
Al_2O_3	17.11	14.04	12.89	6.1-23.3 (9.83)	7.4-11.6 (9.7)	6.1-17.5 (9.74)
Fe_TO_3	7.47	4.48	2.88	2.5-4.8 (3.7)	3.2-4.9 (4.1)	2.6-4.9 (3.78)
MnO	0.15	0.10	0.10	0-0.2 (0.13)	0.1-0.2 (0.15)	0.1-0.3 (0.15)
MgO	3.65	1.97	1.23	0.9-3.5 (2.2)	1.7-3.7 (2.4)	1.5-3.3 (2.3)
CaO	5.83	2.68	2.48	7.5-20.4 (14.5)	9.5-23.6 (14.0)	6.1-24.2 (13.4)
Na_2O	4.10	3.12	2.77	0.5-1.4 (1.0)	1.0-1.9 (1.6)	0.8-2.1 (1.4)
K_2O	1.60	1.89	2.90	1.1-1.7 (1.3)	1.1-1.6 (1.4)	1.1-1.9 (1.5)
P_2O_5	0.26	0.16	0.9	(0.1)	(0.1)	(0.1)
$Fe_2O_3^*$ + MgO	11.73	6.79	4.63	3.5-8.3 (5.9)	5.0-8.1 (6.6)	4.9-8.2 (6.1)
Al_2O_3/SiO_2	0.29	0.20	0.18	0.1-0.5 (0.2)	0.15-.23 (0.2)	0.1-0.35 (0.2)
K_2O/Na_2O	0.39	0.61	0.99	1.0-2.9 (1.5)	0.7-1.4 (0.9)	0.7-1.5 (1.1)
$Al_2O_3/(CaO+Na_2O$	1.72	2.42	2.56	-	-	-

*Total iron as Fe_2O_3

8.5.2 Sandstone Geochemistry and Discriminatory Plots: Bhatia, M. R. (1983) proposed discrimination diagrams for identification of four types of tectonic settings based on average geochemical composition of medium- to fine-grained sandstones, namely, (1) the oceanic island arc (OIA), (2) the continental island arc, (3) the active continental margin (ACM), and (4) the passive margin (PM). The discriminating parameters used are: (i) Fe_tO_3+MgO vs TiO_2; (ii) Fe_tO_3+MgO vs K_2O/Na_2O; (iii) Fe_tO_3+MgO vs Al_2O_3/SiO_2; and (iv) Fe_tO_3+MgO vs Al_2O_3/ (CaO+Na_2O). The geochemical concept behind these discrimination diagrams was based on a general decrease in Fe_tO_3+MgO, TiO_2, and Al_2O_3/SiO_2 and an increase in K_2O/Na_2O and Al_2O_3/ (CaO+Na_2O) as the tectonic setting changes in the sequence OIA-continental island arc-ACM-PM.

Roser and Korsch (1985) took exception to some of Bhatia's (1983) conclusions, claiming that some of the discriminant-function scores are not correct as the effect of grain size on chemical composition was not taken into account. Roser and Korsch (1986) presented their own chemical model on the basis of K_2O/Na_2O ratios and SiO_2 content, which enabled them to discriminate among samples from three major tectonic settings: PM, ACM and OIA.

Recently, Armstrong-Altrin and Verma (2005) evaluated the discrimination diagrams of Bhatia, M. R. (1983) and Roser and Korsch (1986) with a large number of geochemical data on Neogene sediments including 314 samples from a passive margin setting, 86 samples from an active continental margin setting, and 124 samples from an oceanic island arc setting. They also claimed the following discrepancies in the discriminatory plots of Bhatia, M. R. (1983) and Roser and Korsch (1986):

Fe_tO_3+MgO vs TiO_2 plot: Armstrong-Altrin and Verma (2005) pointed out that the Fe_tO_3+MgO vs TiO_2 plot (Fig. 2A in Armstrong-Altrin and Verma, 2005) shows ~0% success for samples selected from the PM setting. Approximately 76% samples of the PM setting plot in the OIA field and ~18% samples plot outside of any field. The same plot for ACM samples (Fig. 3A in Armstrong-Altrin and Verma, 2005) shows only ~5% success and the remaining 95% samples plot outside the expected field of ACM. For samples from the OIA setting (Fig. 4A in Armstrong-Altrin and Verma, 2005), this plot favors ~15% success, and rest of the samples plot outside the designated field.

Fe_tO_3+MgO vs K_2O/Na_2O plot: The Fe_tO_3+MgO vs K_2O/Na_2O plot (Fig. 2B in Armstrong-Altrin and Verma, 2005) shows ~0% success for samples of PM and ~ 96% of samples fall outside any pre-defined field of Bhatia, M. R. (1983). For samples collected from the ACM setting (Fig. 3B in Armstrong-Altrin and Verma, 2005), the same plot is successful to ~9%, and in case of OIA setting (Fig. 4B in Armstrong-Altrin and Verma, 2005), it shows only ~2% success.

Fe_tO_3+MgO vs Al_2O_3/SiO_2 plot: The Fe_tO_3+MgO vs Al_2O_3/SiO_2 plots (Figs. 2C, 3C, and 4C in Armstrong-Altrin and Verma, 2005) amount to ~2% success for the PM setting, ~7% success for ACM and ~23% success for OIA.

Fe_tO_3+MgO vs Al_2O_3/(CaO+Na_2O) plot: The Fe_tO_3+MgO vs Al_2O_3/(CaO+Na_2O) plots (Figs. 2D, 3D, and 4D in Armstrong-Altrin and Verma, 2005) are amounting only to

~0.3%, ~14% and ~9% successes for the samples from PM, ACM and OIA settings, respectively.

Discriminant function diagram: The discriminant functions plot of Bhatia, M. R. (1983) shows ~14% success for samples from PM setting (Fig. 2E in Armstrong-Altrin and Verma, 2005), ~15% success for samples from ACM setting (Fig. 3E in Armstrong-Altrin and Verma, 2005) and ~17% success for samples from OIA setting (Fig. 4E in Armstrong-Altrin and Verma, 2005).

SiO_2 vs log (K_2O/Na_2O) plot: The SiO_2 vs log(K_2O/Na_2O) plot of Roser and Korsch (1986) (Fig. 2F in Armstrong-Altrin and Verma, 2005) amounts to ~52% success for samples compiled from the PM setting with ~47% of the samples plotting in the ACM field and ~1% in the OIA field (Armstrong-Altrin and Verma, 2005). For ACM, the plot (Fig. 3F in Armstrong-Altrin and Verma, 2005) amounts to ~52% success with the remaining 48% samples plotting in the PM and OIA fields. Moreover, for samples compiled from OIA setting (Fig. 4F in Armstrong-Altrin and Verma, 2005), the plot correctly discriminates ~32% of the samples.

Evaluation of discrimination diagrams using average geochemical data: The evaluation of discriminatory plot of Bhatia, M. R. (1983) and Roser and Korsch (1986) was also tested with the average values for PM, ACM and OIA settings and eleven average compositions for PM, 13 for ACM, and 12 for OIA settings were applied (Figs. 5A-F in Armstrong-Altrin and Verma, 2005). The Fe_tO_3+MgO-TiO_2 plot shows ~0% success for the average values of PM setting, ~8% success for ACM setting, and ~17% success for the OIA setting. The Fe_tO_3+MgO vs K_2O/Na_2O plot completely fails to infer the tectonic setting for any of the average values compiled from PM and OIA settings (~0% success) and demonstrates ~8% success for the ACM setting. The Fe_tO_3+MgO vs Al_2O_3/SiO_2 shows ~58% success for the average values of OIA, ~8% success for ACM setting but completely fails to distinguish the PM setting. The Fe_tO_3+MgO vs Al_2O_3/(CaO+Na_2O) plot completely fails for average values compiled from PM but shows ~8% success for ACM and ~25% success for OIA settings (Armstrong-Altrin and Verma, 2005). The discriminant function diagram works with ~15% success for the average values compiled from ACM setting, ~9% success for PM and ~25% success for samples from OIA settings (Armstrong-Altrin and Verma, 2005). In SiO_2 vs log (K_2O/Na_2O) diagram, about 50% of the average values compiled from OIA plots in the correct field, ~62% from ACM and ~54% from PM setting fall in the expected fields (Armstrong-Altrin and Verma, 2005).

Criticized by Armstrong-Altrin and Verma (2005), the discriminatory plots of Bhatia, M. R. (1983), and Roser and Korsch (1985) are still used in a number of more recent works (e.g. Wanas and Abdel-Maguid, 2006; Spalletti et al., 2007), and thereby applied to the present geochemical data.

8.6 Provenance of the Neogene Sandstone of the Kohat Plateau

8.6.1 Kamlial Formation: The Fe_tO_3+MgO vs TiO_2, Fe_tO_3+MgO vs K_2O/Na_2O and Fe_tO_3+MgO vs Al_2O_3/SiO_2 diagrams of Bhatia, M. R. (1983) do not produce clear picture of the provenance for the Kamlial Formation (Figs. 8.4a, 8.4b, 8.4c). As the data is scattered on all the three plots, no conclusion can be drawn confidently. Still, it is obvious that the data dominantly vibrate around the continental island arc (B) and ACM (C) fields. Roser and Korsch (1986) differentiated the sediments derived from OIA, ACM and PM using SiO_2 and K_2O/Na_2O ratio. This plot, when utilized for the data of Kamlial Formation, indicated that most samples of the sandstone fall in the field of ACM (Fig. 8.4d). Three samples show a PM provenance (Fig. 8.4d).

8.6.2 Chinji Formation: The geochemical data of the Chinji Formation appear as group in the Fe_tO_3+MgO vs TiO_2 plot (Fig. 8.5a), as well as in the Fe_tO_3+MgO vs K_2O/Na_2O and Fe_tO_3+MgO vs Al_2O_3/SiO_2 plots (Figs. 8.5b and 8.5c) of Bhatia, M. R. (1983). All these plots of Chinji Formation favor a dominance of continental island arc provenance. A few samples also plot in the field of ACM, indicating some contribution from the ACM setting. The SiO_2 and K_2O/Na_2O plot of Roser and Korsch (1986) clearly suggests an ACM provenance excluding two samples which fall into the field of OIA provenance (Fig. 8.5d).

8.6.3 Nagri Formation: The Nagri Formation follows nearly the same trend as that of the underlying Chinji Formation. The trend is more disciplined on the Fe_tO_3+MgO vs TiO_2 (Fig. 8.6a) and Fe_tO_3+MgO vs K_2O/Na_2O (Fig. 8.6b) plots of Bhatia, M. R. (1983) suggesting a dominance provenance of continental island arc and ACM settings for the Nagri Formation respectively. The Fe_tO_3+MgO vs Al_2O_3/SiO_2 plot of Bhatia, M. R. (1983) though indicates a scatter of data, still dominantly occupy a mixed provenance of continental island arc and ACM settings (Fig. 8.6c). On the other hand, the SiO_2 and K_2O/Na_2O plot of Roser and Korsch (1986) suggests an ACM provenance for the Nagri Formation, excluding one sample which plots in the field of OIA (Fig. 8.6d).

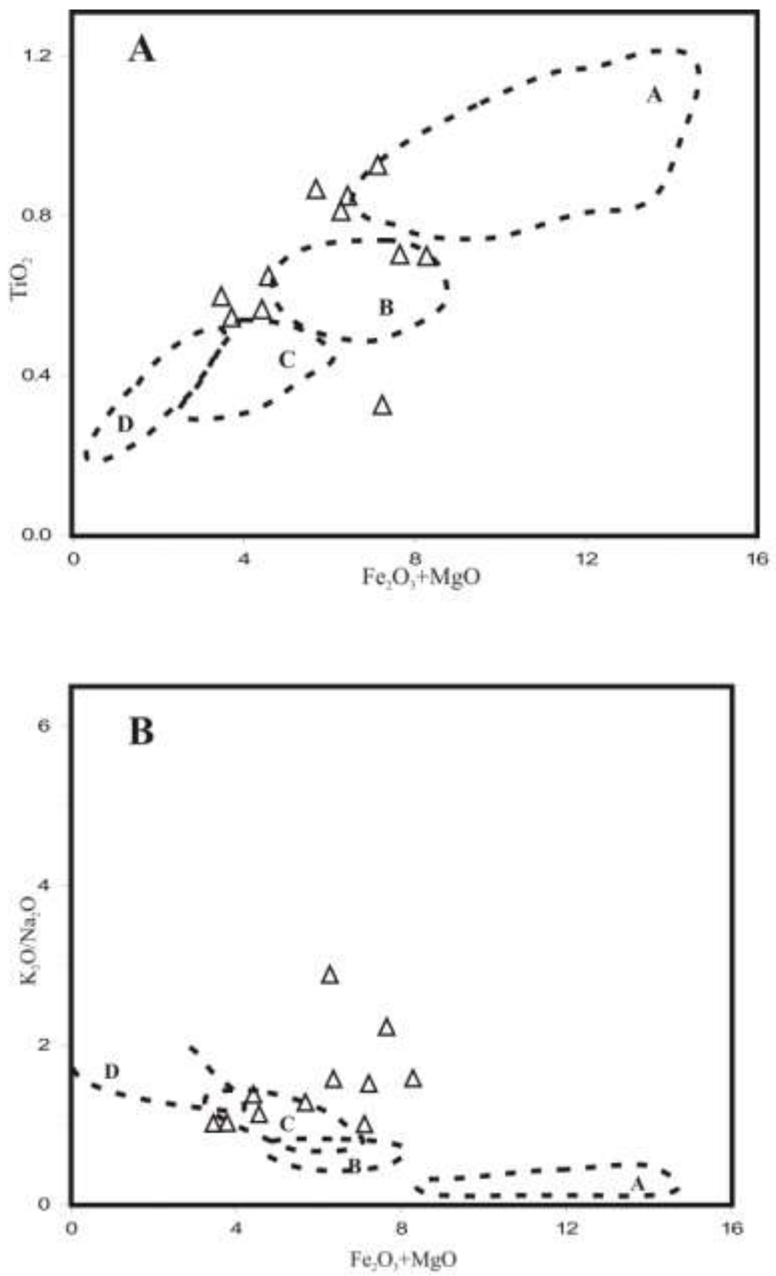

Fig. 8.4 (a) Fe_tO_3+MgO vs TiO_2 diagram after Bhatia, M. R. (1983), for the Kamlial Formation sandstone from Kohat Plateau. X and Y axes are weight percent composition. (b) Plot of Fe_tO_3+MgO vs K_2O/Na_2O (after Bhatia, M. R., 1983) for the Kamlial Formation sandstone from Kohat Plateau. X axis is weight percent composition and Y-axis is ratio of weight percent composition. Fields A= Oceanic island arc, B= Continental island arc, C=Active continental margin and D=Passive margin.

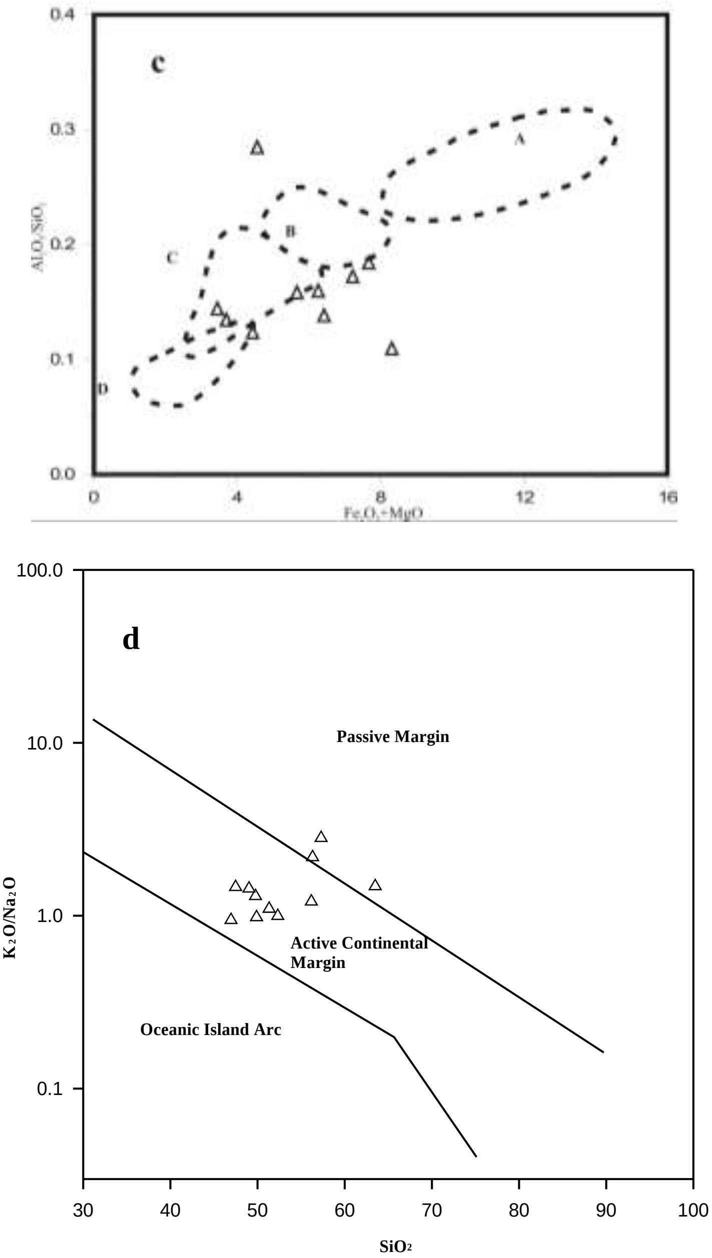

Fig. 8.4 (c) Plots of the Fe_tO_3+MgO vs Al_2O_3/SiO_2 of the Kamlial Formation sandstone of the Kohat Plateau on the tectonic setting discrimination diagrams after Bhatia, M. R. (1983). X axis is weight percent composition and Y-axis is ratio of weight percent composition. Fields A= Oceanic island arc, B= Continental island arc, C=Active continental margin and D=Passive margin. (d) SiO_2–log (K_2O/Na_2O) plot of the Kamlial Formation (Roser and Korsch, 1986). X axis is weight percent composition and Y-axis is log of the ratio of weight percent composition.

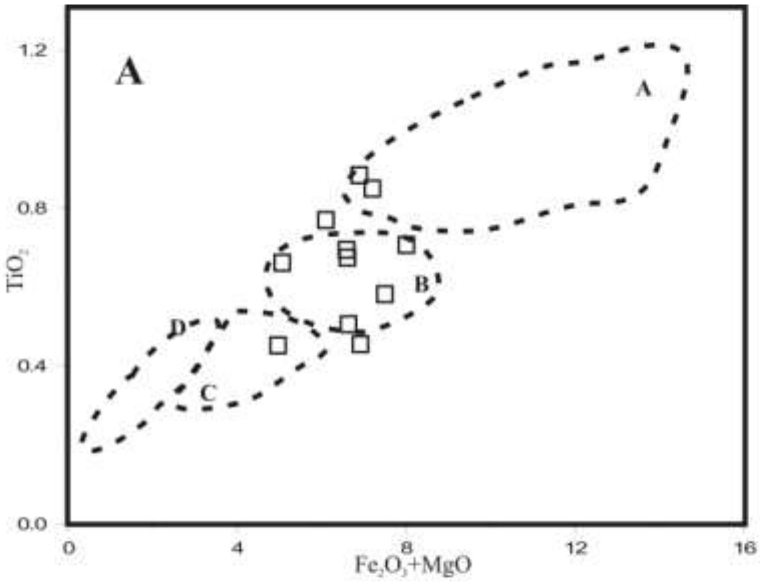

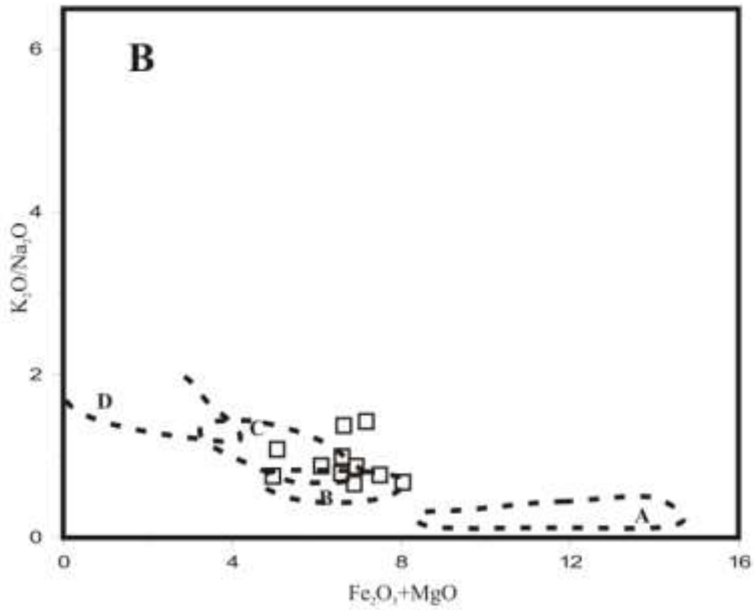

Fig. 8.5 (a) Fe_tO_3+MgO vs TiO_2 diagram after Bhatia, M. R. (1983), for the Chinji Formation sandstone from Kohat Plateau. X and Y axes are weight percent composition. (b) Plot of Fe_tO_3+MgO vs K_2O/Na_2O (after Bhatia, M. R., 1983) for the Chinji Formation sandstone from Kohat Plateau. X axis is weight percent composition and Y-axis is ratio of weight percent composition. Fields A= Oceanic island arc, B= Continental island arc, C=Active continental margin and D=Passive margin.

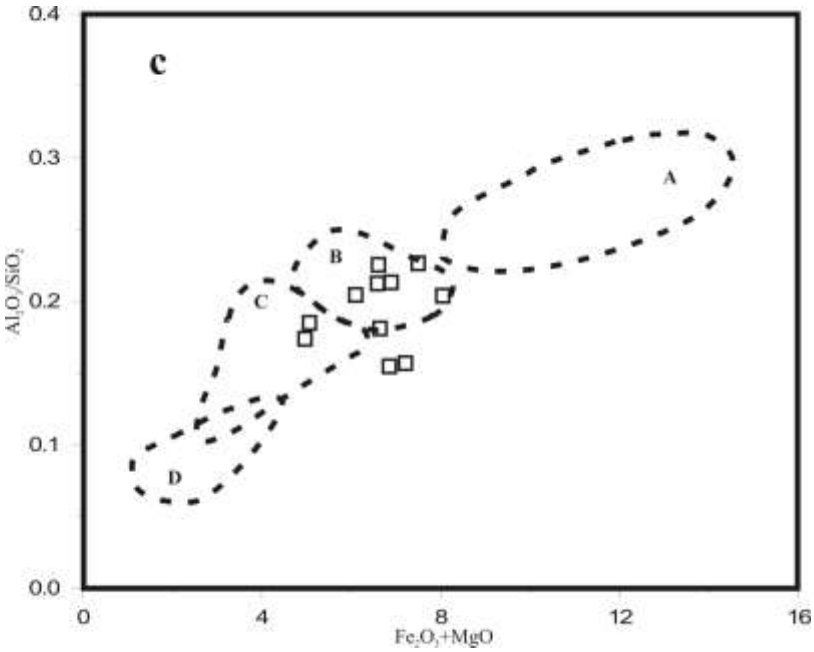

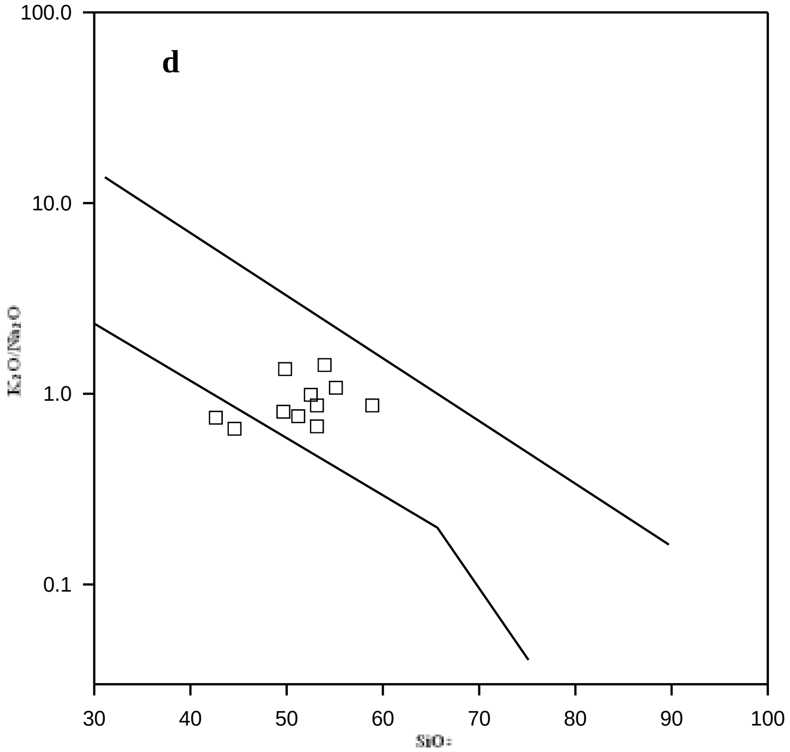

Fig. 8.5 (c) Plots of the Fe_tO_3+MgO vs Al_2O_3/SiO_2 of the Chinji Formation sandstone of the Kohat Plateau on the tectonic setting discrimination diagrams after Bhatia, M. R. (1983). X axis is weight percent composition and Y-axis is ratio of weight percent composition. Fields A= Oceanic island arc, B= Continental island arc, C=Active continental margin and D=Passive margin. (d) SiO_2–log (K_2O/Na_2O) plot of the Chinji Formation (Roser and Korsch, 1986). X axis is weight percent composition and Y-axis is log of the ratio of weight percent composition.

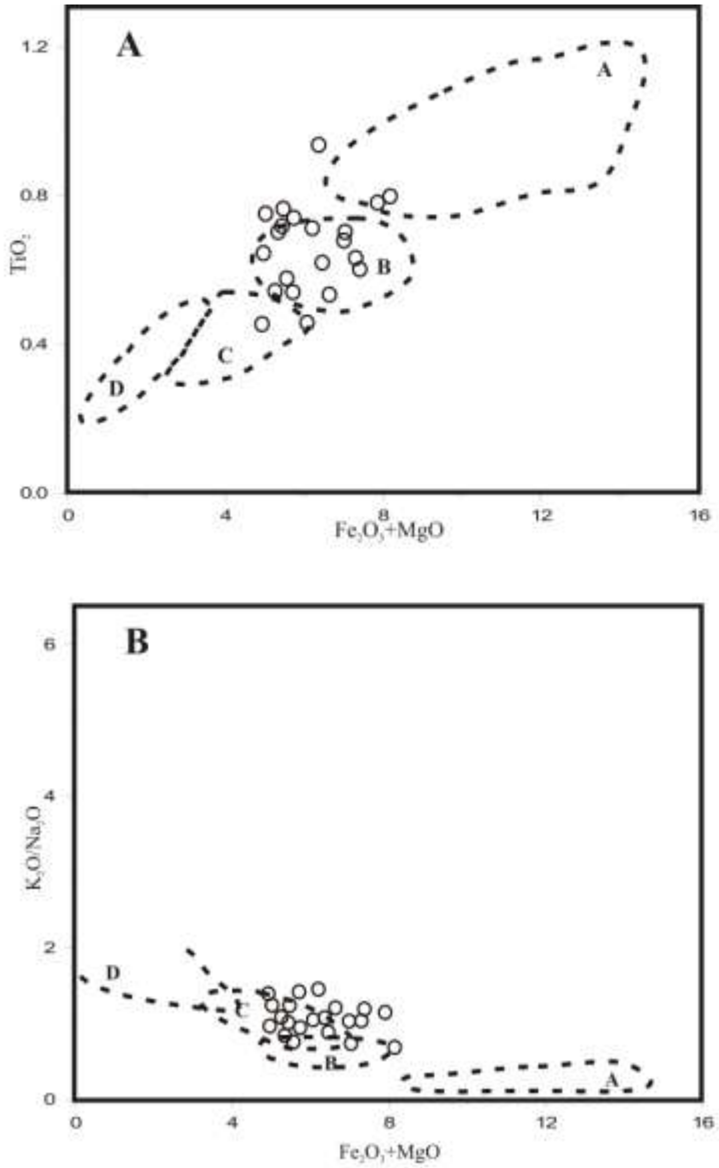

Fig. 8.6 (a) Fe_tO_3+MgO vs TiO_2 diagram after Bhatia, M. R. (1983), for the Nagri Formation sandstone from Kohat Plateau. X and Y axes are weight percent composition. (b) Plot of Fe_tO_3+MgO vs K_2O/Na_2O (after Bhatia, M. R. 1983) for the Nagri Formation sandstone from Kohat Plateau. X axis is weight percent composition and Y-axis is ratio of weight percent composition. Fields A= Oceanic island arc, B= Continental island arc, C=Active continental margin and D=Passive margin.

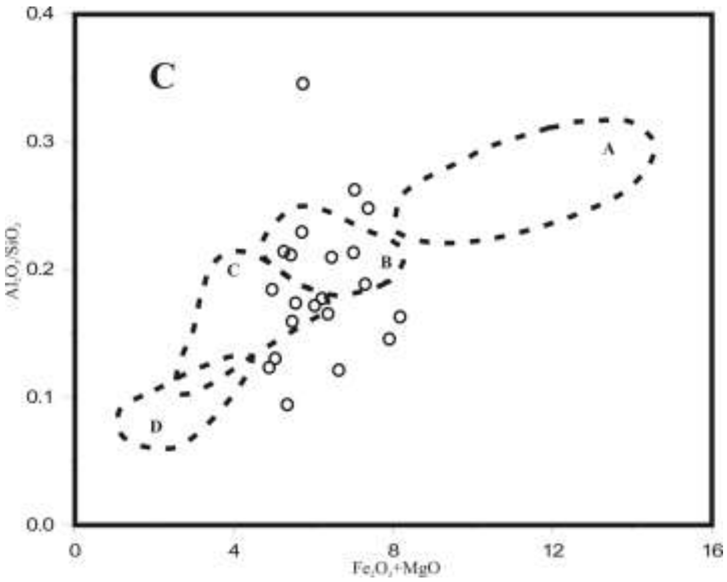

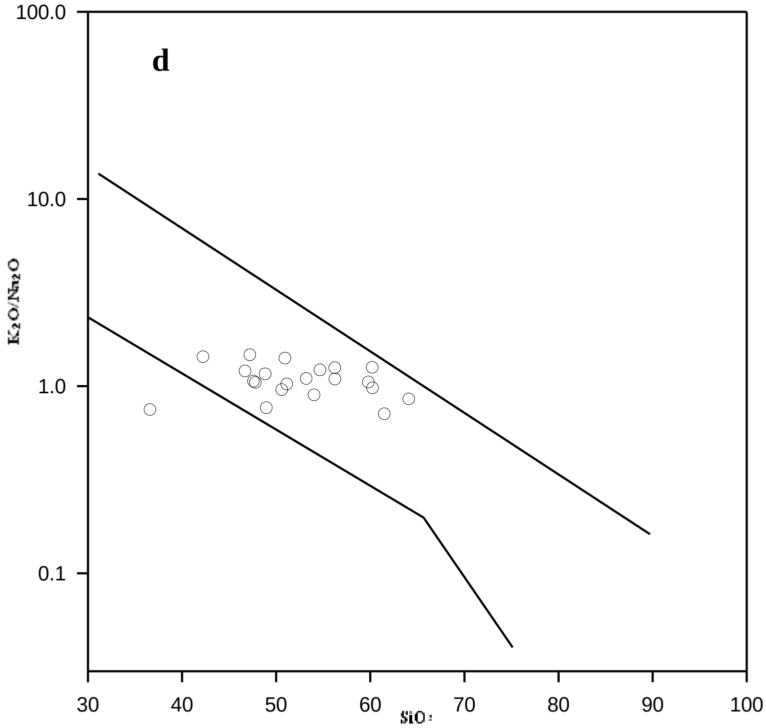

Fig. 8.6 (c) Plots of the Fe_tO_3+MgO vs Al_2O_3/SiO_2 of the Nagri Formation sandstone of the Kohat Plateau on the tectonic setting discrimination diagrams after Bhatia, M. R. (1983). X axis is weight percent composition and Y-axis is ratio of weight percent composition. Fields A= Oceanic island arc, B= Continental island arc, C=Active continental margin and D=Passive margin. (d) SiO_2–log (K_2O/Na_2O) plot of the Nagri Formation (Roser and Korsch, 1986). X axis is weight percent composition and Y-axis is log of the ratio of weight percent composition.

The geochemical data of the Neogene molasse sequence of the Kohat Plateau indicate the consistent continental island arc and ACM provenances for all the three formations with subsidiary input from PM for Kamlial Formation and from OIA for Chinji and Nagri formations. Other geochemical parameters such as Fe_2O_3+MgO, TiO_2 and Al_2O_3/SiO_2 as well as contents of the individual major element oxides except MnO suggest a dominant input from continental island arc with subsidiary contribution from ACM. Average content of MnO of these sediments shows OIA provenance.

8.7 Chemical Index of Alteration (CIA) and Chemical Index of Weathering (CIW)

Major element chemistry can best be employed for determination of weathering extent of the source area after establishment of the general tectonic setting by other means. Both the Chemical Index of Alteration (CIA)

$[\{A1_2O_3/ (AI_2O_3+CaO^*+K_2O+Na_2O)\}\ x100]$

and Chemical Index of Weathering (CIW)

$[\{A1_2O_3/ (AI_2O_3+CaO^*+Na_2O)\}\ x100]$ are based on major elements data.

Where CaO* is the amount of CaO incorporated in the silicate fraction of the rock and the values are in molar proportions to emphasize mineralogical relationship (Nesbitt and Young, 1982). The highly variable values of CaO in the Neogene sandstone of the Kohat, ranging upto 18 wt% in mudstone and upto 23 wt% in sandstone are because of the secondary $CaCO_3$. Fedo et al. (1995) proposed a correction, which involves CO_2 contents in rocks with CaO contributions from non-silicate minerals. In this study we did not analyze for CO_2, and thus there is no easy way to distinguish CaO contributions from carbonates and silicates (feldspars). The main silicate host for CaO, plagioclase is rare in our sandstone samples but albite occurs in mudstone samples, and sphene, the only other Ca-silicate occurs as an accessory mineral is not observed, thus molar CaO* contributions from silicates in the calculation would be negligible. To this effect, CaO* is deliberately omitted from the CIA and CIW calculations and the corresponding indices adopted in this study are designated CIA' and CIW', respectively, which are close and reasonable approximations of the former (Cullers 2000).

The CIA/CIW values may be low, moderate or high. The increasing of CIA/CIW value from low to high is related to the degree of chemical alteration/weathering. Low CIA/CIW values indicate negligible alteration/weathering whereas a moderate or high

CIA/CIW values are correlated with the removal of mobile cations (e.g. Ca^{++}, Na^{+} and K^{+}) relative to the less mobile residual constituents (Al^{+++} and Ti^{+}) (Nesbitt and Young, 1982). Therefore, in case of high values of CIA/CIW much care is required in considering tectonic setting of the source areas.

The CIA values range from about 50 for unweathered upper crust to about 100 for highly weathered residual soils. The CIA value of about 50 generally indicates first-cycle sediments and tends to increase as chemical weathering intensifies (Nesbitt and Young, 1982, 1984). The <50 CIA values of the sediments suggest that the effect of chemical weathering on the composition of these sediments has been negligible (Lee, et al., 2005).

The CIA value of the main rock-forming minerals (quartz, plagioclase, alkali feldspars, pyroxene and olivine) is ≤55 whereas clay minerals yield higher CIA values (usually ≥75) with the highest value of ~100 recorded in kaolinite. High values of the index, >90 indicate extensive conversion of feldspar to clay and hence intense alteration/ weathering. In general, the CIA values in Phanerozoic shales range from 70 to 75, reflecting muscovite, illite and smectite compositions, and a moderately altered/ weathered source, whereas more intense alteration/ weathering results in residual clays such as in kaolinite and gibbsite-rich shales with CIA values close to 100 (Nesbitt and Young, 1982). The CIA value for Post Archian Australian Shale (PAAS) is 69 (Nesbitt and Young, 1984, 1989).

The CIA values of the Neogene molasse sandstone mostly range from 64 to 76 with one sample having a CIA value of 58 (Table 8.1). The CIA values of five samples are between 76 and 86. The dominance of CIA values between 64 to 76, and presence of appreciable amount of feldspar in sandstone favor moderate weathering in the source areas. The presence of sedimentary rock fragments in sandstones reveals that the high CIA values were produced partly by recycling of older sediments rather than by intense weathering as suggested by Lee, Y. I. (2002).

The CIA values of mudstone samples of the Neogene molasse sequence are dominantly in the range of 70 to 80, averaging 75.7 (Table 8.4), which is slightly higher than the CIA value of the PAAS suggesting relatively intense source-area weathering. However, the presence of abundant sedimentary rock fragments in associated sandstones reveals that the high CIA values may probably be due to older sediments rather than by severe weathering (Lee, Y. I., 2002).

Furthermore, the higher values of CIA for the fine sediments are expected, as it generally contains higher proportions of clay. Subramanian et al. (1985) have reported the presence of chlorite and illite in suspended load of the Himalayan rivers. Chlorite and complex clay minerals (smectite, vermiculite and illite) are considered the initial alteration products of the upper crustal rocks (Nesbitt and Young, 1984; Taylor and McLennan, 1985; Graver and Scott, 1995). The possibility of intensive chemical weathering in the Himalayas orogenic belt is highly unlikely, as intense weathering requires tectonic quiescence for a long period, higher temperature and humidity (Kronberg and Nesbitt, 1981; Lasaga et al., 1994).

8.8 Index of Compositional Variability

Cox et al. (1995) proposed a measure of compositional variability, known as the Index of Compositional Variability (ICV), as given below:

$(CaO+K_2O+Na_2O+Fe_2O_3(t) +MgO+MnO+TiO_2)/A1_2O_3$

Where Fe_2O_3 (t) = total iron and CaO includes all sources of Ca. In this index, the weight percents of the oxides rather than moles are used. The value of ICV decreases with increasing degree of weathering. The ICV values of some of the minerals are: pyroxene and amphibole = ~10-100, biotite = ~8, alkali feldspar = ~0.8-1, plagioclase = ~0.6, muscovite and illite = ~0.3, montmorillonite = 0.14-0.3 and kaolinite = ~0.03-0.05 (Cox et al., 1995).

The ICV can be applied to mudrocks as a measure of their compositional maturity. Compositionally immature mudrocks tend to occur in tectonically active settings and are characteristically first-cycle deposits (van de Kamp and Leake, 1985). Compositionally mature mudrocks, on the other hand characterize tectonically quiescent environments where concomitant weathering is active, but may also be the product of intense chemical weathering of first-cycle sediments (Weaver, 1989).

Median ICV values (< 0.6) for mudrocks fall within the range of clay minerals, whereas ICV values >0.7 indicate the presence of a large nonclay fraction. The ICV values of the mudstone of the Neogene sequence are generally greater than 0.7 indicating relatively moderate weathering in the source area. This interpretation is supported by the presence of feldspar in the associated sandstones (Yu et al., 1997; Lee and Sheen, 1998).

Table 8.5. Major and trace element data of the mudstone of the Neogene molasse sequence for whole-rock samples. Major elements concentration is in weight percent, whereas trace element concentrations are in ppm. CIA = Chemical Index of Alteration, CIW = Chemical Index of Weathering, ICV = Index of Compositional Variability. Description of sample number is given in Tables 8.1 and 8.2.

Sample	KCK-8	KCC-12	KCC-13	KCC-16	KCC-23	KAK-41	KAK-43	KAC-53
SiO_2	50.33	51.40	43.83	42.78	55.57	39.68	31.58	55.18
Al_2O_3	12.93	11.75	13.70	11.15	18.21	22.84	10.58	17.26
Fe_2O_3	6.80	5.40	6.39	5.78	6.11	6.67	4.37	7.76
MgO	2.78	3.26	7.05	3.68	3.41	2.96	2.36	3.05
CaO	8.00	10.11	8.27	15.30	2.16	9.63	27.43	4.13
Na_2O	1.09	1.09	0.96	1.13	1.02	1.07	0.99	1.25
K_2O	2.07	1.80	2.34	1.66	1.70	2.24	1.69	2.08
TiO_2	0.97	0.69	0.84	0.78	1.05	1.03	0.52	1.01
P_2O_5	0.10	0.13	0.10	0.11	0.04	0.10	0.10	0.12
MnO	0.11	0.12	0.10	0.13	0.04	0.13	0.13	0.08
LOI	14.61	13.79	16.14	17.65	10.76	13.59	20.35	7.85
Total	99.78	99.54	99.73	100.15	100.06	99.96	100.09	99.75
CIA	76.24	75.85	76.88	75.30	83.82	84.49	75.35	80.06
CIW	0.92	0.91	0.93	0.91	0.95	0.96	0.91	0.93
ICV	1.07	1.05	1.29	1.18	0.73	0.62	0.95	0.88
Trace elements								
Sc	12	11	15	15	9	13	18	11
V	81	79	85	98	90	97	59	102
Cr	92	60	56	121	136	122	56	215
Co	17	16	18	21	19	21	13	23
Ni	68	50	57	122	101	101	25	79
Cu	33	26	32	29	43	33	20	40
Zn	69	56	79	60	69	77	46	71
Ga	13	10	14	10	13	14	8	13
Rb	99	74	115	77	108	117	72	87
Sr	238	205	292	220	121	134	146	149
Y	21	19	18	17	20	17	19	22
Zr	178	143	102	115	179	118	89	155
Nb	12	9	10	11	12	12	8	11
Ag	9	5	3	8	1	2	4	8
Cd	3	2	4	6	4	3	1	6
Sn	3	3	6	5	4	4	1	6
Sb	2	4	-	8	-	-	6	-
Cs	16	8	14	12	6	26	16	7
Ba	134	24	194	212	142	186	205	219
La	37	2	31	32	30	35	34	36
Ce	56	25	48	58	58	52	32	61
Nd	28	25	21	22	33	33	28	40
Sm	7	-	-	1	4	-	-	-
Yb	5	8	3	-	2	6	-	-
Hf	11	1	9	4	3	6	7	8
Ta	-	4	-	1	4	-	-	-
W	41	58	15	44	57	39	28	104
Pb	18	17	23	15	16	17	16	17
Th	12	9	14	9	11	10	9	11
U	5	5	7	4	4	4	3	4

Table 8.5 (Continued)

Sample	KAC-59	KAC-60	KAC-64	KAC-65	KAN-72	KAN-73	KAN-76	KAN-77
SiO_2	43.87	66.97	48.28	49.84	45.54	57.04	54.55	51.19
Al_2O_3	13.69	12.18	11.70	16.11	16.97	9.11	10.13	12.44
Fe_2O_3	7.29	4.61	5.60	6.30	7.87	4.96	4.38	6.67
MgO	3.53	2.00	3.36	2.87	3.96	2.47	2.36	3.14
CaO	13.25	3.20	13.33	8.70	8.21	11.44	11.59	9.53
Na_2O	1.16	0.97	1.02	1.09	1.01	1.18	1.26	1.05
K_2O	2.33	2.17	2.00	2.35	2.37	1.85	1.84	2.36
TiO_2	1.10	0.71	0.69	0.73	1.00	0.42	0.64	1.07
P_2O_5	0.12	0.06	0.12	0.11	0.08	0.11	0.12	0.09
MnO	0.14	0.06	0.13	0.13	0.15	0.12	0.15	0.10
LOI	13.53	7.00	13.75	11.79	12.86	11.22	12.97	12.25
Total	100.01	99.94	100.00	100.02	100.01	99.94	99.98	99.90
CIA	75.55	75.48	75.24	78.80	80.07	69.75	71.39	74.43
CIW	0.92	0.93	0.92	0.94	0.94	0.89	0.89	0.92
ICV	1.14	0.86	1.09	0.84	0.96	1.21	1.05	1.16
Sc	16	12	15	13	15	12	14	13
V	85	76	81	98	97	60	59	80
Cr	80	119	118	83	128	159	57	127
Co	16	16	19	23	26	19	16	30
Ni	62	48	124	68	174	100	26	129
Cu	31	26	26	36	37	20	24	29
Zn	77	51	65	81	85	46	39	67
Ga	13	9	11	15	16	9	8	12
Rb	97	96	84	121	123	74	71	94
Sr	171	136	202	136	145	153	192	253
Y	23	16	20	21	19	19	20	19
Zr	138	181	140	139	118	154	188	136
Nb	12	10	12	12	13	10	8	11
Ag	4	6	7	11	7	6	7	7
Cd	3	5	2	6	6	5	2	1
Sn	5	8	4	8	10	5	5	6
Sb	5	2	1	4	1	4	6	-
Cs	21	11	12	-	7	7	7	9
Ba	222	175	213	210	742	182	222	391
La	31	26	37	38	39	34	28	30
Ce	28	64	48	32	32	29	52	58
Nd	28	27	25	33	27	23	21	31
Sm	-	-	-	-	-	-	-	-
Yb	2	-	1	-	5	-	-	3
Hf	6	7	12	8	6	2	10	-
Ta	-	-	-	-	-	-	3	3
W	25	134	39	60	27	90	117	142
Pb	23	17	19	21	18	13	16	16
Th	12	9	8	13	11	10	9	9
U	5	4	5	4	3	3	4	4

Table 8.5 (Continued)

Sample	KBK-90	KBK-98	KBC-104	KBC-107	KBC-108	KBC-112	KBC-115	KBC-122
SiO_2	47.72	40.47	60.47	66.39	40.36	63.91	51.69	61.37
Al_2O_3	7.52	9.94	11.47	11.06	11.67	14.56	11.36	9.54
Fe_2O_3	6.60	5.24	8.37	8.21	6.16	7.15	8.37	5.69
MgO	5.12	3.41	4.17	2.99	3.99	2.61	3.50	2.57
CaO	11.53	18.61	0.99	0.10	15.62	0.88	6.78	6.81
Na_2O	0.54	0.96	1.14	1.25	0.99	1.08	0.97	0.95
K_2O	1.99	1.46	2.57	2.26	1.98	2.28	3.12	1.82
TiO_2	1.51	1.16	1.61	1.84	0.93	0.95	1.01	0.88
P_2O_5	0.09	0.09	0.10	0.10	0.14	0.09	0.10	0.09
MnO	0.10	0.12	0.11	0.06	0.15	0.05	0.12	0.13
LOI	16.78	18.48	8.93	5.78	18.08	6.48	13.16	10.20
Total	99.51	99.95	99.92	100.03	100.09	100.05	100.16	100.06
CIA	71.16	75.85	71.12	71.09	75.56	77.44	69.59	72.94
CIW	0.93	0.91	0.91	0.90	0.92	0.93	0.92	0.91
ICV	2.11	1.24	1.57	1.50	1.22	0.97	1.50	1.26
Sc	19	15	14	12	21	11	11	13
V	110	71	124	104	80	89	92	78
Cr	97	287	80	129	67	103	71	157
Co	19	22	24	24	21	21	18	20
Ni	79	170	78	79	43	82	66	77
Cu	37	17	50	33	33	32	34	21
Zn	70	50	98	75	75	73	87	55
Ga	12	9	16	14	12	13	16	10
Rb	82	61	126	98	92	106	125	70
Sr	345	140	143	181	189	175	175	143
Y	20	17	20	20	19	23	23	20
Zr	121	163	134	167	99	182	131	195
Nb	10	10	11	11	10	12	13	10
Ag	6	5	5	6	5	5	2	8
Cd	5	3	1	3	3	3	1	5
Sn	4	3	6	6	3	5	7	5
Sb	3	4	1	1	4	-	7	1
Cs	12	5	4	24	2	13	16	11
Ba	173	172	206	221	197	230	223	190
La	27	31	29	32	42	38	38	25
Ce	12	53	48	65	27	61	53	17
Nd	32	48	31	37	28	30	33	17
Sm	6	-	1	-	-	-	-	-
Yb	-	-	4	-	-	8	3	-
Hf	4	4	6	12	4	5	3	17
Ta	1	-	-	-	-	-	5	2
W	18	104	29	144	33	115	15	120
Pb	18	13	22	19	21	19	24	15
Th	10	9	13	11	11	11	14	9
U	6	4	4	4	3	4	5	4

Table 8.5 (Continued)

Sample	KBC-126	KBC-128	KBN-141	KBN-143	KBN-145	KBN-148	KBN-151	KBN-153
SiO_2	54.55	43.44	59.68	59.53	56.40	27.95	60.85	56.86
Al_2O_3	10.21	13.64	12.65	16.92	11.41	5.77	11.45	10.33
Fe_2O_3	7.00	8.00	7.06	7.95	5.42	3.63	5.18	5.07
MgO	3.69	4.73	3.37	3.00	2.93	10.91	3.06	2.94
CaO	6.94	10.11	3.36	0.70	8.18	18.98	5.22	8.93
Na_2O	0.87	0.86	1.00	0.97	0.88	0.66	1.14	0.97
K_2O	2.47	1.98	2.59	2.57	1.93	0.96	1.55	1.36
TiO_2	0.88	0.97	0.90	0.81	0.49	0.00	0.34	0.49
P_2O_5	0.12	0.13	0.11	0.16	0.14	0.09	0.09	0.09
MnO	0.12	0.11	0.08	0.08	0.13	0.15	0.11	0.11
LOI	13.17	16.20	9.24	7.10	12.18	30.71	10.63	12.98
Total	100.03	100.16	100.05	99.79	100.08	99.82	99.61	100.12
CIA	71.29	79.34	73.98	79.48	76.32	73.01	76.32	77.11
CIW	0.92	0.94	0.93	0.95	0.93	0.90	0.91	0.91
ICV	1.47	1.22	1.19	0.91	1.03	2.83	0.99	1.06
Sc	14	13	13	14	14	19	8	12
V	92	142	84	114	77	52	64	66
Cr	69	129	141	102	203	83	175	108
Co	21	21	21	17	23	14	18	18
Ni	60	136	75	65	115	82	78	86
Cu	38	27	33	39	20	11	23	22
Zn	88	74	68	92	55	30	55	53
Ga	16	12	13	17	11	5	12	11
Rb	121	92	112	120	83	30	93	80
Sr	190	147	161	129	159	379	131	128
Y	22	23	19	28	20	10	17	19
Zr	127	123	177	183	168	71	140	166
Nb	13	12	11	16	11	5	11	11
Ag	6	4	10	5	3	7	4	4
Cd	5	2	3	4	2	5	3	3
Sn	7	2	6	7	3	2	5	5
Sb	3	1	-	-	3	6	-	4
Cs	23	4	-	26	13	-	9	-
Ba	233	212	218	309	220	110	228	224
La	39	39	33	37	24	25	26	34
Ce	45	29	60	60	64	11	48	44
Nd	33	24	25	46	29	13	20	20
Sm	-	11	1	-	-	6	-	6
Yb	-	9	-	1	6	-	-	-
Hf	14	4	5	6	5	7	9	7
Ta	-	-	9	2	3	3	-	1
W	22	22	76	50	137	48	66	63
Pb	24	15	17	26	16	8	16	15
Th	15	10	11	15	10	4	8	10
U	4	4	3	4	3	5	3	4

Table 8.6. Ratios of major element oxides and trace elements of the mudstone of the Neogene molasse sequence for whole-rock samples.

Sample	KCK-8	KCC-12	KCC-13	KCC-16	KCC-23	KAK-41	KAK-43	KAC-53
SiO_2/Al_2O_3	3.89	4.37	3.20	3.84	3.05	1.74	2.99	3.20
Al_2O_3/SiO_2	0.26	0.23	0.31	0.26	0.33	0.58	0.33	0.31
Al_2O_3/Na_2O	11.91	10.75	14.22	9.89	17.86	21.25	10.69	13.85
Na_2O/K_2O	0.52	0.61	0.41	0.68	0.60	0.48	0.58	0.60
K_2O/Na_2O	1.91	1.64	2.43	1.48	1.66	2.08	1.71	1.67
K_2O/Al_2O_3	0.16	0.15	0.17	0.15	0.09	0.10	0.16	0.12
Fe_2O_3+MgO	9.58	8.66	13.44	9.46	9.52	9.64	6.73	10.81
La/Th	3.15	0.23	2.23	3.57	2.81	3.40	3.64	3.20
La/Y	1.80	0.11	1.73	1.84	1.54	2.07	1.80	1.62
La/Sc	3.10	0.19	2.08	2.11	3.27	2.64	1.91	3.28
Th/Sc	0.98	0.80	0.93	0.59	1.16	0.78	0.53	1.03
Th/Co	0.70	0.55	0.77	0.43	0.56	0.50	0.74	0.48
Th/Cr	0.13	0.15	0.25	0.07	0.08	0.08	0.16	0.05
Ba/Co	8.05	1.46	10.79	10.23	7.42	8.95	16.42	9.45
Ba/Sc	11.23	2.13	13.04	13.93	15.41	13.89	11.73	20.11
Rb/Cs	6.29	9.33	8.06	6.63	19.56	4.54	4.45	12.44
Y/Ni	0.30	0.37	0.31	0.14	0.19	0.17	0.76	0.28
Ti/Zr	54.39	48.50	82.76	67.80	58.72	87.40	57.76	65.20
Cr/Ti	0.01	0.01	0.01	0.02	0.01	0.01	0.01	0.02
Cr/V	1.13	0.76	0.66	1.24	1.51	1.26	0.96	2.12
V/Cr	0.88	1.32	1.52	0.81	0.66	0.80	1.04	0.47
K/Rb	209.78	243.58	204.53	216.47	157.74	191.13	236.11	238.54
Cr/Ni	1.35	1.20	0.98	1.00	1.34	1.22	2.30	2.73
Cr/Th	7.85	6.64	4.04	13.48	12.68	11.78	6.12	19.22
Cr/Sc	7.72	5.33	3.77	7.98	14.75	9.14	3.22	19.75
Ni/Co	4.11	3.05	3.17	5.88	5.28	4.84	1.96	3.41
Cu/Zn	0.48	0.46	0.41	0.48	0.62	0.43	0.44	0.56
Zr/Th	15.18	15.88	7.30	12.73	16.71	11.34	9.70	13.80
Zr/Sc	14.92	12.76	6.81	7.54	19.43	8.80	5.10	14.18

Table 8.6 (Continued)

Sample	**KAC-59**	**KAC-60**	**KAC-64**	**KAC-65**	**KAN-72**	**KAN-73**	**KAN-76**	**KAN-77**
SiO_2/Al_2O_3	3.20	5.50	4.13	3.09	2.68	6.26	5.38	4.11
Al_2O_3/SiO_2	0.31	0.18	0.24	0.32	0.37	0.16	0.19	0.24
Al_2O_3/Na_2O	11.83	12.50	11.45	14.79	16.80	7.71	8.05	11.87
Na_2O/K_2O	0.50	0.45	0.51	0.46	0.43	0.64	0.68	0.44
K_2O/Na_2O	2.02	2.23	1.96	2.16	2.34	1.57	1.46	2.25
K_2O/Al_2O_3	0.17	0.18	0.17	0.15	0.14	0.20	0.18	0.19
Fe_2O_3+MgO	10.82	6.60	8.96	9.17	11.83	7.44	6.74	9.82
La/Th	2.53	2.87	4.35	3.06	3.47	3.54	3.03	3.23
La/Y	1.36	1.62	1.83	1.79	2.07	1.81	1.40	1.55
La/Sc	1.91	2.19	2.47	2.85	2.50	2.78	2.07	2.40
Th/Sc	0.75	0.76	0.57	0.93	0.72	0.79	0.68	0.74
Th/Co	0.76	0.55	0.44	0.54	0.44	0.49	0.58	0.31
Th/Cr	0.15	0.08	0.07	0.15	0.09	0.06	0.16	0.07
Ba/Co	13.78	10.64	11.01	9.04	29.10	9.40	13.96	12.99
Ba/Sc	13.61	14.79	14.36	15.65	48.19	15.00	16.32	31.28
Rb/Cs	4.55	9.00	6.86	404.33	17.10	10.70	9.97	10.22
Y/Ni	0.37	0.33	0.16	0.31	0.11	0.19	0.77	0.15
Ti/Zr	79.71	39.30	49.33	52.22	84.62	27.23	33.92	79.07
Cr/Ti	0.01	0.02	0.02	0.01	0.01	0.04	0.01	0.01
Cr/V	0.94	1.58	1.46	0.84	1.31	2.66	0.97	1.58
V/Cr	1.06	0.63	0.69	1.19	0.76	0.38	1.03	0.63
K/Rb	241.88	225.70	237.37	193.65	192.14	251.34	259.70	250.76
Cr/Ni	1.29	2.49	0.96	1.22	0.73	1.58	2.18	0.99
Cr/Th	6.53	13.23	14.08	6.61	11.50	16.75	6.13	13.66
Cr/Sc	4.93	10.09	7.99	6.16	8.29	13.15	4.19	10.16
Ni/Co	3.87	2.92	6.41	2.92	6.83	5.20	1.65	4.27
Cu/Zn	0.40	0.50	0.40	0.45	0.43	0.43	0.60	0.43
Zr/Th	11.20	20.07	16.69	11.15	10.66	16.18	20.19	14.60
Zr/Sc	8.45	15.31	9.47	10.40	7.68	12.70	13.81	10.86

Table 8.6 (Continued)

Sample	KBK-90	KBK-98	KBC-104	KBC-107	KBC-108	KBC-112	KBC-115	KBC-122
SiO_2/Al_2O_3	6.35	4.07	5.27	6.00	3.46	4.39	4.55	6.43
Al_2O_3/SiO_2	0.16	0.25	0.19	0.17	0.29	0.23	0.22	0.16
Al_2O_3/Na_2O	13.94	10.34	10.06	8.87	11.74	13.50	11.73	10.00
Na_2O/K_2O	0.27	0.66	0.44	0.55	0.50	0.47	0.31	0.52
K_2O/Na_2O	3.70	1.52	2.25	1.81	1.99	2.11	3.22	1.91
K_2O/Al_2O_3	0.27	0.15	0.22	0.20	0.17	0.16	0.27	0.19
Fe_2O_3+MgO	11.73	8.65	12.54	11.20	10.16	9.76	11.87	8.26
La/Th	2.66	3.43	2.27	3.02	3.67	3.55	2.75	2.93
La/Y	1.32	1.75	1.44	1.58	2.18	1.65	1.67	1.24
La/Sc	1.43	2.10	2.06	2.60	1.99	3.33	3.41	1.91
Th/Sc	0.54	0.61	0.91	0.86	0.54	0.94	1.24	0.65
Th/Co	0.55	0.40	0.54	0.45	0.53	0.51	0.76	0.42
Th/Cr	0.10	0.03	0.16	0.08	0.17	0.10	0.20	0.05
Ba/Co	9.35	7.84	8.62	9.22	9.29	11.18	12.16	9.32
Ba/Sc	9.20	11.89	14.60	17.85	9.43	20.38	19.87	14.41
Rb/Cs	7.04	11.96	28.52	4.12	38.50	8.18	8.08	6.66
Y/Ni	0.26	0.10	0.26	0.26	0.45	0.28	0.35	0.26
Ti/Zr	125.39	71.16	120.51	110.04	94.61	51.95	76.95	45.21
Cr/Ti	0.01	0.02	0.00	0.01	0.01	0.01	0.01	0.02
Cr/V	0.88	4.03	0.64	1.24	0.84	1.16	0.77	2.01
V/Cr	1.14	0.25	1.55	0.81	1.20	0.86	1.29	0.50
K/Rb	242.05	239.96	204.62	230.36	214.00	214.41	248.82	260.60
Cr/Ni	1.23	1.69	1.02	1.64	1.57	1.27	1.08	2.04
Cr/Th	9.62	32.24	6.24	12.06	5.92	9.76	5.10	18.30
Cr/Sc	5.17	19.79	5.67	10.41	3.20	9.16	6.33	11.93
Ni/Co	4.26	7.72	3.28	3.28	2.01	3.97	3.58	3.79
Cu/Zn	0.54	0.34	0.51	0.44	0.45	0.45	0.39	0.39
Zr/Th	11.95	18.30	10.44	15.59	8.73	17.16	9.42	22.69
Zr/Sc	6.42	11.23	9.48	13.45	4.72	16.10	11.70	14.78

Table 8.6 (Continued)

Sample	KBC-126	KBC-128	KBN-141	KBN-143	KBN-145	KBN-148	KBN-151	KBN-153
SiO_2/Al_2O_3	5.34	3.19	4.72	3.52	4.94	4.85	5.32	5.50
Al_2O_3/SiO_2	0.19	0.31	0.21	0.28	0.20	0.21	0.19	0.18
Al_2O_3/Na_2O	11.69	15.92	12.60	17.53	12.92	8.68	10.04	10.64
Na_2O/K_2O	0.35	0.43	0.39	0.38	0.46	0.69	0.74	0.72
K_2O/Na_2O	2.83	2.31	2.58	2.66	2.18	1.44	1.36	1.40
K_2O/Al_2O_3	0.24	0.15	0.20	0.15	0.17	0.17	0.14	0.13
Fe_2O_3+MgO	10.69	12.73	10.44	10.94	8.35	14.54	8.24	8.00
La/Th	2.56	4.03	3.04	2.40	2.44	5.81	3.23	3.44
La/Y	1.74	1.68	1.68	1.30	1.21	2.45	1.56	1.80
La/Sc	2.70	2.89	2.52	2.74	1.73	1.35	3.23	2.80
Th/Sc	1.06	0.72	0.83	1.14	0.71	0.23	1.00	0.81
Th/Co	0.74	0.45	0.52	0.90	0.42	0.31	0.45	0.55
Th/Cr	0.22	0.07	0.08	0.15	0.05	0.05	0.05	0.09
Ba/Co	11.30	9.88	10.52	18.06	9.38	7.87	12.66	12.40
Ba/Sc	16.16	15.78	16.88	22.88	15.69	5.96	28.12	18.24
Rb/Cs	5.31	22.32	-	4.53	6.39	-	10.51	-
Y/Ni	0.37	0.17	0.26	0.44	0.17	0.12	0.22	0.22
Ti/Zr	69.61	78.28	51.13	44.37	29.10	0.00	23.98	29.48
Cr/Ti	0.01	0.01	0.02	0.01	0.04	-	0.05	0.02
Cr/V	0.76	0.91	1.68	0.89	2.63	1.59	2.74	1.63
V/Cr	1.32	1.10	0.59	1.12	0.38	0.63	0.36	0.61
K/Rb	204.19	216.39	232.04	214.85	231.91	315.53	167.44	170.67
Cr/Ni	1.16	0.95	1.88	1.57	1.77	1.02	2.24	1.26
Cr/Th	4.57	13.44	13.21	6.62	20.46	19.34	21.55	10.79
Cr/Sc	4.82	9.63	10.96	7.55	14.47	4.50	21.55	8.78
Ni/Co	2.91	6.34	3.63	3.80	4.89	5.84	4.33	4.72
Cu/Zn	0.43	0.36	0.48	0.42	0.37	0.37	0.42	0.41
Zr/Th	8.34	12.85	16.50	11.88	17.01	16.49	17.30	16.62
Zr/Sc	8.80	9.21	13.69	13.56	12.03	3.83	17.30	13.51

Moderate weathering conditions in the source area for these sediments are also in agreement with compositions indicated by the presence of unstable lithic fragments in interbedded sandstones. It must also be noted that high ICV values of mudrocks are probably due to the presence of calcite cement and high Fe_2O_3 content (Table 8.5), which may be the result of chemical weathering during pedogenesis within the depositional basin. Calcite has been identified as one of the major constituents of mudstone by XRD analysis (See Chapter 7), and the red or maroon color of the mudstone support the presence of high content of Fe_2O_3 (Table 8.5). High ICV values of mudrocks show the dominance of first-cycle detritus, supporting the results of sandstone petrological studies (Lee, Y. I. and Sheen, 1998). Two mudstone samples from Bahadar Khel anticline have ICV values that are slightly greater than 2, which suggest input of first cycle sediment or preferential enrichment of quartz and feldspar during deposition (Joo et al., 2005).

8.9 Major Element Compositions of the Mudstone

The ratio K_2O/Al_2O_3 can be used as an indicator of the original composition of ancient mudrocks. The K_2O/Al_2O_3 ratios for clay minerals and feldspars are markedly different. Values of the K_2O/Al_2O_3 ratio for clay minerals range from 0.0 to 0.3 and those for feldspars from 0.3 to 0.9 (Cox et al., 1995). K_2O/Al_2O_3 ratios of common minerals in the decreasing order are: alkali feldspars (0.4-1), illite (~0.3), and other clay minerals (nearly 0) (Cox et al., 1995). The K_2O/Al_2O_3 ratios of the mudstones of the Neogene molasse sequence of the Kohat area are less than 0.3, suggesting presence of clay minerals relative to other minerals in the original mudstone (Cox et al., 1995).

The high average values of ICV of the Neogene mudstone of the Kohat plateau indicate dominance of nonclay silicate material such as feldspar in these strata. Whereas, the low average values of K_2O/Al_2O_3 of these mudrocks suggest that these rocks are dominated by clay minerals such as illite (Lee, Y. I. and Ko, 1997). Although K has a high aqueous solubility, the chemical stability of illite tends to preserve it. Illite is more resistant to weathering in soils under extreme conditions (Norrish and Pickering, 1983). Thus, high proportions of illite in muds indicate intense chemical weathering concomitant with recycling of older sediments (Potter et al., 1975, 1980).

If maturity is the main controlling factor of Si, Al, Na and K contents in these clastic rocks, then SiO_2/Al_2O_3 should show a positive correlation with K_2O/Na_2O. The Kamlial Formation at Bahadar Khel anticline (r=0.65), mudstone (r= 0.51) and sandstone (r=0.75) of Chinji Formation at Banda Assar syncline and Bahadar Khel anticline, respectively, and sandstone of Nagri Formation at Banda Assar syncline (r= 0.83) show positive correlation and thus suggest that maturity in controlled by Si, Al, Na and K. The Kamlial Formation at Chashmai anticline and Banda Assar syncline, mudstone of Chinji Formation at Chashmai and Bahadar Khel anticlines and Nagri Formation at Chashmai and Bahadar Khel anticlines show no trend in SiO_2/Al_2O_3 and K_2O/Na_2O correlation, and therefore, the concentrations of Si, Al, Na and K are most probably controlled by several processes and should not be modeled by a simple ‘‘maturity’’ process (Kampunzu et al., 2005). Variation in K_2O/Na_2O ratios of sandstone (0.7–2.9) and mudstone (1.4-2.7) of the Neogene molasses sequence of Kohat plateau probably suggest differential Na leaching from these rocks due to chemical weathering (Rashid, S. A., 2002).

Loss on ignition (LOI) of the studied sandstone and mudstone samples varies from 9.61 to 20.73% and 5.77% to 30.71%, respectively, reflecting variable amounts of carbonates and hydrous phases (Liu, 1985; Gu et al., 1997).

8.10 Comparison with PAAS and UCC

The major elements analytical data of the mudstone of the Neogene molasse sequence are presented in Tables 8.5, 8.6 and Figs. 8.7-8.9. Bulk chemical variations of the major elements in the mudstone of the Neogene molasse sequence are plotted on variation diagrams using Al_2O_3 along x-axis and compared with Upper Continental Crust (UCC) and Post-Archaen Australian Shale (PAAS) from Taylor and McLennan (l985).

The SiO_2, Al_2O_3 and Na_2O in the mudstone samples of the Neogene sequence are depleted relative to PAAS and UCC (Figs. 8.7a,b; 8.8a,b; 8.9a,b and Tables. 8.5, 8.7). Two samples contain content of SiO_2 matching the UCC and one sample is between PAAS and UCC (Table. 8.4). The content of Al_2O_3 of five samples is between PAAS and UCC whereas one sample contains high Al_2O_3 relative to PAAS (Tables. 8.5, 8.7). Five of the samples show Na_2O content matching the PAAS (Tables. 8.5, 8.7). K_2O in all mudstone samples of the Neogene molasse sequence is less than PAAS and UCC (Figs. 8.7c, 8.8c, 8.9c and Tables. 8.5, 8.7). P_2O_5 is dominantly less than UCC, however, more than PAAS, excluding a few samples having content similar to PAAS (Figs. 8.7d, 8.8d, 8.9d; Tables. 8.5, 8.7). On the other hands, contents of TiO_2 and Fe_tO_3 of these mudstone are between PAAS and UCC (Figs. 8.7e,f; 8.8e,f; 8.9e,f; Tables. 8.5, 8.7). Three samples of mudstone from Bahadar Khel anticline (one from Kamlial and two from Chinji

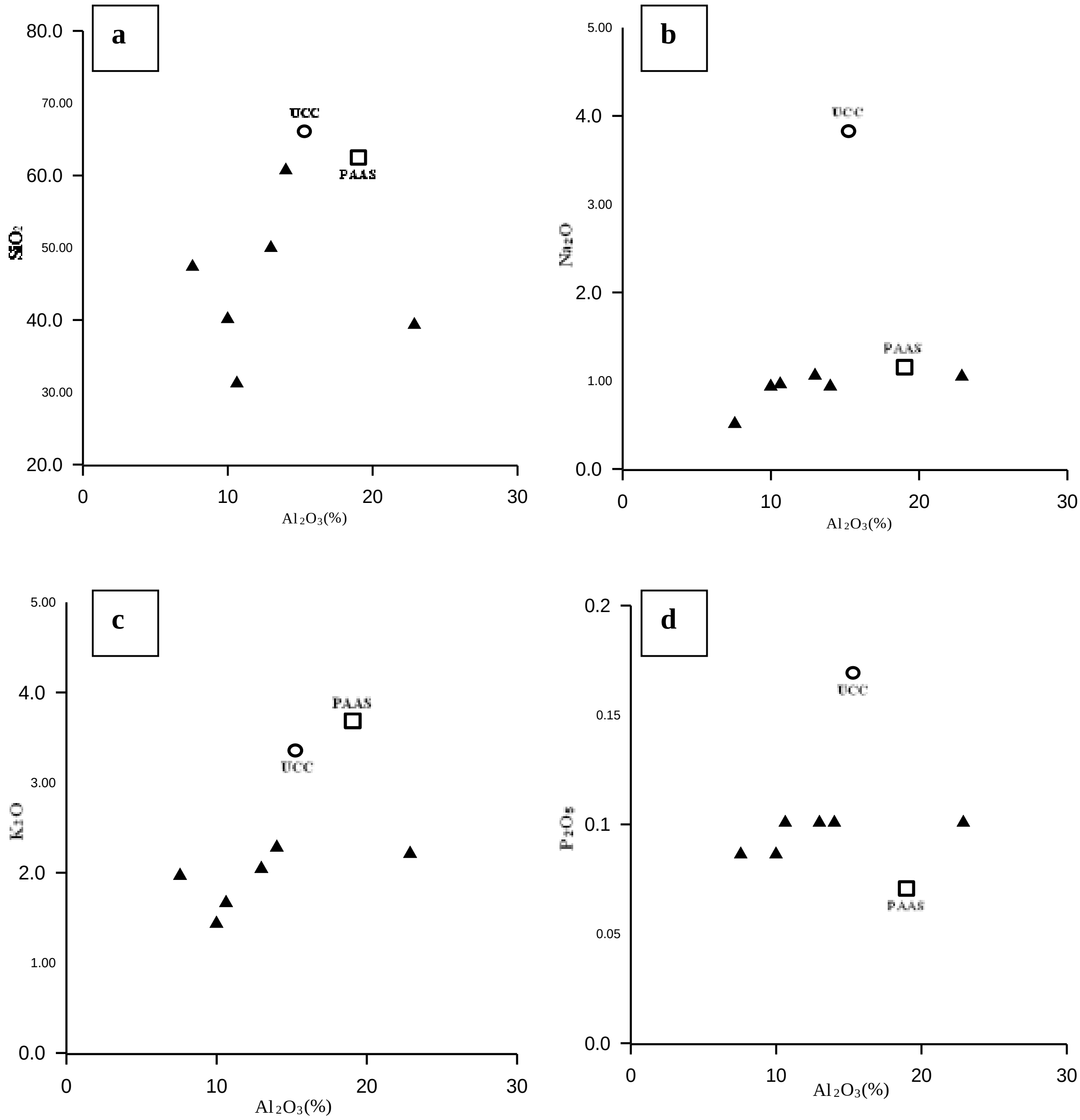

Fig. 8.7. Various oxides of the mudstone of the Kamlial Formation plotted against Al_2O_3. X-axis and Y-axis are weight percent composition. Average data of UCC and PAAS are also plotted for comparison in the binary diagrams.

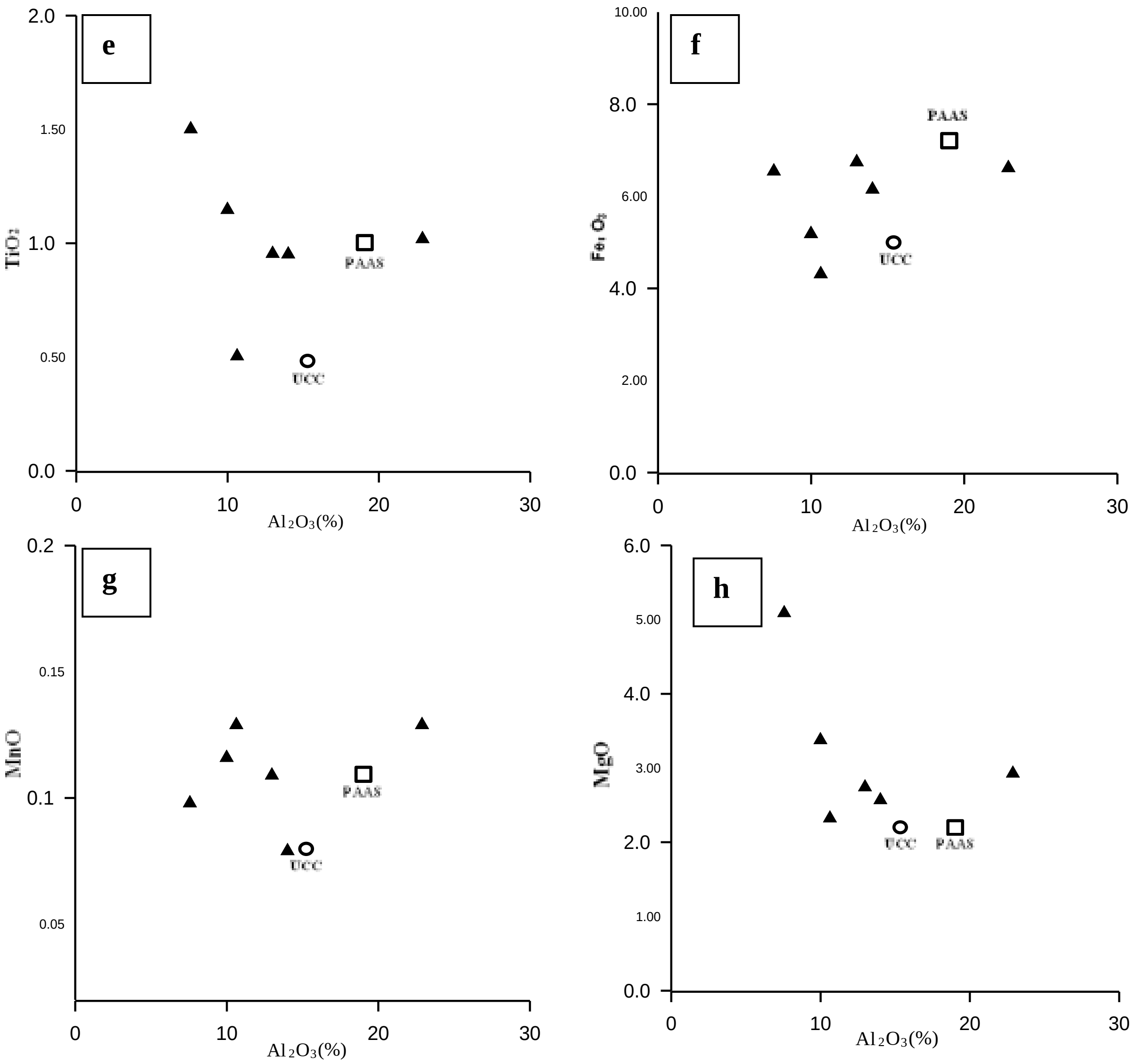
e
f
g
h
TiO₂
Fe₂O₃
MnO
MgO
Al₂O₃(%)
PAAS
UCC

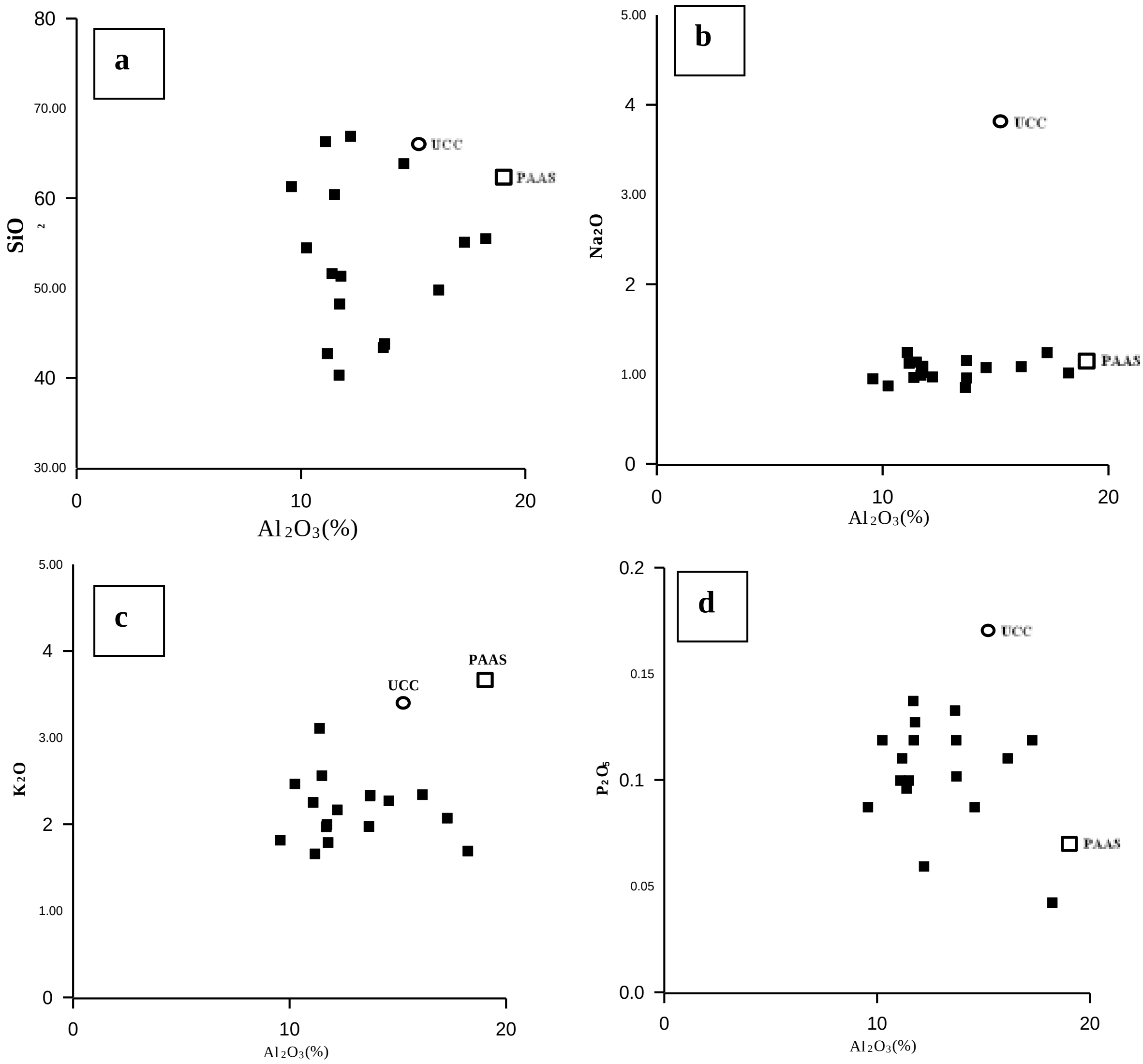

Fig. 8.8. Various oxides of the mudstone of the Chinji Formation plotted against Al_2O_3. X-axis and Y-axis are weight percent composition. Average data of UCC and PAAS are also plotted for comparison in the binary diagrams.

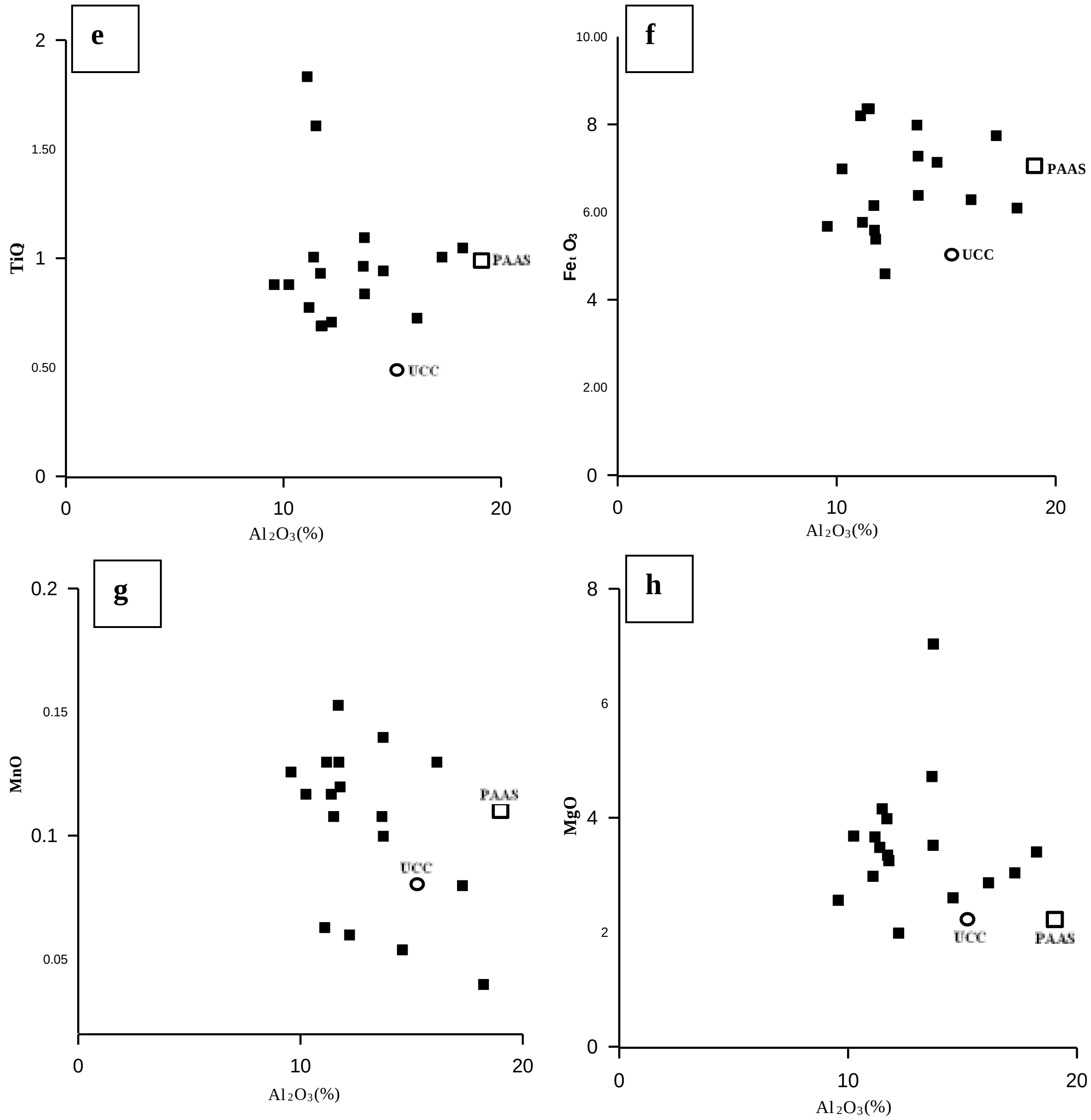
e
TiO
Al₂O₃(%)
PAAS
UCC
f
Feₜ O₃
Al₂O₃(%)
PAAS
UCC
g
MnO
Al₂O₃(%)
PAAS
UCC
h
MgO
Al₂O₃(%)
UCC
PAAS

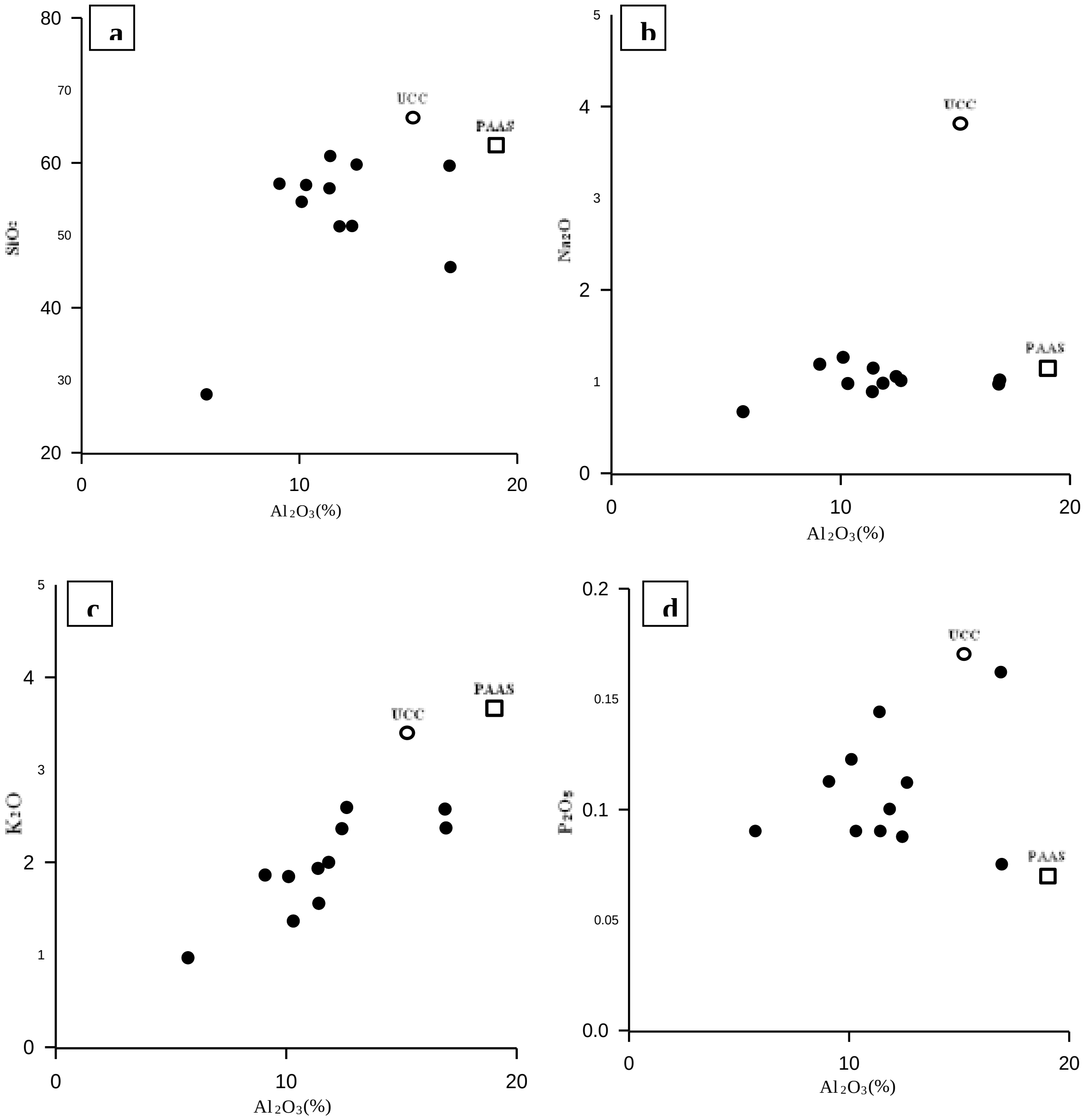

Fig. 8.9. Various oxides of the mudstone of the Nagri Formation plotted against Al_2O_3. X-axis and Y-axis are weight percent composition. Average data of UCC and PAAS are also plotted for comparison in the binary diagrams.

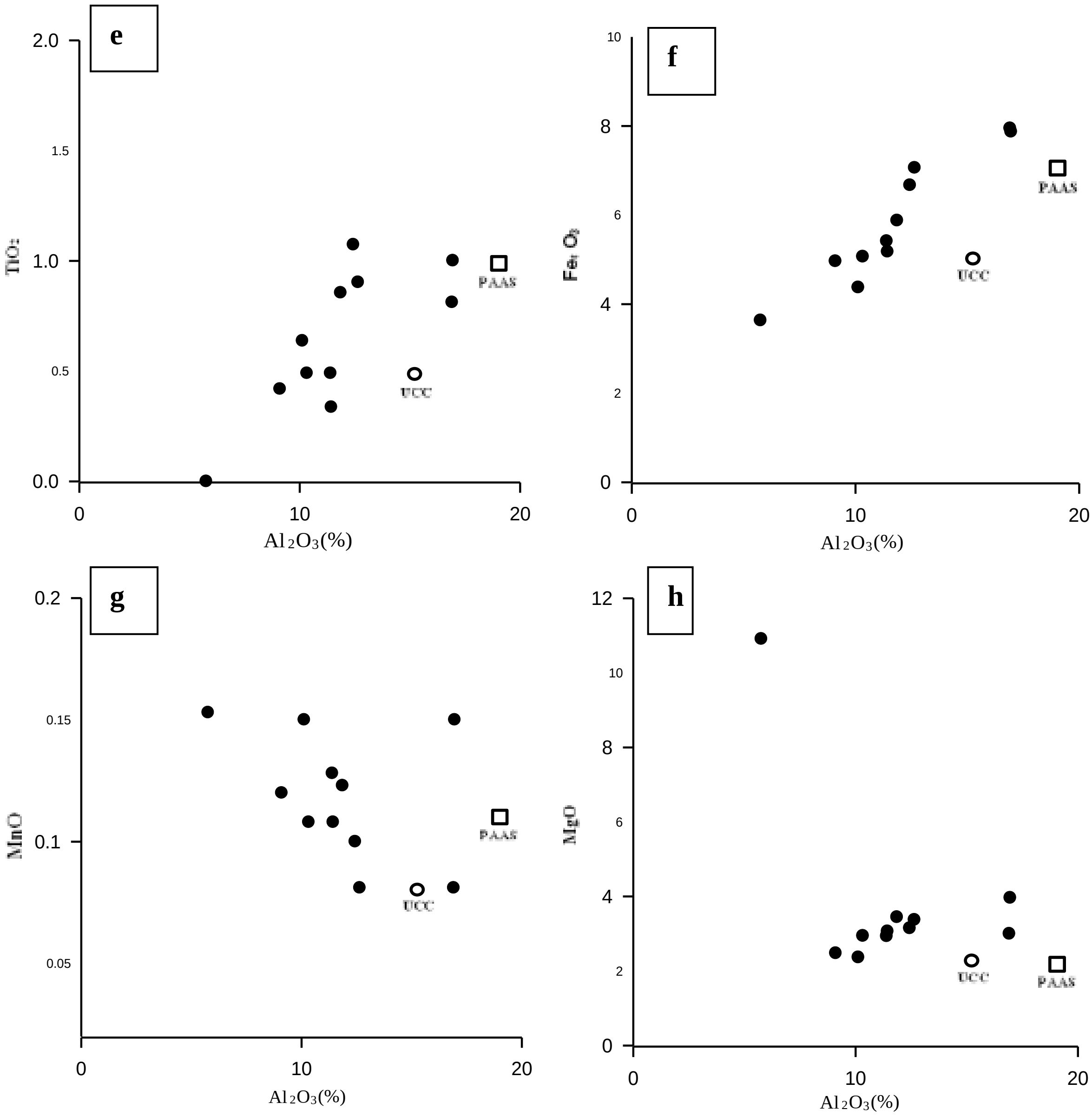

e
TiO2
2.0
1.5
1.0
0.5
0.0
UCC
PAAS
Al2O3(%)
f
Fe2O3
UCC
PAAS
Al2O3(%)
g
MnO
0.2
0.15
0.1
0.05
UCC
PAAS
Al2O3(%)
h
MgO
UCC
PAAS
Al2O3(%)

Table 8.7. Comparison of the average major elements oxides (%) and trace elements (ppm) of the Kamlial (KF), Chinji (CF) and Nagri (NF) formations with UCC and PAAS

	UCC	PAAS	KF Ave	CF Ave	NF Ave
SiO2	65.92	62.80	41.96	52.93	52.96
Al2O3	15.20	18.90	12.76	12.90	11.72
Fe2O3	5.00	7.23	5.94	6.72	5.82
MgO	2.20	2.20	3.33	3.56	3.82
CaO	4.20	1.30	15.04	7.45	8.61
Na2O	3.90	1.20	0.93	1.05	1.01
K2O	3.37	3.70	1.89	2.17	1.94
TiO2	0.50	1.00	1.04	0.98	0.62
P2O5	-	0.16	0.10	0.10	0.11
MnO	0.08	0.11	0.12	0.10	0.12
Trace elements					
Sc	11	16	15	13	13
V	60	150	84	94	75
Cr	35	110	131	106	128
Co	10	23	18	20	20
Ni	20	55	88	78	93
Cu	25	50	28	33	26
Zn	71	85	62	72	59
Ga	-	20	11	13	11
Rb	112	160	86	99	88
Sr	350	200	201	175	183
Y	22	27	19	20	19
Zr	190	210	134	144	150
Nb	14	19	10	11	11
Ag	-	-	5	5	6
Cd	-	-	3	4	3
Sn	-	-	3	5	5
Sb	-	-	3	2	2
Cs	-	15	15	11	8
Ba	550	650	174	195	285
La	30	38	33	32	31
Ce	64	80	41	45	46
Nd	26	32	34	29	25
Sm	4	5	2	1	1
Yb	2	3	2	2	1
Hf	6	5	6	7	6
Ta	-	-	0	1	2
W	-	-	46	61	82
Pb	20	20	16	19	16
Th	11	15	10	11	10
U	3	3	4	4	4

formations) have $TiO_2 \geq 1.5\%$, and one sample of Nagri Formation from the same section is devoid of TiO_2 (Tables. 8.5, 8.7). Four samples of the mudstone show Fe_tO_3 content higher than PAAS and four samples are lower than UCC (Tables. 8.5, 8.7). MnO content is either between PAAS and UCC or higher than PAAS, though three samples have MnO content less than UCC (Figs. 8.7g, 8.8g, 8.9g and Tables. 8.5, 8.7). MgO content of the studied samples is mostly higher than PAAS and UCC excluding four samples whose MgO is less than that of PAAS and UCC (Figs. 8.7h, 8.8h, 8.9h and Tables. 8.5, 8.7). The CaO content is variable and generally higher than PAAS and UCC (Tables. 8.5, 8.7). The CaO content of five samples is between PAAS and UCC whereas four samples from Bahadar Khel anticline show CaO content less than PAAS (Tables. 8.5, 8.7).

The less depleted Na_2O contents in the mudstone of the Neogene molasse sequence compared to the PAAS could be related to the presence of albitic plagioclase and clay minerals. The relatively higher content of CaO may be due to carbonate cement in the sediments. CaO and MgO are usually associated with calcite, dolomite and ferroan carbonates, with the relatively high CaO levels (>5%) being related to dolomitized caliche horizons that formed during pedogenesis (Besly et al. 1993). High CaO and MgO levels together reflect the presence of carbonate minerals, whereas low concentrations are linked to clay minerals (Pearce et al. 2005). The depletion of CaO and Na_2O compared to PAAS reflect moderate to strong weathering, recycling of the source rock, and their removal during transportation (Nesbitt et al. l980; Wronkiewicz and Condie, l987; Condie, l993).

XRD analyses of the mudstone samples of the Neogene molasse sequence indicate the presence of plagioclase, whereas K-feldspar is rare and is identified in a couple of samples. These analyses suggest the dominance of albite from the plagioclase series. In a few samples where albite is absent, the XRD peaks show the presence of orthoclase. Feldspar occurs in more than half of the samples analyzed. Chemically, albite contains Na which is assumed to be the dominant source of Na^+. K^+ is assumed to have been contributed from illite, which occur in majority of the samples analyzed.

8.11 Sedimentary Sorting, Heavy-mineral Accumulation and Trace Elements

Before applying trace elements to monitor provenance of detrital sediments, we need to know which minerals affect the trace element distributions and which lithologies host these minerals. Heavy-mineral accumulation during sedimentary sorting can considerably complicate interpretations of sediment provenance by producing irregular chemical variations in some trace elements (McLennan et al., 1993). This problem can be approached by taking a possible correlation between trace and major elements that monitor the relative abundances of specific minerals. It is known that the REE are generally associated with minerals like zircon, monazite, allanite, etc. (McLennan, 1989). For instance, Zr and Hf may be concentrated in the coarser fraction of the sediment due to zircon accumulation. In the same manner, REE and Th abundances may depend on accumulation of monazite, apatite, zircon or titanite (Crichton and Condie, 1993). Similarly, moderate correlation between the pairs Zr-Yb and Ti-Ta suggests some accumulation of zircon and titanite (Dupuis et al., 2006). Alike, the linear correlation coefficients between REEs and Al_2O_3 suggest that REEs are associated with clay minerals (Condie, 1991).

Zr/Hf ratios in sediments may be used as a good indicator that these ratios are related to zircon or not. Generally, there is no good correlation between Zr and Hf in the Neogene molasses sequence except in sandstone of Kamlial Formation at Banda Assar syncline (r= 0.87) and Chinji Formation at Bahadar Khel anticline (r= 0.75). Furthermore, mean Zr content in the mudstone (145) is usually higher than in the associated sandstones (105), which indicates that sedimentary sorting has not been an important process in controlling Zr concentration. There is poor correlations between Zr and Th in Neogene mudstone except in Nagri Formation at Bahadar Khel anticline (r=0.60). However, there is very significant positive correlation between Zr and Th in the associated sandstones (r=69 to 93), which indicates that zircon has some control over the abundance of Th.

Likewise, to test the influence of grain size on Cr and Zr, the correlation factors of these elements were computed against Al_2O_3. There is no good correlation between Cr and Al_2O_3 in mudstone but significant correlation is observed in sandstones of the Kamlial (r=0.76) and Nagri (-0.72) formations at Banda Assar syncline and Kamlial (r=0.97) and Chinji (r=0.87) formations in Bahadar Khel anticline. Zr shows significant correlation with Al_2O_3 in mudstones of Kamlial Formation at Chashmai (r=0.71), Nagri Formation of Banda Assar syncline (r=-0.78) and Bahadar Khel anticline (r=0.85). In sandstones, significant correlation occurs only in Kamlial Formation in all the three studied sections i.e. Chashmai anticline (r=0.75), Banda Assar syncline (r=0.87) and Bahadar Khel anticline (r=0.74). The correlation factors mentioned show the affinity of these elements to clay minerals.

TiO_2 in sandstone of Kamlial Formation is well correlated to Al_2O_3 at Chashmai (r= 0.65) and Bahadar Khel (0.68) anticlines. In Chinji Formation, TiO_2 shows a strong positive correlation at Chashmai anticline (r= 0.95) and Bahadar Khel anticline (r= 0.85), and V at Banda Assar syncline (r= 0.97) and Bahadar Khel anticline (r= 0.94) with Al_2O_3. Similarly, mudstone of the Nagri Formation also shows a strong correlation of TiO_2 and V, respectively, with Al_2O_3 at Banda Assar syncline (r= 0.78 and r= 0.97) and Bahadar Khel anticline (r= 0.85 and r= 0.93). The fact that V and TiO_2 are well correlated with Al_2O_3 suggests that they are bound to clay minerals and associated phases and, therefore, have been concentrated during weathering processes.

Th/U values of mudstones show strong correlation with weathering intensity for Chinji Formation at Banda Assar syncline (r= 0.82) and Nagri Formation at Bahadar Khel anticline (r= 0.86) thus suggesting an increase with clay content (kaolinite) (McLennan et al., 1990).

8.12 Trace Elements and Weathering

Large ion lithophile elements (LILE): Large ion lithophile elements such as Rb, Sr, Ba, Th, U and Cs behave similarly to related major elements during weathering processes. Like K_2O, Rb and Cs generally incorporate into clays, while like CaO and Na_2O, Sr tends to leach during chemical weathering (Nesbitt et al., 1980). In comparison with UCC and PAAS, mean contents of Rb, Ba and Th in the Neogene mudstone (93, 219 and 10 ppm, respectively) and sandstone (58, 189 and 6 ppm, respectively) are lower than UCC (112, 550 and 10.7 ppm, respectively) and PAAS (160, 650 and 14.6 ppm, respectively). On average, they are slightly enriched in U (mudstone = 4.14 ppm, sandstone = 3.32 ppm, UCC = 2.8 ppm and PAAS = 3.1 ppm). In mudstone units, Rb shows strong positive correlation with Al_2O_3 in Chinji Formation at Chashmai anticline (r = 0.72) and Nagri Formation at Banda Assar syncline (r = 0.98) and Bahadar Khel anticline (r =0 .95). Rb also shows positive correlation with K_2O in Chinji Formation (r = 0.62 at Chashmai anticline, r = 0.82 at Banda Assar syncline and r=0.88 at Bahadar Khel anticline) and Nagri Formation (r = 0.87 at Banda Assar syncline and r=0.91 at Bahadar Khel anticline). Similarly, Rb shows strong positive correlation with Al_2O_3 (r = 0.88 in Kamlial Formation at Banda Assar syncline, r = 0.97 in Chinji Formation at Chashmai anticline, and r = 0.97 and 0.84 in Nagri Formation at Banda Assar syncline and Bahadar Khel anticline, respectively) and K_2O (r = 0.77 in Chinji Formation at Chashmai anticline, r = 0.80 and 0.95 in Kamlial and Nagri formations at Banda Assar syncline, and r = 0.96, 0.52 and 0.97 in Kamlial, Chinji and Nagri formations at Bahadar Khel anticline, respectively) in the sandstone units of the Neogene molasse sequence of the Kohat. These correlations suggest that Rb distribution is mainly controlled by phyllosilicates and illitic phases. The positive correlation between Th and Al_2O_3 in Neogene mudstone (r = 0.73 for Chinji Formation at Banda Assar syncline, and r = 0.87 and 0.96 for Nagri Formation at Banda Assar syncline and Bahadar Khel anticline, respectively) and sandstone (r = 0.62 for Kamlial Formation at both Banda Assar syncline and Bahadar Khel anticline) indicates that it is associated with clays. Similarly, a moderate correlation between Al_2O_3 and La in Neogene mudstone (r = 0.52 for Chinji Formation at Banda Assar syncline, and r = 0.70 and 0.66 for Nagri Formation at Banda Assar syncline and Bahadar Khel anticline, respectively) and sandstone (r = -0.96 and 0.65 for Kamlial Formation at Chashmai and Banda Assar syncline, and r = 0.59 and -0.60 for Nagri Formation at Chashmai and Bahadar Khel anticlines, respectively) indicate that La is controlled in part by clays or micas.

Rb and Cs are very sensitive to climatic influences (Nesbitt et al., 1980) and may become leached during chemical weathering. However, most of the dissolved Rb and Cs may be absorbed and fixed in secondary minerals (Weaver, 1967), and thus enhanced chemical weathering will result in higher Rb and Cs contents. But content of the Rb and Cs in the Neogene mudstone and sandstone is less than the UCC and PAAS, thus suggesting moderate chemical weathering (Yan et al., 2007).

Weathering and sedimentary recycling: U and Th in sedimentary rocks occur in association with several host elements, such as clay minerals, feldspars, heavy minerals, phosphates and organic matter (Ruffell and Worden, 2000). U is highly soluble, even in neutral aqueous solution, however, Th may dissolve in weak acids, such as humic acids (Pierini et al., 2002).

Sedimentary recycling in oxidizing conditions results in a distinct fractionation of Th and U during rock weathering. U^{+4} is readily oxidized to U^{+6}, which forms the highly soluble species, uranyl, that can be removed from the system, whereas Th retains its oxidation state and remains relatively insoluble (McLennan and Taylor, 1980). As a consequence, the Th/U ratio increases due to successive cycles of weathering and redeposition and thus becomes a good marker of these processes. The Th/U ratio of the Neogene molasse sequence of the Kohat Plateau is always less than the average value for the UCC and PAAS, which suggests that these deposits are first cycled. Other evidence of no sedimentary recycling can be envisaged from Rb/Sr ratio that averages 0.29 for sandstone and 0.56 for mudstone of the Neogene molasses sequence of the Kohat Plateau (McLennan et al., 1993).

The Zr/Sc ratio is commonly used as a measure of the degree of sedimentary recycling which leads to the enrichment of the stable mineral zircon in the deposits (Nesbitt and Young, 1982). The Zr/Sc values of the Neogene mudstone (3.83-19.43, averaging 11.17) and sandstone (2.30-14.13, averaging 7.84) are similar or lower as compare to that of the UCC (17.27) and PAAS (13.12) indicating that a recycled sedimentary source was a minor component (Roddaz et al., 2005).

U/Th ratios below 1.25 suggest oxic conditions of deposition, whereas values above 1.25 indicate suboxic and anoxic conditions (Nath et al., 1997). In the Arabian Sea, sediments below the oxygen minimum zone show high U/Th (>1.25) ratios, whereas the sediments above the oxygen minimum zone exhibit low U/Th (<1.25) ratios. The Neogene molasse sequence of this study shows low U/Th ratios (0.27-1.12 for mudstone and 0.22-0.78 for sandstone excluding one anomalous sample of 2.46), which indicate that these sediments were deposited in an oxic environment.

The authigenic uranium content is also considered as an index of bottom water condition in ancient sedimentary sequences (Wignall and Myers, 1988). The authigenic uranium content is calculated as: (authigenic U) = (total U) – Th/3. Values of authigenic U below 5 are thought to represent oxic depositional conditions, while values above 5 are indicative of suboxic and anoxic conditions. In this study, authigenic U contents are low in both mudstone (<3.37 ppm) and sandstone (<2.70 ppm, but 11.96 ppm for the anomalous sample). Thus, the observed low U/Th ratio and low authigenic U content in the studied mudstone and sandstone indicate that these sediments were deposited in an oxic environment.

The V/Cr ratio has also been used as an index of paleooxygenation in many studies (Ernst, 1970; Bjorlykke, 1974; Dill, 1986; Dill et al., 1988). Vanadium may be bound to organic matter by the incorporation of V^{+4} into porphyrins, and is generally found in sediments deposited in reducing environments (Shaw et al., 1990). Cr is mainly incorporated in the detrital fraction of sediments and it may substitute for Al in the clay structure (Bjorlykke, 1974). Ratios > 2 indicate anoxic conditions, whereas values < 2 suggest more oxidizing conditions (Jones and Manning, 1994). In the mudstone of the

Neogene molasse sequence, the V/Cr ratio varies between 0.23 and 1.59, and in sandstone it varies from 0.08 to 1.55, which implies that this sequence was deposited in an oxic depositional environment. Dypvik (1984) and Dill (1986) used the Ni/Co ratio as a redox indicator. Jones and Manning (1994) suggested that Ni/Co ratios < 5 indicate oxic environments, whereas ratios > 5 suggest suboxic and anoxic environments. The sandstone of the Neogene sandstone shows Ni/Co ratio < 5, which suggest that these sediments were deposited in an oxygenated environment. On the other hand, though majority of the mudstone samples of the Neogene sequence show Ni/Co ratio < 5, indicating an oxygenated environment, still in some of the samples, the Ni/Co ratio ranges between 5 and 7, and thus suggests a suboxic environment. In addition, Hallberg (1976) used Cu/Zn as a redox parameter, and high Cu/Zn ratios indicate reducing depositional conditions, while low Cu/Zn ratios suggest oxidizing conditions. The low Cu/Zn ratios for Neogene mudstone (0.34-0.61) and sandstone (0.13-0.60) indicate that this sequence was deposited under well oxidizing conditions.

8.13 Trace Elements and Provenance

The immobile nature of Zr, Nb and Y, and their preferentially enrichment in felsic phases during crystallization and anatexis make them a good provenance indicator (Taylor and McLennan, 1985; Feng and Kerrich, 1990). The Neogene mudstone of the Kohat has Zr ranging from 71 to 195, averaging 144.81 ppm (UCC = 190 ppm, PASS = 210 ppm), Nb ranging from 5 to 16, averaging 10.76 ppm (UCC = 13.7 ppm, PAAS= 19 ppm) and Y ranging from 10 to 28, averaging 19.63 ppm (UCC = 22 ppm, PAA S= 27 ppm). Sandstones of the Neogene molasse sequence show lower Zr, Nb and Y values than the associated Neogene mudstone, UCC and PAAS. Zr ranges from 74 to 184, averaging 104.67 ppm, Nb ranging from 4 to 11, averaging 6.36 ppm and Y ranging from 10 to 21, averaging 14.97 ppm in the Neogene sandstone of the southwestern Kohat. The lower values of Zr, Nb and Y of the studied sequence thus indicate the presence of mafic phases in the source area/s for these sediments.

The suspended sediment load of the Indus River shows distinct negative anomalies for Nb and positive anomalies for Ni, which are similar to the trace element signatures of the arc magmatic rocks exposed in the form of Ladakh/Kohistan island arc as well as the mafic and ultramafic magmatic rocks of the Indus and Shyok suture zones (Honegger et al., 1982, 1989; Rai, 1987; Sharma, 1991; Ahmad, T. et al., 1996) forming the catchment for the Indus river basin. Negative anomalies of Nb are also distinguishing features of subduction-related magmatism (Holm, 1985). The arc magmatic rocks of Ladakh/Kohistan are thought to have formed by the northwards subduction of the Indian Plate beneath the Eurasian Plate along the Indus and Shyok suture zones (Thakur, 1992). The distinct positive Ni anomaly probably reflects the influence of the mafic and ultramafic magmatic rocks of the Indus and Shyok suture zones (Ahmad, T. et al., 1996).

Cullers et al. (1988), Cullers (1994) and Mongelli et al. (1996) used trace element geochemistry for provenance studies of various sediments. In this regard, Co and Sc can be used to distinguish between sediments derived from amphibolites, tonalites and other acidic rocks. Similarly, Ba was used for distinguishing silicic and basic sources of sands. But the best provenance discrimination was obtained by plotting the Ba/Sc and Ba/Co ratios (Cullers et al., 1988). In the present study the low average Ba/Co and Ba/Sc ratios of the Neogene molasses sequence of the Kohat plateau (Ba/Co = 10.81 for mudstone and 4.94 for sandstone, and Ba/Sc = 16.39 for mudstone and 14.36 for sandstone) are significantly lower than the UCC (Ba/Co = 55 and Ba/Sc = 50) and PAAS (Ba/Co = 28.26 and Ba/Sc = 40.62) and thus point to basic rocks as possible source for these lithologies.

Since elements like Cr and Zr are controlled by the chromite and zircon contents, respectively, their ratio may be good indicator of relative influx of komatiite (mafic)/granite (felsic) sources (Wronkiewicz and Condie, 1989). The mudstones of the Neogene molasse sequence of the Kohat plateau have Cr/Zr ratios ranging from 0.30 to 1.76, averaging 0.81 (less than 1), and the sandstones ranging from 0.37 to 4.10, averaging 1.75. The Cr/Zr is >3 in the upper part of the Nagri Formation at Bahadar Khel anticline. The high Cr/Zr ratio in sandstone may be the result of selective sorting of heavy minerals. These ratios are greater than the UCC and PAAS. The Sc/Th ratio of the Neogene sandstone reflects the relative contributions of (basalt + komatiite)/ granite. The average Sc/Th ratio of the sandstones of the Neogene molasse sequence is 2.52, which are greater than UCC and PAAS. The high Cr/Zr and Sc/Th indicate mafic source rocks for the Neogene molasse sequence of the Kohat. Similarly, the high Cr contents (Cr > 110 ppm) of the Neogene molasse sequence may also be interpreted as evidence for derivation from a chromite rich mafic and ultramafic sources.

Low Y/Ni ratios of the mudstone (0.30) and sandstone (0.39) of the Neogene molasses sequence of the Kohat plateau suggest contribution of a mafic to ultramafic component to the Himalayan foreland basin (Huntsman-Mapila et al., 2005). High Cr/V ratio of mudstone (1.4) and sandstone (3.65) also reflect the probable presence of chromite and ultramafic components (Bock et al., 1998) within the molasse sequence that are characteristic of the ophiolitic sequences lying in the north.

Ratios of trace elements such as La/Sc, Th/Sc, Th/Co and Cr/Th are significantly different in felsic and basic rocks and may allow constraints on the average provenance composition (Wronkiewicz and Condie, 1990; Cox et al., 1995; Cullers, 1995). Th/Sc, Th/Co, Cr/Th and La/Sc ratios of mudstone from this study are compared with those of sediments derived from felsic and basic rocks (fine fraction) as well as to UCC and PAAS values (Table 8.8). This comparison shows that the elemental ratios of Th/Sc of the Neogene molasse sequence have more similar values to UCC and PAAS, therefore, they are close to those of the upper continental crust. As the average source of the PAAS is presumed to be derived from granites, this suggests derivation of the Neogene sediments from a source area of felsic composition. Taylor and McLennan (1985) claimed that the Th/Sc ratio is a much more sensitive index for provenance than the La/Th ratio. Ratio of Cr/Th suggests contribution from both silicic and mafic rocks. Furthermore, Th/Co versus La/Sc diagram also indicates dominantly a silicic provenance for the Neogene molasse sequence of the Kohat area (Figs. 8.10-8.12) (Cullers, 2002).

Table 8.8. Range of elemental ratios of the Neogene mudstone and sandstone compared to the ratios of the Upper Continental Crust (UCC), Post Archian Australian Shale (PAAS), sands from silicic rocks, sands from mafic rocks, andesites, granites, ophiolites, Lower Continental Crust (LCC), Oceanic Crust (OC) and average Proterozoic sandstones.

	La/Sc	**Th/Sc**	**Co/Th**	**Cr/Th**
Neogene Mudstone	1.35-3.41	0.51-1.16	1.11-3.23	4.04-19.22
Neogene Sandstone	1.03-3.04	0.20-0.91	3.57-11.11	6.24-75.40
UCC[a]	2.70	0.71	0.9	3.3
PAAS[a]	2.40	0.91	1.58	7.53
Silicic Source[b]	2.50-16.30	0.84-20.50	0.22-1.5	0.40-15.00
Mafic Source[b]	0.43-0.86	0.05-0.22	7.10-8.30	22-500
Andesites[c]	0.90	0.22	4.65	9.77
Granites[c]	80	3.57	0.17	0.44
Ophiolites[c]	0.25	0.02	70	410
LCC[a]	0.30	0.03	33	222
OC[a]	0.10	0.58	214	1227
Ave. Proterozoic Sandstone[c]	4.21	1.75		5.71

[a]Taylor and McLennan (1985), [b]Armstrong-Altrin et al. (2004), [c]Condie (1993)

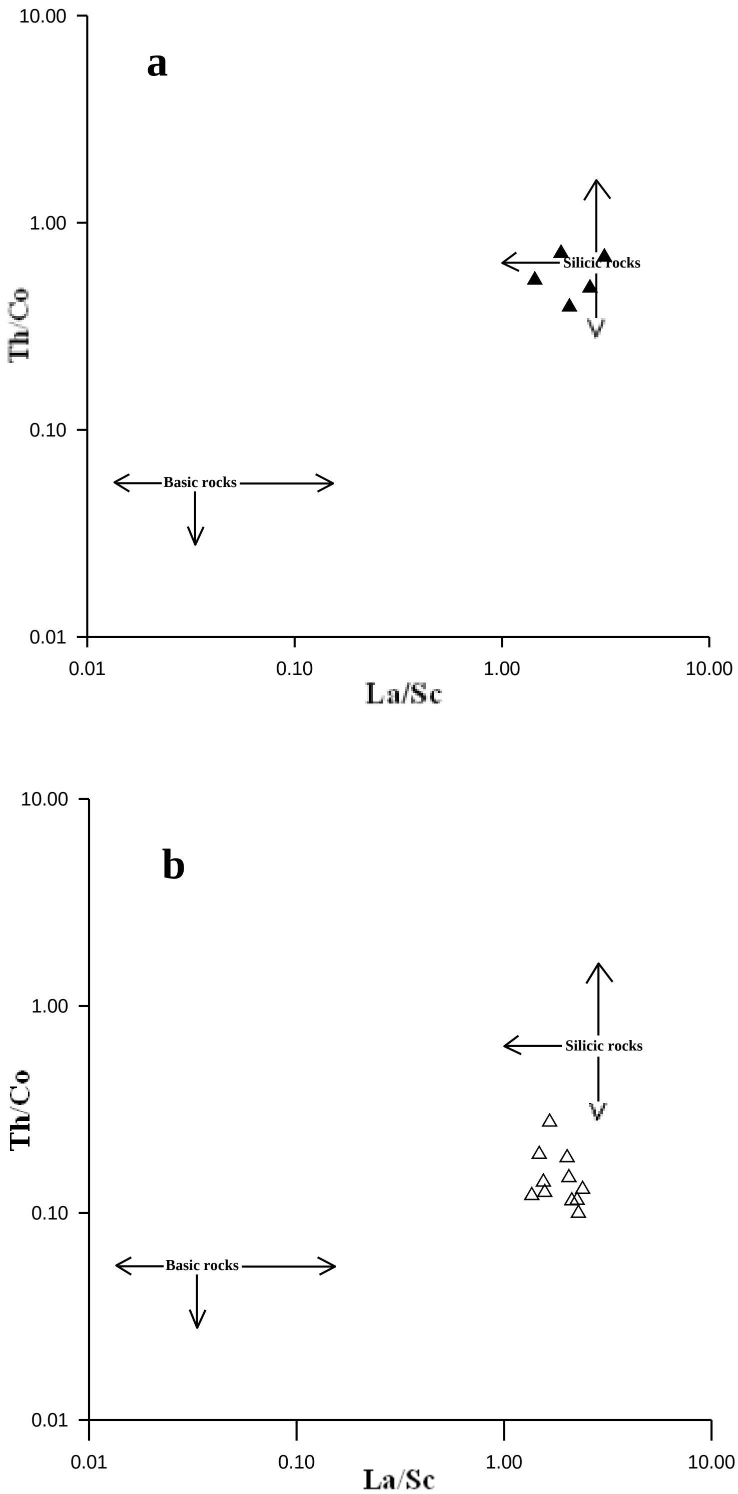

Figs 8.10. Th/Co versus La/Sc diagram for the a) mudstone and b) sandstone samples of the Kamlial Formation. Fields in the diagram are defined after Cullers (2002).

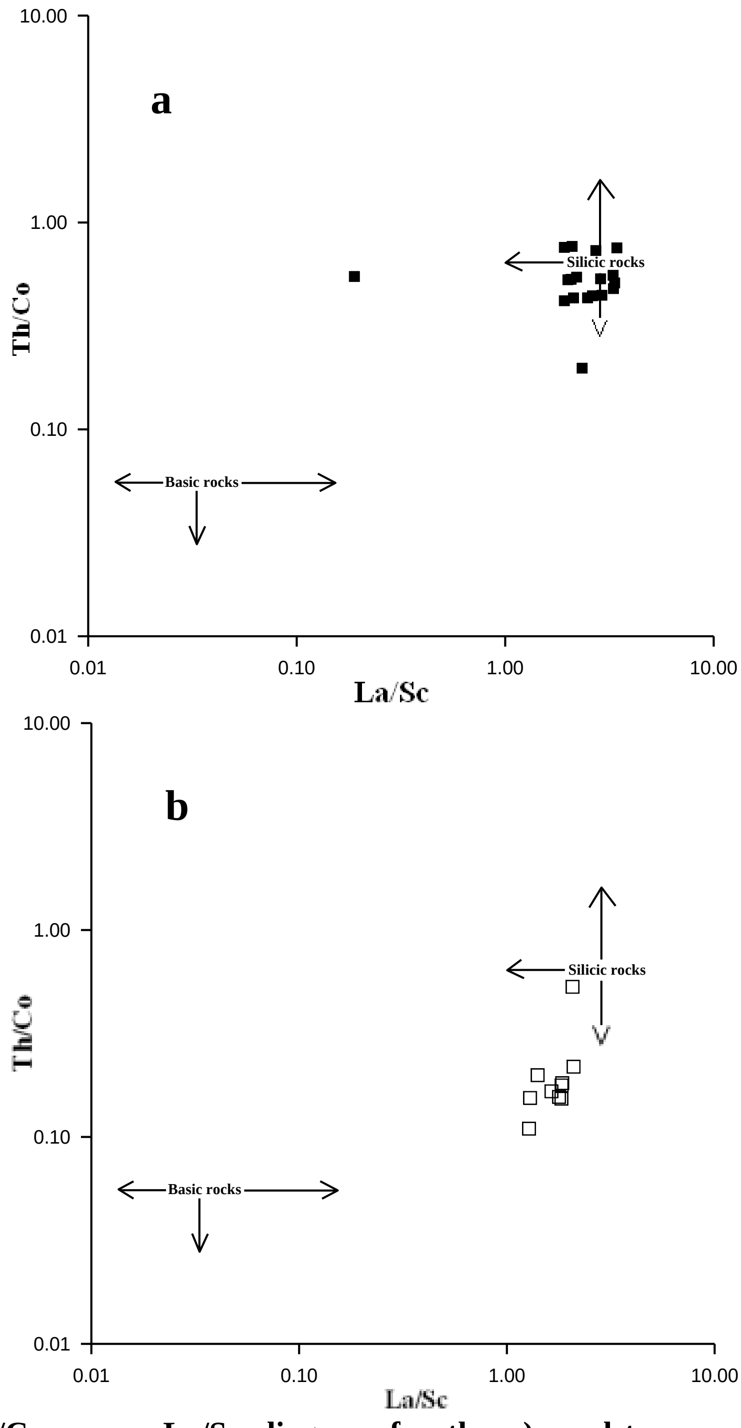

Figs. 8.11. Th/Co versus La/Sc diagram for the a) mudstone and b) sandstone samples of the Chinji Formation. Fields in the diagram are defined after Cullers (2002).

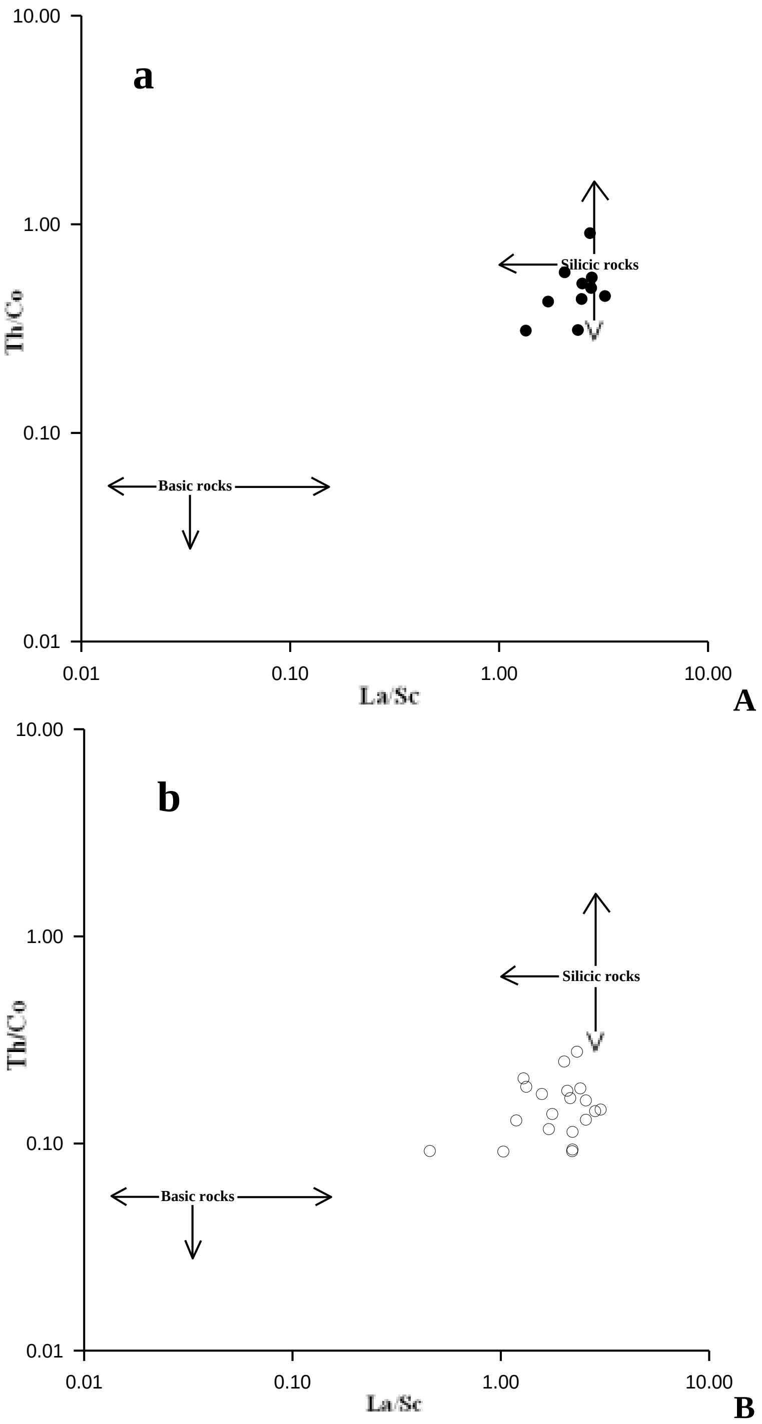

Figs. 8.12. Th/Co versus La/Sc diagram for the a) mudstone and b) sandstone samples of the Nagri Formation. Fields in the diagram are defined after Cullers (2002).

Small differences found in the ratios of Th/Sc, Co/Th and Cr/Th in the mudstone of the different formations and sections may indicate either compositional variations in source area(s) or different oxidation states. The weak correlation of these ratios with the CIA index may suggest moderate chemical weathering, and change in redox conditions during diagenesis (Nagarajan et al., 2007).

Although K and Rb are lithophile elements considered relatively mobile during metamorphism, their absolute values indicate acidic-intermediate igneous precursors, coincident with Th/Sc ratios. Sandstone and mudstone of the Neogene molasse sequence show K/Rb ratios of 249.39 and 223.70, respectively, which are in agreement with the average ratio of the UCC (250), but little higher than PAAS (171) (Shaw, 1968).

8.14 Conclusions

- The geochemical parameters like Fe_2O_3+MgO, TiO_2 and Al_2O_3/SiO_2 of the Neogene molasse sandstone show major provenance from continental island arc and partial influx from active continental margin settings. K_2O/NaO_2 ratio does not signify a particular provenance to these sediments.

- The contents of the major element oxides except MnO of the sandstone of the studied sequences also indicate a dominant continental island arc provenance. The content of MnO of these sandstones suggests a source region composed dominantly of oceanic island arc.

- The Fe_2O_3+MgO vs TiO_2, Fe_2O_3+MgO vs K_2O/Na_2O and Fe_2O_3+MgO vs Al_2O_3/SiO_2 discriminatory plots suggest continental island arc and active continental margin provenances for the Neogene sandstone of the Kohat.

- Discriminatory plot SiO_2 vs log (K_2O/Na_2O) indicates a dominant influx from ACM for the studied sandstone with minor contribution from PM for the Kamlial Formation and oceanic island arc for the Chinji and Nagri formations.

- The CIA values of sandstone of the Neogene sandstone (mostly 64 to 76) and mudstone (mostly 70 to 80) suggest moderate to slightly intense weathering of these sediments. However, ICV values and lower contents of Rb and Cs than UCC and PAAS of the mudstone indicate relatively moderate weathering. Furthermore, the Th/U ratio of the Neogene molasse sequence is lower than the UCC and

PAAS, which also show that these sediments are first cycled in origin. But Zr/Sc ratio proposes minor contribution from recycled sedimentary sources.

- The lower values of Zr, Nb and Y in sandstone and mudstone indicate the consistent presence of mafic phases in the source area.
- Values of the Ba/Sc, Ba/Co, Cr/Zr, Sc/Th and Y/Ni favor the presence of basic/ultrabasic rocks in the source area, still values of La/Th, La/Sc, Th/Zr and plot of Th/Co vs La/Sc propose provenance similar to UCC/PAAS/felsic rocks.
- Generally, there exist a significant positive correlation of TiO_2, Zr, Rb and V with Al_2O_3 indicating their association with clay minerals and associated phases.
- The values of the authigenic U, U/Th, V/Cr, Cu/Zn and Ni/Co of the Neogene molasse sediments show that these sediments were deposited in oxidizing conditions.

CHAPTER 9

Discussion

9.1. The Himalayan Foreland Basin

The Himalayan peripheral foreland basin stretches east–west along the length of the Himalayan orogen, from Pakistan (Pivnik and Wells, 1996) through India (Najman et al., 1997) to Nepal (DeCelles et al., 1998a). A major unconformity separate rocks representing the last marine facies in Eocene times (Mathur, S. N., 1978, 1979; Sakai, 1989; Pivnik and Wells, 1996) from the early continental sediments eroded from the metamorphic rocks of the Himalayan orogen, dated in India younger than mid-Oligocene (Najman et al., 1997) and in Nepal younger than earliest Miocene (DeCelles et al., 2001). The Late Palaeogene alluvial rocks of the Himalayan Foreland Basin are named as the Balakot Formation (Hazara-Kashmir syntaxis) (Bossart and Ottiger, 1989) and the Murree Formation in Pakistan (Shah, 1977), the Dagshai Formation in India (Bhatia, S. B., 1982) and the Dumre Formation in Nepal (Sakai, 1989) (Table 9.1). The younger southern Murree Formation is considered to be Lower Miocene (Fatmi, 1973; Abbasi and Friend, 1989) that is conformably overlain by the Kamlial Formation, magnetostratigraphically dated at 18-14 Ma (Johnson, N. M. et al., 1985).

Table 9.1 Cenozoic stratigraphic units of Himalayan Foreland Basin (from Yin, 2006; Najman, 2006)

<table>
<tr><th></th><th colspan="2">Pakistan</th><th colspan="2">India</th><th>Nepal</th></tr>
<tr><th>Geol Time</th><th>Sulaiman</th><th>Kohat</th><th>Kangra</th><th>Subathu</th><th></th></tr>
<tr><td>L. Pliocene</td><td rowspan="4">Siwalik Gp</td><td rowspan="4">Siwalik Gp</td><td rowspan="4">Siwalik Gp</td><td rowspan="4">Siwalik Gp</td><td rowspan="4">Siwalik Gp</td></tr>
<tr><td>E. Pliocene</td></tr>
<tr><td>L. Miocene</td></tr>
<tr><td>M. Miocene</td></tr>
<tr><td>E. Miocene</td><td>Chitarwata Fm</td><td rowspan="2">Rawalpindi Gp</td><td>Dharamsala Fm</td><td>Kasauli Fm
Dagshai Fm</td><td>Dumre Fm</td></tr>
<tr><td>L. Oligocene</td><td rowspan="3"></td><td rowspan="3"></td><td rowspan="6">Subathu Fm</td><td rowspan="3"></td></tr>
<tr><td>E. Oligocene</td><td rowspan="2"></td></tr>
<tr><td>L. Eocene</td></tr>
<tr><td>M. Eocene</td><td rowspan="2">Kirthar Fm</td><td>Kohat Fm</td><td rowspan="2"></td><td>Bhainskati Fm</td></tr>
<tr><td>E. Eocene</td><td>Mami Khel Fm</td><td></td></tr>
<tr><td>L. Paleocene</td><td>Ghazij Fm</td><td>Ghazij Fm</td><td></td><td>Amile Fm</td></tr>
</table>

On the other hand, the overlying Neogene deposits are termed uniformly "the Siwalik Group" throughout the Himalayan Foreland Basin. The Siwalik Group has been divided into the Lower, Middle and Upper Siwalik sub-groups, broadly recognized as representing mainly mudstone facies, significantly sandstone facies, and sandstone with substantial amount of conglomeratic facies, respectively (Table 9.1), though the first conglomeratic facies are found in the Middle Siwalik sub-group. The foreland basin sequence is mainly located in the Sub Himalaya, however, Palaeogene strata may also occur in the Lesser Himalaya in some regions (specially in Nepal) (Najman, 2006).

9.2 Proposed Depositional Model

The sedimentary succession in the Kamlial, Chinji and Nagri formations of the Kohat Plateau (see sections 5.4 to 5.6) shows multistorey sandstone complex with sheet geometry, and suggest deposition during sheet floods in the braided stream environments (Figs. 9.1-9.3) (Miall, 1978; Rust, 1978a; Gordon and Bridge, 1987; Rust and Jones, 1987). Sedimentological studies of the Siwalik sandstone of the Himalayan Foreland Basin from other sections of the subcontinent also reveal that this complex sandstone was deposited on a fluvial megafan (Kumar, 1993; Kumar and Ghosh, 1994) by a large river system (e.g., Schlunegger et al., 1997, 1998; Horton and DeCelles, 1999), similar to the modern fluvial megafans occurring where modern large Himalayan rivers enter from confined to unconfined areas (Geddes, 1960; Wells and Dorr, 1987; Gohain and Parkash, 1990; Mohindra et al., 1992; Sinha and Friend, 1994; Gupta, S., 1997). Isolated single sandstone bodies between mudstone beds may indicate a single major sheet flood deposit (Gordon and Bridge, 1987).

Siltstone and mudstone units of the studied formations were deposited from suspension, representing slack flood water regime (Figs. 9.1-9.3). The alternate beds of fine sandstone layers and mudstones may probably represent levee deposits in the proximal part of the overbank (Allen, 1965; Elliott, 1974; Kumar and Tandon, 1985). Presence of calcrete concretions and mottling within the mudstone indicates incipient soil formation and limited subaerial exposure of the mudstone facies. Evidences for biological activity including vertical, unlined burrows (skolithos) and surface traces (sinusites) are reported locally from the overbank facies (Kumar et al., 2004).

The vertical stacking of the multistorey sandstone complex with varied facies associations, the sheet geometry, low mudstone content (especially in Nagri Formation), the frequent occurrence of erosional surfaces and palaeoflow consistency (at individual locations) define its deposition in a braided river environment (Miall, 1978; Rust, 1978a; Gordon and Bridge, 1987; Rust and Jones, 1987; Kumar and Nanda, 1989). Vertical stacking of sandstones (multistorey) is the signature of channel bar and channel fill deposits of aggrading low sinuosity streams which migrate laterally across an alluvial plain (Figs. 9.1, 9.3) (Gordon and Bridge, 1987). The base of each storey is marked by a major erosional surface perpendicular to the palaeoflow direction. The large amount of intra-formational breccia in the form of large mudstone blocks along the erosional surface represents cut-bank material due to bank failure, suggesting high current velocity. Lateral and vertical stacking of these sandstone bodies suggests that several channels with high channel density and braided parameter were active during deposition (Rust, 1978b).

According to Gohain and Parkash (1990), multistory channel bodies can form due to climate change, neotectonic activity, differential discharge and sedimentation rates. In present case, it is inferred that the change in fluvial architecture and channel body proportion is due either to uplift of source area, which resulted in an increase in catchment area and high relief, producing more detritus, or altered climatic conditions. In either case, sedimentation patterns suggest a high discharge in large river systems (Kumar et al., 2004).

Channel bars are characteristic of streams of low sinuosity, with steep gradients, variable discharge and abundant sediment supply. They are commonly elongated parallel to the main current direction if the sediment is coarse and poorly sorted, and normal to it if the sediment is finer and better sorted (Figs. 9.1-9.3) (Smith, N. D., 1970). When a channel bar develops in mid-stream, the channel is diverted around it to form two new channels, and by repetition a network of braided channels forms. More commonly, however, braiding seems to be the result of dune migration during floods, followed by dissection during periods of low flow (Mcdonnell, 1974).

The depositional model of the Neogene fluvial system of the Himalayan Foreland Basin can best be represented by a wide channel belt, internally showing a braided morphology of minor channels, wholly enclosed within finer-grained overbank sediments (Figs. 9.1-9.3). Within the surrounding interfluve regions, aggradation was accomplished episodically in response to overbank sheets, channelized splay and flood-derived fines deposition (Smith, N. D. et al., 1989).

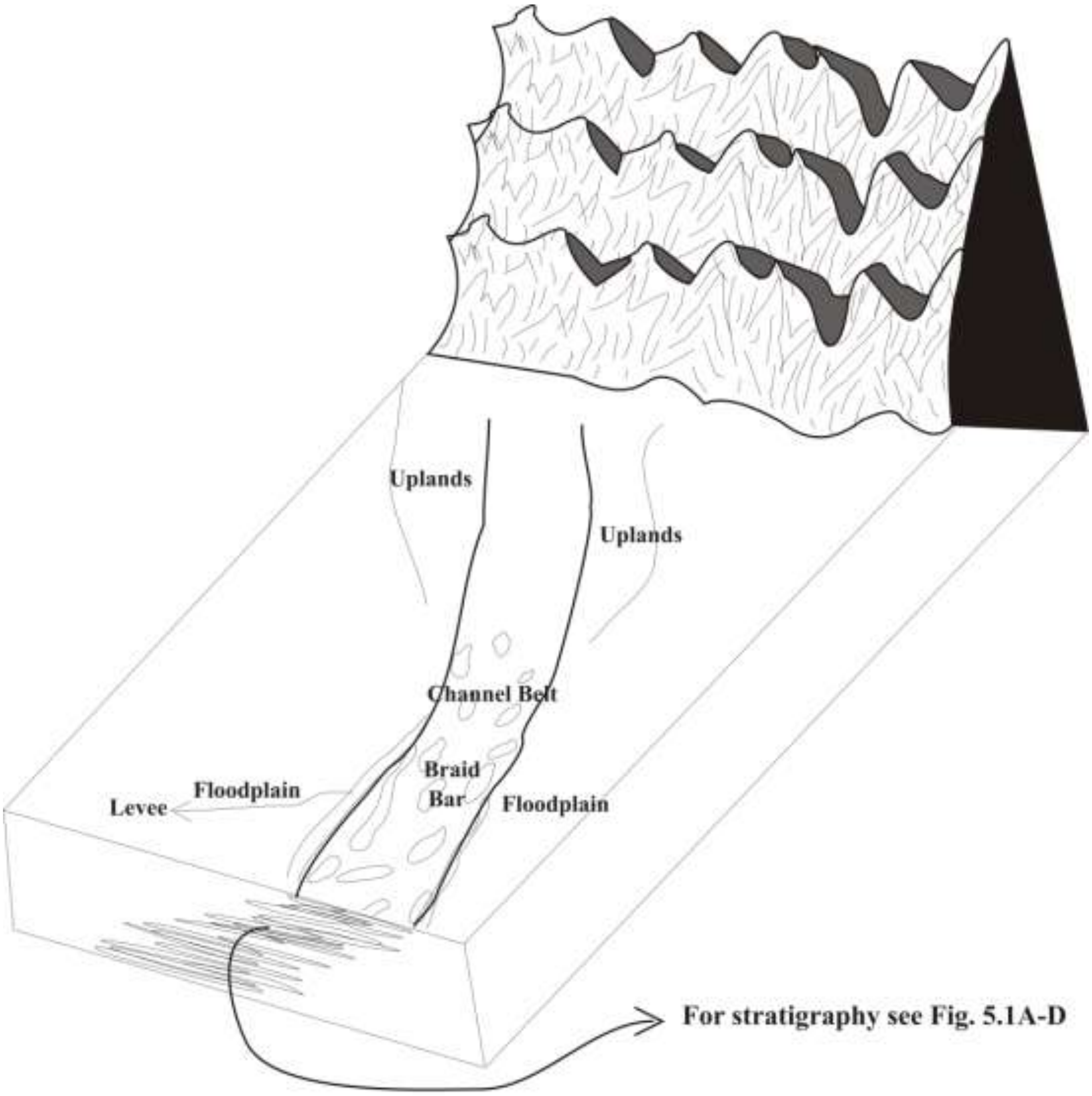

Fig. 9.1. Schematic block diagrams illustrating individual facies associations, their spatial relationship to each other, and depositional models for the Kamlial Formation from southwestern Kohat.

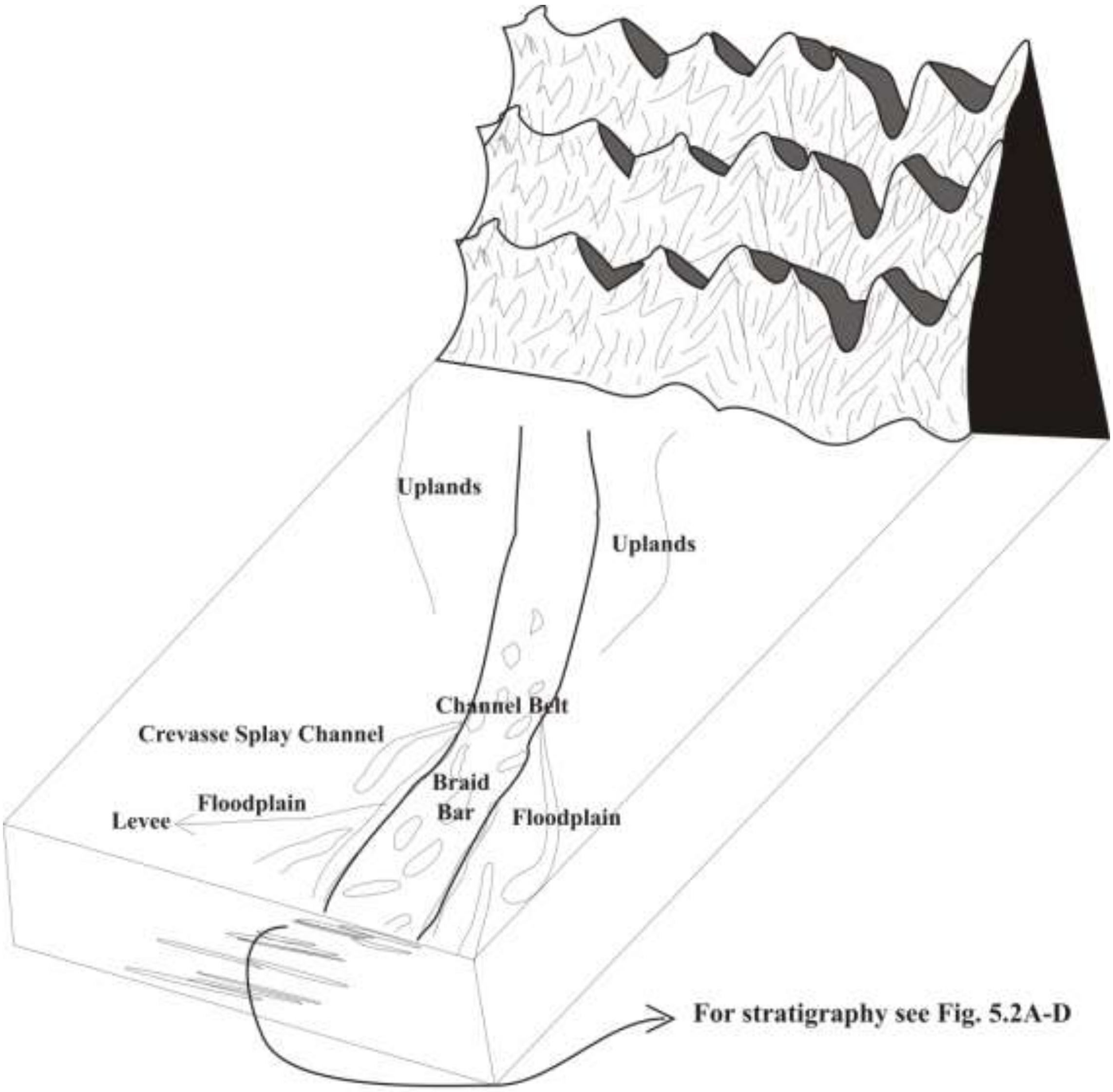

Fig. 9.2. Schematic block diagrams illustrating Chinji Formation, dominantly composed of overbank fine sediments from southwestern Kohat. Deposition of the mud-dominated Chinji Formation was possibly resulted increased tectonic subsidence within the basin.

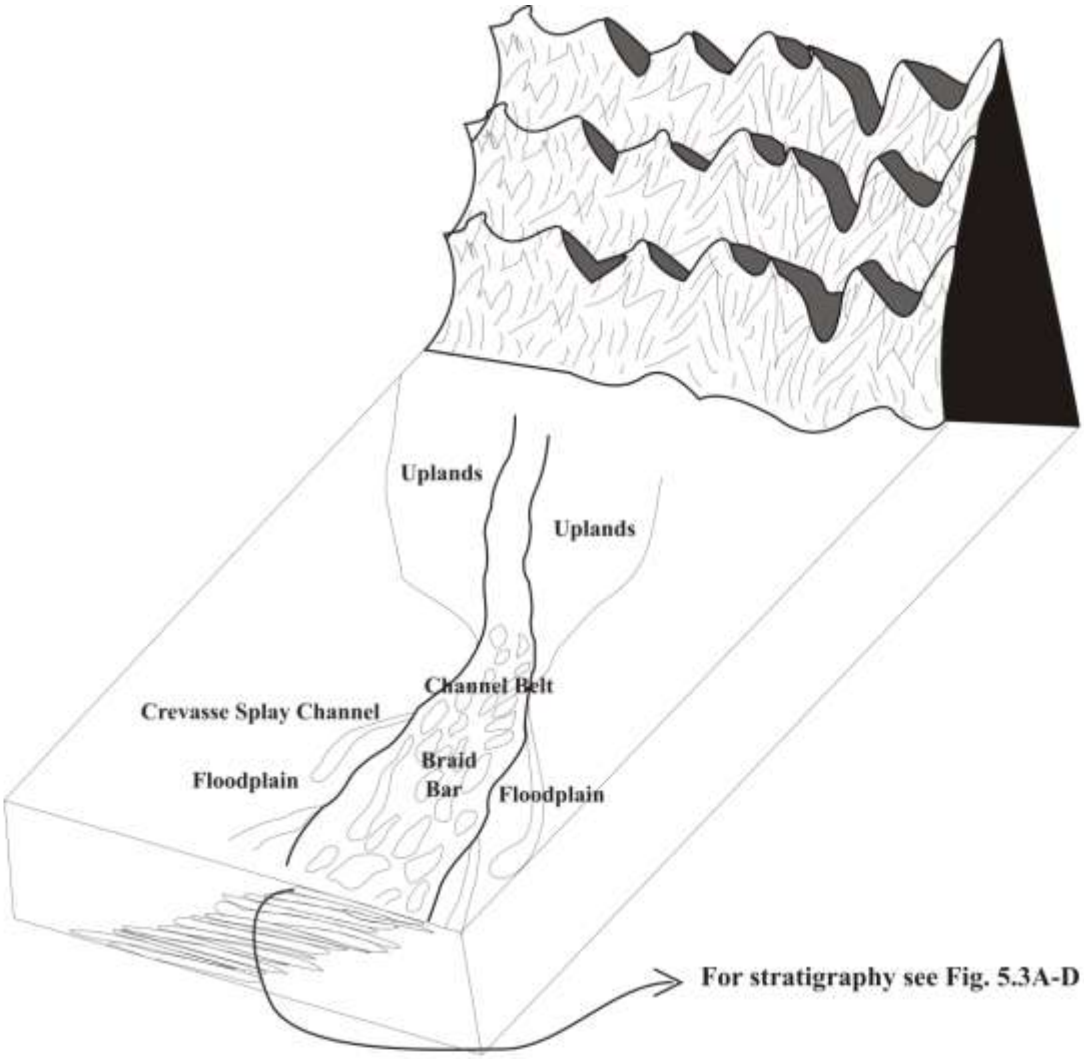

Fig. 9.3. Schematic block diagram of depositional environments and alluvial architectures of the multistorey sandbodies and associated sandstone splays of the Nagri Formation from southwestern Kohat.

The study of Smith, N. D. et al. (1989) also offers a possible explanation of the apparent partitioning and subsequent preservation of fine-grained material out of the braided channels into the interfluve setting. The short lived splay systems of the avulsed South Saskatchewan River rapidly deposited large volumes of fine-grained material across its floodplain (Smith, N. D. et al., 1989). The longer lived splay channels are believed to have shown different hydrodynamic conditions for much of their history, and only the most stable, long lived splay channel evolved to form the new trunk stream after the discrete avulsion event. The Escamilla splay lithofacies associations represent a large volume of the total fluvial sequences preserved, and are interpreted to have been rapidly deposited during episodic avulsion or overbank flooding (Bentham et al., 1993). In rapidly subsiding sedimentary basins, streams of braided character can produce deposits that may have many characteristics of higher sinuosity river deposition. In another braided river model, a channel belt of internally braided character aggrades vertically rather than rapidly expanding laterally through time. The main channel belt changes position within the floodplain by episodic avulsion following a phase of floodplain aggradation. Large volumes of preserved overbank material may well be deposited during these avulsion events (Bentham et al., 1993).

The description of the Donjek River, Canada, by Williams and Rust (1969) shows that the sediments of a braided stream can range from silty clay to pebbles, and that a variety of cross-bedding and ripple structures can be formed whereas fining-upward sequences are attributed to waning current velocities as a channel is gradually infilled.

The minor differences among the studied outcrops could be explained by the presence of short lived sub-parallel fluvial systems flowing across the alluvial plain at the same time. An alternative possibility is that the different sequences were deposited contemporaneously within a single large braided river such as the Brahmaputra where a variety of styles of deposition can be observed within the river at any given moment in time (Bristow, 1987).

The Miocene fluvial deposits of the Siwalik Group are studied in very much detail from the Potwar Plateau (Willis, 1993a; Willis, 1993b; Willis and Behrensmeyer, 1994; Zaleha, 1997a, 1997b; Khan, I. A. et al., 1997). The thick sandstone bodies of the Miocene fluvial system in eastern Potwar are interpreted as deposits of sinuous, braided channels that migrated laterally across an alluvial plain or megafan. Large-scale inclined strata represent deposits of single floods, and their occurrence in sets with basal erosion surfaces represents lateral migration of channel bars and the filling of adjacent channels (Khan, I. A. et al., 1997).

On the other hand, the mudstone-sandstone strata of the Miocene fluvial system in eastern Potwar are interpreted as floodplain (overbank) deposits. The channel-form sandstone bodies are interpreted as deposits of crevasse channels (Khan, I. A. et al., 1997). Pedogenic calcite nodules indicate precipitation of calcium carbonate due to evaporation of groundwater, primarily within the capillary fringe, whereas non-calcareous horizons of paleosols show complete leaching of a calcareous mud (Willis, 1993a; Willis and Behrensmeyer, 1994).

The general decrease in channel-deposit proportion from the Nagri Formation to the Dhok Pathan Formation in the Potwar plateau is interpreted by the changing interaction between two different river systems (Willis, 1993b). However, the lack of a bimodal distribution of major-channel depths and widths in this area does not support an interpretation of two separate and coexisting river systems (Zaleha, 1997a, 1997b). Thus, it is possible that variations in major-channel size in the Nagri and Dhok Pathan formations indicate the degree of activity of different rivers on a single megafan. Furthermore, difference in sediment compositions of different rivers on a single megafan may be related to different sediment sources and/or to different degrees of post-depositional chemical weathering of the deposits (Khan, I. A. et al., 1997).

The low authigenic U contents, and low U/Th, V/Cr, Cu/Zn and Ni/Co ratios (see section 8.12, Table 8.2) in the studied mudstone and sandstone samples of the Neogene sedimentary sequence indicate that these sediments were deposited dominantly in an oxic environment.

9.3 Fluvial Response to Basin Tectonics

Sedimentation in the Kohat area started after the Eocene continent-continent collision (Dewey et al., 1989; Treloar and Coward, 1991) with slow subsidence rate during the deposition of Murree Formation by an ESE flowing fluvial system (Jordan et al., 1988). High degree of interconnectedness of the sandstone bodies and low preservation of overbank fines during the Kamlial Formation times also advocate slow subsidence of the basin. The palaeoflow direction at the time of deposition of Chinji Formation significantly changed because of uplift along the western ranges (Sulaiman

Range) (Abbasi, 1998). Later on, the high uplift rates of the Kohistan Island Arc and adjoining areas such as Nanga Parbat (Zeitler, 1985) increased the subsidence rates and hence sedimentation in the foreland basin (Johnson, N. M. et al., 1985) with abundant sediment supply due to high erosion (Behernsmeyer and Tauxe, 1982; Johnson, N. M. et al., 1985). The Middle Siwalik conglomerates in the Kohat area were deposited by a large river, probably analogous to the present day Indus River (PaleoIndus) flowing to the SSW. The Upper Siwalik conglomerates of the Soan Formation in Potwar area were deposited by a tributary system draining the Sub-Himalaya (Abbasi and Friend, 1989).

In case of present study, the formation-scale variations of the Neogene molasse sequence clearly record different river systems within the Miocene Indo-Gangetic foreland basin. Models which attempt to evaluate the response of alluvial deposition to tectonism generally correlate changes in grain sizes, sediment accumulation rates, slopes and facies migrations with periods of tectonic uplift and quiescence (stability). Formation level changes in the Siwalik Group were caused by tectonism, increase in channel size and bankfull discharge, with mean channel bed slopes remaining generally constant (Willis, 1993b). The Chinji-Nagri transition seems to represent the establishment of a larger river system in the area (Willis, 1993b). Two likely explanations for this change are discussed below.

a) The development of deformational structures at frontal thrust zones, such as faults and antiforms can cause significant river diversion (DeCelles, 1988; Gupta, S., 1993). Such structures were present in the Miocene Himalaya (Coward et al., 1987; Treloar et al., 1991a, 1991b, 1992) and may have developed in association with increased uplift rates. A variety of independent geological data indicate that this uplift varied in space as well as in time and appears to have been greater in regions of the mountain belt to the north-east of the study area compared to those in its north and west (Burbank, 1983; Klootwijk et al., 1985; Zeitler, 1985; Zeitler et al., 1989; Treloar et al., 1989b, 1991a, 1991b; Scharer et al., 1990).

b) Differential uplift could have caused river piracy within the mountain belt thereby increasing the discharge of rivers flowing into the foreland.

In either case, the result would be an increases in channel size and bankfull discharge, increase in sediment accumulation rates (and presumably subsidence rates), and increase in grain size without necessarily causing a change in the direction or magnitude of channel bed slopes. The amount of blue-green hornblende in thick sandstones dramatically increases across the Chinji-Nagri boundary in the western and central Potwar Plateau, but this trend is absent from the eastern Potwar Plateau (Johnson, N. M. et al., 1985; Cerveny et al., 1989). This mineralogical change may be a manifestation of river diversion within the mountain belt.

The upward transition from sandstone- and mudstone-dominant facies (Kamlial and Chinji formations, respectively) to sandstone facies (Nagri Formation) of the Neogene molasse sequence of Kohat suggests a systematic shift from distal to proximal fluvial deposits. Vertical and lateral stacking of the multistorey sandstone bodies in relation to overbank deposits indicate periodic avulsion of the channel belt (Allen, 1965, 1978; Bridge and Leeder, 1979), which suggest an increase in the drainage network in the source area (Kumar et al., 2004). An increase in drainage areas and high relief thus supplied more sediments than small catchment areas having low relief (Pinet and Souridu, 1988). In the Himalayan Foreland Basin, the basin-ward progradation of coarser facies is correlated with either thrusting and/or uplift of the orogenic belt (Burbank and Raynolds, 1988) or a higher rate of sedimentation than of subsidence in the basin (Blair and Bilodeau, 1988; Heller et al., 1988). Similarly, sedimentary basins that occur nearby high relief of active orogenic belts receive large volume of sediment, e.g., rivers draining the orogenic belts of southern Asia supply more than 70% of the sediment load entering the oceans (Milliman and Meade, 1983).

On regional scale, deposition in foreland basins is widely controlled by flexural subsidence resulting from tectonics and sub-lithospheric static and dynamic loading (Beaumont, 1981; Catuneanu et al., 1997, 2000). Tectonic loading is frequently considered to be followed by tectonic unloading resulting from release of lithospheric forces and/or erosion (e.g. Heller et al., 1988; Blair and Bilodeau, 1988; Burbank, 1992; Catuneanu et al., 1997, 2000), which implies that loading/unloading cycles are related to major tectonic events. Catuneanu et al. (1997, 2000) have described a succession of basin-scale loading/unloading cycles controlling second and third order sedimentary sequences with time spans of ~20-25 and 0.4-3 Ma, respectively. In a tectonic loading cycle, the foreland basin system is similar to that of the DeCelles and Giles model (1996) and consists of the four depozones i.e., the wedgetop depozone, the foredeep depozone, the forebulge depozone and the backbulge depozone. The forebulge is thought to be raised and eroded (Jordan, 1995). In a tectonic unloading cycle, the foreland basin system is made up of two depozones (the foresag and the foreslope depozones divided by the flexural hinge line) (Catuneanu et al., 1997). In the unloading stage, the forebulge is missing. Dating the timing of the forebulge uplift indicates the passage from tectonic unloading to tectonic loading. In case of the Himalayan Foreland Basin, the Sargodha High is a basement structure which likely represents the forebulge of the Miocene Ganges basin. Its trend is generally parallel to the trend of the modern Ganges basin. Thickness of the Siwalik rocks dramatically decreases toward this forebulge, but do pass over it. Extensive age-equivalent deposits in both the Indus and Bengal submarine fans and in the Indus and Ganges-Brahmaputra deltas indicate that deposition kept pace with or exceeded subsidence (Kazmi, 1984; Stow et al., 1990; Lindsay, J. F. et al., 1991; Weedon and McCave, 1991).

The drainage pattern of a foreland basin may be indicative of erosionally or tectonically driven uplift of an orogen. According to Burbank (1992), uplift due to active thrusting along the thrust front leads to asymmetric subsidence in the foreland (wedge-shaped basin-fill) whereas erosional unloading leads to regional uplift and hence to a more tabular geometry of the basin-fill. Consequently, a wedge-shaped versus a tabular geometry of the sedimentary strata are indicative of tectonics or erosional uplifts, respectively (e.g. Heller et al., 1988; Jordan and Flemings, 1991, and many others). In the Ganga Plain foreland basin, the sediment fill is asymmetrical, few tens of meters thick in the south and upto 5 km thick in the northernmost part (Agarwal et al., 2002), and thus suggests tectonically induced uplift in the Himalayan orogen. The Neogene molasse strata of the Himalayan Foreland Basin is also asymmetrical, thick in the hinterland and thin in the distal regions, indicating thrust induced uplift in the source area.

Fluvial depositional systems are also sensitive to changes in basin accommodation. The preservation potential of floodplain deposits relative to that of channel-fill sediments depends in large part on variations in this parameter. Where accommodation generation is static or slow, channel systems meander or avulse back and forth across the valley floor through their own deposits, incising laterally into the floodplain and replacing it with the channel fills, which typically consists of sand or gravel. The results may be stacked and laterally-amalgamated channel-fill deposits with few fine-grained intervals. Where accommodation generation is rapid, lateral channel migration is accompanied by stratigraphic climb and, if there is a lengthy return period between successive reoccupations of a given position on the valley floor, significant thicknesses of floodplain deposits may have had time to accumulate (Miall, 2000). The Neogene stratigraphy of the Himalayan Foreland Basin generally indicates rapid accommodation generation during deposition of Kamlial, Chinji and Nagri formations. The Neogene history of the Bengal fan or Indus cone is indicative of persistently overfilled Himalayan Foreland Basin. The overfilled foreland basin suggests that the rate of sediment delivery from the source always exceeded the rate of accommodation of the sediments within the basin (Brozovic and Burbank, 2000).

9.4 Palaeoclimate of the Source Area

The CIA values of mudstone samples of the Neogene sedimentary sequence (see section 8.7, Table 8.5) ranging from 70 to 80 and averaging 75.7 suggest relatively intense weathering at the source area. However, the presence of abundant sedimentary rock fragments in associated sandstones reveals that the high CIA values may probably be due to the presence of recycled sediments rather than a result of severe weathering (Lee, Y. I. 2002). Alike, the ICV values of the mudstone of the Neogene sequence (see section 8.8, Table 8.5) are generally greater than 0.7 indicating relatively moderate weathering in the source area. The limited amount of clay fraction and high contents of quartz and feldspar in mudstones of Neogene sedimentary sequence also indicate limited chemical weathering in the source area. The presence of feldspar in the associated sandstones also supports this interpretation (Yu et al., 1997; Lee, Y. I. and Sheen, 1998). Whereas the dominance of CIA values between 64 to 76 (see section 8.7, Table 8.1) and occurrence of appreciable amount of feldspar and presence of unstable lithic fragments in sandstone also favor moderate weathering in the source areas. Furthermore, the possibility of intensive chemical weathering in the Himalayas orogenic belt is highly unlikely, as intense weathering requires tectonic quiescence for a long period, higher temperature and humidity (Kronberg and Nesbitt, 1981; Lasaga et al., 1994).

The consistent presence of illite in all of the studied mudstone samples from the present study (Appendix A) seems to be the result of chemical weathering of feldspars and micas (Prothero and Schwab, 2003), which indicate humid temperate climate (Einsele, 1992). Kaolinite occurs in most of the studied mudstone samples from the southwestern Kohat Plateau (Appendix A). It results from intense chemical weathering of feldspars and micas in warm and humid climates (Chamley, 1989). Its presence in sedimentary rocks generally indicates the climate of the drainage area rather than the mineralogical composition of the source rocks (Einsele, 1992), though it may be the product of erosion of feldspar-rich granitic rocks. The overall difference in contents of illite and kaolinite in the Neogene sedimentary sequence indicated either variation in the degree of glaciation in the surrounding areas or source areas of different climatic conditions (Kuhlmann et al., 2004).

Absence of chlorite from the studied mudstone samples under discussion indicates absence of slates and schists in the source area, or else it was destroyed during transportation and deposition. However, petrographic studies of the associated sandstone indicate the presence of slates and schists in the source area. Thus, absence of chlorite may either show warm and humid climates (as it is very sensitive to chemical weathering) (Einsele, 1992), or its destruction during low-grade diagenesis.

The presence of labile volcanic and metamorphic lithic fragments in the western regions of the Himalayan Foreland Basin indicates that petrography has not been drastically affected by weathering or diagenesis (Najman and Garzanti, 2000; Najman et al., 2003a). However, alteration of some unstable grains and extensive carbonate replacement has been observed. The low proportion of dense minerals suggests intrastratal solution of unstable mafic material, whilst the high proportions of ultrastables in some sandstone points towards sediment recycling. In contrast, the diagenetic imprint seems to be greater in the sediments deposited further east i.e. in the foreland basin of Nepal and in the Bengal Basin (Najman, 2006).

Ample evidence exists indicating that the climate in northern Pakistan was warm, humid, subtropical to tropical, and influenced by monsoonal circulation throughout the time interval studied (Sahni and Mitra, 1980; Awasthi, 1982; Vishnu-Mittre, 1984; West, 1984; Wright and Thunell, 1988; Ruddiman et al., 1989; Quade and Cerling, 1995). These conditions apparently operated on a regional scale, extending at least as far west as the Arabian Peninsula (Wright and Thunell, 1988; Adams et al., 1990; Hadley et al., 1992), and as far east as south-east Asia (Xianzeng, 1984; Zhichen et al., 1984).

Throughout the Siwalik section in northern Pakistan, independent palaeoenvironmental reconstructions indicate marked seasonality in paleosol formation, discharge variations of individual rivers and the existence of short-lived lakes (Willis, 1993a; Zaleha, 1997a). The gleysols of Ramnagar, Jammu (Ganjoo and Shaker, 2007) and the Khakistari paleosol series of Pakistan of Lower Siwalik (Retallack, 1991) suggest seasonal waterlogging. The hydromorphic paleosols of Lower Siwalik of Ramnagar suggest wet and humid climate, indicative of the beginning of a monsoonal system in Asia caused by uplift of the Tibetan Plateau/Himalaya (Ganjoo and Shaker, 2007). Sedimentary and petrographic evidences indicate an increase in precipitation in the Himalayan region at 10.5 Ma due to major uplift (Zaleha, 1997a, 1997b; Kumar et al., 2003).

It is generally accepted that the Tibetan-Himalayan uplift between 12 and 9 Ma (Amano and Taira, 1992) has led to the intensification of the monsoon system in South Asia (Ruddiman and Kutzbach, 1989; Raymo and Ruddiman, 1992). Based on their "abrupt uplift model", Prell and Kutzbach, (1992) suggested that rapid uplift began at around 10 Ma. After approximately the present elevation (5 km) was attained at about 5 Ma, further uplift ceased. Prell and Kutzbach (1992) also suggested that monsoons as strong as today might have started around at 7-8 Ma, when the elevation was half (2.5 km) of the present one. Evidence in support of this hypothesis comes from both continental and oceanic records. Burbank et al. (1996) also showed that almost all the Siwalik sections recorded acceleration in sedimentation and increase in subsidence rate at around 11 Ma. This shift in sediment flux was probably due to the combined action of intensified monsoonal precipitation and tectonic activity (Sanyal et al., 2004).

Within the resolution of present palaeoclimatic indicators, there is no direct evidence that climatic change within the basin affected deposition. However, this does not preclude a climatic change within the mountain belt, which could have influenced sediment accumulation rates, mean channel grain sizes, river discharges, and/or the number of rivers. The available palaeoclimatic data from the mountain belt though sparse, appear to indicate consistent climatic conditions during the Miocene time (Mathur, Y. K., 1984; Vishnu- Mittre, 1984; West, 1984).

The Nepal Siwalik Group is well studied in the Arung Khola-Tinau Khola area. Komomatsu (1997) identified the inception of moist deciduous monsoonal forest at around 7.5 Ma, and Tanaka (1997) found that C_3 plants changed to C_4 plants at 10.0 Ma. Generally, C_3 plants are trees, shrubs and grasses favoring a cool growth season, while C_4 plants are shrubs and grasses favoring a warm growth season. C_3 and C_4 plants thus indicate semi-deciduous forests and grasslands, respectively. In the Hetauda-Bakiya Khola area, Harrison et al. (1993) identified the change from C_3 plants to C_4 plants at 7.0 to 7.4 Ma. Quade et al. (1995) measured stable isotopes in the Surai Khola area, and concluded that C_3 to C_4 transition occurred at 7.0 Ma in Nepal and northern Pakistan.

Hisatomi and Tanaka (1994) performed facies analysis on the middle to lower part of the Siwalik Group and noted that sediment accumulation began in meandering rivers, changed to meandering rivers of a dominant sheet-splay type at 10.0 Ma, and became braided at 7.5 Ma. Five evolutionary stages of fluvial system in the Arung Khola-Tinau Khola area have been identified: the onset of stage 1 is placed at about 15 Ma, stage 2 (flood flow domination) begins at 10.0 Ma, stage 3 (sandy braided system) at 7.5 Ma, stage 4 (gravelly braided system) from 2.5 Ma, and stage 5 (debris flow domination) from about 1 Ma (Nakayama and Ulak, 1999). Frequent flooding began in the Siwalik foreland at 10.5 to 9.5 Ma, suggesting that the Himalaya uplift was sufficient to cause seasonal precipitation by this time. Based on the evidence from stable isotope studies and plant fossils, monsoon climate was fully established by about 7.0 Ma. However, differences in onset of the individual stages occur among different areas. For example, the onset timing of stage 2 (flood flow domination) ranges from 10.5 to 9.5 Ma; and the sandy braided system of stage 3 shows the largest time difference in onset, between 9.0 and 6.5 Ma (Nakayama and Ulak, 1999).

9.5 Comparison with the Modern Indus Fluvial Basin

The lithofacies of the Kamlial, Chinji and Nagri formations are thought to represent deposits of either the paleo-Indus river or a similar axial fluvial system (Johnson, N. M. et al., 1982; Najman et al., 2003a, b). The multistoreyed channel type sandstone-bodies of the Chinji Formation in southeastern Kohat suggest a consistent flow direction to the SSE (Abbasi, 1998). The sedimentary structures in the overlying Nagri Formation suggest a dominant paleoflow direction to the SSW (Abbasi, 1998). The river system that entered the Kohat area, changed from sandy to silty at the transition from Kamlial to Chinji formations (Abbasi, 1998). Alike, there are broad similarities between channel geometries, discharges and sedimentary characters of Siwalik rivers and modern Indus river system. These include emergence from a mountain belt, generally parallel flow to the basin axis, slopes range from 0.000085 to 0.00018, and bankfull discharges in the order of 10^2-$10^3 m^3 s^{-1}$ (Mackey and Bridge, 1995).

The Miocene Indo-Gangetic foreland seems to be a composite of two distinct basins that are parallel to the Himalayan mountain belt (Zaleha, 1997b). The ancient Ganges and Indus basins were ~ 2000 km and 1000 km long, respectively. Basin widths were ~ 200-300 km along most of their lengths but may have varied from 100-500 km

(Zaleha, 1997b). Broad similarities between the Siwalik rivers and modern fluvial system of the Indo-Gangetic basin are also noteworthy (Zaleha, 1997b). For example, river systems of modern Indo-Gangetic basin are relatively large, mainly braided rivers (e.g., the Indus, Jhelum, Chenab, Yamuna, Ganges) and are spaced on the alluvial plain at intervals of ~60-200 km (Zaleha, 1997b). These rivers merge 300-600 km downstream from the mountain front, being generally oriented transverse to the basin axis near the mountain front but becoming generally parallel to the basin axis.

Similarly, the large volumes of Siwalik-age-equivalent sediments in the Indus and Bengal submarine fans and in the Indus and Ganges-Brahmaputra deltas (Kazmi, 1984; Stow et al., 1990; Lindsay, J. F. et al., 1991; Weedon and McCave, 1991) indicate the coeval existence of significant drainage systems in both the Indus and Ganges Miocene forelands. Dominantly south to south-west palaeocurrents in Siwalik rocks in the Trans-Indus area (Cerveny et al., 1989) further support the existence of an active drainage system there which flowed toward the Indus submarine fan during that time.

9.6 Source Area Tectonic Settings for the Kamlial, Chinji and Nagri Formations

Modal point count data of the Kamlial, Chinji and Nagri formations presented in chapter 6 indicate both dissected magmatic arc and recycled orogen on Q-F-L plots (see sections 6.9-6.11, Figs. 6.5, 6.8, 6.11). Dissected magmatic arc orogen shows extensive cogenetic plutons of magmatic arc exposed as a result of erosional unroofing. A dominant magmatic arc provenance for these formations is also suggested from the Qm-F-Lt plots (see sections 6.9-6.11, Figs. 6.6, 6.9, 6.12). Qp-Lvm-Lsm plot shows magmatic arc as well as magmatic arc and subduction complex provenance for the studied three formations (see sections 6.9-6.11, Figs. 6.7, 6.10, 6.13). Furthermore, the negligible amount of smectite in mudstone of the Neogene sedimentary sequence of the southwestern Kohat Plateau suggests limited exposures of volcanic rocks (dissected magmatic arc) in the source area. Different geochemical plots determined based on whole rock geochemistry of sandstone (presented in chapter 8) indicate active continental margin and continental island arc provenance for the Kamlial, Chinji and Nagri formations (see section 8.6, Figs. 8.4-8.6). The Fe_2O_3+MgO vs TiO_2, Fe_2O_3+MgO vs K_2O/Na_2O and Fe_2O_3+MgO vs Al_2O_3/SiO_2 discriminatory plots suggest continental island arc and active continental margin provenances for the Neogene sandstone of the Kohat. Discriminatory plot SiO_2 vs log (K_2O/Na_2O) indicate a dominant influx from active continental margin for the studied sandstone with minor contribution from PM for the

Kamlial Formation and oceanic island arc for the Chinji and Nagri formations. Alike, the geochemical parameters like Fe_2O_3+MgO, TiO_2 and Al_2O_3/SiO_2 of the Neogene molasse sandstone show major provenance from continental island arc and partial influx from active continental margin settings. The contents of the major element oxides except MnO of the sandstone of the studied sequences also indicate a dominant continental island arc provenance. The content of MnO of these sandstones suggests a source region composed dominantly of oceanic island arc. K_2O/NaO_2 ratio does not signify a particular provenance to these sediments.

In summary, three major tectonic orogens are identified for the said formations based on petrographic and geochemical data:

a) Recycled orogen i.e. the Himalayan Tectonic Units

b) Active continental margin orogen i.e. the Trans-Himalaya and Karakoram

c) Magmatic arc orogen i.e. Kohistan and Ladakh Arc

9.6.1 Sediment Influx from Himalayan Tectonic Units

In Pakistan, the major change from sedimentary to metamorphic provenance occurs between the Eocene marine rocks and the Oligo-Miocene Murree rocks (underlying the Kamlial Formation) (Table 3.1), which marks the first substantial input from the rising Himalayan thrust belt (Critelli and Garzanti, 1994). Detrital minerals with ages <55 Ma indicate erosion from sources affected by the Himalayan metamorphism (Najman, 2006). The dominance of low grade metapelites with significant but subordinate igneous and sedimentary lithic inputs in Balakot Formation of Hazara-Kashmir syntaxis, equivalent to the Murree Formation of the Kohat-Potwar Plateau is interpreted to have been derived from the Indian Plate, Kohistan Arc and suture zone ophiolites (Bossart and Ottiger, 1989; Critelli and Garzanti, 1994). Critelli and Garzanti (1994) described the source of the low-grade metamorphic Indian Plate material as the “proto High Himalaya”. The higher average uplift rate to the south of MMT (0.39 mm/yr) than the average uplift rate to the north of MMT (0.20 mm/yr) during Murree time also supports the same source of origin (Zeitler et al., 1982; Zeitler, 1985). The absence of high grade metamorphic rock fragments implies that the Murree strata do not represent the metamorphosed rocks in the south and that the uplift within the Himalaya was insufficient to expose abundant high grade rocks to erosion (Treloar et al., 1989b; Spencer, 1993).

The petrography of the Balakot Formation shows that the Kohistan Island Arc obducted onto the Indian plate along the MMT and became an area of positive topographic relief thereby exposing it to significant amounts of erosion by the time of deposition of the Balakot Formation after 37 Ma (Najman et al., 2001, 2002). Tectonic exhumation may have been achieved by extensional movement on the MMT (Najman et al., 2002). The mix of Himalayan aged and pre-Himalayan aged detrital micas in the Balakot Formation suggests that exhumation of both basement and cover rocks to the surface occurred early in the thrusting event (Najman et al., 2002). Rivers draining to the foreland basin had catchment areas predominantly within the Himalayan thrust stack during Early Miocene (circa 18 Ma). Correspondingly, the highest proportion of detritus was derived from the Indian crust Himalayan thrust belt (Najman et al., 2003a).

Study of the history of the Himalayan erosion and deposition suggests that the Paleogene Himalayan Foreland Basin received sediments mainly from southern Tibet, the Indus-Tsangpo suture zone, and the supracrustal sections of the ultra-high pressure gneiss terrains in the western Himalaya and possibly the eastern Himalayan syntaxis. In the early Miocene, the foreland basin received sediments from the Tethyan Himalayan cover sequence and metamorphic clasts from the ultra high pressure gneiss terrains in the western Himalaya. The high-grade Greater Himalayan Complex (GHC) became a source of sediments after 11-5 Ma when it got exposed and hence high-grade metamorphic clasts started appearing in the Siwalik Group of the Himalayan Foreland Basin (DeCelles et al., 1998b; Sakai et al., 1999; White et al., 2001). The time of exposure of the GHC at the Earth’s surface is indicated after 10-4 Ma by apatite fission track ages and from ~21 to 17 Ma by the widespread early Miocene leucogranites (e.g., Scaillet et al., 1990, 1995; Murphy and Harrison, 1999; Guillot et al., 1999; Searle et al., 1999; De`zes et al., 1999).

The formation of the Murree Foreland Basin is associated with the initiation of the MMT in latest Paleocene, resulting in the obduction of the Kohistan Island Arc onto the northern margin of the Indian Plate (Tahirkheli et al., 1979), and flexing down of the northwestern Indian lithosphere (Bossart and Ottiger; 1989). Kohat and some parts of the Potwar province uplifted and became nondepositional areas during Middle to Late Eocene, but in the beginning of the Miocene, deposition of the Murree rocks started in this region (Bossart and Ottiger, 1989). The Middle Siwalik (≈ 8.7 Ma) conglomerate with dominantly metamorphic and plutonic clasts at Jawalamukhi in Himachal Pradesh provides an evidence for the late Miocene uplift of the Main Boundary Thrust (Meigs et al., 1995).

The late Neogene deposition in northern Pakistan can be subdivided into two intervals. Prior to about 6.4 Ma, the medial foreland was undeformed, however, the Salt Range experienced its initial deformation, and the nearby river systems were affected between 6.4 and 4.5 Ma (Burbank and Beck, 1989; Mulder and Burbank, 1993). The sandstone that supplanted the white color were produced by a local, northeastwardly flowing river system that carried distinctive clasts of Talchir Granites, derived from Paleozoic strata exposed in the Salt Range. Alike, the probable increase in the abundance of Eocene limestone clasts and their angularity in the Siwalik sections (Burbank and Beck, 1989) more proximal to the Salt Range also support this idea (Mulder, 1991).

Sandstones with abundant quartz and common sedimentary to metamorphic lithics with only minimal evidence of volcanic detritus suggest a recycled orogen for the Kamlial Formation from the eastern Kohat Plateau. However, the Q-F-L plot of Dickinson (1985) places the Kamlial Formation of the Potwar Plateau (Fig. 3.1) dominantly in the field of magmatic arc signature (Najman et al., 2003a), which is significantly different from the Kamlial Formation of the eastern Kohat Plateau (Fig. 3.1) in the west (Abbasi and Friend, 1989). The relative scarcity of arc material and the absence of distinctive blue-green hornblende in the eastern Kohat Plateau indicate that the paleo-Indus River first cut through the arc after deposition of the Kamlial Formation (circa 11 Ma) (Abbasi and Friend, 1989). These along strike variations suggest a regionally extensive tectonic unit providing an apron of sediment to the basin rather than a single point source (Najman et al., 2003a). Furthermore, the appearance of sediment derived from a particular source rock does not necessarily imply early exposure (Copeland, 1993). Rather, it may also indicate the evolving catchment areas of different river systems (Parkash et al., 1980; Willis, 1993b).

The obvious sources for the dominant igneous component in Kamlial Formation of Potwar Plateau are the Kohistan arc and Indus suture zone/MMT. Appropriate sources for the subsidiary sedimentary and very low to medium grade metasedimentary detritus can be found both north and south of the arc, in the Karakoram and Himalayan thrust belts (Najman et al., 2003a). Mica grains of pre-Himalayan age may have been sourced from lithologic units south of the MMT including Cambrian-Ordovician and Permo-Carboniferous igneous and metamorphic rocks. The Himalayan-aged micas (youngest grain aged 14 Ma) on the other hand, may have been eroded from the Indian crust thrust stack and the Kohistan Arc. The rather rarely occurring zero lag time detrital mica in the Kamlial Formation may have been eroded from the rapidly exhumed Nanga Parbat Haramosh Massif (Najman et al., 2003a).

The observed provenance and sedimentological changes at the Murree-Kamlial Formation boundary at Chinji village (Potwar Plateau) have led Najman et al. (2003b) to propose a major change in palaeodrainage i.e., the first routing of the paleo-Indus through the arc to the foreland basin at 18 Ma. The drastic temporal change of the Kamlial Formation from eastern Kohat and Potwar plateaus in terms of hornblende content may be due to diversion of a river that was already carrying hornblende to the Chinji area of Potwar region (Najman et al., 2003b). Possible river diversion, and concurrent increased palaeodischarge, and sediment accumulation rates at 11 Ma, suggest active tectonic deformation due to a significant new thrust load shifting towards the foreland (Willis, 1993a, b; Burbank et al., 1996).

On the other hand, the Siwalik Group rocks from eastern Kohat and Potwar predominantly plot in the recycled orogen, which suggest major influx from medium to high grade metamorphic, with only a subordinate contribution from sedimentary, arc and ophiolites lithologies (Abbasi and Friend, 1989; Critelli and Ingersoll, 1994; Garzanti et al., 1996; Pivnik and Wells, 1996). A comparison of the Th/U and Rb/Sr ratios of the Neogene molasse sequence of the Kohat Plateau with the corresponding average values for the UCC and PAAS argue against sedimentary recycling for these sedimentary deposits (see section 8.10, Tables 8.1, 8.2, 8.5, 8.6) (McLennan et al., 1993). Likewise, the Zr/Sc ratios of the Neogene mudstone and sandstone are similar to or lower than those of the UCC and PAAS indicating that a recycled sedimentary source was a minor component (see section 8.10, Tables 8.1, 8.2, 8.5, 8.6) (Roddaz et al., 2005).

The change in the heavy mineral assemblage, according to Cerveny et al. (1989) and Willis (1993b) was a clear evidence for influx from the blue-schist to amphibolite grade rocks of the Kohistan arc terrain. However, ZFT ages younger than 12 Ma have not yet been obtained from this terrain, and are reported only from the bedrocks of northern Pakistan in the region of the NPHM (Ruiz and Diane, 2006).

The bulk of the Himalayan material now contributing to the Indus River is delivered by the four large rivers of the Punjab (the Sutlej, Ravi, Chennab and Jhelum rivers; Fig. 4.1). Although erosion of the Nanga Parbat massif contributes material of very negative ε_{Nd} values (-22 to -30) (Walker, C. B. et al., 2001), the Indus River immediately downstream of Nanga Parbat has an ε_{Nd} value of around -11, which is far short of the -15 seen at the delta or even in the Pleistocene fan sediments (Clift et al., 2001a, 2002b). The only way to shift the net Indus sediment budget from the pre-5 Ma levels to those seen today is to increase the relative discharge from the Himalayas. This implies that input from the rivers of Punjab before 5 Ma must have been largely non-existent. But it is not true, as reconstruction of the exhumation histories for the western Greater Himalayas shows that these mountains were in existence before 20 Ma ago (Searle, 1996; Walker, C. B. et al., 2001) and foreland sediments demonstrate that these ranges were being rapidly eroded during the Early to Mid-Miocene (Burbank et al., 1996; Najman et al., 2003a). Nonetheless, this erosion does not seem to have been communicated to the Arabian Sea until after 5 Ma ago. The suggested simple explanation for this pattern is as that the ancestral rivers of Punjab were connected to the Ganges and not to the Indus drainage. Support for this model comes from the palaeocurrent measurements by Burbank et al. (1996), which suggest eastward flow during much of the Miocene time in the foreland basin of northeast Pakistan, now occupied by the tributaries of the rivers of Punjab. Data from this study also show that input of sediments from the major tributaries draining the Himalayan litho-tectonic units was negligible at the present-day Kohat region, as is the case with the Modern Indus River system.

Similarly, there is a sharp contrast in composition of the Modern Indus sands upstream and downstream of Tarbela Lake. Indus sand composition from Tarbela Lake indicates strong influx of sediments from active continental margin (81±2 %) followed by 19±2 % from Himalayan tectonic units (Garzanti et al., 2005). Whereas the total Indus budget downstream of Tarbela Lake suggests a bulk bedload contribution of 47±2% from active-margin units (27±3% from Karakoram, 10±3% from Hindu Kush, 3±2% from the Ladakh Arc and South Tibet, and 7±2% from the Kohistan Arc) and 53±2% from Himalayan passive margin units (including 39±4% from Punjab tributaries and 6±3% from Nanga Parbat) to the overall Indus flux (Garzanti et al., 2005).

Paleocurrent data of the Kamlial Formation of the Potwar Plateau demonstrate predominant flow toward the east, east-southeast and southeast (Stix, 1982; Johnson, N. M. et al., 1985) which is different from the more southward-directed paleocurrents further west in the Kohat Plateau (Fig. 4.1) (Abbasi and Friend, 1989). These southeast-directed orientations have been interpreted as indicative of either (1) local slopes on large alluvial fans, not necessarily representative of the main direction of regional flow (Willis, 1993a, b) or (2) axial drainage in the Potwar Plateau region, flowing east toward the Ganges River catchment at these times and afterwards (Raynolds, 1981; Beck and Burbank, 1990; Burbank et al., 1996).

According to the most acceptable evolutionary model for Himalaya, the convergence initiated along the Indus-Tsangpo Suture, followed by the MCT and MBT, while as the convergence shifted to the newly formed younger tectonic structure, the older fault systems became inactive (LeFort, 1975; Sto¨cklin, 1980). This model states that MCT is dormant and MBT is now active, however, according to Validya (2003), the deformation has shifted to the HFT which marks the southernmost limit of the Himalayan orogenic belt. On the other hand, the steady-state model suggests a gradual shift of the deformational front from the hinterland towards south, but indicates that the MBT and MCT are contemporaneous features that are still active (Seeber and Armbruster, 1979; Seeber et al., 1981). This view is supported by several other geological and geomorphological evidences that indicate ongoing tectonic activity along the MCT (Valdiya, 1980; Seeber and Gornitz, 1983) and MBT (Nakata, 1989; Valdiya, 1992; Malik and Nakata, 2003).

Movement involving ductile shearing along the MCT was initiated circa 23 Ma and terminated at circa 16 Ma in Eastern Nepal (Searle et al., 2003). Reactivation of MCT at < 10 Ma, based on Pliocene monazite ages from the footwall of the MCT (Harrison et al., 1997) is interpreted as progressive metamorphism in response to the insertion of thrust sheets within the Lesser Himalaya duplex by Robinson et al. (2003). However, geomorphic studies suggest that the MCT remains active today (Hodges, 2000).

In NW Himalaya, the internal zones of the Indian Plate records an early-Tertiary regional metamorphism with no evidence for a later metamorphic event whereas the central Himalaya preserves the Late Oligocene to Early Miocene main regional metamorphic event associated with displacements along the Main Central Thrust (Hubbard and Harrison, 1989), which overprints an earlier Eocene metamorphic phase (Hodges and Silverberg, 1988; Hodges et al., 1988). The crystalline rocks of the internal zone between the MMT in the north and the Panjal-Khariabad fault (in the Hazara region) and the Batal Thrust (in the Kaghan Valley) in the south have been correlated with the GHC of the central Himalaya (Greco and Spencer, 1993). The Lesser Himalayan Zone equivalent consisting of relatively unmetamorphosed Proterozoic to Eocene sediments crop out in the footwall of the Panjal-Khairabad fault and the Batal Thrust in NW Himalaya (Greco and Spencer, 1993).

Studies in the Everest transect and Bhutan reveal that early movement along the MCT took place at circa 20 Ma (Searle et al., 2003) or 23 Ma (Daniel et al., 2003), respectively, coeval with movement on the South Tibetan Detachment Zone (STDZ). Geochronologic data from Sikkim (Catlos et al., 2003) and southern Tibet to the north of Bhutan (Edwards and Harrison, 1997) indicate that movements along the MCT seem to have been intermittent until about 10 Ma or after 12.5 Ma, respectively. Although it is widely assumed that slip on the STDZ and MCT occurred at least in part simultaneously (Burchfiel et al., 1992; Hodges et al., 1992; Searle et al., 1997), evidence has not yet been documented for such a relationship (Vance et al., 1998).

Whereas most of the Himalayan orogen exhumed at a rate between 0.1 and 1.0 mm/a (Einsele, 1992), the Tibetan Plateau uplifted at an average rate of 0.2 to 0.3 mm/a for about 25 Ma (Zhao and Morgan, 1985), and the High Himalayas uplifted with an average rate of about 1.5 mm/a for the last 20 Ma (Burg et al. 1987). However, the uplift rates may have been considerably higher in such tectonic settings for shorter periods in limited areas. For example, the uplift rates in the Nanga Parbat Haramosh Massif have increased from ≤0.5 mm/a to more than several mm/a during the last 7 Ma (Hurford, 1991).

The clear correlation between high exhumation rates and local structural development suggests that the rate and magnitude of deformation have played an important role in deciding where and how fast Himalayan exhumation occurs (Yin, 2006). The theories proposed for differential denudation in the MCT hanging wall from east to west along Himalayan strike include:

(a) an eastward increase in the magnitude of slip along the MCT due to counter-clockwise rotation of India with respect to Asia during Indo-Eurasian collision (Guillot et al., 1999);
(b) an eastward change in the dip angle of the subducted Indian continent (Guillot et al., 1999); and
(c) an eastward increase in the magnitude of exhumation in response to regional variation of climatic conditions (Finlayson et al., 2002).

Lombardo and Rolfo (2000) report that eclogite facies metamorphism in the Pakistan Himalaya with peak temperatures of 580-600 °C and pressures >23-24 kbar, occurred at ~47-46 Ma (Smith, H. A. et al., 1994; Foster et al., 2002), while exhumation of ultra high pressure rocks to greenschist facies conditions (pressure ~ 4 kbars) was accomplished rapidly between 46 and 40 Ma with an exhumation rate of about 40±30 mm/a for the Kaghan valley (Tonarini et al., 1993; Treloar et al., 2003). Recent review by Yin (2006), however, suggests that the exhumation rate in the Kaghan valley must have been exceedingly slow about 0.33±0.2 mm/a after 40-46 Ma.

The $^{40}Ar/^{39}Ar$ biotite ages decrease systematically from >40 Ma around the margin to 5–0 Ma in the core of the Nanga Parbat syntaxis. This indicates differential exhumation, heat advection, or a combination of both during the development of the syntaxis (Zeitler et al., 2001). Assuming 350 °C, 1 and 5 m.y., and 30 °C/km as the closure temperature of biotite, duration of exhumation and a constant geothermal gradient, respectively, the core of the Nanga Parbat syntaxis has experienced an exhumation at a rate of 7.0±4.5 mm /yr. The exhumation rate in core of the western Himalayan syntaxis is high since latest Miocene time (Zeitler, 1985; Treloar et al., 1989a; George et al., 1995; Winslow et al., 1994, 1995; Schneider et al., 1999), though exhumation rate around the edge of the Nanga Parbat syntaxis was 0.30±0.20 mm/a (Yin, 2006) and the average exhumation rate calculated for the Early and Middle Miocene times was 0.67 mm/a (Zeitler et al., 1989; Treloar et al., 2000).

Current estimates of crustal shortening across the Himalayan orogen indicate an eastward increase in the magnitude of shortening. The overall shortening across the westernmost Himalaya in Pakistan is no more than 200 km (DiPietro and Pogue, 2004). However, the minimum amount of crustal shortening across the central Himalayan orogen ranges from >750 km in southwest Tibet and western Nepal to >326 km in eastern Nepal and south-central Tibet (Hauck et al., 1998).

The age of the Siwalik Group (11.8 to 0.85 Ma) in Shinghar/Surghar Ranges indicates that sedimentation in this area began later than the deposition of basal part in the Potwar Plateau and shows westward transgression of these molasse facies (Khan, M. J. and Opdyke, 1987).

9.6.2 Sediment Influx from the Trans-Himalaya and Karakoram

During the Jurassic, the collision of Lhasa block with the northern Qiangtang block along the Bangong suture made the southern margin of the former Andean-type continental margin, along which considerable volume of oceanic crust was subducted that subsequently resulted in 2500 km long calc-alkaline intrusive continental arc complex i.e. the Trans-Himalayan batholith (O'Brien, 2001). At the end of the Cretaceous, the oceanic Kohistan-Ladakh arc collided with Asia, and was then itself intruded by granites of the Andean-type arc (O'Brien, 2001).

Clearly the Karakoram, Hindu Kush and Lhasa Block have been active margins since as early as 195 Ma ages are known in the Hindu Kush (Hildebrand et al., 2001), and 150-145 Ma and 115 Ma intrusions in the Karakoram (Searle, 1991). The Asian active margin also includes the Kohistan and Ladakh arcs associated with Indo-Asian collision (Hildebrand et al., 2001). The southern margin of Asia is dominantly composed of volcanic and plutonic elements of arc origin and their variably metamorphosed Precambrian-Mesozoic country rocks (Burg et al., 1983; Searle, 1991).

Magmatically and tectonically, there are two differences between the Karakoram and Trans-Himalaya belts. 1) In Karakoram the plutonic activity continues throughout the Eocene timing of the India-Eurasia collision and onward at least up to the Miocene (Debon et al., 1986; Searle et al., 1989), whereas in Trans-Himalaya, the plutonic activity seems to have stopped at about 10 Ma after collision (LeFort, 1988). 2) There is also a difference between the two batholiths in terms of uplift and erosion rates, both being very fast in the Karakoram region (Zeitler 1985).

Geochronologic data for the Trans-Himalayan continental arc suggest that the most intense period of magmatic activity was older (latest Cretaceous) in the west and younger (early Tertiary) in the east. Likewise, the arc magmatism ended earlier in the west (late Paleocene) than in the east (middle Eocene). This observation shows that the Trans-Himalayan arc magmatism corresponds closely in time with the collision of India, which occurred earlier in the west than in the east (Rowley, 1996).

Some researchers have regarded the Karakoram batholith as a westward extension of the Gangdese batholith that has been offset hundreds of kilometers by the Karakoram fault system (Peltzer and Tapponnier, 1988). However, this interpretation is criticized by Searle (1996) who argued that all the available geologic evidence suggests that the

Karakoram fault system developed in Neogene time and displacement along it is not more than 120-150 km.

The backbone of the main Karakoram range is made up of an axial composite batholith intruding Palaeozoic-Triassic sedimentary series lying on the northern side of the range. Plutonic activity of the Karakoram batholith extends from as early as Middle Cretaceous (LeFort, 1988) to as recently as Late Miocene (Debon et al. 1986; Searle et al. 1989).

The implication from the combined data of the Nd and Pb is that much of the sediment in the Indus Fan is derived from rocks lying north of the Indus Suture, mostly the Karakoram. The 5-7 km/Myr exhumation rates in the South Karakoram Metamorphic Belt (SKMB) (Zeitler, 1985; Cerveny et al., 1989; Villa et al., 1996) supports this conclusion, though the Karakoram Batholith has much lower recent rates of exhumation (<1 km/Myr) (Krol et al., 1996). The area of the SKMB is approximately six times that of NPHM (500x35 km versus 100x30 km), and correspondingly six times more material may be derived from this source into the Indus River (Clift et al., 2002b).

The Indus Fan deposits display a weak isotopic signature of the major Himalayan units but a strong input from the Mesozoic arcs in the Karakoram mountains (Clift et al., 2001a, 2002a). Synthesis of seismic reflection data indicates that rapid sediment accumulation in the Indus Fan occurred in two pulses; one in the Middle Miocene and another in the Pleistocene. The former event is related to rapid uplift and exhumation of the Karakoram Mountains (Clift et al., 2002b). The petrographic and geochemical data from this study do not show any change in the provenance of the western Himalayan Foreland Basin sediments since the deposition time of the Kamlial Formation (Figs. 9.4-9.5). Hence it is suggested that the scenario presented by Clift et al. (2002b) for the Middle Miocene remained persistent since the time of deposition of the Kamlial Formation (Figs. 9.4-9.5).

Clift and Gaedicke (2002) attributed much of the Middle Miocene influx of sediments to tectonism and rapid exhumation in the Karakoram range, which forms the dominant source for the Indus Fan. Major events of deformation and granite genesis, dated at 25-20 Ma in the Hindu Kush and Karakoram (Hildebrand et al., 1998; Parrish and Tirrul, 1989; Scharer et al., 1990), were followed by a period of rapid cooling from 17 to 5 Ma (Searle et al., 1989). Further erosion related to the start of transpression along the Karakoram Fault caused >20 km of exhumation between 18-11 Ma (Searle et al., 1998).

Today, the Indus River flows westward along the line of suture zone and then cuts south over the Himalayas, perpendicular to the strike of the orogen, into the foreland basin and finally the Indus Fan (Najman et al., 2003a). Yet, the route of the paleo-Indus remains controversial. Though some researchers consider the path of the Indus River to be antecedent, others suggest that it first cut through the Himalayan belt and debouched into the foreland basin in the Early Miocene, or at 11 Ma, with earlier routing perhaps into the Katawaz remnant ocean basin (Abbasi and Friend, 1989; Qayyum et al., 1996; Brookfield, 1998; Shroder and Bishop, 2000; Clift et al., 2001a). From the Kohat Plateau, which is very close to the modern Indus, composition of sandstone of the Kamlial, Chinji and Nagri formations closely resembles the recent Indus Fan detritus (Figs. 9.4-9.5) (Suczek and Ingersoll, 1985).

The composition of the Indus sands from the Tarbela lake suggest a dominant supply of Indus bedload from the active-margin (81±2% i.e., 60±6% from Karakoram; 6±4% from the Ladakh Arc and South Tibet; 14±4% from the Kohistan Arc), followed by the Himalayan units (19±2% i.e., Nanga Parbat 13±3%; Tethys and Greater Himalaya 6±3%) (Garzanti et al., 2005). At the Salt Range front, the detrital modes of Indus sands reflect extensive recycling of older Indus sediments (54±3%) with subordinate contributions from the Kabul (33±2%), Soan (11±2%), and Kurram, Tochi and Gomal rivers (3±2%) (Garzanti et al., 2005).

Assuming a peak cooling rate of 7 km/Myr (Zeitler, 1985; Zeitler et al., 1993; Winslow et al., 1994) and a temperature gradient of 30°/km, Clift et al. (2001b) predicted that as much as ~20% of the modern Indus bedload could be derived from the NPHM. However, based on proposed peak exhumation rates of 3-7 km/Myr and the perturbed geothermal gradient (Whittington, 1996; Moore and England, 2000), the lower exhumation rates would imply that <10% of the Indus Fan might have been derived from NPHM. Obviously, the erosional record of the Indus Fan is not dominated by erosion from the NPHM, as also concluded by Clift et al. (2002b).

According to Clift and Blusztajn (2005), the source of the Indus sediments was dominated by erosion within and north of the Indus Suture Zone until five million years ago, and after that the river began to receive more erosional products from the Himalayan

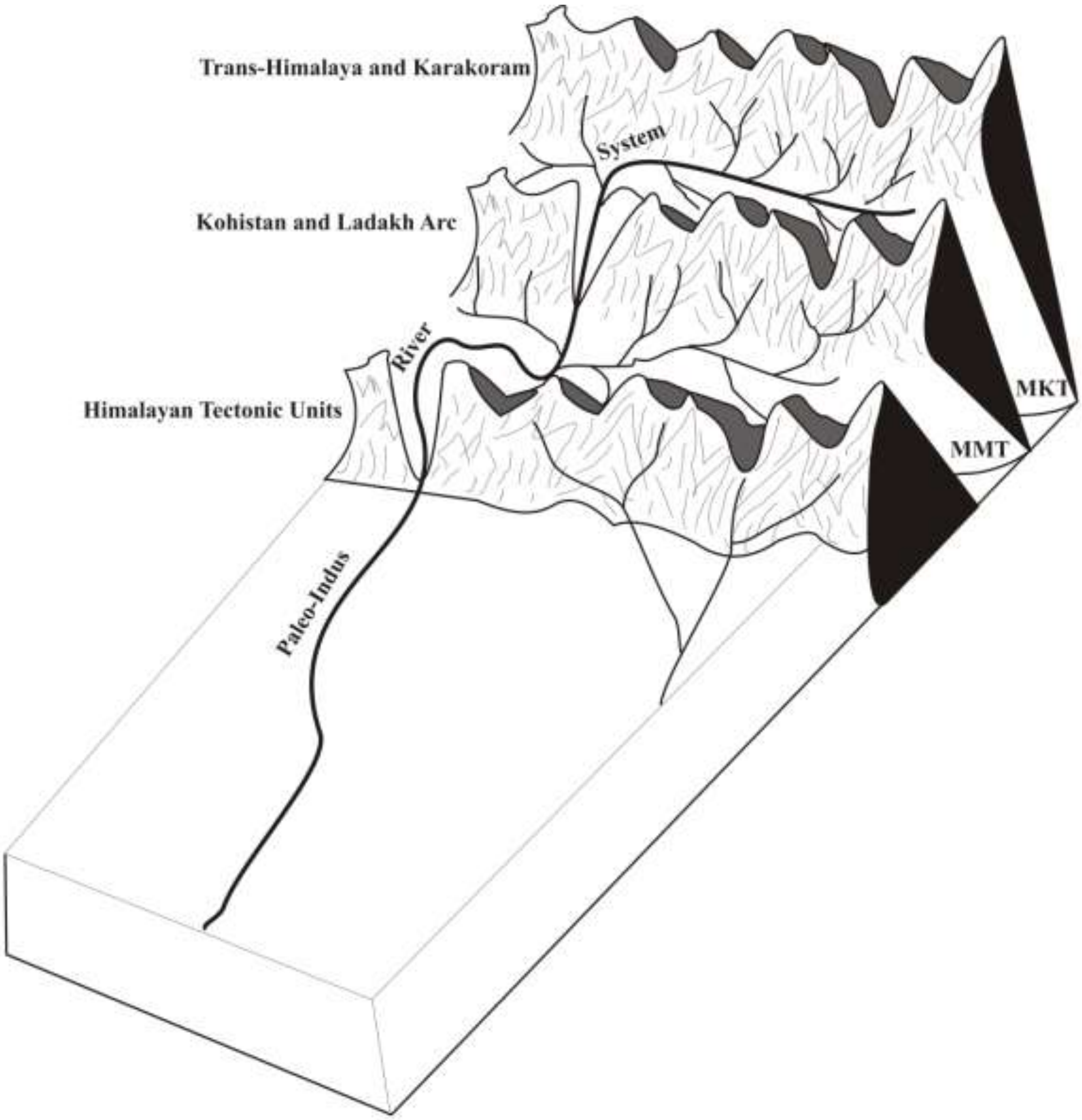

Fig. 9.4. Conceptual reconstruction of the tectonics-drainage pattern of the NW Himalaya at the time of deposition of the Kamlial Formation. MKT= Main Karakoram Thrust; MMT= Main Mantle Thrust.

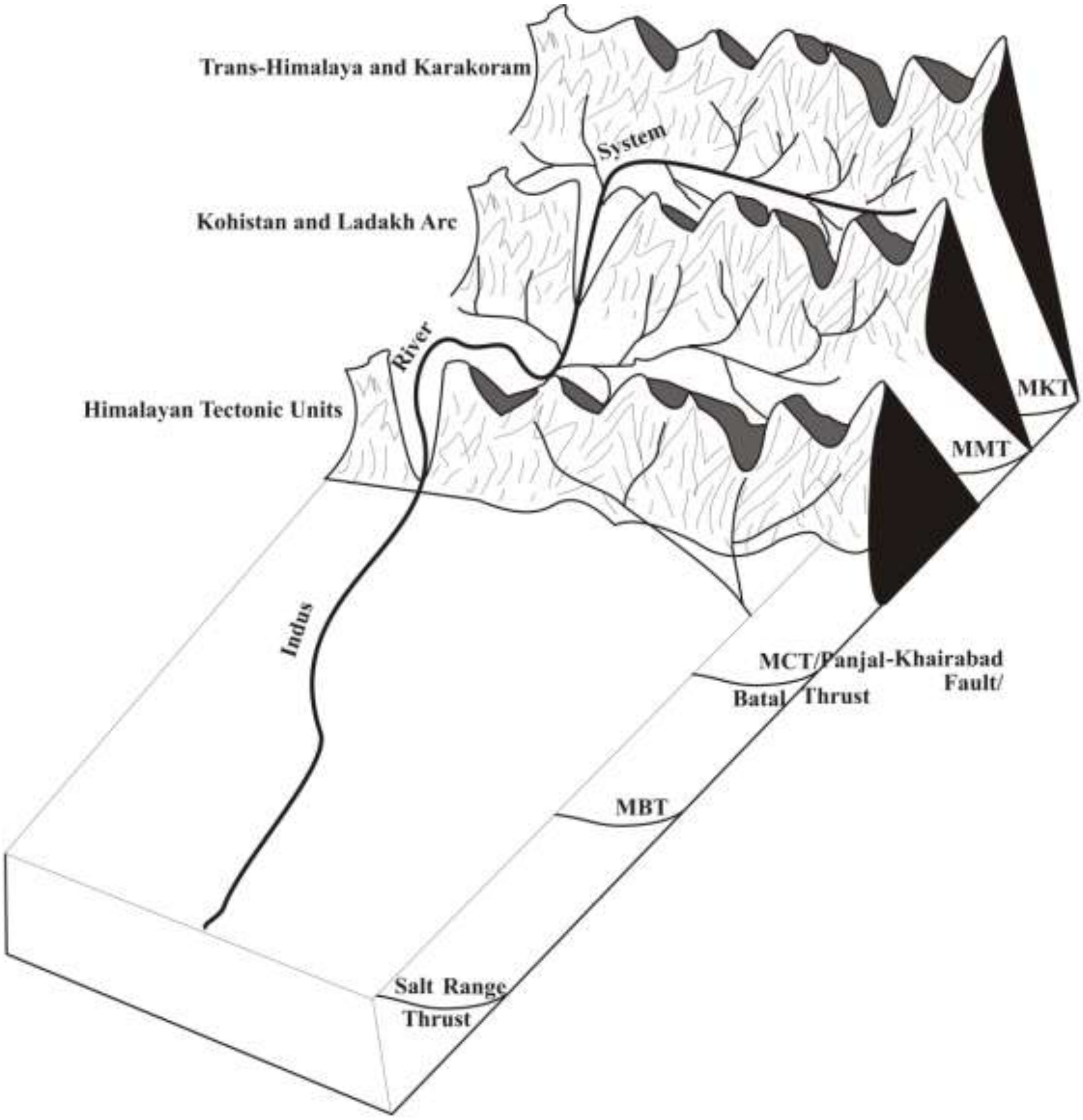

Fig. 9.5. Conceptual reconstruction of the tectonics-drainage pattern of the NW Himalaya at the time of deposition of the Nagri Formation. MKT= Main Karakoram Thrust; MMT= Main Mantle Thrust; MCT= Main Central Thrust; MBT= Main Boundary Thrust.

sources. These authors propose that this change in the erosional pattern is caused by a rerouting of the major rivers of the Punjab into the Indus, which flowed east into the Ganges River before that time.

Consistent with the conclusion based on Nd and Pb isotope data, the trace element composition of individual amphibole grains suggests that the Indus River sediment budget is dominated by erosion of the Southern Karakoram Metamorphic Belt (Clift et al., 2002b). This conclusion is also in conformity with the suggestion that the Nanga Parbat, although rapidly uplifting, does not seem to be the dominant sediment source to the Indus River because of its small area (Lee, J. I. et al., 2003). Material in the Indus River eventually delivered to the Arabian Sea is only moderately diluted by Greater and Lesser Himalaya flux delivered by the tributaries that join it in the foreland basin (Lee, J. I. et al., 2003).

9.6.3 Sediment Influx from Kohistan and Ladakh Arc

In the Himalayan region, where several thousand kilometres of ocean crust was consumed below the Eurasian continent (the Lhasa block), both continental (Trans-Himalayan batholith) and oceanic (Kohistan-Ladakh arc) magmatic arcs can be recognized (O'Brien, 2001). However, Sutre (1990) [ch. Clift et al., 2002] and Rolland et al. (2000) have suggested that the oceanic Kohistan arc in Pakistan was continuous with a continental arc in central and eastern Ladakh, similar to the modern day Aleutian Arc.

The recent data set of Najman et al. (2003a, b) show major arc erosion at 18 Ma, which is inconsistent with the previously held belief that this occurred at 11 Ma. The latter interpretation is based on the increased fluvial discharge and the first appearance of arc-derived hornblende to the foreland basin (Cerveny et al., 1989). However, the late appearance of hornblende may also be due either to (1) gradual erosion through deeper levels of the arc covering or (2) diversion to the region of a river that was already carrying hornblende.

The Pb isotope systematics of K-feldspars from the Indus River in Ladakh and Indus-Zanskar confluence show dominant erosion from the Ladakh Batholith and/or the Paleogene sediments of the Indus Molasse (Clift et al., 2001a; Clift et al., 2002b). The last mentioned itself is largely sourced from the Lhasa Block in the upper part of its stratigraphy (Clift et al., 2001a). At the moment, it is difficult to understand whether and how the Kohistan-Ladakh arc was connected to the Tibetan Asian continental arc (Lhasa block), a region where no evidence of oceanic arc or back-arc basin formations is reported (Coulon et al., 1986).

Geochronologic data suggest that calc-alkalic magmatism in Kohistan and Ladakh began before ca. 100 Ma, and the youngest event occurred at late Paleocene age (Honegger et al., 1982; Scharer et al., 1984; Petterson and Windley, 1985). This age range suggests that, subsequent to collision, the then-newly-accreted Kohistan-Ladakh island-arc complex evolved into a continental arc marking the southern border of Eurasia. Volumetrically, most of the Kohistan and Ladakh batholiths developed in this continental arc setting in latest Cretaceous time. Further in the east, the continental arc is represented principally by the Gangdese batholith of southern Tibet (Hodges, 2000).

From west to east, the arc lava geochemistry shows an evolution from an immature arc to a mature arc. The geochemistry of the east Ladakh Nubra-Shyok area volcanic rocks indicates an evolution towards a more mature volcanic arc in the east (possibly built on continental basement) (Clift et al., 2002b).

Gangdese, Ladakh and Kohistan are all believed to represent the roots of a continental arc along the southern margin of Asia. The character of the Gangdese batholith in these arcs is typical of continental arc intrusions. The Ladakh batholith was either melted from a mantle source and then intruded into the Asian (Karakoram) margin without much reworking of the existing crust, or the basement into which it was emplaced contained a large amount of oceanic material, as is the case in the Kohistan batholith (Clift et al., 2002b).

The Nd isotope compositions and trace element ratios of the Dras 1 Volcanic Formation show significantly more continental contamination than is seen in the Neogene Tonga (Clift et al., 2002b). Comparison of the Nd isotope and trace element data with modern arc complexes (the Izu or Tonga Arcs) indicates that the Dras-Kohistan Arc was less purely oceanic (Clift et al., 2002b). On the other hand, no lava data compares closely with the recent Aegean Arc, which shows strong continental chemical contamination (Clift et al., 2002b).

Sutre (1990) [ch. Clift et al., 2002] suggested that the Dras-Kohistan Arc formed on the continental basement of the Trans-Himalaya that existed as a continental fragment within the Tethys Ocean. On the other hand, Robertson and Degnan (1994) argued that the Trans-Himalaya was separated by a narrow marginal sea from the Karakoram Block and that the Dras-Kohistan Arc originated independently between the Trans-Himalaya and India, above a north-dipping oceanic subduction zone within the Tethyan oceanic crust. Though, Rolland et al. (2000) proposed that the Dras-Kohistan Arc appears to have characteristics of intraoceanic features in the vicinity of Kargil, the arc in the Leh region and further east was emplaced into continental crust. Most recently Rolland et al. (2002) used trace element as well as Nd and Pb isotope chemistry to propose a wholly oceanic origin for the arc above a north-dipping subduction zone during the mid Cretaceous.

Igneous rocks from both the Kohistan and Ladakh display similar geochemical features (Petterson and Windley, 1991; Sullivan et al., 1994; Ahmad, T. et al., 1998). Also an important plutonic activity that lasted until 25 Ma resulted in successive emplacement of more and more differentiated granitoid intrusions. The geochemical affinities of these plutons indicate that the Kohistan-Ladakh arc terrain evolved as an active margin after its accretion to the Asian plate (Petterson and Windley, 1991; Treloar et al., 1996).

Volcanic rocks of Eocambrian and Cambrian age including acidic and basic tuffs, basalts, andesites and felsic rocks occur in the western Tethyan Himalaya (Garzanti et al., 1986). The volcanics include low-K tholeiites with trace element characteristics indicative of an immature arc environment (Garzanti et al., 1986). The 520 to 500 Ma dates on detrital zircon grains analyzed from the Phulchauki Group (Nepal) as well as the arkosic nature of these sediments could reflect input from this arc system (Gehrels et al., 2006). This evidence for Cambrian magmatic arc activity in the Tethyan Himalaya also suggests initiation of subduction along the northern margin of Gondwana and its change from a passive to convergent Andean type margin by ~510 Ma. However, Myrow et al. (2006a, 2006b) had questioned the presence of Cambrian arc and sedimentary environment in this region.

9.7 Source Area Lithologies of the Kamlial, Chinji and Nagri Formations

The presence of an appreciable amount of feldspar in the Kamlial, Chinji and Nagri formations indicates either high relief or arctic climate at the source area (Prothero and Schwab, 2003). The higher proportion of alkali feldspar than plagioclase shows dominance of granite and acidic gneisses in the source area. However, this feature might also be due to the higher chemical stability of alkali feldspar than plagioclase during transportation (Tucker, 2001). The presence of microcline also favors granitic and pegmatitic sources.

The abundance of mica rarely exceeds 10 % of the total framework grains in the Kamlial, Chinji and Nagri sandstones. The flakes of micas are mostly bent thereby suggesting their derivation from metamorphic or deformed assemblages (Michaelsen and Henderson, 2000). A similar provenance is indicated by the presence of lithic grains of metamorphic origin, grains of epidote and garnet. The occurrence of monazite, apatite and rutile, on the other hand, suggests both metamorphic and igneous (plutonic) source rocks (Morton et al., 1992). Chromite may have been derived from unmetamorphosed/ metamorphosed basic to ultrabasic source rocks (Dubey and Chatterjee, 1997). The abundance of volcanic lithics in Nagri sandstone at Chashmai and Banda Assar syncline indicates magmatic-arc settings (Boggs, 1992).

The lower values of Zr, Nb and Y, and the low average ratios of Ba/Co, Ba/Sc and Y/Ni of the studied sequence relative to the Upper Continental Crust (UCC) and Post Archain Austrailian Shale (PAAS) indicate the presence of mafic phases in the source area/s for these sediments (see section 8.10, Tables 8.1, 8.2, 8.5, 8.6). Similarly, the high Cr/Zr, Cr/V and Sc/Th ratios compared to the UCC and PAAS and high Cr contents ($Cr > 110$ ppm) indicate mafic and ultramafic source rocks for the Neogene molasse sequence of the Kohat area (see section 8.10, Tables 8.1, 8.2, 8.5, 8.6).

On the other hand, the elemental ratios of Th/Sc, La/Th, La/Sc, Th/Zr and plot of Th/Co vs La/Sc propose provenance of the Neogene molasse sequence similar to UCC and PAAS. As the average source of the PAAS is presumed to be granitic, the studied Neogene sediments are most probably derived from a source area of felsic composition (see section 8.10, Tables 8.1, 8.2, 8.5, 8.6). Similarly, the Th/Co versus La/Sc relation indicates a dominantly silicic provenance for the Neogene molasse sequence of the Kohat area whereas ratio of Cr/Th suggests contribution from both silicic and mafic rocks (see section 8.10, Tables 8.1, 8.2, 8.5, 8.6) (Cullers, 2002).

The 0.66 P/F value for the Arabian Sea sand indicates its derivation from collision orogenic belts (Suczek and Ingersoll, 1985). Lithic populations of the Arabian Sea sand (metasedimentary and sedimentary), micas (predominantly muscovite and biotite) and amphiboles suggest a source area composed of uplifted basement terrains of granitic to granodioritic composition plus extensive metasedimentary and sedimentary terrains (Suczek and Ingersoll, 1985). The presence of felsitic and andesitic volcanic lithic fragments, however, argues against the derivation of the sand from a magmatic arc (Suczek and Ingersoll, 1985).

All the suggested varieties of source lithologies for the studied sandstones occur in northern Pakistan. For example, the sedimentary/metasedimentary lithologies occur as a part of the Hindu Kush-Karakoram range (Gaetani et al., 1990). The Karakoram and Kohistan batholiths, consisting of unmetamorphosed/ metamorphosed granite-diorites as well as pegmatites and aplites in the north, could be the major sources of plutonic provenance (Jan et al., 1981a). The Jijal-Pattan complex is exposed along the Indus river to the north of MMT and dominantly consists of garnet granulites and ultramafic rocks (Jan, 1985). The Kamila amphibolite to the north of MMT chiefly consists of amphibolite with subordinate amounts of ultramafics, gabbro, diorite, tonalite and granite (Jan, 1988). Similarly, the ~ 100 km wide Tethyan sequence consists of Cambrian to Eocene unmetamorphosed or weakly metamorphosed rocks that extends along the entire length of the Himalayas (Gansser, 1964). The 2500 Km long and discontinuous Indus Suture Zone (ISZ) in northern Pakistan is characterized by the occurrence of a variety of mélanges containing talc carbonate schist, greenstone, greenschist, metagabbro and metasediments (Kazmi et al., 1984).

South of the ISZ, the Indian continental margin is composed of late Precambrian to early Paleozoic gneisses, ortho- and paragneisses of the Besham group and Nanga Parbat syntaxis (Tahirkheli, 1982), granite and granitic gneisses of the Mansehra and Swat areas, pelitic, psammitic and calcareous schists as well as marbles of the Besham, Hazara and Swat areas (Treloar et al., 1989b). Similarly, slates and quartzites are the dominant lithologies of lower Hazara and Attock-Cherat ranges (Calkin et al., 1975; Hussain et al., 1989).

The uplift rates of the Himalayan orogenic belt increased substantially during the Miocene times (Zeitler, 1985) that rapidly exposed deep-seated metamorphic and igneous rocks for denudation. Subsequently, the Himalayan drainage system analogous to the present day river systems of Indus, Ganges and Brahmaputra (Abid et al., 1983) started flowing axially into their respective basins depositing thick detrital sediments. The type of sediments carried by these drainage systems is primarily controlled by the lithologies exposed in their catchment areas. For example, the present day Indus river in northern Pakistan contains sediments consisting of plutoniclastic, metamorphiclastic and sedimentary/metasedimentary grains which represent the lithologies of the Karakoram and Hindu Kush ranges in the region (Garzanti et al., 2005). The Kohistan-Ladakh arc and Nanga Parbat Haramosh Massif supply high-grade quartzofeldspathic sands whereas the Ladakh batholith sheds pure arkosic detritus (Garzanti et al., 2005). Heavy minerals in all these sands are dominated by blue-green to subordinately green and brown hornblende, garnet and epidote (Garzanti et al., 2005). The Soan, Kurram and Tochi rivers carry lithic sands with abundant sedimentary and low-grade metasedimentary components (limestone, shale/slate, sandstone/metasandstone, chert). Heavy minerals, including epidote, garnet, red to coffee-brown chrome spinel, and staurolite, are largely recycled from terrigenous units (Garzanti et al., 2005).

In eastern Kohat, the progressive upsection increase of feldspar in the Siwalik Group is related to uplift and erosion of granitic bodies in the source area since Late Miocene times (Abbasi and Friend, 1989). High content of feldspar from the Surghar Range (Abid et al., 1983), northern Potwar (Krynine, 1937), the Miocene-Pleistocene Indus Cone sediments (Suczek and Ingersoll, 1985), and the high uplift rate of Karakoram batholith (Searle, 1987) and Nanga Parbat (Zeitler, 1985) in the alike period favor the same idea. However, no such trend in increase of feldspar content in sandstones of the Kamlial, Chinji and Nagri formations from southwestern Kohat has been observed. This contrast of the present study with earlier works can be attributed to the variable lithologic units along arc, paleoclimatic conditions in the source area as well as in the depositional sedimentary basin. The low feldspar content (< 13%) within the sandstones of the northern Bowen Basin (Michaelsen and Henderson, 2000), compared to high feldspar content (up to 50%) within the same sandstones in the central and southern part of the Bowen Basin is attributed to along-arc compositional variation (Baker et al., 1993; Ahmad, R. et al.,1994). Alternatively, no major change in modal petrographic point count data, especially no significant increase in feldspar content upsection as observed in other parts of the Himalayan Foreland Basin (DeCelles et al., 1998a, 1998b), show no major change in source lithologic units for sediments deposited in southwestern Kohat from deposition time of the Kamlial Formation till deposition time of Nagri Formation. Instead, this conclusion may show that during the said period there was no major change in paleoclimatic conditions in the source area of the sediments. However, variation of feldspar content in individual samples may show variation in the degree of weathering at relatively short interval of time.

The heavy mineral assemblage of the Chinji and Nagri formations in the Potwar area mainly includes amphibole, chlorite, tourmaline, garnet, epidote, magnetite and pyrite, indicating granodiorite source rock for the constituent sediments. These formations contains 20-300 ppm Cr, 20-200 ppm Ni, 50-400 ppm V indicating basic source rocks; and 50-500 ppm Zr showing that some of the material was also derived from acidic to intermediate rocks, while the presence of alkali feldspar indicates acidic igneous source rocks (Alam et al., 2003).

The heavy mineral analyses of the Siwalik Group indicate a sharp change in the abundance of blue green hornblende. It frequently ranges from 15 % to 38 % at the base of Nagri Formation, 45 % in the Nagri Formation, 65 % in the older Dhok Pathan Formation and 40 % in the Soan Formation in the Trans-Indus section (Cerveny et al., 1989). A similar trend has been reported by Johnson, N. M. et al. (1985) from the Chinji-Nagri boundary in the Chinji area of the Potwar Plateau. Sufficient exposure of the Kohistan Island Arc (KIA) by 11 Ma, which is mainly composed of amphibolite and granulitic norites, and the occurrence of abundant (44%) blue amphibole in the heavy mineral fraction of the Swat River which originates and flows through the exposure of the KIA (Johnson, N. M. et al., 1985) support a northern provenance. The blue green hornblende ranges from 28-40 % with an average of 33±3 % of the total heavy minerals in the present day Indus River followed by kyanite and garnet (Cerveny et al., 1989). This study, however, does not show any significant change in abundance of hornblende from Lower Siwalik to Middle Siwalik.

9.8 The Central and Eastern Himalayas and the Himalayan Foreland Basin

In the Subathu sub-basin of India (Table 9.1, Fig. 3.1), the Dagshai Formation represents the oldest continental facies followed by the Kasauli Formation. Sandstones of these formations consist predominantly of metapelitic detritus. The Himalayan metamorphic detritus first appear in the Dagshai Formation at the close of Oligocene time, whereas sediments of deeper metamorphic levels are seen in the Kasauli Formation at the earliest Miocene time. The occurrence of higher grade metamorphic lithic grains and garnet is in coincidence with the displacement period along the Main Central Thrust and South Tibetan Detachment Zone at Early Neogene time. “Himalayan aged” micas and zircons (Najman et al., 1997, 2004), and Greater Himalayan ε_{Nd} signatures (Najman et al., 2000) attest to Greater Himalayan provenance (Najman and Garzanti, 2000).

Isotopic dating of detrital white micas shows that the Dagshai Formation is probably younger than 28 Ma (Najman et al., 1997). Depositional age is constrained as younger than 28-22 Ma by Ar-Ar dating of detrital micas (Najman et al., 1997) and Early-Middle Miocene by plant fossils for the overlying Kasauli Formation (Fiestmantel, 1882).

Although sandstone composition of the Subathu and lower Dagshai successions is similar to the Balakot and Murree formations of northern Pakistan (Critelli and Garzanti, 1994), compositional time trends differ. Namely, low grade metamorphic (phyllite) grains are abundant at the base of the Balakot Formation and decrease upward, whereas the opposite trend is recorded in India (Najman and Garzanti, 2000). The progressive enrichment in feldspars through time (with gradual decrease of the P/F ratio; Garzanti et al., 1996; Uddin and Lundberg, 1998) is common to all Himalayan foreland basin clastic suites from Pakistan to Nepal, reflecting progressive deepening of erosion into the more deeply seated granitoid crustal rocks at the core of the Himalayan thrust stack (Najman and Garzanti, 2000).

The Kasauli Formation and Lower Dharamsala subgroup sediments of the Subathu sub-basin and Kangra sub-basin, respectively, record in their provenance a gradual unroofing of the metamorphosed Greater Himalaya, as low- to medium-grade metamorphic detritus are common in these sediments (Najman and Garzanti, 2000). But the overlying Upper Dharamsala subgroup shows a predominance of detritus from sedimentary and low-grade metamorphic sources (White et al., 2002). This contrast in provenance indicates individual tectonic histories within the catchment areas. The Subathu sub-basin most probably received sediments from the paleo-Sutlej or paleo-Yamuna rivers, whereas the Kangra basin received sediments draining from the paleo-Beas. If the unroofing of the metamorphic core of the Greater Himalaya occurred synchronously, then the Dagshai Formation sediment eroded from a very low to low grade metamorphic source and that of the Lower Dharamsala subgroup from a low to medium-grade metamorphic source (Najman et al., 2004).

Though limestones and marbles constitute a significant proportion of the Tethys and Greater Himalayan lithologic units, respectively, their rarity in fluvial sands may be the result of wet monsoonal climates, whereby carbonate gets dissolved even in mountain segments (Harris et al., 1998; Galy and France-Lanord, 2001). On the other hand, P/F ratios do not show significant change from mountain streams to the Assam plains, even though Lesser Himalayan and Sub-Himalayan sediments are recycled at the Himalayan front (Singh and France-Lanord, 2002).

Studies from the Bengal Fan indicate several close similarities between the Early Miocene and the present day erosional systems (Galy et al., 1996). These include: (1) the same primary provenance for both the Early Miocene and recent sediments (i.e. the GHC or a geochemically analogous unit), (2) comparable degree of weathering for both the Early Miocene and recent sediments, and (3) similar mean rates of exhumation. Alike, Sr and Nd isotopic compositions of the Early Miocene sediments from the Bengal Fan are similar to those of the present day GHC. All this suggests that the provenance of these sediments has changed little since ca. 20 Ma (France-Lanord et al., 1993; Galy et al., 1996).

The low proportion of Greater Himalayan material in the Indus Fan compared to the Bengal Fan indicates that the drainage basin of the former was concentrated north of the Indus Suture. Although the Greater Himalaya in Zanskar and Lahaul were rapidly exhumed at ~20-23 Ma (Searle, 1991; Searle, 1996; Walker, J. D. et al., 1999), metamorphism in the western Pakistani Greater Himalaya appears to have reached its peak much earlier, ~45 Ma (Treloar et al., 1989a; Searle, 1996). As a result, the modern Ganges-Brahmaputra drainage basin receives more sediment influx than the modern Indus basin from the Greater Himalaya units. Compared to the central and eastern Himalayas, exhumation is fast north of the Indus Suture Zone within the Indus drainage area (western Himalaya) (Clift et al., 2002b).

Whereas the Indus Fan sediments seems to be dominated by the materials of the tectonic units adjacent to the suture zone (Clift et al., 2001b), the Bengal Fan sediments deposited by the Ganges and Brahmaputra rivers show dominant derivation from the rapidly unroofing Himalaya (France-Lanord et al., 1993) with only minor input from the Indian Shield in its distal region (Crowley et al., 1998). The Pb isotopic values of detrital feldspars and the paleocurrent data of the Indus Group suggest the Lhasa Block as being the most likely source component and the basin resulted from a large-scale axial river flowing through the suture shortly after the final marine transgression (Clift, 2001a).

9.9 Tectonic and Climatic Controls on Erosion Rates

High exhumation rates in orogens are generally driven by both tectonic convergence and climatically controlled erosion (Whipple and Tucker, 1999; Willett, 1999). Rock uplift generates topographic relief, thereby enhancing the possibilities for orographic precipitation. Enhanced precipitation (1) controls effective hillslope erosional processes, and (2) increases river discharge (Thiede et al., 2004). In other words, positive feedback between erosion and exhumation over geologic time requires (a) high regional erosion, and (b) coeval replacement of mass by tectonic influx of material (Thiede et al., 2004). However, the nature of this interaction between the distribution of precipitation, regional erosion rates and patterns of rock uplift is still a matter of controversy (Burbank et al., 2003; Reiners et al., 2003; Dadson et al., 2003). For example, in central Nepal, Burbank et al. (2003) suggest that tectonically forced removal of crustal material is the most important factor affecting erosion across a region. Another strong argument for continuous localized erosion over geologic time scales is the complete removal of approximately 10-15 km of the Greater Himalayan crystalline rocks along the Sutlej Valley since the MCT was active, which once covered the rocks of the Lesser Himalayan Zone (Thiede et al., 2004). Similarly, Burbank et al. (1993) suggested that decreasing rates of erosion since 8 Ma, immediately following the commonly accepted age of monsoonal strengthening (Kroon et al., 1991) reflected a stabilizing of slopes due to increased vegetation and the retreat of mountain glaciers. In contrast, Reiners et al. (2003) show strongly varying long-term erosion rates across the Cascade Mountains (USA) closely tracking modern mean annual precipitation. Alike, measured erosion rates in the modern Himalaya are faster in regions where the monsoon is heavier (Galy and France-Lanord, 2001). In addition, during the last glacial stage erosion rates in the Himalaya, inferred from sedimentation rates in the Ganges delta, were higher when the monsoon was stronger (Goodbred and Kuehl, 1999). Modern erosion rates are ~3 times higher in the northernmost parts of the Lesser Himalaya than in the adjacent Greater Himalaya, which are discordant with higher rock uplift rates north of the MCT and are consistent spatially with the peak monsoonal precipitation (Amidon et al., 2005).

According to the stream-power law, river incision rates should be highest in regions with high runoff and steep river gradients. Rivers in the Himalayan region are characterized by (1) large annual runoff variation, (2) strong correlation between discharge and sediment transport, and (3) high sediment flux during peak discharge events (Galy and France-Lanord, 2001; Bookhagen et al., 2005). The monsoonal precipitation in Himalayan orogen exerts a strong control on surface erosional processes, particularly during abnormal monsoon years (higher precipitation) (Bookhagen et al., 2005).

9.10 The Himalayan Drainage System

It has been long noted that the current Himalayan drainage system is asymmetric, with the Indus River system covering about one-fifth of the Himalayan range and by the Ganges and Brahmaputra River systems the rest. Wadia (1953) and DeCelles et al. (1998a) have proposed that the east-west trending Himalayan drainage system in the foreland had reversed its flow direction from the west to the east in the Pliocene after the deposition of the older part of the Siwalik Group. Another model proposed for the evolution of the Indus and Ganges systems considers the current Himalayan drainage systems to have remained approximately the same configuration since the start of the Indo-Eurasian collision (Brookfield, 1998). In a recently published review, Yin (2006) has presented the following speculative model for the evolution of the Himalayan drainage system.

After Indian-Eurasian collision, a longer duration of strain accumulation until 20 Ma, higher magnitude of crustal shortening in the western than in the eastern Himalaya resulted in the northwestward tilting of the Indian continent, which kept the Himalayan Rivers to flow westward (Fig. 28B, in Yin, 2006). During 20-15 Ma, the total amount of crustal shortening increased faster in the eastern than in the western Himalaya due to a faster convergence rate between India and Asia. As a result, the northeastern corner of Indian continent started to tilt northeastward while the majority of northern India remained tilting northwestward. The opposite tilting directions in the northeastern and northwestern parts of India created a drainage divide in the Himalaya (Fig. 28C, in Yin, 2006).

From 15-10 Ma, the total crustal shortening increased faster in the eastern than in the western Himalayan orogen, which caused the Himalayan drainage divide to migrate farther to the west. The migration of the divide might be in discrete jumps possibly due to the dynamic instability of the drainage network that had been constantly affected by Himalayan tectonics (Fig. 28D, in Yin, 2006). Whereas, in the last 10 Ma, an increase in thrust load in the eastern Himalayan orogen forced the Himalayan river system to transport more sediment to the Bengal Fan than to the Indus Fan (Fig. 28E, in Yin, 2006).

The above model makes the following testable predictions:

(1) the Himalayan drainage divide migrates westward in a discrete fashion, and its amplitude increases westward;

(2) the older west-flowing drainages are systematically captured by the younger east-flowing drainages;

(3) the main repository of the Himalayan sediments was the Indus Fan in the Paleogene but the Bengal Fan in the Neogene;

(4) the fluctuation of sedimentary fluxes into the Indus and Bengal fans may be strongly influenced by the development of the foreland basin hinge zone rather than the climate change alone (Burbank et al., 1993).

In the northwestern Himalaya, during Early Paleogene, the uplift of the Himalayas and Kohistan resulted in the formation of a molasse basin in between these two ranges, containing more than 2000 m thick post-Eocene sediments of fluvial and fluvioglacial origin, largely derived from granodioritic Ladakh batholith with subordinate influx from Himalaya (Searle and Owen, 1999). The Paleo-Indus that deposited these sediments with E-W flow direction formed the first submarine fan at the head of the Indian Ocean (at the northeastern corner of the Katwaz remnant; Qayyum et al., 1996). During Early Miocene, the uplift of Mohmand, Waziristan and Baluchistan ranges bordering the Katwaz, and other geomorphic processes diverted the Paleo-Indus drainage system to the south (i.e. the present day Indus drainage system; Qayyum et al., 1997).

At the Early Eocene time, the eastern part of the Himalayan Foreland Basin was comprised of a series of E-W trending tectonic upwarps e.g., Khairabad-Jacobabad high, Panno Aqil graben and Shahpur-Delhi ridge etc. having a series of E-W flowing streams. Along the northern and western margins of the Indus platform, two large depressions known as the Himalayan foredeep and Sulaiman-Kirthar foredeep, respectively, also existed at that time (Kazmi and Abbasi, 2008).

In the Sulaiman-Kirthar foredeep, a sluggish meandering river came into existence at about 22 Ma that deposited the Chitarwata Formation (Waheed and Wells, 1990). The river system was changed into a braided one during Middle Miocene by the sporadic tectonic disturbances and climatic variations, which deposited Vihowa Formation (17.4-

11 Ma; Downing et al., 1993; Raza et al., 2002). During Middle to Late Miocene, renewed tectonic uplift resulted in heavier sediment load to this braided river system, which now deposited Litra Formation (11-6 Ma; Raza et al., 2002).

In the Himalayan foredeep, a large meandering river flowed eastward during Late Oligocene to Early Miocene that deposited the Murree Formation (Stix, 1982; Abbasi and Friend, 2000). During 18.3 to 14.3 Ma, tectonically produced steeper slopes as well as more seasonal rainfall deposited the Kamlial Formation. Concurrent tectonic uplift and climatic variation lead to higher precipitation in the hinterland, and the river system changed into a braided one, depositing Chinji Formation (14.3-10.8 Ma; Kazmi and Abbasi, 2008). With renewed tectonic uplift in the mountain front during 11 to 9 Ma, the river system as made a vigorous one with heavier sediment load and greater discharge capacity that deposited the Nagri Formation (Willis, 1993a, b). In Potwar region, after deposition of Nagri Formation, because of tectonic quience, the river system that deposited the Dhok Pathan Formation (8.1-3.6 Ma) survived in a much subdued form (Khan, I. A. et al., 1997).

Detailed stratigraphic and sedimentologic descriptions of deposits of Late Miocene age from the Potwar and Jhelum re-entrant show at least four different types of fluvial systems.

A) The major axial river with flow direction toward the east-southeast, thick (>10-15 m) channel sandstones with abundant blue green hornblende in its dense mineral assemblage and higher relative proportions of intrusive, volcanic and metamorphic clasts (Mulder, 1991) suggest a fluvial system analogous to the modern Indus River (Burbank et al., 1996).

B) Major tributary rivers as large as the axial river system with considerable source areas within the hinterland are characterized by the brown sandstone, 10-20 m thick and more than 3 km wide. Such southward flowing rivers appear to represent an ancestral Jhelum River carrying clasts distinctive of the Panjal Trap (Burbank and Raynolds, 1988).

C) River systems originating primarily within the foreland are represented by typically brown or "buff" color sandstone channel bodies of small dimensions (< 10 m thick, and 1-5 km in width) with no preferred paleoflow directions (Behrensmeyer and Tauxe, 1982) suggest recycling of previously deposited strata (Burbank et al., 1996).

D) Rivers originating primarily within the foreland, but having source areas controlled by tectonic deformation within the foreland itself with sand bodies considerably smaller in vertical and lateral dimensions (Burbank et al., 1996).

The present study in the light of above discussion suggests that both the paleo-Indus and the east flowing drainage systems were present since the time of deposition of the Kamlial Formation. The dominant magmatic arc provenance based on sandstone petrography, and active continental margin as well as continental island arc provenance on the basis of whole rock geochemistry for all the three studied formations i.e. the Kamlial, Chinji and Nagri formations advocate the presence of a drainage system most likely the present day Indus River system. This study also shows that sediment influx from rivers draining the Himalayan thrusts stack to the southwestern Kohat was negligible at the time of deposition of the studied formations. However, recycled orogen suggested on the basis of sandstone petrography for the Siwalik Group from Potwar and eastern Kohat shows the existence of a river system sourced from the Greater and Lesser Himalayan zones at that time.

CHAPTER 10

Conclusions

- On the basis of field observations and presence of various sedimentary structures, different lithofacies of the Kamlial Formations are identified, namely; Channel Conglomerates Facies (K1), Cross-bedded Sandstone Facies (K2), Interbedded Mudstone, Sandstone and Siltstone Facies (K3) and Mudstone Facies (K4). These facies propose that the Kamlial Formation was possibly deposited by sandy bedload or a major mixed load river. Such rivers, especially during floods, may have heavy load of suspended sediment. Because of highly erodible banks, sinuosity is rather low and braiding is well developed that depends mainly on the availability of sand content.

- In Chinji Formation, based on various sedimentary structures, the following lithofacies are identified; Cross-bedded Channel Sandstone Facies (C1), Cross-bedded and Cross-laminated Sandstone Facies (C2), Interbedded Mudstone, Siltstone and Sandstone Facies (C3) and Mudstone Facies (C4). Sandstone of the Chinji Formation was most probably deposited by mixed-load rivers with significant fine suspended sediment. The floodplain deposits of the Chinji Formation seem to have been deposited by suspended-load rivers during major flood events. Low lateral and vertical connectivity of the sandstone bodies suggest high subsidence rates, resulting in high preservation of overbank fines. The change from thick channel sandstones (Kamlial Formation) to dominantly overbank accumulation with minor, thin, channel-sandstone lenses (Chinji Formation) could be due to a change in climate or the palaeodrainage of the area. Considering the fluvial lithofacies assemblages, the sequences are typical of a braided river system and may be related to S. Saskatchewan type.

- Based on field observations and presence of sedimentary structures in the Nagri Formation, the following lithofacies are identified; Channel Conglomerate Facies (N1), Cross-bedded Channel Sandstone Facies (N2), Interbedded Sandstone, Siltstone and Mudstone Facies (N3) and Mudstone Facies (N4). The Nagri Formation was most probably deposited by sandy bedload rivers. The availability of sand is a major control on braided patterns. The low proportion of mudstone-siltstone facies in Nagri Formation might reflect one or more factors including: (1) low subsidence rates promoting rapid lateral migration of channels, or (2) an arid climatic regime and limited vegetation allowing greater potential for lateral migration of channels, or (3) a strongly seasonal discharge resulting in flash flooding.

- Based on definitions of the sandy and muddy basins, the Himalayan Foreland Basin acted as sandy basin during the times of deposition of the Kamlial and Nagri formations, and as muddy basin during deposition period of the Chinji Formation.

- Red coloration of the Neogene mudstone of the Kohat Plateau most probably indicates deposition under hot, semi-arid and oxidizing diagenetic conditions. Furthermore, the values of the authigenic U, U/Th, V/Cr, Cu/Zn and Ni/Co of the Neogene molasse sediments suggest their deposition in oxidizing conditions.

- The greater abundance of feldspar (plagioclase) than clay minerals in the mudstone suggests high denudation rates or high relief or limited chemical weathering in the source area(s). The CIA values of sandstone of the Neogene sandstone (mostly 64 to 76) and mudstone (mostly 70 to 80) suggest moderate and slightly intense weathering of these sediments, respectively. However, ICV values, and low contents of Rb and Cs of the mudstone relative to UCC and PAAS indicate moderate degree of weathering.

- The presence of illite in the mudstone suggests cold and dry glacier conditions whereas kaolnite indicates warm and humid conditions. This conclusion favors a vast source area having markedly different climates in different parts or alternatively, an alternation between extreme climatic conditions.

- On the basis of modal mineralogy, the sandstones of the Kamlial, Chinji and Nagri formations of the southwestern Kohat Plateau fall into feldspathic and lithic arenites types. However, there appears to be a systematic spatial shift in sandstone composition: all the three formations from the Banda Assar syncline are totally lithic arenite while sandstone of the Chinji Formation from the Chashmai anticline is exclusively feldspathic arenite.

- The dominant petrographic characteristics of quartz in the Kamlial sandstone suggest its derivation partly from medium- and high-grade metamorphic rocks, with subsidiary contribution from low grade metamorphics, whereas quartz from sandstone of the overlying Chinji and Nagri formation indicates a subequal contribution from medium-high grade and low-grade metamorphic rock provenances. Spatial control over types of quartz grains is again noteworthy; the quartz grains from the Chashmai anticline indicate their derivation exclusively form medium- and high-grade metamorphic rocks for all the three formations whereas the quartz grains of all the three formations from the Banda Assar syncline and Bahadar Khel anticline suggest a dominant contribution from low grade metamorphic rocks. The relative dominance of polycrystalline quartz grains composed of 2-3 crystals (Qp_{2-3}) also proposes an origin from metamorphic source rocks. Similarly, the presence of mica and other heavy minerals indicate that the source area was composed of metamorphic rocks. Alike, the presence of illite in mudstone suggests a source area composed of low-grade metamorphic and sedimentary rocks. However, the relatively greater abundance of monocrystalline quartz suggests that the presence of granitic and volcanic rocks in the source areas cannot be ruled out, or else the quartz grains have traveled a longer distance of transportation.

- Spatial and temporal increase in the relative abundance of non-undulatory and undulatory monocrystalline quartz suggests plutonic/volcanic and metamorphic/ tectonically deformed source lithologies, respectively.

- The sandstones of the Neogene molasse sequence of the Kohat Plateau are characterized by the consistent presence of volcanic, sedimentary and low grade metamorphic lithic fragments. The sandstones in which L exceeds F, Q is moderate, and V/L is low are derived from highlands while the sandstones in which F exceeds L, Q is moderate, and V/L is low are derived from deeply eroded areas e.g., plutonic igneous rocks and high grade gneisses.

- The greater abundance of alkali feldspar than plagioclase in sandstone, and dominance of plagioclase in the associated mudstone suggest a major change in source area lithologies at time of erosion of these sediments. Dominance of plagioclase suggests source rocks of basic composition, which more readily alter to clay minerals than acidic rocks. The the lower values of Zr, Nb and Y in sandstone and mudstone indicate the consistent presence of mafic phases in the source area.

- The alkali feldspar is chemically more stable than plagioclase. Its higher abundance in sandstone indicates dominance of granite and acidic gneisses in the source area. Similarly, the relative abundance of different quartz types from the Kamlial, Chinji and Nagri formations is suggestive of a granitic and/or gneissic source.

- The modal composition of sandstone from the Kamlial, Chinji and Nagri formations suggest derivation from Magmatic Arc (MA), Recycled Orogens (RO) and a mixed provenance source.

- Plots of major element geochemical data on a variety of discriminatory diagrams indicate continental island arc and active continental margin (ACM) provenances for the sandstone of the three studied formations of southwestern Kohat. Similarly, discriminatory plot of SiO_2 vs log (K_2O/Na_2O) indicate a dominant influx from ACM for the studied sandstone. Other geochemical parameters like Fe_2O_3+MgO, TiO_2 and Al_2O_3/SiO_2 and contents of the major element oxides except MnO of the Neogene molasse sandstone show major provenance from continental island arc and partial influx from active continental margin settings.

- The content of MnO of these sandstones, however, suggest a source region composed dominantly of oceanic island arc, whereas, K_2O/NaO_2 ratio does not signify any particular provenance to these sediments, and therefore, should be used much carefully.

- The Th/U ratio of the Neogene molasse sequence is lower than the UCC and PAAS, which show that these sediments are first cycled in origin. But Zr/Sc ratio proposes minor contribution from recycled sedimentary sources.

- In regional tectonic scenario of the study area, it is assumed that the recycled orogen sediments are sourced from the Himalayan tectonic units, the active continental margin orogen sediments from the Asian active continental margin (the Trans-Himalaya and Karakoram) and the magmatic arc orogen sediments from the Kohistan-Ladakh arc.

- Ratios of the Ba/Sc, Ba/Co, Cr/Zr, Sc/Th and Y/Ni favor the presence of basic/ultrabasic rocks in the source area, however, those of La/Th, La/Sc, Th/Zr and plot of Th/Co vs La/Sc propose provenance similar to UCC/PAAS/felsic rocks.

- A significantly positive correlation of each of TiO_2, Zr, Rb and V with Al_2O_3 indicate a common association of all these elements with clay minerals and similar phases.

References:

Abbasi, I. A., 1989. Sedimentology and Structure of the Southern Kohat, Trans Indus Ranges, Pakistan. Unpub. Ph. D. Dissertation. Clare Collage, Cambridge.

Abbasi, I. A., 1991. Large scale vertical aggradations of sandstone in the Kamlial Formation of the Kohat Basin, Pakistan. Geol. Bull. Univ. Peshawar 24, 33-44.

Abbasi, I. A., 1994. Fluvial architecture and depositional system of the Miocene molasse sediments, Shakardara Formation, southeastern Kohat, Pakistan. Geol. Bull. Univ. Peshawar 27, 81-98.

Abbasi, I. A., 1998. Major pattern of fluvial facies and evolution of the Himalayan Foreland Basin, southeastern Kohat Plateau, Pakistan. In: Ghaznavi, M. I., Raza, S. M. and Hasan, M. T. (Eds.), Siwaliks of South Asia. Geol. Surv. Pakistan. 59-70.

Abbasi, I. A. & Friend, P. F., 1989. Uplift and evolution of the Himalayan orogenic belt, as recorded in the foredeep sediments. In: Derbyshire, E. and Owen, L. A. (Eds.), The Neogene of the Karakoram and Himalayas. Zeitschrift fur Geomorphologie. Spec. Pub. 76, 75-88.

Abbasi, I. A. & Friend, P. F., 2000. Exotic conglomerate of the Neogene Siwalik succession and their implications for the tectonic topographic evolution of the Western Himalaya. In: Khan, M. A., Treloar, P. J., Searle, M. P. and Jan, M. Q. (Eds.), Tectonics of the Nanga Parbat Syntaxis and the Western Himalaya. Geol. Soc. Lond. Spec. Pub. 170. 455-466.

Abbasi, I. A., Abid, I. A. & Khan, M. A., 1983. Statistical study of the Dhok Pathan Formation, Puki Gudikhel, Surghar Range, Karak. Geol. Bull. Univ. Peshawar 16, 85-96.

Abid, I. A., Abbasi, I. A., Khan, M. A. & Shah, M. T., 1983. Petrography and geochemistry of the Siwalik sandstone and its relationship to the Himalayan orogeny. Geol. Bull. Univ. Peshawar 16, 65-83.

Adams, C. G., Lee, D. E. & Rosen, B. R., 1990. Conflicting isotopic and biotic evidence for tropical sea-surface temperatures during the Tertiary. Palaeo. Palaeo. Palaeo. 77, 289-313.

Adams, J., 1980. Active tilting of the United States mid-continent: Geodetic and geomorphic evidence. Geology 8, 442-446.

Agarwal, K. K., Singh, I. B., Sharma, M., Sharma, S. & Rajagopalan, G., 2002. Extensional tectonic activity in the cratonward parts (peripheral bulge) of the Ganga Plain foreland basin, India. Int. J. Earth Science (Geol Rundsch), 91, 897-905.

Ahmad, R., Tipper, J. C. & Eggleton, R. A., 1994. Compositional trends in the Permian sandstones from the Denison Trough, Bowen Basin, Queensland reflect changing provenance and tectonics. Sediment. Geol. 89, 197-217.

Ahmad, T., Islam, R., Khanna, P. P. & Thakur, V. C., 1996. Geochemistry, petrogenesis and tectonic significance of the basic volcanic units of the Zildat ophiolitic melange, Indus suture zone, eastern Ladakh (India). Geodinamica Acta 9, 222-233.

Ahmad, T., Thakur, V. C., Islam, R., Khanna, P. P. & Mukherjee, P. K., 1998. Geochemistry and geodynamic implications of magmatic rocks from the Trans-Himalayan arc. Geochem. J., 32, 383-404.

Ahmad, T., Harris, N., Bickle, M., Chapman, H., Bunbury, J. & Prince, C., 2000. Isotopic constraints on the structural relationships between the Lesser Himalayan Series and the High Himalayan Crystalline Series, Garhwal Himalaya. Geol. Soc. Am. Bull. 112, 467-477.

A´lava, J. T. & Jaillard, E., 2005. Provenance of the Upper Cretaceous to Upper Eocene clastic sediments of the Western Cordillera of Ecuador: Geodynamic implications. Tectonophysics 399, 279-292.

Alam, M., Alam, M. M., Curray, J. R., Chowdhury, A. L. R. & Gani, M. R., 2003. An overview of the sedimentary geology of the Bengal basin in relation to the regional tectonic framework and basin-fill history. Sed. Geol. 155, 179-208.

Allègre, C. J., Courtillot, V., Tapponnier, P., Wirn, A., Mattauer, M., Coulon, C., Jaeger, J. J., Achache, J., Schaerer, U., Marcoux, J., Burg, J. P., Girardeau, J., Arrnijo, R., Gariepy, C., Goepel, C., Tindong, L., Xuchang, X., Chenfa, C., Guanggin, L., Baoyu, L., Jiwen, T., Naiwen, W., Guorning, C., Tonglin, H., Xibin, W., Wanmjng, D., Huaibin, S., Yougong, C., Ji, Z., Hongrong, Q., Peisheng, B., Songchan, W., Bixiang, W., Yaoxiu, Z. & Xu., R., 1984. Structure and evolution of the Himalaya-Tibet orogenic belt. Nature 307, 17-22.

Allen, J. R. L., 1965. A review of the origin and characteristics of recent alluvial sediments. Sediment. 5, 89-191.

Allen, J. R. L., 1978. Studies in fluviatile sedimentation: An exploratory quantitative model for the architecture of avulsion controlled alluvial suites. Sed. Geol. 21, 129-147.

Allen, J. R. L., 1982. Sedimentary Structures, Their Character and Physical Basis. Elsevier, Amsterdam, 1 and 2, 593 and 663p.

Allen, P. A., Homewood, P. & Williams, G. D., 1986. Foreland basins: An introduction. In: Allen, P. A. and Homewood, P. (Eds.), Foreland Basins. Int. Assoc. Sediment. Spec. Pub. 8, 3-12.

Amano, K. & Taira, A., 1992. Two-phase uplift of Higher Himalayas since 17 Ma. Geology 20, 391-394.

Amidon, W. H., Burbank, D. W. & Gehrels, G. E., 2005. U-Pb zircon ages as a sediment mixing tracer in the Nepal Himalaya. EPSL 235, 244-260.

Anczkiewicz, R. & Vance, D., 2000. Isotopic constraints on the evolution of metamorphic conditions in the Jijal-Patan complex and the Kamila Belt of the Kohistan arc, Pakistan Himalaya. Geol. Soc. Lond., Spec. Pub. 170, 321-331.

Anczkiewicz, R., Burg, J. P., Villa, I. M. & Meier, M., 2000. Late Cretaceous blueschist metamorphism in the Indus Suture Zone, Shangla region, Pakistan Himalaya, Tectonophysics 324, 111-134.

Appel, E., Rosler, W. & Corvinus, G., 1991. Magnetostratigraphy of the Miocene-Pleistocene Surai Khola Siwaliks in western Nepal. J. Geophys. Res. 105, 191-198.

Argles, T. W., 2000. The evolution of the Main Mantle thrust in the Western Syntaxis, Northern Pakistan. In: Khan, M. A., Treloar, P. J., Searle, M. P. and Jan, M. Q. (Eds.), Tectonics of the Nanga Parbat Syntaxis and the Western Himalaya. Geol. Soc. Lond., Spec. Pub. 170, 101-122.

Arita, K., 1983. Origin of the inverted metamorphism of the Lower Himalayas Central Nepal. Tectonophysics 95, 43-60.

Armstrong-Altrin, J. S. & Verma, S. P., 2005. Critical evaluation of six tectonic setting discrimination diagrams using geochemical data of Neogene sediments from known tectonic settings. Sed. Geol. 177, 115-129.

Armstrong-Altrin, J.S., Lee, Y., Verma, S. & Ramasamy, S., 2004. Geochemistry of sandstones from the Upper Miocene Kudanul Formation, southern India: Implications for provenance, weathering and tectonic setting. J. Sed. Res. 74, 167-179.

Ashmore, P. E., 1991. How do gravel-bed rivers braid? Can. J. Earth. Sci. 28,326-341.

Asiedu, D. K., Suzuki, S. & Shibata, T., 2000. Provenance of sandstones from the Lower Cretaceous Sasayama Group, Inner Zone of Southwest Japan. Sed. Geol. 131, 9-24.

Attaullah, M., 1970. The sediment load and measurements for their controlling rivers of West Pakistan. Report prepared for Planning Commission of Pakistan. 1 & 2, 214 & 320 pp.

Awasthi, N., 1982. Tertiary plant megafossils from the Himalaya - a review. The Paleobot 30, 254-267.

Azizullah & Khan, M. A., 1998. Lithostratigrapgy and depositional system of Siwaliks of Shinghar-Surghar Range, Thakhti Nasrati-Shanawah area, district Karak, Pakistan. In: Ghaznavi, M. I., Raza, S. M. and Hasan, M. T. (Eds.), Siwaliks of South Asia. Geol. Surv. Pakistan. 71-80.

Badgley, C. E., 1986. Taphonomy of mammalian fossil remains from Siwalik rocks of Pakistan. Paleobiology 12, 119-142.

Badgley, C. E. & Behrensmeyer, A. K., 1995. Two long geological records of continental ecosystems. Palaeo. Palaeo. Palaeo. 115, 1-11.

Bagati, T. N. & Kumar, R., 1994. Clay mineralogy of the Middle Siwalik sequence in the Mohand area. Dehra Dun: Implication for climate and source area. Him. Geol. 15, 219-228.

Bahlburg, H., 1998. The geochemistry and provenance of Ordovician turbidites in the Argentine Puna. In: Pankhurst, R. J. and Rapela, C.W. (Eds.), The Proto-Andean Margin of Gondwana. Geol. Soc. Lond. Spec. Pub. 142, 127-142.

Baig, M. A. S., 1984. Some observations about changes of fluvial system in Cis-Indus and Trans-Indus exposures of Dhok Pathan Formation. 1st Pakistan Geological Congress. Abstract.

Baker, J. C., Fielding, C. R., De Caritat, P. & Wilkinson, M. M., 1993. Permian evolution of sandstone composition in a complex backarc extensional to foreland basin: the Bowen Basin, Eastern Australia. J. Sediment. Petrol. 63, 881-893.

Bard, J. P., Maluski, H., Matte, P. & Proust, F., 1980. The Kohistan Sequence: Crust and mantle of an obducted island arc. Geol. Bull. Univ. Peshawar 13, 87-94.

Barry, J. C., Johnson, N. M., Raza S. M. & Jacobs, L. L., 1985. Neogene mammalian faunal change in southern Asia: Correlations with climatic, tectonic, and eustatic events. Geology 13, 637-640.

Barry, J. C., Morgan, M. E., Flynn, L. J., Pilbeam, D., Behrensmeyer, A. K., Raza, S. M., Khan, I. A., Badgley, C., Hicks, J. & Kelley, J., 2002. Faunal and environmental change in the late Miocene Siwaliks of northern Pakistan. Paleobiology Memoirs 3, 1-55 (Supplement to Paleobiology 28 (2)).

Basu, A., 1976. Petrology of Holocene fluvial sand derived from plutonic source rocks: Implication to plaeoclimatic interpretations. J. Sed. Pet. 46, 694-709.

Basu, A., 1985. Influence of climate and relief on composition of sands released at source area. In: Zuffa, G. G. (Ed.), Provenance of Arenites: Dordrecht, The Netherlands, Reidel Publishing Company, Nato Advanced Study Institute Series 148, 1-18.

Basu, A., Young, S. W., Suttner, L. J., James, W. C. & Mack, G. H., 1975. Re-evaluation of the use of undulatory extinction in detrital quartz for provenance interpretation. J. Sed. Petrol. 45, 873-882.

Bauluz, B., Mayayo, M. J., Fernandez-Nieto, C. & Lopez, J. M. G., 2000. Geochemistry of Precambrian and Paleozoic siliciclastic rocks from the Iberian Range NE Spain: Implications for source-area weathering, sorting, provenance, and tectonic setting. Chem. Geol. 168, 135-150.

Beaumont, C., 1981. Foreland Basins. Geoph. J. Royal Astronomical Soc. 65, 291-329.

Beck, R. A., & Burbank, R. W., 1990. Continental-scale diversion of rivers: A control of alluvial stratigraphy. Geol. Soc. Am. Abstracts with Programs, 22, 238p.

Beerbower, J. R., 1964. Cyclothems and cyclic depositional mechanism in alluvial plain sedimentation. Kansas Geol. Surv. Bull. 169, 31-42.

Behrensmeyer, A. K., 1987. Miocene fluvial facies and vertebrate taphonomy in northern Pakistan. In: Ethridge, G., Flores, R. M. and Harvey, M. D. (Eds.), Recent Developments in Fluvial Sedimentology. Spec. Pub. Soc. Econ. Paleont. Mineral. 39, Tulsa, 169-176.

Behrensmeyer, A. K. & Tauxe, L., 1982. Isochronous fluvial systems in Miocene deposits of northern Pakistan. Sediment. 29, 331-352.

Bentham, P. A., Talling, P. J. & Burbank, D. J., 1993. Braided stream and floodplain deposition in a rapidly aggrading basin: the Escanilla Formation, Spanish Pyrenees. In: Best, J. L. and Bristow, C. S. (Eds.) Braided Rivers. Geol. Soc. Spec. Pub. 75, 177-194.

Besly, B. M., Burley, S. D. & Turner, P., 1993. The late Carboniferous “Barren Red Bed” play of the Silver Pit area, southern North Sea. In: Parker, J. R. (Ed.), Petroleum Geology of Northwest Europe. Proceedings of the 4th conference. Geol. Soc. Lond., 727-740.

Bhatia, M. R., 1983. Plate tectonics and geochemical composition of sandstones. J. Geol. 91, 611-627.

Bhatia, M. R., 1985a. Composition and classification of Paleozoic flysch mudrocks of eastern Australia: Implication in provenance and tectonic setting interaction. Sed. Geol. 41, 249-268.

Bhatia, M. R., 1985b. Rare earth elements geochemistry of Australian Paleozoic graywackes and mudrocks: Provenance and tectonic control. Sed. Geol. 45, 97-113.

Bhatia, M. R. & Crook, K. A. W., 1986. Trace element characteristics of graywackes and tectonic setting discrimination of sedimentary basins. Contribution Miner. Pet. 92, 181-193.

Bhatia, M. R. & Taylor, S. R., 1981. Trace-element geochemistry and sedimentary provinces: A study from the Tasman geosyncline Australia. Chem. Geol. 33, 115-125.

Bhatia, S. B., 1982. Facies, fauna and flora in the lower Tertiary formations of Northwestern Himalaya: A synthesis: Cenozoic stratigraphy, palynology in India. Palaeontol. Soc. India Spec. Pub. 1, 8-20.

Bignold, S. M. & Treloar, P. J., 2003. Northward subduction of the Indian Plate beneath the Kohistan island arc, Pakistan Himalaya: New evidence from isotopic data. J. Geol. Soc. Lond. 160, 377-384.

Bignold, S. M. & Treloar, P. J., 2006. Changing sources of magma generation beneath intra-oceanic island arcs: An insight from the juvenile Kohistan island arc, Pakistan Himalaya. Chem. Geol. 233, 46-74.

Biju-Duval, B., 2002. Sedimentary Geology. Technip, Paris.

Biscaye, P. E., 1965. Mineralogy and sedimentation of the recent deep-sea clay in the Atlantic Ocean and adjacent seas and oceans. Geol. Soc. Am. Bull. 76, 803-832.

Bjorlykke, K., 1974. Geochemical and mineralogical influence of Ordovician island arcs on epicontinental clastic sedimentation: A study of Lower Palaeozoic sedimentation in the Oslo region, Norway. Sediment. 21, 251-272.

Blair, T. C. & Bilodeau, W. L., 1988. Development of tectonic cyclothems in rift, pull-apart, and foreland basins: Sedimentary response to episodic tectonism. Geology 16, 517-520.

Blatt, H., 1967. Provenance determination and recycling of sediments. J. Sed. Pet. 37, 1031-1044.

Blatt, H., Middleton, G. V. & Murray, R. C., 1980. Origin of Sedimentary Rocks. Prentice Hall Inc., 87.

Bluck, B. J., 1971. Sedimentation in the meandering River Endrick. Scott. J. Geol. 7, 93-138.

Bock, B., McLennan, S. M. & Hanson, G. N., 1998. Geochemistry and provenance of the Middle Ordovician Austin Glen Member (Normanskill Formation) and Taconian Orogeny in New England. Sediment. 45, 635-655.

Boggs, S., 1968. Experimental study of rock fragments. J. Sed. Pet. 38, 1326-1339.

Boggs, S., 1992. Sedimentary Petrology. Blackwell Scientific Publications.

Boggs, S. & Seyedolali, S., 1992. Provenance of Miocene Sandstones from Sites 796, 797 and 799, Japan Sea. In: Pisciotto, K. A., Ingle, J. C, Jr., von Breymann, M. T, Barron, J., 1992. Proceedings of the Ocean Drilling Program, Scientific Results. 127/128.

Bonis, N. R., 1985. Paleomagnetic analysis of Siwaliks strata in the Trans Indus Region, northwestern Pakistan, Unpub. B. A. thesis, Darthmouth Collage, Hanover, N. H. 35p.

Bookhagen, B., Thiede, R. & Strecker, M. R., 2005. Abnormal monsoon years and their control on erosion and sediment flux in the high, arid northwest Himalayas. EPSL 231, 131-146.

Bossart, P. & Ottiger, R., 1989. Rocks of the Murree formation in northern Pakistan: Indicators of a descending foreland basin of Late Paleocene to Middle Eocene age. Eclogae Geologicae Helveticae 82, 133-165.

Breyer J. A. & Bart, H. A., 1978. The composition of fluvial sands in a temperate semiarid region. J. Sed. Pet. 48, 1311-1320.

Bridge, J. S., 1993. The interaction between channel geometry, water flow, sediment transport and deposition in braided rivers. In: Best, J. L. and Bristow, C. S. (Eds.) Braided Rivers. Geol. Soc. Spec. Pub. 75, 13-71.

Bridge, J. S. & Diemer, J. A., 1983. Quantitative interpretation of an evolving river system. Sediment. 30, 599-623.

Bridge, J. S. & Leeder, M. R., 1979. A simulation model of alluvial stratigraphy. Sediment. 26, 617-644.

Bridge, J. S. & Mackey, S. D., 1993. A revised alluvial stratigraphic model. In: Marzo, M. and Puigdefabregas, C. (Eds.), Alluvial Sedimentation. Spec. Pub. Int. Assoc. Sediment. 17, 319-336.

Bristow, C. S., 1987. Brahmaputra River: Channel migration and deposition. In: Ethridge, G., Flores, R. M. and Harvey, M. D. (Eds.), Recent Developments in Fluvial Sedimentology. Spec. Pub. Soc. Econ. Paleont. Mineral. 39, Tulsa, 63-74.

Brookfield, M. E., 1998. The evolution of the great river systems of southern Asia during the Cenozoic India-Asia collision: Rivers draining southwards. Geomorphology 22, 285-312.

Brozovic, N. & Burbank, D. W., 2000. Dynamic fluvial systems and gravel progradation in the Himalayan foreland. Geol. Soc. Am. Bull. 112, 394-412.

Burbank, D. W., 1983. The chronology of intermontane-basin development in the northwestern Himalaya and the evolution of the Northwest Syntaxis. EPSL. 64, 77-92.

Burbank, D. W., 1992. Causes of recent Himalayan uplift deduced from depositional patterns in the Ganges basin. Nature 357, 680-683.

Burbank, D. W. & Beck, R. A., 1989. Early Pliocene uplift of the Salt Range: Temporal constraints on thrust wedge development, northwest Himalaya, Pakistan. In: Malinconico, L. L. Jr. and Lillie, R. J. (Eds.), Tectonics of the Western Himalaya. Geol. Soc. Am. Spec. Paper 232, 113-128.

Burbank, D. W. & Beck, R. A., 1991. Models of aggradation versus progradation in the Himalayan foreland. Geologische Rundschau 80, 623-638.

Burbank, D. W. & Raynolds, R. G. H., 1984. Sequential late Cenozoic structural disruption of the northern Himalayan foredeep. Nature 311, 114-118.

Burbank, D. W. & Raynolds, R. G. H., 1988. Stratigraphic keys to the timing of thrusting in terrestrial foreland basins: Applications to the northwestern Himalaya. In: Kleinspehn, K. L. and Paola, C. (Eds.), New Perspectives in Basin Analysis. Springer-Verlag, New York, 331-351.

Burbank, D. W., Derry, L., & France-Lanord, C., 1993. Lower Himalayan detrital sediment delivery despite an intensified monsoon at 8 Ma. Nature 364, 48-50.

Burbank, D. W., Beck, R. A. & Mulder, T., 1996. The Himalayan Foreland. In: Yin, A. and Harrison, T. M. (Eds.), The Tectonic Evolution of Asia. Cambridge University Press, Cambridge. 149-188.

Burbank, D. W., Blythe, A. E., Putkonen, J., Pratt-Sitaula, B., Gabet, E., Oskin, M., Barros, A. & Ojha, T. P., 2003. Decoupling of erosion and precipitation in the Himalayas. Nature 426 (6967), 652-655.

Burchfiel, B. D., Zhileng, C., Hodges, K. V., Yuping, L., Royden, L. H., Changrong, D. & Jiene, X., 1992. The South Tibetan Detachment System, Himalayan Orogen: Extension contemporaneous with and parallel to shortening in a collisional mountain belt. Geol. Soc. Am. Spec. Paper, 269, 41p.

Burg, J. P., Proust, F.,Tapponnier, P. & Chen, G., 1983. Deformation phases and tectonic evolution of the Lhasa block (southern Tibet, China). Eclogae Geologicae Helvetiae 76, 643-665.

Burg, J. P., Brunel, M., Gapais, D., Chen, G. M. & Liu, G. H., 1984. Deformation of leucogranites of the crystalline main central sheet in southern Tibet (China). J. Struc. Geol. 6, 535-542.

Burg, J. P., Leyreloup, A., Girardeau, J. & Chen, G. M., 1987. Structure and metamorphism of a tectonically thickened continental crust-the Yalu Tsangpo suture zone (Tibet). Philos. Transac. Royal Soc. Lond. Series A 321, 67-86.

Burg, J. P., Chaudhry, M. N., Ghazanfar, M., Anczkiewicz, R. & Spencer, D., 1996. Structural evidence for back sliding of the Kohistan arc in the collisional system of northwest Pakistan. Geology 24, 739-742.

Burnett, A. W. & Schumm, S. A., 1983. Active tectonics and river response in Louisiana and Mississippi. Science 222, 49-50.

Burnett, D. J. & Quirk, D. G., 2001. Turbidite provenance in the Lower Paleozoic Manx Group, Isle of man; implications for the tectonic setting of Eastern Avalonia. J. Geol. Soc. Lond. 158, 913-924.

Butler, R. & Prior, D. J., 1988. Anatomy of a continental subduction zone: The Main Mantle Thrust in North Pakistan. Geol. Rundsch. 77, 239-255.

Buurman, P., 1980. Palaeosols in the Reading Beds (Raleocene) of Alum Bay, Isle of Wight, U.K. Sediment. 27, 593-606.

Calkin, J. A., Offield, T. W., Abdulah, S. K. M. & Tayyab, A. S., 1975. Geology of the southern Himalayan in Hazara, Pakistan, and adjacent areas. USGS Prof. Paper 716-C, 29 pp.

Campbell, J. E. & Hengry, H. E., 1987. Anatomy of a gravelly meander lobe in the Saskatchewan River, near Nipawin Canada. In: Bridge, E. G., Flores, R. M. and Harvey, M. D. (Eds.) Recent Developments in Fluvial Sedimentology. Spec. Pub. Soc. Econ. Paleon. and Mineral. 39, 179-189.

Carroll, D., 1970. Clay minerals: A guide to their X-ray identification. Boulder, Colorado, Geol. Soc. Am. Spec. Paper 126, 80 p.

Catlos, E. J., Harrison, T. M. & Dubey, C. S., 2003. MCT duplex formation in the Sikkim Himalaya. 18th Himalaya-Karakoram-Tibet Workshop, Ascona, Switzerland, Abstract volume, 29.

Catuneanu, O., Beaumont, C. & Waschbusch, P., 1997. Interplay of static loads and subduction dynamics in foreland basins: Reciprocal stratigraphies and the missing peripheral bulge. Geology 25, 1087-1090.

Catuneanu, O., Sweet, A. R. & Miall, A. D., 2000. Reciprocal stratigraphy of the Campanian-Paleocene Western Interior of North America. Sed. Geol. 134, 235-255.

Cerling, T. E., Wang Y. & Quade, J., 1993. Expansion of C4 ecosystems as an indicator of global ecological change in the Late Miocene. Nature 361, 344-345.

Cerveny, P. F., Naeser, N. D., Zeitler, P. K., Naeser, C. W. & Johsnon, N. M., 1988. History of uplift and relief of the Himalaya during the past 18 million years: Evidence from fission-track ages of detrital zircons from sandstones of the Siwalik Group. In: Kleinspehn, K. L. and Paola, C. (Eds.), New perspectives in Basin Analysis. Springer-Verlag Inc., Berlin and New York, 43-61.

Cerveny, P. F., Johnson, N. M., Tahirkheli, R. A. K. & Bonis, N. R., 1989. Tectonic and geomorphic implications of Siwalik Group heavy minerals, Potwar Plateau, Pakistan. In: Malinconico, L. L. and Lillie, R. J. (Eds.), Tectonics and Geophysics of the Western Himalaya. Geol. Soc. Am. Spec. Paper 232, 129-136.

Chamberlain, C. P. & Zeitler, P. K., 1996. Assembly of the crystalline terrains of the northwestern Himalaya and Karakoram, northwestern Pakistan. In: An, Y. and Harrison, M. (Eds.), The Tectonic Evolution of Asia, Cambridge University Press, Cambridge. 138-148.

Chamley, H., 1989. Clay Sedimentology. Springer-Verlag, New York, 623p.

Chaudhry, M. N. & Ghazanfar, M., 1990. Position of the Main Central Thrust in the tectonic framework of Western Himalaya. Tectonophysics 174, 32 1-329.

Clift, P. D., 2002. A brief history of the Indus River. In: Clift, P. D., Kroon, D., Craig, J. and Gaedicke, C. (Eds.), The Tectonic and Climatic Evolution of the Arabian Sea Region. Geol. Soc. Lond. Spec. Pub. 195, 237-258.

Clift, P. D. & Blusztajn, J., 2005. Reorganization of the western Himalayan river system after five million years ago. Nature 438, 1001-1003.

Clift, P. D. & Gaedicke, C., 2002. Accelerated mass flux to the Arabian Sea during the middle to late Miocene. Geology 30, 207-210.

Clift, P. D., Shimizu, N. U., Layne, G. & Blusztajn, J., 2001a.Tracing patterns of unroofing in the Early Himalaya through microprobe Pb isotope analysis of detrital K-feldspar in the Indus molasse, India. EPSL 188, 475-491.

Clift, P. D., Shimizu, N., Layne, G. D., Blusztajn, J., Gaedicke, C., Schluter, H. U., Clark, M. K. & Amjad, S., 2001b. Development of the Indus Fan and its significance for the erosional history of the western Himalaya and Karakoram. Geol. Soc. Am. Bull. 113, 1039-1051.

Clift, P. D., Carter, A., Krol, M. & Kirby, E., 2002a. Constraints on India-Eurasia collision in the Arabian sea region taken from the Indus Group, Ladakh Himalaya, India). In: Clift, P. D., Kroon, D., Craig, J. and Gaedicke, C. (Eds.), The Tectonic and Climatic Evolution of the Arabian Sea Region. Geol. Soc. Lond. Spec. Pub. 195, 97-116.

Clift, P. D., Lee, J. I., Hildebrand, P., Shimizu, N., Layne, G. D., Blusztajn, J., Blum, J. D., Garzanti, E. & Khan, A. A., 2002b. Nd and Pb isotope variability in the Indus River system: Implications for sediment provenance and crustal heterogeneity in the Western Himalaya. EPSL 200, 91-106.

Cojan, I., 1993. Alternating fluvial and lacustrine sedimentation: Tectonic and climatic controls (Provence Basin, S. France, Upper Cretaceous/Paleocene). Spec. Pub. Int. Ass. Sediment. 17, 425-438.

Cojan, I. & Renard, M., 1999. Sedimentology. Oxford and IBH Publishing Co. Pvt. Ltd.

Coleman, J. M., 1969. Brahmaputhra River: Channel processes and sedimentation. Sed. Geol. 3, 129-239.

Collinson, J. D., 1996. Alluvial sediments. In: Reading, H. G. (Ed.), Sedimentary Environments: Processes, Facies and Stratigraphy. Blackwell, Oxford, 37-82.

Condie, K. C., 1991. Another look at rare earth elements in shales. Geochim. Cosmochim. Acta 55, 2527-2531.

Condie, K. C., 1993. Chemical composition and evolution of the upper continental crust: Contrasting results from surface samples and shales. Chem. Geol. 104, 1-37.

Condie, C. K., Noll Jr., P. D. & Conway, C. M., 1992. Geochemical and detrital mode evidence for two sources of Early Proterozoic sedimentary rocks from the Tonto Basin Supergroup, central Arizona. Sediment. Geol. 77, 51-76.

Connor, J. J., 1990. Geochemical stratigraphy of the Yellowjacket Formation (Middle Proterozoic) in the area of the Idaho Cobalt Belt, Lemhi County, Idaho, with Analytical contributions from A.J. Bartel, E. Brandt, P.H. Briggs, S. Danahey, D. Fey, D.B. Hatfield, M. Malcolm, V. Merritt, G. Riddle, S. Roof, K. Stewart, J. Storey, J.E. Taggart, Jr., and R.B. Vaughn. U.S. Geol. Surv. Open-File Report 90-0234 (Part A, Discussion, 29 p.; Part B, Geochemical data files, 1 diskette).

Cook, H. E., Johnson, P. D., Matti, J. C. & Zemmels, I., 1975. Methods of sample preparation and X-ray diffraction data analysis, X-ray mineralogy laboratory, deep sea drilling project, Univ. of California, Riverside. Initial Rep. Deep Sea Drill. Proj. 28, 999-1007.

Copeland, P., 1993. Two-phase uplift of Higher Himalayas since 17 Ma: Comment and reply. Geology 21, 188-190.

Cotter, G. De-P., 1933. Geology of part of the Attock district west of longitude 72° 45 E. Geol. Surv. India. Mem. 55, 63-161.

Coulon, C., Maluski, H., Bollinger, C. & Wang, S., 1986. Mesozoic and Cenozoic volcanic rocks from central and southern Tibet: ^{39}Ar-^{40}Ar dating, petrological characteristics and geodynamical significance. EPSL. 79, 281-302.

Coward, M. P., 1985. A section through the Nanga Parbat Syntaxis, Indus Valley, Kohistan. Geol. Bull. Univ. Peshawar 18, 147-152.

Coward, M. P., Windley, B. F., Broughton, R. D., Luff, I. D., Petterson, M. G., Pudsey, C. J., Rex, D. C. & Khan, M. A., 1986. Collision tectonics in the NW Himalaya. In: Coward, M. P. and Ries, A. C. (Eds.), Collision Tectonics. Geol. Soc. Spec. Pub. 19, 203-219.

Coward, M. P., Butler, R. W. H., Khan, M. A. & Knipe, R. J., 1987. The tectonic history of Kohistan and its implications for Himalayan structure. J. Geol. Soc., Lond., 144, 377-391.

Coward, M. P., Butler, R. W. H., Chambers, A. F., Graham, R. H., Izatt, Khan, M. A., Knipe, R. J., Prior, D. J., Treloar, P. J. & Williams, M. P., 1988. Folding and Imbrication of the Indian crust during the Himalayan collision. Philosoph. Transac. Royal Soc. Lond. 326, 89-116.

Cox, R. & Lowe, D. R., 1996. Quantification of the effects of secondary matrix on the analysis of sandstone composition, and a petrographic-chemical technique for retrieving original framework grain modes of altered sandstones. J. Sed. Res. 66, 548-558.

Cox, R., Lowe, D. R. & Cullers, R. L., 1995. The influence of sediment recycling and basement composition on evolution of mudrock chemistry in the southwestern United States. Geochim. Cosmochim. Acta 59, 2919-2940.

Crichton, J. G. & Condie, K. C., 1993. Trace elements as source indicators in cratonic sediments: A case study from the Early Proterozoic Libby Creek Group, southeastern Wyoming. J. Geology 101, 319-332.

Critelli, S. & Garzanti, E., 1994. Provenance of the Lower Tertiary Murree Redbeds (Hazara-Kashmir Syntaxis, Pakistan) and initial rising of the Himalayas. Sed. Geol. 89, 265-284.

Critelli, S. & Ingersoll, R. V., 1994. Sandstone petrology and provenance of the Siwalik Group (northwestern Pakistan and western-southwestern Nepal). J. Sed. Res. 64, 815-823.

Critelli, S., Le Pera, E. & Ingersoll, R. V., 1997. The effects of source lithology, transport, deposition and sampling scale on the composition of southern California sand. Sediment. 44, 653-671.

Crook, K. A. W., 1974. Lithogenesis and geotectonics, the significance of compositional variations in flysch arenites (graywackes). In: Dott, R. H. and Saver, R. H. (Eds.), Modern and Ancient Geosynclinal Sedimentation. Soc. Econ. Paleont. Mineral. Spec. Pub. 91, 304-310.

Crowley, S. F., Stow, A. D. W. & Croudace, I. W., 1998. Mineralogy and geochemistry of Bay of Bengal deep sea fan sediments, ODP Leg 116. Evidence for an Indian subcontinent contribution to detrital fan sedimentation. In: Cramp, A., Macleod, C. J., Lee, S. V. and Jones, E. J. W. (Eds.), Geological Evolution of Ocean Basins: Results from the Ocean Drilling Program. Geol. Soc. Lond. Spec. Pub. 131, 151-176.

Cullers, R. L., 1988. Mineralogical and chemical changes of soil and stream sediment formed by intense weathering of the Danberg granite, Georgia, U.S.A. Lithos 2I, 301-314.

Cullers, R. L., 1993. The chemical signature of source rocks in size fractions of Holocene stream sediment derived from metamorphic rocks in the Wet Mountains region, Colorado, U.S.A. Chem. Geol. 113, 327-343.

Cullers. R. L., 1994. The controls on the major and trace element variation of shales, siltstones, and sandstones of Pennsylvanian- Permian age from uplifted continental blocks in Colorado to platform sediment in Kansas, USA. Geochim. Cosmochim. Acta. 58, 4955-4972.

Cullers, R. L., 1995. The controls on the major and trace element evolution of shales, siltstones and sandstones of Ordovician to Tertiary age in the Wet Mountain region, Colorado, U.S.A. Chem. Geol. 123, 107-131.

Cullers, R. L., 2000. The geochemistry of shales, siltstones and sandstones of Pennsylvanian-Permian age, Colorado, USA: Implications for provenance and metamorphic studies. Lithos 51, 181-203.

Cullers, R. L., 2002. Implications of elemental concentrations for provenance, redox conditions, and metamorphic studies of shales and limestones near Pueblo, CO, USA. Chem. Geol. 191, 305-327.

Cullers, R. L. & Stone, J., 1991. Chemical and mineralogical comparison of the Pennsylvanian Fountain Formation, Colorado, U.S.A. (an uplifted continental block), to sedimentary rocks from other tectonic environments. Lithos 28, 115-131.

Cullers, R. L., Chaudhuri, S., Kilbane, N. & Koch, R., 1979. Rare earths in size fractions and sedimentary rocks of Pennsylvanian-Permian age from the mid-continent of the U.S.A. Geochim. Cosmochim. Acta. 43, 1285-1302.

Cullers, R. L., Barrett, T., Carlson, R. & Robinson, B., 1987. Rare- earth element and mineralogic changes in Holocene soil and stream sediment: A case study in the Wet Mountains, Colorado, U.S.A. Chem. Geol. 63, 275-297.

Cullers, R. L., Basu, A. & Suttner, L. J., 1988. Geochemical signature of provenance in sand-size material in soils and stream sediments near the Tobacco Root batholith, MT, USA. Chem. Geol. 70, 335-348.

Dabbagh, M. E. & Rogers, J. J., 1983. Depositional environments and tectonic significance of the Wajid Sandstone of southern Saudi Arabia. J. African Earth Sciences 1, 47-57.

Dadson, S. J., Hovius, N., Chen, H. G., Dade, W. B., Hsieh, M. L., Willett, S. D., Hu, J. C., Horng, M. J., Chen, M. C., Stark, C. P., Lague, D. & Lin, J. C., 2003. Links between erosion, runoff variability and seismicity in the Taiwan orogen. Nature 426 (6967), 648-651.

Dahlstrom, C. D. A., 1970. Structural geology in the eastern margin of the Canadian Rocky Mountains. Bull. Can. Petrol. Geol. 18, 332-406.

Daniel, C. G., Hollister, L. S., Parrish, R. R. & Grujic, D., 2003. Exhumation of the Main Central Thrust from lower crustal depths, Eastern Bhutan Himalaya. J. Met. Geol. 21, 317-334.

Davies, D. K. & Etheridge, F. G., 1975. Sandstone composition and depositional environments. Am. Assoc. Petrol. Geol. Bull. 59, 239-264.

De`zes, P. J., Vannay, J. C., Steck, A., Bussy, F. & Cosca, M., 1999. Synorogenic extension: Quantitative constraints on the age and displacement of the Zanskar shear zone (northwest Himalaya). Geol. Soc. Am. Bull. 111, 364-374.

Debon, F., LeFort, P., Sherpard, S. M. F. & Sonet, J., 1986. The plutonic belts of the Transhimalaya and Himalaya-a chemical, mineralogical, isotopic, and chronological synthesis along a Tibet-Nepal section. J. Pet. 27, 219-250.

Debon, F., Le Fort, P., Dautel, D., Sonet, J. & Zimmermann, J. L., 1987. Granites of western and northern Kohistan (Pakistan): A composite Mid-Cretaceous to Upper Cenozoic magmatism. Lithos 20, 19-40.

DeCelles, P. G., 1986. Sedimentation in a tectonically partitioned, nonmarine foreland basin: The Lower Cretaceous Kootenai Formation, southwestern Montana. Geol. Soc. Am. Bull. 97, 911-931.

DeCelles, P. G., 1988. Lithologic provenance modeling applied to the Late Cretaceous synorogenic Echo Canyon Conglomerate, Utah: A case of multiple source areas. Geology 16, 1039-1043.

DeCelles, P. G. & Giles, K. A., 1996. Foreland basin systems. Basin Res. 8, 105-123.

DeCelles, P. G., Gehrels, G. E., Quade, J. & Ojha, T. P., 1998a. Eocene-Early Miocene foreland basin development and the history of Himalayan thrusting, western and central Nepal. Tectonics 17, 741-765.

DeCelles, P. G., Gehrels, G. E., Quade, J., Ojha, T. P., Kapp, P. A. & Upreti, B. N., 1998b. Neogene foreland basin deposits, erosional unroofing and the kinematic history of the Himalayan fold-thrust belt, western Nepal. Geol. Soc. Am. Bull. 110, 2-21.

DeCelles, P. G., Robinson, D. M., Quade, J., Ojha, T. P., Garzione, C. N., Copeland, P. & Upreti, B. N., 2001. Stratigraphy, structure and tectonic evolution of the Himalayan fold-thrust belt in western Nepal. Tectonics 20, 487-509.

Decker, J. & Helmold, K. P., 1985. The effect of grain size on detrital modes: A test of the Gazzi-Dickinson point-counting method-discussion. J. Sed. Pet. 55, 619.

Dewey, J. F., Shackelton, R. M., Chang, C. & Sun, Y., 1988. The tectonic evolution of the Tibetan Plateau. Philosoph. Transac. Royal Soc. Lond. Series A327, 379-413.

Dewey, J. F., Cande, S. & Pitman, W. C., 1989. Tectonic evolution of the India/Eurasia collision zone. Eclogae Geologicae Helvetiae 82, 717-734.

Dickinson, W. R., 1970. Interpreting detrital modes of greywacke and arkose. J. Sed. Pet. 40, 695-707.

Dickinson, W. R., 1974. Plate tectonics and sedimentation. In: Dickinson, W. R. (Ed.), Tectonics and Sedimentation. Soc. Econo. Paleont. Mineral. Spec. Pub. 22, 1-27.

Dickinson, W. R., 1976. Plate Tectonic Evolution of Sedimentary Basins. Am. Assoc. Petrol. Geol. Continuing Education Course Notes Series 1, 62pp.

Dickinson, W. R., 1985. Interpreting provenance relations from detrital modes of sandstones. In: Zuffa, G. G. (Ed.), Provenance of Arenites Dordrecht. The Netherlands, Reidel Publishing Company, NATO Advanced Study Institute Series 148, 333-361.

Dickinson, W. R., 1988. Provenance and sediment dispersal in relation to paleotectonics and paleogeography of sedimentary basins. In: Kleinspehn, K. L. and Paola, C. (Eds.), New Perspectives in Basin Analysis. Springer-Verlag, New York. 3-25.

Dickinson, W. R. & Rich, E. I., 1972. Petrologic intervals and petrofacies in the Great Valley sequence, Sacramento Valley, California. Geol. Soc. Am. Bull. 93, 3007-3024.

Dickinson, W. R. & Suczek, C. A., 1979. Plate tectonics and sandstone composition. Am. Ass. Petrol. Geol. Bull. 63, 2164-2182.

Dill, H., 1986. Metallogenesis of early Paleozoic graptolite shales from the Graefenthal Horst (northern Bavaria-Federal Republic of Germany). Econ. Geol. 81, 889-903.

Dill, H., Teshner, M. & Wehner, H., 1988. Petrography, inorganic and organic geochemistry of Lower Permian Carboniferous fan sequences (Brandschiefer Series) FRG. Constraints to their palaeogeography and assessment of their source rock potential. Chem. Geol. 67, 307-325.

DiPietro, J. A. & Isachsen, C. E., 2001. U-Pb zircon ages from the Indian plate in northeast Pakistan and their significance to Himalayan and pre-Himalayan geologic history. Tectonics 20, 510-525.

DiPietro, J. A. & Pogue, K. R., 2004. Tectonostratigraphic subdivisions of the Himalaya: A view from the west. Tectonics 23, TC5001. doi:10.1029/2003TC001554.

DiPietro, J. A., Hussain, A., Ahmad, I. & Khan, M. A., 2000. The main mantle thrust in Pakistan: Its character and extent. In: Treloar, P. J. and Searle, M. P. (Eds.), Himalayan Tectonics. Geol. Soc. Lond. Spec. Pub. 74, 375-393.

Doeglas, D. J., 1962. The structures of sedimentary deposits of braided rivers. Sediment. 1, 167-190.

Downing, K. F., Lindsay, E. H., Downs, W. R. & Speyer, S. E., 1993. Lithostratigraphy and vertebrate biostratigraphy of the early Miocene Himalayan Foreland, Zinda Pir Dome, Pakistan. Sed. Geol. 87, 25-37.

Dubey, N. & Chatterjee, B. K., 1997. Sandstones of Mesozoic Kachchh Basin: Their provenance and basinal evolution. Indian J. Petrol. Geol. 6, 55-68.

Dupuis, C., He´bert, R., Dubois-Coˆte, V., Guilmette, C., Wang, C. S. & Li, Z. J., 2006. Geochemistry of sedimentary rocks from me´lange and flysch units south of the Yarlung Zangbo suture zone, southern Tibet. J. Asian Earth Sciences 26, 489-508.

Dypvik, H., 1984. Geochemical compositions and depositional conditions of Upper Jurassic and Lower Cretaceous Yorkshire clays, England. Geol. Mag. 121, 489-504.

Eames, F. E., 1952. A contribution to the study of Eocene in the western Pakistan and eastern India, Part A: The geology of the standard section in western Punjab and in Kohat district. Geol. Soc. Lond. Quart. Jour. 107, 159-172.

Edwards, M. A. & Harrison, T. M., 1997. When did the roof collapse? Late Miocene north-south extension in the High Himalaya revealed by Th-Pb monazite dating of the Khula Kangri granite. Geology, 25, 543-546.

Einsele, G., 1992. Sedimentary Basins: Evolution, Facies and Sediment Budget. Springer-Verlag, Berlin Heidelberg New York. 628p.

Einsele, G. & Hinderer, M., 1997. Terrestrial sediment yield and the lifetimes of reservoirs, lakes and larger basins. Geol. Rundsch. 86, 288-310.

Elliott, T., 1974. Interdistributary bay sequences and their genesis. Sediment. 21, 611-622.

Emery, D. & Myers, K. J. (Eds.), 1996. Sequence Stratigraphy. Blackwell Scientific Publication.

Ergin, M., 1995. Effects of fine grain size on distribution in shallow and deep black sea sediments: A comparison between oxic and anoxic depositional environments. Geo-Marine Letters 15, 51-58.

Eriksson, P. G., Schreiber, U. M., Reczko, B. F. & Snyman, C. P., 1994. Petrography and geochemistry of sandstones interbedded with the Rooiberg Felsite Group (Transvaal sequence, south Africa): Implication for provenance and tectonic setting. J. Sed. Res. A64, 836-846.

Ernst, T. W., 1970. Geochemical Facies Analysis. Elsevier, Amsterdam, 152 p.

Ethridge, F. G., Jackson, T. J. & Youngberg, A. D., 1981. Flood-basin sequence of a fine grained meanderbelt subsystem: The coal bearing Lower Wasatch and Upper Fort Union Formations, South Powder River Basin, Wyoming. In: Ethridge, F. G. and Flores, R. M. (Eds.), Recent and Ancient Nonmarine Depositional Environments: Models for exploration. Soc. Econ. Paleon. Mineral. Spec. Pub. 31, 191-212.

Fatmi, A., 1973. Lithostratigraphic units of the Kohat-Potwar Province, Indus Basin, Pakistan. Geol. Surv. Pakistan Mem. 10.

Fedo, C. M. & Cooper, J. D., 1989. Braided fluvial to marine transition: The basal lower Cambrian Wood Canyon Formation, southern Marble Mountains, Mojave Desert, California. J. Sed. Pet. 60, 220-234.

Fedo, C. M., Nesbitt, H. W. & Young, G. M., 1995. Unraveling the effects of potassium metasomatism in sedimentary rocks and paleosols, with implications for paleoweathering conditions and provenance. Geology 23, 921-924.

Feistmantel, C., 1880. Notes on fossil plants from Kattywar, Shaikh Budin and Sirgjuar. India Geol. Surv. Recs. 13 (pt 1), 62-69.

Feng, R. & Kerrich, R., 1990. Geochemistry of fine-grained clastic sediments in the Archean Abitibi greenstones belt, Canada: Implications for provenance and tectonic setting. Geochim. Cosmochim. Acta 54, 1061-1081.

Ferguson, R. I., 1984. Sediment load of the Hunza River In: Miller, K. J. (Ed.), The International Karakoram Project 2, Cambridge Univ. Press., 581-598.

Ferrell, K. M., 2001. Geomorphology, facies architecture, and high resolution, non-marine sequence stratigraphy in avulsion deposits, Cumberland Marshes, Saskatchewan. Sed. Geol. 139, 93-150.

Fiestmantel, O., 1882, Note on the remains of palm leaves from the Tertiary Murree and Kasauli beds in India. Geol. Surv. India Rec. 15, 51-53.

Finlayson, D. P., Montgomery, D. R. & Hallet, B., 2002. Spatial coincidence of rapid inferred erosion with young metamorphic massifs in the Himalayas. Geology 30, 219-222.

Flynn, L. J., Pilbeam, D., Jacobs, L. L., Barry, J. C., Behrensmeyer A. K. & Kappelmen, J. W., 1990. The Siwaliks of Pakistan: Time and faunas in a Miocene terrestrial setting. J. Geol. 98, 589-604.

Folk, R. L., 1974. Petrology of Sedimentary Rocks, 2nd Ed. Hemphill Press, Austin, Texas. 182 pp.

Foster, G., Kinny, P., Vance, D., Prince, C. & Harris, N., 2000. The significance of monazite U-Th-Pb age data in metamorphic assemblages; a combined study of monazite and garnet chronometry. EPSL 181, 327-340.

Foster, G., Vance, D., Argles, T. & Harris, N., 2002. The tertiary collision-related thermal history of the NW Himalaya. J. Met. Geol. 20, 827-843.

France-Lanord, C., Derry, L. & Michard, A., 1993. Evolution of the Himalaya since Miocene time: Isotope and sedimentological evidence from the Bengal fan. In: Treloar, P. J. and Searle, M. P. (Eds.), Himalayan Tectonics. Geol. Soc. Lond. Spec. Pub. No. 74, 603-622.

Frank, W., Grasemann, B., Guntli, P. & Miller, C., 1995. Geological map of the Kishwar-Chamba-Kulu region (NW Himalayas India). Jahrbuch der Geologischen Bundesanstalt 138, 299-308.

Franzinelli, E. & Potter, P. E., 1983. Petrology, chemistry and texture of modern river sands, Amazon River system. J. Geol. 91, 23-40.

Fraser, J., Searle, M. P., Parrish, R. & Noble, S., 2001. Chronology of deformation, metamorphism and magmatism in southern Karakoram mountains, Geol. Soc. Am. Bull. 113, 1443-1455.

Friedman, R., Gee, J., Tauxe, L., Downing, K. & Lindsay, E., 1992. The magnetostratigraphy of the Chitarwata and lower Vihowa Formations of the Dera Ghazi Khan Area, Pakistan. Sed. Geol. 81, 253-268.

Friend, P. F., 1966. Clay fractions and colours of some Devonian red beds in the Catskill Mountains, USA. J. Geol. Soc. Lond. 122, 273-292.

Friend, P. F., 1978. Distinctive features of some ancient river systems. In: Miall, A. D. (Ed.), Fluvial Sedimentology. Can. Soc. Petrol. Geol. Mem. 5, 531-542.

Friend, P. F., Raza, S. M., Baig, M. A. S. & Khan, I. A., 1999. Geological evidence of the ancestral Indus from the Himalayan foothills. In: Meadows, A. and Meadows, P. S. (Eds.), The Indus River, Biodiversity, Resources, Humankind. Oxford Univ. Press, Oxford, 103-113.

Fuller, A. O., 1985. A contribution to the conceptual modeling of pre-Devonian fluvial systems. Geol. Soc. S. Aft. Trans. 88, 189-194.

Gaetani, M. & Garzanti, E., 1991. Multicyclic history of the northern India continental margin (northwestern Himalaya). Am. Assoc. Petrol. Geol. Bull. 75, 1427-1446.

Gaetani, M., Garzanti, E., Jadoul, F., Nicora, A., Tintori, A., Pasini, M. & Kanwar, S. A. K., 1990. The north Karakorum side of the central Asia geopuzzle. Geol. Soc. Am. Bull. 102, 54-62.

Galy, A. & France-Lanord, C., 2001. Higher erosion rates in the Himalaya: Geochemical constraints on riverine fluxes. Geology 29, 23-26.

Galy, A., France-Lanord, C. & Derry, L. A., 1996. The Late Oligocene-Early Miocene Himalayan belt Constraints deduced from isotopic compositions of Early Miocene turbidites in the Bengal Fan. Tectonophysics, 260, 109-118.

Ganjoo, R. K. & Shaker, S., 2007. Middle Miocene pedological record of monsoonal climate from NW Himalaya (Jammu & Kashmir State), India. J. Asian Earth Sciences, 29, 704-714.

Gansser, A., 1964. The Geology of the Himalayas. Wiley Interscience, New York, 289 p.

Gansser, A., 1983. Geology of the Bhutan Himalaya. Birkha¨user Verlag, Boston, 180 p.

Garver, J. I., Royce, P. R. & Smick, T. A., 1996. Chromium and nickel in shale of the Taconic Foreland: A case study for the provenance of fine-grained sediments with an ultramafic source. J. Sed. Res. 66, 100-106.

Garzanti, E. & Van Haver, T., 1988. The Indus clastics: Forearc basin sedimentation in the Ladakh Himalaya (India). Sed. Geol. 59, 237-249.

Garzanti, E., Casnedi, R. & Jadoul, F., 1986. Sedimentary evidence of a Cambro-Ordovician orogenic event in the northwestern Himalaya. Sed. Geol. 48, 237-265.

Garzanti, E., Baud, A. & Mascle, G., 1987. Sedimentary record of the northward flight of India and its collision with Eurasia (Ladakh Himalaya India). Geodynamica Acta 1, 297-312.

Garzanti, E., Critelli, S. & Ingersoll, R. V., 1996. Paleogeographic and paleotectonic evolution of the Himalayan Range as reflected by detrital modes of Tertiary sandstones and modern sands (Indus transect, India and Pakistan). Geol. Soc. Am. Bull. 108, 631-642.

Garzanti, E., Vezzoli, G., Ando, S., Paparella, P. & Clift, P. D., 2005. Petrology of Indus River sands: A key to interpret erosion history of the Western Himalayan Syntaxis. EPSL 229, 287-302.

Gazzi, P., 1966. Le arenarie del flysch sopracretaceo dell'Appennino modenese; correlazioni con il flysch di Monghidoro. Mineralogicae Petrografica Acts 12, 69-97.

Geddes, A., 1960. The alluvial morphology of the Indo-Gangetic plain: Its mapping and geographical significance. Transactions and Papers. Institute of British Geographers 28, 253-276.

Gee, E. R., 1981a. Geological map of Salt Range, Toposheet No. 43 D/13 & 14 and H/1 & 2, scale 1:50000, Punjab, Pakistan. New Geosc. No. 1147, 1148, 1179 and 1180 (Salt Range Ser. Sheet No. 5), Punjab Geol. Map Series Vol. IV, Geol. Surv. Pakistan, Quetta and Overseas Coop. Deptt., UK.

Gee, E. R., 1981b. Geological map of Salt Range, Toposheet No. 43 D/5, 9, 6 & 10, scale 1:50000, Punjab, Pakistan. New Geosc. No. 1080, 1081, 1115 and 1116 (Salt Range Ser. Sheet No. 4), Punjab Geol. Map Series Vol. IV, Geol. Surv. Pakistan, Quetta and Overseas Coop. Deptt., UK.

Gee, E. R., 1981c. Geological map of Salt Range, Toposheet No. 43 H/1, 2, 5 & 6, scale 1:50000, Punjab, Pakistan. New Geosc. No. 1179, 1180, 1210 and 1211 (Salt Range Ser. Sheet No. 6), Punjab Geol. Map Series Vol. IV, Geol. Surv. Pakistan, Quetta and Overseas Coop. Deptt., UK.

Gee, E. R., 1983. Tectonic problems of the sub-Himalayan region of Pakistan. Kashmir J. Geol. 1, 11-18

Gee, E. R. & Gee, D. G., 1989. Overview of the geology and structure of the Salt Range, with observations on related areas of northern Pakistan. Geol. Soc. Am. Spec. Paper 232, 95-112.

Gehrels, G. E., DeCelles, P. G., Ojha, T. P. & Upreti, B. N., 2006. Geologic and geochronologic evidence for early Paleozoic tectonism in the Kathmandu thrust sheet, central Nepal Himalaya. Geol. Soc. Amer. Bull. 118, 185-198.

George, M. T., Harris, B. W. & Butler, R. W. H., 1993. The tectonic implications of contrasting granite magmatism between Kohistan island arc and the Nanga Parbat-Haramosh Massif, Pakistan Himalaya. In: Treloar, P. J. and Searle, P. M. (Eds.), Himalayan Tectonics. Geol. Soc. Spec. Pub., 74, 173-191.

George, M., Reddy, S. & Harris, N., 1995. Isotopic constraints on the cooling history of the Nanga Parbat-Haramosh Massif and Kohistan arc, western Himalaya. Tectonics 14, 237-252.

Gergen, L. D. & Ingersoll, R. V., 1986. Petrology and provenance of Deep Sea Drilling Project sand and sandstone from the north Pacific Ocean and the Bering Sea. Sed. Geol. 51, 29-56.

Ghandour, I. M., Harue, M. & Wataru, M., 2003. Mineralogical and chemical characteristics of Bajocian-Bathonian shales, G. Al-Maghara, North Sinai, Egypt: Climatic and environmental significance. Geochem. J. 37, 87-108.

Ghosh, S. K., 1987. Cyclicity and facies characteristics of alluvial sediments in the Upper Paleozoic Monongahela-Dunkard Group, Central West Virginia. In: Ethridge, G., Flores, R. M. and Harvey, M. D. (Eds.), Recent Developments in Fluvial Sedimentology. Spec. Pub. Soc. Econ. Paleon. and Mineral. 39, Tulsa, 229-239.

Ghosh, S. K., Kumar, R. & Suresh, N., 2003. Influence of Mio-Pliocene drainage re-organisation in the detrital modes of sandstone, Subathu sub-basin, Himalayan foreland basin. J. Him. Geol. 24, 35-46.

Gibson, T. G., Bybell, L. M. & Mason, D. B., 2000. Stratigraphic and climatic implications of clay mineral changes around the Paleocene/Eocene boundary of the northeastern US margin. Sed. Geol. 134, 65-92.

Gingerich, P. D., 2003. Stratigraphic and micropaleontologic constraints on the middle Eocene age of the mammal-bearing Kuldana Formation of Pakistan. J. Verteb. Paleont. 23, 643-651.

Girty, G. H., Mossman, B. J. & Pincus, S. D., 1988. Petrology of Holocene sand, Peninsular Ranges, California and Baja Norte, Mexico: Implications for provenance-discrimination models. J. Sed. Pet. 58, 881-887.

Godin, L., Brown, R. L., Hanmer, S. & Parrish, R., 1999. Back folds in the core of the Himalayan orogen: An alternative interpretation. Geology 27, 151-154.

Gohain, K., & Parkash, B., 1990. Morphology of the Kosi megafan. In: Rachocki, A. H. and Church, M. (Eds.), Alluvial Fans: A Field Approach, Wiley, New York, 151-178.

Goodbred, S. L. & Kuehl, S. A., 1999. Holocene and modern sediment budgets for the Ganges-Brahmaputra river system; evidence for highstand dispersal to flood-plain, shelf, and deep-sea depocenters. Geology 27, 559-562.

Gordon, E. A. & Bridge, J. S., 1987. Evolution of Catskill (Upper Devonian) river systems: Intra and extrabasinal controls. J. Sed. Pet. 57, 234-249.

Govindaraju, K., 1989. Compilation of working values and sample description of 272 geostandards, Geostandards Newsletter 13, 1-113.

Graham, S. A., Dickinson, W. R. & Ingersoll, R. V., 1975. Himalayan-Bengal model for flysch dispersal in the Appalachian-Ouachita system. Geol. Soc. Am. Bull. 86, 273-286.

Graver J. I. & Scott T. J., 1995. Trace elements in shale as indicators of crustal provenance and terrain accretion of the southern Canadian cordillera. Geol. Soc. Am. Bull. 107, 440-453.

Greco, A. & Spencer, D. A., 1993. A section through the Indian Plate, Kaghan valley, NW Himalaya, Pakistan. In: Treloar, P. J. and Searle, M. P. (Eds.), Himalayan Tectonics. Geol. Soc. Lond. 221-236.

Greco, A., Martinotti, G., Papritz, K., Ramsay, J. G. & Rey, R., 1989. The crystalline rocks of the Kaghan valley (NE-Pakistan). Eclogae Geologicae Helvetiae 82, 629-653.

Griffin, J. J., Windom, H. & Goldberg, E. D., 1986. The distribution of clay minerals in the World Ocean. Deep-Sea Res. 15, 433-459.

Gu Z. Y., Lal D., Liu T. S., Guo Z. T., Southon J. & Caffee M. W., 1997. Weathering histories of Chinese loess deposits based on uranium and thorium series nuclides and cosmogenic ^{10}Be. Geochim. Cosmochim. Acta 61, 5221-5231.

Guillot, S., Cosca, M., Allemand, P. & LeFort, P., 1999. Contrasting metamorphic and geochronologic evolution along the Himalayan belt. In: Macfarlane, A., Sorkhabi, R.B. and Quade, J. (Eds.), Himalaya and Tibet: Mountain Roots to Mountain Tops. Geol. Soc. Am. Spec. Papers, 328, 117-128.

Guillot, S., Garzanti, E., Baratoux, D., Marquer, D., Maheo, G. & de Sigoyer, J., 2003. Reconstructing the total shortening history of the NW Himalaya. Geochemistry, Geophysics, Geosystems 4, 1064, doi: 10.1029/2002GC000484.

Gupta, S., 1993. Drainage deflection by actively growing anticlines at the Himalayan mountain front: Implications for Himalayan drainage patterns. In: Yu, B. and Fielding, C. R. (Eds.), Modern and Ancient Rivers: Their Importance to Mankind, Fifth International Conference on Fluvial Sedimentology, Conference Proceedings, Keynote Addresses, and Abstracts, Brisbane, 47.

Gupta, S., 1997. Himalayan drainage patterns and the origin of fluvial megafans in the Ganges foreland basin. Geology 25, 11-14.

Hadley, D. G., Bown, T. M. & Brouwers, E. M., 1992. Late Miocene fluvial and shallow marine paleoenvironments, central and western Abu Dhabi Emirate, United Arab Emirates. Geol. Soc. Am. Abstr. with Programs 24, A360.

Hallberg, R. O., 1976. A geochemical method for investigation of palaeoredox conditions in sediments. Ambio, Spec. Report 4, 139-147.

Harris, N., Bickle, M., Chapman, H., Fairchild, I. & Bunbury, J., 1998. The significance of Himalayan rivers for silicate weathering rates: Evidence from the Bhote Kosi tributary. Chem. Geol. 144, 205-220.

Harrison, T. M., Copeland, P., Hall, S. A., Quade, J., Burner, S., Ojha, T. P. & Kidd, W. S. F., 1993. Isotopic preservation of Himalayan/Tibetan uplift, denudation and climatic histories of two molasse deposits. J. Geol. 101, 157-175.

Harrison, T. M., Copeland, P., Kidd, W. S. F. & Lovera, O. M., 1995. Activation of the Nyainqentanghla shear zone: Implications for uplift of the southern Tibetan Plateau. Tectonics 14, 658-676.

Harrison, T. M., Ryerson, F. J., LeFort, P., Yin, A., Lovera, O. M. & Catlos, E. J., 1997. A Late Miocene-Pliocene origin for the Central Himalayan inverted metamorphism. EPSL. 146, E1-E7.

Hauck, M. L., Nelson, K. D., Brown, L. D., Zhao, W. J. & Ross, A. R., 1998. Crustal structure of the Himalayan orogen at similar to 90 degrees east longitude from Project INDEPTH deep reflection profiles. Tectonics 17, 481-500.

Haughton, P. D. W., 1988. A cryptic Caledonian flysch terrain in Scotland. J. Geol. Soc. Lond. 145, 685-703.

Heim, A. & Gansser, A., 1939. Central Himalaya. Geological Observations of the Swiss Expedition 1936. Hindustan Publishing corporation Delhi. 1-246.

Heins, W. A., 1993. Source rock texture vs. climate and topography as controls on the composition of modern, plutoniclastic sand In: Johnsson, M. J. and Basu, A. (Eds.), Processes Controlling the Composition of Clastic Sediments. Geol. Soc. Am. Spec. Paper 284, 135-146.

Heller, P. L. & Paola, C., 1989. The paradox of Lower Cretaceous gravels and the initiation of thrusting in the Sevier orogenic belt, United States Western Interior. Geol. Soc. Am. Bull. 101, 864-875.

Heller, P. L., Angevine, C. L., Winslow, N. S. & Paola, C., 1988. Two-phase stratigraphic model of foreland basin development. Geology 16, 501-504.

Hemphill, W. R. & Kidwai, A. H., 1973. Stratigraphy of the Bannu and Dera Ismail Khan areas, Pakistan. U. S. Geol. Surv. Prof. Paper 716-B, 36p.

Herron, M. M., 1988. Geochemical classification of terrigenous sands and shales from core or log data. J. Sed. Pet. 58, 820-829.

Hildebrand, P. R., Noble, S. R., Searle, M. P., Parrish, R. R. & Shakirullah, 1998. Tectonic significance of 24 Ma crustal melting in the eastern Hindu Kush, Pakistan. Geology 26, 871-874.

Hildebrand, P. R., Noble, S. R., Searle, M. P., Waters, D. J. & Parrish, R. R., 2001. Old origin for an active mountain range: Geology and geochronology of the eastern Hindu Kush, Pakistan. Geol. Soc. Am. Bull. 113, 625-639.

Hisatomi, K. & Tanaka, S., 1994. Climatic and environmental changes at 9 and 7.5 Ma in the Churia (Siwalik) Group, West Central Nepal. Himalayan Geol. 15, 161-180.

Hodges, K. V., 2000. Tectonics of the Himalaya and southern Tibet from two perspectives. Geol. Soc. Am. Bull. 112, 324-350.

Hodges, K. V. & Silverberg, D. S., 1988. Thermal evolution of the Greater Himalaya, Gahrwal, India. Tectonics 7, 583-600.

Hodges, K. V., Hubbard, M. S. & Silverberg, D. S., 1988. Metamorphic constraints on the thermal evolution of the central Himalayan orogen. Royal Soc. Lond. Philosoph. Transac. 326, 257-280.

Hodges, K. V., Parrish, R. R., Housh, T. B., Lux, D. R., Burchfuel, B. C., Royden, L. H. & Chen, Z., 1992. Simultaneous Miocene extension and shortening in the Himalayan orogen. Science 258, 1466-1470.

Hodges, K. V., Parrish, R. R. & Searle, M. P., 1996. Tectonic evolution of the central Annapurna Range, Nepalese Himalaya. Tectonics 15, 1264-1291.

Holail, H. M. & Moghazi, A. M., 1998. Provenance, tectonic setting and geochemistry of greywackes and siltstones of the Late Precambrian Hammamat Group, Egypt. Sed. Geol. 116, 227-50.

Holm P. E., 1985. The geochemical fingerprints of different tectono-magmatic environments using hygromagmatophile element abundances of tholeiitic basalts and basaltic andesites. Chem. Geol. 51, 303-323.

Homewood, P. & Caron, C., 1982. Flysch of the western Alps. In: Hsu, K. K. (Ed.), Mountain Building Processes. Academic Press Lond. 157-168.

Homewood, P., Allen, P. A. & Williams G. D., 1986. Dynamics of the Molasse Basin of western Switzerland. In Allen, P. A. and Homewood, P. (Eds.), Foreland Basins. Int. Assoc. Sediment. Spec. Pub. 8, 199-217.

Honegger, K., Dietrich, V., Frank, W., Gansser, A., Thoni, M. & Trommsdorf, V., 1982. Magmatism and metamorphism in the Ladakh Himalaya (the Indus Tsangpo Suture Zone). EPSL 60, 253-292.

Honegger, K., Le Fort, P., Mascle, G. & Zimmermann, J. L., 1989. The bluechists along the Indus suture zone in Ladakh, NW Himalaya. J. Met. Geol. 7, 57-72.

Horton, B. K. & DeCelles, P. G., 1999. Modern and ancient fluvial megafans in the foreland basin system of the central Andes, southern Bolivia: Implications for drainage network evolution in fold-thrust belts. Basin Research 13, 43-63.

Hower, J., Eslinger, E. V., Hower, M. E. & Perry, E. A., 1976. Mechanism of burial metamorphism of argillaceous sediments: Mineralogical and chemical evidence. Geol. Soc. Am. Bull. 87, 725-737.

Hsu, K. J., 1970. The meaning of the word flysch–a short historical search. In: Lajoie, J. (Ed.), Flysch Sedimentology in North America. Geol. Assoc. Can. Spec. Paper 7, 1-11.

Hubbard, M. S. & Harrison, T. M., 1989. Ar^{40} /Ar^{39} age constraints on deformation and metamorphism in the main central thrust zone and Tibetan Slab, Eastern Nepal Himalaya. Tectonics 8, 865-880.

Humayun, M., 1986. Petrology of the Swat Amphibolites and the development of a "Lesser Himalayan" Basin. Geol. Bull. Univ. Peshawar 19, 83-100.

Huntsman-Mapila, P., Kampunzu, A. B., Vink, B. & Ringrose, S., 2005. Cryptic indicators of provenance from the geochemistry of the Okavango Delta sediments, Botswana. Sed. Geol., 174. 123-148.

Hurford, A. J., 1991. Uplift and cooling pathways derived from fission track analysis and mica dating: A review. Geol Rundsch 80, 349-368.

Hussain, A., Yeats, R. S. & Pogue, K., 1989. Stratigraphic and structural events around the southern margin of Peshawar Basin. Geol. Bull. Univ. Peshawar 22, 45-54.

Ingersoll, R. V., 1983. Petrofacies and provenance of Late Mesozoic forearc basin, Northern and Central California. Am. Assoc. Petrol. Geol. Bull. 67, 1125-1142.

Ingersoll, R. V., 1990, Actualistic sandstone petrofacies: Discriminating modern and ancient source rocks. Geology 18, 733-736.

Ingersoll, R. V. & Suczek, C. A., 1979. Petrography and provenance of Neogene sand from Nicobar and Bengal fans. DSDP sites 211 and 218. J. Sed. Pet. 49, 1217-1228.

Ingersoll, R. V., Bullard, T. F., Ford, R. L., Grimm, J. P., Pickle, J. D. & Sares, S.W., 1984. The effect of grain size on detrital modes: A test of the Gazzi-Dickinson point counting method. J. Sed. Pet. 54, 103-116.

Ingersoll, R. V., Kretchmer, A. G. & Valles, P. K., 1993. The effect of sampling scale on actualistic sandstone petrofacies. Sediment. 40, 937-953.

Ingersoll, R. V., Graham, S. A. & Dickinson, W. R., 1995. Remnant ocean basins. In: Busby, C. J. and Ingersoll, R. V. (Eds.), Tectonics of Sedimentary Basins. Blackwell Science, Oxford, 363-391.

Jagoutz, O., Burg, J. P., Jagoutz, E., Muntener, O., Petteke, T. & Ulmer, P., 2004. Zoned ultramafic intrusions of the Chilas complex in Kohistan (NE Pakistan): Mantle diapers and km-scale melt conduits in extending island arcs. Himalayan Journal of Sciences (Special Issue Extended Abstracts) 2 (4), 166.

Jan, M. Q., 1985. High-P rocks dong the suture zones around the Indo-Pakistan plate and phase chemistry of blueschist from eastern Ladakh. Geol. Bull. Univ. Peshawar 18, 1-40.

Jan, M. Q., 1988. Geochemistry of amphibolites from the southern part of the Kohistan arc, N. Pakistan. Mineral. Mag. 52, 147-159.

Jan, M. Q. & Howie, R. A., 1980. Ortho- and clinopyroxenes from the pyroxene granulites of Swat Kohistan, northern Pakistan. Mineral. Mag. 43, 715-726.

Jan, M. Q., Asif, M., Tahirkheli, T. & Kamal, M., 1981a. Tectonic subdivision of granitic rocks of north Pakistan. Geol. Bull. Univ. Peshawar 14, 159-182.

Jan, M. Q., Kamal, M. & Khan, M. I., 1981b. Tectonic control over emerald mineralization in Swat. Geol. Bull. Univ. Peshawar 14, 101-109.

Jan, M. Q., Pervez, M. K., Khattak, M. U. K. & Windley, B. F., 1984. The Chilas stratiform complex: Weld and mineralogical aspects. Geol. Bull. Univ. Peshawar 17, 153-169.

Jaume, S. & Lillie, R., 1988. Mechanics of the Salt Range, Potwar Plateau, Pakistan: A fold and thrust belt underlain by evaporites. Tectonics 5, 57-71

Jenkinson, R., Rendell, H., Dennell, R. W., Jah, M. A. & Sutherland, S., 1989. Upper Siwalik Palaeo-environments and paleoecology in the Pabbi Hills, Northern Pakistan. Zeitschrift fur Geomorphologie 33, 417-428.

Johnson, D. D. & Beaumount, C., 1995. Preliminary results from a planform kinematic model of orogen evolution surface processes and the development of clastic foreland basin stratigraphy. In: Dorobek, S. L. and Ross, G. M. (Eds.), Stratigraphic Evolution of Foreland Basins. Spec. Pub. Soc. Econ. Paleon. Mineral. 52, 3-24.

Johnson, G. D., 1977. Paleopedology of ramapithecus-bearing sediments, North India. Geologische Rundschau 66, 192-216.

Johnson, G. D., Zeitler, P. K., Naeser, C. W., Johnson, N. M., Summers, D. M., Frost, C. Opdyke, N. D. & Tahirkheli, R. A. K., 1982. The occurrence and fission-track ages of late Neogene and Quaternary volcanic sediments, Siwalik Group, northern Pakistan. Palaeo. Palaeo. Palaeo. 37, 63-93.

Johnson, G. D., Opdyke, N. D., Tandon, S. K. & Nanda, A. C., 1983.The magnetic polarity stratigraphy of the Siwalik Group at Haritalyangar (India) and a new last appearance datum for Ramapithecus and Sivapithecus in Asia. Palaeo. Palaeo. Palaeo. 44, 223-249.

Johnson, N. M., Opdyke, N. D., Johnson, G. D., Lindsay, E. H. & Tahirkheli, R. A. K., 1982. Magnetic polarity stratigraphy and ages of Siwalik Group rocks of the Potwar Plateau, Pakistan. Palaeo. Palaeo. Palaeo. 37, 17-42.

Johnson, N. M., Stix, J., Tauxe, L., Cerveny, P. F. & Tahirkheli, R. A. K., 1985. Palaeomagnetic chronology, fluvial processes and tectonic implications of the Siwalik deposits near Chinji Village, Pakistan. J. Geol. 93, 27-40.

Johnson, S. Y., 1984. Cyclic fluvial sedimentation in a rapidly subsiding basin, northwest Washington. Sed. Geol. 38, 361-391.

Johnsson, M. J., 1990. Tectonic versus chemical-weathering controls on the composition of fluvial sand in tropical environments. Sediment. 37, 713-726.

Johnsson, M. J., 1993. The system controlling the composition of clastic sediments. In: Johnsson, M. J. and Basu, A. (Eds.), Processes Controlling the Composition of Clastic Sediments. Geol. Soc. Am. Spec. Paper 284. Boulder, Colorado, 1-19.

Jones, B. & Manning, D. C., 1994. Comparison of geochemical indices used for the interpretation of paleo-redox conditions in Ancient mudstones. Chem. Geol. 111, 111-129.

Joo, Y. J., Lee, Y. I. & Bai, Z., 2005. Provenance of the Qingshuijian Formation (Late Carboniferous), NE China: Implications for tectonic processes in the northern margin of the North China block. Sed. Geol. 177, 97-114.

Jordan, T. E., 1981. Thrust loads and foreland basin evolution, Cretaceous western United States. Am. Assoc. Petrol. Geol. Bull. 65, 2506-2520.

Jordan, T. E., 1995. Retroarc foreland and related basins. In: Busby, C. J. and Ingersoll, R. V. (Eds.), Tectonics of Sedimentary Basins. Blackwell Science, Oxford, 331-362.

Jordan, T. E. & Flemings, P. B., 1991. Large-scale stratigraphic architecture, eustatic variation, and unsteady tectonism: A theoretical evaluation. J. Geophys. Res. 96, 6681-6699.

Jordan, T. E., Flemings, P. B. & Beer, J. A., 1988. Dating thrust fault activity by use of foreland basin strata. In: Kleinspehn, K. and Paola, C. (Eds.), New perspectives in

Basin Analysis. Frontiers in Sedimentary Geology. Springer-Verlag, New York. 307-330.

Jorgensen, D. W., Harvey, M. D., Schumm, S. A. & Flam, L., 1993. Morphology and dynamics of the Indus River: Implications for the Mohen Jo Daro site. In: Shroder, J, F. (Ed.), Himalaya to Sea: Geology, Geomorphology and the Quaternary. Routledge Press, Lond. 288-326.

Kadri, I. B., 1995. Petroleum Geology of Pakistan. Ferozsons (Pvt.) Ltd., Lahore. 275p.

Kampunzu, A. B., Cailteux, J. L. H., Moine, B. & Loris, H. N. B. T., 2005. Geochemical characterization, provenance, source and depositional environment of Roches Argilo-Talqueuses (RAT) and Mines Subgroups sedimentary rocks in the Neoproterozoic Katangan Belt (Congo): Lithostratigraphic implications. J. African Earth Sciences 42, 119-133.

Karim, A., 1998. Hydrogeochemistry and Isotope Systematics of the Indus River Basin. Unpub. Ph. D. thesis. Deptt. of Earth Sciences, Univ. of Ottawa. 210p.

Karunkaran, C. & Rao, A. R., 1979. Status of exploration for hydrocarbon in the Himalayan region-Contributions to stratigraphy and structure. Geol. Surv. India Miscell. Pub. 41, 1-66.

Kazmi, A. H., 1984. Geology of the Indus delta. In: Haq, B. U. and Milliman, J. D. (Eds.), Marine Geology and Oceanography of Arabian Sea and Coastal Pakistan. Van Nostrand Reinhold, New York, Pt. B, 71-84.

Kazmi, A. H. & Abbasi, I. A., 2008. Stratigraphy and Historical Geology of Pakistan. National Center of Excellence in Geology, Univ. Peshawar, Peshawar.

Kazmi, A. H. & Jan, M. Q., 1997. Geology and Tectonics of Pakistan. Graphic Publishers, Karachi. 554p.

Kazmi, A. H. & Rana, R. A., 1982. Tectonic map of Pakistan. Geol. Surv. Pakistan, Quetta. Scale 1:2000000.

Kazmi, A. H., Lawrence, R. D., Dawood, H., Snee, L. W. & Hussain, S. S., 1984. Geology of the Indus suture zone in the Mingora-Shangla area of Swat, N. Pakistan. Geol. Bull. Univ. Peshawar 17, 127-144.

Keller, W. D., 1970. Environmental aspects of clay minerals. J. Sed. Pet. 40, 785-813.

Kempe, D. R. C. & Jan, M. Q., 1970. An Alkaline Igneous Province in the NW Frontier Province, West Pakistan. Geol. Mag. 107, 395-398.

Khan, I. A., Bridge, J. S., Kappelman, J. & Wilson, R., 1997. Evolution of Miocene fluvial environments, eastern Potwar plateau, northern Pakistan. Sediment. 44, 221-251.

Khan, M. A., Ahmed, R., Raza, H. A. & Kemal, A., 1986. Geology of petroleum in Kohat-Potwar depression, Pakistan. Am. Assoc. Petrol. Geol. Bull. 70, 396-414.

Khan, M. A., Jan, M. Q., Windley, B. F., Tarney, J. & Thirlwall, M. F., 1989. The Chilas Mafic-Ultramafic Igneous Complex: The root of Kohistan island arc in the Himalaya of northern Pakistan. In: Malinconico, L. L. and Lillie, R. J., (Eds.), Tectonics of the Western Himalayas. Geol. Soc. Am. Spec. Paper, 232, 75-94.

Khan, M. A., Jan, M. Q. & Weaver, B. L., 1993. Evolution of the lower arc crust in Kohistan, N. Pakistan: Temporal arc magmatism through early, mature and intra-arc rift stages. In: Treloar, P. J. and Searle, M. P. (Eds.), Himalayan Tectonics. Geol. Soc. Lond. Spec. Pub. 74, 123-138.

Khan, M. J. & Ahmad, W., 1991. Stratigraphy and sedimentology of the Upper Siwalik Group, Sakhi Sarwar area, Southern Zindapir Anticline, Sulaiman Range, Pakistan. Geol. Bull. Univ. Peshawar 24, 45-61.

Khan, M. J. & Opdyke, N. D., 1987. Magnetic-Polarity stratigraphy of the Siwalik Group of the Shinghar and Surghar ranges, Pakistan. Geol. Bull. Univ. Peshawar 20, 111-127.

Khan, M. J. & Opdyke, N. D., 1993. Position of the PaleoIndus as revealed by the magnetic stratigraphy of the Shinghar and Surghar ranges, Pakistan. In: Shroder, J, F. (Ed.), Himalaya to Sea: Geology, Geomorphology and the Quaternary. Routledge Press, Lond. 198-212.

Khan, M. J., Opdyke, N. D. & Tahirkheli, R. A. K., 1988. Magnetic stratigraphy of the Siwalik Group, Bhittani, Marwat, and Khisor ranges, northwestern Pakistan and the timing of Neogene tectonics of the Trans Indus. J. Geoph. Res. 93, 11,773-11,790.

Khan, T., Khan, M. A. & Jan, M. Q., 1994. Geology of a part of the Kohistan terrain between Gilgit and Chilas, northern areas, Pakistan. Geol. Bull. Univ. Peshawar 27, 99-112.

Kirschbaum, M. A. & McCabe, P. J., 1992. Controls on the accumulation of coal and on the development of anastomosed fluvial systems in the Cretaceous Dakota Formation of southern Utah. Sediment. 39, 581-598.

Klootwijk, C. T., Conaghan, P. J. & Powell, C. M., 1985. The Himalayan arc: Large-scale continental subduction, oroclinal bending, and back-arc spreading. EPSL 75, 316-319.

Klootwijk, C. T., Gee, J. S., Pierce, J. W. & Smith, G. W., 1991. Constraints on the India-Asia convergence: Paleomagnetic results from the ninety east ridge. In: Weissel, J., Pierce, J., Taylor, J. W. and Alt, J. (Eds.), Proceedings of the Ocean Drilling Program, Scientific Results: College Station, Texas A & M University Press, p. 777-884.

Komomatsu, M., 1997. Miocene leaf-fossils assemblages of the Churia (Siwalik) Group in Nepal and their paleoclimatic implication. J. Geol. Soc. Japan 103, 265-274.

Kraus, M. J. & Middleton, L. T., 1987. Contrasting architecture of two alluvial suites in different structural settings. In: Ethridge, G., Flores, R. M. and Harvey, M. D. (Eds.), Recent Developments in Fluvial Sedimentology. Spec. Pub. Soc. Econ. Paleon. and Mineral. 39, Tulsa, 253-262.

Kravtochenko, K. N., 1964. Soan Formation-upper unit of the Siwalik Group in Potwar. Sci. and Ind. 3, 230-233.

Krol, M. A., Zeitler, P. K., Poupeau, G. & Pecher, A., 1996. Temporal variations in the cooling and denudation history of the Hunza plutonic complex, Karakoram Batholith, revealed by $^{40}Ar/^{39}Ar$ thermochronology. Tectonics 15, 403-415.

Kronberg B. I. & Nesbitt H. W., 1981. Quantification of weathering, soil geochemistry and soil fertility. J. Soil Science 32, 453.

Kroon, D., Steens, T. & Troelstra, S. R., 1991. Onset of Monsoonal related upwelling in the western Arabian Sea as revealed by planktonic foraminifers. Proc. Ocean Drilling Program Sci. Results 117, 257-263.

Krynine, P. D., 1937. Petrography and genesis of the Siwalik Series. Am. J. Sci. 34, 422-426.

Krynine, D., 1950. Petrology, stratigraphy, and origin of the Triassic sedimentary rocks of Connecticut. Conn. State Geol. Nat. Hist. Surv. Bull. 73, 239 pp.

Kuhlmann, G., de Boer, P. L., Pedersenc, R. B. & Wonga, T. E., 2004. Provenance of Pliocene sediments and paleoenvironmental changes in the southern North Sea region using Samarium-Neodymium (Sm/Nd) provenance ages and clay mineralogy. Sed. Geol. 171, 205-226.

Kumar, R., 1993. Coalescence megafan: Multistorey sandstone complex of the Late-Orogenic (Mio-Pliocene) sub-Himalayan belt, Dehra Dun, India. Sed. Geol. 85, 327-337.

Kumar, R. & Ghosh, S. K., 1994. Evolution of the Mio-Pleistocene alluvial fan system in the Siwalik Foreland Basin, Dehra Dun, India. In: Kumar, R., Ghosh, S. K. and Phadtare, N. R. (Eds.), Siwalik Foreland Basin of Himalaya. Himal. Geol. 15, 143-159.

Kumar, R. & Nanda, A. C., 1989. Sedimentology of the Middle Siwalik sub-Group of Mohand area, Dehra Dun valley, India. J. Geol. Soc. India 34, 597-616.

Kumar, R. & Tandon, S. K., 1985. Sedimentology of Plio-Pleistocene Late Orogenic deposits associated with intraplate subduction-the Upper Siwalik Subgroup of a part of Panjab Sub-Himalaya, India. Sed. Geol. 42, 105-158.

Kumar, R., Ghosh, S. K. & Sangode, S. J., 1999. Evolution of a fluvial system in a Himalayan foreland basin, India. In: Macfarlane, A., Sorkhabi, R. B. and Quade, J. (Eds.), Himalayan and Tibet: Mountain Roots to Mountain Tops. Geol. Soc. Am. Spec. Paper 328, 239-256.

Kumar, R., Ghosh, S. K. & Sangode, S. J., 2003. Mio-Pliocene sedimentation history in the northwestern part of the Himalayan foreland basin, India. Current Science, 84, 1006-1113.

Kumar, R., Sangode, S. J. & Ghosh, S. K., 2004. A multistorey sandstone complex in the Himalayan Foreland Basin, NW Himalaya, India. J. Asian Earth Sciences 23, 407-426.

Kutzbach, J. E., Prell, W. E. & Ruddiman, W. F., 1993. Sensitivity of Eurasia climate to surface uplift of the Tibetan Plateau. J. Geol. 101, 177-190.

Lacassie, J. P., Roser, B., Solar, J. R. D. & Herve´, F., 2004. Discovering geochemical patterns using self-organizing neural networks: A new perspective for sedimentary provenance analysis. Sed. Geol. 165, 175-191.

Lasaga, A. C., Soler J. M., Ganor J., Burch T. E. & Nagy K. L., 1994. Chemical weathering rate laws and global geochemical cycles. Geochim. Cosmochim. Acta 58, 2361-2386.

Latif, M. A., 1970. Explanatory notes on the geology of the southern Hazara to accompany the revised geological map. Wien Jahrb. Geol. Bundesanst. 15, 5-20

Laury, R. L., 1971. Stream bank failure and rotational slumping; preservation and significance in the geologic record. Geol. Soc. Am. Bull. 82, 1251-1266.

Lave´, J. & Avouac, J. P., 2000. Active folding of fluvial terraces across the Siwaliks Hills, Himalayas of central Nepal. J. Geoph. Res. 105, 5735-5770.

Lawerence, R. D. and 15 others, 1989. Tectonics south of the suture, northern Pakistan. 28th International Geological Congress, Washington, Abstract 2, 265.

LeFort, P., 1975. Himalayas, the collided range: Present knowledge of the continental arc. Am. J. Science 275-A, 1-44.

LeFort, P., 1988. Granites in the tectonic evolution of the Himalaya, Karakoram and southern Tibet. Philosoph. Transac. Royal Soc. Lond. A326, 281-299.

LeFort, P., 1996. Evolution of the Himalaya. In: Yin, A. and Harrison, T. M. (Eds.), The Tectonic Evolution of Asia, Cambridge University Press, Cambridge. 95-109.

LeFort, P., Michard, A., Sonet, J. & Zimmermann, J. L., 1983. Petrography, geochemistry and geochronology of some samples from the Karakoram axial batholith (northern Pakistan). In: Shams F.A. (Ed.), Granites of Himalayas, Karakoram and Hindu Kush. Institute of Geology, Punjab Univ., Lahore, Pakistan, 377-387.

Le Maitre, R. W., 1982. Numerical Petrology: Statistical Interpretation of Numerical Data. Elsevier, Amsterdam. 281 pp.

Le Pera, E. & Critelli, S., 1997. Sourceland controls on the composition of beach and fluvial sand of the northern Tyrrhenian coast of Calabria, Italy: Implications for actualistic petrofacies. Sed. Geol. 110, 87-97.

Lee, J. I., Clift, P. D., Layne, G., Blum, J. & Khan, A. A., 2003. Sediment flux in the modern Indus River inferred from the trace element composition of detrital amphibole grains. Sed. Geol. 160, 243-257.

Lee, J. I., Park, B-K., Jwa, Y-J., Yoon, H. I., Yoo, K. C. & Kim, Y., 2005. Geochemical characteristics and the provenance of sediments in the Bransfield Strait, West Antarctica. Marine Geol. 219, 81-98.

Lee, Y. I., 2002. Provenance derived from the geochemistry of Late Paleozoic-Early Mesozoic mudrocks of the Pyeongan supergroup, Korea. Sed. Geol. 149, 219-235.

Lee, Y. I. & Ko, H. K., 1997. Illite crystallinity and fluid inclusion analysis across a Paleozoic disconformity in central Korea. Clays and Clay Miner. 45, 147-157.

Lee, Y. I. & Sheen, D-H., 1998. Detrital modes of the Pyeongan Supergroup (Late Carboniferous-Early Triassic) sandstones in the Samcheog coalfield, Korea: Implication for provenance and tectonic setting. Sed. Geol. 119, 219-238.

Leeder, M., 1999. Sedimentology and Sedimentary Basins. Blackwell Science Limited.

Lepichon, X., Fournier, M. & Jolivet, L., 1992. Kinematics, topography, shortening, and extrusion in the India-Eurasia collision. Tectonics 11, 1085-1098.

Lewis, 1937. “A new Siwalik correlation (India).” Am. J. Sci. Ser. 5, No.195, V.33, 191-204.

Lillie, R. J., Johnson, G. D., Yousaf, M., Zamin, A. S. H. & Yeats, R. S., 1987. Structural development within the Himalayan fold-and-thrust belt of Pakistan. In: Beaumont, C. and Tankard, A. J. (Eds.), Sedimentary Basins and Basin-forming Mechanisms. Can. Soc. Petrol. Geol. Memoir 12, 379-392.

Lindsey, D. A., Tysdal, R. G. & Taggart, J. E. Jr., 2003. Chemical Composition and Provenance of the Mesoproterozoic Big Creek, Apple Creek, and Gunsight Formations, Lemhi Group, Central Idaho [Chapter B of: Russell G. Tysdal, David A. Lindsey, and Joseph E. Taggart, Jr. Correlation, Sedimentology, Structural Setting, Chemical Composition, and Provenance of Selected Formations in Mesoproterozoic Lemhi Group, Central Idaho]. USGS Prof. Paper 1668-B.

Lindsay, E. H. & Downs, W. R., 2000. Age assessment of the Chitarwata Formation. Himalayan Geology 21, 99-107.

Lindsay, E. H., Flynn, L. J., Cheema, I. U., Barry, J. C., Downing, K. F., Rajpar, A. R. & Raza, S. M., 2005. Will Downs and the Zinda Pir Dome. Palaeontologia Electronica 8, 19A, 18p.

Lindsay, J. F., Holliday, D. W. & Hulbert, A. G., 1991. Sequence Stratigraphy and the evolution of the Ganges-Brahmaputra Delta Complex. Am. Assoc. Petrol. Geol. Bull. 75, 1233-1254.

Liu, T. S., 1985. Loess and the Environment. China Ocean Press, Beijing.

Lombardo, B. & Rolfo, F., 2000. Two contrasting eclogite types in the Himalayas: Implications for the Himalayan orogeny. J. Geodynamics 30, 37-60.

Mack, G. H., 1984. Exceptions to the relationship between plate tectonics and sandstone composition. J. Sed. Pet. 54, 212-220.

Mack, G. H. & Suttner, L. J., 1977. Paleoclimate interpretation from petrographic comparison of Holocene sands and the Fountain Formation (Pennsylvanian) in the Colorado Front Range. J. Sed. Pet. 47, 89-100.

Mack, G. H., Leeder, M. R., Perez-Arlucea, M. & Bailey, B. D. J., 2003. Early Permian silt-bed fluvial sedimentation in the Orogrande basin of the Ancestral Rocky Mountains, New Mexico, USA. Sed. Geol. 160, 159-178.

Mackey, S. D. & Bridge, J. S., 1995. Three-dimensional model of alluvial stratigraphy: Theory and application. J. Sed. Res. 65, 7-31.

Mackie, W., 1986. Sand and sandstones of the eastern Moray. Edinburgh Geology Society Transactions 7, 148-172.

Makaske, B., Smith, D. G. & Berendsen, H. J. A., 2002. Avulsions, channel evolution and floodplain sedimentation rates of the anastomosing upper Columbia River, British Columbia, Canada. Sediment. 49, 1049-1071.

Malik, J. N. & Nakata, T., 2003. Active faults and related Late Quaternary deformation along the northwestern Himalayan Frontal Zone, India. Annals of Geophysics 46, 917-936.

Maluski, H. & Matte, P., 1984. Ages of Alpine tectonometamorphic events in the NW Himalaya (N. Pakistan) by the $^{40}Ar/^{39}Ar$ method. Tectonics 3, 1-18.

Marsaglia K. M. & Ingersoll, R. V., 1992. Compositional trends in arc-related, deep-marine sand and sandstone: A re-assessment of magmatic-arc provenance, Geol. Soc. Am. Bull. 104, 1637-1649.

Massari, F., 1983. Tabular cross-bedding in Messinian fluvial channel conglomerates, southern Alps, Italy. In: Collinson, J. and Lewin, J. (Eds.), Modern and Ancient Fluvial Systems. Int. Assoc. Sedimentol. Spec. Publ. 6, 287-300.

Mathur, N. S., 1978. Biostratigraphical aspects of the Subathu Formation, Kumaun Himalaya. Recent Researches in Geology 5, 96-112.

Mathur, N. S., 1979. Palaeoecology of the Subathu Formation, Kumaun Himalaya. Indian Geol. Soc. Bull. 12, 81-90.

Mathur, Y. K., 1984. Cenozoic palynofossils, vegetation, ecology and climate of the north and northwestern subhimalayan region, India. In: Whyte, R. O. (Ed.), The Evolution of the East Asian Environment. Univ. of Hong Kong, 504-551.

Maynard, J. B., Valloni, R. & Yu, H. S., 1982. Composition of modern deepsea sands from arc-related basins. In: Legget, J. K. (Ed.), Trench-Forearc Geology: Sedimentation and Tectonics on Modern and Ancient Active Plate Margins. Geol. Soc. Lond. Spec. Pub. 10, 551-561.

McBride, E. F., 1985. Diagenetic processes that affect provenance determinations in sandstone, In: Zuffa, G. G. (Ed.), Provenance of Arenites. Dordrecht, The Netherlands, Reidel Publishing Company, NATO Advanced Study Institute Series 148, 95-113.

McBride E. F. & Picard, M. D., 1987. Downstream changes in sand composition, roundness, and gravel size in a short-headed high-gradient stream, north western Italy. J. Sed. Pet. 57, 1018-1026.

McCabe, P. J., 1977. Deep distributary channels and giant bedforms in the Upper Carboniferous of the Central Pennines, northern England. Sediment. 24, 271-290.

McCarthy, P. J., Martini, I. P. & Leckie, D. A., 1997. Anatomy and evolution of a Lower Cretaceous alluvial plain: Sedimentology and paleosols in the upper Blairmore Group, south-western Alberta, Canada. Sediment. 44, 197-220.

Mcdonnell, K. L., 1974. Depositional Environments of the Triassic Gosford Formation, Sydney Basin. J. Geol. Soc. Australia, 21, 107-132.

McKee, E. D., Crosby, E. J. & Berryhill, H. L., 1967. Flood deposits, Bijou Creek, Colorado, June, 1965. J. Sed. Pet. 37, 829-851.

Mclane, M., 1995. Sedimentology. Oxford University Press.

McLennan, S. M., 1989. Rare earth elements in sedimentary rocks: Influence of provenance and sedimentary process. Reviews in Mineralogy 21, 169-200.

McLennan, S. M., 2001. Relationships between the trace element composition of sedimentary rocks and upper continental crust. Geochemistry Geophysics Geosystems 2, C000109.

McLennan, S. M. & Taylor, S. R., 1980. Th and U in sedimentary rocks: Crustal evolution and sedimentary recycling. Nature 285, 621-624.

McLennan, S. M., Taylor, S. R. & Kroner, A., 1983. Geochemical evolution of Archean shales from South Africa: I. The Swaziland and Pongola Supergroups. Precamb. Res. 22, 93-124.

McLennan, S. M., Taylor, S. R., McCulloch, M. T. & Maynard, J. B., 1990. Geochemical and Nd-Sr isotopic composition of deep sea turbidites: Crustal evolution and plate tectonic associations. Geochim. Cosmochim. Acta 54, 2015-2050.

McLennan, S. M., Hemming, S., McDaniel, D. K. & Hanson, G. N., 1993. Geochemical approaches to sedimentation, provenance and tectonics. In: Johnsson, M. J. and

Basu, A. (Eds.), Processes Controlling the Composition of Clastic Sediments. Geol. Soc. Am. Spec. Paper 284. Boulder, Colorado, 21-40.

Medlicott, H. B., 1864. On the geological structure and relations of the southern portion of the Himalayan ranges between the river Ganges and the Ravee. Memoir Geol. Surv. India 3, 1-212.

Meigs, A. J., Burbank, D. W. & Beck, R. A., 1995. Middle-late Miocene (>10Ma) formation of the Main Boundary thrust in the western Himalaya. Geology 23, 423-426.

Meissner, C. R., Hussain, M., Rashid, M. A. & Sethi, U. B., 1969. Geology of the Parachinar Quadrangle, Pakistan. USGS Prof. Paper 716-G, 20 p.

Meissner, C. R., Master, J. M., Rashid, M. A. & Hussain, M., 1974. Stratigraphy of the Kohat Quadrangle, Pakistan. USGS Prof. Paper 716-D, 89 p.

Meissner, C. R., Hussain, M., Rashid, M. A. & Sethi, U. B., 1975. Geology of the Parachinar quadrangle, Pakistan. USGS. Prof. Paper, 716-F, 24p.

Metcalfe, R. P., 1993. Pressure, temperature and time constraints on metamorphism across the Main Central Thrust zone and High Himalayan slab in the Garhwal Himalaya. In: Treloar, P. J. and Searle, M. P. (Eds.), Himalayan Tectonics. Geol. Soc. Spec. Pub. 74, 485-509.

Miall, A. D., 1977. A review of the braided river depositional environment. Earth Sci. Rev. 13, 1-62.

Miall, A. D., 1978. Lithofacies types and vertical profile models in braided river deposits. In: Miall, A. D. (Ed.), Fluvial Sedimentology, Calgary. Can. Soc. Petrol. Geol., Mem. 5, 597-604.

Miall, A. D., 1996. The Geology of Fluvial Deposits: Sedimentary Facies, Basin Analysis and Petroleum Geology. Springer-Verlag Inc., Heidelberg, 582p.

Miall, A. D., 2000. Principles of Sedimentary Basin Analysis. Springer, Berlin, 616p.

Michaelsen, P. & Henderson, R. A., 2000. Sandstone petrofacies expressions of multiphase basinal tectonics and arc magmatism: Permian-Triassic north Bowen Basin, Australia. Sed. Geol. 136, 113-136.

Mikoshiba, M. U., Takahashi,Y., Takahashi,Y., Kausar, A., Khan, T., Kubo, K. & Shirahase, T., 1999. Rb-Sr isotopic study of the Chilas Igneous Complex, Kohistan, northern Pakistan. In: Macfarlane, A., Sorkhabi, R. B. and Quade, J., (Eds.), Himalaya and Tibet: Mountain Roots to Mountain Tops. Geol. Soc. Am., Spec. Paper 328, 47-57.

Milliman, J. D. & Meade, R. H., 1983. World wide delivery of river sediment to the oceans. J. Geol. 91, 1-21.

Milliman, J. D., Quraishee, G. S. & Beg, M. A. A., 1984. Sediment discharge from the Indus River to the ocean: Past, present, and future In: Haq B. U. and Milliman, J. D. (Eds.), Marine Geology and Oceanography of the Arabian Sea and Coastal Pakistan. Van Nostrand Reynolds, New York, 65-70.

Mohindra, R., Parkash, B. & Prasad, J., 1992. Historical geomorphology and pedology of the Gandak megafan, middle Gangetic plains, India. Earth Surface Process and Landforms 17, 643-662.

Molnar, P., 1984. Structure and tectonics of the Himalaya: Constraints and implications of geophysical data. Annu. Rev. Earth Planet. Sci. 12, 498-518.

Molnar, P. & Tapponnier, P., 1975. Cenozoic tectonics of Asia: Effect of continental collision. Science 189, 419-426.

Mongelli, G., Cullers, R. L. & Muelheisen, S., 1996. Geochemistry of Late Cretaceous-Oligocene shales from the Varicolori Formation, southern Apennines, Italy: Implications for mineralogical, grain-size control and provenance. Eur. J. Miner. 8, 733-754.

Moore, M. A. & England, P. C., 2000. On the inference of denudation rates from cooling ages of minerals. EPSL 185, 265-284.

Morgan, M. E., Kingston, J. D. & Marino, B. D., 1994. Carbon isotopic evidence for the emergence of C4 plants in the Neogene from Pakistan and Kenya. Nature 367, 162-165.

Morton, A. C. & Johnsson, M. J., 1993. Factors influencing the composition of detrital heavy mineral suites in Holocene sands of the Apure river drainage basin, Venezuela. In: Johnsson M. J. and Basu, A. (Eds.), Processes Controlling the Composition of Clastic Sediments, Boulder, Colorado. Geol. Soc. Am. Spec. Paper 284, 171-185.

Morton, A. C., Davies, J. R. & Waters, R. A., 1992. Heavy minerals as a guide to turbidite provenance in the Lower Paleozoic Southern Welsh Basin: A pilot study. Geol. Mag. 129, 573-580.

Mulder, T. J., 1991. Isochronous paleogeographies and stratigraphic evolution of the northwest Himalayan foredeep, 8.5-5 Ma, central and eastern Potwar Plateau, Pakistan. Unpub. MS Thesis. Los Angeles, Univ. of Southern California, 107p.

Mulder, T. J. & Burbank, D. W., 1993. The impact of incipient uplift on patterns of fluvial deposition: An example from the Salt Range, Northwest Himalayan Foreland, Pakistan. In: Marzo, M. and Puigdefabregas, C. (Eds.), Alluvial Sedimentation. Oxford, Blackwell Scientific Publications 17, 521-539.

Munoz-Jimenez, A. & Casas-Sainz, A. M., 1997. The Rioja Trough (N Spain): Tectonosedimentary evolution of a symmetric foreland basin. Basin Res. 9, 65-85.

Murphy, M. A. & Harrison, T. M., 1999. Relationship between leucogranites and the Qomolangma detachment in the Rongbuk Valley, south Tibet. Geology 27, 831-834.

Myrow, P. M., Snell, K. E., Hughes, N. C., Paulsen, T. S., Heim, N. A. & Parcha, S. K., 2006a. Cambrian depositional history of the Zanskar valley region of the Indian Himalaya: Tectonic implications. J. Sed. Res. 76, 364-381.

Myrow, P. M., Thompson, K. R., Hughes, N. C., Paulsen, T. S., Sell, B. K. & Parcha, S. K., 2006b. Cambrian stratigraphy and depositional history of the northern Indian Himalaya, Spiti Valley, north-central India. Geol. Soc. Am. Bull. 118, 491-510.

Nagarajan, R., Madhavaraju, J., Nagendra, R., Armstrong-Altrin, J. S. & Moutte, J., 2007. Geochemistry of Neoproterozoic shales of the Rabanpalli Formation, Bhima Basin, Northern Karnataka, southern India: Implications for provenance and paleoredox conditions. Revista Mexicana de Ciencias Geológicas 24, 150-160.

Naidu, A. S., 1966. Lithological and chemical facies changes in the recent deltaic sediments of the Godavari River, India. In: Shirly, M. L. (Ed.), Deltas in Their Geologic Framework. Geol. Soc. Houston, 125-158.

Naini, B. R. & Kolla, V., 1982. Acoustic character and thickness of sediments of the Indus Fan and the continental margin of western India. Marine Geol. 47, 181-185.

Najman, Y., 2006. The detrital record of orogenesis: A review of approaches and techniques used in the Himalayan sedimentary basins. Earth Sci. Rev. 74, 1-72.

Najman, Y. & Garzanti, E., 2000. Reconstructing early Himalayan evolution and paleogeography from Tertiary foreland basin sedimentary rocks, Northern India. Geol. Soc. Am. Bull. 112, 435-449.

Najman, Y., Pringle, M. S., Johnson, M. R. W., Robertson, A. H. F. & Wijbrans, J. R., 1997. Laser Ar^{40}/Ar^{39} dating of single detrital muscovite grains from early foreland-basin sedimentary deposits in India: Implications for early Himalayan evolution. Geology 25, 535-538.

Najman, Y., Bickle, M. & Chapman, H., 2000. Early Himalayan exhumation: Isotopic constraints from the Indian foreland basin. Terra Nova 12, 28-34.

Najman, Y., Pringle, M., Godin, L. & Oliver, G., 2001. Dating of the oldest continental sediments from the Himalayan foreland basin. Nature 410, 194-197.

Najman, Y., Pringle, M., Godin, L. & Oliver, G., 2002. A reinterpretation of the Balakot Formation: Implications for the tectonics of the NW Himalaya, Pakistan. Tectonics 21, 7-18.

Najman, Y., Garzanti, E., Pringle, M., Bickle, M., Stix, J. & Khan, I., 2003a. Early-Middle Miocene paleodrainage and tectonics in the Pakistan Himalaya. Geol. Soc. Am. Bull. 115, 1265-1277.

Najman, Y., Pringle, M., Bickle, M., Garzanti, E., Burbank, D., Ando, S. & Brozovic, N., 2003b. Non-steady-state exhumation of the Higher Himalaya, N.W. India: Insights from a combined isotopic and sedimentological approach. Geoph. Res. Abstracts 5 (abstr 04551).

Najman, Y., Johnson, C., White, N. M. & Oliver, G., 2004. Constraints on foreland basin and orogenic evolution from detrital mineral fission track analyses and sediment facies of the Himalayan foreland basin, NW India. Basin Res. 16, 1-24.

Nakata, T., 1989. Active faults of the Himalaya of India and Nepal. Geol. Soc. Am. Spec. Paper 232, 243-264.

Nakayama, K. & Ulak, P. D., 1999. Evolution of fluvial style in the Siwalik Group in the foothills of the Nepal Himalaya. Sed. Geol. 125, 205-224.

Nath, B. N., Bau, M., Ramalingeswara Rao, B. & Rao, Ch. M., 1997. Trace and rare earth elemental variation in Arabian Sea sediments through a transect across the oxygen minimum zone. Geochim. Cosmochim. Acta 61, 2375-2388.

Nesbitt, H. W. & Young, G. M., 1982. Early Proterozoic climates and plate motions inferred from major element chemistry of lutites. Nature 299, 715-717.

Nesbitt, H. W. & Young, G. M., 1984. Prediction of some weathering trends of plutonic and volcanic rocks based on Thermodynamic and Kinetic considerations. Geochim. Cosmochim. Acta 48, 1523-1534.

Nesbitt, H. W. & Young, G. M., 1989. Formation and diagenesis of weathering profile. J. Geol. 97, 129-147.

Nesbitt, H. W. & Young, G. M., 1996. Petrogenesis of sediments in the absence of chemical weathering: Effects of abrasion and sorting on bulk composition and mineralogy. Sediment. 43, 341-358.

Nesbitt, H. W., Markovics, G. & Price, R. C., 1980. Chemical processes affecting alkalis and alkaline earths during continental weathering. Geochim. Cosmochim. Acta 44, 1659-1666.

Nesbitt, H. W., Young, G. M., McLennan, S. M. & Keays, R. R., 1996. Effects of chemical weathering and sorting on the petrogenesis of siliciclastic sediments, with implication for provenance studies. J. Geol. 104, 525-542.

Net, L. I., Alonso, M. S. & Limarino, C. O., 2002. Source rock and environmental control on clay mineral associations, Lower Section of Paganzo Group (Carboniferous), Northwest Argentina. Sed. Geol. 152, 183-199.

Norrish, K. & Pickering, J. G., 1983. Clay minerals. In: CSIRO, a Division of Soils (Ed.), Soils: An Australian Viewpoint. Commonwealth Scientific and Industrial Research Organization/ Academic Press, 281-308.

O'Brien, P. J., 2001. Subduction followed by collision: Alpine and Himalayan examples. Physics of the Earth and Planetary Interiors, 127, 277–291.

Okada, H., 1971. Classification of sandstones: Analysis and proposals. J. Geol. 79, 509-525.

Oldham, R. D., 1893. Manual of the Geology of India. 2nd Edition, Govt. of India, Calcutta, 543p.

Ori, G. G. & Friend, P. F., 1984. Sedimentary basins formed and carried piggyback on active thrust sheets. Geology 12, 475-478.

Ori, G. G., Roveri, M. & Vannoni, F., 1986. Plio-Pleistocene sedimentation in the Apenninic-Adriatic foredeep (Central Adriatic Sea, Italy). In Allen, P. A. and Homewood, P. (Eds.), Foreland Basins. Int. Assoc. Sediment. Spec. Pub. 8, 183-198.

Orton, G. J. & Reading, H. G., 1993. Variability of deltaic processes in terms of sediment supply, with particular emphasis on grain size. Sediment., 40, 475-512.

Osae, S., Asiedu, D. K., Banoeng-Yakubo, B., Koeberl, C. & Dampare, S. B., 2006. Provenance and tectonic setting of Late Proterozoic Buem sandstones of southeastern Ghana: Evidence from geochemistry and detrital modes. J. African Earth Sciences 44, 85-96.

Ouchi, S., 1985. Response of alluvial rivers to slow active tectonic movement. Geol. Soc. Am. Bull. 96, 504-515.

Paola, C., 1988. Subsidence and gravel transport in alluvial basins. In: Kleinspehn, K. L. and Paola, C. (Eds.), New Perspectives in Basin Analysis. Springer-Verlag, New York, 231-243.

Parkash, B., Sharma, R. P. & Roy, A. K., 1980. The Siwalik Group (Molasse) sediments shed by collision of continental plates. Sed. Geol. 25, 127-159.

Parrish, R. R. & Hodges, K. V., 1996. Isotopic constraints on the age and provenance of the Lesser and Greater Himalayan Sequences, Nepalese Himalaya. Geol. Soc. Am. Bull. 108, 904-911.

Parrish, R. R. & Tirrul, R., 1989. U-Pb age of the Baltoro granite, northwest Himalaya, and implications for monazite systematics. Geology 17, 1076-1079.

Pascoe, E. H., 1963. "A manual of geology of India and Burma." vol. III: Ibid., Calcutta: 1344-2130.

Peˆcher, A., 1989. The metamorphism in the central Himalaya. J. Met. Geol. 7, 31-41.

Pearce, T. J., Wray, D., Ratcliffe, K., Wright, D. K. & Moscariello, A., 2005. Chemostratigraphy of the Upper Carboniferous Schooner Formation, southern North Sea. In: Collinson, J. D., Evans, D. J., Holliday D. W. and Jones N. S. (Eds.), Carboniferous Hydrocarbon Resources: The southern North Sea and surrounding onshore areas. The Occasional Publications series of the Yorkshire Geol. Soc. 7, 147-164.

Peltzer, G. & Tapponnier, P., 1988. Formation and evolution of strike-slip faults, rifts and basins during the India-Asia collision: An experimental approach. J. Geophys. Res. 93, 15095-15117.

Petterson, M. G. & Treloar, P. J., 2004. Volcanostratigraphy of arc volcanic sequences in the Kohistan arc, North Pakistan: Volcanism within island arc, back-arc basin, and intra-continental tectonic settings. J. Volcanol. Geotherm. Res. 130, 147-178.

Petterson M. G. & Windley, B. F., 1985. Rb-Sr dating of the Kohistan arc-Batholith in the Trans-Himalaya of N. Pakistan and tectonic implications. EPSL, 74, 45-75.

Petterson, M, G. & Windley, B. F., 1991. Changing source regions of magmas and crustal growth in the Trans-Himalayas: Evidence from the Chalt volcanics and Kohistan batholith, Kohistan, northern Pakistan. EPSL, 102, 326-341.

Pettijohn, F.J., Potter, P.E. & Siever, R., 1987. Sand and Sandstone. 2nd Ed. Springer, New York, 553p.

Pierini, C., Mizusaki, A. M. P., Scherer, C. M. S. & Alves, D. B., 2002. Integrated stratigraphic and geochemical study of the Santa Maria and Caturrita formations (Triassic of the Parana´ Basin), southern Brazil. J. South Am. Earth Sciences 15, 669-681.

Pilbeam, D. R., Behrensmeyer, A. K., Barry, J. C. & Shah, S. M. I., (Eds.). 1979. Miocene Sediments and Faunas of Pakistan. Postilla. 179, 45p.

Pilgrim, G. E., 1910. Preliminary notes on a revised classification of the Tertiary freshwater deposits of India. India Geol. Surv. Recs. 40, 185-205.

Pilgrim, G. E., 1913. "The correlation of the Siwaliks with mammal horizon of Europe." Geol. Surv. India, Rec. 43, 137-160.

Pilgrim, G. E., 1919. Suggestions concerning the history of the drainage of northern India, arising out of the study of the Siwalik Boulder Conglomerate. J. Astatic Soc. Bengal. NS 15, 81-99.

Pinet, P. & Souridu, M., 1988. Continental erosion and large-scale relief. Tectonics 7, 563-582.

Pinfold, E. S., 1918. Notes on structure and stratigraphy in the North-West Punjab. India Geol. Surv. Recs. 49, 137-160.

Pivnik, D. A. & Sercombe W. T., 1993. Compression and transpression-related deformation in the Kohat plateau, NW Pakistan. In: Treloar, P. T. and Searle, M. P. (Eds.), Himalayan Tectonics. Geol. Soc. Lond. Spec. Publ. 74, 559-580.

Pivnik, D. A. & Wells, N. A., 1996. The transition from Tethys to the Himalaya as recorded in northwest Pakistan. Geol. Soc. Am. Bull. 108, 1295-1313.

Pognante, U. & Spencer, D. A., 1991. First report of eclogites from the Himalayan belt, Kaghan valley (northern Pakistan). Europ. J. Mineral. 3, 613-618.

Pogue, K. R., Hylland, M. D., Yeats, R. S., Khattak, W. U. & Hussain, A., 1999. Stratigraphic and structural framework of Himalayan foothills, northern Pakistan. In: Macfarlane, A., Sorkhabi, R. B. and Quade, J. (Eds.), Himalaya and Tibet: Mountain Roots to Mountain Tops. Geol. Soc. Am. Spec. Papers 328, 257-274.

Pollack, J. M., 1961. Significance of compositional and textural properties of south Canadian river channel sands, New Mexico, Texas, and Oklahoma, J. Sed. Pet. 31, 15-37.

Potter, P. E., 1978. Petrology and chemistry of modern big river sands, J. Geol. 86, 423-449.

Potter, P. E., 1984. South American modern beach sand and plate tectonics. Nature 311, 645-648.

Potter, P. E., 1986. South American and a few grains of sand: Part 1 beach sands. J. Geol. 94, 301-319.

Potter, P. E., Heling, D., Shimp, N. F. & Van Wie, W., 1975. Clay mineralogy of modern alluvial muds of the Mississippi River basin. Bull. Cent. Rech. Pau. 9, 353-389.

Potter, P. E., Maynard, J. B. & Pryor, W. A., 1980. Sedimentology of Shale. Springer-Verlag, Berlin, 400p.

Potter, P. E., Maynard, J. B. & Depetris, P. J., 2005. Mud and Mudstones. Springer-Verlag, Berlin Heidelberg.

Powell, C. M., 1979. A speculative tectonic history of Pakistan and surroundings: Some constraints from the Indian Ocean. In: Farah, A. and DeJong, K. A. (Eds.), The geodynamics of Pakistan. Geol. Surv. Pakistan, Quetta, 5-24.

Powell, C. M. & Conaghan, P. J., 1973. Plate tectonics and the Himalayas. EPSL 20, 1-12.

Powers, P. M., Lillie, R. J. & Yeats, R. S., 1998. Structure and shortening of the Kangra and Dehra Dun re-entrants, Sub-Himalaya, India. Geol. Soc. Am. Bull. 110, 1010-1027.

Prell W. L. & Kutzbach, J. E., 1992. Sensitivity of the Indian monsoon to forcing parameters and implications for its evolution. Nature 360, 647-652.

Prince, C. I., Foster, G., Vance, D., Harris, N. & Baker, J., 1999. The thermochronology of the High Himalayan crystallines in the Garhwal Himalaya; prograde history of a polymetamorphic slab. Terra Nostra 99, 119-120.

Prothero, D. R. & Schwab, F. L., 2003. Sedimentary Geology. W H Freeman & Co. 99-126.

Pudsey, C. J., 1986. The Northern Suture, Pakistan: Margin of a Cretaceous island arc. Geol. Mag. 123, 405-423.

Qayyum, M., Niem, A. R. & Lawrence, R. D., 1996. Newly discovered Paleogene deltaic sequence in the Katawaz basin, Pakistan and its tectonic implications. Geology 24, 835-838.

Qayyum, M., Lawrence, R. D. & Niem, A. R., 1997. Discovery of the paleo-Indus delta-fan complex. J. Geol. Soc. Lond. 154, 753-765.

Qayyum, M., Niem, A. R. & Lawrence, R. D., 2001. Detrital modes and provenance of the Paleogene Khojak Formation in Pakistan: Implications for early Himalayan orogeny and unroofing. Geol. Soc. Am. Bull. 113, 320-332.

Quade, J. & Cerling, T. E., 1995. Expansion of C4 grasses in the Late Miocene of Northern Pakistan: Evidence from stable isotopes in paleosols. Palaeo. Palaeo. Palaeo 115, 91-116.

Quade, J. & Roe, J. L., 1999. The stable isotope composition of early ground water cements from sandstone in paleoecological reconstruction. J. Sed. Res. 69, 667-674.

Quade, J., Cerling, T. E. & Bowman, J. R., 1989. Development of Asian monsoon revealed by marked ecological shift during the Latest Miocene in northern Pakistan. Nature 342, 163-166.

Quade, J., Cerling, T. E., Barry, J. C., Morgan, M. E., Pilbeam, D. R., Chivas, A. R., Lee-Thorp, J. A. & Van der Merwe, N. J., 1992. A 16-Ma record of paleodiet using carbon and oxygen isotopes in fossil teeth from Pakistan. Chem. Geol. (Isotope Geoscience Section) 94, 182-192.

Quade, J., Cater, J. M. L., Ojha, I. P., Adam, J. & Harrison, T. M. J., 1995. Late Miocene environmental change in Nepal and the Northern Indian subcontinent: Stable isotope evidence from Paleosols. Geol. Soc. Am. Bull. 107, 1381-1397.

Rafiq, M., 1987. Petrology and geochemistry of the Ambela granitic complex, N.W.F.P. Pakistan. Unpub. Ph.D. Thesis, Univ. of Peshawar.

Rai, H., 1987. Geochemical study of volcanics associated with Indus ophiolitic melange in western Ladakh, Jammu and Kashmir. Ofioliti 12, 71-82.

Raiverman, V., 2002. Foreland Sedimentation in Himalayan Tectonic Region: A Relook at the Orogenic Process. Bishen Singh Mahendra Pal Singh, Dehra Dun, India, 378p.

Raiverman, V. & Suresh, N., 1997. Clay mineral distribution in the Cenozoic sequence of the western Himalayan Foothills. J. Indian Assoc. Sediment. 16, 63-75.

Raiverman, V., Kunte, S. V. & Mukherjea, A., 1983. Basin geometry, Cenozoic sedimentation and hydrocarbon in north western Himalaya and Indo-Gangetic plains. Petrol. Asia Journal 6, 67-92.

Rashid, M. A., 1965. Mineral deposits of Eastern Kohat region, West Pakistan. Pakistan Geol. Surv. Recs., 13, pt. 2.

Rashid, S. A., 2002. Geochemical characteristics of Mesoproterozoic clastic sedimentary rocks from the Chakrata Formation, Lesser Himalaya: Implications for crustal evolution and weathering history in the Himalaya. J. Asian Earth Sciences 21, 283-293.

Ratschbacher, L., Frisch, W., Liu, G. & Chen, C., 1994. Distributed deformation in southern and western Tibet during and after India-Eurasia collision. J. Geoph. Res. 99, 19917-19945.

Raup, D. M. & Sepkoshi, J. J. Jr., 1984. Periodicity of extinction in geologic past. National Academy of Sciences Preceedings 81, 801-805.

Raymo, M. E. & Ruddiman, W. F., 1992. Tectonic forcing of Late Cenozoic climate. Nature 359, 117-122.

Raynolds, R. G. H., 1981. Did the ancestral Indus flow into the Ganges drainage? Geol. Bull. Univ. Peshawar 14, 141-150.

Raynolds, R. G. H. & Johnson, G. D., 1985. Rates of Neogene depositional and deformational processes, northwest Himalayan foredeep margin, Pakistan. In: Snelling, N. J. (Ed.), The Chronology of the Geological Record. Geol. Soc. Lond. Memoir 10, 291-311.

Raza, S. M., Cheema, I. U., Downs, W. R., Rajpar, A. R. & Ward, S. C., 2002. Miocene stratigraphy and mammal fauna from the Sulaiman Range, Southwestern Himalayas, Pakistan. Palaeo. Palaeo. Palaeo. 186, 185-197.

Reading, H. G., 1972, Global tectonics and the genesis of flysch successions. 24th International Geological Congress Proceedings, Section 6, 59-66.

Reading, H. G., 1996. Sedimentary Environments: Process, Facies and Stratigraphy. Blackwell Science. 688 pp.

Rehman, S. S., Sabir, M. A. & Khan, J., 1997. Discharge characteristics and suspended load from rivers of Northern Indus Basin, Pakistan, Geol. Bull. Univ. Peshawar 30, 325-336.

Reiners, P. W., Ehlers, T. A., Mitchell, S. G. & Montgomery, D. R., 2003. Coupled spatial variations in precipitation and long-term erosion rates across the Washington Cascades. Nature 426 (6967), 645-647.

Retallack, G. J., 1986. Fossil soils as grounds for interpreting long term controls on ancient rivers. J. Sed. Pet. 56, 1-18.

Retallack, G. J., 1988, Field recognition of paleosols. In: Reinhardt, J. and Sigleo, W. R. (Eds.), Paleosols and Weathering Through Geologic Time: Principles and Applications. Geol. Soc. Am. Spec. Paper 216, 1-20.

Retallack, G. J., 1991. Miocene Paleosols and Ape Habitats of Pakistan and Kenya. Oxford University Press, New York.

Retallack, G. J., 1997. A Color Guide to Paleosols. Wiley, Chichester. 175 pp.

Robertson A. H. F. & Collins A. S., 2002. Shyok suture Zone, N. Pakistan: Late Mesozoic-Tertiary evolution of a critical suture separating the oceanic Ladakh Arc from the Asian continental margin. J. Asian Earth Sciences 20, 309-51.

Robertson, A. H. F. & Degnan, P. J., 1993. Sedimentology and tectonic implications of the Lamayuru Complex: Deep water facies of the Indian Passive margin. In: Treloar, P. J. and Searle, M. P. (Eds.), Himalayan Tectonics. Geol. Soc. Lond. Spec. Pub. 74, 299-322.

Robertson A. H. F. & Degnan P. J., 1994. The Dras arc complex: Lithofacies and reconstruction of a Late Cretaceous oceanic volcanic arc in the Indus Suture Zone, Ladakh Himalaya. Sed. Geol. 92, 117-45.

Robinson, D. M., DeCelles, P. G., Garzione, C. N., Pearson, O. N., Harrison, T. M. & Catlos, E. J., 2003. Kinematic model for the Main Central thrust in Nepal. Geology 31, 359-362.

Roddaz, M., Viers, J., Brusset, S., Baby, P. & He´rail, G., 2005. Sediment provenances and drainage evolution of the Neogene Amazonian foreland basin. EPSL 239, 57-78.

Rolland Y., Pecher A. & Picard C., 2000. Middle Cretaceous back-arc formation and arc evolution along the Asian margin; the Shyok suture zone in northern Ladakh (NW Himalaya). Tectonophysics, 325, 145-73.

Rolland, Y., Mahéo, G., Guillot, S. & Pêcher, A., 2001. Tectono-metamorphic evolution of the Karakorum Metamorphic complex (Dassu-Askole area, NE Pakistan): Exhumation of mid-crustal HT-MP gneisses in a convergent context. J. Met. Geol. 19, 717-737.

Rolland, Y., Picard, C., Pecher, A., Lapierre, H., Bosch, D. & Keller, F., 2002. The Cretaceous Ladakh arc of NW Himalaya; slab melting and melt-mantle interaction during fast northward drift of Indian Plate. Chem. Geol. 182, 139-78.

Roser, B. P. & Korsch, R. J., 1985. Plate tectonics and geochemical composition of sandstones: A discussion. J. Geol. 93, 81-84.

Roser, B. P. & Korsch, R. S., 1986. Determination of tectonic setting of sandstone-mudstone suites using SiO_2 content and K_2O/Na_2O ratio. J. Geol. 94, 635-650.

Roser, B. P. & Korsch, R. J., 1988. Provenance signatures of sandstone-mudstone suites determined using discriminant function analysis of major-element data. Chem. Geol. 67, 119-139.

Rowley, D. B., 1996. Age of initiation of collision between India and Asia: A review of stratigraphic data. EPSL 145, 1-13.

Ruddiman, W. F. & Kutzbach, J. E., 1989. Forcing of the late Cenozoic Northern Hemisphere climate by plateau uplift in southeast Asia and the American southwest. J. Geoph. Res. 94, 18409-18427.

Ruddiman, W. F., Prell, W. L. & Raymo, M. E., 1989. Late Cenozoic uplift in southern Asia and the American West: Rationale for general circulation modeling experiments. J. Geoph. Res. 94, 18379-391.

Ruffell, A. & Worden, R., 2000. Palaeoclimate analysis using spectral gamma-ray data from the Aptian (Cretaceous) of southern England and southern France. Palaeo. Palaeo. Palaeo. 155, 265-283.

Ruiz, G. & Diane, S., 2006. The Punjab foreland basin of Pakistan: A reinterpretation of zircon fission-track data in the light of Miocene hinterland dynamics. Terra Nova, 18, 248-256.

Rumelhart, P. E. & Ingersoll, R. V., 1997. Provenance of the upper Miocene Modelo Formation and subsidence analysis of the Los Angeles basin, southern California: Implications for paleotectonic and paleogeographic reconstructions. Geol. Soc. Am. Bull. 109, 885-899.

Rust, B. R., 1978a. Depositional models for braided alluvium. In: Miall, A. D. (Ed.), Fluvial Sedimentology. Can. Soc. Petrol. Geol. Mem. 5, 605-625.

Rust, B. R., 1978b. Depositional models for braided alluvium. In: Miall, A. D. (Ed.), Fluvial Sedimentology. Can. Soc. Petrol. Geol. Mem. 5, 605-626.

Rust, B. R. & Jones, B. G., 1987. The Hawkesbury Sandstone south of Sydney, Australia. Triassic analogue for the deposits of large braided rivers. J. Sed. Pet. 57, 222-233.

Rust, B. R. & Koster, E. H., 1984. Coarse alluvial deposits. In: Walker, R. G. (Ed.), Facies Models. Geol. Assoc. Canada. 53-69.

Sahni, A. & Mitra, H. C., 1980. Neogene palaeobiogeography of the Indian subcontinent with special reference to fossil vertebrates. Palaeo. Palaeo. Palaeo. 31, 39-62.

Sakai, H., 1989. Rifting of Gondwanaland and uplifting of the Himalayas recorded in Mesozoic and Tertiary fluvial sediments in the Nepal Himalayas. In: Taira, A. and Masuda, F. (Eds.), Sedimentary Facies in the Active Plate Margin. Terra Scientific Publishing Company, Tokyo, 723-732.

Sakai, H., Takigami, Y., Nakamuta, Y. & Nomura, H., 1999. Inverted metamorphism in the Pre-Siwalik foreland basin sediments beneath the crystalline nappe, western Nepal Himalaya. J. Asian Earth Sciences 17, 727-739.

Sanyal, P., Bhattacharya, S. K., Kumar, R., Ghosh, S. K. & Sangode. S. J., 2004. Mio-Pliocene monsoonal record from Himalayan foreland basin (Indian Siwalik) and its relation to vegetational change. Palaeo. Palaeo. Palaeo. 205, 23-41.

Sanyal, P., Bhattacharya, S. K. and Prasad, M., 2005. Chemical diagenesis of Siwalik sandstone: Isotopic and mineralogical proxies from Surai Khola section, Nepal. Sed. Geol. 180, 57-74.

Savage, K. M. & Potter, P. E., 1991. Petrology of modern sands of the Rios, Gauviare and Inirida, southern Colombia: Tropical climate and sand composition. J. Geol. 99, 289-298.

Scaillet, B., France-Lanord, C., & LeFort, P., 1990. Badrinath-Gangotri plutons (Garhwal, India): Petrological and geochemical evidence for fractionation processes in a High Himalayan leucogranite. J. Volcanology and Geothermal Res. 44, 163-188.

Scaillet, B., Peˆcher, A., Rochette, P. & Champenois, M., 1995. The Gangotri granite (Garhwal Himalaya): Laccolithic emplacement in an extending collisional belt. J. Geoph. Res. 100, 585-607.

Scharer, U., Xu, R. H. & Alle`rgre, C. J., 1984. U-Pb geochronology of Gangdese (Transhimalaya) plutonism in the Lhasa-Xigaze region, Tibet. EPSL 69, 311-320.

Scharer, U., Copeland, P., Harrison, T. M. & Searle, M. P., 1990. Age, cooling history and origin of postcollisional leucogranites in the Karakoram Batholith, N. Pakistan: A multi-system isotope study. J. Geol. 98, 233-251.

Schelling, D. & Arita, K., 1991. Thrust tectonics, crustal shortening, and the structure of the far-eastern Nepal, Himalaya. Tectonics 10, 851-862.

Schlunegger, F., Jordan, T. E. & Klaper, E. M., 1997. Controls on erosion denudation in the orogen on foreland basin evolution: The Oligocene central Swiss Molasse Basin as an example. Tectonics 16, 823-840.

Schlunegger, F., Slinerland, R. & Matter, A., 1998. Crustal thickening and crustal extension as controls on the evolution of drainage network of the central Swiss Alps between 30 Ma and present: Constraints from the stratigraphy of the Northern Alpine Foreland Basin and the structural evolution of the Alps. Basin Res. 10, 197-212.

Schneider, D. A., Edwards, M. A., Kidd, W. S. F., Khan, M. A., Seeber, L. & Zeitler, P. K., 1999. Tectonics of Nanga Parbat, Western Himalaya; Synkinematic plutonism within the doubly vergent shear zones of a crustal-scale pop-up structure. Geology 27, 999-1002.

Shroder, J. F. & Bishop, M. P., 1999. Indus to the sea: Evolution of the system and Himalaya geomorphology. In: Meadows, A and Meadows, P. S. (Eds.). The Indus River, Biodiversity, Resources, Humankind. Oxford Univ. Press, Oxford, 231-248.

Shroder, J. F. & Bishop, M. P., 2000. Unroofing of the Nanga Parbat Himalaya. In: Khan, M. A., Treloar, P. J., Searle, M. P. and Jan, M. J. (Eds.), Tectonics of the Nanga Parbat Syntaxis and the Western Himalaya. Geol. Soc. Lond. Spec. Pub. 170, 163-179.

Schumm, S. A., 1986. Alluvial river response to active tectonics. Active Tectonics, Washington D. C. National Academy Press, 80-94.

Schwab, F. L., 1971. Geosynclinal composition and the new global tectonics. J. Sed. Pet. 41, 928-938.

Schwab, F. L., 1975. Framework mineralogy and chemical compositional of continental margin-type sandstone. Geology 3, 487-490.

Schwartz, R. K. & DeCelles, P. G., 1988. Cordilleran Foreland Basin evolution in response to interactive Cretaceous thrusting and foreland partitioning, Southwestern Montana. Geol. Soc. Am. Mem. 171, 489-513.

Searle, M. P., 1983. Stratigraphy, structure and evolution of the Tibetan-Tethys zone in Zanskar and the Indus suture zone in the Ladakh Himalaya. Royal Soc. Edinburgh Transac. Earth Sciences 73, 205-219.

Searle, M. P., 1987. Thrust related origin and emplacement of crustly derived leucogranites of the High Himalaya, from Zanskar and Gangotri. Abstract. T. S. G. annual meeting. P. 57.

Searle, M. P., 1991. Geology and Tectonics of the Karakoram Mountains. John Wiley and Sons Inc.

Searle, M. P., 1996. Cooling history, erosion, exhumation, and kinematics of the Himalaya-Karakorum-Tibet orogenic belt. In: Yin, A. and Harrison, T. M. (Eds.), The Tectonic Evolution of Asia, Cambridge Univ. Press, 110-137.

Searle, M. P. & Khan, M. A., 1996. Geological Map of North Pakistan and Adjacent Areas of Northern Ladakh and Western Tibet, Scale 1:650,000. Oxford University, Oxford, England.

Searle, M. P. & Owen, L. A., 1999. The evolution of the Indus River in relation to topographic uplift, erosion, climate and geology of western Tibet, the Trans-Himalaya and High Himalaya ranges. In: Meadows, A. and Meadows, P. S.

(Eds.), The Indus River, Biodiversity, Resources, Humankind. Oxford Univ. Press, Oxford, 208-230.

Searle, M. P. & Rex, A. J., 1989. Thermal model for the Zanskar Himalaya. J. Met. Geol. 7, 127-134.

Searle, M. P., Rex, A. J., Tirrul, R., Rex, D. C., Barnicoat, A. & Windley, B. F., 1989. Metamorphic, magmatic, and tectonic evolution of the central Karakoram in the Biafo-Baltoro-Hushe regions of northern Pakistan. In: Malinconico, L. L. and Lillie, R. J. (Eds.), Tectonics of the Western Himalaya. Geol. Soc. Am. Spec. Paper 232, 47-73.

Searle, M. P., Khan., M. A., Jan M. Q., Dipietro., J. A., Pogue, K. R., Pivnik, D. A., Sercombe, W. J., Izatt, C. N., Blisniuk, P. M., Treloar, P. J., Gaetani, M. & Zanchi, A., 1996. Geological Map of North Pakistan and adjacent areas of northern Ladakh and western Tibet, Scale 1: 650,000.

Searle, M. P., Corfield, R. I., Stephenson, B. & McCarron, J., 1997. Structure of the north Indian continental margin in the Ladakh-Zanskar Himalayas: Implications for the timing of obduction of the Spontang ophiolite, India-Asia collision and deformation events in the Himalaya. Geol. Mag. 134, 297-316.

Searle, M. P., Weinberg, R. F. & Dunlap, W. J., 1998. Transpressional tectonics along the Karakoram fault zone, northern Ladakh: Constraints on Tibetan extrusion. In: Holdsworth, R. E., Strachan, R. A. and Dewey, J. F. (Eds.), Continental Transpressional and Transtensional Tectonics. Geol. Soc. Lond. Spec. Pub. 135, 307-326.

Searle, M. P., Nobles, S. R., Hurford, A. J. & Rex, D. C., 1999. Age of crustal melting, emplacement and exhumation history of the Shivling leucogranite, Garhwal Himalaya. Geol. Mag. 136, 513-525.

Searle, M. P., Simpson, R. L., Law, R. D., Parrish, R. R. & Waters, D. J., 2003. The structural geometry, metamorphic and magmatic evolution of the Everest massif, High Himalaya of Nepal-South Tibet. J. Geol. Soc. Lond. 160, 345-366.

Seeber, L. & Armbruster, J., 1979. Seismicity of the Hazara Arc in Northern Pakistan: Decollement vs. basement faulting. In: Farah, A. and De Jong, K. A. (Eds.), Geodynamics of Pakistan. Geol. Surv. Pakistan, Quetta, 131-142.

Seeber, L. & Armbruster, J. G., 1981. Great detachment earthquakes along the Himalayan arc and long-term forecasting. In: Simpson, D. W. and Richards, P. G. (Eds.), Earthquake Prediction: An International Review. Am. Geol. Union 4, 259-279.

Seeber, L. & Gornitz, V., 1983. River profiles along the Himalayan arc as indicators of active tectonics. Tectonophysics 92, 335-367.

Seeber, L., Armbruster, J. G. & Quittmeyer, R. C., 1981. Seismicity and continental subduction in the Himalayan arc. AGU, Geodynamics Series 5, Washington, D.C.

Selley, R. C., 1966. Tertiary fumaroles on the island of Raasay, Inverness-shire. Geol. Mag. 103, 558-564.

Selley, R. C., 1970. Ancient Sedimentary Environments. Chapman and Hall, Lond.

Sengupta, S. M., 1994. Introduction to Sedimentology. A. A. Balkema/Rotterdan/ Brookfield.

Shah, S. M. I., 1977. Stratigraphy of Pakistan. Geol. Surv. Pakistan Memoir 12, 138p.

Shao, L., Stettegger K. & Garbe-Schoenberg C. D., 2001. Sandstone petrology and geochemistry of the Turpan basin (NW China): Implications for the tectonic evolution of a continental basin. J. Sed. Res. 71, 37-49.

Sharma K. K., 1991. Petrochemistry and tectonic environment of Dras, Shyok, Khardung and Chushul volcanics of Indus Suture zone, Ladakh: A comparative study. In: Sharma K. K. (Ed.), Geology and Geodynamic Evolution of the Himalayan Collision Zone. Part 1. Pergamon Press. 133-153.

Shaw, D. M., 1968. A review of K-Rb fractionation trends by covariance analysis. Geochim. Cosmochim. Acta 32, 573-602.

Shaw, T. J., Geiskes, J. M. & Jahnke, R. A., 1990, Early diagénesis in differing depositional environments: The response of transition metals in pore water. Geochim. Cosmochim. Acta 54, 1233-1246.

Simpson, R. L., Parrish, R. R., Searle, M. P. & Waters, D. J., 2000. Two episodes of monazite crystallization during metamorphism and crustal melting in the Everest region of the Nepalese Himalaya. Geology 28, 403-406.

Singh, S. K. & France-Lanord, C., 2002. Tracing the distribution of erosion in the Brahmaputra watershed from isotopic compositions of stream sediments. EPSL 202, 645-662.

Sinha, R. & Friend, P. F., 1994. River systems and their sediment flux, Indo-Gangetic plains, northern Bihar, India. Sediment. 41, 825-845.

Smith, D. G., 1976. Effect of vegetation on lateral migration of anastomosed channels of a glacier meltwater river. Geol. Soc. Am. Bell. 87, 857-860.

Smith, D. G., 1983. Anastomosed fluvial deposits; modern examples from Western Canada. In: Collinson, J. D. and Lewin, J. (Eds.), Modern and Ancient Fluvial Systems. Int. Assoc. Sediment. Spec. Pub. 6, 155-168.

Smith, D. G., 1986. Anastomosing river deposits, sedimentation rates and basin subsidence, Magdalena River, northwestern Columbia, South America. Sed. Geol. 46, 177-196.

Smith, D. G. & Smith, N. D., 1980. Sedimentation in anastomosed river systems: Examples from alluvial valleys near Banff, Alberta. J. Sed. Pet. 50, 157-164.

Smith, H. A., Chamberlain, C. P. & Zeitler, P. K., 1994. Timing and duration of Himalayan metamorphism within the Indian Plate, northwest Himalaya, Pakistan, J. Geol. 102, 493-508.

Smith N. D., 1970. The braided stream depositional environment: Comparison of the Platte River with some Silurian clastic rocks, north central Appalachians. Geol. Soc. Am. Bull. 81, 2993-3014.

Smith, N. D. & Smith, D. G., 1984. William River: An outstanding example of channel widening and braiding caused by bed-load addition. Geology 12, 78-82.

Smith, N. D., Cross, T. A., Dufficy, J. P. & Clough, S. R., 1989. Anatomy of an avulsion. Sediment. 36, 1-24.

Sorkhabi, R. B. & Macfarlane, A., 1999. Himalaya and Tibet: Mountain roots to mountain tops. In: Macfarlane, A., Sorkhabi, R. B. and Quade, J. (Eds.), Himalaya and Tibet: Mountain Roots to Mountain Tops, Geol. Surv. Am. Spec. Paper 328, 1-8.

Spalletti, L. A., Queralt, I., Matheos, S. D., Colombo, F. & Maggi, J., 2007. Sedimentary petrology and geochemistry of siliciclastic rocks from the Upper Jurassic Tordillo Formation (Neuquen Basin, western Argentina): Implications for provenance and tectonic setting. J. South American Earth Sciences dio: 10.1016/j.jsames.

Spencer, D. A., 1993. What was the timing of the Himalayan continent-continent collision (45, 50, 55, 60 or 65 Ma)? Constraints from eclogites. Geol. Soc. Am. Abstracts with programs, 25, No.6, A-121.

Stanley, S. M., 1984. Temperature and biotic crises in the marine realm. Geology 12, 205-208.

Staubli, A., 1989. Polyphase metamorphism and the development of the Main Central Thrust. J. Met. Geol. 7, 73-93.

Stix, J., 1982. Stratigraphy of the Kamlial Formation near Chinji Village, Northern Pakistan. M. Sc. Dissertation, Hanover, New Hampshire, Dartmouth College, 17p.

Sto¨cklin, J., 1980. Geology of Nepal and its regional frame. J. Geol. Soc. Lond. 137, 1-34.

Stow, D. A. V., Amano, K., Balson, P. S., Brass, G. W., Corrigan, J., Raman, C. V., Tiercelin, J-J., Townsend, M. & Wijazananda, N. P., 1990. Sediment facies and processes on the distal Bengal Fan, Leg 116. Proc. Ocean Drilling Program, Scientific Results, 116, 377-396.

Stratigraphic Committee of Pakistan, 1964a. Minutes of the sixth meeting [February]: Pakistan Geol. Surv. Open File Report.

Stratigraphic Committee of Pakistan, 1964b. Minutes of the seventh meeting [April]: Pakistan Geol. Surv. Open File Report.

Streif, H. (Ed.), 1996. Deutsche Beitrage aur Quartarforschung in der sudlichen Nordsee, Geologisches Jahrbuch, Heft 146, Reihe A.E. Schweizerbart'sche Verlagsbuchhandlung, Hannover. 244 pp.

Subramanian, V., Van't Dack, L. & Van Grieken, R., 1985. Chemical composition of river sediments from the Indian subcontinent. Chem. Geol. 48, 271-279.

Suczek, C. A. & Ingersoll, R. W., 1985. Petrology and provenance of Cenozoic sand from the Indus Cone and the Arabian Basin, DSDP sites 211, 222 and 224. J. Sed. Pet. 55, 340-346.

Sullivan, M. A., Windley, B. F., Saunders, A. D., Haynes, J. R. & Rex, D. C., 1994. A paleogeographic reconstruction of the Dir Group: Evidence for magmatic arc migration within Kohistan, N. Pakistan. In: Treloar, P. J. and Searle, M. P. (Eds.), Himalayan Tectonics. Geol. Soc. Lond. Spec. Pub. 74, 139-160.

Suresh, N., Ghosh, S. K., Kumar, R. & Sangode, S. J., 2004. Clay-mineral distribution patterns in late Neogene fluvial sediments of the Subathu sub-basin, central sector of Himalayan foreland basin: Implications for provenance and climate. Sed. Geol. 163, 265-278.

Sutre, E., 1990. Les formations de la marge nord Neotethysienne et les mélanges ophiolitiques de la zone de l'Indus en Himalaya du Ladakh. PhD Thesis, Univ. of Poitiers, Poitiers, France.

Sutter, L. J., Langford, R. D. & Mack, G. H., 1985. Guide to the field study of alluvial fan and fan-delta deposits in the Fountain Formation (Pennsylvanian-Permian), Colorado. In: Ferm, J. C. and Horne, J. C. (Eds.), Carboniferous Depositional Environments in the Appalachian Region. Univ. of South Carolina, Columbia, S. C., 65-86.

Sutter, M. W. & Steidtmann, J. R., 1987. Fluvial-sandstone architecture and thrust-induced subsidence, northern Green River Basin, Wyoming. In: Ethridge, G., Flores, R. M. and Harvey, M. D. (Eds.), Recent Developments in Fluvial Sedimentology. Spec. Pub. Soc. Econ. Paleon. Mineral. 39, Tulsa, 279-285.

Suttner, L. J., 1974. Sedimentary Petrographic provinces: An evaluation. In: Ross, C. A. (Ed.), Paleogeographic Provinces and Provinciality. Spec. Pub. Soc. Econ. Paleon. Mineral. 21, 75-84.

Suttner, L. J., Basu, A. & Mack, G. H., 1981. Climate and the origin of quartzarenite. J. Sed. Pet. 51, 1235-1246.

Tahirkheli, R. A. K., 1979. Geology of Kohistan and adjoining Eurasian and Indo-Pakistan continents, Pakistan. Geol. Bull. Univ. Peshawar Spec. Issue 11, 1-30.

Tahirkheli, R. A. K., 1982. Geology of the Himalaya, Karakoram and Hindu Kush in Pakistan. Geol. Bull. Univ. Peshawar Spec. Issue, 15, 51p.

Tahirkheli, R. A. K., Mattauer, M., Proust, F. & Tapponier, P., 1979. The India-Eurasia suture zone in northern Pakistan: Synthesis and interpretation of data at plate scale, In: Farah, A. and DeJong, K. (Eds.), Geodynamics of Pakistan. Geol. Surv. Pakistan, Quetta. 125-130.

Tamburi, A. J., 1974. Geology and the water resources of the Indus Plains. Unpub. Ph. D. dissertation, Colorado State University, Fort Collins, CO.

Tanaka, S., 1997. Uplift of the Himalaya and climate changes at 10 Ma evidence from records of the carbon stable isotopes and fluvial sediments in the Churia Group Nepal. J. Geol. Soc. Japan. 103, 253-264.

Tandon, S. K. & Narayan, D., 1981. Calcrete conglomerate, casehardened conglomerate and cornstone-a comparative account of pedogenic and non-pedogenic carbonates from the continental Siwalik Group, Punjab, India. Sediment. 28, 353-367.

Tandon, S. K. & Varshney, S. K., 1991. Origin of selective carbonate cemented (concretionary) layers within multistoried sandstone bodies of the Neogene Middle Siwalik Subgroup, NW Himalaya, India. Abstract, Birbal Sahni Birth Centenary Symposium on the Siwalik Basin, WIHG, Dehra Dun, India, 45.

Tanoli, S. K., Abbasi, I. A., Riaz, M., Rahman, O., Iqbal, H. & Akhtar, M. K., 1993. Sedimentology of the Eocene sequence in the Kohat Basin. Unpub. Collaborative research project of National Center of Excellenece in Geology, Univ. of Peshawar And Exploration Studies & Research Department, Oil & Gas Development Corporation, Islamabad. 87p.

Tapponnier, P., Peltzer, G., Le Dain, A.Y., Armijo, R. & Cobbold, P., 1982. Propagating extrusion tectonics in Asia: New insights from simple experiments with plasticine. Geology 10, 611-616.

Tate, E. L. & Farquharson, F. K., 2000. Simulating reservoir management under the threat of sedimentation: The case of Tarbela Dam on the River Indus. Water Resour. Manag. 14, 191-208.

Taylor, S. R. & McLennan, S. M., 1985. The Continental Crust: Its Composition and Evolution. Blackwell Scientific Publications, Oxford. 312pp.

Tewari, V. C., 1993. Precambrian and Lower Cambrian stromatolites of the lesser Himalaya. Geophytology 23, 19-39.

Thakur, V. C., 1992, Geology of the Western Himalaya. Oxford, Pergammon Press. 363p.

Thakur, V. C. & Rawat, B. S., 1992. Geological Map of Western Himalaya, 1: 1,000,000. Wadia Institute of Himalayan Geology, Dehra Dun, India.

Thiede, R. C., Bookhagen, B., Arrowsmith, J. R., Sobel, E. R. & Strecker, M. R., 2004. Climatic control on rapid exhumation along the Southern Himalayan Front. EPSL 222, 791-806.

Thiry, M., 2000. Palaeoclimatic interpretation of clay minerals in marine deposits: An outlook from the continental origin. Earth Sci. Rev. 49, 201-221.

Tonarini, S., Villa, I. M., Oberli, F., Meier, M., Spencer, D. A., Pognante, U. & Ramsay, J. G., 1993. Eocene age of eclogite metamorphism in Pakistan Himalaya: Implications for India-Eurasian collision. Terra Nova 5, 13-20.

Tortosa, A., Palomares, M. & Arribas, J., 1991. Quartz grain types in Holocene deposits from the Spanish Central System: Some problems in provenance analysis. Geol. Soc. Lond. Spec. Pub. 57, 47-54.

Toulkeridis, T., Clauer, N., Krfner, A., Reimer, T. & Todt, W., 1999 Characterization, provenance and tectonic setting of Fig Tree greywackes from the Archean Barberton Belt, South Africa. Sed. Geol. 124, 113-129.

Treloar, P. J., 1989. Imbrication and unroofing of the Himalayan thrust stack of the north Indian plate, north Pakistan. Geol. Bull. Univ. Peshawar 22, 25-44.

Treloar, P. J. & Coward, M. P., 1991. Indian Plate motion and shape: Constraints on the geometry of the Himalayan orogen. Tectonophysics 191, 189-198.

Treloar, P. J. & Searle, M. P. (Eds.), 1993. Himalayan Tectonics. Geol. Soc. Spec. Pub. 74, 630p.

Treloar, P. J., Rex, D. C., Guise, P. G., Coward, M. P., Searle, M. P., Windley, B. F., Petterson, M. G., Jan, M. Q. & Luff, I. W., 1989a. K/Ar and Ar/Ar geochronology of the Himalayan collision in NW Pakistan: Constraints on the timing of suturing, deformation, metamorphism and uplift. Tectonics 8, 881-909,

Treloar, P. J., Broughton, R. D., Williams, M. P., Coward, M. P. & Windley, B. F., 1989b. Deformation, metamorphism and imbrication of the Indian plate, south of the main mantle Thrust, north Pakistan. J. Met. Geol. 7, 111-125.

Treloar, P. J., Brodie, K. H., Coward, M. P., Jan, M. Q., Khan, M. A., Knipe, R. J., Rex, D. C. & Williams, M. P., 1990. The evolution of the Kamila shear zone, Kohistan, Pakistan. In: Salisbury, M. H. and Fountain, D. M. (Eds.), Exposed Cross-sections of the Continental Crust. Kluwer Academic Press, Amsterdam, 175-214.

Treloar, P. J., Potts, G. J., Wheeler, J. & Rex, D. C., 1991a. Structural evolution and asymmetric uplift of the Nanga Parbat syntaxis, Pakistan Himalaya. Geologische Rundschau 80, 411-428.

Treloar, P. J., Rex, D. C. & Williams, M. P., 1991b. The role of erosion and extension in unroofing the Indian Plate thrust stack, Pakistan Himalaya, Geol. Mag. 128, 465-478.

Treloar, P. J., Coward, M. R., Chambers, A. F., Izatt, C. N. & Jackson, K. C., 1992. Thrust geometries, interferences and rotations in the Northwest Himalaya. In: McClay, K. R. (Ed.), Thrust Tectonics. Chapman and Hall, New York, 325-342.

Treloar, P. J., Petterson, M. G., Jan, M. Q. & Sullivan, M. A., 1996. A re-evaluation of the stratigraphy and evolution of the Kohistan arc sequence, Pakistan Himalaya: Implication for magmatic and tectonic arc building processes. J. Geol. Soc. Lond. 153, 681-93.

Treloar, P. J., Rex, D. C., Guise, P. G., Wheeler, J., Hurford, A. J. & Carter, A., 2000. Geochronological constraints on the evolution of the Nanga Parbat syntaxis, Pakistan Himalaya. In: Khan, M. A., Treloar, P. J., Searle, M. P. and Jan, M. Q. (Eds.), Tectonics of the Nanga Parbat Syntaxis and the Western Himalaya. Geol. Soc. Lond. Spec. Pub. 170, 137-162.

Treloar, P. J., O'Brien, P. J., Parrish, R. R. & Khan, M. A., 2003. Exhumation of early Tertiary, coesite-bearing eclogites from the Pakistan Himalaya. J. Geol. Soc. Lond. 160, 367-376.

Tucker, M. E., 2001. Sedimentary Petrology: An Introduction to the Origin of the Sedimentary Rocks. 3rd Ed. Blackwell Sci. Publ., Oxford. 262 pp.

Turner, P., 1980. Continental Red Beds. Developments in Sedimentology 29. Elsevier. 562 pp.

Uddin, A. & Lundberg, N., 1998. Cenozoic history of the Himalayan-Bengal system: Sand composition in the Bengal basin, Bangladesh. Geol. Soc. Am. Bull. 110, 497-511.

Valdiya, K. S., 1980. Geology of the Kumaon Lesser Himalaya. Wadia Institute of Himalaya, Dehra Dun, India. 291pp.

Valdiya, K. S., 1992. The Main Boundary Thrust Zone of Himalaya, India. Annals Tectonicae 6, 54-84.

Validya, K. S., 2003. Reactivation of Himalayan frontal fault: Implications. Current Science 85, 1013-1040.

Valdiya, K. S. & Bhatia, S. B. (Eds.), 1980. Stratigraphy and Correlations of Lesser Himalayan Formations. Hindustan Publishing Corporation, India. 330p.

Valloni, R. & Maynard I. B., 1981. Detrital modes of recent deep sea sands and their relation to tectonic setting: A first approximation. Sediment. 28, 75-84.

Valloni, R. & Mezzadri, G., 1984. Compositional suites of terrigenous deep-sea sands of the present continental margins. Sediment. 31, 353-364.

Vance, D., Ayres, M., Kelley, S. & Harris, N., 1998. The thermal response of a metamorphic belt to extension: Constraints from laser Ar data on metamorphic micas. EPSL 162, 153-164.

Van de Kamp, P. C. & Leake, B. E., 1985. Petrography and geochemistry of feldspathic and mafic sediments of the northeastern Pacific margin. Trans. R. Soc. Edinburgh: Earth Sci. 76, 411-449.

Van de Kamp, P. C. & Leake, B. E., 1994. Petrology, geochemistry, provenance and alteration of Pennsylvanian-Permian arkose, Colorado and Utah. Geol. Soc. Am. Bull. 105, 1581-1582.

Van Houten, F. B., 1973. Meaning of molasse. Geol. Soc. Am. Bull. 84, 1973-1975.

Van Houten, F. B., 1981. The odyssey of molasses. In Miall, A. D. (Ed.), Sedimentation and Tectonics in Alluvial Basins. Geol. Assoc. Can. Spec. Paper 23, 35-48.

Vance, D. & Harris, N., 1999. Timing of prograde metamorphism in the Zanskar Himalaya. Geology 27, 395-398.

Villa, I. M., Lemennicier, Y. & LeFort, P., 1996. Late Miocene to Early Pliocene tectonometamorphism and cooling in south-central Karakorum and Indus-Tsangpo suture, Chogo Lungma area (NE Pakistan). Tectonophysics, 260, 201-214.

Virdi, N. S., 1979. On the geodynamic significance of mega-lineaments in the Outer and Lesser regions of western Himalaya. Himalayan Geology 9, 79-99.

Vishnu-Mittre, 1984. Floristic change in the Himalaya (southern slopes) and Siwaliks from the mid-Tertiary to Recent times. In: Whyte, R. O. (Ed.), The Evolution of the East Asian Environment. Univ. of Hong Kong.483-503.

Wadia, D. N., 1926. The geology of Poonch State (Kashmir) and adjacent portions of the Punjab. Geol. Surv. India Mem. 51, pt 2, 185-370.

Wadia, D. N., 1931. The syntaxis of the NW Himalaya. Rec. Geol. Surv. India. 65/2: 189-223.

Wadia, D. N., 1953. Geology of India. 3rd edition. MacMillan and Co. Limited, Lond. 553pp.

Waheed, A. & Wells, N. A., 1990. Changes in paleocurrents during the development of an obliquely convergent plate boundary (Sulaiman fold-belt, southwestern Himalayas, west-central Pakistan). Sed. Geol. 67, 237-261.

Walker, C. B., Searle, M. P. & Waters, D. J., 2001. An integrated tectonothermal model for the evolution of the High Himalaya in western Zanskar with constraints from thermobarometry and metamorphic modeling. Tectonics 20, 810-833.

Walker, J. D., Martin, M. W., Bowring, S. A., Searle, M. P., Waters, D. J. & Hodges, K. V., 1999. Metamorphism, melting, and extension; age constraints from the High Himalayan slab of Southeast Zanskar and Northwest Lahaul. J. Geol. 107, 473-495.

Walker, R. G. & Cant, D. J., 1984. Sandy fluvial systems. In: Walker, R. G. (Ed.), Facies Models. Geol. Assoc. Canada. 71-89.

Walker, T. R., 1967. Formation of red beds in modern and ancient deserts. Geol. Soc. Am. Bull. 78.

Wanas, H. A. & Abdel-Maguid, N. M., 2006. Petrography and geochemistry of the Cambro-Ordovician Wajid Sandstone southwest Saudi Arabia: Implications for provenance and tectonic setting. J. Asian Earth Sciences 27, 416-429.

Weaver, C. E., 1967. Potassium, illite and the ocean. Geochim. Cosmochim. Acta 31, 2181-2196.

Weaver, C. E., 1989. Clays, Muds, and Shales. Elsevier, Amsterdam. 819 pp.

Weedon, G. P. & McCave, I. N., 1991. Mud turbidites from the Oligocene and Miocene Indus Fan at Sites 722 and 731 on the Owen Ridge. Proc. Ocean Drilling Program, Scientific Results 117, 215-220.

Welcomme, J. L., Benammi, M., Crochet, J. Y., Marivaux, L., Metais, G., Antoine, P. O. & Baloch, I., 2001. Himalayan forelands: Paleontological evidence for Oligocene detrital deposits in the Bugti Hills (Balochistan, Pakistan). Geol. Mag. 138, 397-405.

Wells, N. A., 1983. Transient streams in sand-poor redbeds: Early-middle Eocene Kuldana Formation of northern Pakistan. Spec. Pub. Int. Assoc. Sediment. 6, 393-403.

Wells, N. A., 1984. Marine and Continental Sedimentation in the Early Cenozoic Kohat Basin and Northwestern Indo-Pakistan. Unpub. Ph.D. Thesis, Univ. of Michigan, Ann Arbor, 465p.

Wells, N. A. & Dorr, J. A., 1987. Shifting of the Kosi River, Northern India. Geology 15, 204-207.

West, R. M., 1984. Siwalik faunas from Nepal: Paleoecologic and paleoclimatic implications. In: Whyte, R. O. (Ed.), The Evolution of the East Asian Environment. Centre for Asian Studies, Univ. of Hong Kong. 724-44.

Whipple, K. X. & Tucker, G. E., 1999. Dynamics of the stream power river incision model: Implications for height limits of mountain ranges, landscape response time scales and research needs. J. Geophys. Res. 104, 17661-17674.

White, N., Parrish, R. R., Bickle, M. J., Najman, Y. M. R., Burbank, D. & Maithani, A., 2001. Metamorphism and exhumation of the northwest Himalaya constrained by U-Th-Pb analysis of detrital monazite grains from early foreland basin sediments. J. Geol. Soc. Lond. 158, 625-635.

White, N. M., Pringle, M., Garzanti, E., Bickle, M., Najman, Y., Chapman, H. & Friend, P., 2002. Constraints on the exhumation and erosion of the High Himalayan Slab, NW India, from foreland basin deposits. EPSL 195, 29-44.

Whitmore, G. P., Crook, K. A. W. & Johnson, D. P., 2004. Grain size control of mineralogy and geochemistry in modern river sediment, New Guinea collision, Papua New Guinea. Sed. Geol. 171, 129-157.

Whittington, A., 1996. Exhumation overrated at Nanga Parbat, northern Pakistan. Tectonophysics 206, 215-226.

Wignall, P. B. & Myers, K. J., 1988. Interpreting the benthic oxygen levels in mudrocks, a new approach. Geology 16, 452-455.

Willett, S. D., 1999. Orogeny and orography: The effects of erosion on the structure of mountain belts. J. Geophys. Res. 104, 28957-28982.

Williams, P. F. & Rust, B. R., 1969. The sedimentology of a braided river. J. Sed. Pet. 39, 649-679.

Willis, B., 1993a. Ancient river systems in the Himalayan foredeep, Chinji Village area, northern Pakistan. Sed. Geol. 88, 1-76.

Willis, B., 1993b. Evolution of Miocene fluvial systems in the Himalayan foredeep through a two kilometer-thick succession in northern Pakistan. Sed. Geol. 88, 77-121.

Willis, B. & Behrensmeyer, A. K., 1994. Architecture of Miocene overbank deposits in northern Pakistan. J. Sed. Res. B64, 60-67.

Willis, B. & Behrensmeyer, A. K., 1995. Fluvial systems in Siwalik Miocene and Wyoming Paleogene. Palaeo. Palaeo. Palaeo. 115, 13-35.

Winchester, J. A. & Max, M. D., 1989. Tectonic setting discrimination in clastic sequences: An example from the Late Proterozoic Erris Group, NW Ireland. Precamb. Res. 45, 191-201.

Windley, B. F., 1995, The Evolving Continents. 3rd Ed. John Wiley & Sons, Chichester, 526pp.

Winslow, D. M., Zeitler, P. K., Chamberlain, C. P. & Hollister, L. S., 1994. Direct evidence for a steep geotherm under conditions of rapid denudation, western Himalaya, Pakistan. Geology 22, 1075-1078.

Winslow, D. M., Chamberlain, C. P. & Zeitler, P. K., 1995. Metamorphism and melting of the lithosphere due to rapid denudation, Pakistan Himalaya. J. Geology 103, 395-408.

Wright, J. D. & Thunell, R. C., 1988. Neogene planktonic foraminifera1 biogeography and paleoceanography of the Indian Ocean. Micropaleont. 34, 193-216.

Wright, V. P. & Tucker, M. E., 1991. Calcrete. Reprint Series of the Int. Assoc. Sediment. 2, 352p.

Wronkiewicz, D. J. & Condie, K. C., 1987. Geochemistry of Archean shales from the Witwatersrand Supergroup, South Africa: Source-area weathering and provenance. Geochim. Cosmochim. Acta 51, 2401-2416.

Wronkiewicz, D. J. & Condie, K. C., 1989. Geochemistry and provenance of sediments from the Pongola Supergroup, South Africa: Evidence for a 3.0 Ga old continental craton. Geochim. Cosmochim. Acta 53, 1537-1549.

Wronkiewicz, D. J. & Condie, K. C., 1990. Geochemistry and mineralogy of sediments from the Ventersdorp and Transvaal Supergroups, South Africa: Cratonic evolution during the early Proterozoic. Geochim. Cosmochim. Acta 54, 343-354.

Wynne, A. B., 1874. Notes on the geology of neighborhood of Mari hill station in the Punjab. Ibid. Recs. 7, 64-74.

Wynne, A. B., 1879. A geological reconnaissance from the Indus at Khushalgargh to the Kurran at Thal on the Afghan frontier. Geol. Surv. India. Rec. 12, 100-114.

Xianzeng, W., 1984. The paleoenvironment of China from the Tertiary. In: Whyte, R. O. (Ed.), The Evolution of the East Asian Environment. Univ. of Hong Kong. 472-482.

Yamamoto, H. & Nakamura, E., 1996. Sm-Nd dating of garnet granulites from the Kohistan complex, northern Pakistan. J. Geol. Soc. Lond. 153, 965-969.

Yamamoto, H. & Nakamura, E., 2000. Timing of magmatic and metamorphic events in the Jijal complex of the Kohistan arc deduced from Sm-Nd dating of mafic granulites. In: Khan, M. A., Treloar, P. J., Searle, M. P. and Jan, M. Q. (Eds.), Tectonics of the Nanga Parbat Syntaxis and the Western Himalaya. Geol. Soc. Lond. Spec. Pub., 170, 313–319.

Yan, Y., Xia, B., Lin, G., Cui, X., Hu, X., Yan, P. & Zhang, F., 2007. Geochemistry of the sedimentary rocks from the Nanxiong Basin, South China and implications for provenance, paleoenvironment and paleoclimate at the K/T boundary. Sed. Geol. 197, 127-140

Yeats, R. S. & Lillie, R. J., 1991. Contemporary tectonics of the Himalayan frontal fault system: Folds, blind thrusts and the 1905 Kangra earthquake. J. Struct. Geol. 13, 215-225.

Yeats, R. S. & Lawrence, R. D., 1984. Tectonics of the Himalayan thrust belt in northern Pakistan. In: Haq, B. U. and Milliman, J. D. (Eds.), Marine Geology and Oceanography of Arabian Sea and Coastal Pakistan. Van Nostrand, Reinhold, New York. 177-198.

Yin, A. 2006. Cenozoic tectonic evolution of the Himalayan orogen as constrained by along-strike variation of structural geometry, exhumation history, and foreland sedimentation. Earth Sci. Rev. 76, 1-131.

Yin, A., Harrison, T. M., Ryerson, F. J., Chen, W., Kidd, W. S. F. & Copeland, P., 1994. Tertiary structural evolution of the Gangdese thrust system, southeastern Tibet. J. Geophys. Res. 99, 18175-18201.

Young, S. W., 1976. Petrographic textures of detrital polycrystalline quartz as an aid to interpreting crystalline source rocks. J. Sed. Pet. 46, 595-603.

Young, S. W., Basu, A., Suttner, L. J., Mack G. H. & Darnell, N. A., 1975. Use of size composition trends in Holocene soil and fluvial sand for palaeoclimate interpretation. Proceedings IX International Sedimentological Congress, Nice, France 1, 201-209.

Yoxall, W. H., 1969. The relationship between falling base level and lateral erosion in experimental streams. Geol. Soc. Am. Bull. 80, 1379-1384.

Yu, K. M., Lee, G. H. & Boggs Jr., S., 1997. Petrology of Late Paleozoic-Early Mesozoic Pyeongan group sandstones, Gohan area, South Korea and its provenance and tectonic implications. Sed. Geol. 109, 321-338.

Zaleha, M. J., 1997a. Fluvial and lacustrine paleoenvironments of the Miocene Siwalik Group, Khaur area, northern Pakistan. Sediment. 44, 349-368.

Zaleha, M. J., 1997b. Intra- and extra-basinal controls on fluvial deposition in the Miocene Indo-Gangetic foreland basin, northern Pakistan. Sediment. 44, 369-390.

Zeitler, P. K., 1985. Cooling history of the NW Himalaya, Pakistan. Tectonics 4, 127-51

Zeitler, P. K., Tahirkheli, R. A. K., Naesser, C., Johnson, N. & Lyon, J., 1980. Preliminary fission-track ages from Swat valley, northern Pakistan. Geol. Bull. Univ. Peshawar 13, 23–29.

Zeitler, P. K., Johnson, N. M., Naeser, C. W. & Tahirkheli, R. A. K., 1982. Fission-track evidence for Quaternary uplift of the Nanga Parbat region, Pakistan. Nature 298, 255-257.

Zeitler, P. K., Sutter, J. F., Williams, I. S., Zartman, R. & Tahirkheli, R. A. K., 1989. Geochronology and temperature history of the Nanga Parbat-Haramosh Massif, Pakistan. In: Malinconico, L. L. and Lillie, R. J. (Eds.), Tectonics of the Western Himalaya. Geol. Soc. Am. Spec. Paper 232, 1-22.

Zeitler, P. K., Chamberlain, C. P. & Smith, H. A., 1993. Synchronous anatexis, metamorphism, and rapid denudation at Nanga Parbat (Pakistan Himalaya). Geology 21, 347-350.

Zeitler, P. K., Koons, P. O., Bishop, M. P., Chamberlain, C. P., Craw, D., Edwards, M. A., Hamidullah, S., Jan, M. Q., Khan, M. A., Khattak, M. U. K., Kidd, W. S. F., Mackie, R. L., Meltzer, A. S., Park, S. K., Pecher, A., Poage, M. A., Sarker, G., Schneider, D. A., Seeber, L. & Shroder, J. F., 2001. Crustal reworking at Nanga Parbat, Pakistan: Metamorphic consequences of thermal-mechanical coupling facilitated by erosion. Tectonics 20, 712-728.

Zhao, W. L. & Morgan, W. J., 1985. Uplift of Tibetan plateau. Tectonics 4, 359-369.

Zhao, W. L., Nelson, K. D. and the Project INDEPTH Team, 1993. Deep seismic reflection evidence for continental underthrusting beneath southern Tibet. Nature 366, 557-559.

Zhichen, S., Haomin, L., Yahui, Z. & Gengwu, L., 1984. The Miocene floristic regions of east Asia. In: Whyte, R. O. (Ed.), The Evolution of the East Asian Environment. Univ. of Hong Kong, 448-460.

Zimmermann, U. & Bahlburg, H., 2003. Provenance analysis and tectonic setting of the Ordovician clastic deposits in the southern Puna Basin, NW Argentina. Sediment. 50, 1079-1104.

Zuffa, G. G., 1980. Hybrid arenites: Their composition and classification. J. Sed. Pet. 50, 21-29.

Appendix A. XRD diagrams generally observed in most of the mudstone samples of the Kamlial, Chinji and Nagri formations of the southwestern Kohat.

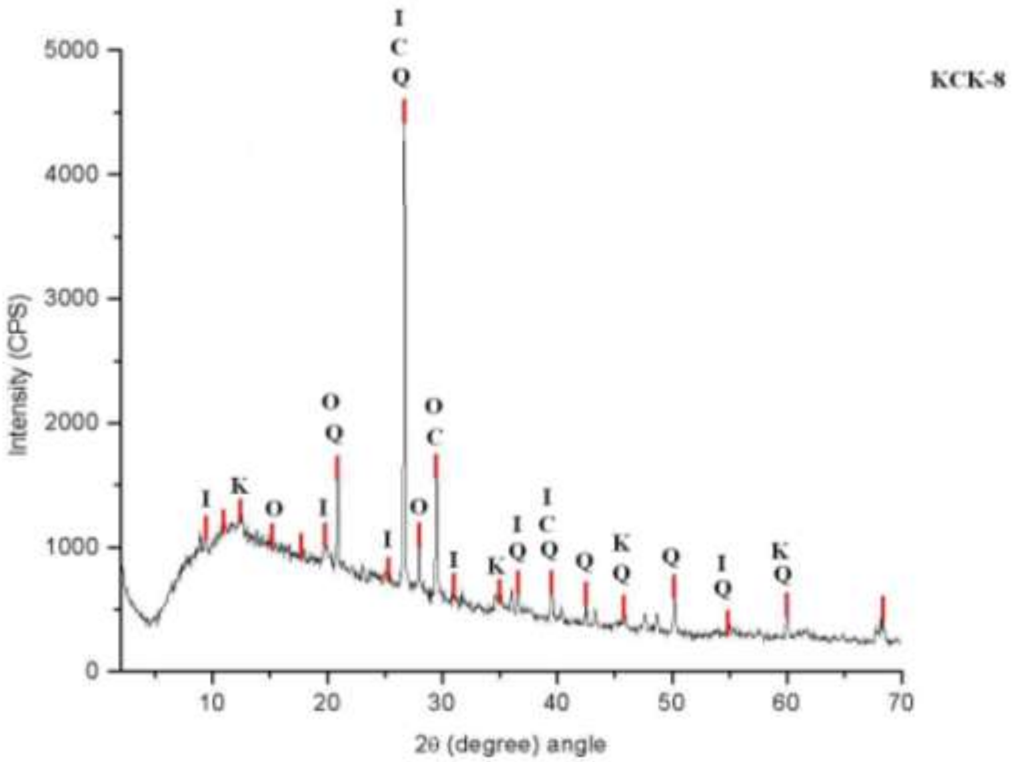

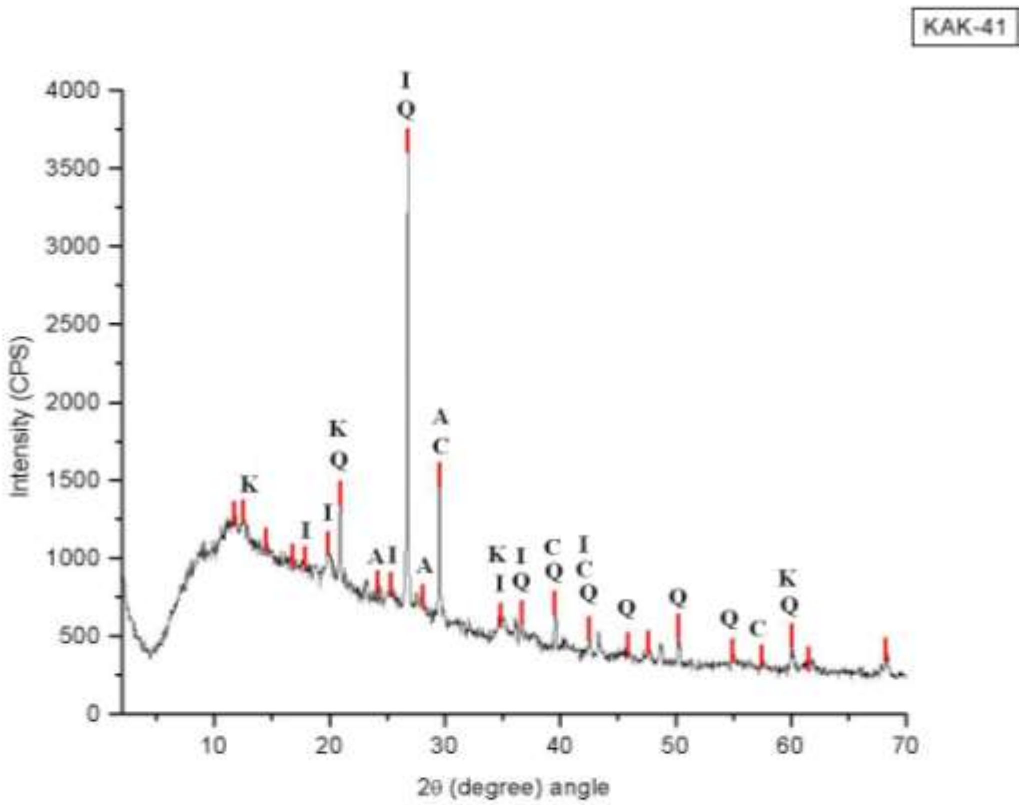

Selected mudstone samples of the Kamlial Formation I = Illite, K = Kaolinite, Q = Quartz, C = Calcite, O = Orthoclase, A = Albite.

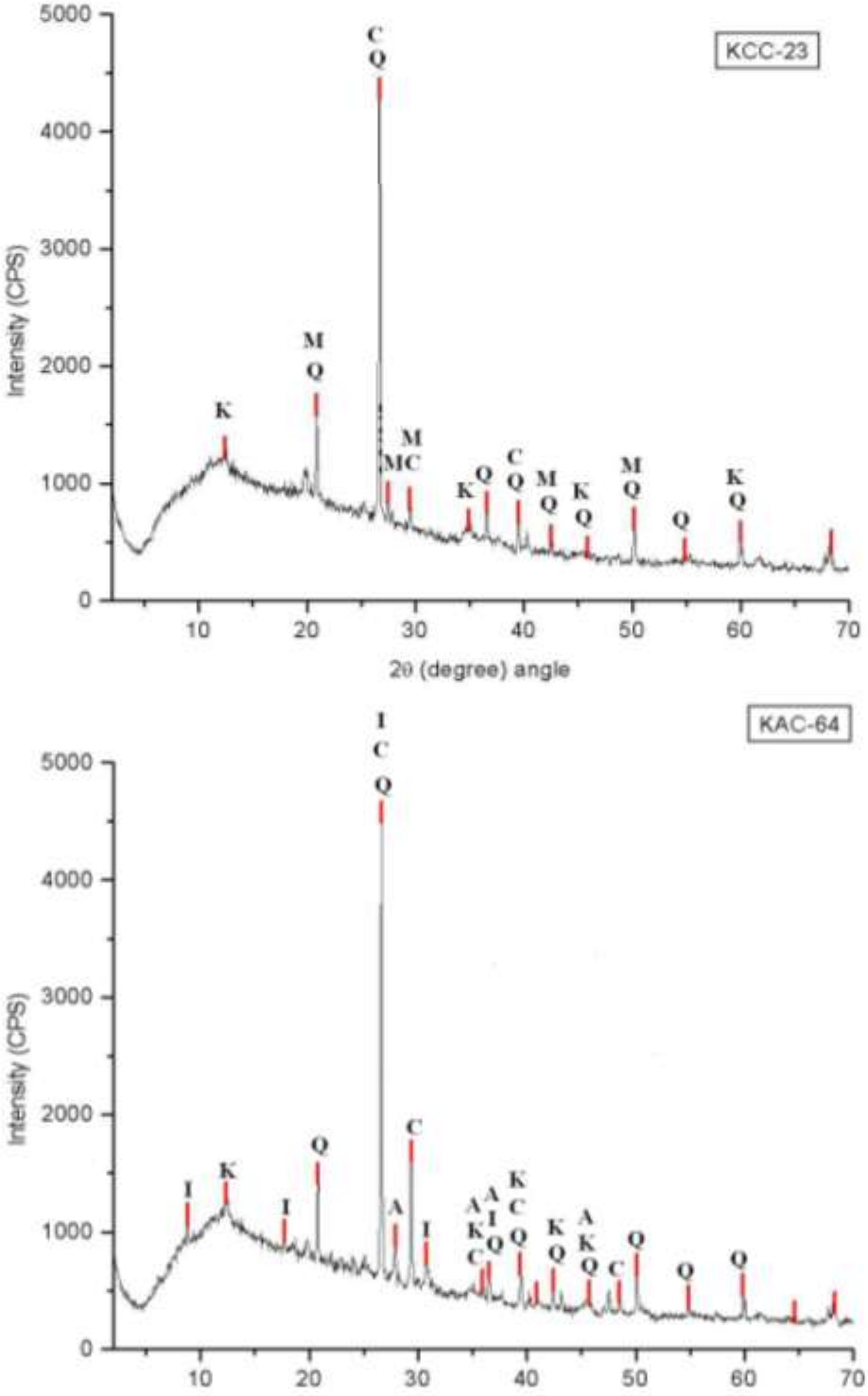

Selected mudstone samples of the Chinji Formation. I = Illite, K = Kaolinite, Q = Quartz, C = Calcite, M = Microcline, A = Albite.

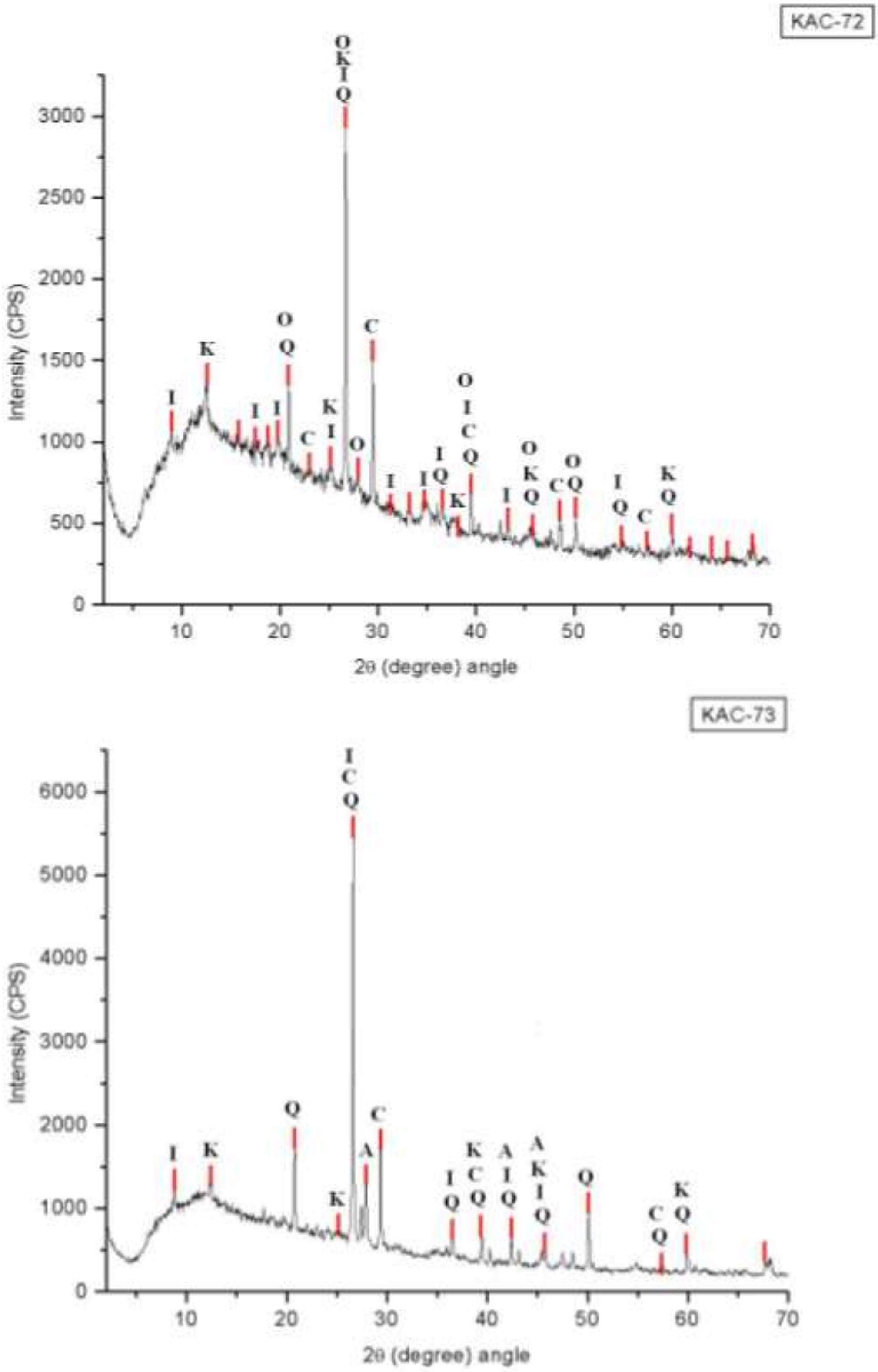

Selected mudstone samples of the Chinji Formation from Banda Assar syncline Illite (I), Kaolinite (K), Quartz (Q), Calcite (C), Orthoclase (O) and Albite (A).

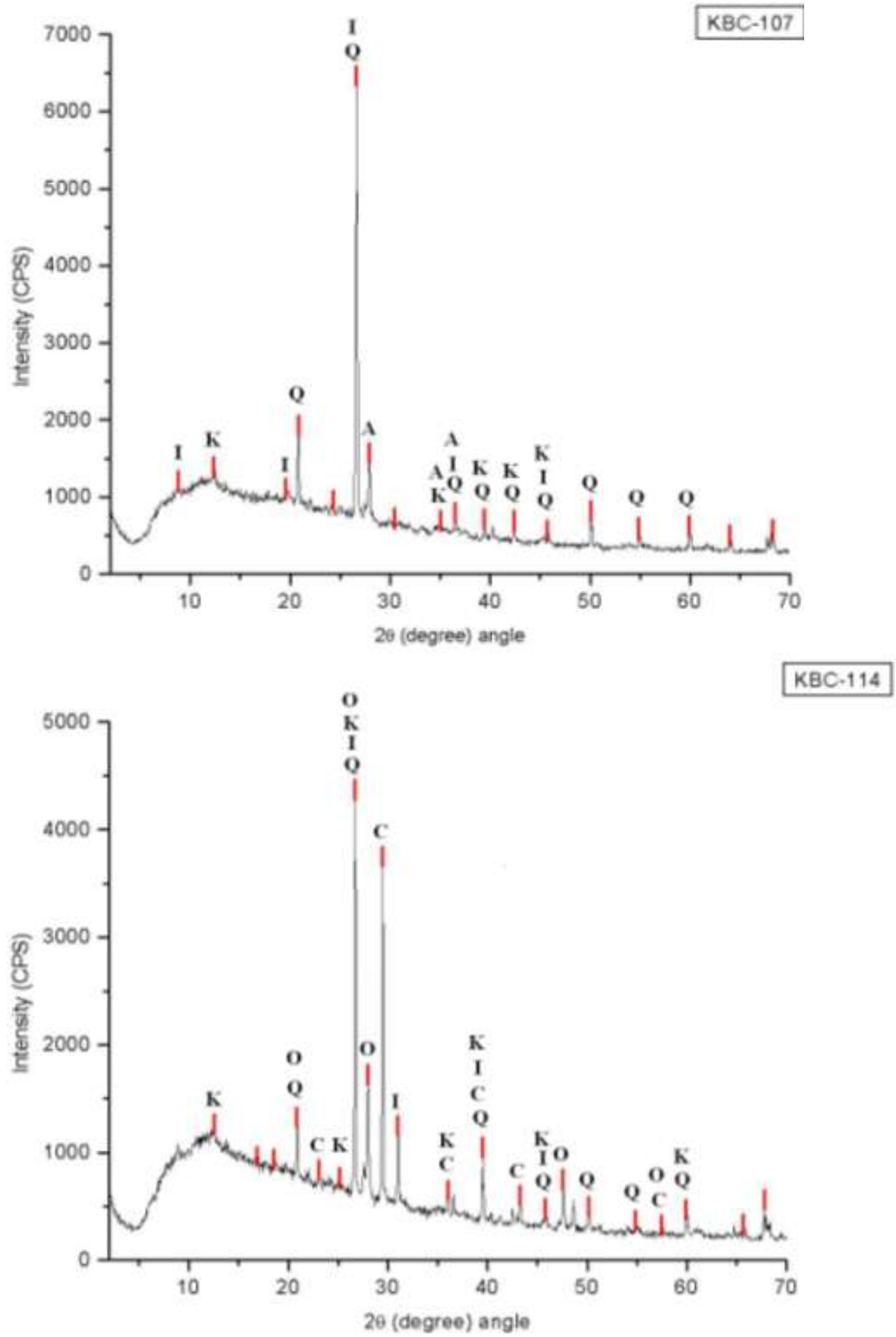

Selected mudstone samples of the Chinji Formation from Bahadar Khel anticline. I = Illite, K = Kaolinite, Q = Quartz, C = Calcite, O = Orthoclase, A = Albite.

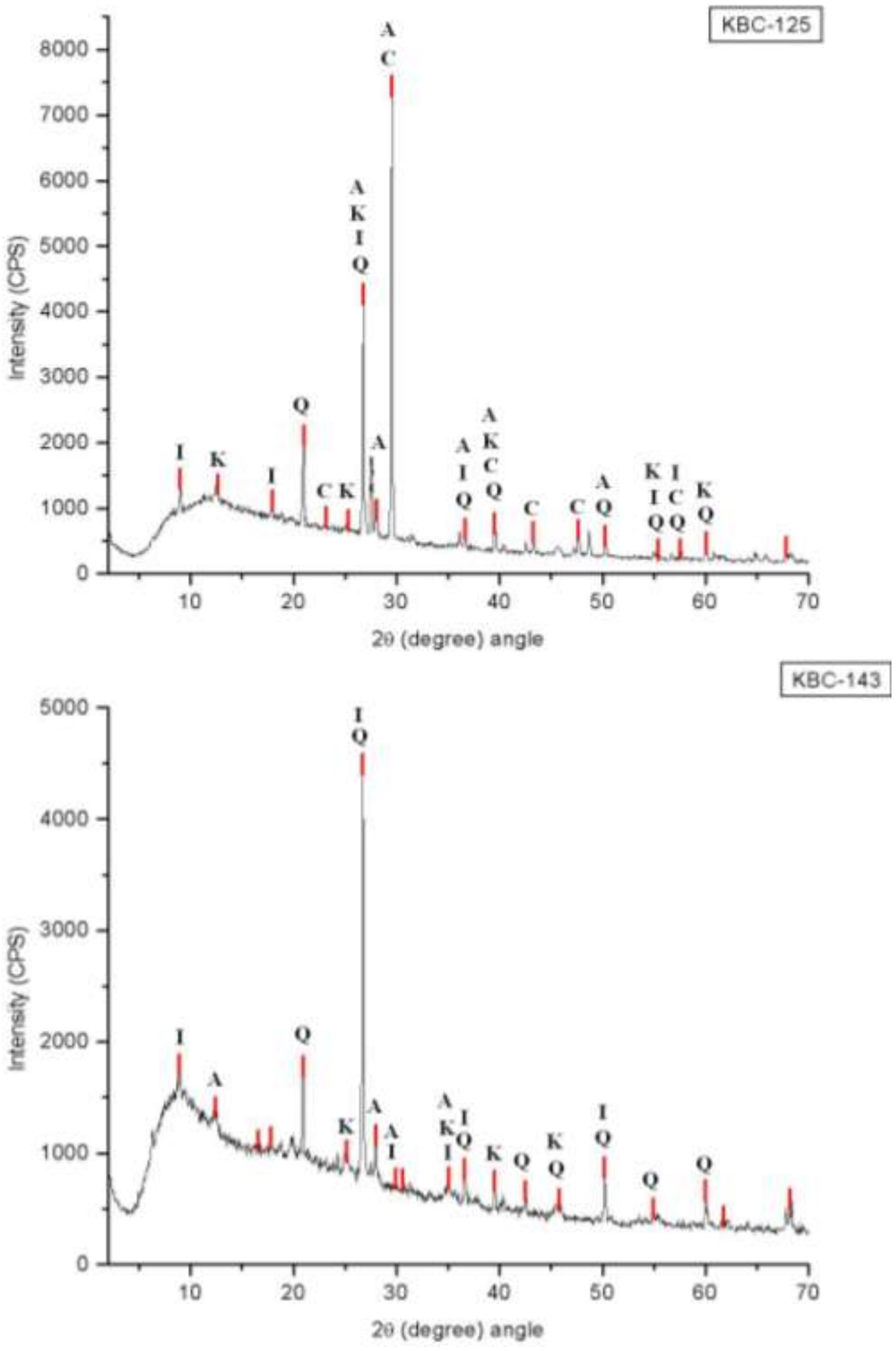

Selected mudstone samples of the Chinji Formation from Bahadar Khel anticline Illite (I), Kaolinite (K), Quartz (Q), Calcite (C) and Albite (A). However, Fig. 7.10 shows absence of calcite cement.

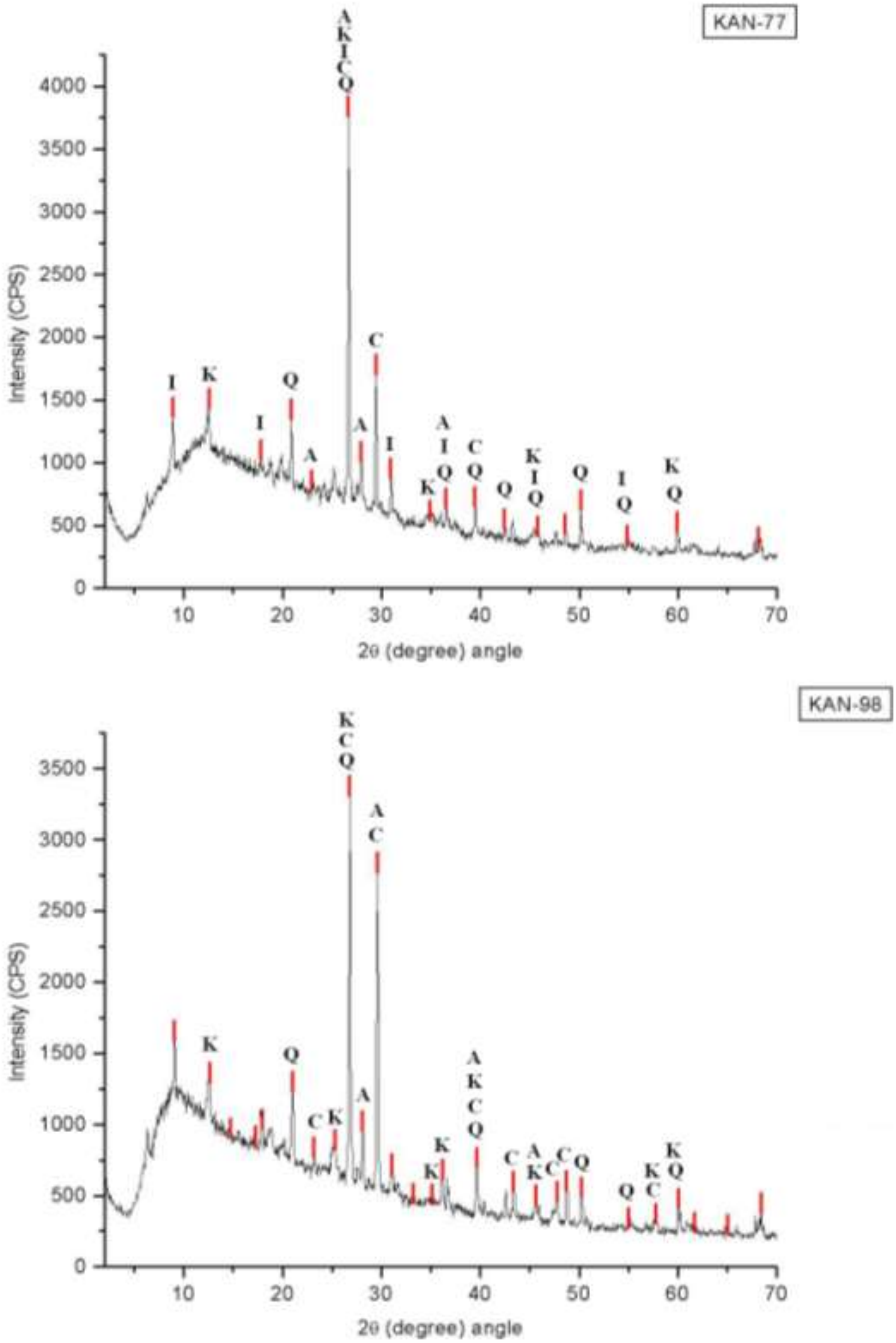

Selected mudstone samples of the Nagri Formation from Banda Assar syncline. Illite (I), Kaolinite (K), Quartz (Q), Calcite (C) and Albite (A).

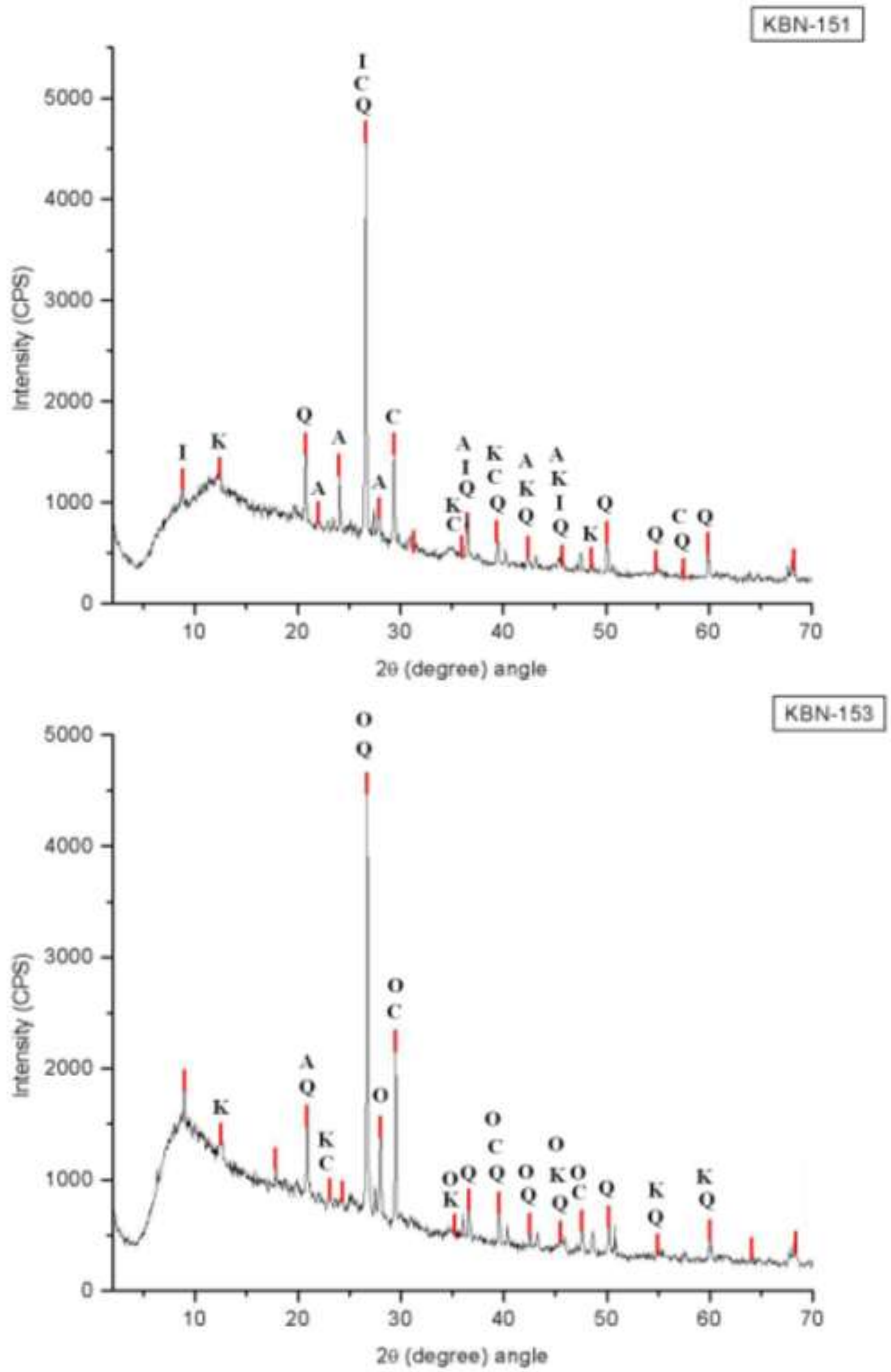

Selected mudstone samples of the Nagri Formation from Bahadar Khel anticline. I = Illite, K = Kaolinite, Q = Quartz, C = Calcite, O = Orthoclase, A = Albite.

Appendix B. XRD data of the selected mudstone samples of the Neogene sedimentary sequence of the southwestern Kohat.

Sample KAK-41		ICDD No. 30419 Quartz		ICDD No. 20629 Calcite		ICDD No. 20056 Illite		ICDD No. 30052 Kaolinite		ICDD No. 90456 Albite	
2θ	D	2θ	D	2θ	D	2θ	D	2θ	D	2θ	D
11.75	7.52512										
12.5	7.07525							12.470	7.092		
14.5	6.10354	-	-	-	-	-	-	-	-	-	-
16.8	5.27275	-	-	-	-	-	-	-	-	-	-
17.9	4.95113					17.813	4.975				
19.9	4.45781					19.871	4.464				
20.95	4.2367	20.858	4.255					19.961	4.444		
24.15	3.68207									24.188	3.676
25.35	3.51043					25.906	3.436				
26.75	3.3298	26.631	3.344			26.813	3.322				
28.1	3.17282									28.085	3.175
29.55	3.02034			29.543	3.021					29.634	3.012
34.85	2.57219					35.057	2.558	35.057	2.558		
36.65	2.44988	36.541	2.457			36.634	2.451				
39.55	2.27667	39.529	2.278	39.529	2.278						
42.55	2.12284	42.355	2.132	43.209	2.092	42.355	2.132				
45.9	1.97539	45.784	1.980								
47.65	1.90685										
50.25	1.81411	50.034	1.821								
54.95	1.66954	54.955	1.669								
57.5	1.60141			57.557	1.600						
60.05	1.53936	59.988	1.541					59.988	1.541		
61.55	1.50539										

Sample KCC-12		ICDD No. 50490 Quartz, Low		ICDD No. 30596 Calcite		ICDD No. 310968 Illite-1M		ICDD No. 30059 Kaolinite		ICDD No. 90457 Albite, Ord	
2θ	D	2θ	D	2θ	D	2θ	D	2θ	D	2θ	D
8.9	9.92743					8.836	10.00				
10.8	8.18482	-	-	-	-	-	-	-	-	-	-
12.55	7.04717							12.559	7.042		
15.35	5.76741	-	-	-	-	-	-	-	-	-	-
20.85	4.2568	20.858	4.255								
22.05	4.02777									22.026	4.032
23.1	3.84701			23.196	3.831						
25.2	3.53098							25.092	3.546		
26.65	3.34206	26.631	3.344	26.631	3.344	26.631	3.344	26.722	3.333	26.540	3.356
27.95	3.1895									27.994	3.185
29.45	3.03037			29.452	3.030						
30.9	2.8914					30.823	2.899				
36.55	2.45636	36.541	2.457			36.355	2.469			36.355	2.469
39.45	2.28221	39.435	2.283	39.341	2.288						
42.45	2.12761	42.450	2.128								
45.8	1.97947	45.784	1.980			45.592	1.988	45.784	1.980		
47.55	1.91062			47.321	1.919						
50.15	1.81749	50.131	1.818								
54.9	1.67094	54.855	1.672								
59.95	1.54169	59.988	1.541					59.988	1.541		
64.0	1.45354										

continued.

Sample KCC-23		ICDD No. 50490 Quartz, Low		ICDD No. 30596 Calcite		ICDD No. 30052 Kaolinite		ICDD No. 190926 Microcline, Ordered	
2θ	D	2θ	D	2θ	D	2θ	D	2θ	D
12.45	7.10355					12.470	7.092		
20.9	4.24673	20.858	4.255					21.037	4.219
26.7	3.33592	26.631	3.344	26.631	3.344				
27.45	3.24645							27.448	3.247
29.45	3.03037			29.452	3.030			29.452	3.030
34.95	2.56506					35.057	2.558		
36.6	2.45312	36.541	2.457						
39.5	2.27944	39.435	2.283	39.341	2.288				
42.5	2.12522	42.450	2.128					42.640	2.119
45.9	1.97539	45.784	1.980			45.592	1.988		
50.15	1.81749	50.131	1.818					50.229	1.815
54.9	1.67094	54.855	1.672						
60.0	1.54052	59.988	1.541			59.988	1.541		
68.35	1.37125								

Sample KCC-64		ICDD No. 50490 Quartz, Low		ICDD No. 30596 Calcite		ICDD No. 310968 Illite-1M		ICDD No. 50143 Kaolinite		ICDD No. 90466 Albite, Ordered	
2θ	D	2θ	D	2θ	D	2θ	D	2θ	D	2θ	D
8.85	9.9834					8.836	10.00				
12.35	7.16084							12.382	7.143		
17.7	5.00662					17.635	5.025				
20.8	4.26692	20.858	4.255								
26.6	3.34823	26.631	3.344	26.631	3.344	26.631	3.344				
27.9	3.1951									27.903	3.195
29.4	3.03541			29.452	3.030						
30.75	2.90516					30.823	2.899				
35.95	2.49597			36.077	2.488			36.077	2.488	35.984	2.494
36.5	2.45961	36.541	2.457			36.355	2.469			36.541	2.457
39.4	2.28499	39.435	2.283	39.341	2.288			39.435	2.283		
40.9	2.20459										
42.4	2.13	42.450	2.128					42.450	2.128		
45.75	1.98152	45.784	1.980					45.688	1.984	45.784	1.980
48.5	1.87539			48.383	1.880						
50.1	1.81919	50.131	1.818								
54.85	1.67234	54.855	1.672								
59.9	1.54285	59.988	1.541								
64.65	1.44049										

continued.

Sample KAC-72		**ICDD No. 50490 Quartz, Low**		**ICDD No. 240027 Calcite**		**ICDD No. 240495 Illite-2M2**		**ICDD No. 30059 Kaolinite**		**ICDD No. 20534 Orthoclase**	
2θ	D	2θ	D	2θ	D	2θ	D	2θ	D	2θ	D
8.95	9.87208					8.570	10.309				
12.55	7.04717							12.559	7.042		
15.8	5.60415	-	-	-	-	-	-	-	-	-	-
17.5	5.06339					17.545	5.051				
18.8	4.71609	-	-	-	-	-	-	-	-	-	-
19.8	4.4801					19.782	4.484				
20.9	4.24673	20.858	4.255							20.858	4.255
23.0	3.86351			23.106	3.846						
25.15	3.53789					25.272	3.521	25.092	3.546		
26.7	3.33592	26.631	3.344			26.631	3.344	26.722	3.333	26.722	3.333
28.0	3.18392									27.994	3.185
29.45	3.03037			29.452	3.030						
31.35	2.85091					31.189	2.865				
33.2	2.69615										
34.75	2.57936					34.687	2.584				
36.6	2.45312	36.541	2.457			36.634	2.451				
38.25	2.351							38.405	2.342		
39.5	2.27944	39.435	2.283	39.435	2.283	39.435	2.283			39.341	2.288
43.25	2.09009					43.399	2.083				
45.85	1.97743	45.784	1.980					45.784	1.980	45.592	1.988
48.55	1.87358			47.610	1.908						
50.15	1.81749	50.131	1.818							50.034	1.821
54.9	1.67094	54.855	1.672			55.054	1.667				
57.5	1.60141			57.356	1.605						
60.0	1.54052	59.988	1.541					59.988	1.541		
61.85	1.49881										

Sample KAC-73		**ICDD No. 50490 Quartz, Low**		**ICDD No. 30596 Calcite**		**ICDD No. 310968 Illite-1M**		**ICDD No. 30052 Kaolinite**		**ICDD No. 90466 Albite, Ordered**	
2θ	D	2θ	D	2θ	D	2θ	D	2θ	D	2θ	D
8.8	10.04001					8.836	10.00				
12.45	7.10355							12.470	7.092		
20.8	4.26692	20.858	4.255								
25.15	3.53789							24.820	3.584		
26.6	3.34823	26.631	3.344	26.631	3.344	26.631	3.344				
27.9	3.1951									27.903	3.195
29.4	3.03541			29.452	3.030						
36.5	2.45961	36.541	2.457			36.355	2.469				
39.4	2.28499	39.435	2.283	39.341	2.288			39.154	2.299		
42.4	2.13	42.450	2.128			42.166	2.141			42.545	2.123
45.75	1.98152	45.784	1.980			45.592	1.988	45.592	1.988	45.784	1.980
50.1	1.81919	50.131	1.818								
57.4	1.60396			57.155	1.610						
59.9	1.54285	59.988	1.541					59.988	1.541		

continued.

Sample KBC-106		**ICDD No. 20471 Quartz**		**ICDD No. 30612 Calcite**		**ICDD No. 30059 Kaolinite**		**ICDD No. 100393 Albite, Disordered**	
2θ	D	2θ	D	2θ	D	2θ	D	2θ	D
9.05	9.76322	-	-	-	-	-	-	-	-
12.55	7.04717					12.559	7.042		
13.15	6.72694	-	-	-	-		-	-	-
16.7	5.3041	-	-	-	-	-	-	-	-
18.05	4.91032	-	-	-	-	-	-	-	-
19.5	4.54835	-	-	-	-	-	-	-	-
21.0	4.22673								
23.2	3.83065			23.106	3.846				
24.35	3.65228							24.459	3.636
26.8	3.3237	26.813	3.322			26.722	3.333		
28.15	3.16729							28.085	3.175
29.6	3.01536			29.634	3.012			29.634	3.012
34.65	2.58658								
36.2	2.4793					36.169	2.481		
39.6	2.27391	39.529	2.278	39.529	2.278	39.716	2.268	39.716	2.268
43.35	2.0855			43.684	2.070				
45.65	1.98563	45.784	1.980			45.784	1.980	45.592	1.988
48.65	1.86996								
50.3	1.81242	50.034	1.821						
55.05	1.66674	54.955	1.669			55.253	1.661		
57.6	1.59887			57.960	1.590				
60.1	1.5382	59.988	1.541			59.988	1.541		

Sample KBC-107		**ICDD No. 50490 Quartz, Low**		**ICDD No. 310968 Illite-1M**		**ICDD No. 50143 Kaolinite**		**ICDD No. 20515 Albite**	
2θ	D	2θ	D	2θ	D	2θ	D	2θ	D
8.85	9.9834			8.836	10.00				
12.35	7.16084					12.382	7.143		
19.6	4.52536			19.603	4.525				
20.85	4.2568	20.858	4.255						
24.3	3.65968								
26.6	3.34823	26.631	3.344	26.631	3.344				
27.9	3.1951							27.812	3.205
30.5	2.9284								
35.1	2.55444					35.150	2.551	35.150	2.551
36.55	2.45636	36.541	2.457					36.634	2.451
39.45	2.28221	39.435	2.283			39.435	2.283		
42.45	2.12761	42.450	2.128			42.450	2.128		
45.75	1.98152	45.784	1.980	45.592	1.988	45.688	1.984		
50.1	1.81919	50.131	1.818						
54.85	1.67234	54.855	1.672						
59.95	1.54169	59.988	1.541						
64.0	1.45354								

continued.

Sample KBC-112		ICDD No. 50490 Quartz, Low		ICDD No. 310968 Illite-1M		ICDD No. 30052 Kaolinite		ICDD No. 90457 Albite, Ord	
2θ	D	2θ	D	2θ	D	2θ	D	2θ	D
8.85	9.9834			8.836	10.00				
12.45	7.10355					12.470	7.092		
20.8	4.26692	20.858	4.255						
23.55	3.77451	-	-	-	-	-	-	-	-
26.6	3.34823	26.631	3.344	26.631	3.344			26.540	3.356
27.95	3.1895							27.994	3.185
34.9	2.56862					35.057	2.558		
36.5	2.45961	36.541	2.457	36.355	2.469			36.355	2.469
39.45	2.28221	39.435	2.283			39.154	2.299		
42.5	2.12522	42.450	2.128						
45.75	1.98152	45.784	1.980	45.592	1.988	45.592	1.988		
50.1	1.81919	50.131	1.818						
54.85	1.67234	54.855	1.672						
59.9	1.54285	59.988	1.541			59.988	1.541		
63.95	1.45456								

Sample KBC-114		ICDD No. 50490 Quartz, Low		ICDD No. 20629 Calcite		ICDD No. 310968 Illite-1M		ICDD No. 30059 Kaolinite		ICDD No. 20534 Orthoclase	
2θ	D	2θ	D	2θ	D	2θ	D	2θ	D	2θ	D
12.55	7.04717							12.559	7.042		
16.85	5.25722	-	-	-	-	-	-	-	-	-	-
18.55	4.77908	-	-	-	-	-		--	-	-	-
20.9	4.24673	20.858	4.255							20.858	4.255
23.1	3.84701			23.106	3.846						
25.15	3.53789							25.092	3.546		
26.7	3.33592	26.631	3.344			26.631	3.344	26.722	3.333	26.722	3.333
28.0	3.18392									27.994	3.185
29.5	3.02535			29.543	3.021						
31.0	2.8823					30.823	2.899				
36.05	2.48927			36.077	2.488			36.169	2.481		
39.5	2.27944	39.435	2.283	39.529	2.278	39.716	2.268	39.716	2.268		
43.25	2.09009			43.209	2.092						
45.8	1.97947	45.784	1.980			45.592	1.988	45.784	1.980		
47.6	1.90873									47.610	1.908
50.15	1.81749	50.131	1.818								
54.9	1.67094	54.855	1.672								
57.45	1.60268			57.557	1.600					57.557	1.600
59.95	1.54169	59.988	1.541					59.988	1.541		
65.7	1.41999										

continued.

Sample KBC-125		**ICDD No. 30444 Quartz**		**ICDD No. 20629 Calcite**		**ICDD No. 20056 Illite**		**ICDD No. 30059 Kaolinite**		**ICDD No. 100393 Albite, Disordered**	
2θ	D	2θ	D	2θ	D	2θ	D	2θ	D	2θ	D
9.0	9.81735					8.836	10.00				
12.65	6.99269							12.559	7.042		
17.95	4.93745					17.813	4.975				
21.0	4.22673	21.127	4.202								
23.15	3.83881			23.106	3.846						
25.3	3.51725							25.092	3.546		
26.75	3.3298	26.813	3.322			26.813	3.322	26.722	3.333	27.721	3.215
28.1	3.17282									28.085	3.175
29.55	3.02034			29.543	3.021					29.634	3.012
36.65	2.44988	36.820	2.439			36.634	2.451			36.634	2.451
39.55	2.27667	39.716	2.268	36.077	2.488			39.716	2.268	39.716	2.268
43.3	2.08779			43.209	2.092						
47.65	1.90685			47.321	1.919						
50.25	1.81411	50.326	1.812							50.131	1.818
55.4	1.65704	55.652	1.650			55.253	1.661	55.253	1.661		
57.55	1.60014	57.557	1.600	57.557	1.600	57.557	1.600				
60.05	1.53936	59.988	1.541					59.988	1.541		

Sample KBC-143		**ICDD No. 30427 Quartz**		**ICDD No. 150603 Illite**		**ICDD No. 120447 Kaolinite**		**ICDD No. 90457 Albite, Ord**	
2θ	D	2θ	D	2θ	D	2θ	D	2θ	D
8.9	9.92743			8.570	10.30				
12.4	7.13208					12.382	7.143		
16.6	5.33583	-	-	-	-	-	-	-	-
17.85	4.96489	-	-		-	-	-	-	-
20.95	4.2367	20.858	4.255						
25.15	3.53789					25.001	3.559		
26.7	3.33592	26.631	3.344	26.722	3.333				
28.0	3.18392							27.994	3.185
29.95	2.98091			29.817	2.994			29.999	2.976
30.6	2.91906	-	-	-	-	-	-	-	-
35.05	2.55797			35.057	2.558	35.150	2.551	35.150	2.551
36.6	2.45312	36.634	2.451	36.634	2.451				
39.55	2.27667					39.435	2.283		
42.5	2.12522	42.640	2.119						
45.85	1.97743	45.784	1.980			45.688	1.984		
50.2	1.8158	50.326	1.812	50.326	1.812				
54.95	1.66954	54.955	1.669						
60.0	1.54052	59.988	1.541						
61.8	1.4999								
68.2	1.3739								

continued.

Sample KAN-77		**ICDD No. 50490 Quartz, Low**		**ICDD No. 30596 Calcite**		**ICDD No. 310968 Illite-1M**		**ICDD No. 30059 Kaolinite**		**ICDD No. 90457 Albite, Ord**	
2θ	D	2θ	D	2θ	D	2θ	D	2θ	D	2θ	D
8.9	9.92743					8.836	10.00				
12.55	7.04717							12.559	7.042		
17.8	4.97872					17.635	5.025				
20.9	4.24673	20.858	4.255								
22.95	3.87181									23.016	3.861
26.65	3.34206	26.631	3.344	26.631	3.344	26.631	3.344	26.722	3.333	26.540	3.356
27.95	3.1895									27.994	3.185
29.45	3.03037			29.452	3.030						
30.95	2.88684					30.823	2.899				
34.95	2.56506							35.057	2.558		
36.55	2.45636	36.541	2.457			36.355	2.469			36.355	2.469
39.45	2.28221	39.435	2.283	39.341	2.288						
42.45	2.12761	42.450	2.128								
45.8	1.97947	45.78	1.98			45.592	1.988	45.784	1.980		
48.55	1.87358										
50.15	1.81749	50.131	1.818								
54.9	1.67094	54.855	1.672			55.652	1.650				
59.95	1.54169	59.988	1.541					59.988	1.541		
68.15	1.37478										

Sample KBN-151		**ICDD No. 50490 Quartz, Low**		**ICDD No. 30596 Calcite**		**ICDD No. 310968 Illite-1M**		**ICDD No. 50143 Kaolinite**		**90466 Albite, Ordered**	
2θ	D	2θ	D	2θ	D	2θ	D	2θ	D		
8.8	10.04001					8.836	10.00				
12.4	7.13208							12.382	7.143		
20.8	4.26692	20.858	4.255								
22.05	4.02777									22.026	4.032
24.05	3.69716									24.098	3.690
26.6	3.34823	26.631	3.344	26.631	3.344	26.631	3.344				
27.9	3.1951									27.903	3.195
29.4	3.03541			29.452	3.030						
31.35	2.85091										
36.0	2.49261			36.077	2.488			36.077	2.488		
36.5	2.45961	36.541	2.457			36.355	2.469			36.541	2.457
39.4	2.28499	39.435	2.283	39.341	2.288			39.435	2.283		
42.45	2.12761	42.450	2.128					42.450	2.128	42.545	2.123
45.75	1.98152	45.784	1.980			45.592	1.988	45.688	1.984	45.784	1.980
48.55	1.87358							48.771	1.866		
50.1	1.81919	50.131	1.818								
54.85	1.67234	54.855	1.672								
57.55	1.60014	57.255	1.608	57.155	1.610						
59.95	1.54169	59.988	1.541								
68.3	1.37213										

continued.

Sample KCK-8		ICDD No. 50490 Quartz, Low		ICDD No. 30596 Calcite		ICDD No. 240495 Illite-2M2		ICDD No. 30052 Kaolinite		ICDD No. 20534 Orthoclase	
2θ	D	2θ	D	2θ	D	2θ	D	2θ	D	2θ	D
9.4	9.40046					8.570	10.309				
11	8.03645										
12.45	7.10355							12.470	7.092		
15.2	5.82399									15.138	5.848
17.75	4.99263	-	-	-	-	-	-	-	-	-	-
19.8	4.4801					19.782	4.484				
20.9	4.24673	20.858	4.255							20.858	4.255
25.3	3.51725					25.272	3.521				
26.7	3.33592	26.631	3.344	26.631	3.344	26.631	3.344			26.722	3.333
28	3.18392									27.994	3.185
29.5	3.02535			29.452	3.030						
31	2.8823					31.189	2.865				
35	2.56151							35.057	2.558		
36.6	2.45312	36.541	2.457			36.634	2.451				
39.5	2.27944	39.435	2.283	39.341	2.288	39.435	2.283				
42.5	2.12522	42.450	2.128								
45.85	1.97743	45.784	1.980					45.592	1.988		
50.2	1.8158	50.131	1.818								
54.9	1.67094	54.855	1.672			55.054	1.667				
60	1.54052	59.988	1.541					59.988	1.541		
68.35	1.37125										